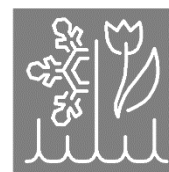




Universität Hamburg

DER FORSCHUNG | DER LEHRE | DER BILDUNG

Fachbereich
Chemie



Valorization of biogenic raw materials by selective catalytic oxidation using polyoxometalate catalysts and efficient downstream processing via nanofiltration

Cumulative Dissertation

with the aim of achieving a doctoral degree

Doctor rerum naturalium (Dr. rer. nat.)

at the Faculty of Mathematics, Informatics and Natural Sciences

Department of Chemistry

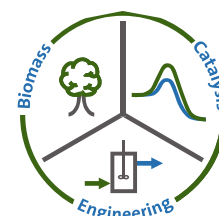
Institute of Technical and Macromolecular Chemistry

University of Hamburg

submitted by

Tobias Esser

Hamburg 2024



1. Evaluator Prof. Dr.-Ing. habil. Jakob Albert
Department of Chemistry
Institute of Technical and Macromolecular Chemistry
University Hamburg
2. Evaluator Prof. Dr.-Ing. Mirko Skiborowski
Department of Process and Chemical Engineering
Institute of Process Systems Engineering
Hamburg University of Technology
1. Examiner Prof. Dr.-Ing. habil. Jakob Albert
Department of Chemistry
Institute of Technical and Macromolecular Chemistry
University Hamburg
2. Examiner Prof. Dr. Lisa Vondung
Department of Chemistry
Institute of Inorganic and Applied Chemistry
University Hamburg
3. Examiner Dr. Thomas Hackl
Department of Chemistry
Scientific Service – NMR Spectroscopy
University Hamburg

Date of Disputation: 06.12.2024

This study was conducted between October 2020 and September 2023 at the Institute of Technical and Macromolecular Chemistry of the University Hamburg under the supervision of Prof. Dr.-Ing. habil. Jakob Albert.

List of Publications

Parts of this work and other studies have already been published in the following journals or presented as contributions at conferences.

Journals

- T. Esser, M. Huber, D. Voß, J. Albert, *Development of an efficient downstream process for product separation and catalyst recycling of a homogeneous polyoxometalate catalyst by means of nanofiltration membranes and design of experiments*, Chemical Engineering Research and Design, **2022**, 185, 37-50.
- A. Wassenberg, T. Esser, M. Poller, J. Albert, *Investigation of the Formation, Characterization, and Oxidative Catalytic Valorization of Humins*, Materials, **2023**, 16, 2864-2882.
- J. C. Raabe, T. Esser, F. Jameel, M. Stein, J. Albert, M. Poller, *Study on the incorporation of various elements into the Keggin lacunary-type phosphomolybdate $[PMo_9O_{34}]^{9-}$ and subsequent purification of the polyoxometalates by nanofiltration*, Inorganic Chemistry Frontiers, **2023**, 10, 4854-4868.
- T. Esser, A. Wassenberg, J. C. Raabe, D. Voß, J. Albert, *Catalytic valorization of humins by selective oxidation using transition-metal substituted Keggin-type polyoxometalate catalysts*, ACS Sustainable Chemistry and Engineering, **2024**, 12, 543-560.
- T. Esser, A. Wassenberg, D. Voß, J. Albert, *Selective catalytic oxidation of humins to carboxylic acids using $H_4[PVMo_{11}O_{40}]$ Keggin-type polyoxometalate enhanced by alcohol doping and solubilizer*, RSC Reaction Chemistry and Engineering, **2024**, 7, 357-375.
- A. Wassenberg, T. Esser, M. Poller, D. Voß, J. Albert, *Humin-free synthesis of levulinic acid from fructose using heteropolyacid catalysts*, Biofuels Bioproducts Biorefining, **2024**, 115, 139-152.

VIII | *List of Publications*

- J. C. Raabe, T. Esser, M. Poller, J. Albert, *Synthesis and characterization of V substituted Anderson-type telluro-molybdates and tungstates for catalytic oxidation of furan derivatives to formic and maleic acid*, *Catalysis Today*, **2024**, 441, 114899.
- T. Esser, A. Wassenberg, D. Voß, J. Albert, *Process optimization for the selective catalytic oxidation of humins to carboxylic acids and application of an efficient downstream process by the means of nanofiltration*, *Chemical Engineering and Research Design*, **2024**, 209, 311-322.

Conferences

- T. Esser, D. Voß, J. Albert, *Efficient downstream processing in green processes using homogenous polyoxometalate catalysts by means of nanofiltration membranes*, Presentation, 14th European Congress of Chemical Engineering, **2023**, Berlin/Germany.
- D. Voß, T. Esser, A. Wassenberg, J.C: Raabe, J. Albert, *Reaction engineering meets catalyst recycling: An innovative approach for combined humin valorization and homogeneous polyoxometalate recycling*, Poster, 57. Jahrestreffen Deutscher Katalytiker, **2024**, Weimar/Germany

Table of Content

LIST OF PUBLICATIONS	VII
LIST OF ABBREVIATIONS AND SYMBOLS.....	XIII
1 ZUSAMMENFASSUNG	1
2 ABSTRACT	5
3 INTRODUCTION	8
3.1 MOTIVATION	8
3.2 OBJECTIVE OF THE DISSERTATION	9
3.3 STRUCTURE OF THE DISSERTATION.....	10
4 THEORETICAL BACKGROUND	11
4.1 BIOGENIC RAW MATERIALS	11
4.1.1 <i>Structure of Primary Biomass</i>	12
4.1.1.1 Carbohydrates.....	13
4.1.1.2 Lignocellulose.....	14
4.1.1.3 Triglycerides	15
4.1.2 <i>Energetic and Technical Use of Biomass</i>	16
4.2 SELECTED PROCESSES FOR BIOMASS VALORIZATION.....	17
4.2.1 <i>The Biofine Process</i>	17
4.2.1.1 Formation of Humins	19
4.2.1.2 Structure of Humins.....	21
4.2.2 <i>The OxFA Process</i>	23
4.2.2.1 Fundamentals of the OxFA Process.....	23
4.2.2.2 Technical Execution of the OxFA Process	26
4.3 POLYOXOMETALATES.....	29
4.3.1 <i>Properties of Keggin-type Polyoxometalates</i>	32
4.3.2 <i>Applications of Polyoxometalates</i>	34
4.4 SELECTED CARBOXYLIC ACIDS OF INDUSTRIAL INTEREST	36
4.4.1 <i>Formic Acid</i>	37
4.4.1.1 Properties of Formic Acid	37
4.4.1.2 Production of Formic Acid	37
4.4.1.3 Applications for Formic Acid	40
4.4.2 <i>Acetic Acid</i>	41
4.4.2.1 Properties of Acetic Acid	41
4.4.2.2 Production of Acetic Acid.....	41
4.4.2.3 Applications for Acetic Acid	42
4.4.3 <i>Maleic Acid</i>	42
4.4.3.1 Properties of Maleic Acid.....	43
4.4.3.2 Production of Maleic Acid	43
4.4.3.3 Applications for Maleic Acid.....	44
4.4.4 <i>Levulinic Acid</i>	44

X | Table of Content

4.4.4.1 Properties of Levulinic Acid	45
4.4.4.2 Production of Levulinic Acid	45
4.4.4.3 Applications of Levulinic Acid	46
4.5 MEMBRANE TECHNOLOGY FOR HOMOGENEOUS CATALYST RECYCLING	47
4.5.1 Operating Principle for Membrane Separation	47
4.5.2 Driving Forces in Membrane Separation	51
4.5.3 Resistances in Membrane Separation.....	53
4.5.4 Nanofiltration.....	55
5 EXPERIMENTAL PART	57
5.1 10-FOLD BATCH REACTOR	58
5.2 3-FOLD BATCH REACTOR	59
5.3 600 ML BATCH REACTOR.....	60
5.4 NANOFILTRATION SYSTEM – POMMEM	62
5.5 ANALYTICS FOR QUALITATIVE & QUANTITATIVE MEASUREMENTS	63
5.6 CALCULATION BASES	66
5.6.1 Calculation of Reaction Key Figures using HPLC	66
5.6.2 Calculation of Reaction Key Figures using Quantitative ¹ H-NMR	68
5.6.3 Calculations for Solid Reaction Residues using CHNS.....	69
5.6.4 Calculations for Gaseous Reaction Products using GC.....	69
5.6.5 Calculations for Membrane Separation	70
5.7 CHEMICALS & GASES.....	70
6 CUMULATIVE PART OF THE DISSERTATION.....	74
6.1 DEVELOPMENT OF AN EFFICIENT DOWNSTREAM PROCESS FOR THE RECYCLING OF HOMOGENEOUS POLYOXOMETALATE CATALYSTS	75
6.2 SELECTIVE CATALYTIC OXIDATION OF FURAN DERIVATES AS MODEL SUBSTANCES FOR HUMINS.....	91
6.3 FROM MODEL SUBSTRATES TO REAL HUMINS - A NOVEL APPROACH FOR HUMIN VALORIZATION.....	112
6.4 PROCESS OPTIMIZATION FOR THE HUMIN VALORIZATION AND APPLICATION OF AN EFFICIENT DOWNSTREAM PROCESS USING NANOFILTRATION.....	133
7 COMPREHENSIVE DISCUSSION OF RESEARCH RESULTS	147
8 REFERENCES	163
9 APPENDIX	187
9.1 LIST OF HAZARDOUS SUBSTANCES	187
9.2 LIST OF FIGURES	190
9.3 LIST OF TABLES	192
9.4 LIST OF SCHEMES.....	193
9.5 SUPPORTING INFORMATION (ESI).....	194
9.5.1 ESI of 1 st Publication (Chapter 6.1)	194
9.5.2 ESI of 2 nd Publication (Chapter 6.2)	203
9.5.3 ESI of 3 rd Publication (Chapter 6.3)	229
9.5.4 ESI of 4 th Publication (Chapter 6.4)	240

ACKNOWLEDGMENTS..... 243
DECLARATION ON OATH..... 245

List of Abbreviations and Symbols

Acronym	Meaning
AA	Acetic acid
ATR	Attenuated total reflection
BT	Benzothiophene
CHNSO	Elemental analysis
CSTR	Continuous stirred tank-reactor
CV	Cyclic voltammogram
DBT	Dibenzothiophene
DFG	Deutsche Forschungsgemeinschaft
DFT	Density functional theory
DHH	2,5-dioxo-6-hydroxyhexanal
DME	Dimethyl ether
DMM	Dimethoxy methanol
e.g.	For example
ECODN	Extraction-coupled oxidative denitrification
ECODO	Extraction-coupled oxidative deoxygenation
ECODS	Extraction-coupled oxidative desulfurization
ESI	Electronic supplementary information
et al.	And other (Latin: et alia)
EtOH	Ethanol
FA	Formic acid
FDCA	2,5-furandicarboxylic acid
FID	Flame ionization detector
FT-IR	Fourier transform infrared spectroscopy
Gas	Gas/Gaseous
GC	Gas chromatography
GI	Glucose (glucose-based humin)
HDS	Hydrodesulfurization
HMBC	Heteronuclear multiple bond correlation
5-HMF	5-Hydroxymethylfurfural
HPA	Heteropolyanion
HPA-1 blue	Completely reduced HPA-1 ($H_4[PVMo_{11}O_{40}]$)
HPA-2 blue	Completely reduced HPA-2 ($H_5[PV_2Mo_{10}O_{40}]$)
HPA-n	Heteropolyanion substituted by n vanadium atoms ($H_{(3+n)}[PV_nMo_{12-n}O_{40}]$)

XIV | List of Abbreviations and Symbols

Acronym	Meaning
HPLC	High performance liquid chromatography
HSAB	Hard-Soft-Acid-Base concept
HSQC	Heteronuclear single quantum coherence
i	Variable component
ICP-OES	Optical emission spectrometry with inductively coupled plasma
IPA	Isopolyanion
j	Variable component
LeA	Levulinic acid
LHPA	Lacunary Keggin-type phosphormolybdate anion
LMCT	Ligand-to-metal-charge-transfer
LOHC	Liquid organic hydrogen carrier
M	Metal (transition metal)
MA	Maleic acid
MeOH	Methanol
MF	Microfiltration
MM	Methoxy methanol
MOF	Metal organic framework
MS	Model substance
MWCO	Molecular weight cut-off
NF	Nanofiltration
NH ₃ -SCR	Selective catalytic reduction using NH ₃
NMR	Nuclear magnetic resonance
NS	Number of scans
OA	Oxalic acid
ODS	Oxidative desulfurization
OxFA	Oxidative conversion of biomass to formic acid
PDA	Photodiode array detector
PFR	Plug flow reactor
pH	Pondus Hydrogenii, negative decadic logarithm of the hydrogen ion concentration
pK _a	Negative decadic logarithm of the acid constant (acid dissociation constant)
POM	Polyoxometalate
POMMem	Polyoxometalate membrane system
PrOH	Iso-propanol
PTFE	Polytetrafluoroethylene
pTSA	Para-Toluenesulfonic acid
R	Rest group

Acronym	Meaning
RID	Reflection index detector
SAA	Sulfoacetic acid
2-SBA	2-Sulfobenzoic acid
SCO	Selective catalytic oxidation
SEM	Scanning electron microscopy
SWV	Square wave voltammograms
TBA	Tetrabutylammonium
TCD	Temperature conductivity detector
TD	Time domain
TGA	Thermogravimetric analysis
UF	Ultrafiltration
vol.	Volume
wt.	Weight
X	Heteroatom
XRD	X-ray diffraction

Acronym (Flow Diagram)	Meaning
B	Tank
CV	Check valve
FIRC	Flow indicating, recording, and controlling
M	Motor
MC	Membrane cell
MFC	Mass flow controller
P	Pump
PI	Pressure indicating
PIR	Pressure indicating and recording
R	Reactor
SV	Safety valve (pressure relief valve)
TIC	Temperature indicating and controlling
TIR	Temperature indicating and recording
V	Valve

XVI | *List of Abbreviations and Symbols*

Formula Symbol	Meaning	Unit
A	Area	m ²
c	Molar concentration	mol L ⁻¹
E	Electrostatic potential	V
F	Faraday constant	C mol ⁻¹
h	Planck constant	J s
J	Permeate flux	kg h ⁻¹ m ⁻²
m	Mass	kg
M	Molecular mass	g mol ⁻¹
n	Molar amount	mol
N	Quantity	-
O/C	Ratio of the mass fraction of oxygen and carbon	-
p	Pressure	bar
R	Rejection	%
S	Selectivity	%
t	Time	s
T	Temperature	°C or K
V	Volume	m ³
w	Mass fraction	%
X	Conversion	%
Y	Yield	%
z	Charge number	-
α	Activity	mol L ⁻¹
γ	Molar fraction in gaseous phase	%
β	Mass concentration	kg L ⁻¹
δ	Chemical shift	ppm
μ	Chemical potential	kJ
ν	Frequency	Hz
π	Osmotic pressure	Pa
ρ	Density	kg m ⁻³

Index / Exponent	Meaning
0	Initial value (t=0)
C	Carbon
cat	Catalyst
Com i	Component i
End	At the end
Feed	Feed solution
H	Hydrogen

Index	Meaning
i	Variable number
liq	Liquid
n	Variable number
M	Metal (transition metal)
Mem	Membrane
MS	Model substance
ox	Oxidated
Per	Permeate
Pro i	Product i
red	Reduced
Ret	Retentate
sol	Solvent
Stand	Standard
Sub	Substrate
theo	Theoretical
V	Vanadium
k	Variable number for heteroatoms in HPA structure
m	Variable number for oxygen atoms in HPA structure
y	Variable charge number complex anions
x	Variable number

1 Zusammenfassung

Die selektive katalytische Oxidation von lignocellulotischer Biomasse stellt eine Schlüsseltechnologie dar, mit welcher biobasierte Chemikalien und Energieträger hergestellt werden können. In sogenannten *Bioraffinerien* bilden sich jedoch häufig auch komplexe unerwünschte Nebenprodukte, die als *Humine* bezeichnet werden. Dadurch wird die vollständige Verwertung aller Rohstoffkomponenten verhindert und die Wirtschaftlichkeit dieser Prozesse vermindert. Dabei kann die stoffliche Verwertung von Huminen durch selektive katalytische Oxidation einen Beitrag leisten die Rohstoffeffizienz in Bioraffinerien zu steigern.

Um die Umsetzung der Humine untersuchen zu können, wurden zunächst verschiedene Generationen an Humin-ähnlichen Modelsubstraten anstelle der komplexen Humine umgesetzt. In diesem Kontext wurde zuerst die Umsetzung von Furfural als Modelsubstanz der ersten Generation mit homogenen Polyoxometallat (POM) Katalysatoren der *Keggin*-Struktur zu industrierelevanten Carbonsäuren unter milden Bedingungen (90 °C, 30 bar O₂) in wässriger Phase untersucht. In den eingesetzten POM-Katalysatoren wurde Molybdän als Addenda-Atom in der Phosphormolybdänsäure (H₃[PMo₁₂O₄₀]) mit unterschiedlichen Übergangsmetallen substituiert und auf diese Weise modifiziert. Die Ergebnisse zeigen, dass die elektrochemischen Eigenschaften der Katalysatoren mit dem Umsatz von Furfural korrelieren und eine Anpassung des Redoxpotentials erzielt werden konnte. Hierdurch war es möglich, sowohl den Umsatz als auch die Selektivität zu beeinflussen. Der einfach Vanadium-substituierte Katalysator H₄[PVMo₁₁O₄₀] erwies sich hinsichtlich der katalytischen Aktivität und der Ausbeute an Maleinsäure sowie Ameisensäure als überlegen. Des Weiteren wurde demonstriert, dass eine mehrfache Substitution von Addenda-Atomen mit bis zu sechs Vanadium-Atomen die katalytische Aktivität drastisch steigert, jedoch auf Kosten der Selektivität. Demnach stellte der H₄[PVMo₁₁O₄₀] Katalysator den besten Kompromiss aus Aktivität und Selektivität dar.

Im Weiteren wurden verschiedene kommerzielle Monofuran-Derivate, darunter 2-Methylfuran, 2-Furfurylalkohol, 2(5H)-Furanon, 5-Hydroxymethylfurfural (5 HMF) und 2-Furan-carbonsäure mit dem ausgewählten Katalysator unter sonst gleichen Bedingungen umgesetzt. Hieraus konnten Struktur-Aktivitäts-Selektivitätsbeziehungen abgeleitet werden. Gemäß dieser Beziehungen ist eine geeignete Funktionalisierung der Substrate mit Sauerstoff entscheidend für eine effiziente

Umwandlung. Dies zeigte sich insbesondere im Fall des 5-HMF, das als bifunktionelles Substrat (hohe Sauerstofffunktionalisierung) vollständig zu den Hauptprodukten Ameisensäure, Maleinsäure und CO₂ umgesetzt werden konnte. Basierend auf den Ergebnissen wurden Reaktionspfade abgeleitet, in denen die Eliminierung von Ameisensäure durch oxidative C-C Bindungsspaltung und Elektronenübertragung auf den Katalysator den initialen Schritt darstellt. Anschließend zum initialen Schritt wird der Katalysator reoxidiert und dabei 5-Hydroxyfuran-2(5H)-on als Intermediat gebildet, das anschließend zu Maleinsäure oxidiert wird. Analog zu diesem postulierten Reaktionspfad konnte auch 2-Furancarbonsäure umgewandelt werden. Jedoch kann die oxidative C-C Bindungsspaltung nur durch die Decarboxylierung von 2-Furancarbonsäure erfolgen, die erheblich weniger effizient ist, weshalb deutlich geringere Umsätze, aber hohe Selektivitäten zu Maleinsäure erzielt wurden. Die postulierten Reaktionspfade konnten auch bei komplexeren Modellschubstanzen der zweiten Generation, die aus unterschiedlich verknüpften oder verzweigten Furan-Derivaten bestanden, beobachtet werden. Die Modellschubstanzen der zweiten Generation verfügen über verschiedene C-C oder C-O-C Bindungen, die unter anderen einzelne Furan-Ringe miteinander verknüpfen. Interessanterweise stellten Verbindungen mit einer geringeren Sauerstofffunktionalisierung und mehr C-C Bindungen eine erheblich größere Herausforderung als Substrate dar, jedoch konnten trotzdem alle ausgewählten Substanzen zu Ameisensäure und Maleinsäure umgewandelt werden.

Die gewonnenen Erkenntnisse wurden auf die Oxidation eines Glucose-basierten Humins in wässriger Phase übertragen. Hierdurch wurde demonstriert, dass der H₄[PVMo₁₁O₄₀]-Katalysator auch bei der Umsetzung der komplexen Humine einen relativen Selektivitätsvorteil gegenüber höher substituierten Katalysatoren hat. Hierbei sollte der Einsatz verschiedener alkoholischer Additive die Bildung von CO₂ weiter hemmen und so die Effizienz des Prozesses steigern. Bereits eine Zugabe von 5 Vol-% Methanol erwies sich dabei als effizient und ermöglichte eine starke Inhibierung der CO₂ Bildung, wodurch zum ersten Mal mehr Wertprodukte (Carbonsäuren) als CO₂ bei der Oxidation von Huminen gebildet wurde. Dieser beachtenswerte Effekt konnte sogar bei erhöhten Reaktionstemperaturen von 120 °C und damit bei einer gesteigerten Aktivität erzielt werden.

Als alternativer Ansatz wurde der Einsatz von para-Toluolsulfonsäure (pTSA) als Lösungsvermittler und Reaktionspromoter untersucht. Durch eine optimierte Zugabe

von 1,5 mmol pTSA, konnte die Aktivität der Umsetzung bereits bei einer Temperatur von 90 °C gesteigert werden. Erstaunlicherweise wurden auch ohne die CO₂ inhibierende Wirkung von Methanol Carbonsäuren und CO₂ fast äquivalent gebildet. Durch eine höhere Reaktionstemperatur von 120 °C stieg die Aktivität nochmals drastisch an, jedoch dominierte hierbei die Bildung von CO₂. Aus diesem Grund wurde die synergetische Kombination von Methanol zur Inhibierung der CO₂ Bildung und pTSA zur Steigerung der Aktivität bei 120 °C untersucht. Der neuartige Ansatz war allen bisher entwickelten Reaktionssystemen zur Oxidation von Huminen hinsichtlich Aktivität und Selektivität überlegen.

Im Anschluss wurden zeitaufgelöste Experimente durchgeführt, die zeigten, dass sich in den ersten Stunden der Sauerstoffanteil in den festen Rückständen der Reaktion stark erhöht. Gemäß dieser Beobachtung und Analysen via *Fourier-Transformation-Infrarotspektrometer* (FT-IR) werden zuerst sauerstofffunktionalisierte Bindungen gespalten, wodurch insbesondere kurzkettige Produkte wie Ameisensäure, Essigsäure und CO₂ entstehen. Dieser Prozess induziert neue Sauerstofffunktionalisierungen an vorher nicht funktionalisierten Kohlenstoffatomen, weshalb der Sauerstoffanteil steigt, und der Kohlenstoffanteil sinkt. Aufgrund dieses Mechanismus waren größere Fragmente der Humine nicht zugänglich. Nachfolgende Experimente an Huminen, die auf verschiedenen Zuckern basierten, sollten die Übertragbarkeit des Ansatzes auf unterschiedliche Humin-Strukturen demonstrieren. Hierbei konnte die effiziente und selektive Umsetzung dieser verschiedenen Humine mit dem neuen Reaktionssystem erfolgreich durchgeführt werden. Darüber hinaus ermöglichte das neue System den Einsatz des höher substituierten H₅[PV₂Mo₁₀O₄₀] Katalysators, wodurch eine höhere Aktivität und Ausbeute an Wertprodukten bei einer gleichzeitig gesenkten Reaktionstemperatur von 90 °C erreicht wurde.

Um dem Ziel eines nachhaltigen Prozesses gerecht zu werden, muss auch eine effiziente Rückgewinnung des homogenen Katalysators aus den Reaktionslösungen untersucht werden. Zu diesem Zweck wurde ein Nanofiltrations-Setup entwickelt und optimiert. Eine Besonderheit dieses Setups ist, dass es im Membranmodul einen integrierten Rührer besitzt, der für eine effiziente Überströmung der Membran verantwortlich ist, wodurch sich dieses System von der klassischen Cross-Filtration abhebt. Die Optimierung des entwickelten Systems erfolgte durch eine Versuchsreihe basierend auf der statistischen Versuchsplanung gemäß eines *Box-Hunter-Hunter*

Versuchsplans. Die Ergebnisse dieser Versuchsreihe identifizierten die Rührgeschwindigkeit als einflussreichsten Parameter für einen effizienten Rückhalt der Katalysatorkomponenten. Unter Anwendung der optimierten Parameter konnten hohe Rückhalte der Katalysatorkomponenten Vanadium (97 %) und Molybdän (99 %) sowie niedrige Rückhalte für Ameisensäure (3 %) und Essigsäure (10 %) erreicht werden. Im Anschluss wurde der Einfluss einer Anreicherung des Katalysators auf seine strukturelle Integrität untersucht. Die Experimente zur Aufkonzentrierung des Katalysators demonstrierten, dass sich dieser ohne Verlust der strukturellen Integrität anreichern lässt. Hierdurch war die Entfernung von über 80 % der Carbonsäuren aus den Reaktionslösungen möglich. Die Erkenntnisse wurden erfolgreich auf verschiedene POM-Katalysatoren übertragen. Um die Effizienz des Prozesses zu steigern, wurde eine Reihe an kommerziellen Nanofiltrationsmembranen unter Verwendung einer Modelllösung, basierend auf der Produktlösung der Oxidation der Humine gescreent. Hierbei erwies sich die säurestabile XN45 Membran der Firma *Mann+Hummel* als vielversprechend und ermöglichte einen Rückhalt der Katalysatorkomponenten Molybdän und Vanadium von über 99 % sowie einen gewünschten Rückhalt für Ameisensäure von 0 %.

Im Sinne der Nachhaltigkeit muss der Membranprozess lange Prozesszeiten ermöglichen, ohne sichtlichen Verlust der Trennleistung. Hierzu wurden Langzeitversuche durchgeführt, die zeigten, dass die ausgewählte Membran eine effiziente Trennung über eine Betriebszeit von 168 h ohne Verlust der Performance ermöglichte. In finalen Rezyklierungsstudien wurde der Katalysator nach Aufbereitung mittels Nanofiltration mehrfach in konsekutiven Oxidationsexperimenten an Huminen erfolgreich rezykliert. Dabei zeigten Messungen mittels ^{51}V -NMR, dass die Katalysatorstruktur erhalten blieb und damit auch die katalytische Aktivität. Dies war darauf zurückzuführen, dass die Oxidationsprodukte erfolgreich entfernt und folglich der pH-Wert auf Werte über 1 stabilisiert wurde. Ohne diese Stabilisierung des pH-Wertes, fiel dieser unter pH 1, wodurch es zum erheblichen Verlust der katalytischen Aktivität aufgrund der vermehrten Bildung weniger substituierter Katalysatorisomere kam. Dadurch konnte die Effizienz des entwickelten Nanofiltrationsprozesses demonstriert und somit eine Grundlage für einen kontinuierlichen Prozess geschaffen werden.

2 Abstract

The selective catalytic oxidation of lignocellulosic biomass is a key technology for the bio-based production of chemicals and energy carriers. In so-called *biorefineries*, complex undesired by-products, known as *humins*, can form. This prevents the complete utilization of all raw material components. The material utilization of humins through selective catalytic oxidation could contribute to increasing raw material efficiency of biorefineries.

In order to investigate the efficient conversion of humins, different generations of humin-like model substrates were initially used instead of the complex humins. In this context, furfural was converted as first-generation model substance to industrially relevant carboxylic acids using homogeneous *Keggin*-type polyoxometalate catalysts (POMs) under mild conditions (90 °C, 30 bar O₂) in aqueous phase. The POM-catalysts used were modified by the substitution of molybdenum as an addenda atom in the *Keggin*-type phosphomolybdic acid (H₃[PMo₁₂O₄₀]) by various other transition metals. A correlation between the electrochemical properties and the conversion of furfural was found and an adjustment of the redox potential was achieved. Due to this adjustment, it was possible to influence the conversion and selectivity. The singly vanadium-substituted H₄[PVMo₁₁O₄₀] catalyst was found to be superior in terms of catalytic activity and yields of maleic and formic acid. Multiple substitution of addenda atoms with up to six vanadium atoms drastically increased the catalytic activity, but at the expense of selectivity. Accordingly, the H₄[PVMo₁₁O₄₀] catalyst represented the best compromise between activity and selectivity.

Several commercially available monofuran derivatives, including 2-methylfuran, 2-furfuryl alcohol, 2(5H)-furanone, 5-hydroxymethylfurfural (5-HMF) and 2-furoic acid, were converted using the selected catalyst under otherwise identical conditions. Structure-activity-selectivity relationships were derived from these experiments. According to the relationships, a suitable functionalization of the substrates with oxygen is crucial for their efficient conversion. 5-HMF as a bifunctional substrate (high oxygen functionalization) could therefore be completely converted to the main products formic acid, maleic acid and CO₂. From the results, reaction pathways were derived in which the elimination of formic acid by oxidative C-C bond cleavage and electron transfer to the catalyst represents the initial step. 5-Hydroxyfuran-2(5H)-one is formed as intermediate by reoxidation of the catalyst, which is ultimately converted to maleic

acid. Analogous to the postulated reaction pathway, 2-furoic acid was also converted to maleic acid. However, the oxidative C-C bond cleavage can only occur by decarboxylation of 2-furoic acid, which is considerably less efficient causing significantly lower conversions. Both, 2-furoic acid and 2(5H)-furanone were selectively converted to maleic acid. The postulated reaction pathways could also be observed in oxidizing experiments using more complex model substances. These second-generation model substances consisted of differently linked or branched furan derivatives owning C-C or C-O-C bonds. The conversion of second-generation model substances also yielded in formic and maleic acid, although substrates with lower oxygen functionalization and C-C bonds represented a greater challenge.

The knowledge gained was transferred to the oxidation of glucose-based humins in aqueous phase. It was shown that the $H_4[PVMo_{11}O_{40}]$ catalyst has a relative selectivity advantage over more highly substituted POM-catalysts as predicted by the preliminary tests on model substances. Various alcoholic additives were tested as inhibitors to further decrease CO_2 formation. An addition of 5 vol% methanol proved to be the most efficient and enabled a strong inhibition of CO_2 formation, whereby for the first time more value-added products (carboxylic acids) than CO_2 were formed during the oxidation of humins. This remarkable effect could even be achieved at elevated reaction temperatures of 120 °C and thus at increased activity.

As an alternative approach, the use of para-toluenesulfonic acid (pTSA) as a solubilizer and reaction promoter was investigated. Using an optimized addition of 1.5 mmol pTSA, the activity of the reaction was increased already at a temperature of 90 °C. Surprisingly, almost equivalent yields of carboxylic acids and CO_2 were obtained even without the CO_2 -inhibiting effect of methanol. Increasing the reaction temperature to 120 °C allowed to drastically increase the activity, but the formation of CO_2 dominated. For this reason, the synergistic combination of methanol to inhibit CO_2 formation and pTSA to increase the activity at 120 °C was investigated. The new approach was superior to all previously developed reaction systems for the oxidation of humins in terms of activity and selectivity.

Time-resolved experiments showed that the oxygen content in the solid residues of the reaction increases significantly in the first hours of the reaction. According to this observation and *Fourier*-transform infrared spectroscopy (FT-IR) analyses, oxygen-functionalized bonds are initially cleaved, forming short-chain products such as formic acid, acetic acid, and CO_2 . This process induces new oxygen functionalization on

previously non-functionalized carbons. Consequently, the oxygen content increases and the carbon content decreases. Due to this mechanism, larger fragments of humin structure were not accessible. The efficient and selective conversion of several humins based on different sugars was conducted applying the new reaction system. Furthermore, the new system enabled the use of the higher substituted $H_5[PV_2Mo_{10}O_{40}]$ catalyst, which led to a higher activity and yield of value-added products even at a lower reaction temperature of 90 °C.

For the recovery of the homogeneous POM-catalysts, a nanofiltration system was developed and optimized. The used system has an integrated stirrer within the membrane cell, which is responsible for sufficient cross-flow of the membrane and therefore differs from classic cross-filtration. Through statistical design of experiments following a *Box-Hunter-Hunter* experimental plan, stirring speed was identified as the most influential parameter. Applying the optimized parameters, a high rejection for the catalyst components vanadium (97 %) and molybdenum (99 %) as well as a low rejection for formic acid (3 %) and acetic acid (10 %) were achieved. Enrichment experiments showed that the catalyst could be enriched without loss of structural integrity. In this process, over 80 % of carboxylic acids were removed from the reaction solution. The developed nanofiltration process was successfully transferred to various POM-catalysts. To increase the efficiency of the process, several commercial nanofiltration membranes were screened using a model solution based on the product solution of the selective catalytic oxidation of humins. The acid-stable XN45 membrane of *Mann+Hummel* proved to be promising, enabling high rejection of over 99 % for the catalyst components Molybdenum and Vanadium as well as a desirable low rejection for formic acid of 0 %.

Duration tests showed that the selected membrane enabled efficient separation over an operating time of 168 h without loss in performance. In final recycling studies, the catalyst was successfully recycled several times in consecutive oxidation experiments of humins after processing using nanofiltration. Measurements using ^{51}V -NMR showed that the catalyst structure and thus the catalytic activity are retained. This is due to the removal of the oxidation products and the stabilization of the pH value in an optimal range between 1.2 to 1.4. If the pH value was not stabilized and dropped below pH 1, significant loss of catalytic activity could be determined due to the increased formation of less substituted catalyst isomers. Hence, the efficiency of the nanofiltration process was demonstrated and the basis for a continuous process was created.

3 Introduction

The introduction is divided into three sections, in which the motivation, the objective and the structure of the present work are described in more detail.

3.1 Motivation

Today's society is consuming a dramatically increasing amount of fossil carbon sources including natural gas and petroleum to meet the constantly growing demand for energy, chemicals, and materials. The foreseeable shortage of fossil raw materials and the social, economic, and ecological problems associated with their use resulting in intensive research into bio-based alternatives. A major problem caused by the excessive dependence on fossil fuels is the contribution to the increase in greenhouse gas emissions and thus to climate change.¹⁻⁴

Accordingly, the use of lignocellulosic biomass as a sustainable and abundant source of energy and raw materials as well as the only source of renewable carbon plays a key role in supplying a highly developed industrial society of the future. Biomass originates from CO₂ and water that was converted by photosynthesis utilizing solar energy and is produced in tremendous amounts each year. Hence, biomass can be regarded as stored solar energy, which leads to a carbon neutral usage. Therefore, industry and research are striving to develop bio-based processes for the conversion of these often very complex biogenic raw materials. Compared to fossil resources, biomass exhibits a complex macromolecular structure and an over-functionalization. More precisely, lignocellulosic biomass contains up to 43 wt.-% of oxygen, while fossil resources such as crude oil only contain 0 wt.-% to 1.5 wt.-%.^{5,6} From a petrochemical point of view, the "excess" oxygen must be removed and the biomass defunctionalized in order to be able to use well-established processes. Alternatively, new process routes have to be developed that enable the direct use of complex biomass to produce bio-based chemicals and energy carriers. However, the over-functionalized character of biomass still obligates the application of a number of intricate process steps. Consequently, the production of value-added products through the valorization of biogenic feedstock is the most complex and least developed operation.^{2,3,5-7}

In this regard, novel approaches for sustainable bio-based processes can be summarized under the generic term "biorefineries". In biorefineries, almost all types of biomass are converted into bio-based chemicals and energy carriers using a

combination of different conversion technologies. In addition to the complex process structures, the establishment of biorefineries is hampered by the fact that so far either only low-value products have been provided or complex product mixtures as well as undesired by-products have been produced. As a result, only a few technologies for converting biomass into value-added products have been established to date.⁸⁻¹²

One example for the successful establishment of a biorefinery technology is the continuous production of biogenic levulinic acid through the acid-catalyzed hydrolysis of biomass in the so-called *Biofine process*. The Biofine process is one of the most advanced large-scale biorefinery technologies. Unfortunately, this process also produces an insoluble polymeric solid called *humin* due to thermally initiated reactions of intermediates. The humins formed diminish the carbon efficiency by up to 30 %, which is in direct contradiction to the biorefinery's claim to fully utilize all raw material components.¹¹ Humins represent a highly complex class of materials, wherefore their chemical utilization to increase process and carbon efficiency in biorefineries is proving to be a challenge. *Mearten et al.*⁸ investigated the chemical utilization of humins by the oxidative conversion to short chain carboxylic acids such as formic acid and acetic acid using homogenous polyoxometalate catalysts in aqueous phase.^{8,10-13}

Formic acid has numerous applications in the animal feed, leather, textile, and pharmaceutical industries. Furthermore, formic acid can also be viewed as a carbon dioxide-carried hydrogen equivalent, whereby via catalytic decomposition the stored hydrogen can be released again. On the other hand, the thermal decomposition of formic acid produces carbon monoxide and water. Based on this product spectra, formic acid can be considered as syngas equivalent that has convenient handling, storage, and transportation characteristics.¹⁴⁻¹⁸

3.2 Objective of the dissertation

The main objective of the present work was to deepen the understanding of the oxidative valorization of humins and its further development as well as optimization. For this purpose, homogeneous polyoxometalate catalysts and oxygen as oxidizing agent were used in aqueous phase. One point of investigation was the modification of the catalysts by substitution with different transition metals and different degrees of substitution in oxidation experiments on model substances that occur as structural motifs in humins. In this process, the most suitable catalyst for the selective catalytic oxidation of humins to carboxylic acids should be identified. Furthermore, structure-

activity-selectivity relationships should also be derived from the experiments. Another objective was the transfer of the insights to real humins and the optimization of their selective catalytic oxidation through adapted reaction conditions as well as the employment of additives that increase both activity and selectivity. The final objective was the development, optimization, and application of an efficient downstream process by means of nanofiltration. This should facilitate an energy-saving and highly selective process enabling the recycling of the homogeneous catalysts.

3.3 Structure of the dissertation

The present dissertation comprises a total of 10 chapters, which include the summary (Chapter 1 & 2), a general introduction (Chapter 3), the theoretical background (Chapter 4), the experimental part (Chapter 5) and the cumulative (Chapter 6) as well as a comprehensive discussion of all results and publications of this work (Chapter 7).

The theoretical background initially describes biogenic raw materials and relevant processes for their conversion. Subsequently, polyoxometalates as the catalysts used in this work and plausible biogenic products from the selective catalytic oxidation of humins are explained in more detail. The theoretical background ends with an introduction of membrane processes and a comprehensive discussion of nanofiltration as an efficient downstream technology for polyoxometalates as well as value-added products produced in the present work. In the following chapter the employed process/test facilities and analytical devices are described. The cumulative part includes the results of the experimental studies conducted in this work and their discussion in published specialist articles. Each article is introduced with a synopsis at the beginning, where all synopses together reflect the successive development and achievements on selective catalytic oxidation of humins. The conclusion is a cross-publication discussion of all results.

4 Theoretical Background

In the following chapter, the theoretical background for the present dissertation is discussed. At the beginning, biomass as a renewable source of carbon, its classification, and main components as well as selected processes for its valorization are presented. The substance class of polyoxometalates is introduced and an overview of their classification, the various structures and catalytic applications is given. Subsequently, the basic principles of the processes relevant to this dissertation are explained. On the one hand, the selective catalytic oxidation of lignocellulosic biomass is explicated as a key technology by the means of the *OxFA process*. On the other hand, the acid-catalyzed hydrolysis of carbohydrates in the so-called *Biofine process* is discussed. Thereby, the formation and structure of humins as an undesired by-product are described. In addition, humins are considered as a source of renewable hydrocarbons. Afterwards, the properties and applications of selected industrially relevant carboxylic acids are explained, which are considered here as potential products from a sustainable humin valorization process. Finally, nanofiltration is discussed as an efficient downstream process.

4.1 Biogenic Raw Materials

Potential options for the substitution of fossil energy sources currently being explored include energy from wind, solar, geothermal sources, and biomass. In comparison, the latter is not only a renewable source of energy, but also the only regenerative source of carbon providing a tremendous substitution potential for fossil carbon sources. Moreover, biomass is abundant, which predestines it for the sustainable production of energy and chemicals. Every year, approximately 120 to 170 billion tons of biomass are generated worldwide, yet only 3.5 % of this enormous resource is used by mankind.^{2,3,6} Biomass is photosynthetically stored solar energy through the decisive reaction of carbon dioxide and water with the release of oxygen. Thus, the solar energy stored in biomass can be used locally and temporarily independent of instantaneous solar radiation.^{2,3,5,6}

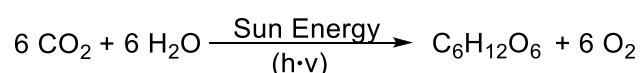
According to *Kaltschmitt*⁵, biomass is defined as the entity of all substances of organic origin comprising by definition both living and dead (but not yet fossilized) phyto- and zoomass as well as their residues. In addition, substances that resulted from a

technical or material conversion are also counted as biomass. These include, for example, paper, vegetable oils and organic household waste.⁵

Biomass can be divided into primary, secondary, and tertiary biomass, depending on whether solar energy is used directly or indirectly. Essentially, primary biomass includes all plant mass, plant residues, and products/by-products of the processing industry that have resulted from the direct photosynthetic use of solar energy. In contrast, if the energy was obtained only indirectly from the sun, it is classified as secondary biomass. Hereby, decomposition and transformation of organic substances takes place and thus secondary biomass comprises all zoo mass and excreta. Substances produced from primary or secondary biomass by one or more further technical processing steps such as pulp, paper or humins are referred to as tertiary biomass.^{2,5}

4.1.1 Structure of Primary Biomass

In dried state, plant biomass consists mainly of the elements carbon (42 – 47 %), oxygen (40 – 44 %) and hydrogen (up to 6 %).⁵ Plant biomass is produced by direct use of solar energy in the process of photosynthesis. In photosynthesis, energy-rich organic substances, namely carbohydrates, are produced from energy-poor substances such as carbon dioxide from the air and water utilizing solar energy. Scheme 4.1 shows an example of the formation of glucose by photosynthesis.^{3,6}



Scheme 4.1: Photosynthetic formation of glucose.

Triglycerides and lignocellulose as well as carbohydrates represent the main components of plant biomass. Proteins and nucleic acids represent a smaller part of plant biomass.^{3,5,6} The following section deals with the major components of plant biomass.

An intermolecular reaction between several monosaccharides can produce long polymeric, linear, or branched chains giving the structure of polysaccharides. Examples for polysaccharides are starch and cellulose. Here, the individual monomer units are linked to one another via α - or β -1,4-glycosidic bonds.^{6,19}

4.1.1.2 Lignocellulose

The main component of terrestrial biomass is a complex structural material called lignocellulose, which consists of cellulose (40 - 50 %), hemicellulose (20 - 30 %) as well as lignin (15 - 20 %), as illustrated in Figure 4.1.^{21,22} Due to its high availability, lignocellulose gains crucial importance as an abundant carbon-neutral renewable source. Depending on the plant species and growth conditions, the specific composition can vary, which influences the structural properties of the different plants.^{20–25}

Cellulose consists of repeated 1,4-D-glucopyranose units linked by β -1,4-glycosidic bonds and can be found as an essential structural component in cell wall of plants. In general, the homopolysaccharide formed by hundreds to many thousands of monomer units, can be described by the formula $(C_6H_{10}O_5)_n$.^{21–24,26}

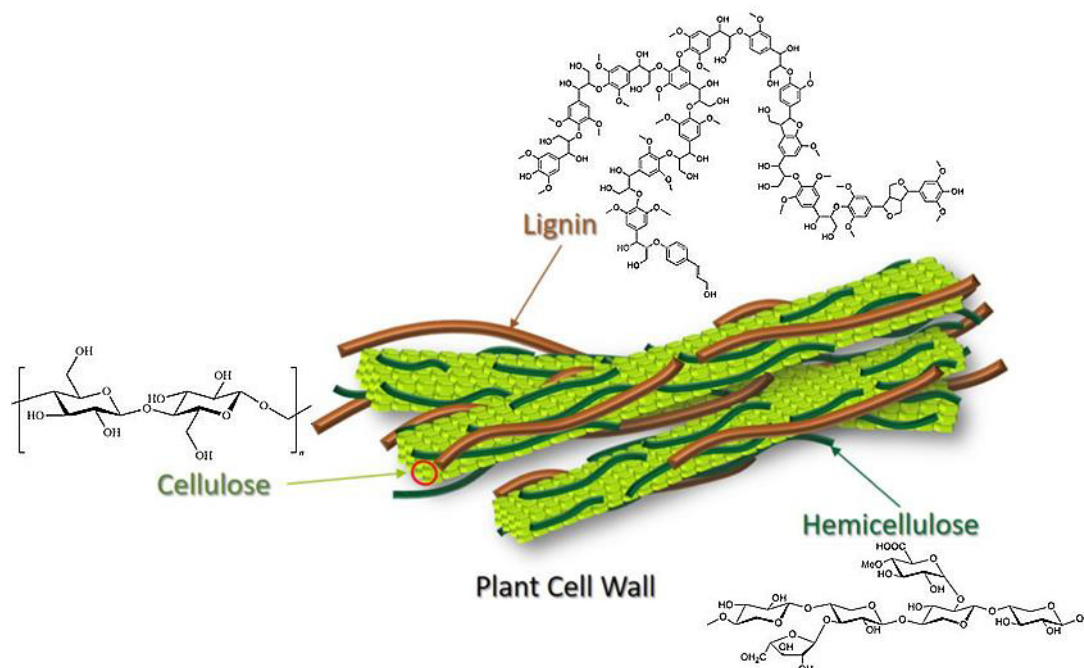


Figure 4.1: Composition and structure of lignocellulosic biomass.²¹

The number of polymerized units varies depending on the plant species and is called the degree of polymerization. Intermolecular hydrogen bonds hold the individual cellulose strands together, forming a fibrillar structure with crystalline and amorphous regions. Thus, a tight network of intra- and intermolecular hydrogen bonds lead to a stiffening of the structure.^{21–24,26}

In contrast to the homopolysaccharide cellulose, hemicelluloses are matrices of polysaccharides consisting of various monosaccharides such as pentoses (e.g., xylose), hexoses (e.g., glucose) and other carbon-based components. Hemicellulose as collection of fully amorphous and branched heteropolysaccharides with shorter chains is structurally less stable. Thus, it is easier to break and dissolve than cellulose.^{21,24,26}

Phenyl-propane derivatives are the base for the highly complex, three-dimensional, and hydrophobic polymer lignin. This large molecule, built by more than 10,000 units, consists of the phenolic main components sinapyl alcohol, coniferyl alcohol and p-coumaryl alcohol, the so-called (mono-) lignols.^{5,24} The aromatic macromolecule results from radical polymerization/cross-linking of these monolignols building carbon (C-C) and ether (C-O-C) bonds. Due to radical polymerization, lignin is chemically diverse and not defined. Analogous to hemicellulose, the proportion of monomers and thus lignin's composition as well as structure varies depending on the respective plant species. Lignin acts as a composite material in cell walls being secondarily intercalated between cellulose microfibrils, giving the plants stability and mechanical strength.^{5,6,20,21,24,26}

4.1.1.3 Triglycerides

Another component of plant biomass are fats and fatty oils, which are esters of the trivalent alcohol glycerol and three often different fatty acids. Fatty acids are higher mono carboxylic acids (containing eight or more carbon atoms) that can be either saturated (without double bonds) or unsaturated (with double bonds). Lauric acid (C₁₂, saturated) and palmitic acid (C₁₆, saturated) are two well-known representatives of fatty acids. The structure of the esterified fatty acids including chain length and number of double bonds determines the characteristic of triglycerides. Thus, triglycerides such as palm or coconut oil containing unsaturated and short-chain fatty acids, are solid at room temperature. In contrast, triglycerides such as rapeseed oil containing long-chain branched fatty acids are liquid at room temperature.^{5,6,27}

Storage and structural lipids are distinguished in plant biomass. On the one hand, storage lipids are reserve or storage compounds in oil plants. On the other hand, structural lipids (membrane lipids) form the fundamental framework of the cell membrane. In industry, fats and oils can be used to produce several products. In particular, the short-chain C₁₂ and C₁₄ fatty acids in coconut oil and palm kernel oil, so-called laurics (from lauric acid), are used to produce special surfactants.^{5,6,27}

4.1.2 Energetic and Technical Use of Biomass

As expounded in the previous sections (*vide supra*, 4.1), biomass is a sustainable energy source, but also the only renewable carbon source. Therefore, several approaches for utilization processes exist that aim for the substantial and energetic use of biomass. In the simplest case, biomass is burned directly to generate heat. A more advanced approach are thermo-chemical conversion processes. In thermo-chemical conversion such as gasification, slow pyrolysis or hydrothermal conversion, secondary energy sources are produced from solid bioenergy sources primarily under the influence of heat. The supply of vegetable oil-based energy sources through mechanical processes or extraction is categorized as physico-chemical conversion. If microorganisms are used to convert biomass into secondary energy sources or energy, this is referred to as biochemical conversion.^{5,20,25}

If the aforementioned conversion processes are used to produce fuels, these fuels are divided into three categories depending on the converted substrate. Accordingly, fuels from energy crops such as starch or oil-containing crops are designated as first-generation biofuels. As a result, these fuels are in direct competition with food production. Indirect competition with food production exists for second-generation biofuels based on lignocellulosic biomass. The indirect competition is explained by the provision of arable land for the cultivation of lignocellulosic plants. However, in the case of third-generation biofuels that are obtained from microorganisms or algae there are no competing uses.^{20,25,27}

In literature, numerous approaches for the chemo-catalytical valorization of biomass to produce platform chemicals are discussed.^{25,26,28–30} In the following section, selected processes for biomass valorization are expatiated in more detail.

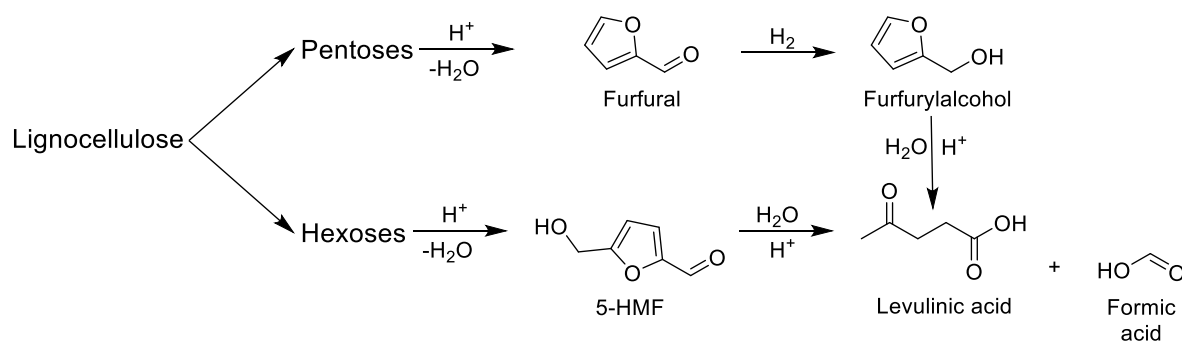
4.2 Selected Processes for Biomass Valorization

Synthetic products, including the vast majority of chemicals and materials, are originated from fossil resources such as petroleum. The finite nature of these fossil resources and the environmental problems associated with their use promote the sustainable development of novel processes towards bio-economies of modern society. Establishing integrated biorefinery technologies that valorize various non-eatable biogenic feedstocks into bio-based chemicals is essential.^{2,10,12,28,31–34}

In this context, important process routes are the hydrolysis and oxidation of complex biomass. The following sections introduce the *Biofine process*, one of the most advanced and commercially viable biorefinery technologies for fractionating lignocellulosic biomass (*vide infra*, 4.2.1). Another promising approach is the selective catalytic oxidation of biomass to formic acid (FA) in the so-called *OxFA process*. The OxFA process is an important approach for the presented dissertation and in general a key technology for the sustainable production of formic acid. Therefore, the OxFA process is explained in the following section (*vide infra*, 4.2.2).^{2,12,28,35,36}

4.2.1 The Biofine Process

The *Biofine process* is an integrated process involving the acid-catalyzed hydrolysis of complex polysaccharides to their monomeric components that are subsequently continuously converted into value-added platform chemicals. The simplified process route of the Biofine process is shown in Scheme 4.3. Herein, lignocellulosic fractionating occurs under the influence of sulfuric acid to produce monomer units like fructose and glucose. For this purpose, a 3.5 wt-% sulfuric acid solution is mixed with the lignocellulosic biomass forming a slurry (at 30 % solids content).^{10,12} This slurry is continuously supplied to a reactor operating at about 215 °C and 25 bar.¹² In multiple acid-catalyzed and consecutive reactions hexoses as well as pentoses of polysaccharides are converted to 5-hydroxymethylfurfural (5-HMF) and gaseous furfural, respectively. Furfural can be recovered from the gaseous phase with a purity of 98 wt-%.¹² The slurry containing the intermediate 5-HMF is fed into a second reactor where it is subjected to an operating temperature of about 195 °C and a pressure of 14 bar.^{10,12,32,34}



Scheme 4.3: Simplified process route of levulinic acid from lignocellulose in the Biofine process, according to *Climent et al.*¹⁰.

In this last process step, levulinic acid is produced with a yield of about 50 % based on the hexose content of the substrate.³² Equimolar amounts of formic acid as by-product are produced. Distillation is a conventional method for the purification of levulinic acid. To this end, levulinic acid is vacuum distilled at 0.1 bar and steam stripped at 1.0 bar resulting in a commercial grade levulinic acid with a purity of 98 wt-%.¹² Levulinic acid is considered as one of the top 14 bio-based platform molecules due to its high functionality resulting from its keto- and carboxylic acid group (*vide infra*, 4.4.4). Valorizing inexpensive lignocellulosic waste in the Biofine process enables the production of levulinic acid at competitive cost of about 0.06 € to 0.18 € per kilogram.¹⁰ Furfural as by-product of the acid-catalyzed hydrolysis of pentose, could be hydrogenated to furfuryl alcohol in an additional process step and further processed into levulinic acid (Scheme 4.3). However, this case will not be discussed further in this section. A simplified process flow diagram of the Biofine process for producing biogenic levulinic acid is shown in Figure 4.2.^{10–12,32,33}

A drawback of the acid-catalyzed hydrolysis of complex biomass to the reactive intermediate 5-HMF is the undesired formation of large amounts of insoluble polymerization products in the biofine process. These insoluble and highly complex polymers, called humins, account for up to 30 % of the converted carbon.¹¹ Thus, the carbon and overall process efficiency is strongly decreased.^{10,12,32,34,37} The utilization of humins is crucial for a high process efficiency and hence a deeper understanding of their formation and structure is essential. For this reason, the following subsections deal with humins in more detail.

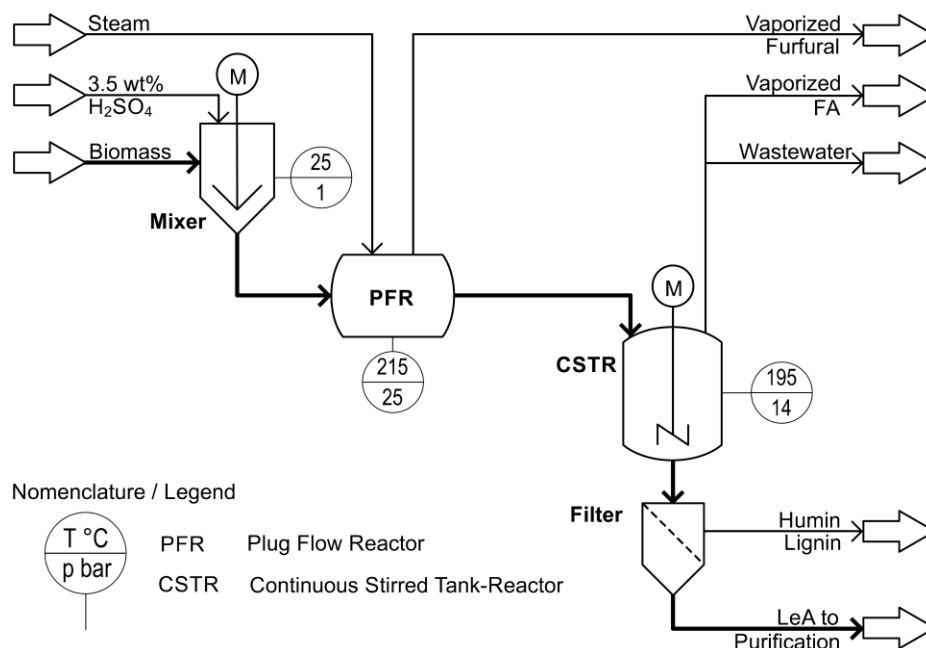
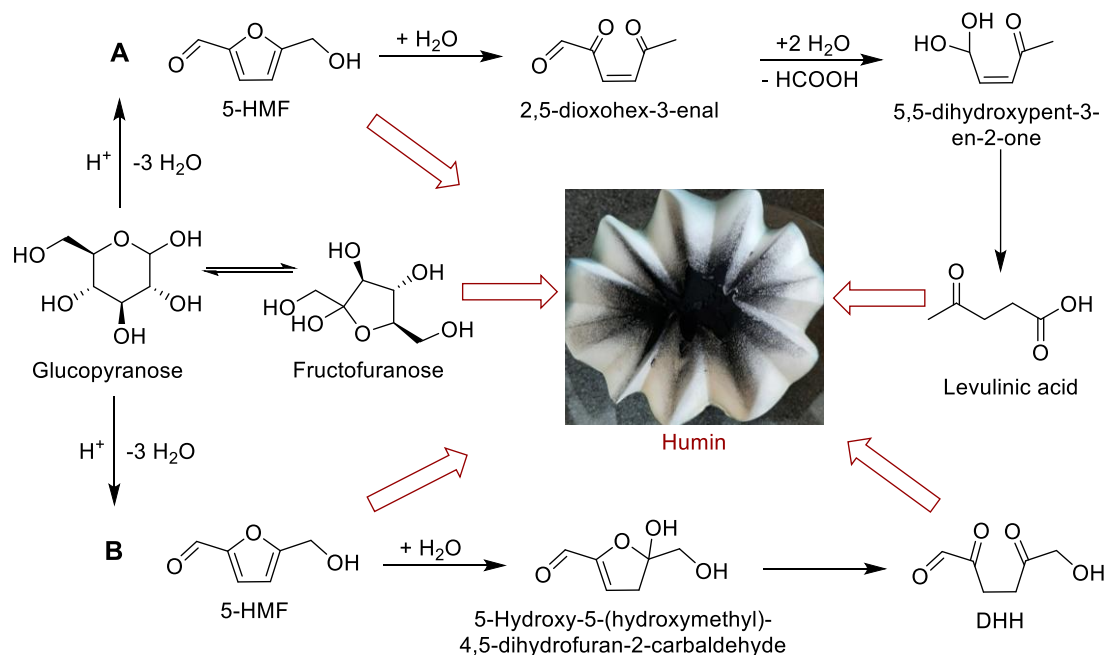


Figure 4.2: Simplified process flow diagram for the Biofine process, according to *Kapanji et al.*¹².

4.2.1.1 Formation of Humins

The formation of humins is a challenge in biorefinery and especially in the Biofine process hampering efficient use of resources. Hence, the formation and structure of humin has attracted attention of researchers in recent years. Numerous studies were conducted to gain a deeper understanding of the mechanism of humin formation and their structure.^{8,9,37–52}

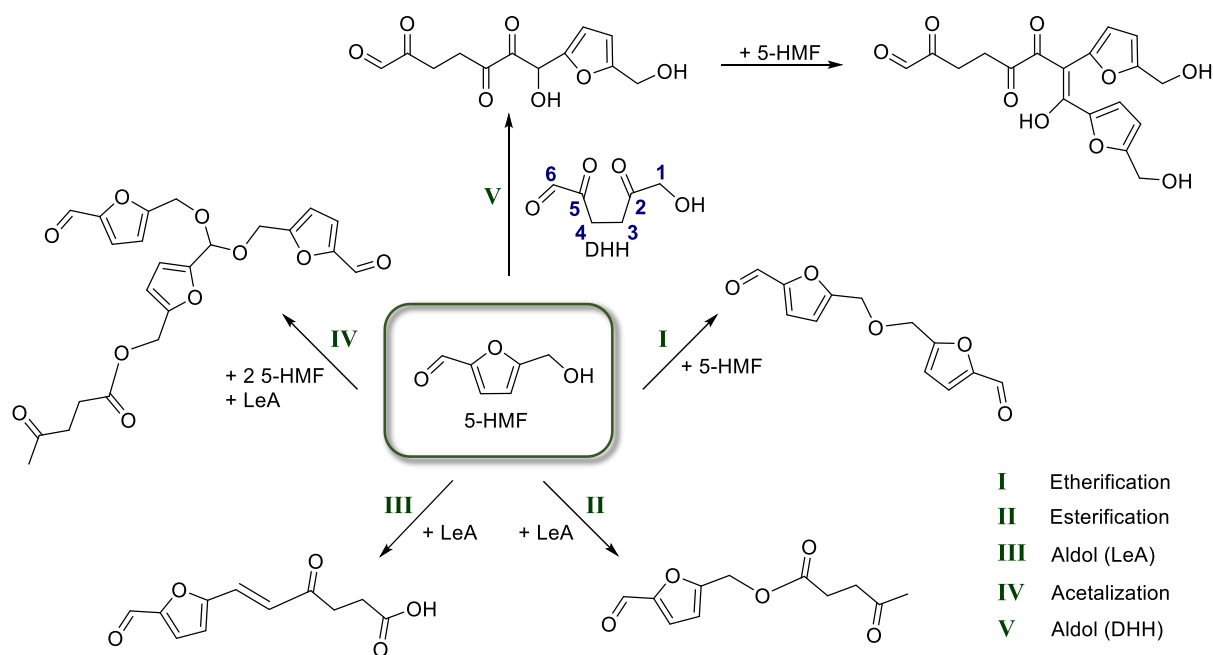
In order to better understand the formation of humins, knowledge of the intermediates and by-products that are formed during the hydrolysis of 5-HMF to levulinic acid is helpful. For this reason, Scheme 4.4 shows the routes from glucose over 5-HMF to levulinic acid and 2,5-dioxo-6-hydroxyhexanal (DHH). In all routes, the hydrolysis of complex biomass and the subsequent dehydration of glucose to 5-HMF by removing three equivalents of water is the starting point. Levulinic acid and formic acid are produced in parallel from 5-HMF passing the intermediates 2,5-dioxohex-3-enal and 5,5-dihdropent-3-en-2-one by rehydration and ring opening (Scheme 4.4, A). Starting from 5-HMF, the by-product DHH can also be formed by addition of water to the intermediate 5-hydroxy-5-(hydroxymethyl)-4,5-dihydrofuran-2-carbaldehyd and subsequent ring opening (Scheme 4.4, B). It can be clearly seen that all intermediates as well as by-products are multifunctional and therefore capable of various reactions.^{9,40,46,49,53,54}



Scheme 4.4: Schematic presentation of the reaction pathway from glucose to levulinic acid and formation of humins. A. Pathway to levulinic acid, B. Pathway to DHH, according to literature^{9,46,53–55}.

Multifunctionality allows a series of elemental reactions such as etherification, esterification, aldol condensation and acetylation. In this process, 5-HMF can form ethers with itself as well as esters, aldol products or complex structures by acetylation reacting with levulinic acid (LeA), as illustrated in Scheme 4.5. The products of such reactions still possess functional groups that allow further reactions and thus finally polymerization to humins. In addition, 5-HMF and DHH can be linked via one of its four enols by an aldol reaction followed by condensation. Since there is no $\alpha\text{-H}$ atom at the aldehyde function of 5-HMF, the aldol reaction with subsequent condensation can only take place in positions 3, 4 and 6 (Scheme 4.5, V). This creates a new target for another aldol reaction and condensation.^{9,37,45–47,52,53}

Although there are already very tangible ideas about the formation mechanism of humins, their exact structure has not yet been fully elucidated due to their high complexity. Rather, structural motifs and elementary components of the structure have been identified and discussed in literature so far.^{39,42,45,46,51,56} These structural elements could be helpful as model substances for material utilization of humins to gain a better understanding. In the following section, the individual structural elements are explained in more detail and appropriate model substances are discussed.



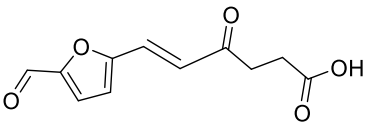
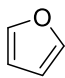
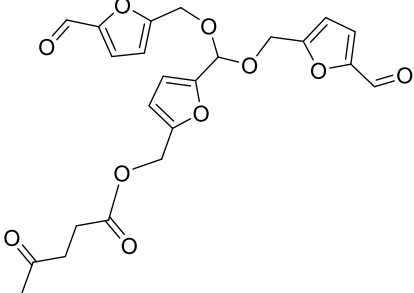
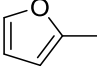
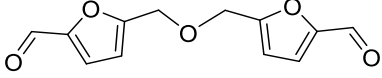
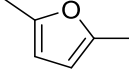
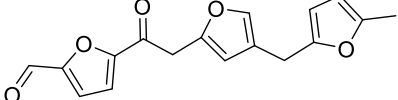
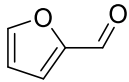
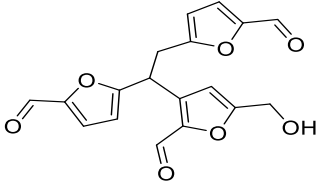
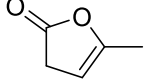
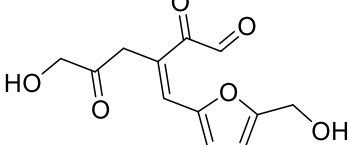
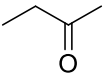
Scheme 4.5: Reaction types of 5-HMF leading to the formation of humins, according to literature^{9,45,53,54}.

4.2.1.2 Structure of Humins

Although the exact structure of humins is not known yet, a vast majority of conducted studies conclude that humins are based on furan-rich polymer networks. This also seems plausible considering the possible formation mechanisms previously discussed (*vide supra*, 4.2.1.1). Consequently, it also seems evident that up to 60 % of the humin structure is based on furan rings.³⁸ On the one hand, the results of studies and the formation mechanisms indicate that the furan rings within the network are linked via oxygen-functionalized bonds (C-O-C). On the other hand, linkage via aliphatic carbon bonds (C-C) and acetyl groups (O=C-C) are also being discussed. A coexistence of both linkage types cannot be excluded. In Table 4.1 confirmed fragments of humin structure are listed. Already suspected fragments that result from the postulated formation mechanisms were confirmed by literature (Table 4.1, Entries 1-3). These fragments are representatives of the strongly oxygen-functionalized networks. Studies have also confirmed fragments in which linking of the furan rings does not require a high degree of oxygen functionalization (Table 4.1, Entries 4-6). In addition, less complex fragments including predominantly monofuran derivatives, can also be detected (Table 4.1, Entries 7-12). These include commercially available substances such as furan, 2-methylfuran, 2,5-dimethylfuran, furfural, α -angelicalactone and 2-butanone.^{8,37-40,42-48,51}

Accordingly, in a potential humin valorization process, a variety of functionalities and binding types have to be processed. This requires interaction with oxygen-functionalized bonds such as ethers and esters, but also interaction with single and double carbon bonds. The complex and undefined structure of humins makes a targeted valorization process difficult. Consequently, the use of model substances can be helpful for an initial understanding. A recurring fragment is the furan ring, which represents an essential structural motif for potential model substances.

Table 4.1: Fragments of humin structure and components of pyrolysates confirmed by mass spectroscopy.

Entry	Fragment	Reference	Entry	Fragment	Reference
1		39,48	7		44
2		45	8		44
3		40,45,47	9		44
4		42	10		44
5		39	11		44
6		39,56	12		44

An important key technology for the valorization of complex biomass is the OxFA process, which forms the basis for the selective catalytic oxidation of humins developed in this dissertation. The following section describes the OxFA process in more detail.

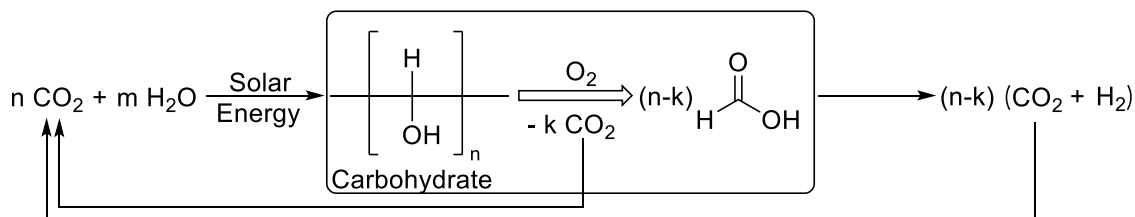
4.2.2 The OxFA Process

In the *OxFA process* (Oxidative Conversion of Biomass to Formic Acid) biomass is partially catalytically oxidized to formic acid under mild reaction conditions by the means of reaction temperatures of less than 100 °C and pressures below 30 bar. The fundamental idea of the OxFA process is the production of formic acid, a bulk chemical of industrial relevance that can also be regarded as a storable and transportable secondary energy carrier. To this end, formic acid can selectively be decomposed to hydrogen using metal catalysts. *Wölfe*⁵⁷ and *Albert*³⁶ at the Department of Chemical Reaction Engineering at Friedrich-Alexander-Universität Erlangen-Nürnberg developed and optimized the process. It has been demonstrated that biomass can be converted from a variety of sources, compositions, and humidities. As sole by-product, easily separable CO₂ is produced in the gas phase. The separation of formic acid is feasible using 1-hexanol or 1-heptanol as extraction agent in *in-situ* or *ex-situ* extraction. In addition to the discontinuous mode of operation, the continuous mode of operation was also comprehensively investigated. In 2015, the *OxFA GmbH* was founded as a joint venture between *JBACH GmbH* and *EnviTec Biogas AG* aiming for a commercialization of the OxFA process.^{29,35,36,57–65}

The following section takes a closer look at the OxFA process and discusses its fundamentals, the process system, including product separation.

4.2.2.1 Fundamentals of the OxFA Process

As described above, the OxFA process pursues the production of formic acid (FA) as a hydrogen or energy storage molecule from biomass by oxidative conversion producing CO₂ as sole by-product. The produced CO₂ during the OxFA process and the subsequent decomposition of formic acid to hydrogen was originally absorbed from the atmosphere by photosynthesis in the biomass's growth process, resulting in a CO₂-neutral cycle for the overall process. Therefore, the OxFA process represents a sustainable method for the indirect use of solar energy. This cycle is shown in simplified form in Scheme 4.6.⁵⁷



Scheme 4.6: Indirect hydrogen production from solar energy by converting biomass to formic acid, adapted from *Wölfel et al.*⁵⁷.

A sufficient catalyst must be used together with molecular oxygen to oxidatively convert biomass into FA under mild conditions. On the one hand, the catalyst should decrease the activation energy for the oxidation of the biomass resulting high FA yields. In addition, direct electron transfer between molecular oxygen as an oxidizing agent and the biogenic substrate without using a catalyst is not feasible under these mild reaction conditions due to high energy barriers. On the other hand, the choice of catalyst is essential to avoid the thermodynamically favored total oxidation of biogenic feedstock to CO_2 and water influencing the process efficiency and sustainability. In Figure 4.3 the qualitative energy diagram of the OxFA process is illustrated. The term "usable energy difference" refers to the energy difference between FA and the products of total oxidation CO_2 as well as H_2O . The exothermic process can be catalyzed by a homogeneous catalyst and takes place in aqueous phase using molecular oxygen as oxidant. For the OxFA process, *Keggin*-type polyoxometalate catalysts are used, which are described in the following section (*vide infra*, 4.3). Oxidation occurs through the transfer of electrons from the substrate to the catalyst, which is thereby reduced. The catalyst is then reoxidized by molecular oxygen.^{57,66,67}

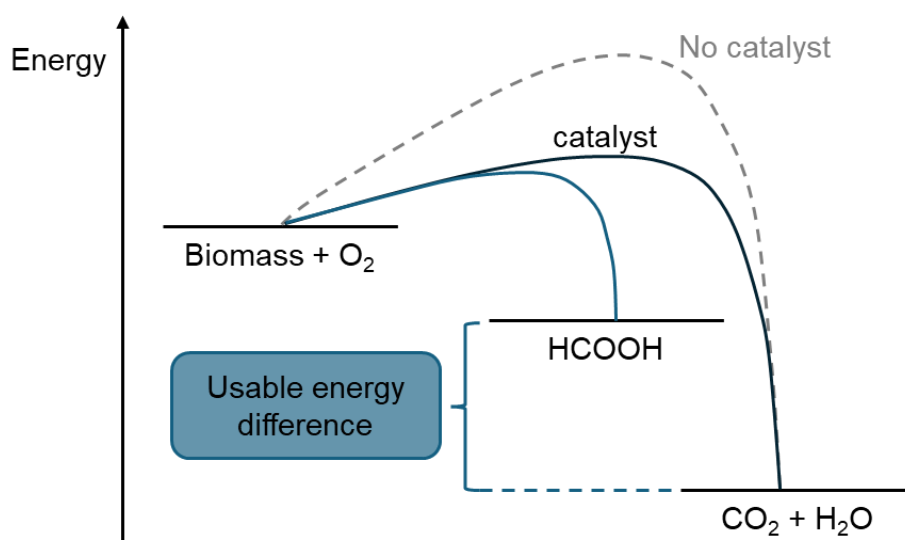


Figure 4.3: Qualitative energy diagram of the OxFA process, according to *Albert*⁶⁷.

The catalytic cycle of the OxFA process is shown schematically in Figure 4.4. The POM catalyst's reoxidation is the rate-determining step at low oxygen pressure. However, the higher partial pressure of oxygen, the faster the reoxidation of the catalyst. Thus the oxidation of the biomass becomes the rate-determining step at higher oxygen partial pressures.^{57,66,67}

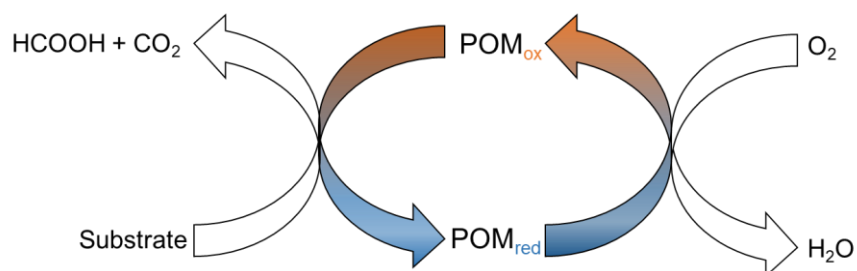
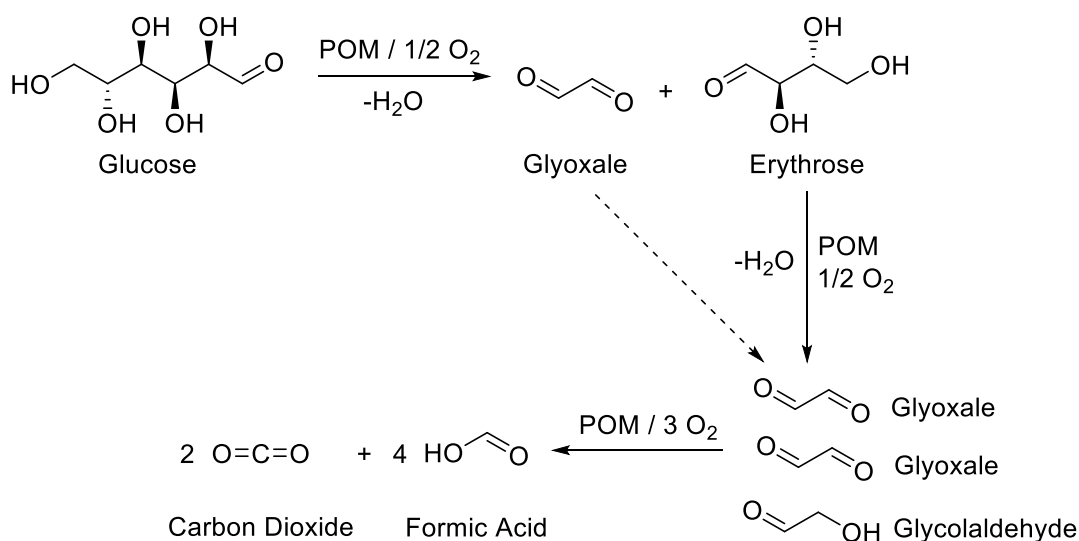


Figure 4.4: Schematic catalytic cycle of the OxFA process, adapted from literature^{61,67}.

The substrate is converted by oxidative C-C bond cleavage enabled by the catalyst under mild reaction conditions. With each oxidative cleavage that occurs during the degradation of carbon skeletons, the newly produced terminal carbon atoms' oxidation number rises. *Albert*⁶⁷ postulated a three-step degradation mechanism to the C₁ chemicals FA and CO₂ using glucose as example. Scheme 4.7 depicts this degradation mechanism schematically. The POM catalyst initiates the first oxidative C-C bond cleavage between two hydroxyl groups in acidic environment. Under water cleavage, glyoxal and erythrose are produced as intermediates.^{57,67,68}



Scheme 4.7: Proposed reaction mechanism for the POM catalyzed oxidation of glucose to formic acid, adapted from literature^{67,69}.

The latter is subsequently converted to the C₂ molecules, glyoxal and glycolaldehyde by an additional oxygen atom that is transferred from the POM catalyst eliminating water. In the final reaction step, the three C₂ molecules are converted to FA and CO₂ in a stoichiometric ratio of 4:2 by POM-catalyzed oxidation.^{57,67,68}

4.2.2.2 Technical Execution of the OxFA Process

In the initial studies of *Wölfel et al.*⁵⁷, the double vanadium-substituted phosphomolybdic acid H₅[PV₂Mo₁₀O₄₀] was investigated as catalyst. Here, glucose was used as a water-soluble model substrate in a batch autoclave at an oxygen partial pressure of 30 bar ensuring that the catalyst is present in oxidized form during the reaction. The oxidation of glucose to formic acid was successfully conducted in a temperature range of 70 °C to 90 °C. On the one hand, temperatures below 70 °C proved to be too low to ensure catalytic activity. On the other hand, temperatures above 90 °C threatened to promote the thermal decomposition of formic acid and were therefore not used.^{57,70}

Subsequently to the studies of *Wölfel et al.*⁵⁷, the catalyst system and the batch operation of the process were extensively investigated and optimized by *Albert et al.*^{66,67,71}. In these subsequent studies, it was proved that the five times vanadium-substituted H₈[PV₅Mo₇O₄₀] catalyst is more selective and more active. Furthermore, a reaction temperature of 90 °C and a reaction oxygen pressure between 20 bar and 30 bar were specified since the catalyst proved to be highly active at this temperature and the formic acid produced does not thermally degrade below 100 °C. Apart from the effective conversion of many potential intermediates such as erythrose, glyoxal, or glycolaldehyde for mechanistic clarification, humins as an undesired by-product of biomass valorization could also be oxidized to FA.^{53,57,64,66,67,70}

*Reichert et al.*⁶³ developed a two-phase reaction system using an additional organic phase for *in-situ* extraction, which enables a further system optimization. Specifically, studies indicated that the linear alcohols 1-hexanol and 1-heptanol are appropriate extraction agents for FA. On the one hand, the elaborated process of separating the azeotropic product mixture of FA and water can be avoided by *in-situ* extraction. On the other hand, the FA selectivity significantly increased applying *in-situ* extraction. More specifically, the FA yield and selectivity in the oxidative conversion of glucose using H₈[PV₅Mo₇O₄₀] catalyst as well as 1-hexanol as extractant at 90 °C and 20 bar oxygen partial pressure reached 85 % after 48 hours of reaction, with glucose being

completely converted. In comparison, in a single-phase system under the same reaction conditions, a FA yield and selectivity of about 53 % was achieved under complete conversion of glucose. This optimization can be explained by the fact that the extraction of the formed FA led to an increase of the pH in the aqueous catalyst phase reaching values above 2.5. Thus, the ideal pH range for the catalyst, which has already been documented in the literature⁷² was reached. The concept of *in-situ* extraction and its potential implementation in continuous OxFA process is schematically represented in Figure 4.5.^{63,72}

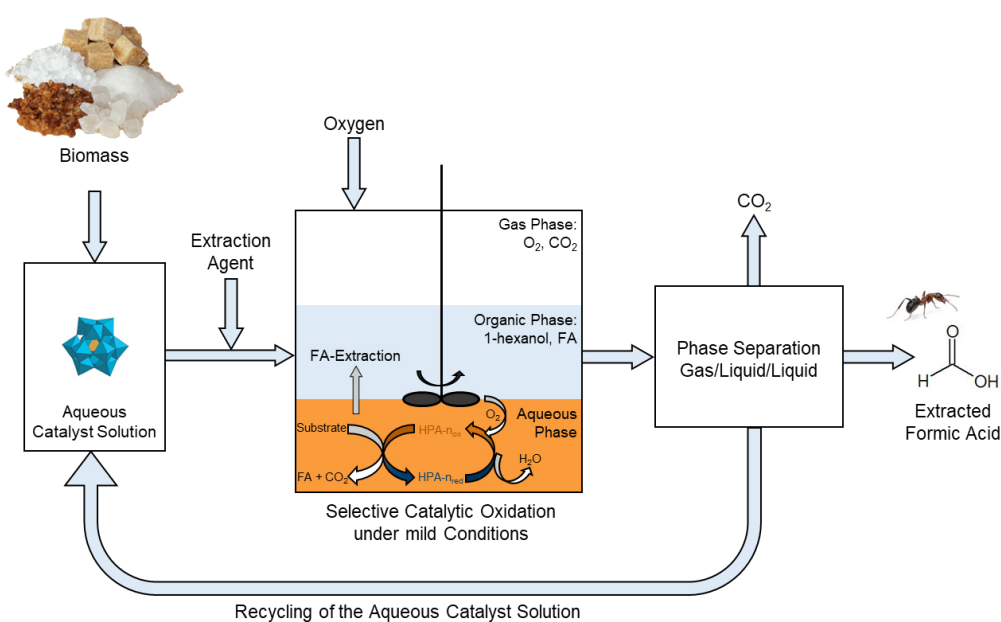


Figure 4.5: Schematic representation of the concept of *in-situ* extraction and its potential implementation in continuous OxFA process, adapted from Voß⁶¹.

Building on the previous results reported in literature, Voß *et al.*²⁹ aimed at the development of a continuous process as the next step towards a potential technical application of selective biomass oxidation to FA. On a 2 L-scale, continuous FA production from biomass in the liquid phase, including catalyst recycling and product separation in a mini plant, was demonstrated. In Figure 4.6 a simplified process flow diagram of the continuous mini plant for the OxFA process developed by Voß *et al.*^{29,61} is shown. The *upstream process* includes receiver tanks as well as pumps and other dosing equipment supplying all input streams, such as liquid phase or gas. The aqueous substrate and catalyst solution is stored in a receiver tank under ambient conditions. The continuous supply of fresh substrate and extraction agent is provided by two additional receiver tanks. Immediately before entering the reactor, the substrate and catalyst solution is combined with the extraction agent in a heated tube and pumped into the reactor.^{29,61}

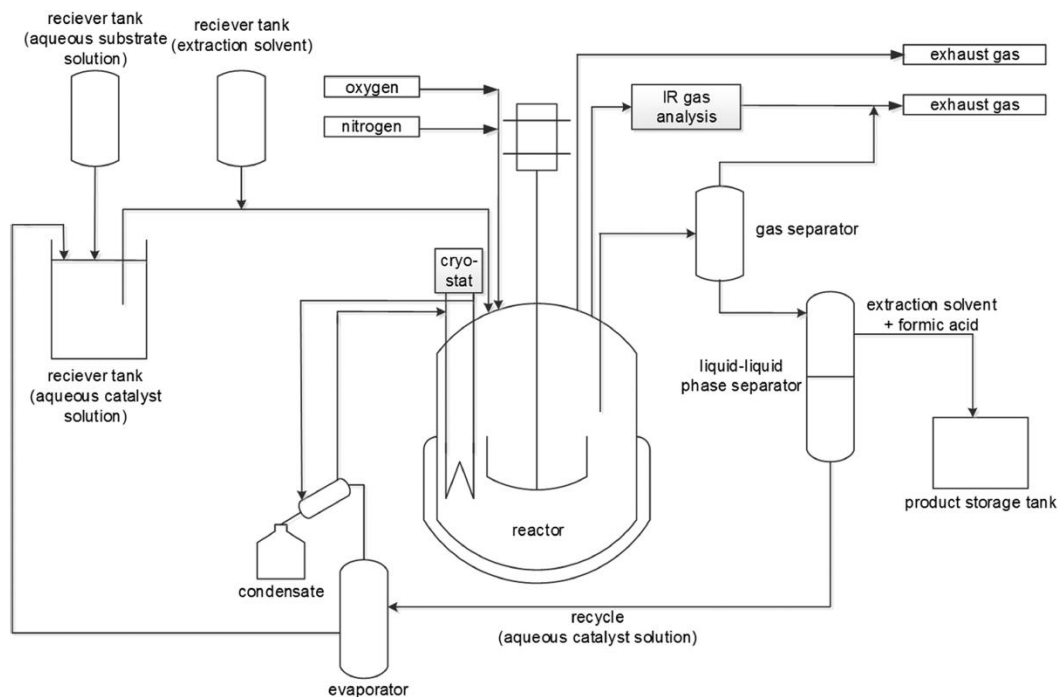


Figure 4.6: Simplified process flow diagram of OxA process (mini plant).²⁹

A continuous stirred tank reactor (CSTR) with a capacity of 2 L equipped with gas entrainment stirrer was selected as reactor enabling an intensive dispersion of the reaction mixture. Thus, effective *in-situ* extraction of the FA into the extractant and optimal oxygen input into the reaction solution were made feasible.^{29,61}

In the *downstream process*, the gas dissolved in the reaction mixture is first expelled by increasing the surface area via a gas separator and subsequently the two liquid phases are removed via a siphon. The aqueous catalyst solution is separated from the organic product phase in a liquid-liquid separator. Excess water that was introduced by the aqueous substrate solution is removed from the catalyst solution via an evaporator. Finally, the concentrated catalyst solution is collected in the receiver tank, where it is mixed with fresh substrate.^{29,61}

*Voß et al.*²⁹ were able to demonstrate a stationary process after 22 h. In the steady state of the process, the substrate sucrose was converted reaching a FA yield of 62 % with a selectivity of 71 % at 90 °C, 20 bar oxygen partial pressure, $H_8[PV_5Mo_7O_{40}]$ as catalyst and 1-hexanol as extractant. Furthermore, constant catalytic activity over 670 h time-on-steam with an average FA yield of 58 % could be obtained.^{29,61}

Based on the results described above, the *OxFA GmbH* is pursuing the industrialization of the OxFA process. Two processes are used for product separation and catalyst recovery. Product solutions with an FA content of >30 wt.-% can be achieved using flash distillation. Alternatively, an FA content of >95 wt.-% can be achieved by using extraction. Unlike previously described, the *OxFA GmbH* has patented a process in 2020, wherein polar extraction agents such as N-(n-hexadecyl)formamide, N-di-n-acetamide or an N,N-diakylcarboxamide are used.^{73,74}

As shown in this section, polyoxometalate catalysts represent a promising class of substances for the oxidative valorization of biomass and are therefore described in more detail in the following section.

4.3 Polyoxometalates

In general, polyoxometalates (POMs) are a unique class of inorganic compounds based on metal oxide units that form mostly anionic polynuclear metal-oxo cluster. These metal oxide units consist of early transition metals (M) such as molybdenum (Mo) as well as tungsten (W) in their highest oxidation state. They can be described by the general formula $[MO_x]$, where the number of oxygen atoms (x) can vary between four and seven. Depending on the number of oxygen atoms, different structures such as tetrahedra ($x = 4$) or heptahedra ($x = 7$) are formed for the oxo-anion. The polycondensation of the metal oxide units as a result of protonation leads to linkage of the individual units at corners, edges and faces forming three-dimensional highly symmetric structures.^{75–83}

The formation of those polyanions is strongly influenced by the synthesis conditions such as pH, concentration, and temperature. In particular, pH can affect the assembly of the polyoxometalate structure due to the pH-dependent formation of different metal species in solution. For example, the $[Mo_7^{VI}O_{24}]^{6-}$ anion is predominating in an aqueous molybdate solution at pH 7. Even slight changes in pH or of the synthesis conditions in general can shift equilibria, allowing the synthesis of an enormous variety of complex compounds. This enables a flexible design of the composition, size, shape, and properties of the synthesized structures. Due to the immense variety of possible structures, some of them are shown in Figure 4.7, a classification is useful.^{75–83}

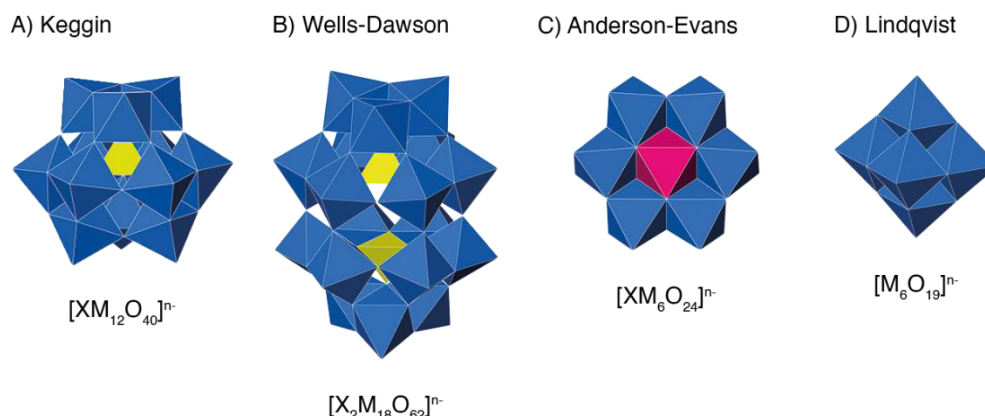


Figure 4.7: Polyhedral representation of different polyoxometalate structures. Octahedra of metal oxide units are blue, tetrahedra of heteroatoms are yellow and octahedrally coordinated heteroatoms are magenta.⁸⁴

The polyoxometalate structures shown in Figure 4.7 consist of corner-sharing and edge-sharing pseudo-octahedral MO_6 units (blue), in which the metal atoms are commonly referred to as addenda atoms. A rough but widely accepted classification system divides these POMs into two groups. On the one hand, the polycondensation of several $[\text{MO}_4]^{2-}$ units of the same species (addenda atoms) forms the so-called isopolyanions (IPAs). IPAs can be described by the general formula $[\text{M}_n\text{O}_{(4n-m)}]^{(2n-m)-}$ with condensation degrees $n \geq 6$. On the other hand, polycondensation of metal units around a central heteroatom X (X = P, As, Si, Ge) or a foreign metal species (yellow or magenta) forms the so-called heteropolyanions (HPAs). These complexes are described by the general formula $[\text{X}_k\text{M}_n\text{O}_m]^{y-}$.^{81–83,85,86}

Polyanions described by the general molecular formula $[\text{M}_6\text{O}_{19}]^{y-}$ referred to as Lindqvist form the most important structural type in the group of IPAs (Figure 4.7 D). The Lindqvist structure is an octahedral arrangement that in turn consists of six small edge-sharing octahedra. In total, the individual metal oxide units are connected via twelve oxygen atoms, each of them link two metals together. In the center is an oxygen atom, which is connected to all six metal atoms. In addition, each metal atom has a terminal oxygen atom that is bonded to only one metal atom. Typical counter cations for the anion are K^+ , Na^+ or NH_4^+ .^{78,87–89}

In comparison to IPAs, HPAs are more stable due to the heteroatom and the associated interaction within the complex (Figure 4.7 A-C). The ratio of heteroatoms X (yellow/magenta) and metal atoms M (blue) determines the structure of the complex formed. Thus, HPAs can be further subdivided into subgroups.^{82,85,86}

Among the HPAs, the *Keggin* structure is the best studied structure, which can be described by the general molecular formula $[XM_{12}O_{40}]^{y-}$ (Figure 4.7 A). The ratio of heteroatom to metal atoms is therefore 1/12. The tetrahedrally coordinated heteroatom in the center of the complex is surrounded by twelve octahedral $[MO_6]$ units. Three of these octahedral units can be summarized as so-called triades $[M_3O_{13}]$, of which a total of four are arranged around the central heteroatom, forming the characteristic structure $[(XO_4)M_{12}O_{36}]^{y-}$.^{79,81,82,86,89,90}

If the *Keggin* structure is truncated by removing a cap (M_3 ring) at the polar regions, a defect $[XM_9O_{34}]^{y-}$ POM structure is formed, also known as lacunary POM. The Dawson structure is based on the assembly of two of those fragments forming a symmetrical $[X_2M_{18}O_{62}]^{y-}$ cluster (Figure 4.7 B), where the X/M-ratio is 2/18. In the local pseudo-octahedral environment of the Dawson structure, the eighteen metal atoms are arranged in four parallel rings of three (pol), six (equator), six (equator), and three (pol) metal ions. Due to the arrangement in the Dawson structure, there are also dimetallic $[M_2O_{10}]$ groups in addition to the mentioned trimetallic $[M_3O_{13}]$ groups. Hence, different electronic structures prevail in the Dawson anion between the equator region and the cap region.^{81,82,86,91,92}

The so-called *Anderson-Evans* structure, which is another type of heteropolyanion, is described by the general molecular formula $[XM_6O_{24}]^{y-}$, corresponding to a X/M-ratio of 1/6 (Figure 4.7 C). Unlike the first two HPA structures, the central heteroatom exists as an octahedral $[XO_6]$ group (magenta) and is annular surrounded by six $[MO_6]$ octahedra, leading to the characteristic planar shape of these heteropolyanions.^{87,89,90}

Due to the structural diversity of POMs and the possibility to manipulate them, POMs can be adapted for many applications. For example, a desired modification can be achieved by partial substitution of addenda atoms with other transition metals. Such modified *Keggin*-type polyanions proved to be interesting catalysts that have already been used in numerous applications, including the OxFA process. In addition, their use for the valorization of humins is also promising. Therefore the properties of substituted *Keggin*-type POMs are described in more detail in the following section.^{36,66,71,93–95}

4.3.1 Properties of *Keggin*-type Polyoxometalates

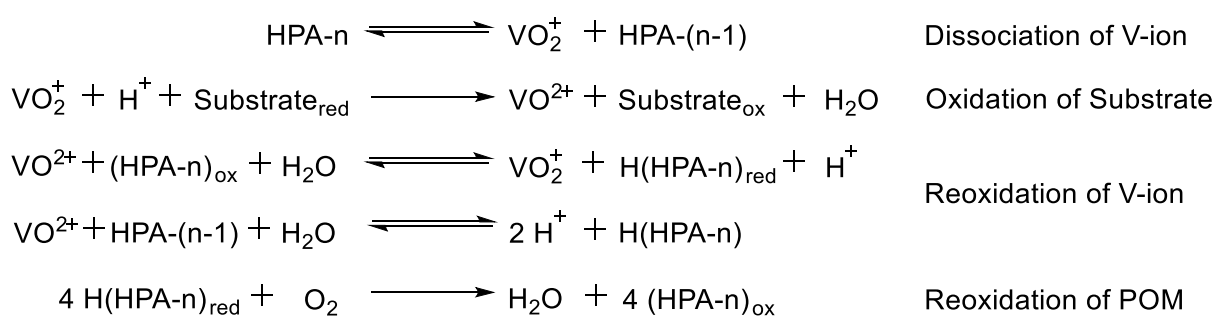
As already mentioned above, POMs are characterized by unique properties and are therefore of high research interest. POMs are soluble in commonly used polar solvents, stable over a wide range of conditions and are insensitive to oxidants. Furthermore, they are multifunctional catalysts that simultaneously act as strong Brønsted acids and redox catalysts. Their redox activity originates from their high capacity to bear and release electrons and thus enables multiple electron transfer. As a result, electrochemically fast redox systems are created that can take part in many cycles. The targeted substitution of addenda atoms using other redox-active metals can enhance these properties. In particular, the use of vanadium (V) as a high redox-active metal for substitution in *Keggin*-type POMs has attracted scientific attention in recent decades. Accordingly, the substitution of individual molybdenum (Mo) atoms in the *Keggin*-type phosphomolybdic acid $H_3[PMo_{12}O_{40}]$ using vanadium leads to a significant increase in redox activity of the newly formed $H_{(3+n)}[PV_nMo_{12-n}O_{40}]$ heteropoly acid. The vanadium-substituted heteropoly acids can be abbreviated as HPA- n , where n is the degree of substitution. In Table 4.2 the different vanadium-substituted HPAs in dependency of the degree of substitution are listed.^{66,71,79,81,82,96,97}

Table 4.2: Vanadium-substituted *Keggin*-type heteropoly acids based on phosphomolybdic acid.^{84,98}

Entry	Abbreviation	Formula	Number of isomers
1	HPA-0	$H_3[PMo_{12}O_{40}]$	1
1	HPA-1	$H_4[PVMo_{11}O_{40}]$	1
2	HPA-2	$H_5[PV_2Mo_{10}O_{40}]$	5
3	HPA-3	$H_6[PV_3Mo_9O_{40}]$	13
4	HPA-4	$H_7[PV_4Mo_8O_{40}]$	27
5	HPA-5	$H_8[PV_5Mo_7O_{40}]$	38
6	HPA-6	$H_9[PV_6Mo_6O_{40}]$	48

Due to their reversible oxidative properties, vanadium-substituted HPAs are used in liquid-phase oxidations under mild conditions. Vanadium changes its oxidation state ($V^{5+} \rightleftharpoons V^{4+}$), which is responsible for redox activity. Monomeric pervanadyl (VO_2^+), which dissociates from the HPA-n structure under strongly acidic conditions, forms the catalytically active species upon oxidation of the substrate. The subsequent reoxidation by molecular oxygen can only occur within the HPA structure. In Scheme 4.8 the resulting reaction mechanisms from dissociation of pervanadyl, substrate oxidation to subsequent reoxidation is shown. During the catalytic cycle, the structural integrity of the catalyst is given. Typically, the change between oxidized and reduced forms of the catalyst is associated with a color change. This color change occurs due to the intense d-d transitions as well as interval charge transfer and usually results in a characteristic deep blue color of the POMs, hence called “poly-blues” or “heteropoly-blues”. This phenomenon can be observed particularly well with vanadium-substituted *Keggin*-type POMs, which are intensely orange in oxidized state. Interestingly, higher vanadium-substituted HPAs in particular have proven to be extremely active. According to *Poller et al.*⁹⁹ higher substituted HPAs are able to form peroxo ligands between neighboring vanadium atoms, decreasing the activation energy of oxidation reaction.^{77,79,81,82,99,100}

In addition to pervanadyl, other vanadium species can also be formed in aqueous solutions, depending on the pH value, as illustrated in Figure 4.8. The formation of vanadium species depends not only on the pH value, but also on the vanadium concentration. It can be seen that the catalytically active pervanadyl is formed at pH values below 3.8.¹⁰¹



Scheme 4.8: Pervanadyl-catalyzed oxidation of substrate and subsequent reoxidation of catalyst.^{102–104}

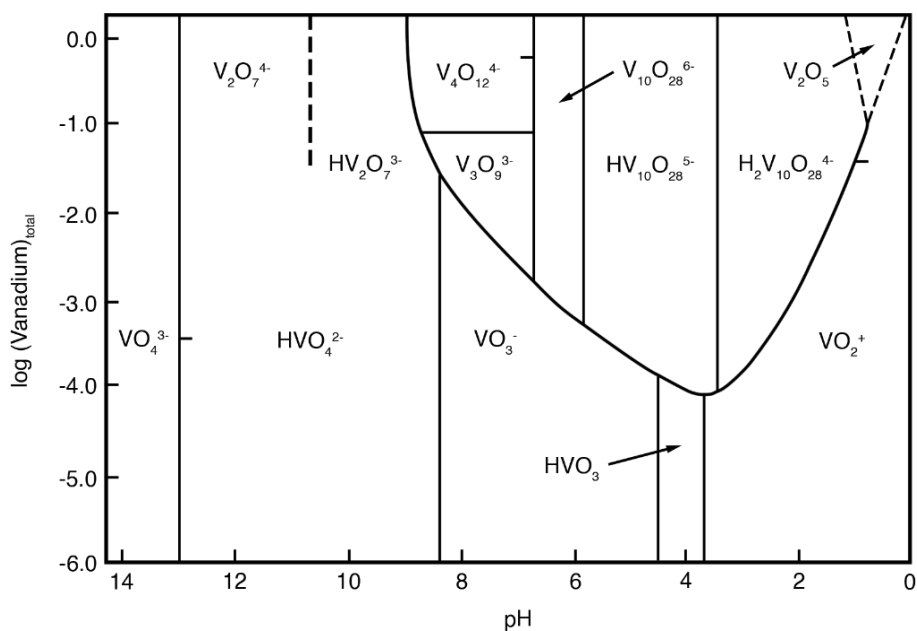


Figure 4.8: Dependency of vanadium species on pH value in predominance diagram.¹⁰¹

Another interesting field of research is the influence of alcoholic additives on catalysis using vanadium-substituted HPAs. Several studies have impressively shown that alcoholic additives have an impact on vanadium-substituted POM-catalysts in the selective catalytic oxidation of biomass.^{69,105,106} In particular, methanol (MeOH) as an additive enables a remarkable inhibition of CO₂ formation. According to the literature, this property is due to the action of methanol as a radical scavenger, stabilizer of reactive groups and promoter of new catalytic V-species. One conjecture is the formation of the vanadium ester $[\text{VO}(\text{OMe})\text{O}_2]^{2-}$, which is more selective and inhibits the overoxidation of the substrate to CO₂.^{69,105,106}

4.3.2 Applications of Polyoxometalates

Based on the above-mentioned structural diversity and controllable properties of POMs, there is a wide range for their application. Beyond use in catalysis, POMs are attractive for applications in electrochemistry, biochemistry, biotechnology, nanotechnology, medicine, and material science. POMs are used to combat some types of tumors or to treat Alzheimer's disease.^{79,81,95,107–109}

However, for the studies of the present dissertation, the application of POMs in catalysis as Brønsted acid and redox catalysts is interesting and important. *Keggin*-type vanadium-substituted POMs are particularly characterized by their unique properties such as increased redox activity. Here, applications as homogeneous but also heterogeneous catalysts are conceivable. For example, the selective catalytic

reduction of nitrogen monoxide (NO) using ammonia (NH₃) as reductant (NH₃-SCR) can be catalyzed by heterogeneously supported POM-catalysts. In homogeneous applications, a five times vanadium-substituted *Keggin*-type POM (HPA-5) can be used as catalyst for the sustainable desulfurization of fuels in *extraction-coupled oxidative desulfurization* (ECODS). Furthermore, it could be demonstrated that *extractive oxidative denitrification* (ECODN) as well as *deoxygenation* (ECODO) is also feasible. In the review by *Raabe et al.*³⁰ a comprehensive overview of possible applications of HPA-5 can be found.^{110–114}

Another relevant area of application for POMs is the use in the valorization of biogenic raw materials and complex biomass. This includes the oxidation of the platform chemicals such as 5-HMF and furfural, which are available from biogenic sources, into industry-relevant products such as maleic acid (MA) and 2,5-furandicarboxylic acid (FDCA). *Zhong et al.*⁷⁵ collated an overview of the possible applications in the valorization of biomass in their review.^{75,115}

The mentioned OxFA process, wherein formic acid can be produced from biomass, is also one of the possible applications. The development of the OxFA process is well advanced and has already been demonstrated in continuous operation. Simple biogenic substrates but also complex substrates can be converted applying the OxFA process. It was shown that the conversion of insoluble complex biomass can be optimized by using additives such as para-toluenesulfonic acid (pTSA) as solubilizer. In addition, the selectivity and catalytic performance of the catalysts in the OxFA process can be influenced by alcoholic additives such as methanol and ethanol.^{29,35,36,69,75,106,115–117}

In the following sections, the carboxylic acids relevant to this work industry are presented in more detail. Specifically, formic acid, acetic acid, maleic acid and levulinic acid are described more deeply as potential value-added products. The essential properties and manufacturing processes of these carboxylic acids are considered.

4.4.1 Formic Acid

Methanoic acid, also called formic acid (*Acidum formicium*) is the simplest carboxylic acid and is described by the formula HCOOH . Its name is derived from its natural occurrence in the glands of ants (*Formicidae*), from which the acid can be obtained by distillation. Formic acid is also contained in the stinging hairs of nettles.^{121–125}

4.4.1.1 Properties of Formic Acid

With a melting point of 8.3 °C and a boiling point of 100.8 °C (at 1013 hPa), formic acid is a colorless, corrosive liquid with a pungent odor that is miscible with many polar solvents as well as in any ratio with water.^{122,123} Due to the intermolecular hydrogen bonds and the resulting association as dimers, the boiling point for such a short-chain organic compound is relatively high. Dimerized formic acid makes up 95 % of the formic acid vapor at ambient temperature and atmospheric pressure causing a significant deviation from ideal gas.¹²² Formic acid is a strong organic acid, actually the strongest unsubstituted carboxylic acid with a pK_a of 3.74 and is corrosive to the skin when undiluted.¹²² In combination with water, it forms a high boiling azeotrope that contains 22.4 wt-% water and 77.6 wt-% formic acid.¹²² This azeotropic mixture boils at 107.6 °C and 1013 hPa.^{118,119,121–126}

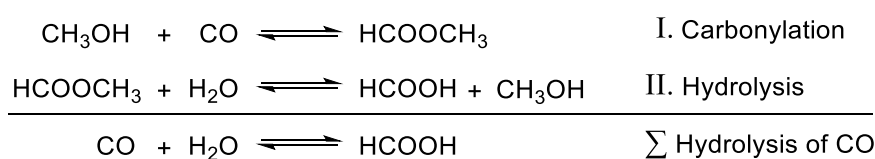
Many of the usual chemical characteristics and typical reactions of the aliphatic carboxylic acids, such as esterification and amidation, are present in formic acid. In contrast to higher homologues, simple esterifications do not require the use of mineral acid catalysts and are faster due to the high acidity of formic acid. Another crucial difference between formic acid and higher homologues arises from the fact that in addition to the carboxyl group, formic acid also has an aldehydic carbonyl group. Therefore, it can have a reducing effect analogous to aldehydes.^{121–123,125,126}

4.4.1.2 Production of Formic Acid

The global production capacity of formic acid was valued at 950 thousand tons per year in 2014 and even reached one million tons per year in 2019.^{60,123} A typical

production site annually produces 20 thousand to 100 thousand tons of formic acid.⁶⁰ According to *Dutta et al.*¹²³ and *Bulushev et al.*¹²⁷, it is estimated that the market for formic acid is growing by 3.0 % to 5.6 % annually.^{14,122,123,125,127}

The industrial production of formic acid is essentially based on two process routes, the acidolysis of its salts (formates) or the hydrolysis of methyl formate. The latter is the dominant process with a market share of 80 % to 90 %.^{122,127} In Scheme 4.9 the reaction system of methyl formate hydrolysis to formic acid is shown. This process route is based on two process stages. The first stage is the carbonylation of methanol to methyl formate, which is typically proceeded at an elevated temperature of 80 °C and a pressure of 45 bar in presence of a basic catalyst such as sodium (NaOCH₃) or potassium methoxide (KOCH₃).^{122,125} Hereby, the carbonylation achieves a conversion of around 95 % for carbon monoxide (CO) and around 30 % for methanol, which can be increased to an almost quantitative conversion by recycling methanol.¹²² In the second stage, the methyl formate formed during carbonylation is hydrolyzed to formic acid, which also acts as hydrolysis catalyst (autocatalysis). In order to shift the hydrolysis equilibrium in favor of the formation of formic acid and methanol in the second step, an excess of water is used. Another approach for shifting the hydrolysis equilibrium is the use of additives such as tertiary amines, which form adducts with formic acid and therefore remove the free acid from the equilibrium. The first stage receives the methanol liberated in the second stage.^{18,122,125,127}



Scheme 4.9: Reaction system of methyl formate hydrolysis to formic acid, according to literature^{18,121,125}.

Formally, the sum of the applied reaction sequence depicts the hydrolysis of carbon monoxide to formic acid. However, this approach is unfavorable from an industrial perspective and thus the detour via the intermediate methyl formate is used.^{122,125,127}

Another conventional process, which is far less significant, is the acidolysis of formates using mineral acids such as sulfuric or phosphoric acid. In the process, sulfates or phosphates are formed as by-products with the counterions (sodium or calcium) of the formate anion. However, this process is now only used by manufacturers in Sweden and smaller Chinese manufacturers.¹²²

The high availability of carbon dioxide and environmental regulations are stimulating companies and scientists to develop new innovative approaches for the utilization of captured carbon dioxide as a raw material. In this scenario, various routes of producing carbon dioxide-based formic acid are being explored. These process routes to produce formic acid from carbon dioxide include approaches such as electrochemical conversion in alkaline medium or catalytic hydrogenation. In particular, either heterogeneously or homogeneously catalyzed hydrogenation of carbon dioxide to formic acid is the counterpart of current research. The heterogeneously catalyzed hydrogenation can typically take place on nanostructured metal catalysts involving noble metals such as Pd, Ru and Au. *Sun et al.*¹²⁸ present a comprehensive overview of various heterogeneous systems for the hydrogenation of carbon dioxide in their review. *Klankermayer et al.*¹⁵ and *Thijis et al.*¹²⁵ have compiled an extensive compilation of homogeneous reaction systems in their reviews. The homogeneous reaction systems investigated are based, among other, on Ir(III)-pincer complexes or non-precious multidentate NP₃ (tris(2-(diphenylphosphino)ethyl)amine) ligand in combination with nickel(II) salts.^{14–17,125,128,129}

In addition to the use of captured carbon dioxide, the production of formic acid from biogenic raw materials is investigated. One approach is the hydrolysis of biomass with all its components, including hemicellulose, cellulose, lignin and vegetable oils. In this process the biomass is depolymerized into its essential components. For example, hemicellulose can be converted into formylated and acetylated xylose oligomers, which are further hydrolyzed to formic acid and acetic acid. Furfural, the actual main product of this process, is also formed via hydrolysis of xylose oligomers. A comparable process approach is already known from the Biofine process, whereby levulinic acid and formic acid are produced via the intermediate 5-HMF (*vide supra*, 4.2.1). Consequently, formic acid is only a co-product and not the actual main product in these hydrolysis approaches of biomass.^{127,130–132}

A more targeted attempt to convert biomass into formic acid is given with the partial oxidation of biogenic raw materials. In the early 1980s, *McGinnis et al.*^{133–135} already oxidized various types of wood without the use of a catalyst at 33 bar of O₂ and 190 °C yielding about 20 % formic acid. By using FeSO₄ as a catalyst, the yield of formic acid could be increased in this process. Significant progress has been achieved through the selective catalytic oxidation of carbohydrates in the aqueous phase catalyzed by polyoxometalate catalysts under mild reaction conditions as presented by

Wölfel *et al.*⁵⁷ (*vide supra*, 4.2.2). The previously introduced OxFA process and its optimization have been the subject of research since then. Optimized catalyst systems, the expansion of possible substrates, the use of additives and the design of a continuous process are being investigated. The optimization of the OxFA process enables almost complete carbon valorization of the biomass used making it a promising approach to produce biogenic formic acid.^{29,35,69,106,116,133–138}

4.4.1.3 Applications for Formic Acid

Formic acid has a wide range of applications as a food additive, preservative in silage and animal feed, as well as in the textile, leather, and rubber industries. The use of formic acid is helpful in ensiling as it lowers the pH and promotes the growth of lactic acid bacteria, thereby preventing other unwanted microbial growth. In the textile industry, formic acid is used as a pH regulator to produce synthetic fibers or to neutralize alkaline solutions. Various pharmaceuticals and food compounds, such as synthetic insulin (purification of recombinant insulin), caffeine, aspartame, and vitamin B1, employ formic acid as a synthetic intermediary.^{15,122,123,127}

The interesting properties of formic acid may be important for energy storage in addition to its material use in various industries. The inherent advantages of formic acid include its relatively low toxicity, low flammability, and the fact that it is liquid at ambient conditions, which makes it a promising material for hydrogen storage. Hydrogen could thus be stored in liquid form under ambient conditions, which means that formic acid can be considered as a hydrogen carrier. Gravimetrically, about 4.4 wt-% hydrogen is stored in the formic acid molecule, which approaches the Department of Energy's target of 5.5 wt-% for efficient storage materials.¹²⁷ However, due to its high density of 1.22 g mL⁻¹, formic acid achieves a high volumetric storage density and stores up to 53 g of hydrogen per liter, which corresponds to 1.77 kW.^{123,122} Furthermore, the dehydrogenation of formic acid has a low enthalpy of reaction compared to most other systems, allowing hydrogen to be produced under moderate conditions (< 100 °C). The reaction can be catalyzed with metals such as platinum, copper, or nickel. In addition, the use of formic acid as fuel for a direct formic acid fuel cell is also conceivable and is being researched.^{14,58–60,62,123,125,139}

4.4.2 Acetic Acid

Ethanoic acid, better known as acetic acid, is one of the most important organic carboxylic acids and is described by the formula CH_3COOH . It is found in diluted form in many plant and animal systems and is formed during the fermentation of ethanol using acetic acid bacteria (*Bacterium aceti*). The fermentation of wine into acetic acid was already known and practiced over 5,000 years ago.^{121,140,141}

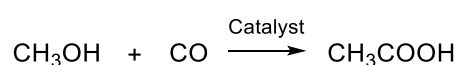
4.4.2.1 Properties of Acetic Acid

As the next higher homologue to formic acid, acetic acid has similar properties. With a melting point of 16.8 °C and a boiling point of 117.9 °C (at 1013 hPa), it is also a clear, colorless, corrosive liquid with a pungent odor.¹⁴⁰ The typical vinegar-like odor is already noticeable at just 1 ppm. Acetic acid is miscible in any ratio with water, ethanol, diethyl ether, hydrocarbon tetrachloride and chloroform. Analogous to formic acid, intermolecular hydrogen bonds can be formed between individual acetic acid molecules, resulting in cyclic dimers. In contrast to formic acid, acetic acid has an additional methyl group, which increases the electron density on the functional group through inductive effects and thus leads to a lower pK_a of 4.77.^{121,140}

4.4.2.2 Production of Acetic Acid

The demand for acetic acid was already high at 13 million tons per year in 2015 and rose to over 18 million tons per year by 2020.^{141,142} It is estimated that the acetic acid market is annually growing by around 5 %.^{140–142}

Acetic acid can be industrially produced via synthetical or biological routes via bacterial fermentation. Although the latter is only responsible for around 10 % of global production, it remains due to its importance as a food of organic origin.¹⁴¹ However, the synthesis routes in conventional chemical processes are significantly faster and more productive. Among the synthetic routes, methanol carbonylation is widely accepted and the method of choice, as described in Scheme 4.10.^{121,140–143}



Scheme 4.10: General reaction equation for the carbonylation of methanol to acetic acid.

The carbonylation of methanol on a rhodium-based carbonyl catalyst at a temperature of 150 °C to 200 °C and a pressure of 30 bar to 50 bar is also called the *Monsanto process*.^{140,142} Using an iodide promoter, selectivity of up to 99 % can be achieved in the Monsanto process.^{140,144} As solvent a mixture of acetic acid and water is preferred. Within the catalytic cycle, water is also needed for the hydrolysis of intermediates to acetic acid and regeneration of the promoter. A further development of the process and the associated replacement of the rhodium-based catalyst with an iridium catalyst could be demonstrated. In the so-called *Cativa process*, the iridium catalyst allows the use of less water and the suppression of water-gas shift reaction, enabling high yields of acetic acid of up to 85 %.^{140,142,144}

4.4.2.3 Applications for Acetic Acid

Acetic acid is in demand as a platform chemical with a wide range of applications such as the production of pharmaceuticals, rubber accelerators, cosmetics and in the plastics industry. The plastics industry requires the largest proportion of acetic acid produced worldwide for the synthesis of polymers. The synthesis of vinyl acetate monomer to produce polyvinyl acetate is of particular industrial importance. Vinyl acetate monomer and its polymers, in turn, can be extensively used in paints, coatings, resins and textiles.^{140,142}

4.4.3 Maleic Acid

Cis-Butenedioic acid, also known as maleic acid, is an industrially important C₄ dicarboxylic acid, described by the formula C₂H₂(COOH)₂. The structure of maleic acid, its anhydride, and trans isomer, fumaric acid, are shown in Figure 4.10. It can be seen that each molecule contains a double bond in the α,β-position. Unlike the industrially relevant carboxylic acids presented so far, maleic acid does not occur in nature.^{145–148}

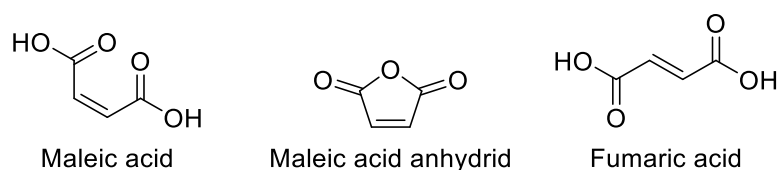


Figure 4.10: Structural formula of maleic acid, its anhydride, and its trans-isomer fumaric acid.

However, its name is derived from the naturally occurring malic acid (2-hydroxybutanedioic acid) found in apples (*Malum*). On the other hand, fumaric acid occurs naturally in many plants such as climbing annual plant (*Fumaria officinalis*), after which it is named.^{145–148}

4.4.3.1 Properties of Maleic Acid

Maleic acid is a solid with a melting point of 130.5 °C that crystallizes in the form of monoclinic prisms.¹⁴⁶ The dissociation constant K_1 of the first stage in water (25 °C) is at a value of $1.14 \cdot 10^{-2}$ and is therefore about twelve times higher than that for fumaric acid at a value of $9.57 \cdot 10^{-4}$.^{145,146} About 78.9 g of maleic acid can be dissolved in 100 g of water at 25 °C and is hence readily soluble in water.¹⁴⁶ This property is due to the local proximity of carboxyl groups, which allows the formation of intramolecular hydrogen bonds that stabilize the anion. Accordingly, the maleic acid anion of the first dissociation stage is more stable than that of fumaric acid, which means that the second dissociation stage is more hindering for maleic acid than for fumaric acid. Thus, the second stage dissociation constant K_2 of $4.13 \cdot 10^{-5}$ is higher for fumaric acid than for maleic acid at a value of $5.95 \cdot 10^{-7}$.¹⁴⁵ Due to the two carboxyl groups and the double bond of maleic acid, it is a multifunctional molecule that enables various chemical reactions. These include classic reactions of carboxylic acids such as esterification or amidation. Involving the double bond, addition reactions are possible such as the addition of water, which lead to the formation of malic acid. Due to the proximity of the carboxyl groups to one another, intramolecular elimination reactions can occur (> 100 °C), leading to the formation of the anhydride.^{145–148}

4.4.3.2 Production of Maleic Acid

Maleic acid is produced primarily from its anhydride by heating it in small amounts of water. After the reaction, the solid product is separated from the cooled mother liquor and dried in vacuum. As a diluted solution, the mother liquor can be recycled back into the hydration stage or can also be processed in the dehydration stage of the maleic anhydride production. Since the production of maleic acid depends on the production of maleic anhydride, this process must also be reviewed. The industrial production of maleic anhydride is based on the catalytic gas phase oxidation of suitable hydrocarbons such as benzene, which has dominated the market for a long time as a raw material for this process. In recent years, the use of C₄ hydrocarbons has become

increasingly important. For example, most of Europe has already converted from benzene-based maleic anhydride technology to butane-based. To produce maleic anhydride, the hydrocarbon is fed into a tubular reactor in a homogeneous mixture with preheated air at around 2.5 bar and up to 500 °C.¹⁴⁶ The tubular reactor consists of a multiplicity of vertical tubes arranged in parallel, whereby the V₂O₅ and MoO₃ catalyst is located as a fixed bed. Subsequent to the reactor, the reaction mixture is fed into a liquid partial condensation where maleic acid anhydride condenses at around 55 °C. Depending on the raw material used, the design of the process can vary. An overview of the possible technological implementations was published by *Felthouse et al.*¹⁴⁵. As shown, the conventional production of maleic anhydride and maleic acid requires the use of fossil raw materials.^{145,146,149}

The high availability of biogenic raw materials is driving industry and science to develop new process routes to enable sustainable process chains, such as to produce maleic acid and its derivatives. In this context, the platform chemicals furfural and 5-HMF have attracted attention, as they can be obtained from biogenic raw materials such as corn cobs, corn stocks, rice husks and sawdust. One example is the production of furfural by the Biofine process, wherein pentoses from lignocellulosic biomass are converted into furfural by hydrolysis, as already described (*vide supra*, 4.2.1). Sustainably produced malic acid can be obtained by oxidizing biogenic furfural. For this purpose, numerous studies have been carried out around the world investigating oxidation of furfural to maleic acid on catalysts such as sulfated zirconia, vanadium pentoxide or polyoxometalates using oxidizing agents such as air and hydrogen peroxide.^{148,150–163} Electrochemical process variants have also been investigated in the literature.^{164–166}

4.4.3.3 Applications for Maleic Acid

Maleic acid is a crucial raw ingredient used in the production of copolymers, surface coatings, lubricant additives, flavorants, unsaturated polyester resins, and agrochemicals. Global industrial demand for maleic acid was estimated at around 1.8 million tons per year in 2021.^{154,157–162,164,166}

4.4.4 Levulinic Acid

Levulinic acid is the simplest and most important oxocarboxylic acid, which are classified according to the relative positions of the oxo and carboxyl groups. Accordingly, α -, β -, γ - and δ -oxocarboxylic acids are distinguished. Therefore, levulinic

acid is γ -oxocarboxylic acid, as shown in Figure 4.11. Levulinic acid is also systematically called 4-oxopentanoic acid and can be described by the formula $\text{CH}_3\text{CO}(\text{CH}_2)_2\text{COOH}$.¹⁶⁷

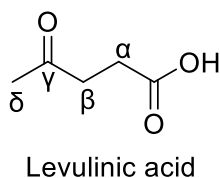


Figure 4.11: Structural formula of levulinic acid.

4.4.4.1 Properties of Levulinic Acid

With a melting point of 37 °C and a boiling point of 246 °C (at 1013 hPa), levulinic acid forms colorless crystals at room temperature that are readily soluble in water, ethanol, or diethyl ether. Due to its interesting chemical structure, levulinic acid can react as a ketone and as a carboxylic acid. The further distance between the carbonyl group and the carboxyl group stabilize levulinic acid against degradation by decarboxylation compared to other representatives of the oxocarboxylic acids with lower relative distances of functional groups.¹⁶⁷

4.4.4.2 Production of Levulinic Acid

As early as the 1940s, levulinic acid was already produced by acid-catalyzed hydrolysis of starch using sulfuric acid.¹⁶⁸ This was the antecedent of today's Biofine process, which has already been discussed in detail in Section 4.2.1. In Table 4.3, various modifications of the Biofine process to produce levulinic acid from different biogenic raw materials are listed. Depending on the used biogenic raw material, it may be necessary to adapt the reaction conditions in order to be able to use a wide variety of biogenic raw materials for the efficient production of levulinic acid. Key factors include acid concentration, temperature, solvent concentration and reaction time. In principle, an increased concentration of acid can increase the yield, but there are limits to this effect depending on the other process conditions and the raw material. The yield of levulinic acid increases with increasing reaction temperature, with an optimum usually being found between 200 °C and 220 °C, above which humin formation is favored.¹⁶⁸ If the amount of solvent is not chosen optimally, the hydrolysis process can be inhibited.^{13,167–175}

Table 4.3: Different process approaches and their yields to produce levulinic acid from various raw materials.

Entry	Raw material	Catalyst	Operating temperature /°C	Yield of levulinic acid / mol%	Reference
1	Glucose	5 wt-% H ₂ SO ₄	170	80.7	171
2	Starch	6 wt-% H ₂ SO ₄	200	66.4	172
3	Paper	> 5 wt-% H ₂ SO ₄	< 240	59.8	173
4	Wheat straw	4.5 wt-% HCl	220	79.6	174
5	Bagasse	4.5 wt-% HCl	220	82.7	174

This optimum depends strongly on the acid concentration but is generally above 90 wt-%. The optimal reaction time depends on the settings of the process conditions mentioned above. At higher reaction temperatures, prolonged reaction times (> 45 min) lead to increased formation of by-products.^{13,167–175}

4.4.4.3 Applications of Levulinic Acid

Levulinic acid was chosen as one of the top 12 sugar-derived chemicals based on criteria from the *National Renewable Energy Laboratory*, which consider a component's industrial adaptability, economics, market size, and capacity to serve as a platform for the synthesis of biogenic derivatives. Due to the multifunctionality of levulinic acid, which makes it a potentially extremely versatile building block to produce a variety of organic (bulk) chemicals, it has earned a place on this list. The diverse areas of application also include the use as specialty chemicals in polymer resins, textile dyes, in the food as well as flavor and fragrance industry, as solvents, herbicides, additives or plasticizers. For example, levulinic acid can be used to produce chemicals such as γ -valeroacetone, 1,4-butanediol and tetrahydrofuran, which are used as agrochemicals as well as pharmaceuticals, plasticizers, or solvent, respectively. In total, there are up to 60 potentially relevant derivatives of levulinic acid. Nevertheless, the production of levulinic acid and its use in various areas are still developing quite slowly. Global annual production is currently estimated at around 17.5 thousand tons, while the potential production capacity worldwide is estimated at 450 thousand tons.^{11,12,167,176–180}

4.5 Membrane Technology for Homogeneous Catalyst Recycling

The previous sections served as an introduction to the basics of sustainable processes. In detail, this means: biomass as a sustainable raw material, examples of green processes, polyoxometalates as promising catalysts and possible relevant products that could be produced using the first mentioned points. Thus, the substrate (humins) derived from biogenic sources, the catalyst class and the target products were defined for the present work. The only operation missing for the development of a sustainable process for the selective catalytic oxidation of humins is an efficient downstream process. Here, the homogeneous nature of polyoxometalate catalysts represents a particular hurdle.

One promising technology to overcome this hurdle are membrane processes, which have gained increasing interest in recent years. The increasing interest is due to their relative sustainability advantage and economic benefits over other separation technologies. A preliminary study by *Bertleff et al.*¹¹² successfully demonstrated the potential of membrane processes in the recovery of homogeneous polyoxometalate catalysts and product separation.^{112,181–185} In the following sections, membrane processes are therefore viewed in more detail as a possible downstream process for the recovery of homogeneous polyoxometalate catalysts and product separation. This includes a description of the basic mode of operation, a discussion of the driving forces, their classification, and the areas of application.

4.5.1 Operating Principle for Membrane Separation

The membrane is at the core of every membrane separation process and is usually arranged in a closed unit, the membrane module. The membrane module's schematic structure can be seen in Figure 4.12. In the module, the membrane serves as a partially permeable, or semi-permeable, separating layer between two chambers. Semi-permeability is the fundamental property of membranes which describes the ability to selectively control the permeation rate of individual components / species of a substance mixture. A different permeation rate of two components enables the separation of these components. Since the membrane is permeable to at least one of the components on the inlet side, this component (i) permeates through the membrane into the second chamber. The remaining or rejected component(s) (j) on the inlet side cannot pass through the membrane and consequently accumulate in the first chamber.^{181,184–189}

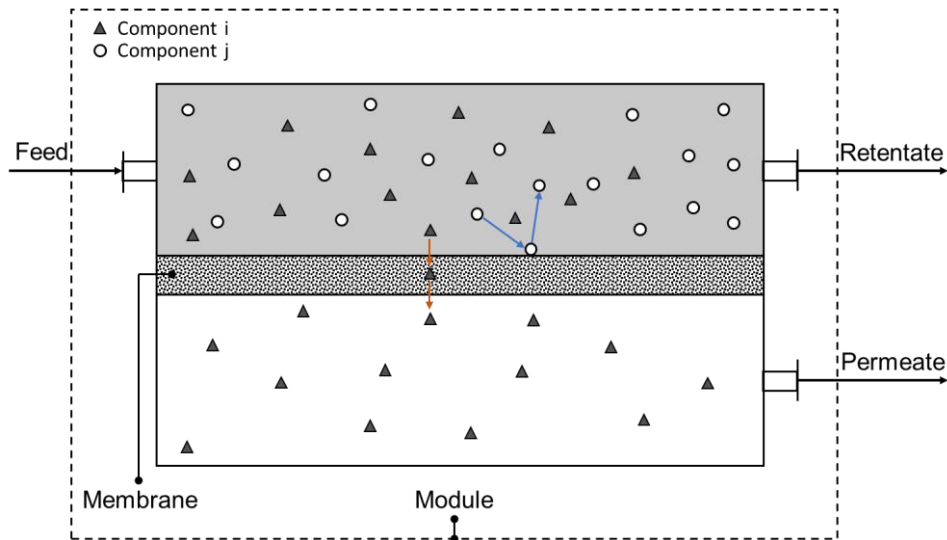


Figure 4.12: Schematic illustration of a membrane module naming the essential components, according to *Merlin et al.*¹⁸⁴.

The flow of the rejected component(s) is referred to as retentate, while the flow of the permeating component is referred to as permeate. In the context of membrane processes, important parameters that describe the process are the permeate flux and the rejection.^{181,184–189}

The permeate flux J is defined as the mass m_{Perm} or volume V_{Perm} of permeate that permeates across the active membrane surface A_{Mem} through the membrane in a certain time t , as described in Equation (4.1).

$$J = \frac{m_{Perm}(\text{or } V_{Perm})}{A_{Mem} \cdot t} \quad (4.1)$$

The selectivity essentially results from the different rejections R of the respective components. It is defined as the ratio of the mass concentration of a component i in the permeate $\beta_{Perm,i}$ and in the feed $\beta_{Feed,i}$, as described in Equation (4.2). Any other concentration measure can be used instead of the mass concentration. The local or integral concentration measures can differ considerably in some cases. However, in most cases the integral values are used to calculate the performance parameters of a membrane process, as the measurement of them is simpler than of the locally resolved concentration values.^{181,184}

$$R_i = \left(1 - \frac{\beta_{Perm,i}}{\beta_{Feed,i}}\right) \cdot 100 \% \quad (4.2)$$

If a component cannot penetrate the membrane and is therefore completely rejected, the rejection reaches its maximum value of 100 %. Conversely, a rejection of 0 % means that a component cannot be rejected and is therefore removed as an aliquot without any change in concentration. A special case is represented by rejection values below 0 %, where active transmembrane transport takes place for the respective component. This special case is discussed in more detail in Section 4.5.4. Additionally, the rejection can be used to derive the *molecular weight cut-off* (MWCO) as further parameter for characterizing membranes. MWCO describes the minimum molecular weight for which 90 % of a component is rejected by the membrane. This value is commonly specified by the manufacturer of a membrane, but is not universally valid, as the MWCO depends strongly on the component, its molecular structure, its substance-specific interaction with the membrane and the solvent, which in turn influences these interactions.^{184,190}

The membrane process, the rejection of components or their permeation through the membrane, depends on transport phenomena that can basically be described by a simplified transport approach. Here, the flux through a membrane can be defined as the ratio of a driving force that leads to transmembrane mass transport and the resistance that opposes it, as shown in Equation (4.3).^{184,191,192}

$$Flux = \frac{Driving\ Force}{Resistance} \quad (4.3)$$

For an efficient separation process regarding a target component *i*, the flow of this component through the membrane must be higher than for a component *j* to be separated. According to Equation (4.3), there are two possibilities to enable different permeation rates:

- Different driving forces (*i*-preferring)
- Different resistances (*j*-disadvantaging)

Classic separation processes such as distillation are based on rapid equilibration and therefore increasingly follow the driving force approach. Thus, they are thermodynamically based. The kinetics only dictate the time required and the dimensions of the process. On the other hand, membrane processes achieve their separation performance through different transport resistances for the components of a mixture and are therefore kinetically based. Consequently, in most membrane processes, resistance plays a more important role in the success of the separation

process then driving forces. For example, this means that the difference in rejection for components i and j of the binary mixture ij must be as large as possible in order to ensure selective separation. Nevertheless, driving forces also contribute to the overall process and must be taken into account because they are important for both the time-scale and dimensioning of the separation process. A detailed discussion of the driving forces and resistances in membrane separation is provided in the following sections (*vide infra*, 4.5.2 and 4.5.3).^{181,184,191,192}

In addition to their importance in industry as downstream processes, membranes can also be found in many natural applications where they fulfill elementary functions. For example, in plants, animals and humans, (cell) membranes selectively regulate the transport of oxygen, nutrients and toxins. In industries, membrane processes can be used for a variety of separation tasks, whereby a wide range of membrane processes specially optimized for the most diverse applications were developed. Optimization criteria include the permeate flux as well as the rejection of the individual components and thus the selectivity of separation process. Membrane processes are particularly popular in water treatment. Basically, membrane processes offer inherent advantages in industrial separation processes:^{184,193}

- Since separation does not need a phase change, it is more energy efficient than e.g. distillation.
- Separation by membrane processes can be conducted under mild conditions and thus it is suitable for sensitive products.
- Unlike adsorptive separation processes, it may operate continuously under steady-state conditions without requiring regeneration cycles.
- Unlike traditional clarifying, which often depends on the addition of chemical coagulants and flocculants, resulting in restricted sludge generation, little to no chemical addition is needed.
- Membrane processes are compatible with other separation processes.
- Membranes can be adjusted for a specific application.
- Up-scale of membrane processes is easy.

These and further advantages using membrane processes can be realized depending on the separation task and the selected design of the membrane process.

4.5.2 Driving Forces in Membrane Separation

The driving forces arise from varying process parameters or thermodynamic variables. In membrane processes, the difference in pressure p , concentration c , electric potential E , or temperature T between two phases separated by the membrane form the framework for the processes. In response to the forces resulting from the differences in these parameters, the transmembrane flow of mass, heat and electricity arises. Table 4.4 shows a collection of different membrane processes classified according to the applied driving forces and involved phases. The pressure-driven membrane processes are of particular interest for the present work. The differential pressure results from an overpressure on the inlet side or a negative pressure on the permeate side. In practice it is quite possible for several driving forces to act simultaneously.^{184,187,191–195}

During the membrane process, a loss or change of driving force and the associated decrease in transmembrane mass transport or in selectivity is possible. For example, the pressure loss in the membrane module has a decreasing effect on the driving force. In addition, deposits can form on the membrane (fouling), which increase the transport resistance and thus decrease the transmembrane flow. Furthermore, the enrichment of the rejected component(s) on the membrane surface, also called *concentration polarization*, leads to a higher driving force for the permeation of the component(s).^{181,184,191,192,196}

Table 4.4: Examples of membrane processes with different driving forces and phases of the material systems to be processed, according to literature^{184,187,191,192}.

Entry	Process	Phases	Driving Force	Example of Application
1	Filtration, Reverse Osmosis	Liq/Liq	Δp , Feed up to 200 bar	Desalination of water
2	Dialysis	Liq/Liq	Δc	Artificial kidney
3	Osmosis	Liq/Liq	Δc	Cell membrane
4	Electrodialysis	Liq/Liq	E	Separation of ions from aqueous solutions
5	Pervaporation	Liq/Gas	Δp (Δp_i), decreased on permeate side	Separation from trace substances
6	Gas permeation	Gas/Gas	Δp , high feed or decreased permeate pressure	Separation: H_2/N_2 CO_2/CH_4

Consequently, the selectivity of the separation decreases. For the present work, the following obstacles can be derived applying a membrane-based downstream process for the selective catalytic oxidation of biomass (e.g. humins) using homogeneous POM catalysts:

- Strong enrichment of the POM catalyst (concentration polarization) on the membrane surface effecting separation selectivity.
- The enrichment of the catalyst leads to low pH values and consequently to its precipitation or structural changes.
- Partially dissolved complex biomass or cleaved components of it precipitate and lead to fouling.

By cleverly designing the membrane module, the concentration polarization and related fouling can be minimized. Figure 4.13 shows different filtration methods and the associated flow types. In *dead-end filtration*, the membrane surface is exposed to a vertical feed flow that is pressed through the membrane by a pressure gradient, for example. Both the feed flow and the driving force are perpendicular to the membrane surface in dead-end filtration. During the filtration process, the rejected component(s) form a covering layer that influences the separation process. If particles are deposited on the membrane surface and form a layer of particles, also known as a *filter cake*, the pressure loss increases progressively. Thus, this method is usually operated discontinuously. In view of the points mentioned above, this method is not suitable for the continuous separation envisaged in this work. In comparison, the feed is injected tangentially to the membrane surface so that the feed flow is orthogonal to the driving force.^{181,184,191,192,196}

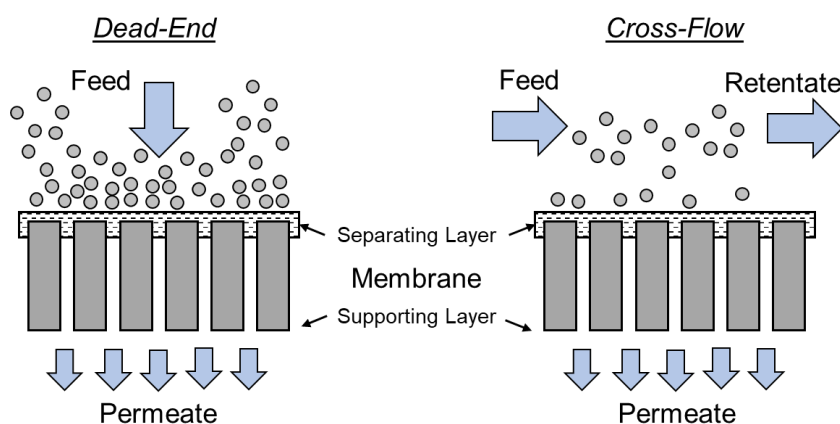


Figure 4.13: Possible flows in membrane modules for dead-end filtration (left) and cross-flow filtration (right), adapted from literature^{184,186}.

Due to the cross-flow, shear forces are generated that lead to a decrease of the covering layer. This means that in cross-flow filtration there is an interplay between the mass transport to the membrane surface due to the driving force and the transport back into the core flow. Overall, the formation of a filter cake or, in general, the enrichment of the rejected component(s) (concentration polarization) is severely restricted or even prevented. Thus, cross-flow filtration achieves steady-state distribution of particles or solutes at the interface and can therefore be operated continuously. The disadvantage of this *modus operandi* is that the creation of a turbulent flow increases the energy demand. However, the additional energy demand is still lower than using dead-end filtration.^{181,184,192,195}

4.5.3 Resistances in Membrane Separation

Basically, the membrane represents a transport resistance whose different strengths for the respective components enable their separation. Two main mechanisms can be used to describe membrane separation: the *solution-diffusion model* and the *pore-flow model*, as displayed in Figure 4.14. The solution-diffusion model is used for microscopically pore-free membranes, so-called dense membranes. These include membranes with pore diameters below 0.5 nm, meaning that the diameter is within the range of thermal motion of the polymer chains that make up the membrane. Solution-diffusion membranes appears less suitable for the present work, wherefore only the pore-flow model is further considered. This kind of membranes also describes the experiments of performed by *Bertleff et al.*¹¹² in their study on membrane separation of POM catalysts. The pore-flow model is used for porous membranes with large permanent free volume and pore diameters up to 100 nm.^{112,181,184,197–199}

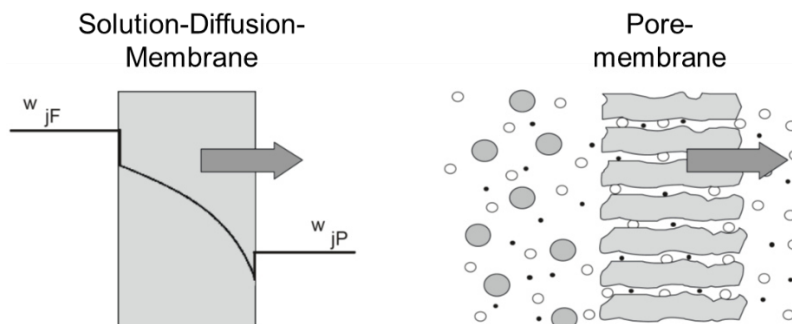


Figure 4.14: Idealized model for molecular transport across membranes, adapted from *Merlin et al.*¹⁸⁴.

The transition range between dense membranes and porous membranes is between 0.5 nm and 1 nm. The porous structure consists of a network of narrow pores. According to the pore flow model, mass transport in the porous structure occurs through convection. The separation occurs through the filter effect, which is based on size exclusion. This means that the structure of the pore network can determine the prevailing resistance for the respective component and thus enable selective separation.^{181,184,197–199}

When separating using porous membranes, the pore diameter is of crucial importance for the possible separation processes. For this reason, a classification of membranes and the resulting membrane processes according to pore size seems sensible, as can be seen in Figure 4.15. In particular, the pressure-driven membrane processes in combination with porous membranes are relevant to the present work. These include *nanofiltration* (NF), *ultrafiltration* (UF) and *microfiltration* (MF). NF has several unique properties and advantages that make it a promising technology for the separation of homogeneous polyoxometalate catalysts, which is one objective of the present work. Thus, in view of the preliminary work by *Bertleff et al.*¹¹² and the given separation task, the following section explains the special features of NF in more detail.^{191,193,200}

Contaminant size	Ionic range		Molecular range		Macromolecular range	Microparticle range
Pore size (nm)	1		10		100	1000 10,000
Molecular weight (g/mol)	100	200	1000	100 000	500 000	
Solutes	Aqueous salt		Virus		Bacteria	
	Inorganic contaminants		Proteins		Micro plastics	
	MICROS (<1 nm) Pharmaceuticals, steroid hormones, personal care products, pesticides, low molecular weight acids and neutrals, etc.		Microsolutes		Humic acids	
			MACROS (>1 nm) Proteins, humic substances, natural organic matter, biopolymers, nanoparticles, viruses			
Membrane separation process	Electrodialysis		Membrane bioreactor			
	Reverse osmosis		Membrane distillation			
	Nanofiltration		Microfiltration			
	Pervaporation		Ultrafiltration			

Figure 4.15: Classification of liquid phase membrane processes according to their pore size and possible areas of application, adapted from *Schäfer et al.*²⁰⁰.

4.5.4 Nanofiltration

Nanofiltration fills an important gap between reverse osmosis and UF enabling the rejection of relatively low molecular weight organic solutes and fractionation of ions. Characteristically, molecules with molecular weights above 300 g mol^{-1} can be rejected and monovalent can be separated from polyvalent ions through electrostatic interactions with the membrane material and its typical pore size of 1 nm .^{181,184,191,200}

NF has received great attention in recent years as a prospective separation technique. Intensive research has led to a wide range of different NF membranes that are stable in a variety of media and enable low-energy separation/purification in a wide MWCO range from 150 Da to 1000 Da . With a thin top layer resting on a porous support, the majority of these membranes have an asymmetric structure. The nanometer-scale pores lead to an extremely complex process depending on micro-hydrodynamics as well as interfacial events that take place on the membrane surface and in the nanopores of the membrane. As a result, the separation mechanism in NF cannot always be explained only by size exclusion effects. Steric, electrostatic, dielectric, and transport effects can all contribute to rejection of components by NF membranes. This is particularly true when separating ions in aqueous solution, which is required for the separation of homogenous polyoxometalate catalysts of the present work.^{200–202}

For instance, different charges and the associated differences in the size of hydration shell provide the mechanism for the separation of monovalent and multivalent ions. Ions with a larger hydration shell (usually polyvalent ions) would have to shed their shell to enter the membrane pore and are therefore rejected. In addition, ions polarize media at the interface according to their dielectric constant. The dielectric constant of the membrane is lower than that of the solvent causing repulsion. Furthermore, changes in the dielectric constant within the pores provide an extra energy barrier for ion solvation, which results in the ions being rejected. This phenomenon is also known as *dielectric exclusion*.^{200,203}

Polymeric NF membranes in contact with aqueous solution can slightly be charged due to dissociation of ionizable surface functional groups or adsorption of charged solute based on a weak ion-exchange capacity of NF membranes. This slight surface charge can lead to a phenomenon known as *electrostatic repulsion* or *Donnan exclusion*, which affects monovalent and polyvalent ions differently. It is well known that the Donnan exclusion is more pronounced on polyvalent ions.^{201–204}

Given the characteristic properties of NF and the composition of possible product solutions for selective catalytic oxidation processes by homogeneous POMs, NF appears predestined as a downstream process. *Bertleff et al.*¹¹² pursued this very promising approach in their study on the separation of POM catalysts from product solutions of the ECODS process (*vide supra* 4.3.2). The suitability of NF as downstream in ECODS and analogous processes is supported by numerous facts. On the one hand, the possible products of the selective catalytic oxidation such as FA as well as AA have molecular weights substantially below 300 g mol^{-1} and therefore may penetrate the membrane unhindered. On the other hand, the *Keggin*-type polyoxometalate catalysts usually have molecular weights above 1800 g mol^{-1} . Therefore, a selective separation of products and catalysts appears feasible. It should be noted that the catalysts are inorganic molecules of heavy elements and thus the resulting molecular size, which is crucial for separation using NF, is not comparable to organic molecules of the same molecular weight. Nevertheless, the difference in molecular weights is so large it can be assumed that the molecular sizes also differ greatly from one another. In addition, the products are monovalent ions (formate, acetate), while the catalysts are polyvalent molecules with valences of up to eight. Hence, it can be assumed that there is a significant difference in the size of hydration shell, in dielectric exclusion and Donnan exclusion enabling efficient separation of products and catalyst. The results of *Bertleff et al.*¹¹² confirm these assumptions and prove that a selective separation of FA and AA from POM catalysts is possible. While the catalyst was almost completely rejected, FA and AA were able to penetrate the membrane almost unhindered.¹¹² It is to be expected that the selective catalytic oxidation of humins will produce a similar product spectrum and thus a separation comparable to the product solutions of the ECODS process could be possible. Overall, NF is not only a promising downstream process for oxidative valorization of humins in terms of a high possible selectivity but is also characterized by low costs and energy demand.

5 Experimental Part

The studies and experiments in this dissertation were conducted in various test facilities on a laboratory-scale. Depending on the used system, the test phase and objective, the experimental procedure, methodology, analytics, and calculation basis varies. A detailed description of the respective procedure, analytics (devices) and calculation can be found in the section of the corresponding study (*vide infra*, 6). The analytical procedure is therefore not discussed further in this section, but the descriptions of the test setups used are presented here in more detail. Screening experiments for catalyst selection and determination of the structure-activity-selectivity relationships of different humin-like substrates were conducted in a batch reactor system consisting of ten reactors connected in parallel, each with a total volume of 20 mL (*10-fold batch reactor*). Oxidation experiments on humins and optimization experiments on humin conversion were carried out in 100 mL autoclaves. The system used consists of three autoclaves connected in parallel (*3-fold batch reactor*). The final developed process was scaled up in a 600 mL autoclave (*600 mL batch reactor*). This system was also used for the reactions in the recycling study. There, a nanofiltration unit was developed, built, and used as a downstream process for the separation of POM-catalyst and products (*POMMem*). The process development matrix, which shows the structure and successive sequence of the investigations using the test facilities and the associated objectives, is summarized in Figure 5.1.

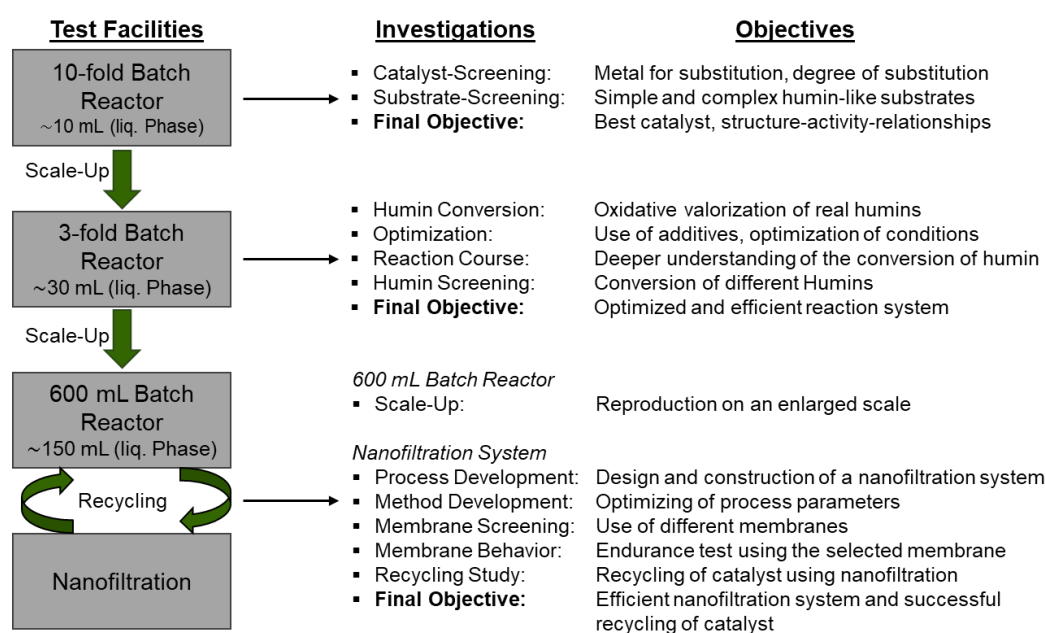


Figure 5.1: Process development matrix for the selective catalytic oxidation of humins.

5.1 10-fold Batch Reactor

The 10-fold batch reactor consists of ten 30 mL Hastelloy (C276) autoclaves from *Parr Instruments*. Glass inlets were used in all autoclaves to improve the handling of solid residues. All tubes, fittings and valves were made of stainless steel (EN 1.471). In Figure 5.2, pictures of the setup (A) and an individual autoclave (B) consisting of a head and digester as well as a schematic process flow diagram (C) are shown. The connection of the head and digester was sealed using sealing rings made of polytetrafluoroethylene (PTFE). Reaction temperatures up to 200 °C could be achieved using a heating block that has suitable recesses for a maximum of ten autoclaves. The heating was controlled by a controller from *Horst GmbH*. The stirring speed of the magnetic stirrer was controlled between 0 rpm and 1000 rpm using a magnetic stirring plate from *IKA®-Werke GmbH & CO. KG*. The pressure could be monitored analogically via pressure gauges or digitally employing pressure sensors from *Keller AG*. Bursting disks for each autoclave limited the pressure to a maximum of 100 bar \pm 10 bar (at 20 °C).

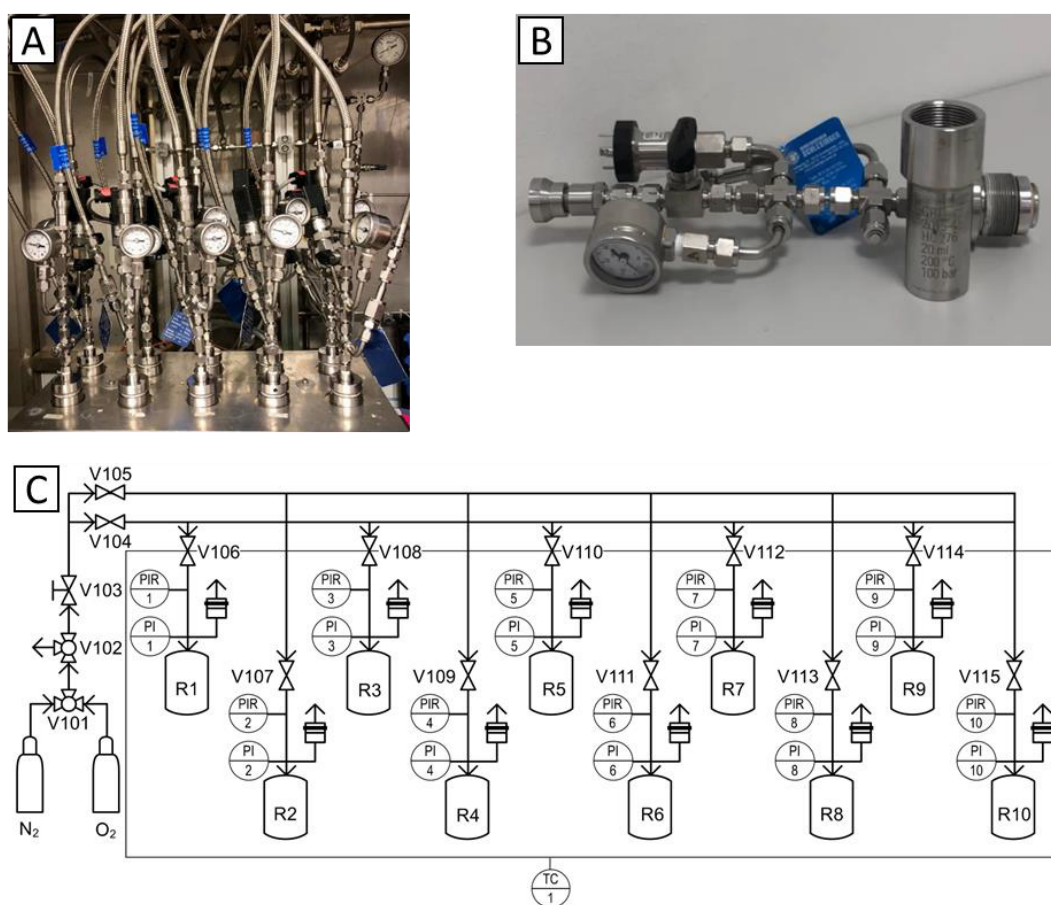


Figure 5.2: 10-fold batch reactor A) picture of the system with all reactors, B) picture of one reactor and C) process flow diagram.

The autoclaves were connected to a supply line that enabled the supply of oxygen or nitrogen. By adjusting valve V101, it was possible to select between oxygen and nitrogen gas supply, the pressure could be adjusted via the fine metering valve V103 (Figure 5.2 C). The system could be vented via valve V102. Due to the high number of autoclaves, the gas supply was divided into two lines, which could be shut off separately by valves V104 and V105. In addition, each autoclave had a shut-off valve (V106 to V115) which allows the autoclave to be closed separately. The experimental procedure using the 10-fold batch reactor can be found in the corresponding part of Section 6.2.

5.2 3-fold Batch Reactor

The 3-fold batch reactor consists of three identical 100 mL autoclaves made of stainless steel (EN 1.471). Glass inlets were used in the autoclaves to protect against corrosion and for improved handling of solid residues. In contrast to the 10-fold batch reactor, each autoclave was equipped with its own heating jacket and a gas entrainment impeller. Thus, it was feasible to conduct simultaneous experiments at different reaction temperatures up to 200 °C. Figure 5.3 shows a picture of the 3-fold batch reactor (A) and the schematic process flow diagram (B). The stirrers were driven via a Ministar control from *IKA®-Werke GmbH & CO KG* coupled by a compact A3040HC3 magnetic stirrer from *Parr Instrument GmbH*. By adjusting valve V101, it was possible to select between oxygen and synthetic air gas supply. The supply of reaction gases and thus also the pressure in the autoclave could be regulated individually for each autoclave via the metering valves V102 to V104. Nitrogen could be filled into the reactors via an additional supply line, the supply could be regulated separately for each autoclave using the metering valves V105 to V107. Gas could be released into the exhaust gas or taken as a gas sample via valves V108 to V110 or V111 to V113, respectively. The pressure could be monitored analogically via pressure gauges PI1 to PI3 or digitally using pressure sensors PIR1 to PIR3. The system was controlled using a *Eurotherm* controller. For safety reasons, each autoclave was equipped with a bursting disk that protect the setup for inadmissible overpressure by limiting the pressure to 120 bar \pm 12 bar (at 20 °C). In addition, each autoclave was equipped with a pressure relief valve (SV101 – SV103) that limits the pressure to 65 bar. The experimental procedure using the 3-fold batch reactor can be found in the corresponding part of Section 6.3 and 6.4.

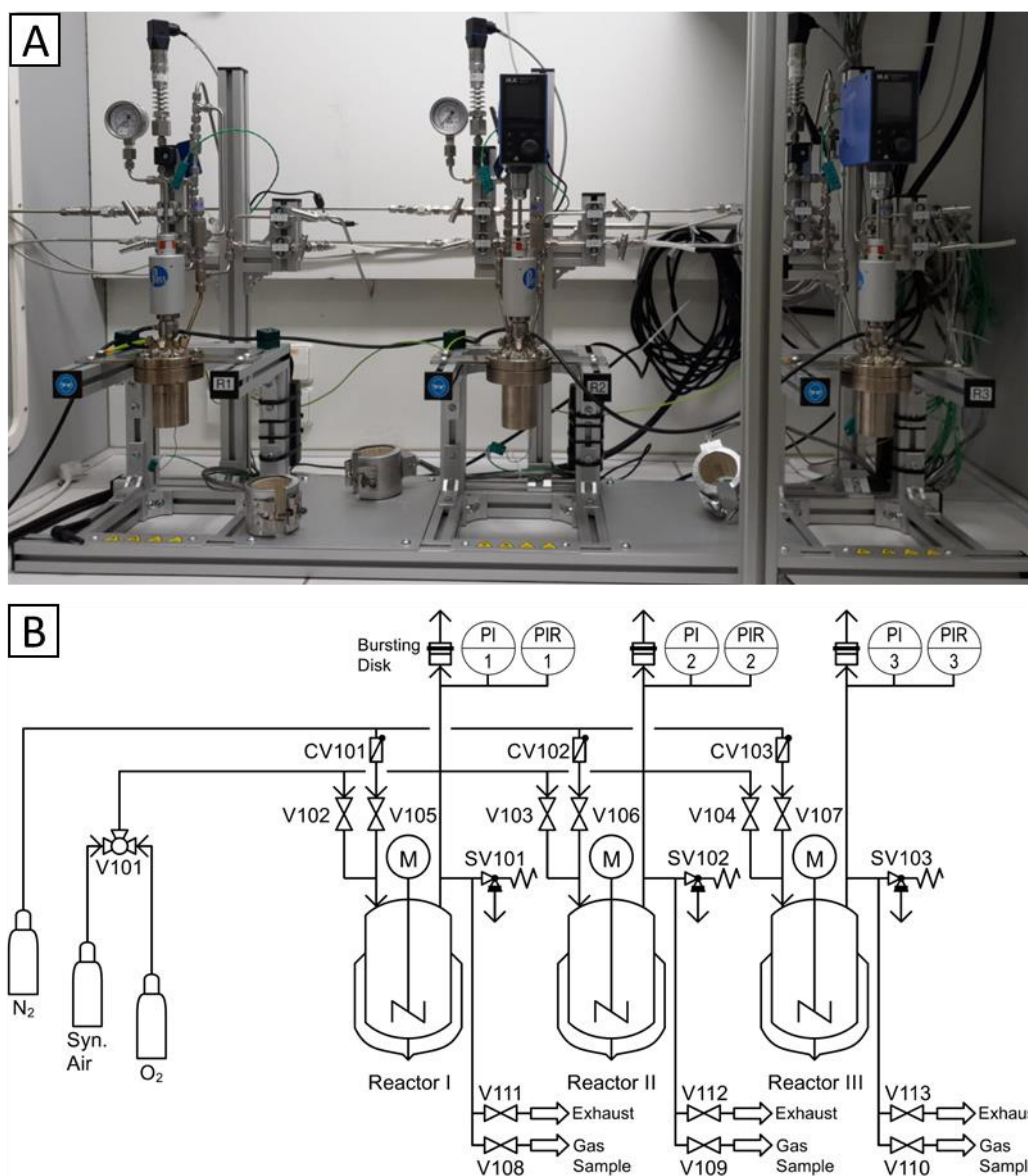


Figure 5.3: 3-fold batch reactor A) picture of the system with all reactors, B) process flow diagram.

5.3 600 mL Batch Reactor

The 600 mL high pressure autoclave made of Hastelloy (C276) purchased from *Parr Instrument GmbH* was equipped with a gas entrainment stirrer driven by a controllable three-phase motor from *Cemp International*. The reaction solutions were weighed into a glass inlet, which was subsequently placed in the autoclave. Both, the Pt100 thermocouple and the stirrer were constructed from Hastelloy (C276) ensuring high chemical resistance. Other components and pipes were made of stainless steel (EN 1.4571) and the seals used were made of PTFE. Figure 5.4 shows a picture of the 600 mL batch reactor (A) and the schematic process flow diagram (B).

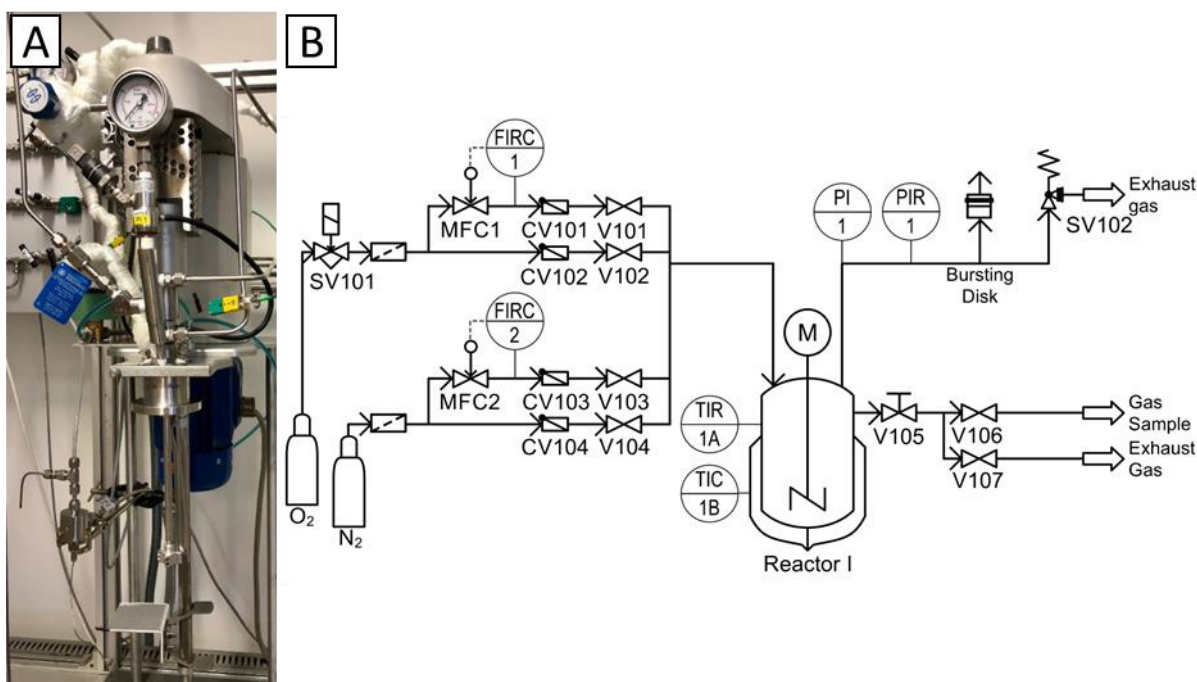


Figure 5.4: 600 mL batch reactor A) picture of the system, B) process flow diagram.

A heating jacket from *Horst GmbH* with an integrated Pt100 thermocouple (TIC1B) was used to heat the reactor. The pressure could be monitored analogically via pressure gauge PI1 or digitally using the electrical pressure sensor PIR1 from *Ashcroft Inc.* All process data as well as the heating were processed or controlled by controllers purchased from *Eurotherm Germany GmbH*. The oxygen supply could be controlled either manually or electronically using the mass flow controller MFC1 from *Bronkhorst Deutschland GmbH*. The same function was available for nitrogen via the mass flow controller MFC2. All supply lines were equipped with inline filters, check valves (CV101-104) and separate shut-off valves (V101-104). Since oxygen is an active gas, the oxygen line also had a magnetic safety valve (SV101) that stops the gas supply in the event of malfunctions or impermissible operating parameters. Further safety devices against overpressure were a bursting disk that limited the pressure to $100 \text{ bar} \pm 10 \text{ bar}$ (at $20 \text{ }^\circ\text{C}$) and a pressure relief valve (SV102) that opens when 50 bar is exceeded. In addition, the system was equipped with a cryostat from *LAUDA Dr. R. Wobser GmbH & CO. KG*, which was able to actively counter-cool. Using the metering valve V105, gas samples could either be taken or the reactor could be ventilated. The experimental procedure using the 600 mL batch reactor can be found in the corresponding part of Section 6.4.

5.4 Nanofiltration System – POMMem

Figure 5.5 shows images (A, B) as well as the corresponding process flow diagram (C) of the membrane system that was designed, constructed, and used for nanofiltration experiments. More information on the development and special features of this system as well as the components selected can be found in publication²⁰⁵ (Section 6.1). The heart of the membrane system is the HPLC pump purchased from *Bischoff Analysetechnik u. -geräte GmbH*, which is responsible for generating a constant pressure in the system and the membrane cell in which the actual separation process takes place. Adjusting either the fine metering valve V102 or the pressure relief valve V106, the pressure could be set to the desired value (Figure 5.5, C). An integrated stirrer within the membrane cell ensured sufficient flow across the membrane, which is unique compared to classic cross-flow filtration using overflow pumps. This special design was developed and patented²⁰⁶ by *PS Prozesstechnik GmbH*. Further details on the design of the system and the experimental procedure for membrane screening, duration tests and recycling study can be found in Section 6.1 and Section 6.4.

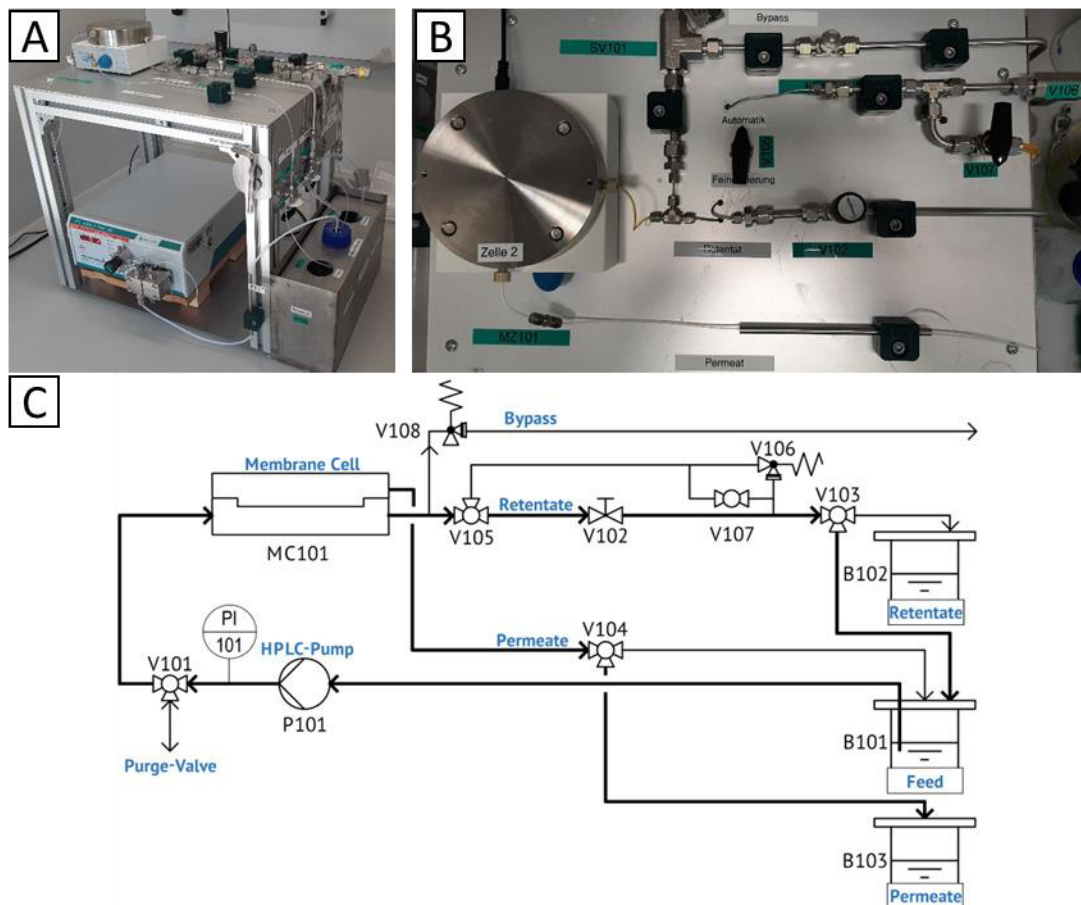


Figure 5.5: Nanofiltration system (POMMem) A) picture of entire system, B) picture from above C) process flow diagram, adapted from *Esser et al.*²⁰⁵.

5.5 Analytics for Qualitative & Quantitative Measurements

The analytical devices and methods used depends on the experiment performed and are described in more detail in the respective study of Section 6 in which they were used. For this reason, only a list of the analytical devices used, and their essential features is given in Table 5.1 for gases, Table 5.2 for liquid phase and Table 5.3 as well as Table 5.4 for solid analysis.

The composition of the gas phase after the oxidation experiments was analyzed by *gas chromatography* (GC). Qualitative and quantitative analyses of the liquid reaction solutions were measured by *nuclear magnetic resonance* (NMR) of the nuclei ^1H and ^{13}C as well as their coupling in 2D-NMR such as *heteronuclear single quantum coherence* (HSQC) and *heteronuclear multiple bond correlation* (HMBC). In addition, NMR measurements were used to verify the catalysts structures (^{51}V , ^{31}P). Further quantitative analyses of the liquid reaction solutions were carried out using *high-performance liquid chromatography* (HPLC). The composition of the catalysts and their quantitative detection in membrane solutions were determined using *optical emission spectrometry with inductively coupled plasma* (ICP-OES). Furthermore, the catalysts were structurally examined using *single X-ray crystal structure analysis*, *powder X-ray diffraction* (XRD) and their water content was determined using *thermogravimetric analysis* (TGA). Additional analysis for catalysts and solids included *attenuated total reflection Fourier transform infrared spectroscopy* (ATR-FTIR), *elemental analysis* (CHNSO) and *scanning electron microscope* (SEM) analysis.

Table 5.1: Analytical device for gas phase analysis.


Picture	Description
<p>GC</p> 	<p>Variant 450-GC, offline gas chromatography</p> <ul style="list-style-type: none"> ▪ Shin-Carbon-ST-column (2 m x 0.75 mm) ▪ 250 μL sample loop ▪ 4.82 bar argon as carrier gas ▪ Flame ionization detector (FID) ▪ Thermal conductivity detector (TCD) ▪ Galaxy Chromatography Data Systems as operating software

Table 5.2: Analytical devices for liquid phase analysis.







Picture	Description
<div style="display: flex; justify-content: space-around;"> <div style="text-align: center;"> <p>500 MHz NMR²⁰⁷</p>  </div> <div style="text-align: center;"> <p>600 MHz NMR²⁰⁷</p>  </div> </div>	<p>Bruker Avance I 500 MHz (AVIII600)²⁰⁷</p> <ul style="list-style-type: none"> ▪ Base frequency 500.13 MHz ▪ 5 mm BBI sample head with ATM and z-gradient ▪ Sample changer B-ACS (120 samples) ▪ TOPSPIN 2.1 <p>Bruker Avance III HD 600 MHz (AVIII600)²⁰⁷</p> <ul style="list-style-type: none"> ▪ Base frequency 600.13 MHz ▪ 5 mm BBFO sample head (Smart Probe) with ATM and z-gradient ▪ Sample changer SampleXpress Lite (16 samples) ▪ TOPSPIN 3.6.4
<p style="text-align: center;">HPLC</p> 	<p>SHIMADZU HPLC</p> <ul style="list-style-type: none"> ▪ Refraction index detector (RI) ▪ Photo diode array detector (PDA) ▪ Autosampler (168 samples) ▪ Aminex HPX-87H 300 mm x 7.8 mm BIORAD column
<p style="text-align: center;">ICP-OES²⁰⁸</p> 	<p>Fa. Spectro Ametek Model Arcos.²⁰⁸</p> <ul style="list-style-type: none"> ▪ Inductively coupled plasma optical emission spectroscopy ▪ ORCA-Optic 130 nm to 770 nm
<p style="text-align: center;">Potentiostat²⁰⁹</p> 	<p>Metrohm - Autolab PGSTAT101²⁰⁹</p> <ul style="list-style-type: none"> ▪ C3 cell stand ▪ Working electrode: Glassy carbon electrode (diameter: 3 mm) ▪ Reference electrode: Ag/Ag⁺ electrode ▪ Counter electrode: platinum electrode
<p style="text-align: center;">pH-Measurement</p> 	<p>Winlab pH meter (Windaus-Labortechnik GmbH & Co. KG.)</p> <ul style="list-style-type: none"> ▪ Excellent Line pH meter ▪ pH/T30 electrode

Table 5.3: Analytical devices for solid analysis – part 1.

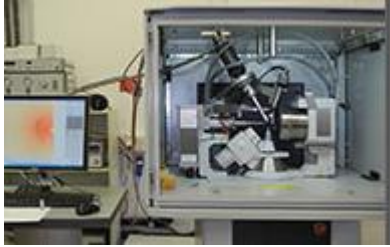





Picture	Description
<p data-bbox="204 331 689 367">Single X-ray crystal structure analysis²¹⁰</p> 	<p data-bbox="724 331 1187 367">Agilent Technologies X-ray analyzer²¹⁰</p> <ul data-bbox="772 376 1385 600" style="list-style-type: none"> ▪ 4-circle single crystal diffractometer SuperNova from Oxford Diffraction ▪ Molybdenum and copper source (dual instrument), microfocus tubes ▪ Cryostream-700 Plus nitrogen steam cooling, 100 K - 500 K (Oxford Cryosystems)
<p data-bbox="347 645 545 680">Powder-XRD²¹⁰</p> 	<p data-bbox="724 645 1283 680">X'Pert Pro diffractometer (PANalytical Corp.)²¹⁰</p> <ul data-bbox="772 689 1334 913" style="list-style-type: none"> ▪ Cu-Kα radiation ($\lambda = 1.5418 \text{ \AA}$) ▪ PIXcel detector with 256 channels (angular range: $-3.12^\circ (2\theta)$) ▪ $0.5 - 150.0^\circ (2\theta)$ as maximum angle range ▪ Automatic 45-fold sample changer ▪ Anton-Paar XRK 900 reaction
<p data-bbox="414 1003 475 1039">TGA</p> 	<p data-bbox="724 1003 1043 1039">NETSCH TG 209 F1 Libra</p> <ul data-bbox="772 1048 1391 1227" style="list-style-type: none"> ▪ Duran-glass crucible ▪ Micro oven made from high-performance ceramics ▪ Temperature ranges up to $1100 \text{ }^\circ\text{C}$ with heating rates up to 200 K min^{-1}
<p data-bbox="379 1361 510 1397">ATR-FTIR</p> 	<p data-bbox="724 1361 995 1397">SHIMADZU ATR-FTIR</p> <ul data-bbox="772 1406 1359 1541" style="list-style-type: none"> ▪ IRSpirit ▪ attenuated total reflection (ATR) ▪ QATRTM-S single-reflection ATR ▪ Fourier transform infrared spectrophotometer
<p data-bbox="319 1653 571 1688">CHNSO-Analyzer²⁰⁸</p> 	<p data-bbox="724 1653 1187 1688">Fa. EuroVector / Hekatech analyzer²⁰⁸</p> <ul data-bbox="772 1697 1257 1809" style="list-style-type: none"> ▪ CHNS-O ▪ EuroEA Elemental Analyzer ▪ HT oxygen-analyzer from HEKAtech

Table 5.4: Analytical devices for solid analysis – part 2.

Picture	Description
<div style="display: flex; justify-content: space-around;"> <div style="text-align: center;"> <p>SEM²¹¹</p>  </div> <div style="text-align: center;"> <p>FEI Quanta 3D FEG²¹¹</p> <ul style="list-style-type: none"> ▪ Field emission gun with acceleration Voltage: 0.2 kV - 30 kV ▪ Resolution of 1.2 nm ▪ Everhart-Thornley (detector) ▪ Backscattered electron detector (BSED) ▪ Low vacuum secondary electron detector (LV-SED) ▪ Gaseous secondary electron detector (GSED) </div> </div>	

5.6 Calculation Bases

Depending on the analytics and substrates used as well as test series conducted, the calculation bases for the calculation of reaction key figures varied, which are explained in more detail in the respective study of Section 6. Since the calculation bases are essential for interpreting the results of the test series, they are also discussed in detail in the following sections. It can be said in advance that all yields of the individual products are based on the molar amount of carbon atoms in the respective components. This is done against the background that the objective of the present work is the utilization of biogenic carbon and thus the efficiency of the developed process is measured by its conversion into value-added products.

5.6.1 Calculation of Reaction Key Figures using HPLC

In initial studies of the present work, furan derivatives were used as humin model substances and converted by selective catalytic oxidation. Thereby, the model substances differed in their complexity and water solubility and thus the calculation basis varied slightly depending on the substrate. Equation (5.1) was used to determine each water-soluble substrate's conversion in the oxidation studies:²¹²

$$X_{Sub\ i} = \frac{c_{0,Sub\ i} - c_{Sub\ i}}{c_{0,Sub\ i}} \quad (5.1)$$

The quantity of substrate *i* converted is represented by the difference between the initial concentration $c_{0,Sub\ i}$ of substrate *i* and the concentration $c_{Sub\ i}$ at the end of reaction. HPLC was used for the determination of the concentration values before and

after the reaction. The ratio of the concentration at the end of the reaction to the initial concentration was used to calculate the conversion $X_{Sub,i}$ of substrate i . For the determination of the conversion of water insoluble substrates the total yield of all products was used. Using Equation (5.2), the yield of each product in the liquid phase was calculated:²¹²

$$Y_{Pro\ i} = \frac{c_{Pro\ i}}{c_{Pro\ i,theoretical}} = \frac{c_{Pro\ i}}{c_{0,Carbon}/N_{Carbon,Pro\ i}} \quad (5.2)$$

All products in the liquid phase were water soluble and could therefore be determined using HPLC. The ratio of the measured concentration $c_{Pro\ i}$ of the product i to its theoretical maximum concentration $c_{Pro\ i,theoretical}$ results the yield $Y_{Pro\ i}$ of a product i . Dividing the initial concentration of carbon $c_{0,Carbon}$ by the number of carbons $N_{Carbon,Pro\ i}$ in the product, the theoretical maximum concentration of a product i is obtained.

Since a stock solution could not be prepared for water-insoluble model substances (MS) and it was therefore not possible to determine their initial concentration using HPLC, the calculation of the yield had to be modified. Consequently, the mass fraction, not the concentrations, was the basis for the calculation. The initial amount of carbon $n_{0,Carbon}$ was calculated according to Equation (5.3):²¹²

$$n_{0,Carbon} = \frac{w_{C,MS\ i} \cdot m_{MS\ i}}{M_{Carbon}} \quad (5.3)$$

Here, the mass fraction $w_{C,MS\ i}$ of carbon in the corresponding model substance i and the weighed-in mass of model substance i , $m_{MS\ i}$, were multiplied to determine the mass of carbon. The initial quantity of carbon $n_{0,Carbon}$ was calculated using the molar mass of carbon M_{Carbon} . Equation (5.4) describes the theoretical maximum mass fraction $w_{Pro\ i,theoretical}$ of a product i :²¹²

$$w_{Pro\ i,theoretical} = \frac{m_{Pro\ i,theoretical}}{m_{total}} = \frac{n_{0,Carbon}/N_{Carbon,Pro\ i} \cdot M_{Pro\ i}}{m_{MS\ i} + m_{cat} + m_{sol}} \quad (5.4)$$

The ratio of the initial amount of carbon $n_{0,Carbon}$ to $N_{Carbon,Pro\ i}$ in the product i multiplied by the product's molar mass $M_{Pro\ i}$ was used to determine the theoretical maximum mass $m_{Pro\ i,theoretical}$ of a product i . The theoretical maximum mass fraction $w_{Pro\ i,theoretical}$, was obtained by dividing the maximum mass of the product by the initial total mass m_{total} in the reactor, which is the sum of the weighed-in masses of model substance $m_{MS\ i}$, catalyst m_{cat} and solvent m_{sol} . It was assumed that the liquid reaction phase's mass would remain constant. Mass was lost in the liquid phase as a result of the carbon

partly entering the gas phase as gaseous products. However, the mass shift was anticipated to be little because the starting mass fraction of the substrates (carbon) was relatively low, at around 5 %. Furthermore, in the liquid phase, oxidation products were created that bind extra mass brought on by oxygen. All things considered; a negligible mass change could be expected. The achieved mass fraction $w_{Pro\ i}$ of a product i was calculated according to Equation (5.5):²¹²

$$w_{Pro\ i} = c_{Pro\ i} \cdot \rho_{liquid} \cdot M_{Pro\ i} \quad (5.5)$$

Here, the achieved mass fraction $w_{Pro\ i}$ is the product of the measured concentration $c_{Pro\ i}$ of a product i , the density ρ_{liquid} of the liquid reaction phase (after filtration), and the molar mass $M_{Pro\ i}$ of product i . Finally, the ratio of the actual mass fraction $w_{Pro\ i}$ to the theoretical mass fraction $w_{Pro\ i, theoretical}$ was used to calculate the yield $Y_{MS, Pro\ i}$, as described by Equation (5.6):²¹²

$$Y_{MS, Pro\ i} = \frac{w_{Pro\ i}}{w_{Pro\ i, theoretical}} \quad (5.6)$$

The selectivity S results from the ratio of the yield to the conversion, as shown in Equation (5.7):²¹²

$$S = \frac{Y}{X} \quad (5.7)$$

5.6.2 Calculation of Reaction Key Figures using Quantitative ¹H-NMR

A 10 wt% tert.-butanol solution in D₂O was utilized as a reference solution for quantification by ¹H-NMR. Since the mass fraction and molar mass of the added standard solution were precisely measured, the molar quantity of tert-butanol in the sample could be determined. A product's molar amount $n_{Pro\ i}$ was determined by multiplying the known molar amount of the standard n_{Stand} by the ratio of its measured area $A_{Pro\ i}$ to the area of the standard A_{Stand} . As done in Equation (5.8), the measured areas need to be normalized by the number of protons N_H that produce respective signal in ¹H-NMR:²¹³

$$n_{Pro\ i} = \frac{A_{Pro\ i}/N_{H, Pro\ i}}{A_{Stand}/N_{H, Stand}} \cdot n_{Stand} \quad (5.8)$$

Using the calculated molar amount of product i and the mass of the sample, its mass fraction can be calculated by known relationships. Analog to Equation (5.3) and (5.4), the initial molar amount of carbon and the theoretical maximum mass fraction of the product i was calculated. Finally, the yield was calculated according to Equation (5.6)

5.6.3 Calculations for Solid Reaction Residues using CHNS

The solid reaction residues were filtered and washed using Soxhlet extraction. Subsequently, the dried as well as weighted solids were analyzed using CHNS to determine the mass fraction of carbon w_{Carbon} . Knowing the total mass m_{solid} of the solid residue and the mass fraction of carbon, the molar amount of carbon in the residue was calculated using Equation (5.9):^{212,213}

$$n_{\text{Carbon,solid}} = \frac{w_{\text{Carbon}} \cdot m_{\text{solid}}}{M_{\text{Carbon}}} \quad (5.9)$$

The ratio between the molar amount of carbon in the solid residue and the initial amount of carbon in the reactor results the yield of solid.

5.6.4 Calculations for Gaseous Reaction Products using GC

The molar fraction γ_i of the gaseous products CO and CO₂ was determined using GC. Assuming the validity of the ideal gas law, the total molar amount $n_{\text{total,gas}}$ of gas molecules in the reactor could be determined. By multiplying the total molar amount of gas and the molar fraction of CO or CO₂ the molar amount of the respective gaseous product is obtained. Since each gaseous product contains exactly one carbon atom per molecule, the molar amount of product is equal to the molar amount of carbon in this product. According to these relationships, the yield $Y_{\text{gas},i}$ of products in the gas phase could be calculated using Equation (5.10):^{212,213}

$$Y_{\text{gas},i} = \frac{p_{\text{Sample}} \cdot V_{\text{gas}}}{RT} \cdot \gamma_i \cdot \frac{1}{n_{0,\text{Carbon}}} \quad (5.10)$$

The volume V_{gas} of the gas phase in the reactor is known. Furthermore, the pressure p_{Sample} was also determined before sampling.

5.6.5 Calculations for Membrane Separation

As described in Section 4.5.1, one of the most important evaluation criteria for a membrane process or membrane is the rejection R of a specific component, which can be determined according to Equation (4.2). The concentration values were determined by ICP-OES for the catalyst components and by HPLC for the valuable products.^{205,213}

Based on the ratio of the feed volume V_0 at the start of the experiment to the feed volume V_{End} at the end, the volumetric enrichment E_V was calculated. Equation (5.11) allows the calculation of the theoretical enrichment $E_{theo,i}$ of a component i based on the volumetric enrichment.²¹³

$$E_{theo,i} = \left(\frac{V_0}{V_{End}} \right)^{R_i} \quad (5.11)$$

The real measured enrichment E_i of a component i was calculated by the ratio of the determined mass concentration of the component at the end and at the beginning of the experiment.

5.7 Chemicals & Gases

The chemicals used as well as the synthesis of model substances, humins and catalysts can be found in the corresponding sections of the experimental studies (*vide infra*, Section 6). In addition, a list of hazardous substances can be found in Section 9.1. For reasons of clarity, all chemicals used for all published studies are overarchingly listed in this section. All chemicals were acquired commercially and used without further purification. To synthesize humins, acetic acid as an acid catalyst and various sugars were used, which are listed in Table 5.5.

Table 5.5: List of used chemicals for the synthesis of humins.

Entry	Name	CAS	Type	Purity	Supplier
1	Acetic acid	64-19-7	Catalyst	Glacial	VWR Chemicals
2	D(-)-fructose	57-48-7	Substrate	Biochemistry	Merck Millipore
3	D(+)-glucose	50-99-7	Substrate	Biochemistry	Merck Millipore
4	D(+)-xylose	25990-60-7	Substrate	Biochemistry	Merck Millipore
5	Sucrose	57-50-1	Substrate	99.0 %	Alfa Aesar

All chemicals used for the synthesis of complex model substances are listed in Table 5.6. Furthermore, various POM catalysts were prepared for oxidation experiments, which required a number of precursors and other chemicals listed in Table 5.7 and Table 5.8.

Table 5.6: List of used chemicals for the synthesis of complex model substances.

Entry	Name	CAS	Type	Purity	Supplier
1	2-Ethyl-furoate	614-99-3	Substrate	99.0 %	Alfa Aesar
2	5-HMF	67-47-0	Substrate	97.0 %	Carl Roth
3	Amberlyst-15	39389-20-3	Catalyst	100.0 %	VWR Chemicals
4	Chloroform	67-66-3	Solvent	99.0 %	VWR Chemicals
5	Ethyl acetate	141-78-6	Substrate	99.8 %	VWR Chemicals
6	Ethyl bromo-acetate	105-36-2	Substrate	98.0 %	VWR Chemicals
7	Furfural	98-01-1	Substrate	98.0 %	Sigma Aldrich
8	Furfuryl alcohol	98-00-0	Substrate	98.0 %	VWR Chemicals
9	Furoic acid	88-14-2	Substrate	98.0 %	Sigma Aldrich
10	Tetrahydro-furan	109-99-9	Solvent	99.5 %	Carl Roth
11	Tri-n-buthyl-phosphine	998-40-3	Catalyst	95.0 %	VWR Chemicals

Table 5.7: List of used chemicals for the synthesis of POM catalysts (part I).

Entry	Name	CAS	Type	Purity	Supplier
1	Cobalt(II) acetate	71-48-7	Precursor	99.9 %	ABCR Chemical
2	Divanadium pentoxid	1314-62-1	Precursor	99.5 %	Alfa Aesar
3	Hydrochloric acid	7647-01-0	pH-regulator	37.0 %	VWR Chemicals
4	Hydrogen peroxide	7722-84-1	Solvent	30.0 %	VWR Chemicals
5	Manganese(II) acetate	638-38-0	Precursor	98.0 %	Alfa Aesar
6	Molybdenum trioxide	1313-27-5	Precursor	99 %	Alfa Aesar

Table 5.8: List of used chemicals for the synthesis of POM catalysts (part II).

Entry	Name	CAS	Type	Purity	Supplier
1	Nickel(II)acetate	373-02-4	Precursor	99.0 %	Aldrich Chemistry
2	Niobium(V)oxide	1313-96-8	Precursor	99.5 %	Alfa Aesar
3	Phosphoric acid	7664-38-2	Precursor	85.0 %	Grüssing
4	Sodium acetate	127-09-3	Buffer	99.0 %	Merck
5	Sodium carbonate	497-19-8	pH-regulator	99.0 %	Grüssing
6	Sodium molybdate dihydrate	10102-40-6	Precursor	99.5 %	Carl Roth
7	Sodium vanadium(V)oxide	13718-26-8	Precursor	96.0 %	Alfa Aesar

Various chemicals were used for substrate and catalyst screening, including furan derivatives, additives and standards for calibration. All chemicals are listed in Table 5.9 and Table 5.10.

Table 5.9: List of used chemicals for the oxidation experiments (part I).

Entry	Name	CAS	Type/Use	Purity	Supplier
1	2-Methylfuran	534-22-5	Substrate	99.0 %	Sigma Aldrich
2	4-methoxyphenol	150-76-5	Substrate	99.0 %	Sigma Aldrich
3	5-HMF	67-47-0	Substrate/Product/ Calibration	97.0 %	Alfa Aesar
4	5-Hydroxyfuran-2(5H) one	14032-66-7	Product/Calibration	96.0 %	AmBeed
5	Acetic acid	64-19-7	Substrate/Product/ Calibration	Glacial	VWR Chemicals
6	Benzofuran	271-89-6	Substrate	99.3 %	Apollo Scientific
7	Deuterium oxide	7789-20-0	Solvent (NMR)	99.9 %	Deutero GmbH
8	Dimethoxy methane	109-87-5	Product/Calibration	98.0 %	Alfa Aesar
9	Ethanol	64-17-5	Substrate/Additive/ Calibration	99.8 %	VWR Chemicals

Table 5.10: List of used chemicals for the oxidation experiments (part II).

Entry	Name	CAS	Type/Use	Purity	Supplier
1	Formic acid	64-18-6	Substrate/Product/ Calibration	97.0 %	VWR Chemicals
2	Fumaric acid	110-17-8	Product/Calibration	99.0 %	Merck
3	Furan-2(5H)-one	497-23-4	Substrate/Product/ Calibration	95.0 %	abcr GmbH
4	Furfural	98-01-1	Substrate/Calibration	98.0 %	Sigma Aldrich
5	Furfuryl alcohol	98-00-0	Substrate	98.0 %	VWR Chemicals
6	Furoic acid	88-14-2	Substrate/Calibration	98.0 %	Sigma Aldrich
7	Levulinic acid	123-76-2	Product/Calibration	98.0 %	Sigma Aldrich
8	Maleic acid	110-16-7	Substrate/Product/ Calibration	99.0 %	Sigma Aldrich
9	Methanol	67-56-1	Substrate/Additive/ Calibration	99.8 %	VWR Chemicals
10	pTSA monohydrate	6192-52-5	Substrate/Additive	98.0 %	Carl Roth
11	Succinic acid	110-15-6	Product/Calibration	99.0 %	Merck
12	Sulfuric acid	7664-93-9	Eluent	95.0 %	Grüssing
13	Tert.-butanol	75-65-0	Calibration (NMR)	99.9 %	VWR Chemicals

The used gases are listed in Table 5.11. Oxygen was used as the reactive gas (oxidizing agent) in oxidation experiments. Nitrogen was used to inert or to produce synthetic air. Hydrogen was used as the fuel gas for the flame of the flame ionization detector (FID) of the GC. Argon was used as the carrier gas in the GC measurements.

Table 5.11: List of used gases.

Entry	Gas	CAS	Type	Purity	Supplier
1	Oxygen	7782-44-7	Reaction gas	99.999 %	Westfalen AG
2	Hydrogen	1333-74-0	Torch gas	99.999 %	Linde AG
3	Nitrogen	7727-37-9	Inert gas	99.999 %	Linde AG
4	Argon	7440-37-1	Carrier gas	99.999 %	Linde AG

6 Cumulative part of the dissertation

This chapter is dedicated to the exploration of the selective catalytic oxidation of humins to short-chain carboxylic acids under mild conditions combined with an efficient downstream processing. The fundamental objective of the investigations is the development of a sustainable process for the valorization of complex humins using homogeneous POM- catalysts. The homogeneous nature of POM catalysts makes them difficult to recover and recycle, which has an impact not only on sustainability but ultimately also on the economic viability of a potential process. Therefore, a comprehensive study on the efficient separation of homogeneous POM catalysts from value-added oxidation products is required. To this end, the Section 6.1 deals with the conception, development, construction, and testing of a nanofiltration process. More specifically, Section 6.1 is dedicated to the development of the nanofiltration system and the associated experimental methodology using a model reaction system.

In parallel, the selective catalytic oxidation of humins is successively developed and optimized in the Sections 6.2 to 6.4, which are encompassed by this chapter. Section 6.2 focuses on the investigation of structure-activity-selectivity relationships in the oxidation of humins and the identification of an appropriate *Keggin*-type polyoxometalate catalyst using commercial and synthesized complex furan derivatives as model substances. In Section 6.3, the findings are transferred to real humins and further developed. This also includes the optimization of the selective catalytic oxidation of humins to carboxylic acids by adjusting the reaction conditions using reaction or selectivity enhancing additives. In Section 6.4, the efficiency of the optimization measures for the selective catalytic oxidation of humins is demonstrated and transferred to an optimized catalyst system. Finally, the further development and adaption of the nanofiltration-based downstream process for the novel reaction system is processed.

6.1 Development of an Efficient Downstream Process for the Recycling of Homogeneous Polyoxometalate Catalysts

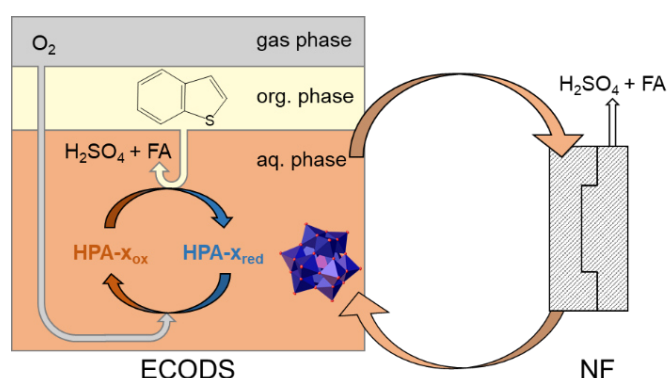
P1

Development of an efficient downstream process for product separation and catalyst recycling of a homogeneous polyoxometalate catalyst by means of nanofiltration membranes and design of experiments

Tobias Esser, Michael Huber, Dorothea Voß, Jakob Albert

Esser, T.; Huber, M.; Voß, D.; Albert, J.: Development of an efficient downstream process for product separation and catalyst recycling of a homogeneous polyoxometalate catalyst by means of nanofiltration membranes and design of experiments. *Chemical Engineering Research and Design*, **2022** (185), 37–50. DOI: 10.1016/j.cherd.2022.06.045.

Formic acid (FA) and acetic acid (AA) are recurring products from the oxidative valorization of biogenic raw materials using homogeneous POM-catalysts in aqueous media. Separating valuable products from the homogeneous catalyst represents a challenge, especially if sustainability criteria for the downstream process used are met. Such criteria include low energy demand and the avoidance of additional additives or solvents (e.g., extractants). In addition, the accumulation of acidic oxidation products and the associated acidification of the reaction solution can have a detrimental effect on the process. An example of this phenomenon is the extraction-coupled oxidative desulfurization (ECODS), in which the accumulation of FA and AA massively inhibits or even negates the catalytic performance of the POM-catalyst. Not only does the acidification of the reaction solution appear to be problematic, but it is also suspected that FA can mechanistically inhibit the catalyst. For this reason, the present section deals with the development of an efficient nanofiltration process for the separation of oxidation products and homogeneous POM-catalysts using the ECODS process as example. This includes the selection of components and the construction of the system as well as the development of a suitable methodology through process optimization. Moreover, this also includes attempts to enrich and recycle the POM-catalyst. The developed downstream process, experimental method, and insights on enrichment as well as recycling of POM-catalyst form the basis for the nanofiltration experiments in Section 6.4. Further supporting information can be found in Appendix 9.5.1.²⁰⁵ The following section is reproduced from Ref.²⁰⁵ published in *Chemical Engineering Research and Design, Elsevier*.



Publication: *Development of an efficient downstream process for product separation and catalyst recycling of a homogeneous polyoxometalate catalyst by means of nanofiltration membranes and design of experiments.*²⁰⁵

Available online at www.sciencedirect.com

Chemical Engineering Research and Design

journal homepage: www.elsevier.com/locate/cherd


Development of an efficient downstream process for product separation and catalyst recycling of a homogeneous polyoxometalate catalyst by means of nanofiltration membranes and design of experiments

Tobias Esser, Michael Huber, Dorothea Voß, Jakob Albert*

Institute of Technical and Macromolecular Chemistry, Universität Hamburg, Bundesstraße 45, 20146 Hamburg, Germany

ARTICLE INFO

Article history:

Received 13 April 2022

Received in revised form 2 June 2022

Accepted 28 June 2022

Available online 1 July 2022

Keywords:

Nanofiltration membrane

Polyoxometalate

Homogenous catalysis

Design of experiments

Catalyst recycling

ABSTRACT

Extractive coupled oxidative desulfurization (ECODS) is a promising technology for efficient deep desulfurization of fuels with integrated product separation. The main objective of this contribution is the development of an efficient downstream process for the separation and recovery of the molecular HPA-5 ($H_8PV_5Mo_7O_{40}$) catalyst by means of nanofiltration membranes. We obtained optimized parameter settings for the membrane separation process using a Box, Hunter & Hunter design of experiments leading to higher rejection of catalyst components above 99%. The optimized parameters were successfully applied for recycling experiments in ECODS. In detail, model gasoline consisting of benzothiophene in iso octane could be efficiently desulfurized in six consecutive runs with product separation by the means of nanofiltration between the individual runs. Distinct changes of the catalyst structure were indicated by ^{51}V NMR and ^{31}P NMR spectroscopy after the second recycling step due to acidification of the aqueous reaction solution. Based on these results, we predict that a continuous process with a coupled nanofiltration separation could push the ECODS technology to industrially relevant technology readiness levels.

© 2022 Institution of Chemical Engineers. Published by Elsevier Ltd. All rights reserved.

1. Introduction

Air pollution is still a major problem for our environment. Therefore, the European Union has decided on a limit of 10 ppmw sulfur for all fuels used for land-based purposes (Europäische Union, Amtsblatt der Europäischen Union, 2009). The most established method for removing sulfur from fuel is still the mature technology of hydrodesulfurization (HDS). The organic sulfur compounds are removed as H_2S from the

oil mixture by catalytic hydrogenation. Non-aromatic sulfur compounds such as mercaptans, sulfides and disulfides are easily removed using the HDS process. However, for aromatic sulfur-containing compounds, such as dibenzothiophene (DBT) and its alkylated analogues, the HDS has to be run under much harsher reaction conditions. These need higher temperature and higher hydrogen pressure to effectuate the conversion for deep desulfurization (Babich, 2003; Gates and Topsøe, 1997).

An interesting alternative approach to HDS is oxidative desulfurization (ODS). This process uses oxidants instead of hydrogen and operates at lower temperatures for deep desulfurization. Used oxidants are organic peroxides, hydrogen peroxide (Campos-Martin et al., 2010), superoxide anions

* Corresponding author.

E-mail address:

jakob.albert@chemie.uni-hamburg.de (J. Albert).

<https://doi.org/10.1016/j.cherd.2022.06.045>

0263-8762/© 2022 Institution of Chemical Engineers. Published by Elsevier Ltd. All rights reserved.

(Mjalli et al., 2014) and molecular oxygen (Ismagilov et al., 2011; Tang et al., 2012, 2015; Ma et al., 2007; Venkateshwar Rao et al., 2007; Zhang et al., 2014). Suitable catalysts for the ODS with molecular oxygen are water-soluble vanadium containing polyoxometalates (POMs) (Tang et al., 2015; Lu et al., 2007; Liao et al., 2017). The sulfones usually formed in the course of the ODS reaction have to be extracted from the hydrocarbon matrix either by a downstream separation process or by in situ extraction (Bosmann et al., 2001; Zhao and Baker, 2015; Jiang et al., 2015; Yazu et al., 2001; Ramírez-Verduzco et al., 2004). Due to the very low solubility of sulfones in water, the latter has not yet been considered as an extraction agent for ODS.

Moreover, because water is a cheap and green solvent, a promising method was developed to use the latter as in situ extracting agent in the so called “extractive coupled oxidative desulfurization (ECODS)”. This process oxidizes the sulfur components using a molecular $H_8PV_5Mo_7O_{40}$ (HPA-5) POM catalyst in aqueous solution to gaseous (CO_2 and CO) as well as water-soluble products such as sulfuric acid, formic acid (FA), acetic acid (AA), oxalic acid (OA), but also to sulfur-containing intermediates such as sulfoacetic acid (SAA) and 2-sulfobenzoic acid (2-SBA). Because the products are gaseous or water soluble, they can be extracted in situ from the hydrocarbon matrix (Bertleff et al., 2017, 2018a; Claufñitzer et al., 2020). The ECODS process can even be used for nitrogenous organic compounds (Bertleff et al., 2020).

The fact that the ECODS process allows deep desulfurization under drastically milder conditions than HDS (120 °C vs. > 300 °C) and uses cheaper raw materials such as molecular oxygen and water, makes the process a pioneering technology. However, some of the reaction products influence the catalytic activity of the HPA-5 catalyst. On the one hand, the pH of the aqueous reaction solution decreases with increasing desulfurization rate due to the formation of the above mentioned acidic species. This causes higher V-substituted species to rearrange to lower V-substituted species and free pervanadyl (VO_2^+), which has a lower catalytic activity [20]. On the other hand, the produced organic acids (especially FA) form stable complexes with the HPA-5 catalyst, lowering its catalytic activity (Bertleff et al., 2018b). Consequently, a sufficient downstream process for the effective separation and recycling of the catalyst is necessary. This could prevent the accumulation of acidic oxidation products, maintaining catalytic activity in ECODS.

Membrane systems gained increasing interest as a result of their relative sustainability advantage over other technologies in recent years (Sikdar and Criscuolo, 2017). This advantage stems mostly from cost savings as well as safe and easy operation (Sikdar and Criscuolo, 2017). Consequently, the growth of membrane market is rapid (Buonomenna, 2013). In particular, nanofiltration (NF) membranes have been used for several applications owing to its unique characteristics, such as enhanced selectivity towards divalent / polyvalent ions while enabling permeability of monovalent ions and small molecules (Ahmad et al., 2022). As a result, using NF in downstream processing can provide an efficient and sustainable concept for recycling and recovery of valuable substances such as homogeneous POM-catalysts (Ahmad et al., 2022).

Previous findings by Bertleff et al. using acid-stable nanofiltration membranes of the DK series membrane-type (GE Power water & Process technologies) in a commercially available METcell Cross-Flow System (Evonik MET LTD) to retain the

POM catalyst in aqueous media showed promising results (Bertleff et al., 2018b). The experimental setup used was based on a classical crossflow process with high feed flows generated by a recycling pump. In common cross-flow membrane filtration (micro to nanofiltration) a high overflow of the membrane surface is required in order to limit the accumulation of rejected components on the membrane (concentration polarization) (Melin and Rautenbach, 2007; Schirg, 2009). This overflow is several times higher than the permeate flux through the membrane. In consequence, low concentration factors are allowed with a given membrane area and an increased energy consumption caused by the overflow pumps. For an efficient recycling process, the catalyst must be highly enriched and a large amount of oxidation products must be separated.

The experimental setup used by Bertleff et al. consisted of three 2,5" cross-flow filtration cells with a hold-up volume of 40 mL and is pressurized with high pressure gas such as nitrogen (Bertleff et al., 2018b; Evonik Resource Efficiency GmbH, 2017). Therefore, the availability of an adequate high-pressure cylinder or gas supply in general and appropriate tubing for the connection to the cell must be ensured (Evonik Resource Efficiency GmbH, 2017). The system was equipped with a gear pump for liquid re-circulation and designed for a minimum working volume of 150 mL (Evonik Resource Efficiency GmbH, 2017). The process was afflicted by typical disadvantages of a classical crossflow process in terms of high feed volume flows and the need for a large membrane area for high retentate enrichment.

However, while the DK series membrane-type could effectively retain the POM catalyst and showed nearly negligible rejection for FA and AA, it could not efficiently separate the sulfuric reaction products sulfuric acid, SAA and 2-SBA from the POM catalyst as these were also mainly retained (> 80%) in the nanofiltration setup. This caused a slight catalyst deactivation during several recycling runs.

A redesign of the experimental setup should overcome this obstacle and strengthen the economic benefits of the membrane processing. A further development of the previous results and an evaluation of the feasibility for a membrane-based downstream process in recycling experiments is still pending. Therefore, the main objective of this contribution was the development of an efficient downstream process for the separation and recovery of the molecular HPA-5 catalyst by means of nanofiltration membranes. Here, industrial requirements concerning recyclability of the catalyst in ECODS and an efficient design should be considered.

2. Results and Discussion

2.1. Development of a membrane setup for efficient HPA-5 catalyst recycling

An efficient downstream process for recovery of the homogeneous HPA-5 catalyst is distinguished by low catalyst losses. For this purpose, a maximum rejection of the HPA-5 components such as molybdenum (Mo)-, vanadium (V)- and phosphorous (P) in aqueous solution is a key aspect of catalyst recycling. Furthermore, the accumulation of reaction intermediates and polar products in the aqueous phase lead to catalyst deactivation in the ECODS process. Therefore, a high permeation of polar oxidation products is necessary (Bertleff et al., 2018b). Consequently, an experimental setup

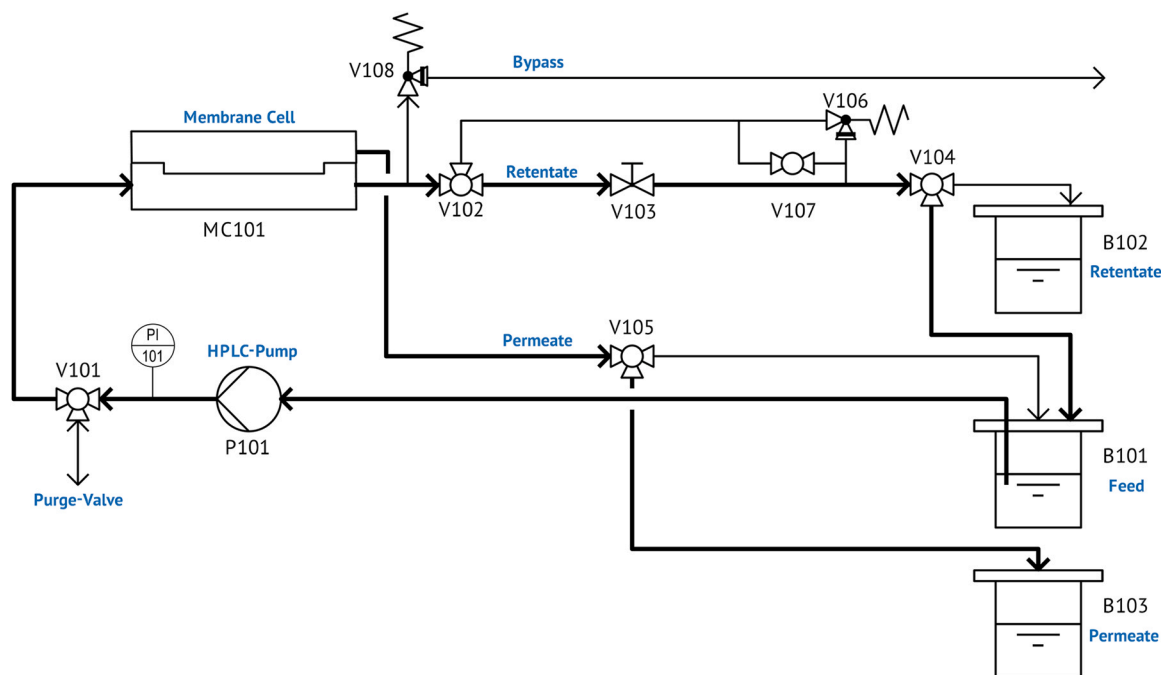


Fig. 1 – Experimental setup for nanofiltration experiments.

has to be developed, enabling a variation and systematic investigation of various process parameters by means of a Design of Experiments (DoE) study. Therefore, we have pursued an alternative downstream approach and designed a new experimental setup for the development of an efficient recovery process for the HPA-5 catalyst at lab scale using flat sheet membranes. The developed experimental setup is shown in Fig. 1.

This setup was perfectly adapted to the requirements for efficient recycling of high molecular weight catalysts in strongly acidic aqueous media. Hence, the setup was designed regarding the following criteria:

- Low working and hold-up volumes allowing small sample amounts (cost savings for valuable substances), enabling high enrichment factors
- Compact system design (possible retrofitting in existing test setups)
- Great flexibility concerning process parameters, enabling systematic investigations
- Safe operation, easy handling and controlling enabling cost effective design

The setup was designed for a minimum working volume of 30 mL and variable pressures up to 50 bar at ambient temperature. A high ratio of membrane area to minimal working volume is reached by the designed setup.

2.2. Preliminary experiments on run-in characteristics and process time

Our first set of experiments was conducted using a feed mixture, representing an aqueous product solution containing HPA-5, FA, AA and sulfuric acid as its major components. The exact composition is given in the experimental section. The purpose of the initial experiments was to examine the run-in characteristics and to determine a sufficient process time for the new experimental setup. These

investigations should result in a standard operating procedure (SOP), which forms the basis for further optimizations. The experiments were performed with a semi-commercial membrane system (see previous section) and a pre-wetted membrane of DK series membrane-type (GE Power water & Process technologies). Table 1 summarizes the determined values for the rejection of catalyst components.

The results show a clear dependency for the rejection of the catalyst components on the process time during the first 60 min (Entries 1,2). Within 60 min, the rejection increases from approximately 95–99% for Mo, 93–97% for V and 78–84% for P, respectively. After the initial 60 min, the rejection of the components stabilizes with negligible fluctuations (Entries 2 – 4). This effect can be attributed to the wetting and swelling of the membrane. When using new or dry membranes a conditioning time is required before a stationary separation behaviour is reached (Melin and Rautenbach, 2007). According to the results, 60 min were needed for the used membrane type. It is noticeable that the rejection of Mo is higher than for the other components. In particular for P, the lower rejection is most likely caused by free phosphate which is not incorporated into the catalyst framework. The presence of free phosphate can be indicated with a characteristic signal around 0 ppm in ^{31}P NMR. Spectra of ^{31}P NMR can be found in the supporting information (Figure S1) Due to proteolysis of HPA-5 in strong acidic media, smaller vanadium oxide species can be formed, which pass the membrane better than the parent HPA-5 (Pobe and Scully, 1975; Zhizhina et al., 2008; Odyakov et al., 2015).

In order to shorten the duration of experiments, further experiments with 15 min process time were carried out on a new pre-wetted membrane cut-out. For this purpose, the newly installed membrane was rinsed with water at a transmembrane pressure of 30 bar for 60 min and emptied afterwards. In this way, a sufficient conditioning of the membrane should be ensured. The aqueous catalyst solution was filled into the membrane system and then processed. All process streams were completely recycled back into the feed

Table 1 – Rejection of catalyst metals and phosphorus, depending on process time.

Entry	Process time / h	Rejection / % ^a		
		Molybdenum ^b	Vanadium ^b	Phosphorus ^b
1	15	95.4	92.5	78.4
2	60	98.8	96.5	84.0
3	105	98.7	96.2	83.2
4	150	98.8	96.5	84.4

Experimental Conditions: DK-series membrane, ambient temperature, 30 bar transmembraneous pressure, 15 mL min⁻¹ pump flow, medium stirring speed, 2.5 mmol HPA-5 in 500 mL water (9.4 g mL⁻¹), 13.2 g L⁻¹ formic acid, 3.1 g L⁻¹ acetic acid and 8.8 g L⁻¹ sulfuric acid a) calculated as described in the corresponding section of the experimental part b) Determined with ICP-OES

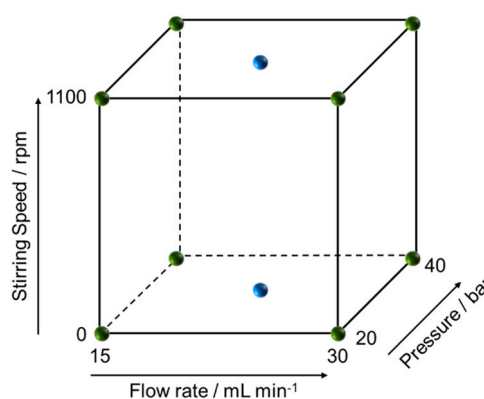
vessel for 15 min. After the initial 15 min, samples were taken and analyzed. The determined rejection was 99%, 96%, 81% for Mo, V and P, respectively.

At the end of the experiment, the membrane system was emptied with air to flush out residual catalyst solution and rinsed with water for final cleaning. After 24 h the experiment was repeated without refreshing the membrane with water. The results are comparable to the previous experiment. Both results indicate that a single pretreatment of the membrane and a process time of 15 min are sufficient. Consequently, this pretreatment and process time were incurred for further experiments.

2.3. Parameter optimization using Box, Hunter & Hunter DoE

Based on the statistical method of Box, Hunter and Hunter a detailed sensitivity analysis was performed for the DoE (Kleppmann, 2016). The purpose of the sensitivity analysis was to decrease the catalyst content in the permeate. This is intended to avoid loss of catalyst for a possible industrial application. Furthermore, the catalyst can interfere with subsequent analysis, hence catalyst concentration in the product solutions (permeates) must be as low as possible.

Analogous to the experiments in the previous section, an aqueous catalyst model solution was used. The influence of the three parameters transmembraneous pressure, flow rate of the pump, and speed of the stirrer were investigated. Transmembrane pressure is the main driving force for transmembrane mass transfer and has a universal effect on all components. Therefore, this parameter is expected to play a significant role in permeate flux and selectivity. For this reason, transmembrane pressure was chosen as an optimization parameter. It is well-known that a gradient of the fluid flow velocity is formed from the flow core (bulk-fluid) to the membrane surface (Baker et al., 1997). At the membrane surface, the velocity is essentially zero and a boundary layer is formed. Rejected components accumulate at the membrane surface and negatively influence the selectivity of the membrane process by concentration polarization (Baker, 2012). Therefore, all rejected components must be transported back to the bulk-fluid. For this purpose, the stirring speed was chosen as an optimization parameter, since it was assumed that the back transport of the rejected components from the membrane surface to the bulk-fluid would be affected by hydrodynamic effects. Shear-induced effects due to enhanced velocity gradients are worth mentioning here

**Fig. 2 – Schematic drawing of experimental points.**

(Melin and Rautenbach, 2007). Equally important is the flow rate of the pump as parameter in a classic cross-flow process, therefore it was also investigated.

The parameters were varied between 20 bar and 40 bar for the pressure, 15 mL min⁻¹ and 30 mL min⁻¹ for the flow rate, as well as 0 rpm and 1100 rpm for the stirring speed, respectively. The intervals are indirectly determined and limited by the equipment used. On the one hand, the practicable pressure is determined by a sufficient permeate flux. On the other hand, the applied maximum pressure of 40 bar is set by tolerances of the used membrane. Furthermore, the setup used represents an alternative to the classic cross-flow processes and is intended to ensure sufficient overflow of the membrane surface without high flow rates of overflow pumps. Therefore, the design only allows variation of the flow rate within a narrow range. The three factors were optimized regarding the rejection of Mo, V and P. In addition, the influence of the parameter variations on the rejection of non-catalyst components such as FA, AA and sulfuric acid, were analyzed. Fig. 2 shows a schematic depiction of the parameter combinations as points on the edges of the cube.

The average values of parameters were used as conditions of center points (blue points in Fig. 2). Since the stirring speed cannot be defined in precise interstages, this parameter was treated as a qualitative parameter. Thus, the stirrer setting only varied between off (0 rpm) and maximum speed (1100 rpm). As a result, two center points are required for both possible stirrer settings. Table 2 shows the settings of all conducted experiments regardless of their chronological order. The center points were executed twice to determine the quality of the experiments (Entries 9 – 12). In addition, the experimental design was randomized to compensate effects of irrelevant or uncontrollable conditions that could affect the results of the experiment.

The Statistica 64© Software Version 13 of Dell Inc. was used to evaluate the results (Dell Inc, 2015). The model used to calculate the effects was optimized by fitting it to the exceeding probability (p-value) of the parameters. Accordingly, parameters with a p-value below 0.05 are considered significant. All parameters and interactions with a p-value greater than 0.05 were successively removed from the model, starting with the highest p-value. Consequently, the effects of significant parameters were evaluated as precisely as possible.

Fig. 3 summarizes the effects of the stirring speed and pressure on the rejection of catalyst components such as Mo, V and P. The stirring speed is the most significant parameter

Table 2 – Experiments of the parameter optimization using Box, Hunter & Hunter DoE.

Entry	Randomized order	Flow rate /mL min ⁻¹	Stirring speed /rpm	Pressure /bar
1	9	15.0	0	20
2	4	30.0	0	20
3	11	15.0	1100	20
4	7	30.0	1100	20
5	6	15.0	0	40
6	2	30.0	0	40
7	3	15.0	1100	40
8	10	30.0	1100	40
9	8	22.5	0	30
10	12	22.5	0	30
11	1	22.5	1100	30
12	5	22.5	1100	30

Experimental conditions: pre-wetted DK-series membrane, ambient temperature, 10 mmol H₅PV₅Mo₇O₄₀ catalyst in 2000 mL water (9.4 g L⁻¹), 13.2 g L⁻¹ formic acid, 3.1 g L⁻¹ acetic acid and 8.8 g L⁻¹ sulfuric acid.

for the rejection of all components. At maximum stirring speed the highest rejection of the components can be achieved. This can be explained by considerably improved overflow of the membrane and minimized concentration polarization. Several factors are known in literature to affect concentration polarization (Baker, 2012). One of them is the boundary layer thickness. Decreasing the boundary layer thickness by increasing the turbulent mixing at the membrane surface exponentially diminishes concentration polarization (Baker, 2012). As expected, the flow generated by the stirrer decreases the laminar boundary layer, increases the turbulent mixing at the membrane surface as well as the back-transport of the components. In this manner, the rejection is maximized at maximum stirring speed. Hence, it can be shown that an integrated stirrer in the membrane cell ensures an efficient overflow of the membrane for our separation task. Hereby, an advantage over classic membrane modules, which operate at high fluid flow velocities generated by recirculation or overflow pumps could arise. Liquid recirculation pumps already account for a significant portion of a plant's capital cost and consume 20 – 40% of the power utilized for separation in industrial membrane systems (Baker, 2012).

At maximum stirring speed the rejection of Mo can be increased from 98.8% to 99.4% on average (Fig. 3, a) at low flow rates of the pump. In particular, the positive effect of an increased stirring speed is noticeable for the rejection of V. Here, the average rejection can be increased from 95% to almost 98% (Fig. 3, b). This is equal to an average decrease of the V concentration by 50% in the permeate at maximum stirring speed compared to no stirring.

No significant influence of the transmembrane pressure for Mo could be determined in the studied range. In comparison, the rejection of the remaining components V and P showed a significant dependence on the pressure. For both components, the rejection increases with increasing pressure. At first glance, these insights contradict with theoretical principles.

The transmembrane pressure is the non-selective driving force behind the transmembrane mass transfer. Hereby, it can be deduced that a higher pressure should lead to a higher permeability of the components. However, the observed

results show the opposite effect. It can be assumed that the pore structure of the membrane was compacted by the pressure. This decreases the exclusion size and thus increases the rejection. Membrane compaction as physical compression of polymeric membranes by high pressure is a phenomenon that has already been observed and studied in literature (Stade et al., 2015; Volkov, 2014). A compacted membrane structure can affect the rejection behavior and may even result in a lower molecular weight cut-off (Stade et al., 2015). Such a positive effect by membrane compaction can be reversible (elastic), partially reversible or irreversible (plastic) (Stade et al., 2015; Volkov, 2014).

For Mo as largest species, which is already rejected very well, the compaction of pores has no significant influence on its rejection (Fig. 3, a). Here, an elastic and plastic compaction, very probably a mixture of both, is conceivable. Both the center point experiments at 1100 rpm and 0 rpm show a trend towards higher rejections of catalyst components over the proceeding experimental study. In the supporting information, the achieved rejections of the study and the randomized order of experiments are lodged (Table S1).

In addition, the randomized order can be found in Table 2. The raw residuals depending on the real chronological order of experiments can be determined using Statistica 64®. Accordingly, there is a slightly increasing disturbance variable towards higher rejections. This argues for a hysteresis and thus for a plastic change in the pore structure of the membrane due to compression and relaxation cycles between the individual experiments.

The experiments can be divided into pairs in which only the pressure was varied. In Table 2, the experiments in entries 1 and 5, 2 and 6, 3 and 7 as well as 4 and 8 correspond in this way. Due to randomization of the order, experiments at 40 bar (Entries 5 – 7) were performed before their corresponding low-pressure experiments at 20 bar (Entries 1 – 3). In all cases, the rejection for the catalyst components is lower at 20 bar than at 40 bar. Therefore, it can be assumed that there must also be a high elastic (reversible) compaction of the pore structure. Thus, the found effect of pressure can be confirmed. Furthermore, the influence on the significance of the stirring speed can be evaluated. In the first performed experiment (center point, Table 2, Entry 11), a rejection for V of 97.3% was reached at a stirring speed of 1100 rpm. In the last experiment (center point, Table 2, Entry 10) a rejection of vanadium about 95.0% was reached at a stirring speed of 0 rpm. Despite several experiments at 40 bar, a significant lower rejection could be achieved. Hence, the assumption of a less important role of plastic compaction and the high significance of the stirring speed for the rejection can be verified.

The flow rate of the pump had no significant effect neither on Mo nor on P rejection with p-values from 0.07 to 0.67. This is due to the fact that the flow profile in the membrane cell is dominated by the influence of the stirrer, whereas the flow rate can hardly change the flow conditions in the set variation range. However, there is a slight inverse dependence of the rejection of V on the flow rate. This could be explained by a minor negative influence of the membrane incident flow at higher flow rates. Overall, the flow rate of the pump seems not to be a relevant parameter in the investigated area.

The accumulation of polar oxidation products such as FA or AA in the aqueous catalyst solution poses a problem for catalyst recycling concerning the catalytic activity. Therefore, the rejection of acidic products was also

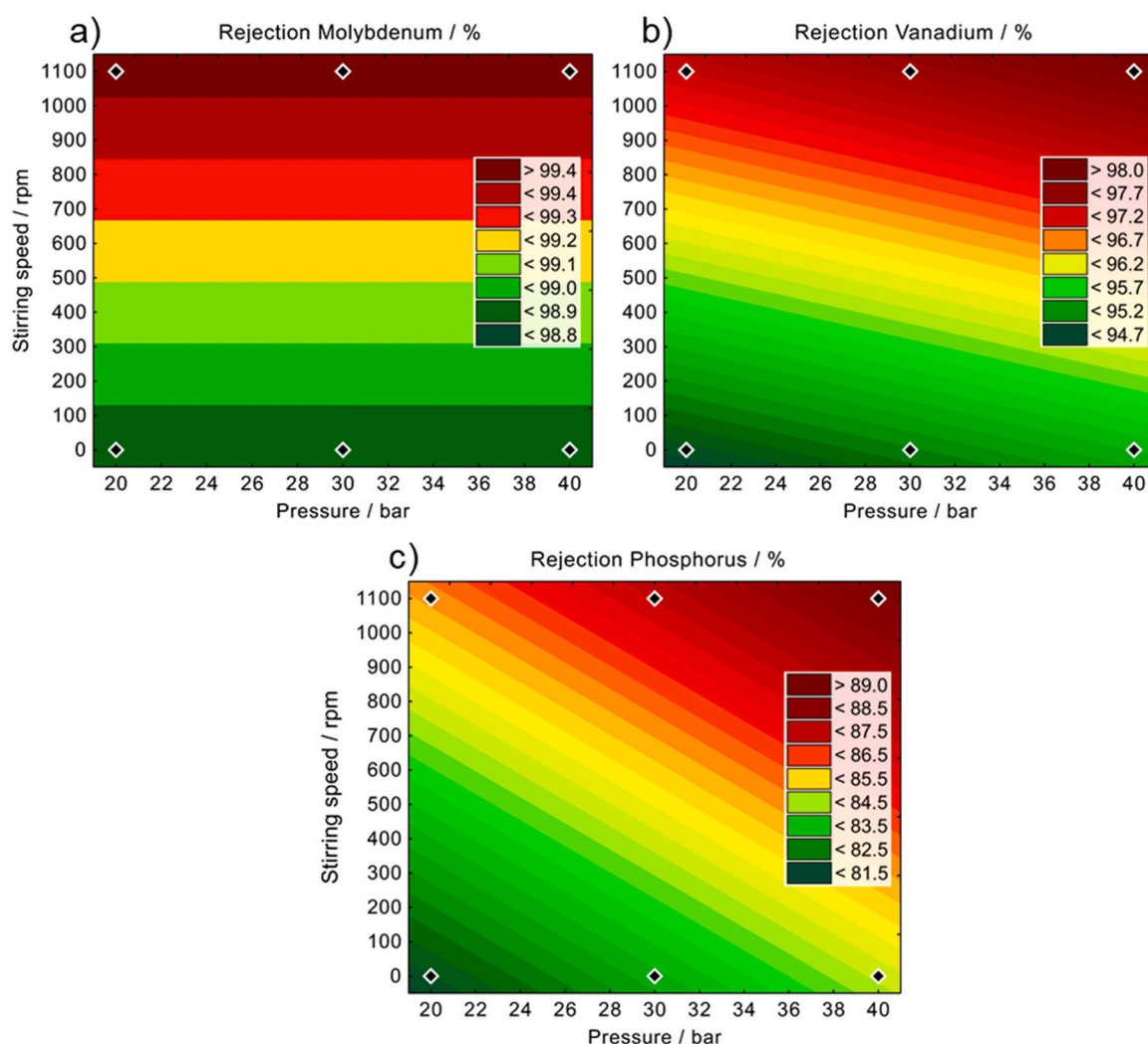


Fig. 3 – Effects of the pressure (abscissa) and stirring speed (ordinate) on the rejection of a) molybdenum, b) vanadium and c) phosphorus.

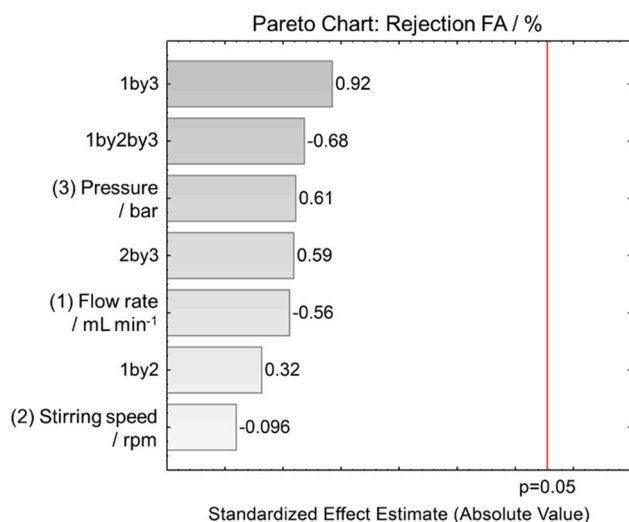


Fig. 4 – Pareto chart for the standardized effect estimation of varied parameters on the rejection of formic acid.

determined in the experiments of the sensitivity study. Fig. 4 shows the results of the sensitivity study for the rejection of FA. The three main parameters flow rate (1), stirring speed (2) and pressure (3) as well as their interactions are shown (Fig. 4). Here, the double interactions (1) with (2), (1) with (3)

and (2) with (3) as well as the triple interactions of (1), (2) and (3) are to be mentioned. Ideally, FA freely permeates the membrane preventing accumulation. According to the sensitivity study, the process parameters have no significant influence on the rejection in the investigated range. FA or rather formate as a small and singly charged molecule penetrates the membrane almost without rejection (<5%). Thus, accumulation in the retentate can be prevented.

The results for AA and sulfuric acid are shown in Fig. 5. The rejection of AA shows a dependence only for the stirring speed. Increasing the stirring speed also increases the rejection (Fig. 5, a). However, with a value of less than 10% the rejection of AA is still low. The rejection of sulfuric acid (Fig. 5, b), here primarily as sulphate ion, is analogous to P (Fig. 3, c). By increasing the pressure as well as the stirring speed, the rejection of sulfuric acid also increases (Fig. 5, b).

These insights can be explained by the facts already discussed for the catalyst components. For the final parameter settings, a compromise between the individual targets must be made. Accordingly, the targets were weighted differently. It is assumed that Mo, as part of the catalyst's framework, most closely represents the complete catalyst. Therefore, the rejection of Mo was considered to be one of the most important target values. On the other hand, V is contemplated as the active component in the catalytic system. It is known that smaller V species can be formed by proteolysis, which

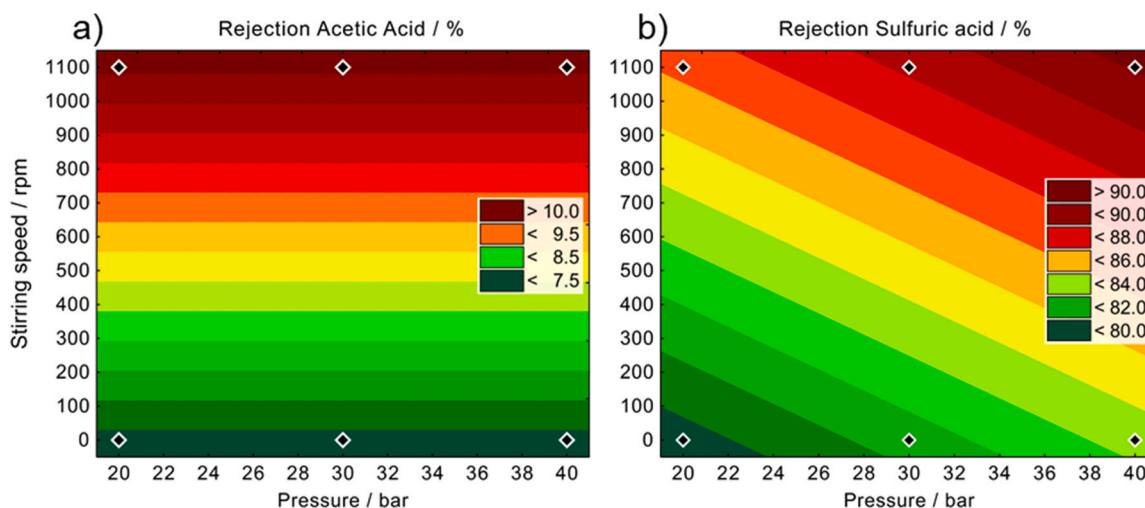


Fig. 5 – Effects of the pressure (abscissa) and stirring speed (ordinate) on the rejection of a) acetic acid and b) sulfuric acid.

have higher permeability than the initial HPA-5 catalyst [20]. In this way a loss of activity would also be possible. Consequently, the rejection of V is as important as the rejection of Mo. Due to an excess of free phosphate, the rejection of P only plays a minor role. FA is considered as the most harmful by-product of oxidation, since its accumulation has an immensely negative effect on the catalytic activity. Here, the rejection of FA is unaffected by the parameter variation, it is no longer taken into account for the further optimization.

Among the varied parameters the stirring speed has the highest significance and impact on the rejection of all components. An increase of the stirring speed also increases the rejection of the catalyst components, which corresponds to the objective of this study. This is most probably due to hydrodynamic effects, which decrease the laminar boundary layer, intensify turbulent mixing at the membrane surface and promote the back transport of the rejected catalyst components. However, a higher stirring speed also enlarges the undesired rejection of AA and sulfuric acid. Both of these oxidation products should be separated from the reaction solution. Though, the rejection of catalyst components is prioritized. The rejection of AA is still low at maximum stirring speed. Therefore, the maximum stirring speed of 1100 rpm was selected as optimum value. Increasing the transmembrane pressure enhances the rejection of V, P as well as sulfuric acid. Here, essentially reversible compaction of the membrane was discussed in detail as a possible cause for the observed change in rejection behavior. Likewise, a higher operation pressure causes a greater risk of damage and decreasing the working life of the membrane. The use of the tested DK-series membrane is permitted up to a pressure of 40 bar, which is consistent to the performed upper interval limit of pressure. As a compromise between high rejection of V, low rejection of sulfuric acid and low risk of damaging as well as a long-life of the membrane, a transmembrane pressure of 30 bar was chosen as optimum value.

The flow rate of the pump does not affect the rejection of most components in the investigated area and has just a minor effect on the rejection of V. In order to ensure the highest possible rejection of the latter and high concentration factors, a minimum flow rate of 15 mL min^{-1} was selected. Lower flow rates are difficult to process concerning pressure control.

In addition to the optimization of the process parameters, another important aspect is the investigation of the operating behavior of the membrane. For this purpose, the mass balance is a helpful tool, as it provides information about possible precipitation or adsorption of catalyst species by the membrane. The mass balance of an experiment was calculated as described in the corresponding section of the experimental part. As an example, an experiment with the optimized parameters using a flow rate of 15 mL min^{-1} , a transmembrane pressure of 30 bar and a stirring speed of 1100 rpm is used. The composition of the model solution (feed) and samples (permeate, retentate) determined by ICP-OES, the volumes of samples and the calculated mass balance for the catalyst components are shown in Table 3.

The mass balance reaches high values of at least 94% for all catalyst components. Here, tolerances within the overall analytical process may play a role in the missing percentage values. Nevertheless, the balance cannot be completely closed, which means that adsorption of catalyst components cannot be completely ruled out at this stage. This is an important subject of investigation for further studies dealing with long-term process behavior.

2.4. Enrichment of the catalyst using the optimized parameters

In order to prevent deactivation of the catalyst, especially FA and AA have to be removed from the aqueous product solution. However, with a single pass through the membrane system, only small amounts of acids can be removed from the solutions. The advantage of the experimental setup compared to a classic crossflow process is the significantly smaller ratio of total feed flux and permeate flux. Hereby, a higher enrichment of catalyst is possible with a given membrane area. A high concentration factor of 1.3 is achieved for our experimental setup by passing through the membrane once. This allows the acids to become stronger diluted when the solution is refilled back to its original volume. Nevertheless, with a concentration factor of 1.3, still insufficient amounts of acids can be removed from the solution in a single pass through the membrane system. The amount of removed acids can be optimized by a larger membrane area.

Table 3 – Calculation of mass balance.

Entry	Species	Concentration ^a $\beta_{n,Feed}$ / mg L ⁻¹	Sample	Volume ^b / mL	Concentration ^a $\beta_{n,Found}$ / mg L ⁻¹	Mass balance ^c
1	Mo	3640	Permeate	8	32	> 95%
2			Retentate	29		
3	V	1366	Permeate	8	38	> 94%
4			Retentate	29		
5	P	204	Permeate	8	26	> 94%
6			Retentate	29		

Experimental conditions: pre-wetted DK-series membrane, ambient temperature, 30 bar transmembrane pressure, 15 mL min⁻¹ flow rate, 1100 rpm stirring speed, HPA-5, FA, AA, H₂SO₄ a) determined by ICP-OES b) measured with graduated measuring glass c) calculated as described in the corresponding section of the experimental part.

Otherwise, the effect of a larger membrane area can also be achieved by recycling the retentate and thus passing it through the membrane several times. For this purpose, enrichment experiments were carried out in order to achieve sufficient depletion of the acidic components. Furthermore, the loss of catalyst for the individual concentration factors was determined. This was done using the rejection as an evaluation criterion. A lower rejection is equal to a higher concentration of catalyst in the permeate and hence indicates a higher loss of catalyst.

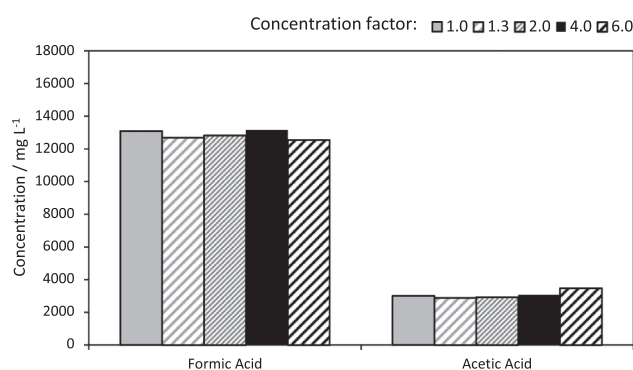
Values of 1.3, 2.0, 4.0 and 6.0 were selected as concentration factors. The concentration factor of 1.3 is the reference experiment for higher concentration factors. For the other factors, the retentate was recycled and permeate withdrawn until the initial volume is decreased to half, a quarter or a sixth, respectively. In all experiments (factors) the accumulated permeate was analyzed and the rejection calculated. The rejection is related to the initial concentration and the concentration of the accumulated permeate at the end of the process. In this way, the rejection reflects the entire enrichment process. The results are shown in Table 4.

With the enrichment in the solution, a decrease in the rejection for the catalyst components could be observed. The rejection decreases from 99.5% to 99.1% for Mo, from 97.6% to 96.3% for V and from 85.2% to 79.8% for P, respectively. Due to the volumetric enrichment, the concentrations of the catalyst components increased continuously. As a result, higher concentrations were also achieved in the permeates. However, the rejection of Mo and thus of the HPA-catalyst is still high with a value of above 99%. Despite enrichment, the large catalyst molecule can poorly penetrate the pore system of the membrane. Therefore, the catalyst is rejected very efficiently even at high concentrations. Smaller V and P species also accumulate in the permeate due to the enrichment. As already mentioned, the P in the permeate is most likely phosphate originated from an excess in catalyst synthesis. Hence, decreased rejection of P is unlikely to have any impact on catalytic activity. The loss of V increases with enrichment. On the other hand, a higher enrichment results in a higher removal of acids, which is essential for maintaining catalytic activity. For this reason, a concentration factor of 6.0 is considered sufficient with a still high rejection of V of 96.3%. Fig. 6 shows the development of the concentrations of FA and AA in the retentate depending on the concentration factors. For both acids the concentration slightly fluctuates around the initial concentration of 1300 mg L⁻¹ (FA) and 3000 mg L⁻¹ (AA), respectively. Consequently, the concentration factor corresponds to the dilution of acids when refilling to the original feed volume. Thus, almost 85% of FA and about 82% of AA can be removed with a

Table 4 – Development of rejections of catalyst components depending on the volumetric enrichment.

Entry	Species	Volumetric enrichment ^a	Rejection ^b / %
1	Mo	1.3	99.5
2		2.0	99.4
3		4.0	99.3
4		6.0	99.1
5	V	1.3	97.6
6		2.0	97.5
7		4.0	96.9
8		6.0	96.3
9	P	1.3	85.2
10		2.0	84.8
11		4.0	81.9
12		6.0	79.8

Experimental conditions: pre-wetted DK-series membrane, ambient temperature, 30 bar transmembrane pressure, 15 mL min⁻¹ flow rate, 1100 rpm stirring speed, HPA-5, FA, AA, H₂SO₄ a) determined by volumetric measurement with graduated measuring glass b) determined with ICP-OES for catalyst components and calculated as described in the corresponding section of the experimental part.

**Fig. 6 – Comparison of several enrichment experiments concerning the development of FA and AA concentration in the retentate depending on the concentration factors.**

concentration factor of 6.0. More than 30% of sulfuric acid can also be removed in this way. A visualization of the development of sulfuric acid concentration can be found in the supporting information (Figure S2).

Maintaining the catalyst structure is also important for the suitability of high concentration factor and the membrane system as downstream process. ⁵¹V NMR spectra of the feed before and the retentate after the enrichment experiments are shown in Fig. 7.

The signals of the different vanadium species are assigned by means of data reported by Evtuguin et al.,

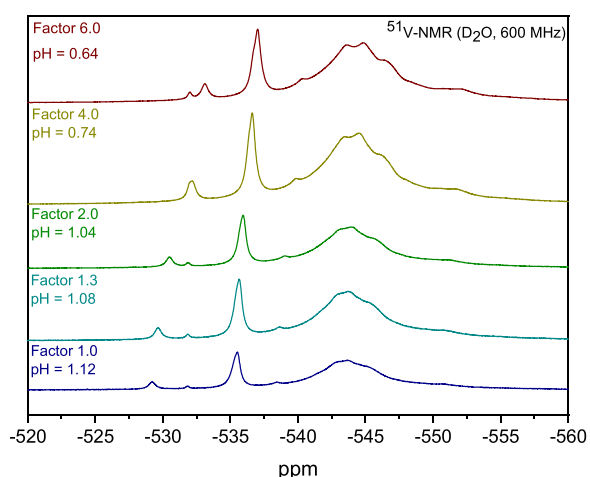


Fig. 7 – ^{51}V NMR spectra (600 MHz) of the liquid phase before and after enrichment via nanofiltration membrane. (Conditions: DK-Series membrane, 15 mL min^{-1} flow rate, 30 bar pressure, 1100 rpm stirrer speed, concentration factors from 1.0 to 6.0 Feed: $2.5\text{ mmol HPA-5 catalyst in } 500\text{ mL water } (9.4\text{ g L}^{-1})$, 13.0 g L^{-1} formic acid, 3.1 g L^{-1} acetic acid and 8.4 g L^{-1} sulfuric acid.)

Petterson et al. and Shatalov et al (Evatugin,1998; Petterson et al., 1994; Shatalov et al., 2000). The ^{51}V NMR spectra of the feed solution before enrichment (concentration factor 1.0) serves as reference. Lower substituted HPA isomers HPA-1 ($\text{H}_4\text{PVMo}_{11}\text{O}_{40}$) and HPA-2 ($\text{H}_5\text{PV}_2\text{Mo}_{10}\text{O}_{40}$) are represented by the signals at $\delta_{\text{V}} - 533\text{ ppm}$ and $- 537\text{ ppm}$. In the range from $\delta_{\text{V}} - 540\text{ ppm}$ to $- 550\text{ ppm}$, more highly substituted HPA isomers induce a broad signal.

A decrease in pH value due to the enrichment can result in slightly different chemical shifts. It can be seen that no structural changes to the catalyst occur as a result of enrichment. The results of ^{31}P NMR measurements can corroborate these insights. ^{31}P NMR spectra are attached to the supporting information (Figure S3). Overall, the results confirm that enrichment by nanofiltration in the studied range is capable of removing the polar oxidation products without affecting the catalyst.

Due to numerous experiments conducted so far (DoE to enrichment) under highly variable experimental conditions, the membrane was partly exposed to a harsh environment. Here, pressure cycles of up to 40 bar, extremely low pH values of less than 1 and greatly increased catalyst concentrations as well as sulfuric acid as crucial component should be mentioned. These conditions, as well as a possible adsorption and precipitation of catalyst components on the membrane, may lead to fouling and affect the service life of the membrane. Long-term stability as one aspect to increase technical readiness level still needs to be investigated. In order to obtain initial indications of possible long-term stability, a control experiment was carried out after completion of the enrichment experiments. For this purpose, the conditions of the first center point (Table 2, Entry 11) from the DoE experiments were used. In the control experiment, a rejection of 99.4% for molybdenum, 97.3% for vanadium and 85.7% for phosphorus was achieved. In comparison, the rejection values of the center point (Table 2, Entry 11) were 99.3% for molybdenum, 97.3% for vanadium and 84.5% for phosphorus, respectively. Consequently, separation efficiency of the membrane as performance indicator shows no

process-relevant changes within the observation period of an accumulated time-on-stream of about 50 h and suggest long-term stability for the time being. It should be noted that in the current set-up the batchwise enrichment of the products is simulated. In contrast, in a continuous process, the continuous mode of operation prevents the enrichment of the products. As a result, the process conditions in a continuous process will be much milder (e.g. pH-value) than in previous experiments. This can have a positive effect on the service life of the membrane. An extension of the observation period and an examination of the membrane after a longer service life are reasonable and will be part of further investigations in a continuous process set-up.

2.5. Recycling of the HPA-5 catalyst with removal of intermediate and decomposition products by nanofiltration membrane

To investigate the catalyst recyclability and the suitability of nanofiltration as downstream process in ECODS, we conducted catalyst recycling experiments. For this purpose, an organic phase consisted of 2,2,3-trimethylpentane (iso-octane) as model fuel with benzothiophene (BT) as sulfur-containing substrate (15900 ppmw) was treated with an aqueous catalyst solution in ECODS. The aqueous catalyst solution was recycled five times in overall six consecutive runs. Between each run the aqueous phase was treated with the membrane system for product separation. The initial run is referred to as run zero and the recycling experiments are designated as run one to run five. The reactions were performed in a high-pressure autoclave. A detailed description of the setup and procedure as well as the exact compositions are given in the experimental section.

The organic phase was analyzed by elemental CHNSO analysis after the reaction. Therefore, the efficiency of desulfurization was monitored for the six consecutive runs. Before and after each reaction, samples of the aqueous phase for NMR were taken to elucidate changes in the catalytic system. In addition, samples of the aqueous phase were analyzed by ICP-OES before each reaction (after membrane separation) to determine any losses of catalyst. Furthermore, all permeates from the membrane separation were analyzed using ICP-OES and IC. Hereby, any catalyst losses could be examined more precisely for their cause and the acid concentrations are monitored.

Fig. 8 shows the development of the V concentration and the values relativized to the initial concentration depending on the recycling run. The V concentration decreases from an initial value of about 730 mg L^{-1} to 510 mg L^{-1} in the last run. This is equal with a decrease of 30%. The decrease in concentration shows linear behavior with a coefficient of determination greater than 0.99. This is a strong indication of the reproducible execution of the experiment. A comparable trend can also be observed for molybdenum, which can be found in the corresponding section of the supporting information (Figure S4). Here the concentration decreases from the initial value of about 2135 mg L^{-1} to 1630 mg L^{-1} , which is equal to a decrease of approximately 24% in the last run. The difference between losses of molybdenum and vanadium may be explained by different rejections.

Analysis of the permeates shows that about 12% of the V and about 5% of the Mo were discharged in the permeate over the entire series of experiments. This corresponds to an average V-loss of about 2% and a Mo-loss of about 1% per

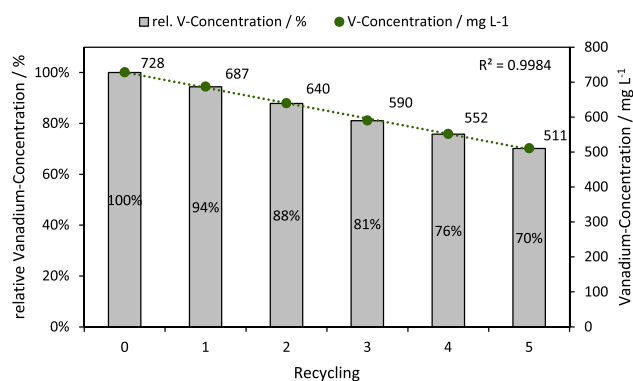


Fig. 8 – Development of vanadium concentration in aqueous catalyst solution depending on the recycling. Determined by ICP-OES.

membrane separation. The relative losses of V and Mo in the permeate can be found in the supporting information (Figure S5, Figure S6). Approximately 18% of V and 19% of Mo are lost most probably due to sampling and peripheral losses. In particular, the latter is most likely responsible for a large part of losses. The reaction and separation do not represent a closed system as they are coupled with each other in batches. Consequently, high losses of V in pipes, glass devices and other peripherals are plausible. Nevertheless, precipitation and adsorption of catalyst species on the membrane cannot be completely ruled out. For this purpose, a precise examination of the membrane after longer time-on-stream is reasonable and will be part of further investigations into the long-term behavior of the membrane process. Losses of V decrease the desulfurization efficiency and counteract the effects of the product separation. Therefore, an evaluation of the suitability of nanofiltration as downstream process to prevent chemical deactivation of the catalyst is falsified.

It has been shown that proteolysis can result in smaller vanadium oxide species that pass the membrane better than the parent HPA-5 (Pobe and Scully, 1975; Zhizhina et al., 2008; Odyakov et al., 2015). Since vanadium is the active component of the catalyst, the loss of vanadium reflects the decrease of catalytic activity much better than other species. In order to be able to carry out an adjusted evaluation, the degree of desulfurization was normalized to the catalyst quantity, which was calculated based on the measured V concentration. The exact calculation bases can be found in the corresponding part of the experimental section. In Fig. 9 the results of desulfurization are shown. The supporting information is accompanied by a consideration based on measured Mo concentrations (Figure S7), for which the following remarks apply almost identically. According to the results, a normalized degree of desulfurization greater than 90% was achieved in the first three runs (Fig. 9, Recycling 0–2).

Despite a double recycling of the catalyst solution, the degree of desulfurization remains almost constant. This is an indication that no chemical deactivation of the catalyst occurs during the first two recycling experiments and the polar oxidation products are sufficiently removed. Nevertheless, a distinct decrease in the degree of desulfurization can be observed from the third recycling (Fig. 9, Recycling 3–5). Here, the degree of desulfurization decreases linearly from 70% at Recycling 3 to around 30% at Recycling 5. In order to evaluate the effects of recycling and polar oxidation products on the catalyst, the measured ⁵¹V NMR spectra before the reactions

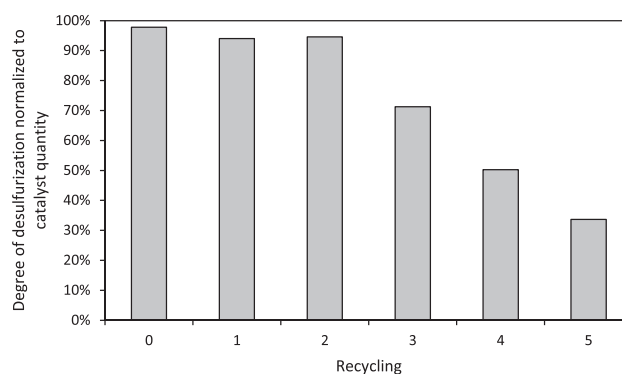


Fig. 9 – Normalized degree of desulfurization with reused aqueous catalyst solution. (Reaction conditions: 0.5 mmol HPA-5 in 200 mL water, 13.8 mmol benzothiophene in 40 mL 2,2,4-trimethylpentane (15900 ppmw S, 120 °C, 20 bar O₂, 1000 rpm, 6 h).

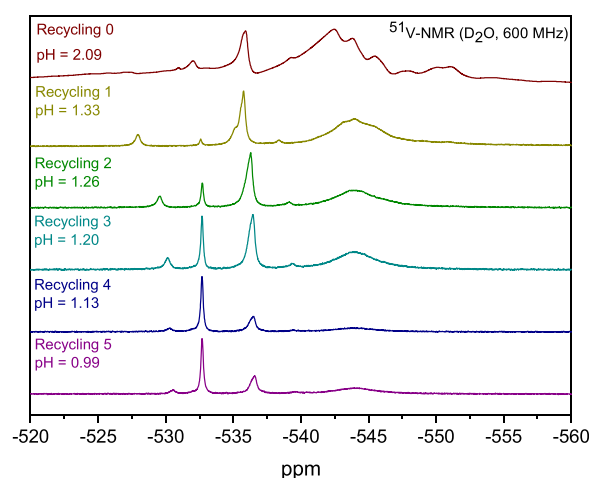


Fig. 10 – ⁵¹V NMR spectra (600 MHz) of the liquid phase before reaction (after nanofiltration). (Reaction conditions: 0.5 mmol HPA-5 in 200 mL water, 13.8 mmol benzothiophene in 40 mL 2,2,4-trimethylpentane (15900 ppmw S, 120 °C, 20 bar O₂, 1000 rpm, 6 h).

are compared in Fig. 10. The signal intensity of the lower substituted HPA-1 isomer at about δ_V – 533 ppm increases with the number of recycles. The change between the second and third recycling is particularly significant. Furthermore, it can be seen that the signal of HPA-2 at δ_V – 536 ppm changes drastically in the last three cycles. The ³¹P NMR spectra attached to the supporting information also indicate a strong change in the catalyst structure (Figure S8). Here, a clear decrease in the number of P-isomers is observed from the beginning to the end of the recycling experiment. Comparing ⁵¹V NMR spectra before and after processing in the membrane system, it can be concluded that the membrane process is not involved in the structural change of the catalyst (see supporting information, Figure S9 to Figure S13). Based on these insights, it is obvious that less active V-species are formed with several ECODS runs. This phenomenon is particularly high for the last three recycling runs. Due to the process time and the processing in batches the solution between recycling 2 and recycling 3 had a longer storage time.

We assume that the long storage time with the accumulated reaction products benefit and enhance the formation of less active catalyst species. These storage times would be omitted in a real continuous process. In addition, batch

operation enables the reaction products to be enriched, since there is no continuous purification. In a continuous process this would be prevented and the catalytic activity could be obtained.

Overall, two successful recycling experiments could be performed and the efficiency of a membrane based downstream process for separation of polar oxidation products was demonstrated. The results are particularly promising for a continuous process in which the polar oxidation products are continuously separated by nanofiltration.

3. Conclusion

The main scope of this study was the development of an efficient downstream process for the homogenous catalyzed extractive oxidative desulfurization of fuels by means of nanofiltration membranes. Here, industrial requirements concerning recyclability of the catalyst in ECODS and an efficient design should be considered.

An alternative concept to the classic crossflow system was chosen for the experimental setup. By using a 3" MiniMem membrane cell (PS Prozesstechnik GmbH) with an integrated stirrer, a high overflow of the membrane and thus an efficient membrane process even with small feed volume flows should be ensured. For the experiments, acid-stable nanofiltration membranes of DK series membrane-type (GE Power water & Process technologies) were used. First experiments with an aqueous model solution of $H_5PV_5Mo_7O_{40}$ catalyst (HPA-5) containing polar oxidation products such as formic acid, acetic acid and sulfuric acid showed promising results. We obtained optimized parameter settings for the membrane separation process using Box, Hunter & Hunter design of experiments with a number of 12 experiments. Consequently, the optimized parameters led to higher rejection of catalyst components compared to the initial experiments. At the same time, both formic acid as well as acetic acid were hardly rejected, thus accumulation together with the catalyst was prevented in the retentate.

For the catalyst recycling, we investigated the feasibility of different concentration factors regarding structural conservation and low losses of catalyst. ^{51}V NMR spectroscopy indicated no significant changes in catalyst structure. At high concentration factors, high rejection of catalyst could still be achieved determined by ICP-OES. The high concentration factors applied allowed efficient decrease of formic acid and acetic acid in the aqueous model solution. The optimized parameters were applied for recycling experiments in ECODS. Here, a model fuel consisting of 2,2,3-trimethylpentane (iso octane) with benzothiophene as sulfur containing substrate (15900 ppmw) as model gasoline were treated with the aqueous catalyst solution. We conducted six consecutive runs with product separation by the means of nanofiltration between the individual runs. The efficiency of desulfurization was monitored by elemental CHNSO analysis for the six runs. Two recycling experiments were successfully conducted without losses of catalytic activity. Further recycling experiments showed significant decrease of desulfurization, due to storage time and accumulation in batch process. Distinct changes of the catalyst structure were indicated by ^{51}V NMR and ^{31}P NMR spectroscopy. Finally, we assume that a continuous process with a coupled nanofiltration separation could prevent this obstacle. In this context, the alternative membrane system shows advantages over the classic crossflow process. As a result, a cost-efficient

design is enabled. We were able to show that the alternative membrane system is competitive with the classic crossflow process in terms of catalyst rejection.

4. Experimental details

4.1. Chemicals

4.1.1. All chemicals were obtained commercially and used without further purification

Benzothiophene was obtained from Thermo Scientific with a purity higher than 98%. 2,2,4-Trimethylpentane was purchased from Acros Organics with a purity higher than 99%. Trans-Decahydronaphthalene was purchased from Merck with a purity for synthesis.

The HPA-5 catalyst $H_8PV_5Mo_7O_{40}$ was synthesized according to the literature (Zhizhina and Odyakov, 2008; Albert et al., 2014). The catalyst was characterized with ICP-OES (38.2 wt% Mo, 14.8 wt% V, 2.3 wt% P).

Formic acid and acetic acid used for model product solutions were obtained from VWR Chemicals with a purity higher than 97% and of 100%, respectively. Sulfuric acid was purchased from Grüssing GmbH with a purity of 95–97%.

4.2. Experimental setup & typical work-up procedure

For the reactions a 600 mL Hastelloy (C-276) autoclave with gas entrainment impeller was used for the desulfurization experiments. All reactants were charged into the vessel. Afterward, the system was purged three times with 30 bar oxygen to remove the air from the gas phase. An inlet pressure of 15 bar and then a stirring speed of 300 rpm was set. Subsequently the reactor was heated to reaction temperature. When the desired reaction temperature was reached, the oxygen pressure was increased to 20 bar and the stirring speed was set to 1000 rpm. At the end of the reaction, the gas phase was analyzed via heated online sampling using a micro-GC. The heating was then switched off and the system was cooled at a stirring speed of 300 rpm. After the system had reached room temperature, the aqueous and organic phases were sampled.

In a typical experiment, the aqueous feed solution containing the catalyst and water-soluble products is pumped out of vessel B101 by the pump P101 into the membrane cell MC101. The flow area of the retentate containing pipe can be decreased by the needle valve V103 with a low flow coefficient (C_v -value) of 0.004. By decreasing the flow area, pressure can be applied and systematically adapted. At the three-way valve V104 retentate is extracted into vessel B102 or recycled into vessel B101. In the same manner, permeate, which passes the membrane, can be drawn off via valve V105 into vessel B103. A bypass with the proportional relief valve V108 protects the system from inadmissible pressure of more than 50 bar in the manual operating mode.

Besides the flexible manual operating mode, the system also has an automatic mode with a fixed pressure setting. Through bypassing valve V103 with valve V102 the pressure is automatically adapted at a preset value by the proportional relief valve V106.

The experimental setup is equipped with a serial double piston pump model 3350 with the preparative pump head 2200 0400 (Bischoff Analysentechnik und -geräte GmbH). The pump has an integrated electronic control and pressure sensor using a high-resolution stepper motor for accurate

flows between 0.1 mL min⁻¹ to 40 mL min⁻¹ and pressures up to 100 bar (Bishoff Analysentechnik u. -geräte GmbH, 2019).

The core piece of the membrane system is a commercially available 3" MiniMem membrane cell (PS Prozesstechnik GmbH) with an active membrane area greater than 30 cm² (PS Prozesstechnik GmbH, 2022). A special feature of this cell is a patented magnetic stirrer implemented within the membrane cell (Schirg, 2009). Even at low volume flows the integrated stirrer ensures an efficient overflow of the membrane.

Additionally, the membrane is arranged overhead, so the feed flows beneath the membrane that further inhibits accumulation on the membrane surface (Schirg, 2009). As a result, the setup can be operated at low volume flows. Due to the low volume flow and overall high ration of membrane area to minimal working volume high concentration factors are feasible. Furthermore, the low working avoids waste of valuable testing material.

All valves are purchased from Swagelok and manufactured from stainless steel. Sealings and capillaries are manufactured from fluorinated plastics such as perfluoro rubber, ethylene tetrafluoroethylene or polytetrafluoroethylene to ensure a high chemical resistance.

The membrane separation experiments were performed with 3" MiniMem membrane cell (PS Prozesstechnik GmbH) equipped with a DK series membrane-type (GE Power water & Process technologies) in a self-designed experimental setup. A detailed description of the experimental setup is given in the results and discussion section. In a typical experiment, the product solution (max. 100 mL at once) is filled into the feed tank. The is pump is switched on and a flow of 15 mL min⁻¹ is set. When the solution reaches the membrane cell, the integrated stirrer is set to maximum speed and the process is operated for five minutes without pressure. During this period, no samples are taken and all flows are recycled back to the feed vessel. After 5 min, the pressure can be adjusted to 30 bar either manually by a needle valve or automatically by a relief valve. Once stable operation has been established (after 15 min), samples can be taken.

4.3. Analytics

The organic phase was analyzed with a gas chromatograph (GC) on an Agilent 8860 GC System with a DB-WAX Ultra Inert column (30 m length, 0.25 mm diameter, 0.25 μm film thickness) using an Agilent 5977B GC/MSD as Detector.

Elemental CHNS analysis of the organic phase were performed with an analyzer of Fa. EuroVector, Model EA-3000. Oxygen in the organic phase was measured with an Oxygen-Analyzer, Fa. HekaTech high temperature pyrolysis furnace.

Gas chromatography of the gaseous phase was conducted on a 2-module Micro-GC Fusion from INFICON Holding AG. The GC-samples are split and measured on two columns. Module A uses a 5 Å molecular sieve column with a cross-section of 0.25 mm and a length of 10 m. A backflush with 1.0 μL is also preceded. Module B uses a Rt-Q-Bond column with a cross-section of 0.25 mm and a length of 8 m. Each module is connected with a thermal conductivity detector (TCD).

The pH-value was measured using an Excellent Line pH meter and a pH/T30 electrode from Winlab.

The Oxygen content of the aqueous phase was determined using an OXY-1 SMA with a metal flow cell FTM-PSt3 from PreSens Precision Sensing GmbH.

The catalyst components in aqueous phase were analyzed with an ICP-OES spectrometer, Fa. Spectro Ametek Model

Arcos. Samples were measured without digestion at a 1:100 dilution.

The Division of NMR Spectroscopy in the Department of Chemistry measured NMR spectra on a Bruker Avance III HD 600 MHz spectrometer. The samples were prepared by blending 0.4 mL D₂O with 0.2 mL reaction solution.

Acid concentrations in the aqueous phase were determined by IC, Fa. Thermo, Model Integriion equipped with analytical column Dionex Ion Pac AS11-HC 2*250 mm; front column Ion Pac AG11-HC 2*50 mm. Samples were measured with a 1:500 dilution for acetate or diluted 1:1000 as well as 1:500 for formate and the values were averaged.

Quantitative analyses of the aqueous phase were carried out using a HPLC system from SHIMADZU equipped with an Aminex HPX-87 H 300 mm × 7.8 mm BIORAD Column and a refractive index detector. 5 mmol of an aqueous sulfuric acid solution was used as eluent.

4.4. Formulas for calculations

The rejection R for a component x was calculated using the following equation and the measured mass concentration of component x $\beta_{x,Permeate}$ and $\beta_{x,Feed}$ in the permeate or feed, respectively:

$$R_x = 1 - \frac{\beta_{x, Permeate}}{\beta_{x, Feed}}$$

For the determination of the degree of desulfurization in the organic phase the mass fractions of sulfur in ppm were measured after the reaction. The quotient of the mass fraction of sulfur after reaction $w_{sulfur,n}$ and before reaction $w_{sulfur,no}$ gives the degree of desulfurization. In order to assess the efficiency of desulfurization, the degree of desulfurization is normalized to the amount of catalyst, hence catalyst losses do not falsify the evaluation. Therefore, the degree of desulfurization is multiplied with the quotient of the catalyst amount for the individual recycling experiment $n_{HPA-5,n}$ and the initial amount of catalyst in the first experiment $n_{HPA-5,0}$. In the following the equation is summarized:

$$\text{normalized Degree} = \left(1 - \frac{w_{sulfur, n}}{w_{sulfur, n_0}} \right) \cdot \frac{n_{HPA-5, 0}}{n_{HPA-5, n}}$$

The following equation was established to calculate the mass balance of the individual system components:

$$\frac{m_{n, found}}{m_{n, fed}} = \frac{V_{Retentat} \cdot \beta_{n, Retentat} + V_{Permeate} \cdot \beta_{n, Permeate}}{(V_{Retentat} + V_{Permeate}) \cdot \beta_{n, Feed}} \cdot 100 \%$$

The mass balance results from the ratio between the found mass $m_{n,found}$ of a component n and the mass $m_{n,fed}$ fed by the feed. The mass found is calculated via the sum of the volumes of retentate $V_{Retentat}$ or permeate $V_{Permeate}$ multiplied by the corresponding concentration of component n in the retentate $\beta_{n,Retentat}$ or permeate $\beta_{n,Permeate}$, respectively. This sum, divided by the product of the total volume and the concentration of the component n in the feed, multiplied by 100, results the mass balance in percent.

Declaration of Competing Interest

The authors declare that they have no known competing financial interests or personal relationships that could have appeared to influence the work reported in this paper.

Acknowledgements

We thank the central analytics department of the Department of Chemistry for carrying out NMR, ICP, CHNS and IC measurements. J.A. and M.H. acknowledge financial support from Deutsche Forschungsgemeinschaft (DFG) (AL 2130/3–2).

Appendix A. Supporting information

Supplementary data associated with this article can be found in the online version at doi:10.1016/j.cherd.2022.06.045.

References

- Ahmad, N.N.R., Ang, W.L., Teow, Y.H., Mohammad, A.W., Hilal, N., 2022. Nanofiltration membrane processes for water recycling, reuse and product recovery within various industries: a review. *J. Water Process Eng.* 45.
- Albert, J., Lüders, D., Bösmann, A., Guldi, D.M., Wasserscheid, P., 2014. Spectroscopic and electrochemical characterization of heteropoly acids for their optimized application in selective biomass oxidation to formic acid. *Green. Chem.* 16 (1), 226–237.
- Babich, I., 2003. Science and technology of novel processes for deep desulfurization of oil refinery streams: a review. *Fuel* 82 (6), 607–631.
- Baker, R.W., 2012. *Membrane Technology and Applications*. John Wiley & Sons Ltd, pp. 590.
- Baker, R.W., Wijmans, J.G., Athayde, A.L., Daniels, R., Ly, J.H., Le, M., 1997. The effect of concentration polarization on the separation of volatile organic compounds from water by pervaporation. *J. Membr. Sci.* 137 (1–2), 159–172.
- Bertleff, B., Claußnitzer, J., Korth, W., Wasserscheid, P., Jess, A., Albert, J., 2017. Extraction coupled oxidative desulfurization of fuels to sulfate and water-soluble sulfur compounds using polyoxometalate catalysts and molecular oxygen. *ACS Sustain. Chem. Eng.* 5 (5), 4110–4118.
- Bertleff, B., Claußnitzer, J., Korth, W., Wasserscheid, P., Jess, A., Albert, J., 2018a. Catalyst activation and influence of the oil matrix on extractive oxidative desulfurization using aqueous polyoxometalate solutions and molecular oxygen. *Energy Fuels* 32 (8), 8683–8688.
- Bertleff, B., Goebel, R., Claußnitzer, J., Korth, W., Skiborowski, M., Wasserscheid, P., Jess, A., Albert, J., 2018b. Investigations on catalyst stability and product isolation in the extractive oxidative desulfurization of fuels using polyoxometalates and molecular oxygen. *ChemCatChem* 10 (20), 4602–4609.
- Bertleff, B., Haider, M.S., Claußnitzer, J., Korth, W., Wasserscheid, P., Jess, A., Albert, J., 2020. Extractive catalytic oxidative denitrogenation of fuels and their promoting effect for desulfurization catalyzed by vanadium substituted heteropolyacids and molecular oxygen. *Energy Fuels* 34 (7), 8099–8109.
- Bishoff Analysenteknik u. -geräte GmbH, HPLC Pumpe 3350 (Dosierpumpe). In 2019; Vol. 2022.
- Bosmann, A., Datsevich, L., Jess, A., Lauter, A., Schmitz, C., Wasserscheid, P., 2001. Deep desulfurization of diesel fuel by extraction with ionic liquids. *Chem. Commun. (Camb.)* 23, 2494–2495.
- Buonomenna, M.G., 2013. Membrane processes for a sustainable industrial growth. *RSC Adv.* 3, 17.
- Campos-Martin, J.M., Capel-Sanchez, M.C., Perez-Presas, P., Fierro, J.L.G., 2010. Oxidative processes of desulfurization of liquid fuels. *J. Chem. Technol. Biotechnol.* 85 (7), 879–890.
- Claußnitzer, J., Bertleff, B., Korth, W., Albert, J., Wasserscheid, P., Jess, A., 2020. Kinetics of triphase extractive oxidative desulfurization of benzothiophene with molecular oxygen catalyzed by HPA-5. *Chem. Eng. Technol.* 43 (3), 465–475.
- Dell Inc, Dell Statistica (data analysis software system). In 2015; Vol. Version 13.
- Europäische Union, Amtsblatt der Europäischen Union, 2009. 52, L140/88–L140/113.
- Evatugin, Oxidative delignification in the presence of molybdo-vanadophosphate heteropolyanions" mechanism and kinetic studies. *Applied Catalysis A: Genera* 167, 123–139, 1998.
- Evonik Resource Efficiency GmbH, The METcell Range. In 2017; Vol. 2022.
- Gates, B.C., Topsøe, H., 1997. Reactivities in deep catalytic hydrodesulfurization: challenges, opportunities, and the importance of 4-methylthiophene and 4,6-dimethylthiophene. *Polyhedron* 16 (18), 3213–3217.
- Ismagilov, Z., Yashnik, S., Kerzhentsev, M., Parmon, V., Bourane, A., Al-Shahrani, F.M., Hajji, A.A., Koseoglu, O.R., 2011. Oxidative desulfurization of hydrocarbon fuels. *Catal. Rev.* 53 (3), 199–255.
- Jiang, W., Zhu, W., Li, H., Wang, X., Yin, S., Chang, Y., Li, H., 2015. Temperature-responsive ionic liquid extraction and separation of the aromatic sulfur compounds. *Fuel* 140, 590–596.
- Kleppmann, W., *Versuchsplanung - Produkte und Prozesse optimieren*. Carl Hanser GmbH: 2016.
- Liao, X., Wu, D., Geng, B., Lu, S., Yao, Y., 2017. Deep oxidative desulfurization catalyzed by (NH₄)_xH₄-xPMo₁₁VO₄₀ (x = 1, 2, 3, 4) using O₂ as an oxidant. *RSC Adv.* 7 (76), 48454–48460.
- Lu, H., Gao, J., Jiang, Z., Yang, Y., Song, B., Li, C., 2007. Oxidative desulfurization of dibenzothiophene with molecular oxygen using emulsion catalysis. *Chem. Commun. (Camb.)* 2, 150–152.
- Ma, X., Zhou, A., Song, C., 2007. A novel method for oxidative desulfurization of liquid hydrocarbon fuels based on catalytic oxidation using molecular oxygen coupled with selective adsorption. *Catal. Today* 123 (1–4), 276–284.
- Melin, T.; Rautenbach, R., *Membranverfahren*. Springer Berlin Heidelberg: 2007.
- Mjalli, F.S., Ahmed, O.U., Al-Wahaibi, T., Al-Wahaibi, Y., AlNashef, I.M., 2014. Deep oxidative desulfurization of liquid fuels. *Rev. Chem. Eng.* 30, 4.
- Odyakov, V.F., Zhizhina, E.G., Rodikova, Y.A., Gogin, L.L., 2015. Mo-V-phosphoric heteropoly acids and their salts: aqueous solution preparation – challenges and perspectives. *Eur. J. Inorg. Chem.* 2015 (22), 3618–3631.
- Pettersson, L., Andersson, I., Selling, A., Grate, J., 1994. Multicomponent Poly-anions. 46. Characterization of the isomeric keggin decamolybdovanadophosphate ions in aqueous solution by ³¹P and ⁵¹V NMR. *Inorg. Chem.* 33, 982–993.
- Pobe, M.T., Scully, T.F., 1975. Geometrical isomerism arising from partial substitution of metal atoms in isopoly and heteropoly complexes. Possibilities for the keggin structure. *Inorg. Chem.* 14, 953–954.
- PS Prozesstechnik GmbH, MiniMem - the smallest lab membrane filtration unit - Batchsize 20–2000ml. In Vol. 2022.
- Ramírez-Verduzco, L.F., Torres-García, E., Gómez-Quintana, R., González-Peña, V., Murrieta-Guevara, F., 2004. Desulfurization of diesel by oxidation/extraction scheme: influence of the extraction solvent. *Catal. Today* 98 (1–2), 289–294.
- Schirg, P. *Verfahren und Vorrichtung zur Filtration von Produktgemischen*. EP2078556A2, 2009.
- Shatalov, A.A., Evtuguin, D.V., Pascoal Neto, C., 2000. Cellulose degradation in the reaction system O₂/heteropolyanions of series [PMo(122n)VnO₄₀](31n)₂. *Carbohydr. Polym.* 43, 23–32.
- Sikdar, S.K., Criscuolo, A., 2017. Sustainability and how membrane technologies in water treatment can be a contributor. *Sustain. Membr. Technol. Water Wastewater Treat.* 1–21.
- Stade, S., Kallioinen, M., Tuuva, T., Mänttäri, M., 2015. Compaction and its effect on retention of ultrafiltration membranes at different temperatures. *Sep. Purif. Technol.* 151, 211–217.
- Tang, N., Zhang, Y., Lin, F., Lu, H., Jiang, Z., Li, C., 2012. Oxidation of dibenzothiophene catalyzed by [C₈H₁₇N(CH₃)₃]₃H₃V₁₀O₂₈ using molecular oxygen as oxidant. *Chem. Commun. (Camb.)* 48 (95), 11647–11649.
- Tang, N., Jiang, Z., Li, C., 2015. Oxidation of refractory sulfur-containing compounds with molecular oxygen catalyzed by vanadoperiodate. *Green. Chem.* 17 (2), 817–820.

- Venkateshwar Rao, T., Sain, B., Kafola, S., Nautiyal, B.R., Sharma, Y.K., Nanoti, S.M., Garg, M.O., 2007. Oxidative desulfurization of HDS diesel using the aldehyde/molecular oxygen oxidation system. *Energy Fuels* 21 (6), 3420–3424.
- Volkov, A., 2014. Membrane compaction. In: *Encycl. Membr.* 1–2.
- Yazu, K., Yamamoto, Y., Furuya, T., Miki, K., Ukegawa, K., 2001. Oxidation of dibenzothiophenes in an organic biphasic system and its application to oxidative desulfurization of light oil. *Energy Fuels* 15 (6), 1535–1536.
- Zhang, W., Zhang, H., Xiao, J., Zhao, Z., Yu, M., Li, Z., 2014. Carbon nanotube catalysts for oxidative desulfurization of a model diesel fuel using molecular oxygen. *Green. Chem.* 16 (1), 211–220.
- Zhao, H., Baker, G.A., 2015. Oxidative desulfurization of fuels using ionic liquids: a review. *Front Chem. Sci. Eng.* 9 (3), 262–279.
- Zhizhina, E.G., Odyakov, V.F., 2008. Alteration of the physico-chemical properties of catalysts based on aqueous solutions of Mo-V-P heteropoly acids in redox processes. *React. Kinet. Catal. Lett.* 95 (2), 301–312.
- Zhizhina, E.G., Odyakov, V.F., Simonova, M.V., 2008. Catalytic oxidation of organic compounds with oxygen in the presence of Mo-V-phosphoric heteropoly acid solutions. *Kinet. Catal.* 49 (6), 773–781.

6.2 Selective Catalytic Oxidation of Furan Derivates as Model Substances for Humins

P2

Catalytic valorization of humins by selective oxidation using transition-metal-substituted Keggin-Type polyoxometalate catalysts

Tobias Esser, André Wassenberg, Jan-Christian Raabe, Dorothea Voß, and Jakob Albert

Esser, T.; Wassenberg, A.; Raabe, J.-C.; Voß, D.; Albert, J.: Catalytic Valorization of Humins by Selective Oxidation Using Transition-Metal-Substituted Keggin-Type Polyoxometalate Catalysts. *ACS Sustainable Chem. Eng.*, **2024** (12), 543–560. DOI: 10.1021/acssuschemeng.3c06539.

This section deals with the investigation of structure-activity-selectivity relationships in the selective catalytic oxidation of humins. Since the structure of humins is not yet fully understood, their chemical conversion represents a challenge. Furan rings, which form the complex humin structure through various bonds and functional groups, are a confirmed structural element (*vide supra*, 4.2.1.2). Therefore, various commercial as well as synthesized complex furan derivatives as model substances and different synthesized *Keggin*-type polyoxometalate catalysts were tested in the following study in order to gain an initial model and a deeper understanding of the conversion of humins. Figure 6.1 shows a model humin and the associated structural elements that can be represented by appropriate model substances. In the simplest form, only individual furan rings with different functionalities are considered as model substances, which represent the least complex model substances of the first-generation. Several linked furan rings and furan rings with branched side chains form the more complex model substances of the second-generation. Various functionalities are conceivable here, which are discussed in detail in the following study²¹².

In a first step, furfural was selected as a model substance for selective catalytic oxidation at 90 °C and 30 bar O₂ in aqueous phase. Here, the influence of various transition metals in mono-substituted phosphomolybdic acids and the degree of substitution were tested to identify the most suitable catalyst with enhanced activity for the selective ring opening of furfural and oxidation to industrially relevant carboxylic acids such as maleic acid, acetic acid, and formic acid.²¹²

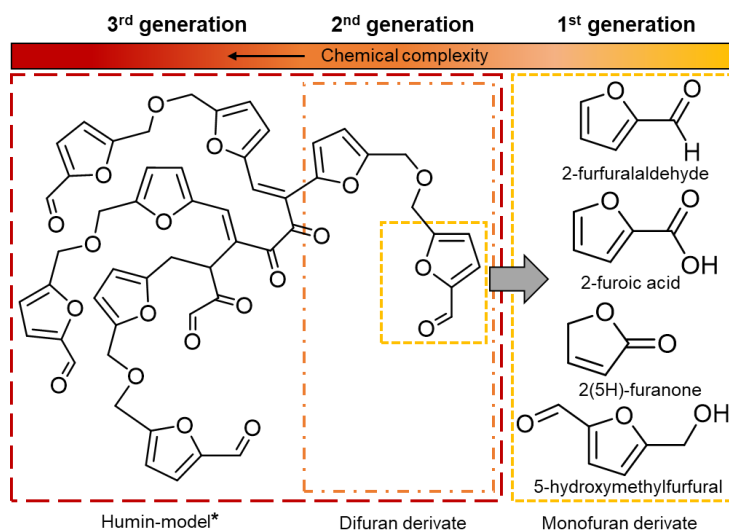
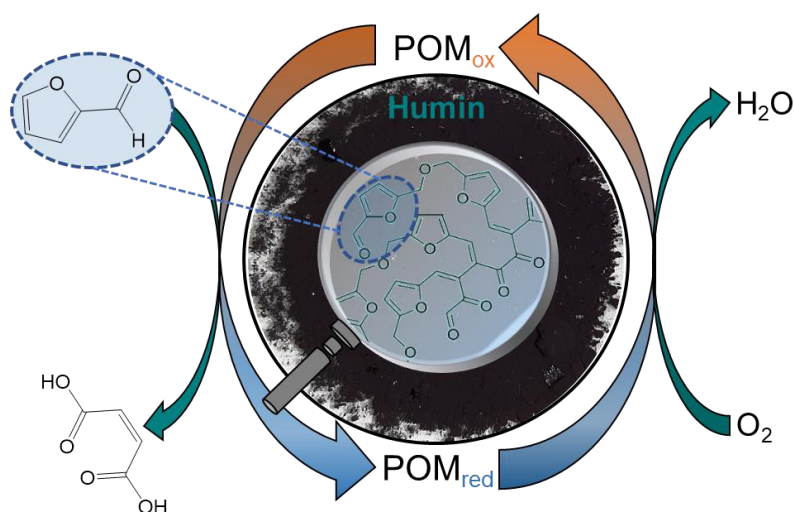


Figure 6.1: Classification of humin model substances according to their chemical complexity: From monofuran derivatives (first-generation) over difuran derivatives (second-generation) to humins (model according to **Maerten et al.*⁸).²¹²

A correlation between the electrochemical properties and the conversion of furfural was demonstrated and an adjustment of the redox activity was obtained. The vanadium-substituted $H_4[PVMo_{11}O_{40}]$ POM-catalyst proved to be superior in terms of the trade-off between selectivity and activity. Subsequently, the structure-activity-selectivity relationships for the selected catalyst were investigated by a substrate screening. Different side chains or functionalizations were tested on the furan rings. In addition, the oxidation process for benzene and phenol derivatives was investigated, which may also be present to a lesser extent in the humin structure. Based on the product composition, a plausible reaction mechanism was postulated. In a final step, complex furan derivatives, which mostly consist of differently linked difuran derivatives, were processed. Oxygen and non-oxygen functionalized bond types were tested as well. Further supporting information can be found in Appendix 9.5.2.²¹² Reprinted from Ref.²¹² with permission of the *American Chemical Society*. Copyright 2023 *American Chemical Society*.



Publication: *Catalytic valorization of humins by selective oxidation using transition-metal substituted Keggin-type polyoxometalate catalysts.*²¹²

Catalytic Valorization of Humins by Selective Oxidation Using Transition-Metal-Substituted Keggin-Type Polyoxometalate Catalysts

Tobias Esser, André Wassenberg, Jan-Christian Raabe, Dorothea Voß, and Jakob Albert*

Cite This: *ACS Sustainable Chem. Eng.* 2024, 12, 543–560

Read Online

ACCESS |



Metrics & More



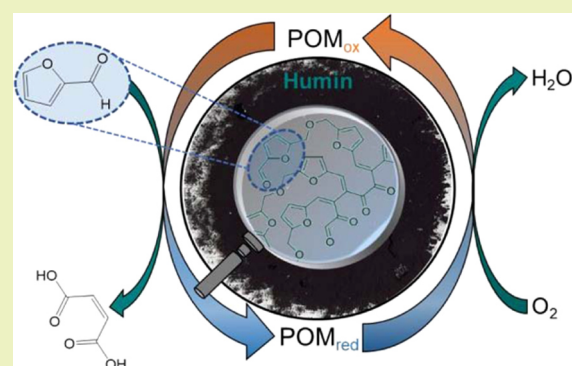
Article Recommendations



Supporting Information

ABSTRACT: The main objective of this study was to gain a deeper understanding of oxidative valorization of humins using polyoxometalate (POM) catalysts. Based on experiments using individual monofuran derivatives as a substrate, evident reaction pathways for the conversion to maleic acid were postulated. By analogous routes, difuran derivatives or branched furan rings could also be converted to maleic acid and formic acid, respectively. Hereby, the monovanadium-substituted catalyst was found to be superior compared to other structures in terms of activity and selectivity due to its unique electrochemical properties. In detail, $H_4[PVMo_{11}O_{40}]$ showed the lowest peak potential in Square-Wave-Voltammetry measurements, achieving the highest activity and carboxylic acid selectivity. Hereby, a deeper understanding of the selective oxidation of humin model substrates like furan derivatives of varying complexity could be achieved. Therefore, helpful conclusions can be drawn for the transformation of humins representing a decisive step toward efficient processes for their valorization.

KEYWORDS: biomass, polyoxometalate catalysts, humin, selective oxidation, maleic acid



INTRODUCTION

The depletion of fossil hydrocarbon resources stimulates innovative approaches in science for the research of sustainable energy sources and feedstock for the cost-effective production of platform chemicals in green processes.^{1–5} Plant biomass, such as lignocellulose, is considered as the main source of renewable carbonaceous feedstock due to its large abundance and availability.^{1,6,7} Furthermore, lignocellulosic biomass is not in direct conflict with food supply like in the case of starch and vegetable oils. Therefore, the conversion of lignocellulose to value-added chemicals is an important and challenging topic. Accordingly, the development of novel biobased process technologies comparable to today's petroleum refining, commonly referred to as biorefinery, has received considerable attention in recent years.^{8–10} Hayes et al.,¹¹ Cherubini,⁸ and Maity⁹ provide a comprehensive overview of various biorefinery technologies. However, in comparison to processes available for fossil resources, the valorization of renewable feedstock to value-added chemicals is the least developed and most complex of all biorefinery operations.^{12,13}

One promising approach is the acid-catalyzed hydrolysis of cellulose as part of lignocellulosic biomass to valuable chemicals.^{4,5,14} In this context, the Biofine process for the continuous production of biogenic levulinic acid by acid-catalyzed hydrolysis is one of the most advanced large-scale biorefinery technologies.^{15–17} However, a major deficit of acid-

catalyzed conversion of cellulose and its derivatives in the liquid phase is the formation of undesirable polymeric byproducts.^{6,14} In fact, processing monosaccharides and their derivatives derived from cellulose results in the coproduction of dark-colored solids known as humins.¹⁸ Unfortunately, due to the kinetic nature of the reaction, the formation of humins cannot be completely prevented, especially on a large reaction scale.^{4,19} In recent years, numerous studies using various analytical techniques have been conducted in order to further elucidate the humin structure.^{4,6,20–22} It is reported that basic building blocks are most probably furan rings bridged by various aliphatic functional groups.^{6,23} According to the literature, these furan rings can account for up to 60% of the humin structure, while aliphatic linkers account for up to 20%.^{24,25} Phenolic and benzofuran derivatives are also discussed as another component of the humin structure, which may only account for a small proportion of the total structure.^{7,25,26} Table 1 lists examples of confirmed humin

Received: October 15, 2023

Revised: December 11, 2023

Accepted: December 12, 2023

Published: December 25, 2023

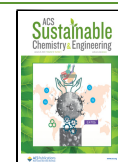
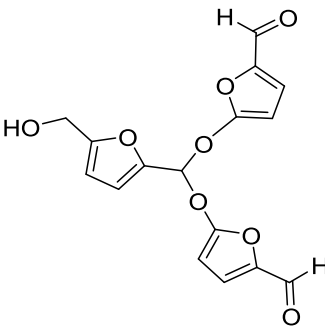
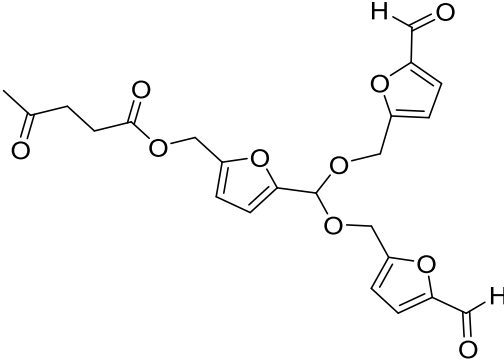
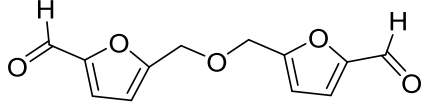
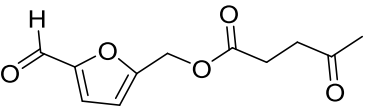
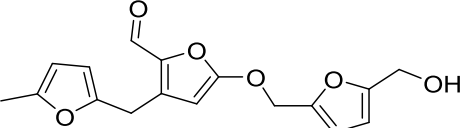


Table 1. Overview of Confirmed Humin Fragments Reported in the Literature

Entry	Humin fragments	Reference
1		24,27
2		23
3		23,26,28
4		23
5		29

fragments from the literature. A comprehensive overview of current insights on various humin fragments and structures confirmed by mass spectroscopy is given by Liu et al.⁶ It can be clearly seen that these fragments, and therefore the humin structure, are based on a complex interplay of different functionalities such as ethers and esters, and also aldehyde and keto groups are conceivable. In this way, the humin structure can be simplified into smaller structural motifs based on different multifuran derivatives that need to be converted or further broken down en route to value-added products.

In the case of the Biofine process, the cross-reaction of intermediates leads to the formation of insoluble humins, accounting for up to 30% of the carbon yield.^{10,15,16} In terms of high efficiency, economy, and sustainability, the usage of byproducts is required. Therefore, the utilization of humins is inevitable both for ecological and economic reasons. So far, some attempts for humin valorization have been reported, but there is still a lack of knowledge on their material potential.⁶

On the one hand, the chemical use of humins in green processes is hampered by their virtually insoluble nature in commonly known solvents.^{4,25} On the other hand, too little is known so far about the structure of humins, which makes it difficult to tailor catalysts and processes for selective conversion into value-added products.²⁵

As mentioned and discussed above as well as supported by a large number of studies, the humin structure exists of a furan-rich polymer network.^{4,6,7,27,28,30,31} Numerous results indicate a linkage of these furan rings via oxygen-functionalized C–O–C bonds.^{4–6,23,25,28,29} However, aliphatic C–C bonds are also under discussion.^{7,25,27,31} Hoang et al.⁷ and Shi et al.³⁰ suggest that the furan rings are also linked via aliphatic acetyl groups as well as via CH₂ bonds. Both linkages via C–O–C and C–C bonds are plausible and coexistence in the real humin structure cannot be excluded either. An exemplary structural motif that allows both types of bonds was recently suggested by Wassenberg et al.²⁹ and corroborated via mass spectroscopic

analyses (Table 1, entry 5). Nevertheless, we can conclude that the complex structure of humins has not been fully elucidated to date. Furthermore, a dependence of the humin structure and morphology on the reaction conditions including temperature, pH, catalyst, and reaction time during their formation can be assumed.⁶ Consequently, not only one specific humin exists but also this material class represents an extremely undefined substrate. Starting with the highly complex humin without the knowledge of its polymeric structure, experiments are difficult to interpret, and to develop conversion processes is obstructive. Maerten et al.⁴ pioneered this field and reported for the first time the selective catalytic oxidation of humins to short-chain carboxylic acids such as formic acid (FA) and acetic acid (AA). The conversion of humins using homogeneous polyoxometalate (POM) catalysts was demonstrated under very mild reaction conditions in aqueous media.⁴ However, further studies are required to optimize the still low yield and selectivity of liquid-phase products.

POMs are a fascinating group of anionic metal-oxide clusters with a broad variety of structural properties and several catalytic applications, especially in the conversion of bioderived platform chemicals.^{32,33} They can act simultaneously as strong Brønsted acids and Redox catalysts, allowing multiple electron transfer, making them useful bifunctional catalysts.³² Due to their controllable catalytic properties, POMs have found application in many fields.^{34,35} Furthermore, POMs exhibit high reactivity and stability over a wide range of conditions.³⁶ Consequently, POMs are attractive for catalysis in novel approaches for reactions under mild conditions in the liquid phase using molecular oxygen, leading to clean, environmentally friendly processes.^{37,38} For example, they can be used as homogeneous catalysts in the valorization of lignocellulosic biomass to FA, as novel heterogeneous supported catalysts for the selective catalytic reduction of NO with NH₃ (NH₃-SCR), or for the oxidative desulfurization of fuels in extraction-coupled oxidative desulfurization (ECODS).^{37–39}

The main objective of this contribution is to gain a deeper understanding of the structure–activity–selectivity relationships in the selective catalytic oxidation of furan derivatives, which form structural motifs in humins. For this purpose, a study on the selective catalytic oxidation of humin-like substances in the form of several mono- and difuran derivatives using homogeneous POM catalysts in aqueous media was conducted. In addition, various transition metals have been used to substitute molybdenum atoms in Keggin-type polyoxometalate to modify the redox behavior.

EXPERIMENTAL SECTION

Chemicals. For the study presented here, different POM catalysts were synthesized and tested. In particular, numerous Keggin-type POMs substituted with different transition metals, which can be described by the formulas H_z[PMMo₁₁O₄₀] with M = Mn^{II}, Co^{II}, Ni^{II}, Fe^{III}, Nb^V, V^V and z = 4, 6, and 7 were used. In addition, the degree of substitution was also varied, giving POMs according to H_{3+x}[PV_xMo_{12-x}O₄₀] with x = 1 to 6. The catalysts were essentially synthesized according to the literature.^{40–43}

In a typical synthesis of monosubstituted phosphomolybdate catalysts, molybdenum(VI) oxide (11 equiv) was suspended in water and a 25% solution of phosphoric acid in water (1 equiv) was added. The reaction mixture was heated to reflux for 30 min, and a yellow, clear solution was formed (solution 1). For the vanadium-substituted H₄[PVMo₁₁O₄₀] catalyst, divanadium(V) oxide (0.5 equiv) was suspended in water and cooled to 4 °C in a parallel batch. A 30% solution of hydrogen peroxide in water (11.91 equiv)

was added dropwise. After stirring, a brown solution was formed from which oxygen gas evolution was observed. In the next step, a 25% solution of phosphoric acid in water (0.174 equiv) was added and the reaction solution was stirred at room temperature (solution 2). Solution 2 was added dropwise to refluxing solution 1, resulting in a color change from yellow to orange. After complete addition, the solution was refluxed for 1 h. It was cooled to room temperature, filtered, and the solvent was removed under reduced pressure, yielding an orange powder. For the synthesis of higher-substituted catalysts, the ratios of the precursors were adjusted to the desired value.⁴³

The catalysts substituted by manganese, nickel, and cobalt were prepared in an analogous process. In the case of Mn(II), the procedure has already been published in a previous publication.⁴² Compared to the vanadium-substituted catalysts, manganese(II) acetate, cobalt(II) acetate tetrahydrate, and nickel(II) acetate tetrahydrate (1 equiv) were used as precursors instead of divanadium(V) oxide.⁴²

The incorporation of niobium (Nb) into the POM catalyst was achieved by a novel synthesis approach using a lacunary Keggin-type structure according to the literature.⁴⁴ According to this procedure, sodium molybdate dihydrate (9 equiv) and disodium hydrogen phosphate (1 equiv) were dissolved in water. The pH was adjusted to 1 by adding a 37% solution of hydrochloric acid in water dropwise, turning the solution yellow (solution 1). Parallel potassium hexaniobate (0.167 equiv) was dissolved in an aqueous 1.5% hydrogen peroxide solution (solution 2). Solution 2 was added to solution 1. Sodium molybdate dihydrate (2 equiv) was added. The yellow solution was refluxed for 2 h. After cooling to room temperature, the solution was filtered and purified according to our previously published nanofiltration approach.⁴⁴ All synthesized catalysts used were extensively characterized, as described below (*vide infra*, catalyst characterization).

The model substrates (MS) used were synthesized on a laboratory scale. MS1 was synthesized with a one-pot, fluoride-promoted Wittig reaction after Fumagalli et al.⁴⁵ In our case, 5.8 mL of ethyl α -bromoacetate dissolved in 50 mL of tetrahydrofuran (THF) and 12.5 mL of *n*-Bu₃P was used for the reaction mixture with 7.13 g of 5-HMF in 60 mL of 1 molar THF/Bu₄NF solution as a substrate. The product was purified by column extraction using chloroform as the solvent. MS2 was synthesized after the procedure used by Abid et al.⁴⁶ using 9 g of the substrate ethyl 2-furoate, 2.82 mL of the substrate acetone and 9 mL of the acidic catalyst sulfuric acid. The product was dissolved in 125 mL of ethyl acetate and afterward neutralized in a separation funnel using saturated NaHCO₃. The organic layer was then concentrated in a rotary evaporator and the resulting organic liquid purified through column chromatography using chloroform as a solvent. MS3 was synthesized using the procedure described by Simeonov et al.⁴⁷ to synthesize 5-HMF. Here, 6 g of fructose, 12.4 g of TEAB and 1.32 mL of water were used to form the ionic liquid for the reaction with 600 mg of powdered Amberlyst-15 as a catalyst. After using the described purification method, the organic residue was filled into a sublimation device and sublimated over 3 days at 130 °C. Afterward, the yellow residue was scraped off the coldfinger and washed with water to remove the residual 5-HMF. The yellow powder was then left to dry at 80 °C overnight. MS4 was synthesized according to Nielson et al.⁴⁸ Here, 0.5 g of sodium was added to 2.2 mL of furfuryl alcohol and 7.5 mL of toluene in a round-bottom flask. After the reaction of sodium, 12 mL of furfural was slowly added to the mixture. The mixture was then stirred for 18 h at room temperature. Afterward, the mixture was washed with a saturated NaCl solution inside a separatory funnel. The resulting organic layer was then concentrated using a rotary evaporator and then purified using column chromatography with a 1:6 mixture of petrolether and chloroform. All model substances were analyzed by CHNS, and the results can be found in Table S4. In addition, the structure of the model substances was verified by ¹H NMR measurements, which can also be found in Figures S15–S18.

All other chemicals were purchased commercially and used without further purification. 5-HMF (97%) was purchased from Alfa Aesar. Furfural (98%), 2-methylfuran (99%), 2-furoic acid (98%),

acid (>99%), and 4-methoxyphenol (99%) were obtained from Sigma-Aldrich. Furan-2(5H)-one (95%) was purchased from abcr GmbH. The supplier for benzofuran (99.3%) was Apollo Scientific and VWR for 2-furfuryl alcohol (98%). For NMR reference spectra, additional commercially available chemicals were used. Formic acid (97%) and acetic acid (100%) were purchased from VWR Chemicals. 5-Hydroxyfuran-2(5H)-one (>96%) was obtained from Ambeed. The precursors for the catalyst synthesis including molybdenum(VI) oxide, divanadium(V) pentoxide, manganese(II) acetate, and niobium(V) oxide were purchased from Alfa Aesar. Cobalt(II) acetate as well as sodium molybdate phosphate were obtained from Carl Roth. Sigma-Aldrich was the supplier of phosphomolybdic acid and nickel(II) acetate. Hydrogen peroxide (30% in water) and hydrochloric acid (37% in water) were supplied by VWR Chemicals.

Experimental Setup and Typical Working Procedure. For the experiments on the oxidation of first- and second-generation substrates, a 10-fold screening plant consisting of ten 20 mL autoclaves made of Hastelloy C276 in batch mode were used. Teflon was chosen as the material for gaskets due to its high chemical resistance. Valves, fittings, and pipes were manufactured of stainless steel 1.4571. The plant was equipped with a heating plate, allowing reaction temperatures up to 200 °C and a magnetic stirrer. All reactors were connected to an oxygen supply line. Each autoclave was also connected to a burst disk due to safety reasons, which limit the maximum pressure to 90 bar.

In a typical experiment on the oxidation of first-generation substrates, each autoclave was filled with 0.14 mmol vanadium (or other transition metal) in the form of a POM catalyst and 10 mL of a substrate solution containing 240 mmol L⁻¹ furfural. Thus, the substrate in the solution provided 12.5 mmol carbon per reactor. This results in a carbon to transition metal *M* (used for substitution) ratio of about 90 mol_{Carbon} mol_M⁻¹. To ensure a pure oxygen atmosphere, the reactors were purged three times with 10 bar oxygen each, thus removing all residual air from the reactors. Subsequently, the reactors were pressurized to a prepressure of about 26 bar and the heating plate was set to 90 °C. For better heat transfer from the reactor wall to the reaction solution, the stirrer was set to 300 rpm. The stirrer was set to 1000 rpm when the desired reaction temperature of 90 °C (115 or 140 °C in some experiments) was reached and the pressure increased to the required value of 30 bar. From this point on, the reaction time of 15 h began.

In the experiments using the second-generation substrates, the test procedure was slightly modified since these highly viscous systems tend to form solids and heavily soil the reactors. For better handling, the tests were carried out in glass liners, which ensure an easier cleaning and sampling (solids). Due to the smaller volume of the glass liners, the reaction volume was reduced to 7.5 mL. Consequently, the amount of substrate was also adjusted. Along with a decreased amount of transition metal, the carbon to transition metal ratio of about 90 mol_{Carbon} mol_M⁻¹ remained constant.

Catalyst Characterization. The stoichiometry of the synthesized and tested catalysts was verified by inductively coupled plasma optical emission spectrometry (ICP-OES) as well as by thermogravimetric analysis (TGA) for determining the content of hydration water. The results can be found in Table S5. For the selected H₄[PVMo₁₁O₄₀] catalyst, a stoichiometry of 1.23 P/0.97 V/11 Mo and a hydration water content of 7 mol per mol catalyst were determined.

Analysis of the catalyst components was performed using a Fa. Spectro Ametek Model Arcos ICP-OES spectrometer. Samples were measured by the Division for Central Element Analytics (ZEA) in the Department of Chemistry. For the determination of the elements Mo, P, V, Nb, and Mn by ICP-OES, different sample preparations were performed depending on the sample. The catalysts H₄[PVMo₁₁O₄₀], H₇[PCoMo₁₁O₄₀], and H₇[PNiMo₁₁O₄₀] were dissolved in water (5 mL), a 65% solution of nitric acid in water was added (100 μL), and the solution was diluted in a volumetric flask with water to 25 mL before measurement. The H₇[PMnMo₁₁O₄₀] catalyst was also dissolved in water (5 mL) and acidified using a 37% solution of hydrochloric acid in water (4 mL) and diluted with water in a volumetric flask to 50 mL. The niobium-substituted catalyst was

dissolved in 25 mL of water without subsequent acidification. Elements Co and Ni were measured using an AAS-F from Fa. Thermo, type Solar S Series (method: F AES without HKL).

TGA measurements were done using a TG 209 F1 Libra of NETZSCH. All data were processed with the software Proteus from NETZSCH. For this purpose, about 20 mg (tare) of the sample was weighted into a Duran-glass crucible and the change in mass was measured during application of the temperature program. This temperature program started with heating to 30 °C, applying a heating rate of 10 K min⁻¹. The temperature of 30 °C was kept constant for 15 min. After this plateau, the temperature was increased to 350 °C at a heating rate of 10 K min⁻¹. The temperature of 350 °C was maintained for 30 min. Afterward, the sample was cooled to room temperature. During all measurements, a nitrogen flow of 20 mL min⁻¹ was passed through the instrument.

The integrity of POM structures was verified using attenuated total reflection Fourier-transform infrared spectroscopy (ATR-FTIR) and ⁵¹V- as well as ³¹P NMR spectroscopy. The results are attached to Figures S19–S25. Nuclear magnetic resonance (NMR) spectra were measured by the division of NMR in the Department of Chemistry employing a Bruker AVANCEII 600 MHz spectrometer. Sample preparation for NMR analysis: POM (70 mg) was dissolved in deionized water (0.7 mL), which had previously been adjusted to pH 1 with a 37% hydrochloric acid solution in deionized water, and acetone-*d*₆ (0.07 mL) was added.

ATR-FTIR spectra were measured in attenuated total reflection (ATR) measurement mode using a QATR-S single-reflection ATR (with a diamond prism). From the obtained data, the baseline was corrected first, and the peaks were determined manually.

To elucidate correlations between structural features and catalytic performance, detailed characterization using single-crystal X-ray diffraction (XRD) was carried out for the monosubstituted POMs. The crystals were obtained by slow evaporation of the solvent under reduced pressure in a desiccator. Single X-ray crystal structure (sc-XRD) analysis was done on a 4-circle single-crystal diffractometer SuperNova from Oxford Diffraction (Agilent Technologies) using a molybdenum and copper source (dual instrument), microfocus tubes, cryostream-700 Plus nitrogen steam cooling, and 100–500 K (Oxford Cryosystems). All structures were solved and refined using Shelxtl⁴⁹ with WinGX^{50,51} as graphical support and Olex2 vl.5.2,⁵³ The results can be found in Figure S26.

The powder XRD diffractograms were measured on an X'Pert Pro diffractometer (PANalytical Corp.) using Cu-K_α radiation (λ = 1.5418 Å) in the range of 5–90°. Data processing was done in the software X'Pert HighScore Plus. The results can be found in Figures S27–S28.

Cyclic voltammogram/square-wave voltammogram (CV/SWV) measurements were performed in an aqueous hydrochloric acid medium at pH 1. The concentration was 1 mmol L⁻¹. Measurements were carried out on a Metrohm-Autolab PGSTAT101. During the measurement, the solution was purged with nitrogen gas. Working electrode: Glassy carbon electrode (diameter: 3 mm); reference electrode: Ag/Ag+ electrode; counter electrode: platinum electrode. All measurements were conducted between -0.6 and 1 V using a scan rate for CV of 100 mV s⁻¹ and 3 scans. SWV measurements were taken with a scan rate of 5 mV s⁻¹, a modulation amplitude of 20 mV and a frequency of 25 Hz. Software IviumSoft.

Analysis of Substrates and Reaction Products. Gaseous CO₂ and CO were quantified using a Varian 450-GC equipped with a TCD-GC detector. A high-performance liquid chromatography (HPLC) system from SHIMADZU equipped with an Aminex HPX-87H 300 mm × 7.8 mm BIORAD column and a refractive index detector were used for quantitative analysis of the aqueous phase. As eluent, an aqueous sulfuric acid solution with a concentration of 5 mmol L⁻¹ was used. Measurements were performed at a temperature of 45 °C, a flow rate of 0.5 mL min⁻¹, and a pressure of 49 bar. An example chromatogram for the reaction of the substrate mixture with H₄[PVMo₁₁O₄₀] can be found in Figure S1.

Nuclear magnetic resonance (NMR) spectra were measured by the division of NMR in the Department of Chemistry using a Bruker AVANCEII 600 MHz spectrometer. ¹H NMR, ¹³C NMR, and ²D-

NMR (HSQC and HMBC) spectra of the reaction solutions were prepared by blending 0.6 mL of the reaction solution with 0.1 mL of a 10 wt % *tert*-butanol solution in D₂O. Software MestReNova. The signals were assigned to the substances using reference spectra calculated in ChemDraw applying an increment system. In addition, reference spectra of the pure substances were recorded and used for comparison. As a result, the influence of the solvent, the pH value, and shielding effects were better considered and thus the assignment is more precise. The reference spectra (¹H NMR, ¹³C NMR) are listed in Figures S29–S34.

An analyzer of Fa. EuroVector, Model EA-3000, was used to perform elemental CHNS analysis.

Formulas for Calculation. The conversion of each water-soluble substrate was calculated using eq 1

$$X_{\text{Sub } i} = \frac{c_{0,\text{Sub } i} - c_{\text{Sub } i}}{c_{0,\text{Sub } i}} \quad (1)$$

The difference between the initial concentration $c_{0,\text{Sub } i}$ of substrate i and the concentration $c_{\text{Sub } i}$ after the reaction corresponds to the amount of substrate i converted. For the calculation of the conversion of the water-insoluble substrates, the total yield was used as conversion. It was assumed that the missing carbon was due to the formation of solids or unreacted substrate (e.g., 2-methylfuran). The yield of each product in the liquid phase was calculated using eq 2

$$Y_{\text{Pro } i} = \frac{c_{\text{Pro } i}}{c_{\text{Pro } i,\text{theoretical}}} = \frac{c_{\text{Pro } i}}{c_{0,\text{Carbon}}/N_{\text{Carbon,Pro } i}} \quad (2)$$

The yield $Y_{\text{Pro } i}$ of product i is calculated using the ratio of the measured concentration $c_{\text{Pro } i}$ of product i after the reaction and the theoretically maximum possible concentration $c_{\text{Pro } i,\text{theoretical}}$ of the product. The theoretically maximum possible concentration was calculated by the ratio of the initial concentration of carbon and the number of carbons $N_{\text{Carbon,Sub } i}$ in the product.

For the second-generation model substances, the calculation of the yield had to be adapted since these are insoluble in water and thus no stock solution could be prepared. Therefore, a determination of the initial concentration by HPLC was excluded. The calculation was based on the mass fraction and not on the concentrations. The initial amount of carbon $n_{0,\text{Carbon}}$ was calculated according to eq 3

$$n_{0,\text{Carbon}} = \frac{w_{\text{C,MS } i} \times m_{\text{MS } i}}{M_{\text{Carbon}}} \quad (3)$$

Here, the mass of carbon was calculated by the product of the mass fraction $w_{\text{C,MS } i}$ of carbon in the respective model substance i and the weighed-in mass of model substance i $m_{\text{MS } i}$. With the molar mass of carbon M_{C} , the initial amount of carbon $n_{0,\text{Carbon}}$ could be calculated. Thus, the theoretical maximum mass fraction $w_{\text{Pro } i,\text{theoretical}}$ of a product i was calculated as shown in eq 4

$$w_{\text{Pro } i,\text{theoretical}} = \frac{n_{0,\text{Carbon}}/N_{\text{Carbon,Pro } i} \times M_{\text{Pro } i}}{m_{\text{MS } i} + m_{\text{cat}} + m_{\text{sol}}} \quad (4)$$

The theoretical maximum possible mass of a product i was calculated from the ratio between the initial amount of carbon $n_{0,\text{Carbon}}$ and the number of carbons $N_{\text{Carbon,Sub } i}$ in the product multiplied by the molar mass $M_{\text{Pro } i}$ of the product. The latter divided by the initial total mass in the reactor, which is the sum of the weighed-in masses of MS $m_{\text{MS } i}$, catalyst m_{cat} , and solvent m_{sol} , gave the theoretically maximum mass fraction $w_{\text{Pro } i,\text{theoretical}}$ of product i . The mass conservation of the liquid reaction phase was assumed. The carbon partially passed into the gas phase in the form of gaseous products, which caused loss of mass in the liquid phase. However, the initial mass fraction of the substrates (carbon) was very small, about 5% (3%), so the mass change was expected to be small. In addition, oxidation products were formed in the liquid phase, which bind additional mass due to oxygen. Overall, a negligible mass change could be expected. The achieved mass fraction $w_{\text{Pro } i}$ of a product i was calculated according to eq 5

$$w_{\text{Pro } i} = c_{\text{Pro } i} \times \rho_{\text{liquid}} \times M_{\text{Pro } i} \quad (5)$$

Here, the achieved mass fraction $w_{\text{Pro } i}$ is the result of multiplying the measured concentration $c_{\text{Pro } i}$ of a product i , the density ρ_{liquid} of the liquid reaction phase (after filtration), and the molar mass $M_{\text{Pro } i}$ of product i . Finally, the yield $Y_{\text{MS,Pro } i}$ of product i was calculated by the ratio of the achieved mass fraction $w_{\text{Pro } i}$ and $w_{\text{Pro } i,\text{theoretical}}$

$$Y_{\text{MS,Pro } i} = \frac{w_{\text{Pro } i}}{w_{\text{Pro } i,\text{theoretical}}} \quad (6)$$

RESULTS AND DISCUSSION

Selection of Suitable Mono- and Difuran Derivatives.

In addition to the already existing functionalities, a modification of the humin structure by catalytic processes is possible. Wassenberg et al.²⁹ demonstrated by CHNS analysis and IR spectroscopy that oxygen is incorporated into the humin structure during their catalytic oxidation. Hence, introducing a certain degree of functionalization at the furan ring by oxidative cleavage of C–C bonds in the humin structure is also within the realm of possibility. Moreover, oxygen-rich bond types between the individual furan rings (Table 1, entries 1 and 2) are particularly predestined to lead to oxygen-rich fragments by oxidative bond cleavage, which are analogous to carboxylic acids, lactones, ketones, or aldehydes. In this way, the humin structure can be further simplified so that humin fragments can be narrowed down to individual furan rings with different functionalizations.⁷ These monofuran derivatives include substances such as 5-hydroxymethylfurfural (5-HMF), 2-furoic acid, 2(*SH*)-furanone, or furfural. The latter is particularly plausible as a building block in humins, since furfural is an intermediate involved in the formation of humins during the conversion of C₅-sugars.^{24,31} Furthermore, complex lignocellulosic biomass also contains pentoses, which form furfural as a byproduct of the Biofine process through acid-catalyzed hydrolysis. This makes the formation of furfural-based humins even more plausible. Another humin precursor is the bifunctional 5-HMF, which is also formed in the Biofine process from the hexoses contained in the lignocellulosic biomass.^{14,23} Due to its bifunctionality, 5-HMF can undergo a variety of reactions leading to some of the high oxygen-functionalized structures listed in Table 1. However, aldol condensation with levulinic acid or 2,5-dioxo-6-hydroxyhexanal (DHH) can lead to structures that have less or only one oxygen functionalization in the immediate vicinity of the furan ring.^{14,23} Hence, these structures might also be an important part of humins. It can be assumed that the monofuran derivatives or analogues are the final precursors in the degradation of the humin structure to low-molecular-weight carboxylic acids. Figure 1 shows in the left part a model of a complex humin structure according to Maerten et al.⁴ and the following simplification of the humin structure to single structural elements. Comparable humin structures can be found in the publications of Hoang et al.,⁷ Maruani et al.,⁵⁴ Shen et al.,²³ and van Zandvoort et al.,²⁵ among others. The simplified structural elements form potential humin-like substrates that can be used to gain a more profound understanding of the catalytic oxidative conversion of humins. In Figure 1, the substrate types derived from the humin structure are sorted according to their complexity. Starting with the monofuran derivatives with the lowest complexity over multifuran derivatives to complex humins, substances are classified chronologically according to their use and increasing complexity into first-, second-, and third-generation substrates.

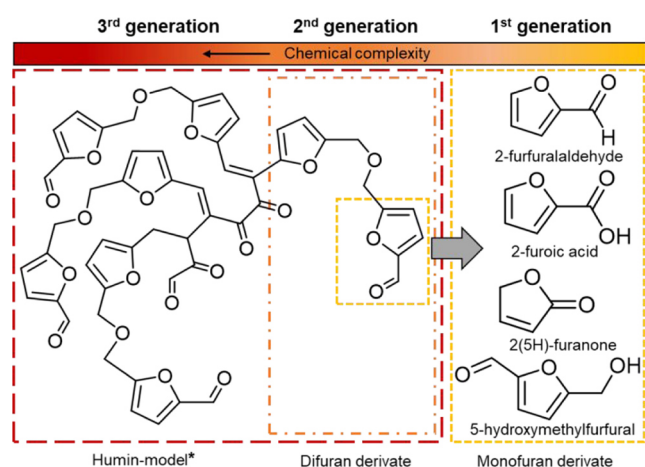


Figure 1. Classification of model substrates for the catalytic oxidation of humins according to their chemical complexity: From simple monofuran derivatives (first-generation) over difuran derivatives (second-generation) to complex model humins (*according to Maerten et al.⁴) as third-generation substrates.

In the first step, a range of different POM catalysts were tested in the oxidative conversion of furfural as a first-generation substrate. In principle, two humin precursors are suitable as first-generation substrates for initial experiments: furfural and 5-HMF. Furfural was chosen because it is significantly involved in the formation of humins, has a lower oxygen functionalization, and thus better reflects the overall functionality in humins and is less water-soluble than 5-HMF. In addition, 5-HMF is likely to be the more reactive and therefore simpler substrate due to its bifunctionality (both are oxygen-functionalized). The extent to which this bifunctionality would be accessible in a real humin is questionable; therefore, the monofunctionality of furfural is so far considered more likely. Nevertheless, 5-HMF is an important structural motif that was also included in the further course of investigations.

Based on the results, a catalyst was selected and used to study the catalytic oxidation of several first-generation substrates such as 5-HMF, 2-furoic acid, 2(5H)-furanone, 4-methoxyphenol, and benzofuran. Thus, different structural motifs and functionalities were investigated in catalytic oxidation experiments. This is used to determine structure–activity–selectivity correlations of the catalyst with these different functional groups and structures. In the second step, the more complex second-generation substrates were used to study the conversion of larger bridged structures and thus the degradation of the humin structure. For this purpose, difuran derivatives were mainly used as they could be synthesized in a more targeted manner. Care was taken to ensure that both oxygen-rich and oxygen-less bond types were represented. In this way, the substrates better represent the real binding conditions in humins and the associated requirements for the catalysts. Furthermore, the selected second-generation substrates are water-insoluble and thus replicate well the properties of humins and the challenges associated with their conversion.

Influence of Transition Metals in Keggin-Type Phosphomolybdates on the Oxidation of Furfural. In order to find a suitable catalyst for a comprehensive study on the catalytic valorization of humins, the transition metal used and thus the redox activity of the POM structure plays a crucial

role. Therefore, several monosubstituted Keggin-type phosphomolybdate POMs $H_x[PMo_{11}O_{40}]$ ($M = Ni, Co, Mn, Nb, V$) were selected for the initial catalyst screening. The Keggin-type heteropolyanion was used for the investigations, since its structure type is already well characterized and synthesis routes are well established.^{41,55} The used transition metals could participate with electron-transfer processes in redox reactions via the redox couples Ni^{II}/Ni^I , Co^{II}/Co^I , Mn^{II}/Mn^I , Nb^V/Nb^{IV} , and V^V/V^{IV} , respectively.⁵⁶ It can be assumed that the substitution of Mo as a framework metal by the described transition metals influences the electronic structure of the POM molecule and thus its redox behavior.⁴² In this regard, the catalysts were compared by means of their activity and selectivity in the oxidation of furfural at 90 °C under 30 bar O_2 for 15 h reaction time. As mentioned before, the complex structures of humins as well as the possible induction of functional groups by the oxidative degradation of these structures require the interaction of potential catalysts with different functionalized furan rings. Reproducing this multifunctionality to a reasonable extent with a well-defined substrate that can be reliably analyzed is proving to be an obstacle. For this reason, furfural was used as a substrate in the first stage. The initial tests were primarily a screening phase to find an active as well as selective catalyst. Subsequently to this screening phase, the selected catalyst was used for individual analysis of structure–activity–selectivity correlations for different substrates. Catalysts that could not convert furfural as the first-generation model substrate of lower chemical complexity were treated unsuitable for the conversion of even more complex second-generation substrates or humins and therefore excluded from further studies.

High-performance liquid chromatography (HPLC) was used to analyze the composition of the reaction solution. An aqueous furfural mixture was used as stock solution in order to close the carbon mass balance. The respective calculations can be found in the corresponding section of the experimental part. An example chromatogram for the reaction of furfural using $H_4[PVMO_{11}O_{40}]$ as a catalyst is attached to Figure S1. Table 2 shows the results of the initial catalyst screening. As a reference, a reaction without catalyst (entry 1, blank) as well as a reaction using unsubstituted phosphomolybdic acid (entry 2) were also carried out. A detailed description of the procedure for the experiments can be found in the corresponding part of

Table 2. Product Yields of Catalyst Screening Experiments Using Monosubstituted POM Catalysts

entry ^a	catalyst ^b	X/% ^c	yield/%			
			MA ^c	FA ^c	AA ^c	CO ₂ ^d
1 ^e	blank	56.4	5.6	7.8	0.6	6.5
2	$H_3[PMo_{12}O_{40}]$	29.6	11.7	4.4	1.8	1.2
3	$H_4[PVMO_{11}O_{40}]$	69.3	22.6	14.7	5.4	5.6
4	$Na_4[PNbMo_{11}O_{40}]$	15.7	4.2	1.6	0.0	1.5
5	$H_7[PMnMo_{11}O_{40}]$	30.6	10.3	3.7	1.1	1.2
6	$H_7[PNI Mo_{11}O_{40}]$	27.3	10.7	3.9	1.3	1.1
7	$H_7[PCoMo_{11}O_{40}]$	24.7	9.4	3.5	1.3	1.0

^aExperimental conditions: 10-fold reaction system, 90 °C, 30 bar O_2 , 15 h, 1000 rpm, 10 mL of stock solution of furfural (12.5 mmol carbon), and 0.14 mmol metal (M) for substitution (90 mol_{carbon} mol_M⁻¹). ^bAnalyzed as described in the corresponding section of the experimental part. ^cDetermined by HPLC-RID. ^dDetermined with GC-TCD. ^eLiquid-phase products determined by ¹H NMR.

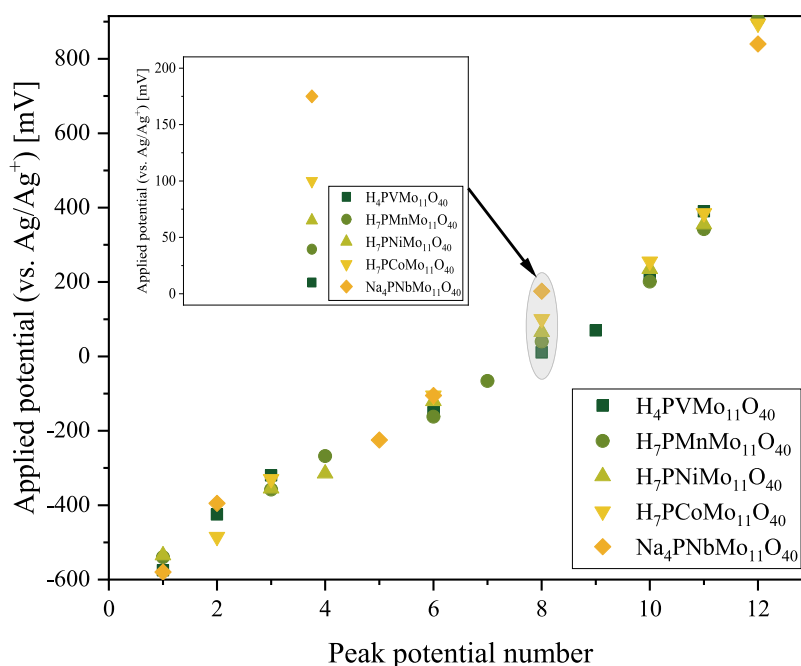


Figure 2. Shift of the peak potentials in the SWV data of $M(z)$ -substituted phosphomolybdates $H_x[PM_YMo_{11}O_{40}]$ with $x = 4, 7$ and $Y = V^{5+}, Nb^{5+}, Mn^{2+}, Ni^{2+}, Co^{2+}$ (concentration 1 mmol L^{-1} , scan rate 100 mV s^{-1} (CV) at pH 1).

the **Experimental Section**. In addition, a graphical comparison of the yields of all products and the corresponding mass balance are attached to **Figure S2**. Interestingly, already the blank without catalyst gave a furfural conversion of around 56% with FA being the main product with around 8% yield. About 7% ended up as CO_2 in the gas phase, which is the highest yield of CO_2 found in all reactions. Furthermore, about 8% 2(*SH*)-furanone was formed (**Figure S2**). 2(*SH*)-Furanone is most probably a stable byproduct based on its structure (**Figure S11**). In addition, a number of unidentified byproducts were formed, accounting for up to 25% of the carbon balance (**Figure S2**). Hence, about 40% of the carbon was lost to undesired byproducts in the reaction without catalyst, indicating low selectivity. Astonishingly, the use of pure phosphomolybdic acid (entry 2) led to a decrease in furfural conversion down to 30%. On the other hand, maleic acid (MA) yield almost doubled up to 12%, while the formation of other carboxylic acids such as FA and AA slightly decreased. Furthermore, the formation of unidentified byproducts was more or less eliminated (**Figure S2**). In this context, catalytic performance does not mean an increase in activity here, but rather a drastic increase in selectivity. The suppression of thermally induced side reactions of furfural or reactive intermediates by influencing the pH and polarity of the solution could have been responsible for this effect. This apparently facilitated the reaction path to maleic acid, reflected by almost doubled yields of MA. According to the results, the incorporation of transition metals such as Mn, Ni, Co, and Nb did not lead to a significant change in this property; therefore, the results of these catalysts were in the same range as the unsubstituted phosphomolybdic acid (entries 4–7). More specifically, furfural conversion of the catalysts substituted with Mn was about 30%, 27% with Ni, 25% with Co, and only 15% for Nb as the substitution metal within the Keggin structure. All of these catalysts achieved MA yields of around 10% except Nb, which corresponds to MA selectivity of 30–40%. Vanadium-substituted $H_4[PVMo_{11}O_{40}]$ achieved by far the

highest conversion (69%) and an MA yield of more than 22% (entry 3). Accordingly, the V-substituted catalyst combines an increase in selectivity using phosphomolybdic acid by suppressing side reactions and promoting of the reaction path to MA with an increase in activity through vanadium.

FA occurs as an additional product in all reactions. In particular, the reaction catalyzed by the V-substituted POM forms the highest amount of FA with a yield of almost 15%. It is conceivable that FA is formed by a cleavage mechanism from C_5 substrates to C_4 products, by side reactions, or by further oxidation of products and intermediates.⁵⁷ Due to the low yields of CO_2 , it can be assumed that the overoxidation of carbon to CO_2 in the tested systems can be neglected. All reactions showed only low yields of AA. It can be assumed that AA is a result of catalytic degradation of intermediates from side reactions or a product of a thermally induced reaction pathway.

The electrochemical investigation of the POM catalysts used should provide deeper insights into how the incorporated metals influence the electrochemical behavior and thus their redox activity. For this purpose, cyclic voltammograms (CV) and square-wave voltammograms (SWV) of the catalysts were recorded. The voltammograms can be found in **Figures S5 and S6**. All maxima, minima, and mean values from the CV data and the maxima from the SWV data are listed in **Tables S1 and S2**, respectively. The CV data were difficult to interpret due to the numerous metals in the POM structure that generate multiple signals. Therefore, the measured SWV were used to further investigate the redox processes. For simplification, the potential maxima were determined from the SWV and depicted in **Figure 2**. At first glance, it is noticeable that most of the peak potentials of the individual catalysts are very close to each other and hardly any clear distinction or tendency can be identified. Only peak potential number 8 (**Figure 2**) shows a difference between the potentials of the individual catalysts. This redox process can be assigned to a two-electron transfer $[PMMo_{11}^{VI}O_{40}]^{z-}/[PMMo_{10}^{VI}Mo^{IV}O_{40}]^{(z+2)-}$ (gener-

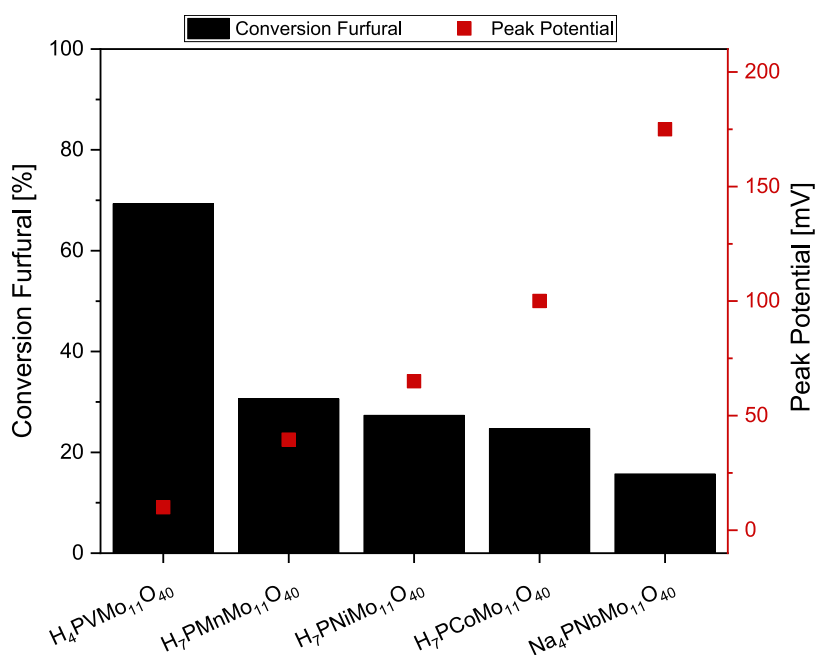


Figure 3. Plot of furfural conversion and peak potentials as a function of the POM catalysts used. Experimental Conditions: 10-fold reaction system, 90 °C, 30 bar O₂, 15 h, 1000 rpm, 10 mL of stock solution with furfural (12.5 mmol carbon), and 0.14 mmol metal (M) for substitution (90 mol_{Carbon} mol_M⁻¹).

ally [POM]^{z-} + 2e⁻ → [POM]^{(z+2)-}.^{42,55,58,59} Compared to H₄[PV^VMo₁₁O₄₀], the peak potentials for the other mono-substituted POMs with Mn^{II}, Ni^{II}, Co^{II}, or Nb^V shift to higher values. Especially, V as a substitution metal generates a significantly lower peak potential of 10 mV compared to other metals. All other metals generate a multiple of this potential. For example, if V is replaced by Mn as metal for substitution, the peak potential already shifts from about 10 to 40 mV, i.e., four times this value. It is plausible that the peak potential is a measure of the reducibility of the metal-POM complex H_x[PMMo₁₁O₄₀] and indicates how well the complex can oxidize a substrate compared to other POM compounds.

Based on the significantly higher activity of H₄[PVMo₁₁O₄₀], it can be assumed that a low potential represents a strong oxidizing ability of the catalyst. In Figure 3, the obtained conversions for furfural are plotted as a function of the peak potentials for the examined catalysts. In comparison, the Nb-substituted POM showed the lowest conversion of furfural. Interestingly, this complex also exhibits the highest peak potential with almost 180 mV. Overall, an opposite trend between activity and peak potential can be deduced from the data presented. This substantiates the thesis formulated at the beginning that a strong oxidizing ability of the catalyst correlates with a low peak potential. Therefore, it is plausible that the incorporation of other transition metals than vanadium did only slightly influence the catalytic properties of unsubstituted phosphomolybdic acid. We can conclude that the catalytic activity is not promoted by the transition metal itself but by the transition-metal-POM complex. Thus, the redox activity of the catalyst can be directly controlled by incorporating different transition metals, which paves the way for an application-oriented production of tailor-made POM catalysts.⁴²

The selective catalytic oxidation of furfural was repeated several times in independent experiments, demonstrating the reproducibility of the results. As an example, the results for the

most promising H₄[PVMo₁₁O₄₀] catalyst can be found in Figure S3. The results could be reproduced for the main products with average yields for MA of 22.1 ± 1.0%, for FA of 14.5 ± 0.4%, for AA of 5.8 ± 0.5%, and for CO₂ of 6.4 ± 0.5%. As an example of one of the less active catalysts, the results of the reproduction experiments using the Nb-substituted catalyst can also be found in Figure S4. Here too, all yields were reproducible.

In addition to quantitative analysis by HPLC, the reaction solutions were qualitatively analyzed by nuclear magnetic resonance (NMR) spectroscopy. For this purpose, one-dimensional NMR measurements such as ¹H NMR and ¹³C NMR as well as two-dimensional NMR measurements such as heteronuclear single quantum coherence (HSQC) and heteronuclear multiple bond correlation (HMBC) were performed. Figure 4 shows an exemplary ¹H NMR spectrum for the reaction solution using H₄[PVMo₁₁O₄₀] as a catalyst. *tert*-Butanol was added to the samples as an internal standard to compare the NMR spectra of different samples. The signals were assigned to the respective protons of the reactants, intermediates, and products. Thereto, the individual protons were named alphanumerically. The numbering was done according to the descending chemical shift within a molecule. For reasons of clarity, only protons that could be seen in the ¹H NMR have been included in the numbering. Protons from hydroxide and carboxylic acid groups were not detectable in aqueous phase. The reason for this can be the proton exchange with the deuterated solvent, which is inactive in the NMR. In addition to the previously mentioned products, the presence of 5-hydroxyfuran-2(*5H*)-one was also confirmed by NMR experiments. 5-Hydroxyfuran-2(*5H*)-one was one major side product or intermediate. The associated ¹³C NMR spectrum and the 2D spectra can be found in Figures S5–S7. In addition, the products identified by HPLC, ¹H NMR, and ¹³C NMR could be successfully detected via respective couplings in 2D experiments (HSQC and HMBC). In the ¹H NMR, further

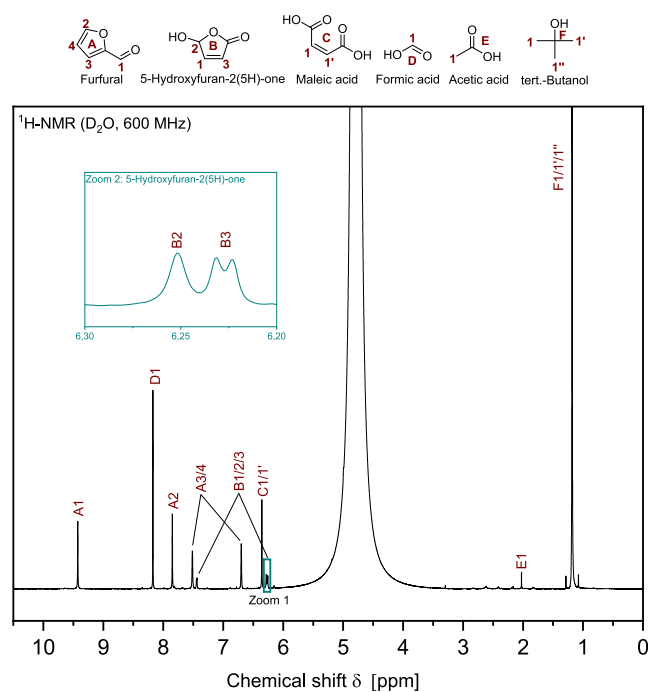


Figure 4. Exemplary ^1H NMR spectra (D_2O , 600 MHz) of the reaction solution of the catalyst screening experiment using $\text{H}_4[\text{PVMo}_{11}\text{O}_{40}]$. Experimental Conditions: 10-fold reaction system, 90°C , 30 bar (O_2), 15 h, 1000 rpm, 10 mL stock solution of furfural (12.5 mmol carbon), and 0.14 mmol metal (M) for substitution ($90 \text{ mol}_{\text{Carbon}} \text{ mol}_{\text{M}}^{-1}$).

small signals can be seen that differ only weakly from the baseline (Figure 4). In particular, a series of signals in the range of a chemical shift δ of 2.1–3.0 ppm should be mentioned. The signals are consistent with succinic acid and levulinic acid, which were also detected in traces via HPLC. However, the concentrations were too low to generate signals in the much less sensitive ^{13}C NMR and consequently, no unequivocal structure elucidation and detection of these molecules was possible. However, the yields of these products were less than 1%. In the area investigated, no influence of various catalysts on the product spectrum can be derived from the experiments.

Influence of the Substitution Degree on the Oxidation of First-Generation Model Substrates. Another possibility for modifying the catalyst arises from the degree of substitution. More precisely, this parameter describes the number of framework metals (Mo) that have been replaced by

a redox-active transition metal (V). It is expected, that the catalytic properties can be influenced by multiple substitutions. In this set of experiments, V-POM complexes of the type $\text{H}_{(3+n)}[\text{PV}_n\text{Mo}_{(12-n)}\text{O}_{40}]$ with $n = 1-6$ have been tested. The detailed description of the synthesis as well as the characterization of the prepared catalysts can be found in the corresponding section of the experimental part. For reasons of comparability, the amount of V and thus the ratio of carbon (substrate) to catalyst was kept constant compared to previous experiments. Consequently, all observations were limited to the effects of the degree of substitution and thereby to the modification of the catalyst. The unsubstituted phosphomolybdic acid $\text{H}_3[\text{PMo}_{12}\text{O}_{40}]$ was also used for a reference experiment. Table 3 shows the conversion as well as the yields of the most interesting products MA, FA, AA, and CO_2 .

The unsubstituted phosphomolybdic acid showed the lowest conversion of only 30% (Table 3, entry 1). It can be deduced that its catalytic activity is not solely based on the Brønsted acidity of the polyoxometalate catalysts, but that redox processes are involved to a crucial extent. These, in turn can be strongly influenced by the incorporation of V, as shown by the aforementioned results. However, the acid had a certain catalytic effect on the reaction, as shown by the achieved MA yield of 11.7%. By increasing the degree of substitution from 0 to 1 or 2, the conversion was increased to 69%, respectively, 100% (Table 3, entries 2 and 3). This affirms the importance of V for the catalytic activity of the tested catalysts. Since the total amount of V was kept constant in these experiments, the effect of a higher degree of substitution must be attributed to the change in the catalyst due to multiple substitution. Poller et al.⁶⁰ have used magnetic and optical spectroscopy in combination with calculations based on density functional theory (DFT) to postulate a mechanism for the catalytic cycle of V-substituted Keggin-type POMs. According to this postulate, adjacent V pairs can be formed in more highly substituted POMs. Upon reoxidation of the POM with molecular oxygen, a peroxy-ligand forms between the adjacent V atoms ($\text{V}^{\text{IV}} \rightarrow \text{V}^{\text{V}}$, $\text{O}^0 \rightarrow \text{O}^{1-}$).⁶⁰ Subsequently, the substrate is further oxidized by the peroxy-species ($\text{O}^{1-} \rightarrow \text{O}^0$). Therefore, the activation energy for the oxidation is lowered due to the single state of the O_2 -POM complex. Overall, it can be assumed that the catalytic activity is significantly enhanced by the possible formation of peroxy-species in multiple substituted POMs for the present reaction compared to the singly substituted POMs.

Table 3. Product Yields of Catalyst Screening Experiments Using POM Catalysts with Different Degrees of V-Substitution of the Type $\text{H}_{(3+n)}[\text{PV}_n\text{Mo}_{(12-n)}\text{O}_{40}]$ with $n = 0-6$

entry ^a	catalyst ^b	X/% ^c	yield/%				
			MA ^c	FA ^c	AA ^c	CO_2 ^d	other ^c
1	$\text{H}_3[\text{PMo}_{12}\text{O}_{40}]$	29.6	11.7	4.4	1.8	1.2	1.6
2	$\text{H}_4[\text{PVMo}_{11}\text{O}_{40}]$	69.3	22.6	14.7	5.4	5.6	12.6
3	$\text{H}_5[\text{PV}_2\text{Mo}_{10}\text{O}_{40}]$	100.0	4.9	40.9	1.5	20.7	22.2
4	$\text{H}_6[\text{PV}_3\text{Mo}_9\text{O}_{40}]$	100.0	0.0	43.0	1.3	26.8	16.0
5	$\text{H}_7[\text{PV}_4\text{Mo}_8\text{O}_{40}]$	100.0	0.0	42.3	1.5	26.4	17.0
6	$\text{H}_8[\text{PV}_5\text{Mo}_7\text{O}_{40}]$	100.0	0.0	42.9	1.3	28.0	13.7
7	$\text{H}_9[\text{PV}_6\text{Mo}_6\text{O}_{40}]$	100.0	0.0	42.7	1.5	30.2	13.3

^aExperimental conditions: 10-fold reaction system, 90°C , 30 bar O_2 , 15 h, 1000 rpm, 10 mL stock solution with furfural (12.5 mmol carbon), and 0.14 mmol vanadium(V) for substitution ($90 \text{ mol}_{\text{Carbon}} \text{ mol}_{\text{Vanadium}}^{-1}$). ^bAnalyzed as described in the corresponding section of the experimental part. ^cDetermined by HPLC-RID. ^dDetermined with GC-TCD.

Interestingly, the MA yield decreased with an increasing degree of V substitution, while the FA yield increased. More precisely, a yield of MA exceeding 22% was achieved in the experiment using the monosubstituted POM (Table 3, entry 2), while for the doubly substituted POM already a significantly lower MA yield of only 5% (Table 3, entry 3), and for all of the more highly substituted catalysts almost no MA could be detected (Table 3, entries 4–7). Basically, it can be assumed that the significantly increased catalytic activity of the higher-substituted POMs leads to the catalytic oxidative degradation of MA and thus MA is no longer a product but an intermediate. Consequently, the yield of FA increases significantly to over 40% (Table 3, entries 4–7). In addition, a significantly increased yield of CO₂ of up to 30% was also obtained using the higher-substituted POMs. A higher degree of substitution seems to promote overoxidation to CO₂. However, a further increase in the degree of substitution higher than three did not lead to a significant change in the product yields of FA and CO₂. At first glance, this does not seem plausible since the statistical probability of V atoms being adjacent increases with the degree of substitution. Consequently, the peroxo-ligand would have to form more frequently and thus the overoxidation would have to increase. However, the amount of V in the reactor was kept constant, which means that the number of POM molecules decreases as the degree of substitution increases. As a result, increasing probability of peroxo-ligands seems to balance with decreasing number of POM molecules. Interestingly, the formation of byproducts and intermediates, which are summarized under “Other”, also increased with increasing degree of vanadium substitution. A graphical comparison of the yields and other byproducts or intermediates is attached to Figure S10. Accordingly, succinic acid and levulinic acid as byproducts were produced as well as 2(*SH*)-furanone and 5-hydroxyfuran-2(*SH*)-one as intermediates. 5-Hydroxyfuran-2(*SH*)-one in particular accounted for a large proportion of other products and intermediates, with yields of around 13% to over 20%. Levulinic acid is a plausible byproduct of the thermally and acid-induced ring-opening of furfural, which also leads to acetic acid through subsequent oxidation. This has already been observed in experiments by Voß et al.⁶¹ in the catalytic oxidation of the C₅ substrate xylose (also xylofuranose), which in its ring form can be regarded as an analogue to furfural. Furanone is also a plausible intermediate from the C₁ elimination of furfural, which can react further to form succinic acid. A discussion of a possible reaction path to succinic acid can be found in the literature.^{62,63} However, with the exception of 5-hydroxyfuran-2(*SH*)-one, yields of only 1–2% were achieved for these byproducts and intermediates.

In summary, the formation of a new, significantly more active species with a higher degree of substitution (>1) in the form of a peroxo-ligand as reported by Poller et al.⁶⁰ is very plausible. On the one hand, furfural conversion could be improved by increasing the degree of substitution from a value of 1 to 2 and higher. On the other hand, the yield of MA decreased considerably with the degree of substitution due to the drastically higher redox activity. We can conclude that a degree of substitution higher than one lowers the yield and hence the selectivity of MA due to overoxidation of the substrate. With regard to selectivity, a degree of substitution of one is chosen as the optimal compromise between activity and selectivity.

Another important point of investigation in advance of further studies on the catalytic oxidation of the first-generation substrates is the stability of the products. Therefore, the main products of the oxidation of the first-generation substrates MA and FA were used as substrates in the next set of experiments. For this purpose, MA and FA were used as substrates, applying the same reaction conditions as in previous experiments using H₄[PVMo₁₁O₄₀] as a catalyst. As reference experiments and to evaluate thermal effects, reactions without the catalyst (blank) have also been performed. The results are shown in Table S3. FA could not be converted thermally or using the selected catalyst under the applied conditions and can be classified as stable. MA could also hardly be thermally oxidized to FA, with a conversion of about only 4%. In comparison, the catalyzed reaction achieved an equally low conversion of 6%. However, the products here consist of approximately 4% FA and 1.7% CO₂. In summary, the main products were treated as stable under the reaction conditions applied.

Extended Study on the Catalytic Oxidation of First-Generation Model Substrates Using H₄[PVMo₁₁O₄₀] as a Catalyst. In the next step, various substrates of the first generation were reacted individually using the selected H₄[PVMo₁₁O₄₀] catalyst to provide more detailed insights into the reaction and an unbiased view of the relationships between structure and activity. In addition, this should enable conclusions to be drawn about possible reaction pathways and thus contribute to a further understanding of the transformation of biobased monofuran derivatives and humin-like substances. The molecular structure of the substrates tested is shown in Figure 5.

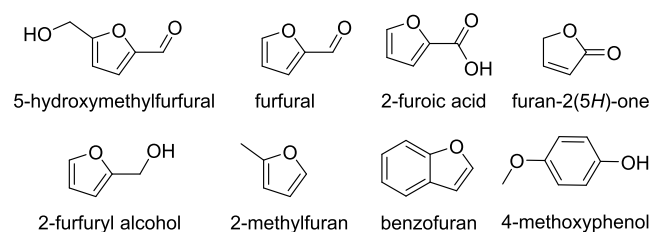


Figure 5. Molecular structure of various first-generation substrates.

Figure 6 shows the conversions upon catalytic oxidation of the first-generation substrates 5-HMF, furfural, 2-furoic acid, 2(*SH*)-furanone, 2-furfuryl alcohol, 2-methylfuran, benzofuran, and 4-methoxyphenol, as well as product yields using H₄[PVMo₁₁O₄₀] as a catalyst (including unreacted substrates). Reference experiments of each substrate without the catalyst (blank) can be found in Figure S11. At first glance, it is obvious that the water-soluble substrates such as 5-HMF, furfural, 2-furoic acid, and 2(*SH*)-furanone form MA as the main oxidation product. These substrates are not only water-soluble but also exhibit oxygen functionalization, which facilitates the removal of C₁ building blocks and leads to structures from which MA can be formed more easily. In this context, the term “oxygen functionalization” is used to describe a side-chain function and excludes oxygen in the heterocyclic furan ring.

The bifunctional substrate 5-HMF provides two oxygen functionalities where the POM catalyst can attack, enabling high substrate conversion of over 98%. A high MA yield of 22.6% was obtained. However, the main product of the catalytic oxidation of 5-HMF was FA with a yield of over 35%. Interestingly, the catalytic oxidation of furfural gave almost the

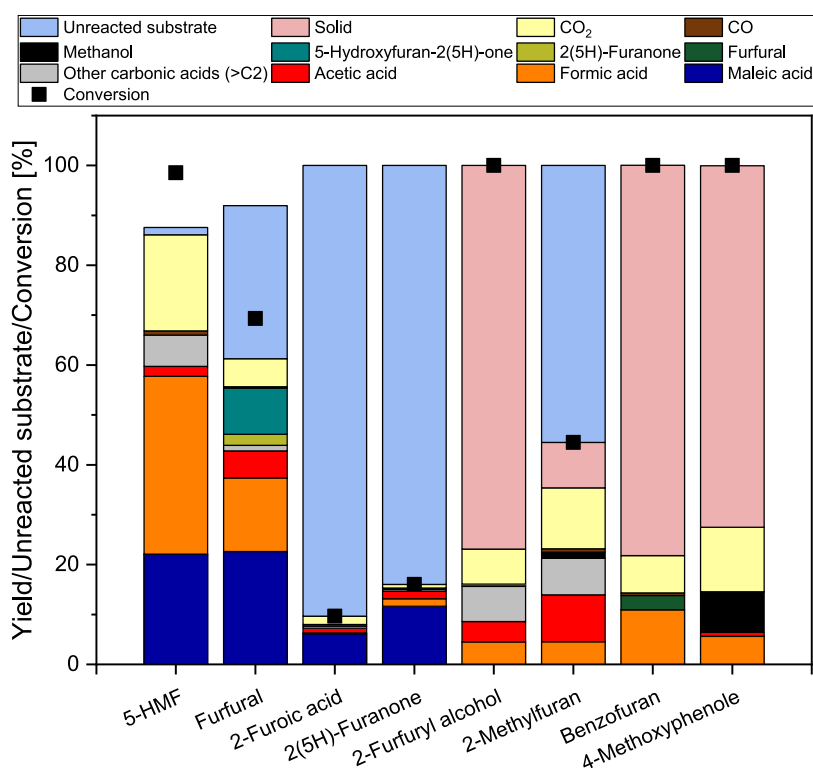


Figure 6. Oxidation of different first-generation substrates using $H_4[PVMo_{11}O_{40}]$ as a catalyst for the determination of activity–functionality–selectivity relationships. Experimental conditions: 10-fold reaction system, 90 °C, 30 bar (O_2), 15 h, 1000 rpm, 10 mL of substrate solution containing 12.5 mmol carbon derived from the respective substrate, and 0.14 mmol vanadium(V) for substitution ($90 \text{ mol}_{\text{Carbon}} \text{ mol}_{\text{Vanadium}}^{-1}$).

same yield of MA with only about 15% yield of FA. This is most likely due to the fact that 5-HMF is a C_6 substrate, which means that two C_1 building blocks must be removed from the molecule to obtain the C_4 product MA. In comparison, furfural is a C_5 substrate, so only half of the number of C_1 building blocks needs to be removed. It is striking that the FA yield in the catalytic oxidation of 5-HMF was more than twice as high as in the oxidation of furfural. This is probably due to the bifunctionality of 5-HMF, which leads to a much more reactive ring structure in bilateral C_1 -bond cleavage than in furfural. Consequently, the oxidation of 5-HMF led to more short-chain oxidation products such as FA and also to total oxidation products such as CO_2 . The CO_2 yield was about 20%, which is almost four times higher than in the oxidation of furfural. Furthermore, 5-hydroxyfuran-2(*SH*)-one with a yield of about 10% was detected in the product solution of the oxidative conversion of furfural.

5-Hydroxyfuran-2(*SH*)-one is probably an intermediate on the pathway to MA, which is formed by the one-time cleavage of a C_1 building block of furfural (aldehyde group). Indeed, neither 5-hydroxyfuran-2(*SH*)-one nor any other possible intermediate could be detected during the oxidative conversion of 5-HMF. Consequently, the hypothesis postulated above can be confirmed that the bilateral C_1 -bond cleavage of 5-HMF leads to significantly more reactive intermediates, which in turn favor the formation of shorter oxidation products. The product spectrum could also be confirmed qualitatively by NMR experiments (^{13}C and 1H) in addition to HPLC. The less functionalized furfural can be oxidized with a conversion of about 70%. This is due to the high reactivity of the aldehyde group of furfural. In fact, more than 56% of furfural could already be thermally converted (Figure S11). However, the

noncatalyzed reaction proved to be far less selective. The situation was similar for the thermal conversion of 5-HMF, where the conversion additionally decreased to about 35%. 2-Furoic acid and 2(*SH*)-furanone pose an even bigger challenge for purely thermal conversion (Figure S11). More specifically, 2-furoic acid with a conversion of at least 0% and 2(*SH*)-furanone with a conversion of only about 3% could not or hardly be thermally converted. It is plausible that these substrates are stabilized by their aromaticity and are not thermally oxidizable at 90 °C because they additionally lack a reactive side chain. In the case of 2-furoic acid, the formation of hydrogen bonds that prevent a purely thermal reaction is also conceivable. Overall, the substrates were hardly or not selectively oxidized in the purely thermal reaction (blank).

Catalytically, 2-furoic acid and 2(*SH*)-furanone also pose a challenge as substrates. Hereby, even using the catalyst, only conversions of 10%, respectively 16%, could be achieved. However, in both cases, the main product was MA with yields of 6.1% for 2-furoic acid and 11.7% for 2(*SH*)-furanone as a substrate. This corresponds to a high selectivity for MA of more than 60% and more than 70% starting from 2-furoic acid or 2(*SH*)-furanone. High selectivity is very important in the oxidative valorization of biomass, as overoxidation of substrates and value-added products is a major challenge. In particular, the oxidation of humins with higher-substituted POM catalysts such as $H_8[PV_5Mo_7O_{40}]$ leads to an increased formation of CO_2 (selectivity up to 80%) as shown by Maerten et al.⁴ For this reason, the results using $H_4[PVMo_{11}O_{40}]$ as catalyst are very promising.

Furfuryl alcohol, another water-soluble furan derivative, tended to form significant amounts of solids (Figure 6). According to CHNS analysis, this solid consists of 57% carbon

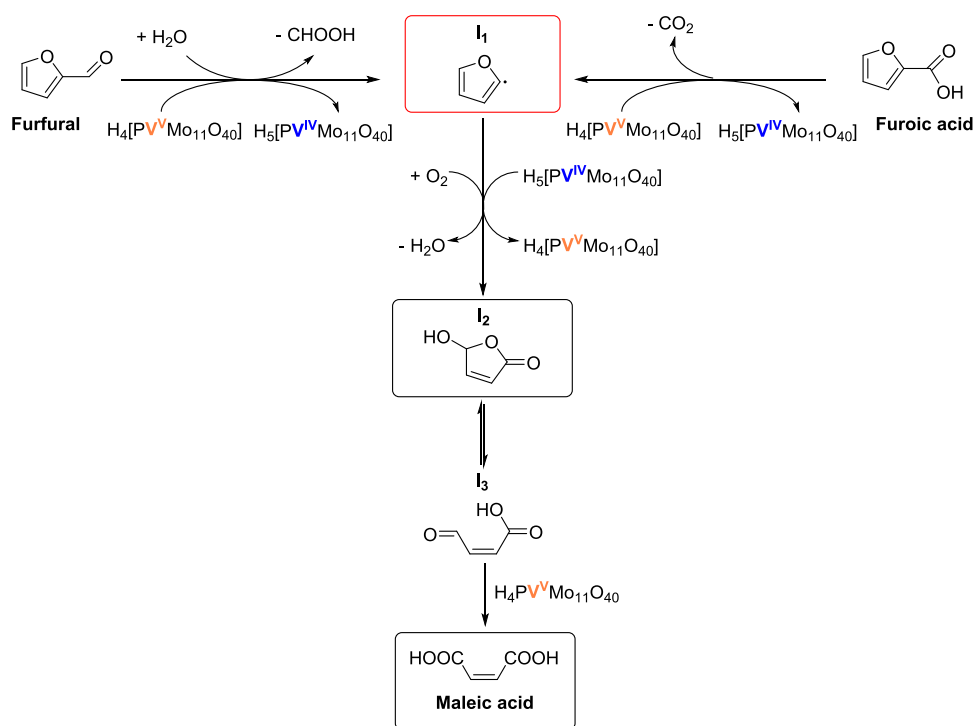


Figure 7. Schematic drawing of the proposed reaction pathways for oxidation of furfural and 2-furoic acid with molecular oxygen using $H_4[P^{VV}Mo_{11}O_{40}]$ in aqueous medium.

on average, which is about 4% less than the initial value of about 61% for furfuryl alcohol. The decrease in carbon content is very small, and it is also conceivable that part of the decrease is due to contamination of the sample by the adsorbed catalyst, which remains despite repeated purification of the solids. It is also plausible that the solids partially consist of dimers of furfuryl alcohol or is based on furan rings coupled/fused building direct furan–furan bonds, which might pose a challenge for oxidative valorization due to low or absence of oxygen functionalization. In particular, direct furan–furan structures are discussed in the literature as part of the humin structure and might be interesting model substances for an optimized reaction system in future studies.^{6,28,64} It can be concluded that furfuryl alcohol was hardly oxidatively converted and the solid was mainly formed from the unoxidized substrate. Thus, no MA was detected in the product spectrum. The major oxidation products obtained were FA, AA, CO_2 , and other carboxylic acids with yields of about 5, 4, 7, and 7%, respectively. Other carboxylic acids include the C_5 product levulinic acid and the C_4 product succinic acid. The last furan derivative tested was 2-methylfuran. Despite the lack of oxygen functionalization and poor water solubility, 2-methylfuran could be catalytically oxidized with a moderate conversion of over 44%. Mainly, short-chain oxidation products such as FA, AA, and CO_2 were formed.

In comparison, the model substrates benzofuran and 4-methoxyphenol, which have a benzene structure, formed less oxidation products with total yields between 20% and 30%. The oxidation products formed were mainly FA and CO_2 . Ultimately, these substrates lack oxygen functionalization, which, in combination with the expected high stability of the benzene ring and low to negligible solubility in water, resulted in less efficient oxidation. In the case of 4-methoxyphenol, the ester function could be partially cleaved by acid-catalyzed

hydrolysis, leading to methanol. Both substrates tended to form significant amounts of solid residues. Interestingly, CHNS analysis showed that the carbon content in the residues is lower than in the substrates before oxidation. The carbon content decreases from about 81 to 64% for benzofuran and from about 68 to 52% for 4-methoxyphenol. Part of the decrease in carbon content could also be due to contamination of the samples by the adsorbed catalyst remaining despite repeated purification of the solids. Nevertheless, it can be concluded that these substrates could also undergo oxidative conversion to a certain extent with the chosen POM catalyst. It should be noted that these structural motifs must have additional side chains in a real humin to be incorporated into the humin network. These side chains could also lead to facilitated conversion. Moreover, the furan ring is discussed in the literature as the predominant structure in humins derived from the humin precursors 5-HMF and furfural.^{4,23–25} In fact, it is also discussed that aromatic compounds such as arenes and phenols are produced only during pyrolysis of humins and are not an elementary part of their structure.²³ For this reason, only furan derivatives such as furfural, 2-furoic acid, and difuran derivatives will be used for mechanistic considerations and further studies in the following.

As the results of the oxidation of furfural using $H_4[P^{VV}Mo_{11}O_{40}]$ had shown, the main products giving yields of about 23 and 15% were MA and FA, respectively. Since MA was found to be stable under the given conditions, the high yield of FA is unlikely to be due to further oxidation of MA. Moreover, a high conversion of about 70% could be achieved with a low yield of CO_2 less than 6%. It is much more likely that FA is a byproduct in the initialization of the reaction to MA. The C_5 substrate furfural must necessarily cleave off a C_1 building block to obtain the C_4 product MA. Due to the low yield of CO and CO_2 , it can be assumed that this step does not take place predominantly in the form of decarbonylation and

decarboxylation as discussed in the literature.^{63,65–67} A mechanism for the oxidation of furfural using H_2O_2 as the oxidant to furoic acid followed by decarboxylation was reported previously.^{63,66} A good overview of the mechanisms discussed in the literature is provided by the work of Gong et al.⁶³ In the experiments performed here, 2-furoic acid could not be detected, which means that decarboxylation must be even more classified as unlikely or as a nondominant reaction pathway. Therefore, the hypothesis that FA is initially eliminated from furfural seems more evident. According to this hypothesis, for each mole of furfural converted, one mole of FA must have been split off. As a result, a theoretical FA yield of about 14% can be calculated by the achieved conversion of furfural to about 70%. This is in excellent agreement with the detected FA yield of 15% in our experiment. 5-Hydroxyfuran-2(*SH*)-one is conceivable as a product of the initial elimination of a C_1 building block from furfural and may act as an intermediate to MA, as frequently discussed in the literature.^{63,65,66,68–70} Another C_4 product detected in the reaction solution and a possible intermediate to MA is 2(*SH*)-furanone. However, the significantly lower MA yield of about 12% in the oxidation of 2(*SH*)-furanone compared to the oxidation of furfural is an indication that 2(*SH*)-furanone is not part of the main reaction pathway. Figure 7 shows the reaction pathway postulated from previous information.

In the literature, the oxidation of furfural using H_2O_2 as an oxidizing agent was widely studied.^{63,68,69,71,72} Here, Baeyer–Villiger (BV) oxidation, in which oxygen is inserted between the carbons of the carbonyl group and the furan ring, seems plausible because of peroxide as the oxidant and the presence of percarboxylic acids. However, BV oxidation without H_2O_2 seems unlikely, so this reaction is excluded for the system presented here. We assume that the elimination of FA occurs under nucleophilic attack of a water molecule in the acidic medium and an electron transfer to the catalyst ($\text{V}^{\text{V}} \rightarrow \text{V}^{\text{IV}}$). Thus, a highly unstable furyl radical (I_1 , Figure 7) is formed and converted to 5-hydroxyfuran-2(*SH*)-one (I_2 , Figure 7) under the action of molecular oxygen and water.

The catalyst is reoxidized during this process ($\text{V}^{\text{IV}} \rightarrow \text{V}^{\text{V}}$). 5-Hydroxyfuran-2(*SH*)-one is in chemical equilibrium with β -formylacrylic acid (I_3 , Figure 7), whose terminal aldehyde group is readily oxidized by the catalyst to a carboxylic acid that forms MA.⁶⁸ Furthermore, we postulate that 2-furoic acid is oxidized to MA via the same pathway. The difference lies in the C_1 component that is eliminated, which is presumably CO_2 . Consequently, for every mole of 2-furoic acid converted to a C_4 product or smaller, one mole of CO_2 would be produced. Therefore, a conversion of 10% results in a theoretical CO_2 yield of 2%, which is in excellent agreement with the achieved yield of 1.7% in our experiment. The considerably lower conversion of 2-furoic acid (10%) suggests that 2-furoic acid is more stable than furfural and decarboxylation is more difficult than the elimination of FA. Hence, decarboxylation is most probably the rate-determining step. As a consequence, the low yield of 5-hydroxyfuran-2(*SH*)-one of less than 1% in the oxidation of 2-furoic acid is plausible since it is converted faster than it is formed. An analogous behavior could be observed for 2(*SH*)-furanone. However, a mechanism without 5-hydroxyfuran-2(*SH*)-one as an intermediate is also discussed in the literature for 2(*SH*)-furanone.^{68,71} The presented results do not allow a clear clarification of the reaction pathway of 2(*SH*)-furanone.

Furfural is considerably better converted than 2-furoic acid and 2(*SH*)-furanone, so it is expected that the reaction to 5-hydroxyfuran-2(*SH*)-one is not the rate-determining step. The high yield of 5-hydroxyfuran-2(*SH*)-one of 9% indicates that the oxidation to MA is most likely the rate-determining step. For this reason, 5-hydroxyfuran-2(*SH*)-one accumulates as it is formed faster than it is oxidized to MA. 5-HMF is expected to follow an analogous mechanism, with the difference that due to bifunctionality, a more reactive intermediate is most likely formed instead of 5-hydroxyfuran-2(*SH*)-one.

Catalytic Oxidation of Second-Generation Substrates Using $\text{H}_4[\text{PVMo}_{11}\text{O}_{40}]$ as a Catalyst. In order to convert complex humins into value-added products, not only the conversion of monofuran derivatives is required but also the interaction with different functionalities of the bonds between the furan ring systems to cleave the humin structure into smaller units. To this end, various second-generation substrates consisting mainly of bridged difuran derivatives were prepared and studied. The exact synthesis method is described in the corresponding section of the experimental part. The more complex second-generation substrates can be divided into two groups. On the one hand, there are substrates with C–C bonds. On the other hand, there are substrates with oxygen-functionalized bonds such as ether and ester. Figure 8 shows the synthesized and tested model substances (MS).

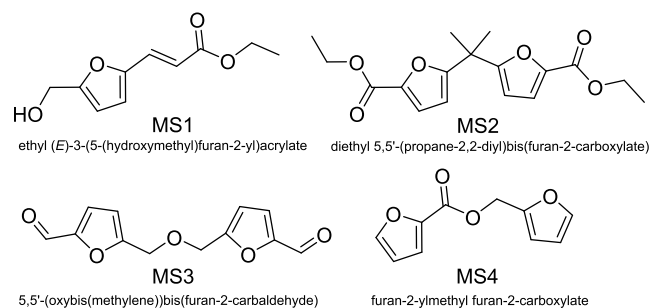


Figure 8. Synthesized second-generation substrates.

Here, MS1 replicates double bonds, MS2 replicates branched single bonds, MS3 replicates ether bonds, and MS4 replicates ester bonds as possible bond types for the cross-linking of furan rings in humins. The influence of these bond types (functionality) on the activity of the catalyst and on the product spectrum was investigated to gain further insights into the conversion of humins. Another important aspect is the water-insoluble character of humins, which was also given by the second-generation substrate. Therefore, the obstacles in the valorization of humins due to their physical properties were taken into account. The catalytic conversion of the model substances was carried out using the selected $\text{H}_4[\text{PVMo}_{11}\text{O}_{40}]$ catalyst employing the reaction conditions of previous studies. The results of the catalytic conversion are summarized in Figure 9. In addition, the reactions were also carried out without a catalyst; the results can be found in Figure S12.

It is obvious that the model substances without oxygen-functionalized bonds (MS1 and 2) were significantly worse converted into smaller oxidation products than the oxygen-functionalized model substances (MS2 and 3). Overall, only about 20% or 6% gaseous and liquid products could be formed during the oxidation of MS1 and MS2, respectively. The highly viscous and water-insoluble second-generation substrates agglomerate at the bottom of the reactor so that the

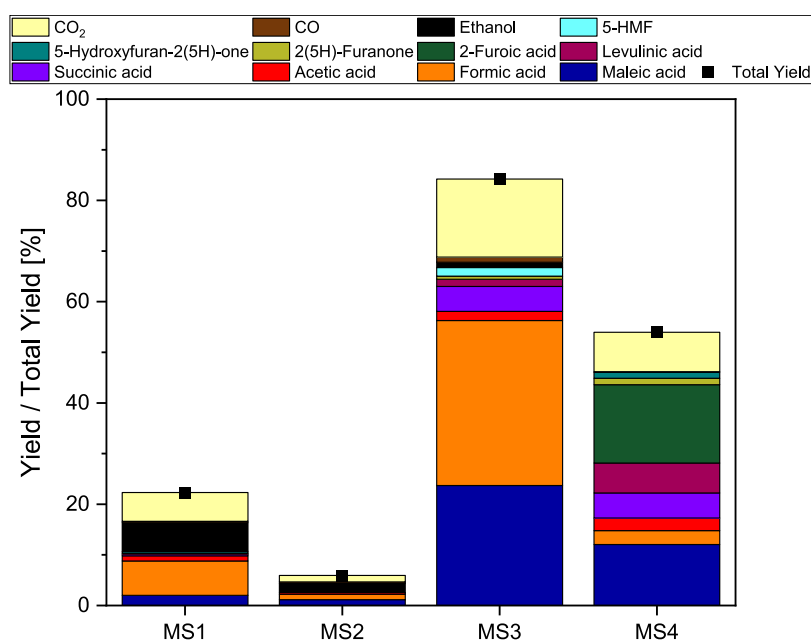


Figure 9. Oxidative conversion of different second-generation substrates using $H_4[PVMo_{11}O_{40}]$ as a catalyst. MS1: Ethyl (E)-3-(5-(hydroxymethyl)furan-2-yl)acrylate, MS2: diethyl 5,5'-(propane-2,2-diyl)bis(furan-2-carboxylate), MS3: 5,5'-(oxybis(methylene))bis(furan-2-carbaldehyde), and MS4: furan-2-ylmethyl furan-2-carboxylate. Experimental conditions: 10-fold reaction system, 90 °C, 30 bar (O_2), 15 h, 1000 rpm, and $H_4[PVMo_{11}O_{40}]$ as the catalyst ($90 \text{ mol}_{\text{Carbon}} \text{ mol}_{\text{Vanadium}}^{-1}$) in 7.5 mL of water.

homogeneous catalyst solution can only interact across the small-phase interface. Consequently, solids were thermally formed, which in turn stuck to the bottom, perpetuating poor accessibility. Thus, the missing yield consists partly of the highly viscous, water-insoluble substrate or predominantly of solids and therefore undesirable byproducts. The yield of solids is not taken into account for further consideration, as these are not value-added products and are treated as unreacted substrates. In addition, the formation of solids or the water insolubility of the unreacted substrate made the determination of conversion difficult. In particular, unreacted substrate accumulates after the reaction as a highly viscous film in the filters. As an example, 1H NMR and ^{13}C NMR spectra of the residue after the experiment converting MS2 compared to the reference spectrum are included in Figures S13 and S14. According to NMR analysis, the spectra are identical, which means that the viscous residue is MS2. Unfortunately, the residues evaporated when the filters dried; therefore, gravimetric determination was not possible. As a result, no conversions could be determined and total yield is used as a performance indicator. Based on the analyses, it seems plausible that the missing carbon is lost solids (periphery) or unreacted substrate so that the total yield roughly corresponds to the conversion.

It appears that the ethoxy residues of the esters were cleaved off at the side chains of MS1 and MS2 and thus converted to ethanol. In this case, an acid-catalyzed reaction using the $H_4[PVMo_{11}O_{40}]$ catalyst, which is a strong Brønsted acid, is plausible. Further oxidation of ethanol to acetic acid, which was also detected, is also conceivable. In particular, a relatively high FA yield of 7% was reached in the reaction of MS1, which can also be explained by the oxidation of side-chain groups such as the alcohol group in the fourth position of the furan ring. However, in MS1, the double bond seems to have been partially broken as MA was detected as a product. Nevertheless, the MA yield is only 3%. Consequently, it can be

assumed that the catalyst interacts poorly with C–C bond types without oxygen.

In comparison, MS3 and MS4 were drastically better converted to liquid-phase and gas-phase products, with total yields of over 80 and 60%, respectively. The main products detected were MA, succinic acid, FA and CO_2 . MS4 is particularly readily oxidized to MA and FA, with yields of 23 and 32%, respectively. Presumably, the ether bond was broken obtaining two molecules of 5-HMF, which could be further converted to MA and FA in a manner analogous to furfural. This assumption is supported by the detection of 5-HMF in the reaction solution for which a yield of 2% was determined. The uncatalyzed reaction reached a much higher yield of 5-HMF of over 7%, where the break of ether bond seems to be more plausible (see Figure S12). Moreover, a levulinic acid yield of 20% was obtained in the noncatalyzed reaction. Levulinic acid is known to be produced from 5-HMF, so the decomposition of MS3 into two moles of 5-HMF seems to be evident. Analogous to MS3, the ester bond of MS4 could be efficiently broken, obtaining 2-furoic acid with a yield of 15%. 2-Furoic acid could be converted to MA with a yield of 12%, analogous to the aforementioned reaction pathway (Figure 7). The yield of MA was lower for the oxidation of MS4 than for MS3, since the reaction proceeds more efficiently via 5-HMF (analogous to furfural) than via decarboxylation of 2-furoic acid. Based on the results of the noncatalyzed reaction, it appears that the ester bond is already easy to break thermally, since a yield of 2-furoic acid of almost 32% was obtained in this reaction (see Figure S12). It is well-known that the thermal conversion of 2-furoic acid is difficult under the applied conditions so that an MA yield of less than 1% could be obtained in the noncatalyzed reaction of MS4.

In summary, the more complex second-generation model substances exhibit a comparable product spectrum and analogous reaction pathway to the products MA and FA as postulated from the results of previous experiments using the

Table 4. Product Yields of Temperature Variation Experiments Using MS1 as a Substrate and $H_4[PVMO_{11}O_{40}]$ as a Catalyst

entry ^a	temperature/°C	catalyst ^b	total yield (gas and liquid)/% ^{cd}	yield/%			
				MA ^c	FA ^c	AA ^c	CO ₂ ^d
1	115		48.4	3.1	8.4	4.2	15.8
2	115	$H_4[PVMO_{11}O_{40}]$	45.4	4.2	9.9	5.1	16.6
3	140		56.0	1.7	8.9	6.7	24.4
4	140	$H_4[PVMO_{11}O_{40}]$	56.0	2.3	8.6	10.8	29.7

^aExperimental conditions: 10-fold reaction system, 115–140 °C, 30 bar (O₂), 30 h, 1000 rpm, MS1, and $H_4[PVMO_{11}O_{40}]$ as the catalyst (90 mol_{Carbon} mol_{Vanadium}⁻¹) in 7.5 mL of water. ^bAnalyzed as described in the corresponding section of the experimental part. ^cDetermined by HPLC-RID. ^dDetermined with GC-TCD.

first-generation substrates. In particular, oxygen-functionalized bonds are efficiently broken by the $H_4[PVMO_{11}O_{40}]$ catalyst. In addition to the redox activity, the Brønsted acidity and the free protons of the catalyst may also play a role. It can be assumed that the latter can activate electron-rich oxygen atoms of ethers and esters by an electrophilic attack. Without oxygen functionalization, this possibility does not exist; therefore, the conversion of bond types as in MS1 is less efficient than in MS3 and MS4. In this matter, MS1 was used to investigate if the conversion of bonds without oxygen functionalization can be optimized by varying the reaction conditions. For this reason, experiments using MS1 were performed at elevated temperatures of 115 and 140 °C and a reaction time of 30 h. The results are shown in Table 4. The total yields of liquid and gaseous products were increased to 45 and 56% at reaction temperatures of 115 and 140 °C, respectively. However, the formation of deep oxidation products such as FA and CO₂ also increased. At a temperature of 115 °C, the yield of CO₂ triples to almost 17%. At a reaction temperature of 140 °C, the CO₂ yield was already 30%. The MA yield reached a maximum of 4% at 115 °C. In contrast, the yield of MA drops to 2% again at 140 °C. We conclude that an increase in temperature and reaction time allows better conversion of MS4 and thus C–C bonds without oxygen. However, this improved activity comes at the expense of value-added products such as MA, which are oxidized to CO₂ at elevated temperatures. It should be noted that temperature must be used very carefully as an optimization parameter in the valorization of humin-like substances and humins; otherwise, overoxidation is favored.

In the experiments of Maerten et al.,⁴ high conversions of humins were obtained with higher-substituted POMs such as $H_8[PV_5Mo_7O_{40}]$ and $K_5[PV_3W_3O_{19}]$, respectively. As already postulated by Poller et al.,⁶⁰ in more highly substituted POMs, peroxy-ligands can be formed on adjacent vanadium atoms, which can increase the activity in oxidation processes. The results obtained so far are in good agreement with this postulate. It remains to be clarified whether more highly substituted POMs allow for a better conversion of bond types as in MS1 and thus a more efficient degradation of humins. For this purpose, MS1 was reacted using $H_8[PV_5Mo_7O_{40}]$ as a catalyst. Figure 10 shows the results of the oxidative conversion of MS1. As expected, the use of $H_8[PV_5Mo_7O_{40}]$ significantly increased the conversion of MS1 to liquid and gaseous oxidation products compared to $H_4[PVMO_{11}O_{40}]$. The product yields increased from about 20% using $H_4[PVMO_{11}O_{40}]$ to almost 40% using $H_8[PV_5Mo_7O_{40}]$ as a catalyst. Similarly, the AA yield increased from 1 to 4%, while the yield of ethanol decreased. The AA probably originates from the degradation of the ethoxy group by the oxidation of ethanol. Likewise, the FA yield had approximately doubled from 7 to 12%, indicating that the side chain with the double bond was increasingly degraded.

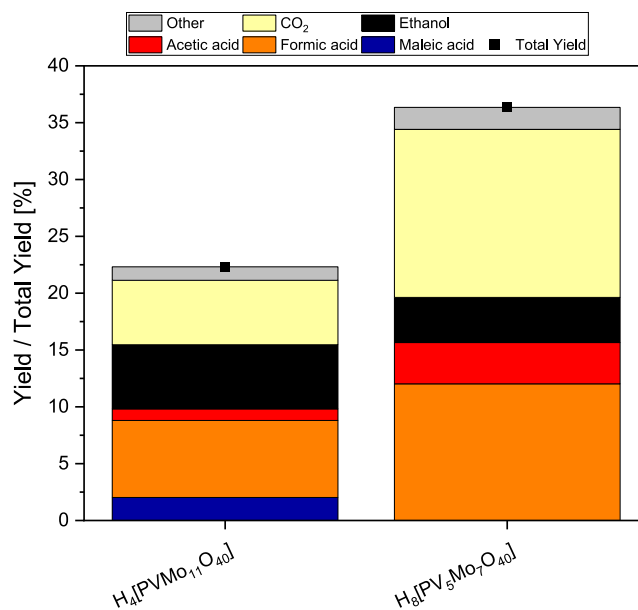


Figure 10. Oxidative conversion of MS1 using $H_4[PVMO_{11}O_{40}]$ and $H_8[PV_5Mo_7O_{40}]$ as catalysts. Experimental conditions: 10-fold reaction system, 90 °C, 30 bar (O₂), 15 h, 1000 rpm, MS1, and POM catalyst with vanadium as the transition metal (90 mol_{Carbon} mol_{Vanadium}⁻¹) in 7.5 mL of water.

Moreover, hardly any C₄–C₆ oxidation products such as 5-HMF or MA were detected. It can be assumed that these were further oxidized to C₁ products due to the increased redox activity of the $H_8[PV_5Mo_7O_{40}]$ catalyst, which can also be deduced from the approximately 3-fold higher yield of CO₂ of 15%. Thus, as in previous experiments, there is a strong tendency to overoxidation when $H_8[PV_5Mo_7O_{40}]$ is used as a catalyst. Other detected products were levulinic acid, succinic acid, and CO, respectively. As in previous experiments, a large amount of solid material was formed at the bottom of the reactor, corresponding to the lack of yield to close the carbon balance.

Overall, a wide variety of structural motifs and complex substrates were examined and catalytically oxidized. This enables to gain important insights into a valorization process of humins. However, there are still further hurdles to overcome that should be addressed in future studies. One challenge is the insolubility of the substrates in water, like humins leading to poor accessibility for the catalyst. This might also be one reason for the just moderate conversion of substrates. Here, further optimization of previous results is conceivable by varying the solvent system and using solubilizers. Furthermore, optimization of the gas entrainment through appropriate stirring elements, reaction conditions, and catalyst based on

previous results might also be beneficial. Such an optimized reaction system could then also be used to investigate more complex substrates with a higher degree of polymerization, other bond types such as direct furan–furan bonds, or real humins. Those investigations will lead to a more efficient and selective process for the valorization of humins and thus facilitating separation processes. Previous studies have shown that nanofiltration is a promising downstream process for homogeneously catalyzed reactions using POMs.^{37,44,73} The use of nanofiltration as a downstream process for the oxidative valorization of humins could also be an integral part of further investigations. Nevertheless, the present comprehensive study provides important insights into structure–activity–selectivity relationships of various functional groups and bonding types as well as the tailoring of POM catalysts, thereby providing a promising basis for further investigations.

CONCLUSIONS

The main objective of this study was to gain a deeper understanding of the oxidative conversion of humins by using model substances like furan derivatives of varying complexity in combination with polyoxometalates as suitable oxidation catalysts in aqueous media. In particular, monofuran derivatives such as furfural are of great interest since they can be obtained directly from numerous biomass feedstocks, thus providing access to value-added products. The oxidative conversion of furan derivatives using molecular oxygen as an oxidant was investigated by an initial catalyst screening using furfural as a substrate. Various transition metals such as V, Mn, Co, Ni, and Nb were used as substitute metals for molybdenum atoms in Keggin-type phosphomolybdates. The effect of certain degrees of substitution in the POM framework on the substrate oxidation has also been studied. A monosubstitution with V was found to be superior compared to the other catalysts tested in terms of activity and yield of the industrially relevant products MA and FA. Moreover, a correlation between the electrochemical properties and the conversion of furfural was revealed and an adjustment of the redox activity could be obtained. The $H_4[PVMo_{11}O_{40}]$ catalyst showed the lowest peak potential in SWV data in combination with the highest activity and lowest CO_2 formation. Based on experiments using the individual monofuran derivatives 5-HMF, furfural, 2-furoic acid, 2(*SH*)-furanone, 2-furfuryl alcohol as well as 2-methylfuran and $H_4[PVMo_{11}O_{40}]$ as a catalyst, structure–activity–selectivity relationships were established and evident reaction pathways for the conversion to MA were postulated. In detail, the C_5 substrate was converted to 5-hydroxyfuran-2(*SH*)-one in a redox process by cleavage of C_1 components such as FA or CO_2 with the participation of the catalyst and finally oxidized to MA. In addition, catalytic oxidation of benzene and phenol derivatives could also be demonstrated, although these structures play a minor role in the transformation of humins. Analogous to the monofuran derivate, difuran derivatives or branched furan rings could also be converted to MA and FA. It was shown that oxygen-functionalized bond types can be converted much better than nonfunctionalized C–C bonds. The use of more highly substituted POMs improved the oxidation of the C–C bonds. In summary, a deeper understanding of the selective oxidation of furan derivatives and tailoring of POMs for this purpose has been gained. From this, helpful conclusions can be drawn for the transformation of humins and a step can be taken toward efficient processes for their valorization. This

could lead to the development of an environmentally friendly and green process for the production of MA.

ASSOCIATED CONTENT

Supporting Information

The Supporting Information is available free of charge at <https://pubs.acs.org/doi/10.1021/acssuschemeng.3c06539>.

Various additional results and analytical data of catalysts and reaction solutions (PDF)

AUTHOR INFORMATION

Corresponding Author

Jakob Albert – Institute of Technical and Macromolecular Chemistry, Universität Hamburg, 20146 Hamburg, Germany; orcid.org/0000-0002-3923-2269; Email: jakob.albert@uni-hamburg.de

Authors

Tobias Esser – Institute of Technical and Macromolecular Chemistry, Universität Hamburg, 20146 Hamburg, Germany

André Wassenberg – Institute of Technical and Macromolecular Chemistry, Universität Hamburg, 20146 Hamburg, Germany

Jan-Christian Raabe – Institute of Technical and Macromolecular Chemistry, Universität Hamburg, 20146 Hamburg, Germany

Dorothea Voß – Institute of Technical and Macromolecular Chemistry, Universität Hamburg, 20146 Hamburg, Germany

Complete contact information is available at:

<https://pubs.acs.org/10.1021/acssuschemeng.3c06539>

Notes

The authors declare no competing financial interest.

ACKNOWLEDGMENTS

J.A., T.E., and A.W. acknowledge financial support from the Deutsche Forschungsgemeinschaft (DFG) via the project AL 2130/5-1. The authors thank the division for NMR spectroscopy and the division for central element analytics of the Department of Chemistry conducting NMR experiments and ICP as well as CHNS measurements. Furthermore, the authors thank the X-ray Service Facility, especially Isabelle Nevoigt, for XRD analyses. The authors also thank Dr. Maximilian J. Poller for his guidance and scientific support.

REFERENCES

- (1) Chernyshev, V. M.; Kravchenko, O. A.; Ananikov, V. P. Conversion of plant biomass to furan derivatives and sustainable access to the new generation of polymers, functional materials and fuels. *Russ. Chem. Rev.* **2017**, *86* (5), 357–387.
- (2) Hou, Q.; Qi, X.; Zhen, M.; Qian, H.; Nie, Y.; Bai, C.; Zhang, S.; Bai, X.; Ju, M. Biorefinery roadmap based on catalytic production and upgrading 5-hydroxymethylfurfural. *Green Chem.* **2021**, *23* (1), 119–231.
- (3) Olsen, K. H. The clean development mechanism's contribution to sustainable development: a review of the literature. *Clim. Change* **2007**, *84* (1), 59–73.
- (4) Maerten, S. G.; Voß, D.; Liauw, M. A.; Albert, J. Selective Catalytic Oxidation of Humins to Low-Chain Carboxylic Acids with Tailor-Made Polyoxometalate Catalysts. *ChemistrySelect* **2017**, *2* (24), 7296–7302.

- (5) Kashparova, V. P.; Chernysheva, D. V.; Klushin, V. A.; Andreeva, V. E.; Kravchenko, O. A.; Smirnova, N. V. Furan monomers and polymers from renewable plant biomass. *Russ. Chem. Rev.* **2021**, *90* (6), 750–784.
- (6) Liu, S.; Zhu, Y.; Liao, Y.; Wang, H.; Liu, Q.; Ma, L.; Wang, C. Advances in understanding the humins: Formation, prevention and application. *App. Energy Combust. Sci.* **2022**, *10*, No. 100062.
- (7) Hoang, T. M. C.; van Eck, E. R. H.; Bula, W. P.; Gardeniers, J. G. E.; Lefferts, L.; Seshan, K. Humins based by-products from biomass processing as a potential carbonaceous source for synthesis gas production. *Green Chem.* **2015**, *17* (2), 959–972.
- (8) Cherubini, F. The biorefinery concept: Using biomass instead of oil for producing energy and chemicals. *Energy Convers. Manage.* **2010**, *51* (7), 1412–1421.
- (9) Maity, S. K. Opportunities recent trends and challenges of integrated biorefinery: Part I. *Renewable Sustainable Energy Rev.* **2015**, *43*, 1427–1445.
- (10) Mukherjee, A.; Dumont, M.-J.; Raghavan, V. Review: Sustainable production of hydroxymethylfurfural and levulinic acid: Challenges and opportunities. *Biomass Bioenergy* **2015**, *72*, 143–183.
- (11) Hayes, D. J.; Hayes, M. H. B. The role that lignocellulosic feedstocks and various biorefining technologies can play in meeting Ireland's biofuel targets. *Biofuels, Bioprod. Biorefin.* **2009**, *3* (5), 500–520.
- (12) Weissermel, K.; Arpe, H.-J. *Industrial Organic Chemistry*, 4th completely rev. ed.; Wiley-VCH, 2003 DOI: 10.1002/9783527619191.
- (13) Bozell, J. J.; Petersen, G. R. Technology development for the production of biobased products from biorefinery carbohydrates—the US Department of Energy's "Top 10" revisited. *Green Chem.* **2010**, *12* (4), 539.
- (14) Patil, S. K. R.; Heltzel, J.; Lund, C. R. F. Comparison of Structural Features of Humins Formed Catalytically from Glucose, Fructose, and 5-Hydroxymethylfurfuraldehyde. *Energy Fuels* **2012**, *26* (8), 5281–5293.
- (15) Climent, M. J.; Corma, A.; Iborra, S. Conversion of biomass platform molecules into fuel additives and liquid hydrocarbon fuels. *Green Chem.* **2014**, *16* (2), 516.
- (16) Hayes, D. J.; Fitzpatrick, S.; Hayes, M. H. B.; Ross, J. R. H. The Biofine Process—Production of Levulinic Acid, Furfural, and Formic Acid from Lignocellulosic Feedstocks. In *Biorefineries-Industrial Processes and Products: Status Quo and Future Directions*; Kamm, B.; Gruber, P. R.; Kamm, M., Eds.; Wiley-VCH Verlag GmbH, 2005; pp 139–164 DOI: 10.1002/9783527619849.ch7.
- (17) Kapanji, K. K.; Haigh, K. F.; Görgens, J. F. Techno-economics of lignocellulose biorefineries at South African sugar mills using the biofine process to co-produce levulinic acid, furfural and electricity along with gamma valeractone. *Biomass Bioenergy* **2021**, *146*, No. 106008.
- (18) Yang, G.; Pidko, E. A.; Hensen, E. J. M. Mechanism of Brønsted acid-catalyzed conversion of carbohydrates. *J. Catal.* **2012**, *295*, 122–132.
- (19) Girisuta, B.; Janssen, L. P. B. M.; Heeres, H. J. Kinetic Study on the Acid-Catalyzed Hydrolysis of Cellulose to Levulinic Acid. *Ind. Eng. Chem. Res.* **2007**, *46* (6), 1696–1708.
- (20) Rasrendra, C. B.; Windt, M.; Wang, Y.; Adisasmito, S.; Makertihartha, I. G. B. N.; van Eck, E. R. H.; Meier, D.; Heeres, H. J. Experimental studies on the pyrolysis of humins from the acid-catalysed dehydration of C6-sugars. *J. Anal. Appl. Pyrolysis* **2013**, *104*, 299–307.
- (21) van Zandvoort, I.; Wang, Y.; Rasrendra, C. B.; van Eck, E. R. H.; Bruijninx, P. C. A.; Heeres, H. J.; Weckhuysen, B. M. Formation, molecular structure, and morphology of humins in biomass conversion: influence of feedstock and processing conditions. *ChemSusChem* **2013**, *6* (9), 1745–1758. Published Online: Jul. 8, 2013
- (22) van Zandvoort, I.; van Eck, E. R. H.; Peinder, P. de.; Heeres, H. J.; Bruijninx, P. C. A.; Weckhuysen, B. M. Full, Reactive Solubilization of Humins Byproducts by Alkaline Treatment and Characterization of the Alkali-Treated Humins Formed. *ACS Sustainable Chem. Eng.* **2015**, *3* (3), 533–543.
- (23) Shen, H.; Shan, H.; Liu, L. Evolution Process and Controlled Synthesis of Humins with 5-Hydroxymethylfurfural (HMF) as Model Molecule. *ChemSusChem* **2020**, *13* (3), 513–519. Published Online: Dec. 10, 2019
- (24) Sumerskii, I. V.; Krutov, S. M.; Zarubin, M. Y. Humins-like substances formed under the conditions of industrial hydrolysis of wood. *Russ J. Appl. Chem.* **2010**, *83* (2), 320–327.
- (25) van Zandvoort, I.; Koers, E. J.; Weingarth, M.; Bruijninx, P. C. A.; Baldu, M.; Weckhuysen, B. M. Structural characterization of 13 C-enriched humins and alkali-treated 13 C humins by 2D solid-state NMR. *Green Chem.* **2015**, *17* (8), 4383–4392.
- (26) Shi, N.; Liu, Q.; Liu, Y.; Chen, L.; Chen, N.; Peng, J.; Ma, L. Formation of Soluble Furanic and Carbocyclic Oxy-Organics during the Hydrothermal Carbonization of Glucose. *Energy Fuels* **2020**, *34* (2), 1830–1840.
- (27) Cheng, Z.; Everhart, J. L.; Tsilomelekis, G.; Nikolakis, V.; Saha, B.; Vlachos, D. G. Structural analysis of humins formed in the Brønsted acid catalyzed dehydration of fructose. *Green Chem.* **2018**, *20* (5), 997–1006.
- (28) Filiciotto, L.; Balu, A. M.; Romero, A. A.; Angelici, C.; van der Waal, J. C.; Luque, R. Reconstruction of humins formation mechanism from decomposition products: A GC-MS study based on catalytic continuous flow depolymerizations. *Mol. Catal.* **2019**, *479*, No. 110564.
- (29) Wassenberg, A.; Esser, T.; Poller, M. J.; Albert, J. Investigation of the Formation, Characterization, and Oxidative Catalytic Valorization of Humins. *Materials* **2023**, *16* (7), 2864 DOI: 10.3390/ma16072864.
- (30) Shi, N.; Liu, Q.; Ju, R.; He, X.; Zhang, Y.; Tang, S.; Ma, L. Condensation of α -Carbonyl Aldehydes Leads to the Formation of Solid Humins during the Hydrothermal Degradation of Carbohydrates. *ACS Omega* **2019**, *4* (4), 7330–7343. Published Online: Apr. 23, 2019
- (31) Cheng, B.; Wang, X.; Lin, Q.; Zhang, X.; Meng, L.; Sun, R.-C.; Xin, F.; Ren, J. New Understandings of the Relationship and Initial Formation Mechanism for Pseudo-lignin, Humins, and Acid-Induced Hydrothermal Carbon. *J. Agric. Food Chem.* **2018**, *66* (45), 11981–11989. Published Online: Nov. 6, 2018
- (32) Zhong, J.; Pérez-Ramírez, J.; Yan, N. Biomass valorisation over polyoxometalate-based catalysts. *Green Chem.* **2021**, *23* (1), 18–36.
- (33) Lechner, M.; Güttel, R.; Streb, C. Challenges in polyoxometalate-mediated aerobic oxidation catalysis: catalyst development meets reactor design. *Dalton Trans.* **2016**, *45* (42), 16716–16726. Published Online: Sep. 7, 2016
- (34) Li, G.; Ding, Y.; Wang, J.; Wang, X.; Suo, J. New Progress of Keggin and Wells-Dawson Type Polyoxometalates Catalyze Acid and Oxidative Reactions. *J. Mol. Catal. A: Chem.* **2007**, *262* (1-2), 67–76, DOI: 10.1016/j.molcata.2006.08.067.
- (35) Voß, D.; Kahl, M.; Albert, J. Continuous Production of Formic Acid from Biomass in a Three-Phase Liquid-Liquid-Gas Reaction Process DOI: 10.1021/acssuschemeng.0c02426.s001.
- (36) Albert, J.; Mehler, J.; Tucher, J.; Kastner, K.; Streb, C. One-step Synthesizable Lindqvist–isopolyoxometalates as Promising New Catalysts for Selective Conversion of Glucose as a Model Substrate for Lignocellulosic Biomass to Formic Acid. *ChemistrySelect* **2016**, *1* (11), 2889–2894.
- (37) Bertleff, B.; Claußnitzer, J.; Korth, W.; Wasserscheid, P.; Jess, A.; Albert, J. Extraction Coupled Oxidative Desulfurization of Fuels to Sulfate and Water-Soluble Sulfur Compounds Using Polyoxometalate Catalysts and Molecular Oxygen. *ACS Sustainable Chem. Eng.* **2017**, *5* (5), 4110–4118.
- (38) Bukowski, A.; Schill, L.; Nielsen, D.; Mossin, S.; Riisager, A.; Albert, J. NH₃-SCR of NO with novel active, supported vanadium-containing Keggin-type heteropolyacid catalysts. *React. Chem. Eng.* **2020**, *5* (5), 935–948.

- (39) Albert, J.; Mendt, M.; Mozer, M.; Voß, D. Explaining the role of vanadium in homogeneous glucose transformation reactions using NMR and EPR spectroscopy. *Appl. Catal., A* **2019**, *570*, 262–270.
- (40) Zhizhina, E. G.; Odyakov, V. Alteration of the physicochemical properties of catalysts based on aqueous solutions of Mo-V-P heteropoly acids in redox processes. *Reaction Kinet. Catal. Lett.* **2008**, *95*, 301–312, DOI: 10.1007/s11144-008-5423-2.
- (41) Albert, J.; Lüders, D.; Bösmann, A.; Guldi, D. M.; Wasserscheid, P. Spectroscopic and electrochemical characterization of heteropoly acids for their optimized application in selective biomass oxidation to formic acid. *Green Chem.* **2014**, *16* (1), 226–237.
- (42) Raabe, J.-C.; Albert, J.; Poller, M. J. Spectroscopic, Crystallographic, and Electrochemical Study of Different Manganese(II)-Substituted Keggin-Type Phosphomolybdates. *Chem. – Eur. J.* **2022**, *28* (49), No. e202201084. Published Online: Jul. 13, 2022
- (43) Raabe, J.-C.; Aceituno Cruz, J.; Albert, J.; Poller, M. J. Comparative Spectroscopic and Electrochemical Study of V(V)-Substituted Keggin-Type Phosphomolybdates and -Tungstates. *Inorganics* **2023**, *11* (4), 138.
- (44) Raabe, J.-C.; Esser, T.; Jameel, F.; Stein, M.; Albert, J.; Poller, M. J. Study on the incorporation of various elements into the Keggin lacunary-type phosphomolybdate [PMo 9 O 34] 9– and subsequent purification of the polyoxometalates by nanofiltration. *Inorg. Chem. Front.* **2023**, *10* (16), 4854–4868.
- (45) Fumagalli, T.; Sello, G.; Orsini, F. One-Pot, Fluoride-Promoted Wittig Reaction. *Synth. Commun.* **2009**, *39* (12), 2178–2195, DOI: 10.1080/00397910802654633.
- (46) Abid, M.; Mhiri, S.; Bougarech, A.; Triki, R.; Abid, S. Preparation, characterization and degradation study of novel sulfonated furanic poly(ester-amide)s. *Des. Monomers Polym.* **2020**, *23* (1), 16–24. Published Online: Feb. 11, 2020
- (47) Simeonov, S. P.; Coelho, J. A. S.; Afonso, C. A. M. An integrated approach for the production and isolation of 5-hydroxymethylfurfural from carbohydrates. *ChemSusChem* **2012**, *5* (8), 1388–1391. Published Online: Jun. 27, 2012
- (48) Nielsen, E. R. Furfuryl Furoate by Condensation from Furfural. *J. Am. Chem. Soc.* **1944**, *66* (7), 1230.
- (49) Bruker. *SHELXTL: Software reference manual*, <https://xray.uky.edu/Resources/manuals/Shellxl-manual.pdf> (accessed 2023–11–15).
- (50) Farrugia, L. J. WinGX suite for small-molecule single-crystal crystallography. *J. Appl. Cryst.* **1999**, *32*, 837–838.
- (51) Farrugia, L. J. WinGX and ORTEP for Windows: an update. *J. Appl. Crystallogr.* **2012**, *45* (4), 849–854.
- (52) Dolomanov, O. V.; Bourhis, L. J.; Gildea, R. J.; Howard, J. A. K.; Puschmann, H. OLEX2: a complete structure solution, refinement and analysis program. *J. Appl. Crystallogr.* **2009**, *42* (2), 339–341.
- (53) Hübschle, C. B.; Sheldrick, G. M.; Dittrich, B. ShelXL: a Qt graphical user interface for SHELXL. *J. Appl. Crystallogr.* **2011**, *44* (Pt 6), 1281–1284. Published Online: Nov. 12, 2011
- (54) Maruani, V.; Narayanin-Richenapin, S.; Framery, E.; Andrioletti, B. Acidic Hydrothermal Dehydration of d -Glucose into Humins: Identification and Characterization of Intermediates. *ACS Sustainable Chem. Eng.* **2018**, *6* (10), 13487–13493.
- (55) Bujanovic, B.; Ralph, S.; Reiner, R.; Hirth, K.; Atalla, R. Polyoxometalates in Oxidative Delignification of Chemical Pulp: Effect on Lignin. *Materials* **2010**, *3* (3), 1888–1903.
- (56) Hollemann, A. F.; Wiberg, N. *Lehrbuch der Anorganischen Chemie*, 102nd ed.; Walter de Gruyter & Co., 2007.
- (57) Voß, D.; Dietrich, R.; Stuckart, M.; Albert, J. Switchable Catalytic Polyoxometalate-Based Systems for Biomass Conversion to Carboxylic Acids. *ACS Omega* **2020**, *5* (30), 19082–19091. Published Online: Jul. 24, 2020
- (58) Hwang, D. Y.; Ha, S. Y.; Kim, S. Electrode-Assisted Wacker Process: Phosphomolybdate-Mediated Oxidation of 1-Butene to Methyl Ethyl Ketone [2]. *Bull. Korean Chem. Soc.* **2001**, *No. 22*, 441–442.
- (59) Sadakane, M.; Steckhan, E. Electrochemical Properties of Polyoxometalates as Electrocatalysts. *Chem. Rev.* **1998**, *98* (1), 219–238.
- (60) Poller, M. J.; Bönisch, S.; Bertleff, B.; Raabe, J.-C.; Görling, A.; Albert, J. Elucidating activating and deactivating effects of carboxylic acids on polyoxometalate-catalysed three-phase liquid–liquid–gas reactions. *Chem. Eng. Sci.* **2022**, *264*, No. 118143.
- (61) Voß, D.; Pickel, H.; Albert, J. Improving the Fractionated Catalytic Oxidation of Lignocellulosic Biomass to Formic Acid and Cellulose by Using Design of Experiments. *ACS Sustainable Chem. Eng.* **2019**, *7* (11), 9754–9762.
- (62) Kang, S.; Tang, P.; Fu, J.; Zhou, H.; Wu, X.; Liao, W.; Liu, S. Sustainable production of organic acids via ozonation of biomass derived 5-hydroxymethylfurfural and furfural. *Sustainable Chem. Pharm.* **2021**, *20*, No. 100383.
- (63) Gong, L.; Agrawal, N.; Roman, A.; Holewinski, A.; Janik, M. J. Density functional theory study of furfural electrochemical oxidation on the Pt (1 1 1) surface. *J. Catal.* **2019**, *373*, 322–335.
- (64) Chen, X.; Guigo, N.; Pizzi, A.; Sbirrazzuoli, N.; Li, B.; Fredon, E.; Gerardin, C. Ambient Temperature Self-Blowing Tannin-Humins Biofoams. *Polymers* **2020**, *12* (11), 2732.
- (65) Lan, J.; Chen, Z.; Lin, J.; Yin, G. Catalytic aerobic oxidation of renewable furfural to maleic anhydride and furanone derivatives with their mechanistic studies. *Green Chem.* **2014**, *16* (9), 4351–4358.
- (66) Román, A. M.; Hasse, J. C.; Medlin, J. W.; Holewinski, A. Elucidating Acidic Electro-Oxidation Pathways of Furfural on Platinum. *ACS Catal.* **2019**, *9* (11), 10305–10316.
- (67) Shao, J.; Ni, Y.; Yan, L. Oxidation of furfural to maleic acid and fumaric acid in deep eutectic solvent (DES) under vanadium pentoxide catalysis. *J. Bioresour. Bioprod.* **2021**, *6* (1), 39–44.
- (68) Murzin, D. Y.; Bertrand, E.; Tolvanen, P.; Devyatkov, S.; Rahkila, J.; Eränen, K.; Wärnå, J.; Salmi, T. Heterogeneous Catalytic Oxidation of Furfural with Hydrogen Peroxide over Sulfated Zirconia. *Ind. Eng. Chem. Res.* **2020**, *59* (30), 13516–13527.
- (69) Alonso-Fagúndez, N.; Agirrezabal-Telleria, I.; Arias, P. L.; Fierro, J. L. G.; Mariscal, R.; Granados, M. L. Aqueous-phase catalytic oxidation of furfural with H 2 O 2: high yield of maleic acid by using titanium silicalite-1. *RSC Adv.* **2014**, *4* (98), 54960–54972.
- (70) Wojcieszak, R.; Santarelli, F.; Paul, S.; Dumeignil, F.; Cavani, F.; Gonçalves, R. V. Recent developments in maleic acid synthesis from bio-based chemicals. *Sustainable Chem. Process.* **2015**, *3* (1), 8325 DOI: 10.1186/s40508-015-0034-5.
- (71) Li, X.; Lan, X.; Wang, T. Selective oxidation of furfural in a biphasic system with homogeneous acid catalyst. *Catal. Today* **2016**, *276*, 97–104.
- (72) Yang, T.; Li, W.; Ogunbiyi, A. T. The effect of Br- and alkali in enhancing the oxidation of furfural to maleic acid with hydrogen peroxide. *Mol. Catal.* **2021**, *504*, No. 111488.
- (73) Esser, T.; Huber, M.; Voß, D.; Albert, J. Development of an efficient downstream process for product separation and catalyst recycling of a homogeneous polyoxometalate catalyst by means of nanofiltration membranes and design of experiments. *Chem. Eng. Res. Des.* **2022**, *185*, 37–50.

6.3 From Model Substrates to Real Humins - A Novel Approach for Humins Valorization

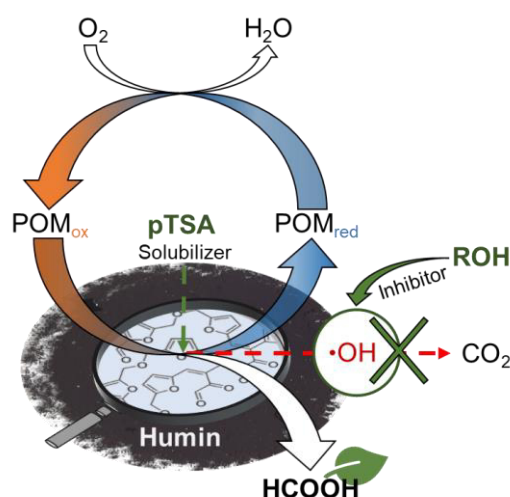
P3

Selective catalytic oxidation of humins to carboxylic acids using the $H_4[PVMo_{11}O_{40}]$ Keggin-type polyoxometalate enhanced by alcohol doping and solubilizer

Tobias Esser, André Wassenberg, Dorothea Voß and Jakob Albert

Esser, T.; Wassenberg, A.; Voß, D.; Albert, J.: Selective catalytic oxidation of humins to carboxylic acids using the $H_4[PVMo_{11}O_{40}]$ Keggin-type polyoxometalate enhanced by alcohol doping and solubilizer. *React. Chem. Eng.*, **2024**, 86 (7), 357. DOI: 10.1039/d3re00672g

As introduced in Section 6.2, the mono-vanadium-substituted $H_4[PVMo_{11}O_{40}]$ POM-catalyst proved to be superior in terms of activity and yield of the industrially relevant products maleic acid and formic acid. In the present section, the transferability of the found insights to real humins is focused. Therefore, a glucose-based humin was chosen as substrate applying the mild reaction conditions used in the previous study.²¹² Again, it could be demonstrated that the $H_4[PVMo_{11}O_{40}]$ POM-catalyst has a relative selectivity advantage over higher substituted catalysts. With the objective of further decreasing the yield of the overoxidation product CO_2 and simultaneously increasing the activity, the use of additives and the optimization of the reaction conditions were investigated. On the one hand, the use of alcoholic additives to inhibit CO_2 formation was tested. On the other hand, the use of para-toluenesulfonic acid (pTSA) as a solubilizer and thus as a reaction promotor was studied. In addition, the synergistic superposition of both additives was tested under optimized reaction conditions. The novel reaction system is characterized by a remarkable CO_2 -inhibiting effect and simultaneously increased activity and has been transferred to other real humins based on different sugars. Further supporting information can be found in Appendix 9.5.3.^{212,213} The following section is reproduced from Ref.²¹³ with permission of the *Royal Society of Chemistry*.



Publication: *Selective catalytic oxidation of humins to carboxylic acids using $H_4[PVMo_{11}O_{40}]$ Keggin-type polyoxometalate enhanced by alcohol doping and solubilizer.*²¹³



Cite this: DOI: 10.1039/d3re00672g

Selective catalytic oxidation of humins to carboxylic acids using the H₄[PVMo₁₁O₄₀] Keggin-type polyoxometalate enhanced by alcohol doping and solubilizer†

Tobias Esser, André Wassenberg, Dorothea Voß  and Jakob Albert *

Oxidative valorization of humins is one promising approach for establishing carbon efficient biomass valorization pathways. In the present contribution, the development of an optimized reaction system for the selective catalytic oxidation (SCO) of water-insoluble and highly complex humins to short-chain carboxylic acids like formic acid (FA) and acetic acid (AA) using Keggin-type polyoxometalates is presented. In detail, the monovanadium-substituted polyoxometalate H₄[PVMo₁₁O₄₀] catalyst exhibited a considerable selectivity advantage in the aqueous phase over state-of-the-art catalysts. More specifically, the yield of the desired products FA and AA (esters) could be drastically improved up to 30%, while undesired side products resulting from thermal-induced decarbonylation and decarboxylation were drastically reduced down to a third. Hereby, alcoholic additives like methanol show a remarkable inhibiting effect on CO₂ formation. It was shown that a temperature of 120 °C represents an optimum where methanol can still inhibit CO₂ formation even at a low alcohol content of 5 vol%. Furthermore, the use of *para*-toluenesulfonic acid (*p*TSA) as solubilizer has been investigated to circumvent the water-insoluble character of humins and to optimize humin conversion. On the one hand, *p*TSA could efficiently promote the activity in the SCO of humins. On the other hand, methanol was far more efficient in inhibiting CO₂ formation, especially at elevated reaction temperatures. The results were reproducible and could even be transferred to various humins based on different sugars. Using the combination of methanol and *p*TSA as additives as well as a singly vanadium-substituted polyoxometalate catalyst provides a highly promising approach for the valorization of complex humins.

Received 12th December 2023,
Accepted 5th March 2024

DOI: 10.1039/d3re00672g

rsc.li/reaction-engineering

In recent years, the industrial valorization of biomass to produce platform chemicals such as levulinic acid has increasingly grown in importance.^{1–5} The driving force behind this development is the increasing demand for energy and chemicals as well as the depletion of fossil hydrocarbon sources. However, only a few bio-based process technologies have been able to establish themselves in industry so far, as they are often more demanding and complex.^{6–8} One deficit is the formation of undesirable by-products by thermal-induced reactions that make such processes inefficient and expensive.^{9,10} In this context, the Biofine process for the acid-catalyzed production of biogenic levulinic acid is one

example.^{11,12} In this process, insoluble black polymeric solids are formed as by-products, the so-called humins.^{5,13,14} Humins are a typical by-product of acid-catalyzed conversion of carbohydrates, decreasing the overall carbon efficiency of such processes.^{9,10,15}

The formation and structure of humins have received much attention in recent years. The humin structure is built by a furan-rich polymer network.¹⁶ Linkage of these furan rings can take place *via* either oxygen functionalized C–O–C bonds or aliphatic C–C bonds.^{17,18} However, there are still controversial discussions about the complex structure of humins that has not been fully elucidated to date.

Several approaches were pursued to suppress the formation of humins in the acid-catalyzed conversion of carbohydrates. However, these approaches fail due to the fast kinetics of humin formation.^{5,14,19,20} Another promising idea is the chemical valorization of humins by catalytic oxidation.^{5,21} Pioneering work in this field was done by Maerten *et al.*,⁵ who demonstrated for the first time the chemical valorization of humins by selective catalytic

Institute of Technical and Macromolecular Chemistry, Universität Hamburg,
Bundesstraße 45, 20146 Hamburg, Germany.

E-mail: jakob.albert@uni-hamburg.de; Tel: (+49) 4042838 4209

† Electronic supplementary information (ESI) available: Various additional results and analytical data of reaction solutions. See DOI: <https://doi.org/10.1039/d3re00672g>



oxidation (SCO) using polyoxometalate (POM) catalysts to short-chain carboxylic acids. POMs are a unique class of inorganic compounds having a wide variety of geometric and electronic structural properties. Moreover, they are ideal prototypes for catalytic applications as they combine the required reactivity and stability at the molecular level.²² More specifically, the study of Maerten *et al.*⁵ showed that a five times vanadium-substituted Keggin-type phosphomolybdic acid $H_8[PV_5Mo_7O_{40}]$ (HPA-5) catalyst could promote humin conversion up to about 89% under very mild conditions of 120 °C and 20 bar oxygen pressure in pure aqueous medium within one hour of reaction time. Unfortunately, CO_2 was the main reaction product with up to 80% yield.⁵ Lowering the reaction temperature down to 90 °C lowers conversion but prevents thermal-induced total oxidation to CO_2 to a certain extent and therefore increased the selectivity of value-added products up to 11% for formic acid (FA) and 5% for acetic acid (AA).⁵ However, only a small fraction of the carbon provided by humins was converted into value-added products, which is so far a major obstacle for catalytic oxidative valorization approaches. Further results published by Wassenberg *et al.*,²¹ where various sugar-derived humins were oxidized in the aqueous phase using HPA-5 showed interesting correlations between humin structure and conversion, showing that ether and ester groups were converted very well by catalytic oxidation, while thioester and ether groups were only poorly oxidized. The furan-containing core structure of the humins remained mostly unaffected by the oxidative treatment. In both studies, humins from different carbohydrates like glucose, fructose or cellobiose were efficiently converted and short-chain carboxylic acids were successfully obtained as value-added products. However, the results showed that vanadium-substituted Keggin-type POMs can be used to oxidize very complex aromatic structures like humins to carboxylic acids. Inspired by the aforementioned results, Esser *et al.*²³ used individual monofuran derivatives like 5-hydroxymethylfurfural (HMF), furfural, 2-furoic acid, 2(5H)-furanone, 2-furfuryl alcohol and 2-methylfuran to gain a deeper understanding of POM-catalyzed humin oxidation. Hereby, they found that the Keggin-type POM-catalyst $H_4[PVMo_{11}O_{40}]$ (HPA-1) can oxidize both monofuran and difuran derivatives or even branched furan rings to maleic acid (MA) and FA, respectively. It was shown that oxygen-functionalized bond types can be converted much better than non-functionalized C–C bonds. The use of more highly V-substituted POMs improved the oxidation of the C–C bonds. However, the MA-yield decreased with an increasing degree of V-substitution, while both FA yield and over-oxidation to CO_2 increased.

Therefore, the main scope of the present study was the optimization of this promising approach for real humin structures. In detail, the use of solubilizers like *para*-toluene sulfonic acid (*p*TSA) and short-chain alcohols as co-solvents in combination with different reaction temperatures on both the kinetics and the selectivity of HPA-1-catalyzed SCO of humins was studied.

Results and discussion

SCO of humins using vanadium-substituted POM catalysts

As results in the literature have shown, vanadium-substituted POM catalysts exhibit remarkable activity in the SCO of complex biomass, including humins.^{5,21,24} In particular, vanadium-substituted phosphomolybdic acid, which forms Keggin-type POM catalysts, proves to be an active catalyst for the oxidative conversion of biomass in aqueous medium. It is plausible that peroxo-ligands located between adjacent vanadium atoms in higher vanadium-substituted POMs are responsible for the enhanced activity, as reported by Poller *et al.*²⁵ In particular, in the SCO of humins, this high activity of catalytic species leads to over-oxidation and thus to increased CO_2 formation.^{5,21}

Analogous findings could be demonstrated by previously published results on the oxidation of mono-furan derivatives and humin-like substances.²³ Here, higher substituted POMs showed significant higher activity for the oxidation of the mono-furan derivative furfural, which was ultimately converted to formic acid (FA) or to CO_2 with yields up to 43% and 30%, respectively. In comparison, the $H_4[PVMo_{11}O_{40}]$ (HPA-1) catalyst was characterized by a much lower tendency to over-oxidation with CO_2 yields of only around 5%. In addition, maleic acid (MA) could be produced as one of the main products with a yield of up to 22%, while higher vanadium-substituted catalysts further degraded the carbon skeleton to FA and CO_2 .

Due to the lower tendency of the HPA-1 catalyst to over-oxidize the carbon skeleton to CO_2 and the resulting selectivity advantage, it was applied for the first time in the SCO of real humins. The substrate used was a glucose-based humin prepared by the acid-catalyzed synthesis of levulinic acid from glucose. The detailed experimental procedure can be found in the corresponding section of the experimental part. Humins are very complex substrates whose structure has not yet been clearly clarified. Various investigations employing diverse analytical methods have been carried out in the past few years to further clarify the humin structure.^{5,9,15,19,20} According to these analyses, numerous studies describe the humin structure as a furan-rich polymer network that is cross-linked *via* both oxygen-functionalized and aliphatic bonds without oxygen.^{4,5,9,16–18,21,26–29} Fig. 1 shows the spectra obtained by Fourier-transform infrared spectroscopy (FTIR) of the glucose-based humin used and the glucose used to produce it. The fundamental frequencies of glucose are caused by the stretching of the hydroxyl groups at about 3300 cm^{-1} , in the range of 2950 cm^{-1} to 2890 cm^{-1} by the aliphatic C–H stretching and by the deformation of the C–O–C and C–O–H bonds at 1460 cm^{-1} to 1340 cm^{-1} . In the range of approx. 1150 cm^{-1} to 990 cm^{-1} , carbohydrate-characteristic vibrations of C–O and C–C can be found. Compared to the spectrum of glucose, the vibrations of the hydroxyl groups are absent, and two new humin-typical signals were detected at around 1600 cm^{-1} and 1700 cm^{-1} . These signals could be assigned to the C=C stretching



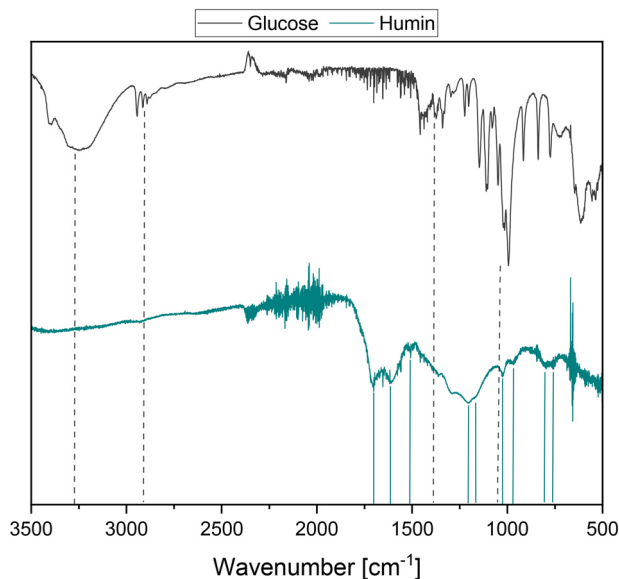


Fig. 1 FTIR spectra of glucose (top, gray) and glucose-based humin (bottom, turquoise).

vibration conjugated with carbonyl at 1600 cm^{-1} and the C=O stretching vibration at 1700 cm^{-1} .^{21,30} The described development of the signals is consistent with the formation mechanisms of humins postulated in the literature.^{16,17,21,30,31} Accordingly, glucose dehydrates under acid catalysis in the first step to 5-hydroxymethylfurfural (5-HMF), which reacts further to obtain levulinic acid (LeA) under ring opening. In the studies by Wassenberg *et al.*,²¹ both intermediates were detected as part of the liquid reaction phase of the acid-catalyzed conversion of hexoses. 2,5-Dioxo-6-hydroxyhexanal (DHH) is also discussed as a possible intermediate, but it has not yet been proven experimentally.^{15,32}

These highly functional molecules can react further in various ways, *e.g.* by aldol condensation. In this process, the hydroxyl groups of glucose were completely converted, while C=C and C=O bonds were formed. Continuing cross-linking can take place through etherification, esterification, acetylation, and further aldol condensations. Shen *et al.*¹⁷ provide a comprehensive overview of reactions and mechanisms involved in the formation of humins. Other characteristic vibrations that indicate the furan-rich network are the C=C stretching vibration of the polysubstituted furans at around 1500 cm^{-1} , the C–O–C deformation of the furan rings at around 1160 cm^{-1} and 1200 cm^{-1} and the C–H vibrations at around 965 cm^{-1} , 800 cm^{-1} and 760 cm^{-1} . A number of structural elements and possible humin structures can be derived from the bonding types and basic building blocks described. Wassenberg *et al.*²¹ provide experimentally proven structural elements of humins in their study. A comprehensive overview of further structural motifs of humins can be found in the review by Liu *et al.*⁹ Furthermore, a detailed discussion of various structural elements, important functional groups and possible humin-

like model substances with regard to a catalytic conversion of humins can be found in previously published results.²³

The morphology of the humin used could also be of interest. For this purpose, the humin produced was examined using scanning electron microscopy (SEM). The results of SEM analysis can be found in Fig. 2. Under traditional conditions, humins mostly consist of agglomerated spherical particles. These interconnected spheres can also be found for the used glucose-based humin (Fig. 2). It can be assumed that the increased participation of LeA in the poly-furanic network presumably prevents the highly ordered stacking orientation by causing more aldol condensations and concurrently esterification.¹⁷ This results in a coexistence of more agglomerated particles with a less layered structure.¹⁷ Due to the high reaction rate at $180\text{ }^{\circ}\text{C}$, larger clusters were preferably formed.

Table 1 shows the results of the SCO of humin using the HPA-1 catalyst in comparison to higher substituted HPA-2 and HPA-5 as well as a Lindqvist-type $\text{K}_5[\text{PV}_3\text{W}_3\text{O}_{19}]$ (IPA-3) POM-catalyst. The results using the HPA-5 and IPA-3 catalysts were published by Maerten *et al.*⁵ and serve to supplement or support the trends identified here. As a reference, an experiment without catalyst (blank) was also carried out in pure aqueous phase. The liquid samples were analyzed by one-dimensional nuclear magnetic resonance (NMR) spectroscopy and the gaseous samples by gas chromatography (GC). The exact procedure can be found in the corresponding section of the experimental part. Furthermore, for the liquid product phase, two-dimensional NMR measurements such as heteronuclear single quantum coherence (HSQC) and heteronuclear multiple bond correlation (HMBC) were performed to exactly reveal the formed structures. Example spectra for the 1D NMR measurements of nuclei ^1H as well as ^{13}C and for the 2D NMR measurements HSQC and HMBC can be found in the ESI† (Fig. S1–S4). In addition, all results could be confirmed by high-performance liquid chromatography (HPLC) measurements summarized in Table S1.†

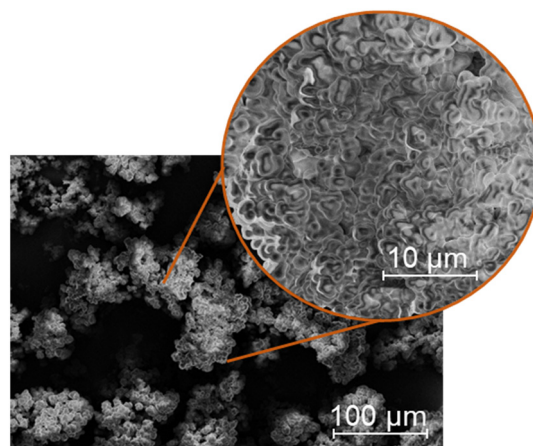


Fig. 2 SEM image of glucose-based humin.



Table 1 Selective catalytic oxidation of humins using different POM catalysts

Entry	Catalyst	Total yield/%	Combined yield/%		Ratio ^e (value : waste)/%
			FA + AA ^c	CO + CO ₂ ^d	
1 ^a	Blank	11.2	3.2	8.0	29 : 71
2 ^a	HPA-1	30.1	10.9	19.2	36 : 64
3 ^a	HPA-2	56.3	7.3	49.1	13 : 87
4 ^b	IPA-3	69.9	11.3	58.6	16 : 84
5 ^b	HPA-5	77.1	12.3	64.8	16 : 84

Experimental conditions: ^a 3-Fold reaction system, 90 °C, 30 bar O₂, 30 h, 1000 rpm, 300 mg solid humin (16.2 mmol carbon), 0.83 mmol of vanadium (V) for substitution (20 mol_{Carbon} mol_V⁻¹) in 30 mL water. ^b Results of Maerten *et al.*⁵ ^c Determined with quantitative ¹H NMR and *tert*-butanol as standard. ^d Determined with GC-TCD. ^e Calculated as described in the corresponding section of the experimental part.

Without the use of a catalyst, the complex humin could hardly be converted, with a total yield of about 11% (Table 1, entry 1). In the gas phase, CO₂ was formed as the main product with a yield of over 7%. FA and AA, which were formed as liquid phase products, were present in approximately equal amounts with yields of 1.5% and 1.8%, respectively.

The combined yield of the gas phase products CO and CO₂ was about 8%, which is 2.5 times higher than the combined yield of the carboxylic acids FA and AA, which was only about 3%. Therefore, the ratio of the value-added products FA as well as AA (value) and the undesired gas-phase products (waste) has reached 29:71. As expected, the use of the HPA-1 catalyst results in a drastic increase in activity, tripling the total yield to over 30% (Table 1, entry 2). The combined yield of the value-added products FA and AA was also increased to almost 11%. Due to the use of the redox-active HPA-1 catalyst, the combined yield of gas phase products increased only up to a value of about 19%. Thereby, the ratio of value-added products to waste slightly improves to 36:64. It can be concluded that the use of the HPA-1 catalyst significantly increases the activity in the SCO of humins but has only a minor effect on the selectivity compared to the uncatalyzed reaction.

As already described, higher vanadium-substituted POM catalysts exhibit increased catalytic activity due to the formation of peroxo-species.^{23,25} Consequently, the use of the double-substituted HPA-2 catalyst led to a fivefold increase in the total yield to about 56% compared to the reaction without catalyst (Table 1, entry 3). Compared to that of the reaction catalyzed by HPA-1, the total yield increased by a factor of more than 2. This confirms the expected increase in activity due to a higher degree of substitution. Considering the results of Maerten *et al.*,⁵ an increase in catalytic activity with increasing degree of substitution could also be observed (Table 1, entries 4 and 5). The total yield increased to about 70% and over 77% using IPA-3 or HPA-5, respectively. According to the results, the application of higher substituted POM catalysts is beneficial concerning the activity. However, the use of a singly vanadium-substituted POM already decreased the formation of CO₂ compared to the results using higher vanadium-substituted catalysts (Table 1, entries 3 and 4). More specifically, the use of the five times

vanadium-substituted HPA-5 resulted in 65% yield of undesired gas-phase products, which is more than three times higher compared to the results using HPA-1.⁵ Moreover, a combined yield of carboxylic acids of about 12% was obtained, which is only slightly more than the results presented here.⁵ Therefore, the use of the HPA-5 catalyst only allows for a considerably less favorable ratio of value-added products and undesired by-products of 16:84. The use of the triple-substituted Lindqvist-type IPA-3 also led to increased CO₂ formation (Table 1, entry 4).⁵ Accordingly, higher vanadium-substituted POM catalysts are much more active, but also promote the overoxidation of humins to CO₂. The tendency of higher substituted POM catalysts to overoxidize the substrate is a well-known and well-studied phenomenon in the literature, yielding CO₂ as the main product.³³⁻³⁶ Consequently, the use of HPA-1 as a catalyst is beneficial concerning the selectivity to short-chain carboxylic acids, which is crucial for a sustainable valorization of humins. Nevertheless, CO₂, whose yields were at least twice that of the value-added products, is the main product in the SCO of humins, regardless of the catalyst used. Hence, it seems reasonable to investigate additional features that can suppress or inhibit CO₂ formation in the SCO of humins. To this end, short-chain alcohols have been discussed in the literature as additives that demonstrated remarkable results in inhibiting CO₂ formation during oxidative conversion of biomass.³⁵⁻³⁷ Short-chain alcohols such as methanol (MeOH) or ethanol (EtOH) succeeded in optimizing oxidation reactions and inhibiting formation of CO₂ using vanadium-based catalysts by acting as radical scavengers, stabilizing reactive groups of substrates and forming new catalytic species as well as increasing the solubility of oxygen.³³⁻³⁷ The transferability of these remarkable effects to the SCO of humins using HPA-1 as a catalyst needs to be further investigated.

Selection of a suitable additive for the suppression of CO₂ formation in the SCO of humins

The suppression of CO₂ formation during the oxidative valorization of biomass by using short-chain alcohols as additives represents a promising approach. Remarkable results have been achieved, especially when methanol was



used.^{34,35,37} Maerten *et al.*³⁵ demonstrated the oxidation of glucose to FA and its ester methyl formate (MF) in nearly perfect selectivity by outstanding CO₂ suppression using methanol as a (co)-solvent. It was reported that the selectivity of FA using glucose as a substrate in an aqueous-methanolic solvent system could be increased from about 50% to over 99% catalyzed by HPA-5.³⁵ Hereby, the undesirable over-oxidation of the substrate to CO₂ was efficiently prevented. Furthermore, it was shown that even a low alcohol content of 10 vol% methanol in aqueous solution allowed for a significant improvement in the yield of carboxylic acids and a very effective suppression of the formation of gaseous by-products.³⁵ Similar results were also obtained by He *et al.*³⁶ and Lu *et al.*³⁴ in their studies. Lu *et al.*³⁴ demonstrated the inhibition of CO₂ formation in oxidative conversion of glucose to FA using H₅[PV₂Mo₁₀O₄₀] (HPA-2) as a catalyst by decreasing the CO₂ yield from about 45% in pure water to less than 4%, even at a low methanol content of at least 10 vol%.

Based on the aforementioned promising results in the oxidative conversion of glucose from the literature, the transferability to the SCO of humins using HPA-1 as a catalyst was further investigated. For this purpose, the SCO of glucose-based humin was studied using an aqueous solution of 10 vol% methanol. In addition, ethanol and isopropanol (iPrOH) were tested as further alcohol additives. For all additives, a stability test was also performed without a substrate under otherwise identical conditions to demonstrate that the carboxylic acids originated only from the carbon in the substrate and not of the organic additive. The results are shown in Table 2.

According to the results shown in Table 2, addition of 10 vol% methanol as an additive led to a significant decrease in yield of the undesired side products CO and CO₂ from above 19% to below 12% compared to a purely aqueous system (Table 2, entries 1 and 2). In an aqueous-alcohol solution, carboxylic acids are partly present as esters, which are formed by esterification with the corresponding alcohol. Due to the low alcohol content and the associated excess water, the equilibrium is on the side of the hydrolysis products. The

yield of carboxylic acids (esters) also increased from under 11% to about 14%. The use of a 10 vol% ethanolic solution also led to a visible inhibition of the formation of gaseous by-products with a yield of about 14% (Table 2, entry 3). Analogously to methanol, the yield of carboxylic acids slightly increased to about 14%. Thus, the ratio of value-added products (carboxylic acids and esters) to undesired by-products (CO/CO₂) was 50:50 and 54:46 when using an ethanolic solution or a methanolic solution, respectively (Table 2, entries 2 and 3). Therefore, addition of methanol is more efficient than addition of ethanol. In this way, the complex humin was converted into more value-added products than into undesired by-products. This is an impressive increase over the reaction without alcohol addition, where the yield of undesired by-products was at least twice that of the value-added products. Addition of isopropanol also showed CO₂-inhibiting effects, but these are less pronounced than that with addition of methanol (Table 2, entry 4).

To exclude formation of carboxylic acids or their esters from alcohols under the reaction conditions, additional experiments without a substrate were conducted. The liquid phase of each experiment was analyzed by NMR and HPLC. The NMR spectra and chromatograms can be found in the ESI (Fig. S5 and S6[†]). It was found that without a substrate no carboxylic acids or esters were formed, confirming the sole origin of FA, MF and AA from the substrate (Table 2, entries 5–7). Comparable results were published by Maerten *et al.*³⁵ and further verified by labeling experiments with ¹³C-labeled glucose. Also, Lu *et al.*³⁴ have investigated the formation of carboxylic acids and esters originated from additives using deuterated alcohols. All detected FA was not D-labeled and thus formed from the substrate.³⁴

Effect of MeOH concentration and reaction temperature on the SCO of humins

It has been shown that an addition of 10 vol% methanol already inhibits the formation of CO₂ in the SCO of humins using HPA-1 as a catalyst. However, the influence of

Table 2 SCO of glucose-based humin using HPA-1 as catalyst in aqueous media with 10 vol% alcohol additive

Entry ^a	Substrate	Additive	Total yield/%	Combined yield/%		Ratio ^{dd} (value:waste)/%
				FA + AA + esters ^b	CO + CO ₂ ^c	
1	Humin (Gl)	—	30.1	10.9	19.2	36 : 64
2	Humin (Gl)	MeOH	25.7	13.8	11.9	54 : 46
3	Humin (Gl)	EtOH	27.8	13.9	13.9	50 : 50
4	Humin (Gl)	iPrOH	24.6	10.7	13.9	44 : 57
5	—	MeOH	0.0	0.0	0.0	—
6	—	EtOH	0.0	0.0	0.0	—
7	—	iPrOH	0.0	0.0	0.0	—

Experimental conditions: ^a 3-Fold reaction system, 90 °C, 30 bar O₂, 30 h, 1000 rpm, 300 mg solid humin (16.2 mmol carbon), 0.83 mmol of vanadium (V) for substitution (20 mol_{Carbon} mol_V⁻¹) in 30 mL aqueous alcohol solution with 10 vol% of the respective alcohol. ^b Determined with quantitative ¹H NMR and *tert*-butanol as standard. ^c Determined with GC-TCD. ^d Calculated as described in the corresponding section of the experimental part.



Table 3 SCO of humin using HPA-1 as catalyst in an aqueous methanolic system with different amounts of methanol

Entry ^a	Catalyst	Amount of MeOH/%	Total yield/%	Combined yield/%		Ratio ^d (value : waste)/%
				FA + AA + esters ^b	CO + CO ₂ ^c	
1	HPA-1	5	27.2	14.7	12.5	54 : 46
2	HPA-1	10	25.7	13.8	11.9	54 : 46
3	HPA-1	20	26.1	12.8	13.4	49 : 51
4	Blank	5	8.6	3.4	5.2	40 : 60

Experimental conditions: ^a 3-Fold reaction system, 90 °C, 30 bar (O₂), 30 h, 1000 rpm, 300 mg solid humin (16.20 mmol carbon), 0.83 mmol of vanadium (V) for substitution (20 mol_{Carbon} mol_V⁻¹) in 30 mL aqueous alcohol solution with 0–20 vol% methanol. ^b Determined with quantitative ¹H NMR and *tert*-butanol as standard. ^c Determined with GC-TCD. ^d Calculated as described in the corresponding section of the experimental part.

methanol content on the inhibition of CO₂ formation for this reaction system has not been investigated so far. For this purpose, further experiments were conducted by adding 5% and 20% methanol to the aqueous solution. The results are shown in Table 3.

According to the results shown in Table 3, the amount of methanol used in the studied range has no significant influence (entries 1–3) on the product selectivity. Concerning the ratio of value-added products to undesired side products, the addition of 5 vol% methanol did not differ from the base experiment with the addition of 10 vol% methanol. Interestingly, the lowest methanol content of 5 vol% enabled the highest combined yield of carboxylic acids of almost 15%, but at the same time the second lowest yield of undesired by-products of around 12% (Table 3, entry 1). Increasing the methanol content up to 20 vol% resulted in slightly lower performance. More specifically, the yield of carboxylic acids decreased to less than 13%, while the yield of gaseous products increased to over 13%. Therefore, further increasing the methanol content is considered inefficient. Furthermore, the methanol content influenced the yield of MF, which increased from 0.9% to 2.8% as the methanol content increased. The methanol content affects the equilibrium of the esterification reaction of FA. However, due to the excess of water and the resulting favored hydrolysis of esters, most of the products were free acids. For further experiments, a methanol content of 5 vol% was chosen because this content enabled the highest yield of carboxylic acids while efficiently inhibiting CO₂ formation. In addition, a lower methanol content is more cost-effective and would therefore have an advantage in a technical-economic system analysis.

The reference reaction without catalyst (blank) also demonstrated the effectiveness of adding 5 vol% methanol for inhibiting CO₂ formation (Table 3, entry 4). Still, the yield of carboxylic acids was more than four times higher when a catalyst was used. Nevertheless, the total yield of about 27% including the combined yield of carboxylic acids of about 15% is still low (Table 3, entry 1). In order to increase the yield of carboxylic acids, experiments were conducted at different reaction temperatures and the influence on the kinetics of the reaction was investigated. The results are shown in Fig. 3. As expected, a strong increase in the activity

was achieved as the reaction temperature increased. The total yield drastically increased from about 27% to over 60% at reaction temperatures of 90 °C and 130 °C, respectively. The highest yield of carboxylic acids of about 29% was achieved at 120 °C, which is almost twice the yield at 90 °C. Increasing the temperature further up to 130 °C, the yield of carboxylic acids remains almost unchanged. Interestingly, the yield of undesired by-products increased from under 29% at 120 °C to about 33% at 130 °C. Consequently, the ratio of value-added products to undesirable by-products shifted in favor of the by-products, resulting in more CO₂ being formed than carboxylic acids. In the temperature range from 90 °C to 120 °C, the combined yields of carboxylic acids and undesirable by-products increased to approximately the same extent with increasing temperature. Hence, the ratio of value-added products to undesirable by-products changed only slightly from 54 : 46 to 50 : 50 in the temperature range between 90 °C and 120 °C. Overall, a reaction temperature of 120 °C is the most efficient concerning the increase in yield of carboxylic

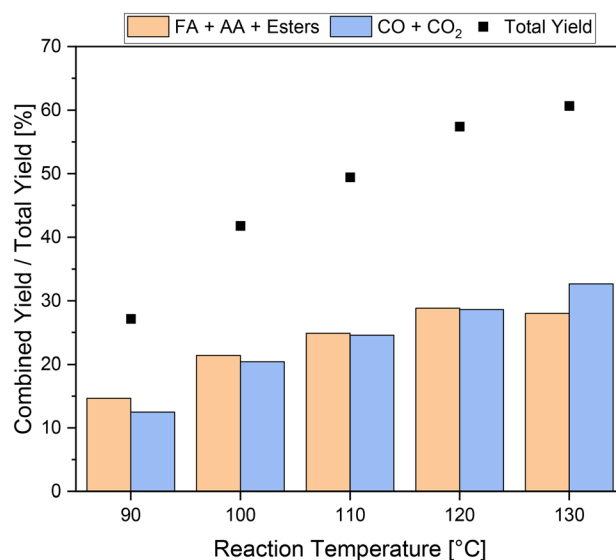


Fig. 3 SCO of humins using HPA-1 as a catalyst at different reaction temperatures in aqueous-methanolic solution. Experimental conditions: 3-fold reaction system, 90–120 °C, 30 bar O₂, 30 h, 1000 rpm, 300 mg solid humin (16.2 mmol carbon), 0.83 mmol of vanadium (V) for substitution (20 mol_{Carbon} mol_V⁻¹) in 5 vol% methanol.



acids and still effective inhibition of CO₂ formation. The stability test with methanol without substrate showed no formation of carboxylic acids up to a reaction temperature of 130 °C, confirming that the value-added products still originated from the humin substrate.

Effect of *p*TSA as solubilizer on the SCO of humins

It is well known that humins are virtually insoluble in commonly known solvents.^{5,21,29} The low solubility of humins hampers their chemical valorization in the liquid phase. In the literature, the use of solubilizers in the oxidative processing of biogenic raw materials and complex biomass is discussed.³⁸ *para*-Toluene sulfonic acid (*p*TSA) has proven to be one of the most promising solubilizers.^{38–44}

The application of *p*TSA for *in situ* solubilization of the substrate and enhancement of activity in the SCO of humins was further investigated. To this end, the oxidation of glucose-based humin was studied using 3 mmol *p*TSA as solubilizer under the initial reaction conditions (90 °C) in aqueous medium. First, the addition of methanol was deliberately avoided in order to be able to assess the influence of *p*TSA as a solubilizer. For the same purpose, the reaction temperature was reset to 90 °C, which also allowed separate consideration of temperature effects on this reaction system. As reference, an experiment was conducted without a catalyst but with the addition of *p*TSA. The results are displayed in Table 4. In the purely thermal reaction without a catalyst, the use of *p*TSA had only a small influence on the activity, with an increase in total yield from about 11% to about 14% compared to the reaction without *p*TSA (Table 4, entries 1 and 2). Interestingly, the combined yield of CO and CO₂ was hardly influenced between these two reactions. However, a combined yield of carboxylic acids of over 7% could be achieved with a combined yield of CO and CO₂ of only 7%, which is almost twice as high as in the reaction without *p*TSA.

It seems evident that the use of *p*TSA resulted in more easily converted humin fragments, which in turn were oxidized into FA and AA. The addition of *p*TSA in the reaction catalyzed by HPA-1 led to analogous results, in which the yield of carboxylic acids increased by almost a factor of two compared to that of the catalyzed reaction without *p*TSA

(Table 4, entries 3 and 4). More precisely, the yield of carboxylic acids increased from over 10% to over 20%, while the yield of undesired by-products remained at a value of 19%. In addition, it was found that more AA than FA was formed with addition of *p*TSA compared to the reaction without addition of *p*TSA. Almost equal yields of about 5.5% for FA and AA were obtained without the addition of *p*TSA. In comparison, the addition of *p*TSA resulted in an AA yield of about 13% and a yield of FA of about 7%. Presumably, the use of *p*TSA as a solubilizer results in better accessibility of the humin to the catalyst, resulting in the C₂ product AA, while the reaction without *p*TSA mainly produces C₁ building blocks, which formed FA and also CO₂.

To exclude that *p*TSA acts as a source for carboxylic acids, the stability of this additive was tested under identical conditions but without the addition of substrate (Table 4, entry 5). The ¹H NMR spectra and HPLC chromatogram indicated no formation of carboxylic acids, as shown in the ESI⁺ (Fig. S7 and S8). Furthermore, the results were confirmed using ¹³C and 2D NMR. In addition, a stability experiment using the reduced form of the catalyst (HPA-1 blue) was conducted. For this purpose, the catalyst was completely reduced using oxalic acid. When completely reduced, the catalyst shows an intense blue color (see Fig. S9[†]). In ⁵¹V NMR spectra, signals are no longer detectable due to the change of V⁵⁺ to V⁴⁺, which is paramagnetic (see Fig. S9[†]). According to ¹H NMR (Fig. S10[†]) and HPLC (Fig. S11[†]), no carboxylic acids could be detected in the stability test using the fully reduced HPA-1 blue catalyst. Comparable results can also be found in the literature.³⁸

Effect of *p*TSA concentration and reaction temperature on the SCO of humins

To further optimize the reaction, the influence of the amount of *p*TSA used and of the reaction temperature was also investigated in analogy to experiments using methanol. For this purpose, two further amounts of *p*TSA, 1.5 mmol and 6 mmol, were tested under otherwise identical reaction conditions. The results are shown in Table 5. The results show a linear dependence of the activity on the used amount of *p*TSA (Table 5, entries 2–4).

Table 4 SCO of humins using HPA-1 as catalyst and *p*TSA as solubilizer in aqueous phase

Entry ^a	Substrate	Catalyst	Additive	Total yield/%	Combined yield/%		Ratio ^d (value : waste)/%
					FA ^b + AA	CO + CO ₂ ^c	
1	Humin (Gl)	—	—	11.2	3.2	8.0	29 : 71
2	Humin (Gl)	—	<i>p</i> TSA	13.9	7.4	6.6	53 : 47
3	Humin (Gl)	HPA-1	—	30.1	10.9	19.2	36 : 64
4	Humin (Gl)	HPA-1	<i>p</i> TSA	39.1	20.1	19.0	51 : 49
5	—	HPA-1	<i>p</i> TSA	0.0	0.0	0.0	—

Experimental conditions: ^a 3-Fold reaction system, 90 °C, 30 bar O₂, 30 h, 1000 rpm, 300 mg solid humin (16.20 mmol carbon), 0.83 mmol of vanadium (V) for substitution (20 mol_{Carbon} mol⁻¹) and 3 mmol *p*TSA in 30 mL water. ^b Determined with quantitative ¹H NMR and *tert*-butanol as standard. ^c Determined with GC-TCD. ^d Calculated as described in corresponding section of the experimental part.



Table 5 SCO of humins using HPA-1 as catalyst and different amounts of *p*TSA

Entry ^a	Amount of <i>p</i> TSA/mmol	Total yield/%	Combined yield/%		Ratio ^d (value : waste)/%
			FA + AA ^b	CO + CO ₂ ^c	
1	0.0	30.1	10.9	19.2	36 : 64
2	1.5	49.9	23.7	26.2	47 : 53
3	3.0	39.1	20.1	19.0	51 : 49
4	6.0	33.1	15.7	17.4	47 : 53

Experimental conditions: ^a 3-Fold reaction system, 90 °C, 30 bar O₂, 30 h, 1000 rpm, 300 mg solid humin (16.20 mmol carbon), 0.83 mmol of vanadium (V) for substitution (20 mol_{Carbon} mol_V⁻¹) and 1.5–6.0 mmol *p*TSA in 30 mL water. ^b Determined with quantitative ¹H NMR and *tert*-butanol as standard. ^c Determined with GC-TCD. ^d Calculated as described in the corresponding section of the experimental part.

According to the results shown in Table 5, the total yield decreased from about 50% to about 33% when 1.5 mmol was used instead of 6.0 mmol, respectively. Therefore, the total yield decreased as the amount of *p*TSA increased. The influence of acid-induced effects and the polarity of the system could play a key role here, both increasing with a larger amount of *p*TSA. When adding more than 1.5 mmol *p*TSA, the pH of the solution drops significantly below pH 1 and thus leaves an adequate pH range, which could also negatively affect the results. This is also reflected in the combined yield of carboxylic acids, which reached its maximum at around 24% when 1.5 mmol *p*TSA was added (Table 5, entry 2). Based on the results, 1.5 mmol *p*TSA was considered as an optimum.

The reaction temperature can highly influence the kinetics of a reaction and thus the yield of carboxylic acids. To this end, experiments were conducted at different reaction temperatures using 1.5 mmol *p*TSA and the HPA-1 catalyst. The results are shown in Fig. 4. As expected, increasing the temperature from 90 °C to 120 °C also increased the total

yield from about 50% to 94%. Unfortunately, the increase in activity mainly affected the yield of products in the gas phase, especially CO₂, which increased from around 26% at 90 °C to about 60% at 120 °C. This corresponds to an increase of a factor of 2.3, which is of a similar magnitude to the increase in total yield. Consequently, the increased activity primarily led to increased CO₂ formation through over-oxidation of the humin. In comparison, the combined yield of carboxylic acid increased only from about 24% to about 34% at 90 °C or 120 °C, respectively. Interestingly, most of this increase was achieved by increasing the reaction temperature from 90 °C to 100 °C, which increased the combined yield of carboxylic acids from about 24% to about 31%. A further increase in reaction temperature had only a minor influence on the combined yield of carboxylic acids and thus is insufficient. In summary, it can be concluded that the addition of *p*TSA as a solubilizer can significantly increase not only the activity but also the combined yield of carboxylic acids even at mild temperatures from 90 °C to 100 °C. Furthermore, the combined yields of carboxylic acid using *p*TSA at mild reaction temperatures could even compete with the yields using methanol at elevated reaction temperatures. However, the addition of *p*TSA did not inhibit CO₂ formation, therefore more undesired by-products than value-added products were formed. In particular, at higher temperatures, this effect was evident. In this regard, the addition of methanol was more beneficial compared to addition of *p*TSA. However, the combination of the effects of both additives could enable a new optimum in the SCO of humins.

Optimization of the SCO of humins by synergetic combination of MeOH and *p*TSA as additives

In order to investigate whether the combination of solubilizer and alcoholic additive leads to synergetic effects, both 5 vol% methanol and 1.5 mmol *p*TSA were added to the reaction solution. The experiment was conducted at 120 °C, since at this reaction temperature the best results and a significantly increased activity were obtained in the experiments using methanol. Moreover, at 120 °C the efficiency of inhibition of CO₂ formation by methanol can be tested, since here the highest CO₂ yield was obtained in the experiments using *p*TSA. The results can be seen in Fig. 5. For comparison, the results for the individual additives at 120 °C are also shown.

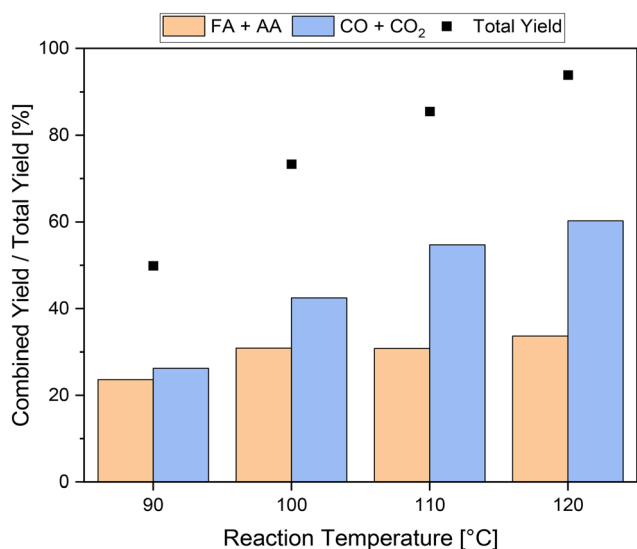


Fig. 4 SCO of humins using HPA-1 as catalyst at different reaction temperatures and *p*TSA as additive. Experimental conditions: 3-fold reaction system, 90–120 °C, 30 bar O₂, 30 h, 1000 rpm, 300 mg solid humin (16.20 mmol carbon), 0.83 mmol of vanadium (V) for substitution (20 mol_{Carbon} mol_V⁻¹) and 1.5 mmol *p*TSA in 30 mL water.



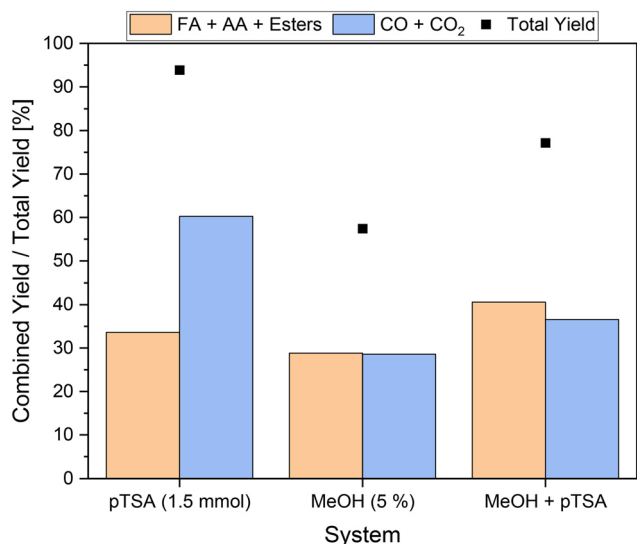


Fig. 5 SCO of humins using HPA-1 as catalyst in aqueous methanolic solution with *p*TSA (combined system). Experimental conditions: 3-fold reaction system, 120 °C, 30 bar O₂, 30 h, 1000 rpm, 300 mg solid humin (16.2 mmol carbon), 0.83 mmol of vanadium (V) for substitution (20 mol_{Carbon} mol_V⁻¹) in 5 vol% methanol with 1.5 mmol *p*TSA.

The results in Fig. 5 show that the total yield of the novel approach was intermediate between the total yields of the individual experiments. More specifically, a total yield of about 77% was achieved, which is almost equal to the average of 76% calculated from the results using the individual additives. This could be an indicator of additive interaction. On the one hand, *p*TSA as an additive increased the activity of the reaction. On the other hand, methanol inhibited CO₂ formation and thus slightly decreased the activity. This seems particularly plausible considering the combined yield of about 37% of undesired by-products, which is even below the average of 44% using the

individual substrates. A combined yield of carboxylic acids of more than 40% was achieved, outperforming the yields obtained using the individual additives. As a result, more value-added products were produced than undesired by-products and significantly higher activity could be enabled.

In comparison to the pioneering experiments by Maerten *et al.*,⁵ which so far represent the benchmark for the SCO of humins, the potential of the newly developed approach can be deduced. The yield of value-added products was increased by a remarkable factor of 3.6, while at the same time the yield of undesired by-products was 1.6 times lower. Three individual reactions were conducted as reproduction experiments to verify the results. It was possible to reproduce the results of liquid phase products with average yields of 26.0% ± 0.2%, 2.5% ± 0.1% and 12.1% ± 0.2% for FA, MF and AA, respectively. Average yields of 2.1% ± 0.1% and 32.8% ± 1.0% were reproduced for the gas phase products CO and CO₂, respectively. The results are found in the ESI† (see Fig. S12). In order to exclude the additives as the origin of carboxylic acids using the novel approach, stability tests were performed without the addition of substrate. According to NMR spectra and HPLC measurements, no carboxylic acids could be detected in the liquid phase after the reaction in these experiments. Furthermore, the formation of CO and CO₂ could not be confirmed by GC measurements.

Of further interest is the stability of the catalyst, as this also has a significant influence on the sustainability and economic effectiveness of the developed reaction system. A comparison of the ⁵¹V NMR and ³¹P NMR spectra of the catalyst before and after the reaction is helpful in this context. The vanadium-substituted POM catalysts can be analyzed structurally based on characteristic signals in the NMR spectra, which have already been discussed in detail in the literature.^{24,39,45–49} Fig. 6 shows both the ⁵¹V NMR spectra and the ³¹P NMR spectra of the used

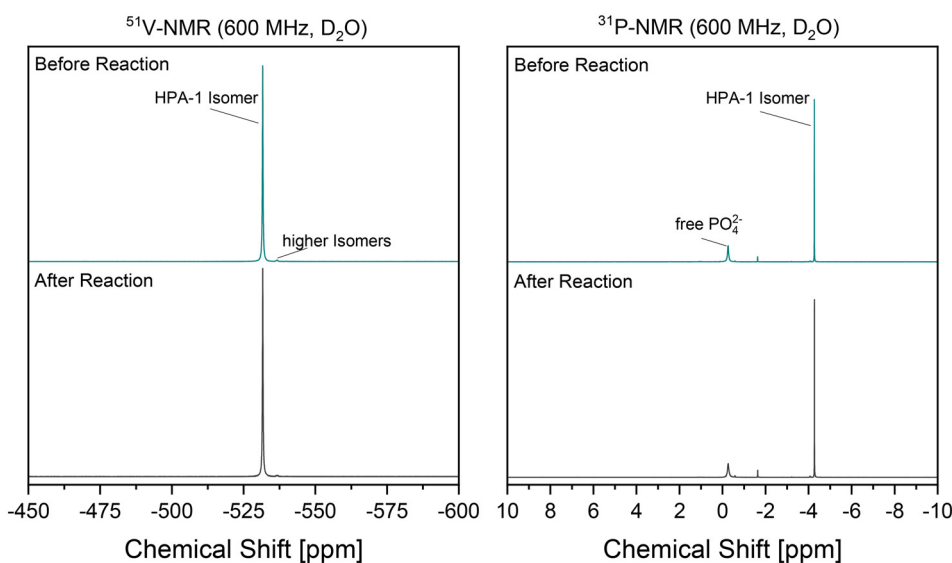


Fig. 6 Comparison of ⁵¹V NMR (left) and ³¹P NMR (right) spectra before and after the reaction. Experimental conditions: 3-fold reaction system, 120 °C, 30 bar O₂, 30 h, 1000 rpm, 300 mg solid humin (16.2 mmol carbon), 0.83 mmol of vanadium (V) for substitution (20 mol_{Carbon} mol_V⁻¹) in 5 vol% methanol with 1.5 mmol *p*TSA.



HPA-1 catalyst in the reaction solution. Due to the low degree of substitution, the spectra are extremely simple, as the number of possible isomers is restricted to almost one.

In addition, the formation of a complex mixture of isomers by dissociation and protolysis of higher substituted isomers is not possible, as these are practically non-existent using HPA-1. The comparison of the ^{51}V NMR spectra before and after the reaction reveal no changes. The signal at about -530 ppm, which can be assigned to the HPA-1 isomer, is retained. The same applies to the signal of the HPA-1 isomer at about -4.2 ppm in the ^{31}P NMR spectra. In particular, a strong increase in free phosphate (at -0.2 ppm) might indicate a decay of the Keggin structure, which was not observed. Overall, the results indicated that the structural integrity of the catalyst is given. In their study, Voß *et al.*⁵⁰ were able to demonstrate a continuous oxidation process in a comparable reaction system using a vanadium-substituted POM catalyst. Analogous to the experiments of Voß *et al.*,⁵⁰ a final evaluation of the catalyst stability and the associated preservation of catalytic activity in the reaction system developed here requires recycling experiments.

Initial investigations by Bertleff *et al.*⁵¹ and previously published results⁵² showed that efficient separation of the acidic oxidation products is essential for stable catalytic activity. In these studies, the decline in catalytic activity without separation of the acidic oxidation products could be attributed, among other things, to the formation of less substituted HPA isomers (HPA-1) at the expense of higher substituted isomers. This would not affect the present system since HPA-1 is already used, but a negative influence of catalysis cannot be ruled out if the oxidation products strongly accumulate. POMs are known to be extremely soluble in polar media, causing them to form a homogeneous phase with the product solution, making efficient separation difficult.^{24,47,53} In this context, nanofiltration proved to be very promising, enabling rejections for the catalyst of over 99%, while carboxylic acids such as FA and AA were almost not rejected.^{51,52}

To gain a deeper insight into the reaction process, the time-resolved reaction profiles were recorded and displayed in Fig. 7. For this purpose, individual reactions with reaction times of 0 h, 2 h, 4 h, 8 h, 16 h and 24 h were conducted and the liquid, gaseous and solid products were analyzed. In the first 4 h of reaction, the formation rate of the liquid phase and gas phase products was the highest and comparable to each other. Both achieved a combined yield of about 16% after 4 h. The amount of solid residue also decreased the strongest during this period. After 4 h, the formation of the products decreases significantly, although this effect is stronger for the gaseous products than for the liquid products. After 8 h, a combined yield of 24% and 20% was achieved for liquid products and gaseous products, respectively. In the subsequent reaction time up to 16 h and onwards, the combined yield of the carboxylic acids increased significantly more slowly, resulting in a very flattened course. The amount of solid residue also behaved similarly depending on the reaction time.

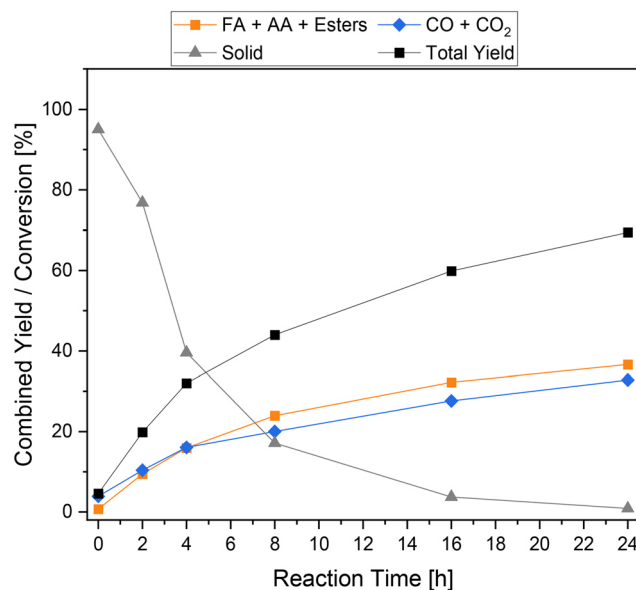


Fig. 7 Reaction course of the SCO of humins using HPA-1 as catalyst in aqueous methanolic solution with pTSA (combined system). Experimental conditions: 3-fold reaction system, 120 °C, 30 bar O₂, 0–30 h, 1000 rpm, 300 mg solid humin (16.20 mmol carbon), 0.83 mmol of vanadium (V) for substitution (20 mol_{Carbon} mol_V⁻¹) in 5 vol% methanol with 1.5 mmol pTSA.

Fig. 8 shows the results of the elemental analysis of the solid residue depending on the reaction time. Of particular interest are the mass fractions of oxygen (O) and carbon (C) and their ratio (O/C). In the first 4 h of reaction, the mass fraction of carbon decreased sharply from over 60% to below 50%, while the mass fraction of oxygen increased from about

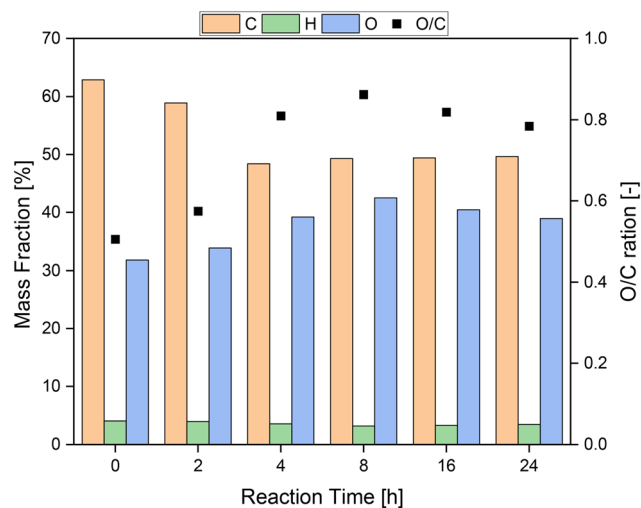


Fig. 8 Elemental analysis of residual humin from the SCO using HPA-1 as catalyst in aqueous methanolic solution with pTSA (combined system) depending on reaction time. Experimental conditions: 3-fold reaction system, 120 °C, 30 bar O₂, 0–24 h, 1000 rpm, 300 mg solid humin (16.20 mmol carbon), 0.83 mmol of vanadium (V) for substitution (20 mol_{Carbon} mol_V⁻¹) in 5 vol% methanol with 1.5 mmol pTSA.



30% to 40%. Hence, the oxygen-carbon ratio increased from about 0.35 to 0.80 in the first 4 h. Therefore, it seems plausible that functional groups were oxidized in the first hours of the reaction, but oxidative C-C bond cleavage also occurred, which induced oxygen-rich functional groups. After 8 h, the ratio of oxygen to carbon reached its peak with a value of almost 0.9. In the following hours the ratio fell slightly again, presumably because more oxygen was removed from the humin structure *via* the oxidation products than was introduced into the humin. This can also be recognized by the almost constant mass fraction of carbon after the first 8 h.

The solid residue was also analyzed by Fourier-transform infrared (FT-IR) spectroscopy to elucidate any structural changes in the humin depending on the reaction time. The results are shown in Fig. 9. Before catalysis, humin typical bands such as substituted furan rings (C=C, C-H vibration) could be observed at 1600 cm^{-1} , 1510 cm^{-1} and 1295 cm^{-1} and additional bands of carbonyl bonds at 1700 cm^{-1} .^{9,21,27,54} During the course of the reaction, the bands corresponding to polysubstituted furan rings (1510 cm^{-1}), aldehydes and ethers (1090 cm^{-1}), and aliphatic chains (1295 cm^{-1}) decreased or disappeared completely.

In the first hours of the reaction, the band corresponding to carbonyl conjugated C=C double bonds (1600 cm^{-1}) became more intense. It can be assumed that the increase in the intensity of this band is due to the oxidation of the insoluble humin residue and thus of alkyl groups or furan rings that could not be cleaved to form double bonds or ketones. Therefore, the number of double bonds conjugated

to carbonyl compounds in humin would increase. The bands corresponding to C=O bonds (1710 cm^{-1}) in acids, aldehydes and ketones behaved in a similar manner. The increase in the mass fraction of oxygen measured by elemental analysis fits these observations. All these observations indicate that oxygen-functionalized bonds and groups were not only converted but also newly induced into the humin structure. Wassenberg *et al.*²¹ described comparable observations in their study. In the range between 950 cm^{-1} and 1050 cm^{-1} new bands occurred, which most likely correspond to M=O bonds and P-O bonds of the catalyst.^{24,55,56} At the end of the reaction, the intensity of all bonds decreased significantly.

Fig. 10 shows a hypothetical mechanism for the SCO of humins. Basically, the discussion of a mechanism is difficult, because despite extensive research, no reliable humin structure exists to date. However, as mentioned above, there are a number of plausible formation mechanisms and proven structural elements for humins, which have led to various models for its structure.^{15–17,29,30,57} According to these models, the furan-rich network is predominantly cross-linked *via* aliphatic bonds and has numerous active oxygen functionalities. In the study by Zandvoort *et al.*,²⁹ 2D NMR spectra were used to demonstrate that the linkers are not simple methylene groups, but rather short aliphatic chains and oxygen-functionalized bonds forming structures similar to levulinic acid, for example. This seems plausible because the formation of humins is most probably based on the aldol condensation of the intermediates 5-HMF, DHH and levulinic acid.¹⁷

In the process, the formation of α,β -unsaturated carbonyl moieties or carbonyl moieties with hydroxy groups in the α -position is possible.^{15,17,21,29} The humin model structure shown in Fig. 10 represents the combination of the various possible bonds and structures in one section. The fundamental framework is based on a model postulated by Filiciotto *et al.*¹⁶ (Fig. 10, A), which was modified by a structural element confirmed by Wassenberg *et al.*²¹ (Fig. 10, B) and a section according to Shen *et al.*¹⁷ (Fig. 10, C).

Based on previously published results dealing with SCO of humin-like model substances, oxygen functionalization is essential for efficient conversion of the structures by POM catalysts.²³ The simplest types of oxygen functions are free functionalities such as aldehydes and carboxylic acids (Fig. 10, pathway 2). These functionalities can be converted directly by the catalyst. Here, an electron transfer (ET) to the catalyst occurs, which is consequently reduced ($V^V \rightarrow V^{IV}$). In this way, an oxidative C-C bond cleavage takes place at the carboxyl function with the elimination of CO_2 . The oxidative C-C bond cleavage on the aldehyde follows a comparable mechanism. We assume that electron transfer is preceded by a nucleophilic attack of a water molecule in acidic medium, resulting in the elimination of FA. Previous publications have used this mechanism to accurately predict the yield of FA and CO_2 in the SCO of humin-like model substances, confirming the plausibility of this mechanism.²³ By eliminating a C_1 building block, a highly unstable furyl

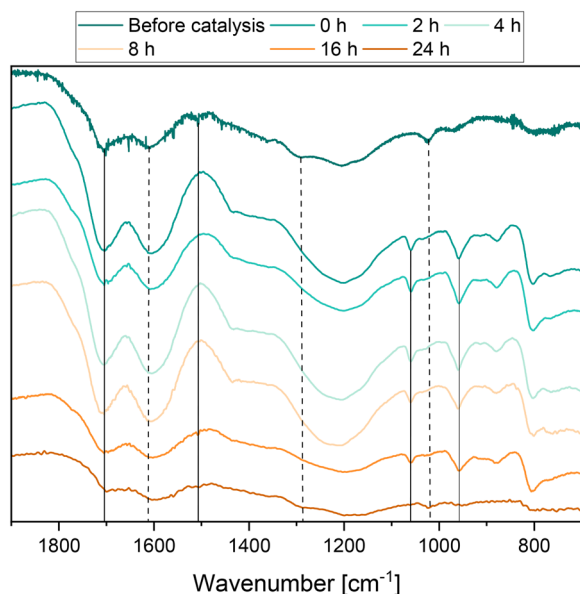


Fig. 9 IR spectra for the reaction course of the SCO of humin using HPA-1 as catalyst in aqueous methanolic solution with *p*TSA (combined system). Experimental conditions: 3-fold reaction system, $120\text{ }^\circ\text{C}$, 30 bar O_2 , 0–24 h, 1000 rpm, 300 mg solid humin (16.20 mmol carbon), $0.83\text{ mmol of vanadium (V)}$ for substitution ($20\text{ mol}_{\text{Carbon}}\text{ mol}_{\text{V}}^{-1}$) in 5 vol% methanol with 1.5 mmol pTSA .



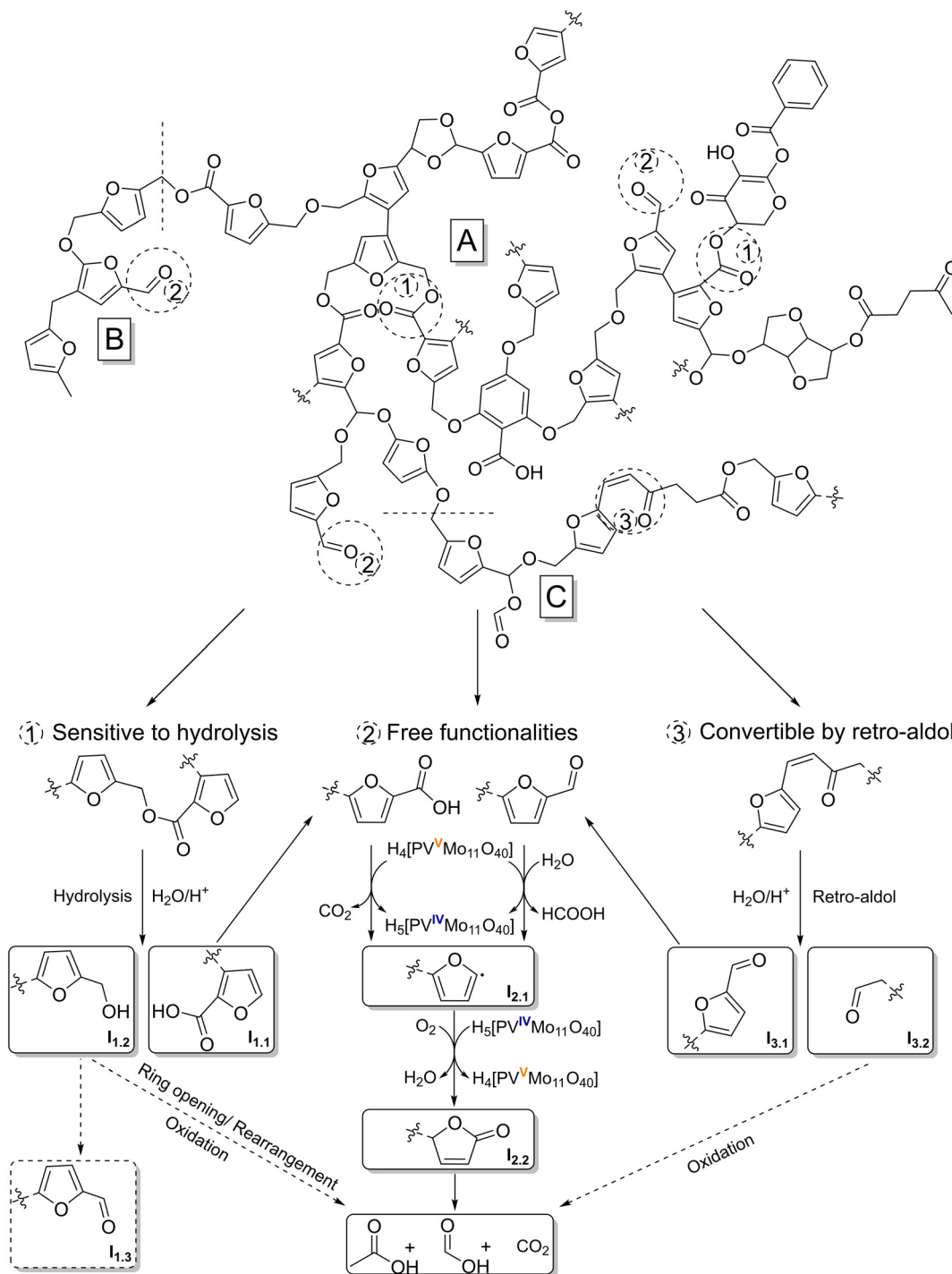


Fig. 10 Reaction mechanism for the selective catalytic oxidation of a modified humin model structure based on structural motifs published by Filiciotto *et al.*¹⁶ (A), Wassenberg *et al.*²¹ (B) and Shen *et al.*¹⁷ (C) by converting humin typical functionalities that are hydrolysis-sensitive (1), free (2) or convertible by retro-aldol (3).

radical (Fig. 10, $\text{I}_{2,1}$) is formed, which is converted to a carbonyl function (Fig. 10, $\text{I}_{2,2}$) under the action of molecular oxygen and water. The catalyst is reoxidized during this process ($\text{V}^{\text{IV}} \rightarrow \text{V}^{\text{V}}$). Intermediate $\text{I}_{2,2}$ is structurally reminiscent of 2(5H)-furanone. In the experiments on the SCO of model substances, both 2(5H)-furanone and mainly 5-hydroxy-2(5H)-furanone as analogous compounds were

detected.²³ Here the intermediate is still bound to the humin by a bond, therefore none of the intermediates could be detected in the reaction solution. The newly formed functionality opens new attack options as well as the possibility of ring opening. It has been demonstrated in previous studies on free furan systems that more strongly oxidized products such as maleic acid are formed as



subsequent products.²³ This is not possible in the present case because the ring system is still integrated into the humin structure, and thus additional C₁ and C₂ building blocks such as FA, AA and CO₂ are oxidatively eliminated. In this way, the humin structure is gradually broken down and new functionalization is repeatedly induced.

Another type of oxygen functionality are hydrolysis-sensitive bonds such as esters (Fig. 10, pathway 1). These bonds can be easily broken by acid catalysis, creating free functionalities (I_{1.1}) that can be converted according to pathway 2. Probably hydroxyl groups are also formed during the hydrolysis of esters (I_{1.2}). Under the prevailing oxidative conditions, the hydroxyl groups could oxidize to carbonyl moieties (I_{1.3}), which in turn can also be converted according to the described pathway 2. The oxidation of primary alcohols by POM catalysts has already been investigated and confirmed in the literature.^{58–61} However, previous results on the free furan system in the form of furfuryl alcohol have shown that the intermediates 2(5*H*)-furanone and 5-hydroxyfuran-(25*H*)-furanone and the final product of this pathway (using free furan systems), maleic acid, were almost not formed.²³ Instead of maleic acid, products such as succinic acid and levulinic acid were detected, indicating a different mechanism.²³ It is known that furfuryl alcohol can rearrange in various ways and even hydrolytic ring openings are possible in aqueous solutions under acidic conditions.^{62–67} Carbonyl moieties, γ -diketone, and conjugated diene structures as well as levulinic acid-like structures can form.^{62–67} Oxidative ring opening is also feasible, leading to conjugated aldehydes.⁶⁷ These structures are more easily converted to short-chain products such as AA, FA and CO₂ by the POM catalyst. This would be consistent with the SCO results for furfuryl alcohol.²³

The α,β -unsaturated carbonyl moieties formed by aldol condensation can also be converted into more accessible structures by acid catalysis (Fig. 10, pathway 3). In a mechanism analogous to that of retro-aldol, these structures are cleaved by protonation of the carbonyl oxygen, nucleophilic attack of a water molecule in the β position and subsequent rearrangement. Comparable mechanisms have already been described in the literature for the SCO of cellulose using POM catalysts.⁶⁸ As a result, easy-to-convert carbonyl moieties near the furan ring (I_{3.1}) are created, which can be converted analogously to pathway 2. The formed aliphatic carbonyl moiety (I_{3.2}) should also be easy to convert, especially since it is usually close to other oxygen functionalities. This causes further C₁ and C₂ building blocks to be cleaved as AA, FA, and CO₂.

Overall, the mechanisms shown represent only a number of possibilities for the SCO of humins. These essentially depend on the actual humin structure, which is not yet completely elucidated. There are also structural models in the literature that stipulate a higher proportion of cross-linking *via* bonds without oxygen functionalization.^{9,26,27,69,70} Ultimately, oxygen functionalization, albeit in lower proportions, enable oxidative degradation. Further mechanistic investigation of the reaction system for the SCO of humins and the integration of future insights on the structure elucidation of humins should be considered in further studies.

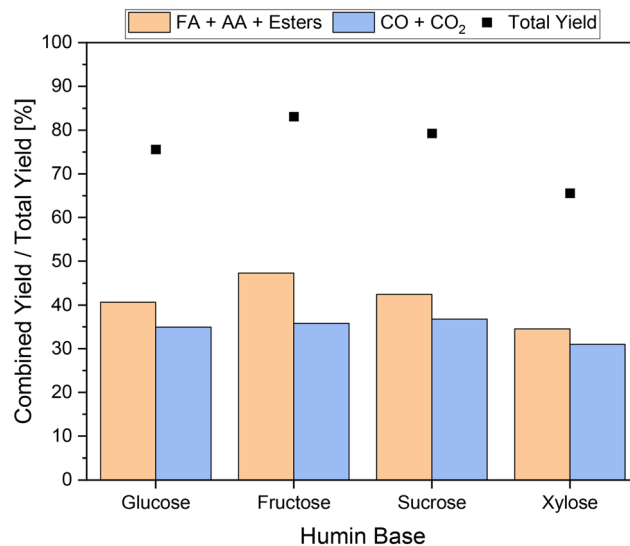


Fig. 11 SCO of various real humins using HPA-1 as catalyst in aqueous methanolic solution with *p*TSA (combined system). Experimental conditions: 3-fold reaction system, 120 °C, 30 bar O₂, 30 h, 1000 rpm, 300 mg solid humin (16.20 mmol carbon), 0.83 mmol of vanadium (V) for substitution (20 mol_{Carbon} mol_V⁻¹) in 5 vol% methanol with 1.5 mmol *p*TSA.

SCO of different real humins using the combined approach

In a final set of experiments, various real humins based on glucose, fructose, sucrose, and xylose were processed to verify the universal effectiveness of the newly developed approach. The results are shown in Fig. 11.

In all experiments, the combined yield of carboxylic acids exceeded the yields of undesired by-products. If a C₆-sugar was used as a substrate for humin synthesis, the yields of undesired by-products were at comparable values of around 36%. In the SCO of the fructose-based humin a combined yield of carboxylic acids of about 47% was achieved. The combined yield of carboxylic acids from the conversion of the sucrose-based humin was between those of glucose- and fructose-based humins. This seems plausible since sucrose is composed of glucose and fructose. Interestingly, the conversion of the xylose-based humin enabled the lowest total yield of only 66% and thus also the lowest combined yield of carboxylic acids below 35%. In contrast to hexoses, humin formation based on pentoses does not occur *via* 5-hydroxymethylfurfural (5-HMF) but *via* furfural; therefore fewer aldol condensations were involved in humin formation.^{9,21} Moreover, the structure of xylose-based humin could be converted less efficiently. Nevertheless, it can be confirmed that the newly developed approach for the selective catalytic oxidation of humins is transferable to various humins and enables their efficient conversion to value-added products. Transferring the insights to higher substituted POM catalysts for the SCO of humins in the newly developed reaction system could be another interesting approach for system optimization. In this process, the use of additives could also help to prevent the over-oxidation of



humins caused by these much more active catalysts. This would allow a decrease in reaction temperature or reaction time, which could increase sustainability and economic viability. However, the question arises as to what extent the effects found are transferable and whether the additives are stable using higher substituted catalysts.

Conclusion

In the presented contribution we focused on the development of an optimized reaction system for the selective catalytic oxidation of water-insoluble and highly complex humins to short-chain carboxylic acid using Keggin-type polyoxometalates. We could demonstrate that a singly vanadium-substituted polyoxometalate catalyst exhibited a considerable selectivity advantage in the aqueous phase over higher substituted catalysts. More specifically, the yield of the undesired by-products CO and CO₂ was drastically decreased to a third, while the yield of carboxylic acids remained almost unchanged compared to that in benchmark experiments. Moreover, we applied alcohol additives with a remarkable inhibiting effect on CO₂ formation, further increasing the efficiency in the SCO of humins. As an alcohol additive, methanol in particular stands out due to the strongest inhibition of CO₂ formation compared to ethanol and isopropanol. For the first time, the oxidative valorization of humins produced more value-added products than undesired by-products such as CO₂. Furthermore, we investigated the influence of alcohol content and reaction temperature on the humin oxidation. It was shown that a temperature of 120 °C represents an optimum where methanol can still inhibit CO₂ formation even at a low alcohol content of 5 vol%. Due to these optimizations, the yield of carboxylic acids could be doubled without formation of CO₂ dominating. Furthermore, the use of *para*-toluenesulfonic acid (*p*TSA) as solubilizer has been investigated to circumvent the water-insoluble character of humins and thus optimize the activity. Using this solubilizer, the water-insoluble humin could be efficiently converted to equal yields of carboxylic acids and undesired by-products even without the CO₂-inhibiting effect of methanol. The activity of the reaction system was enhanced by optimizing the amount of solubilizer and the reaction temperature. However, the drastically increased activity led to a predominant formation of CO₂ and only to a small increase in value-added products. On the one hand, *p*TSA could efficiently promote the activity in oxidative valorization of humins. On the other hand, methanol was far more efficient in inhibiting CO₂ formation, especially at elevated reaction temperatures. Therefore, the combination of both additives at elevated reaction temperature was examined in a final optimization approach in order to exploit possible synergy effects. This novel approach enabled the highest yield of carboxylic acids and simultaneously the lowest yield of CO₂ reported to date in the SCO of humins. The results were reproducible and could even be transferred to various humins based on different sugars. We can conclude that using the combination of methanol and *p*TSA as additives as well as a singly vanadium-substituted

polyoxometalate catalyst provides a highly promising approach in the selective catalytic oxidation of complex humins.

Experimental details

Chemicals

All chemicals were acquired commercially and used without further purification. To synthesize humins, acetic acid as an acid catalyst and various sugars were used. The sugars D(+)-glucose, D(-)-fructose, and D(+)-xylose (all for biochemistry) were purchased from Merck Millipore. Sucrose (99%) was obtained from Alfa Aesar. VWR Chemicals was the supplier of acetic acid (glacial).

For calibrations, reference spectra, and quantification, formic acid (97%) and *tert*-butanol (99%, ultrapure) obtained from VWR Chemicals and Grüssing were used.

For the presented study, singly V-substituted Keggin-type polyoxometalate catalyst, which can be described by the formula H₄[PVMo₁₁O₄₀], was synthesized according to the literature.^{23,39,71–73} In the selective catalytic oxidation of humins, additives were used to optimize the process. Alcohol additives were methanol (99.8%) and ethanol (99.8%) purchased from VWR Chemicals. As solubilizer, *p*TSA monohydrate (98%) obtained from Roth was used.

Catalyst characterization

To verify the stoichiometry of the synthesized H₄[PVMo₁₁O₄₀] catalyst, inductively-coupled optical emission spectrometry (ICP-OES) was used. For the synthesized H₄[PVMo₁₁O₄₀] catalyst, a stoichiometry of 1.23P/0.97V/11Mo was determined. Based on attenuated total reflection Fourier-transform infrared (ATR-FTIR) spectroscopy and ⁵¹V as well as ³¹P NMR spectroscopy, the integrity of the POM structure was verified. The results can be found in the ESI† (Fig. S13–S15).

Using a QATR™-S single-reflection ATR (with a diamond prism), the attenuated total reflection (ATR) FTIR spectrum of the catalyst was measured.

The respective service groups in the Department of Chemistry at Hamburg University conducted the following analyses:

Analysis of the catalyst to determine its stoichiometry was performed using a Fa. Spectro Arcos (Ametek) ICP-OES spectrometer. For the determination of the elemental composition (Mo, P, V) of the catalyst, it was dissolved in water (5 mL). Before measurement, 100 μL of a 65% aqueous nitric acid solution was added and subsequently diluted in a volumetric flask with water to 25 mL.

Nuclear magnetic resonance (NMR) measurements of the catalyst were conducted using a Bruker AVANCEII 600 MHz spectrometer. For the measurement, deionized water was acidified to pH 1 using a 37% aqueous hydrochloric acid solution in which 70 mg of catalyst was dissolved (0.7 mL). As the final preparation step, 0.07 mL of acetone-d₆ was added. Measurements of the ³¹P spectra were conducted in time domain (TD) data size of 32k, with a number of scans (NS) of 2k (=2048), a transmitter frequency offset for channel F1 (O1) and



a spectral width (SW) of -1 and 40 ppm. The settings of the aforementioned parameters for the measurements of the ^{51}V spectra were TD 32k, NS 4k, O1 and SW -520 ppm and 400 ppm and D1 0.5 s.

Experimental setup and general procedure of humin synthesis

Basically, the procedure described by Wassenberg *et al.*²¹ was used for the synthesis of humins. To ensure a better reproducibility, larger batches of humin were prepared to perform oxidation experiments with the same batch. For this purpose, the humin synthesis was scaled up. A 600 mL autoclave made of Hastelloy (C-276) equipped with a gas entrainment impeller was used for the synthesis of large-scale humin batches. The synthesis was conducted under a nitrogen atmosphere, with acetic acid as acidic catalyst and a reaction time of 8 h. For the reaction, an aqueous acetic acid solution was prepared as a stock solution setting a pH value of 2 . For this purpose, about 25 ml of acetic acid (glacial) were mixed with 200 ml of water. Subsequently, 36 g (0.2 mol) of glucose was weighed into a 400 mL glass liner and 200 mL of the acid solution was injected. This acid/solvent/sugar mixture provided a molar ratio of H^+ /sugar of $1:100$. The glass liner was inserted into the 600 mL autoclave, which was then sealed. To ensure a pure nitrogen atmosphere and to avoid oxidation reactions, the autoclave was purged three times with 45 bar nitrogen. Finally, a pre-pressure of 20 bar nitrogen was set. The reaction solution was stirred (300 rpm), the reaction temperature set to 180 °C, and the pressure increased to 45 bar. After 8 h of reaction, the heating jacket was turned off and removed. At a temperature below 30 °C, the autoclave was slowly ventilated and depressurized. The reaction solution containing the solid humin was filtered, rinsed with water, dried, and ground in a mortar. To ensure that no acid remains in the humin, the fine powder was cleaned with water using Soxhlet extraction for 24 h. The cleaned humin was dried for 24 h at 80 °C.

Experimental setup and general procedure of the SCO

For selective catalytic oxidation of synthesized humins a 3-fold reaction system was used. The plant has three identical 100 mL autoclaves made of stainless steel. Each autoclave was equipped with a heating jacket allowing reaction temperatures up to 200 °C, a gas entrainment impeller, and a 45 mL glass liner. All reactors were connected to an oxygen supply line.

In a typical experiment, each glass liner was filled with the appropriate amount of solid catalyst (0.83 mmol of vanadium), 300 mg humin (16.20 mmol carbon) and 30 mL of water. The filled glass liners were inserted into the autoclaves, and these were closed. To ensure a pure oxygen atmosphere, the closed autoclaves were purged three times with 30 bar oxygen. For experiments at a reaction temperature of 90 °C, the autoclaves were pressurized to a pre-pressure of 26.5 bar and the heating jackets were put on. Subsequently, the reaction temperature of 90 °C and a stirring speed of 300 rpm was set. When the desired reaction temperature inside the autoclaves was reached, the

stirring speed was increased to 1000 rpm, which marked the start of the reaction. Due to the increase of temperature, the pressure increased to the desired value of 30 bar. At the end of each experiment, the temperature was set to 0 °C, the heating jackets were taken off and the stirring speed was decreased to 300 rpm, lowering the entrainment of oxygen into the liquid phase. When the temperature inside the autoclaves reached below 30 °C, samples of the gas phase could be taken. After venting the autoclaves, the glass liners were taken out of the autoclaves and the liquid phase was filtered.

In experiments using additives the experimental procedure was slightly adapted. The additive *p*TSA (0.285 g to 1.140 g (1.5 mmol to 6.0 mmol)) was filled into the glass liners in the form of its solid monohydrate. For experiments using alcohol additives, an aqueous solution of the respective alcohol as well as the desired alcohol content was prepared and charged into the glass liners instead of 30 mL water.

Analysis of substrates and reaction products

For quantitative measurement of the liquid phase, a Shimadzu HPLC system equipped with an HPX-87H 300 mm 7.8 mm Bio-Rad column and a refractive index detector was applied. An aqueous sulfuric acid solution at a concentration of 5 mmol L^{-1} was utilized as eluent. Measurements were conducted at a flow rate of 0.5 mL min^{-1} , a pressure of 49 bar, and a temperature of 45 °C.

A Varian 450-GC equipped with a TCD detector was used to measure the amounts of gaseous CO and CO₂.

FT-IR spectra of humins and the solid residue of the oxidation experiments were measured using the already mentioned (ATR) FT-IR device.

The respective service groups in the Department of Chemistry at Hamburg University conducted the following analyses:

A Model EA-3000 analyzer of Fa. EuroVector (Milano, Italy) was used for elemental analyses (CHNSO) of the synthesized humins and the solid residues after oxidation experiments.

NMR spectra of the reaction solutions were conducted using a Bruker AVANCEII 600 MHz spectrometer. The samples of the reaction solutions were prepared by blending 0.6 mL of the reaction solution with 0.1 mL of a 10 wt% *tert*-butanol solution in D₂O. The spectra were evaluated using the software MestReNova®.

Calculations

All calculated yields are based on the carbon provided by the substrate. When quantifying using ^1H NMR, a 10 wt% solution of *tert*-butanol as internal standard in D₂O was used. The molar amount $n_{\text{Pro}i}$ of a product i in the liquid phase can be calculated based on the ratio of its area $A_{\text{Pro}i}$ to the area A_{Stand} of the contained standard. The number of protons N_{H} that generate the signal must be taken into account, as shown in eqn (1). With the known molar amount n_{Stand} of standard in the sample and the mass of the sample, the mass fraction $w_{\text{Pro}i}$ of the respective substance can be calculated.



$$n_{\text{Proi}} = \frac{A_{\text{Proi}} \cdot N_{\text{H,Stand}}}{A_{\text{Stand}} \cdot N_{\text{H,Proi}}} \cdot n_{\text{Stand}} \quad (1)$$

The yield Y_{Proi} of a product i results from the ratio of its measured mass fraction w_{Proi} to its theoretically possible mass fraction $w_{\text{theo,Proi}}$ as shown in eqn (2).

$$Y_{\text{Proi}} = \frac{w_{\text{Proi}}}{w_{\text{theo,Proi}}} \quad (2)$$

The theoretically possible mass fraction $w_{\text{theo,Proi}}$ is calculated by the ratio of the theoretically possible mass of a product i and the sum of the weights of the substrate m_{Sub} , pTSA m_{pTSA} , catalyst m_{Cat} and solvent m_{Sol} (or alcohol-doped solution), as described in eqn (3). Here, the theoretically possible mass of a product i is calculated by the initial molar amount $n_{0,\text{C}}$ of carbon provided by the substrate, the amount $N_{\text{C,Proi}}$ of carbon required for the formation of a product i and its molar mass M_{Proi} .

$$w_{\text{theo,Proi}} = \frac{n_{0,\text{C}} / N_{\text{C,Proi}} \cdot M_{\text{Proi}}}{m_{\text{Sub}} + m_{\text{pTSA}} + m_{\text{cat}} + m_{\text{sol}}} \quad (3)$$

Based on the known mass fraction $w_{\text{C,Sub}}$ of carbon in the substrate, the mass m_{Sub} of substrate and the molar mass M_{C} of carbon, the initial molar amount $n_{0,\text{C}}$ of carbon was calculated, as described by eqn (4).

$$n_{0,\text{C}} = \frac{w_{\text{C,Sub}} \cdot m_{\text{Sub}}}{M_{\text{C}}} \quad (4)$$

Using eqn (5), the measured molar concentration of a product i c_{Proi} was converted to the mass fraction of the product i w_{Proi} for quantification by HPLC:

$$w_{\text{Proi}} = c_{\text{Proi}} \cdot \rho_{\text{liq}} \cdot M_{\text{Proi}} \quad (5)$$

The yield could be calculated analogously to the quantification by NMR using eqn (2). The total yield is the sum of the yields of all products. Based on the total yield, the share of the value-added products (value) in the total yield was calculated according to eqn (6), taking into account the yields of the products formic acid Y_{FA} , methyl formate Y_{MF} and acetic acid Y_{AA} . The share of undesired by-products (waste) was calculated from the difference between 100 and the share of value-added products.

$$\text{Value} = \frac{Y_{\text{FA}} + Y_{\text{MF}} + Y_{\text{AA}}}{\sum_0^i Y_{\text{Proi}}} \times 100 \quad (6)$$

Conflicts of interest

There are no conflicts to declare.

Acknowledgements

J. A. and T. E. acknowledge financial support from the Deutsche Forschungsgemeinschaft (DFG) via the project AL

2130/5-1. Moreover, we thank the division for central element analytics, the division for NMR spectroscopy and the division for electron microscopy of the Department of Chemistry for conducting ICP as well as CHNS measurements, NMR experiments and SEM measurements, respectively. We also thank Jan-Christian Raabe for scientific support.

References

- 1 V. M. Chernyshev, O. A. Kravchenko and V. P. Ananikov, Conversion of plant biomass to furan derivatives and sustainable access to the new generation of polymers, functional materials and fuels, *Russ. Chem. Rev.*, 2017, **86**, 357–387.
- 2 Q. Hou, X. Qi, M. Zhen, H. Qian, Y. Nie, C. Bai, S. Zhang, X. Bai and M. Ju, Biorefinery roadmap based on catalytic production and upgrading 5-hydroxymethylfurfural, *Green Chem.*, 2021, **23**, 119–231.
- 3 K. H. Olsen, The clean development mechanism's contribution to sustainable development: a review of the literature, *Clim. Change*, 2007, **84**, 59–73.
- 4 V. P. Kashparova, D. V. Chernysheva, V. A. Klushin, V. E. Andreeva, O. A. Kravchenko and N. V. Smirnova, Furan monomers and polymers from renewable plant biomass, *Russ. Chem. Rev.*, 2021, **90**, 750–784.
- 5 S. G. Maerten, D. Voß, M. A. Liauw and J. Albert, Selective Catalytic Oxidation of Humins to Low-Chain Carboxylic Acids with Tailor-Made Polyoxometalate Catalysts, *ChemistrySelect*, 2017, **2**, 7296–7302.
- 6 J. J. Bozell and G. R. Petersen, Technology development for the production of biobased products from biorefinery carbohydrates—the US Department of Energy's "Top 10" revisited, *Green Chem.*, 2010, **12**, 539.
- 7 D. J. Hayes and M. H. B. Hayes, The role that lignocellulosic feedstocks and various biorefining technologies can play in meeting Ireland's biofuel targets, *Biofuels, Bioprod. Biorefin.*, 2009, **3**, 500–520.
- 8 K. Weissermel and H.-J. Arpe, *Industrial organic chemistry*, Wiley-VCH, Weinheim, 4th edn, 2003.
- 9 S. Liu, Y. Zhu, Y. Liao, H. Wang, Q. Liu, L. Ma and C. Wang, Advances in understanding the humins: Formation prevention and application, *Appl. Energy Combust. Sci.*, 2022, **10**, 100062.
- 10 S. K. R. Patil, J. Heltzel and C. R. F. Lund, Comparison of Structural Features of Humins Formed Catalytically from Glucose, Fructose, and 5-Hydroxymethylfurfuraldehyde, *Energy Fuels*, 2012, **26**, 5281–5293.
- 11 K. K. Kapanji, K. F. Haigh and J. F. Görgens, Techno-economics of lignocellulose biorefineries at South African sugar mills using the biofine process to co-produce levulinic acid, furfural and electricity along with gamma valeractone, *Biomass Bioenergy*, 2021, **146**, 106008.
- 12 M. J. Climent, A. Corma and S. Iborra, Conversion of biomass platform molecules into fuel additives and liquid hydrocarbon fuels, *Green Chem.*, 2014, **16**, 516.
- 13 G. Yang, E. A. Pidko and E. J. M. Hensen, Mechanism of Brønsted acid-catalyzed conversion of carbohydrates, *J. Catal.*, 2012, **295**, 122–132.



- 14 B. Girisuta, L. P. B. M. Janssen and H. J. Heeres, Kinetic Study on the Acid-Catalyzed Hydrolysis of Cellulose to Levulinic Acid, *Ind. Eng. Chem. Res.*, 2007, **46**, 1696–1708.
- 15 I. van Zandvoort, Y. Wang, C. B. Rasrendra, E. R. H. van Eck, P. C. A. Bruijninx, H. J. Heeres and B. M. Weckhuysen, Formation, molecular structure, and morphology of humins in biomass conversion: influence of feedstock and processing conditions, *ChemSusChem*, 2013, **6**, 1745–1758.
- 16 L. Filiciotto, A. M. Balu, A. A. Romero, C. Angelici, J. C. van der Waal and R. Luque, Reconstruction of humins formation mechanism from decomposition products: A GC-MS study based on catalytic continuous flow depolymerizations, *Mol. Catal.*, 2019, **479**, 110564.
- 17 H. Shen, H. Shan and L. Liu, Evolution Process and Controlled Synthesis of Humins with 5-Hydroxymethylfurfural (HMF) as Model Molecule, *ChemSusChem*, 2020, **13**, 513–519.
- 18 B. Cheng, X. Wang, Q. Lin, X. Zhang, L. Meng, R.-C. Sun, F. Xin and J. Ren, New Understandings of the Relationship and Initial Formation Mechanism for Pseudo-lignin, Humins, and Acid-Induced Hydrothermal Carbon, *J. Agric. Food Chem.*, 2018, **66**, 11981–11989.
- 19 C. B. Rasrendra, M. Windt, Y. Wang, S. Adisasmito, I. G. B. N. Makertihartha, E. R. H. van Eck, D. Meier and H. J. Heeres, Experimental studies on the pyrolysis of humins from the acid-catalysed dehydration of C6-sugars, *J. Anal. Appl. Pyrolysis*, 2013, **104**, 299–307.
- 20 I. van Zandvoort, E. R. H. van Eck, P. de Peinder, H. J. Heeres, P. C. A. Bruijninx and B. M. Weckhuysen, Full, Reactive Solubilization of Humin Byproducts by Alkaline Treatment and Characterization of the Alkali-Treated Humins Formed, *ACS Sustainable Chem. Eng.*, 2015, **3**, 533–543.
- 21 A. Wassenberg, T. Esser, M. J. Poller and J. Albert, Investigation of the Formation, Characterization, and Oxidative Catalytic Valorization of Humins, *Materials*, 2023, **16**(7), 2864.
- 22 J.-C. Raabe, T. Esser, F. Jameel, M. Stein, J. Albert and M. J. Poller, Study on the incorporation of various elements into the Keggin lacunary-type phosphomolybdate [PMo₉O₃₄]⁹⁻ and subsequent purification of the polyoxometalates by nanofiltration, *Inorg. Chem. Front.*, 2023, **10**, 4854–4868.
- 23 T. Esser, A. Wassenberg, J.-C. Raabe, D. Voß and J. Albert, Catalytic Valorization of Humins by Selective Oxidation Using Transition-Metal-Substituted Keggin-Type Polyoxometalate Catalysts, *ACS Sustainable Chem. Eng.*, 2024, **12**(1), 543–560.
- 24 J.-C. Raabe, M. Poller, D. Voß and J. Albert, H₈PV₅Mo₇O₄₀ (HPA-5) - a unique polyoxometalate for acid and RedOx catalysis: synthesis, characterization, and modern applications in green chemical processes, *ChemSusChem*, 2023, e202300072.
- 25 M. J. Poller, S. Bönisch, B. Bertleff, J.-C. Raabe, A. Göring and J. Albert, Elucidating activating and deactivating effects of carboxylic acids on polyoxometalate-catalysed three-phase liquid–liquid–gas reactions, *Chem. Eng. Sci.*, 2022, **264**, 118143.
- 26 N. Shi, Q. Liu, R. Ju, X. He, Y. Zhang, S. Tang and L. Ma, Condensation of α -Carbonyl Aldehydes Leads to the Formation of Solid Humins during the Hydrothermal Degradation of Carbohydrates, *ACS Omega*, 2019, **4**, 7330–7343.
- 27 T. M. C. Hoang, E. R. H. van Eck, W. P. Bula, J. G. E. Gardeniers, L. Lefferts and K. Seshan, Humin based by-products from biomass processing as a potential carbonaceous source for synthesis gas production, *Green Chem.*, 2015, **17**, 959–972.
- 28 Z. Cheng, J. L. Everhart, G. Tsilomelekis, V. Nikolakis, B. Saha and D. G. Vlachos, Structural analysis of humins formed in the Brønsted acid catalyzed dehydration of fructose, *Green Chem.*, 2018, **20**, 997–1006.
- 29 I. van Zandvoort, E. J. Koers, M. Weingarth, P. C. A. Bruijninx, M. Baldus and B. M. Weckhuysen, Structural characterization of ¹³C-enriched humins and alkali-treated ¹³C humins by 2D solid-state NMR, *Green Chem.*, 2015, **17**, 4383–4392.
- 30 H. Shan, L. Li, W. Bai and L. Liu, Evolution Process of Humins Derived from Glucose, *ChemistrySelect*, 2022, **7**(22), 7.
- 31 S. K. R. Patil and C. R. F. Lund, Formation and Growth of Humins via Aldol Addition and Condensation during Acid-Catalyzed Conversion of 5-Hydroxymethylfurfural, *Energy Fuels*, 2011, **25**, 4745–4755.
- 32 J. Horvat, B. Klaić, B. Metelko and V. Šunjić, Mechanism of levulinic acid formation, *Tetrahedron Lett.*, 1985, **26**, 2111–2114.
- 33 S. Wesinger, M. Mendt and J. Albert, Alcohol-Activated Vanadium-Containing Polyoxometalate Complexes in Homogeneous Glucose Oxidation Identified with ⁵¹V-NMR and EPR Spectroscopy, *ChemCatChem*, 2021, **13**, 3662–3670.
- 34 T. Lu, Y. Hou, W. Wu, M. Niu, S. Ren, Z. Lin and V. K. Ramani, Catalytic oxidation of biomass to oxygenated chemicals with exceptionally high yields using H5PV2Mo10O40, *Fuel*, 2018, **216**, 572–578.
- 35 S. Maerten, C. Kumpidet, D. Voß, A. Bukowski, P. Wasserscheid and J. Albert, Glucose oxidation to formic acid and methyl formate in perfect selectivity, *Green Chem.*, 2020, **22**, 4311–4320.
- 36 Z. He, Y. Hou, H. Li, Y. Wang, S. Ren and W. Wu, Novel insights into CO₂ inhibition with additives in catalytic aerobic oxidation of biomass-derived carbohydrates to formic acid, *Renewable Energy*, 2023, **211**, 403–411.
- 37 Z. Tang, W. Deng, Y. Wang, E. Zhu, X. Wan, Q. Zhang and Y. Wang, Transformation of cellulose and its derived carbohydrates into formic and lactic acids catalyzed by vanadyl cations, *ChemSusChem*, 2014, **7**, 1557–1567.
- 38 J. Albert, R. Wölfel, A. Bösmann and P. Wasserscheid, Selective oxidation of complex, water-insoluble biomass to formic acid using additives as reaction accelerators, *Energy Environ. Sci.*, 2012, **5**, 7956.
- 39 J. Albert, D. Lüders, A. Bösmann, D. M. Guldi and P. Wasserscheid, Spectroscopic and electrochemical characterization of heteropoly acids for their optimized application in selective biomass oxidation to formic acid, *Green Chem.*, 2014, **16**, 226–237.



- 40 J. Albert, A. Jess, C. Kern, F. Pöhlmann, K. Glowienka and P. Wasserscheid, Formic Acid-Based Fischer-Tropsch Synthesis for Green Fuel Production from Wet Waste Biomass and Renewable Excess Energy, *ACS Sustainable Chem. Eng.*, 2016, **4**, 5078–5086.
- 41 J. Albert and P. Wasserscheid, Expanding the scope of biogenic substrates for the selective production of formic acid from water-insoluble and wet waste biomass, *Green Chem.*, 2015, **17**, 5164–5171.
- 42 P. Preuster and J. Albert, Biogenic Formic Acid as a Green Hydrogen Carrier, *Energy Technol.*, 2018, **6**, 501–509.
- 43 J. Reichert, B. Brunner, A. Jess, P. Wasserscheid and J. Albert, Biomass oxidation to formic acid in aqueous media using polyoxometalate catalysts – boosting FA selectivity by in-situ extraction, *Energy Environ. Sci.*, 2015, **8**, 2985–2990.
- 44 J. Reichert and J. Albert, Detailed Kinetic Investigations on the Selective Oxidation of Biomass to Formic Acid (OxFA Process) Using Model Substrates and Real Biomass, *ACS Sustainable Chem. Eng.*, 2017, **5**, 7383–7392.
- 45 J. Albert, M. Mendt, M. Mozer and D. Voß, Explaining the role of vanadium in homogeneous glucose transformation reactions using NMR and EPR spectroscopy, *Appl. Catal., A*, 2019, **570**, 262–270.
- 46 A. A. Shatalov, D. V. Evtugin and C. Pascoal Neto, Cellulose degradation in the reaction system O₂/heteropolyanions of series [PMo_(12±n)V_nO₄₀]^{(3±n)-}, *Carbohydr. Polym.*, 2000, 23–32.
- 47 V. F. Odyakov, E. G. Zhizhina, Y. A. Rodikova and L. L. Gogin, Mo-V-Phosphoric Heteropoly Acids and Their Salts: Aqueous Solution Preparation – Challenges and Perspectives, *Eur. J. Inorg. Chem.*, 2015, **2015**, 3618–3631.
- 48 L. Pettersson, I. Andersson, J. H. Grate and A. Selling, Multicomponent Polyanions. 46. Characterization of the Isomeric Keggin Decamolybdoivanadophosphate Ions In Aqueous Solution by 31P and 51V NMR, *Inorg. Chem.*, 1994, 982–993.
- 49 D. V. Evtugin, C. Pascoal Neto, J. Rocha and J. D. Pedrosa de Jesus, *Appl. Catal.*, 1981, **1**, 97–105.
- 50 D. Voß, M. Kahl and J. Albert, Continuous Production of Formic Acid from Biomass in a Three-Phase Liquid-Liquid-Gas Reaction Process, *ACS Sustainable Chem. Eng.*, 2020, **8**, 10444–10453.
- 51 B. Bertleff, R. Goebel, J. Claußnitzer, W. Korth, M. Skiborowski, P. Wasserscheid, A. Jess and J. Albert, Investigations on Catalyst Stability and Product Isolation in the Extractive Oxidative Desulfurization of Fuels Using Polyoxometalates and Molecular Oxygen, *ChemCatChem*, 2018, **10**, 4602–4609.
- 52 T. Esser, M. Huber, D. Voß and J. Albert, Development of an efficient downstream process for product separation and catalyst recycling of a homogeneous polyoxometalate catalyst by means of nanofiltration membranes and design of experiments, *Chem. Eng. Res. Des.*, 2022, **185**, 37–50.
- 53 N. I. Gumerova and A. Rompel, Polyoxometalates in solution: speciation under spotlight, *Chem. Soc. Rev.*, 2020, **49**, 7568–7601.
- 54 G. Tsilomelekis, M. J. Orella, Z. Lin, Z. Cheng, W. Zheng, V. Nikolakis and D. G. Vlachos, Molecular structure, morphology and growth mechanisms and rates of 5-hydroxymethyl furfural (HMF) derived humins, *Green Chem.*, 2016, **18**, 1983–1993.
- 55 J.-C. Raabe, J. Aceituno Cruz, J. Albert and M. J. Poller, Comparative Spectroscopic and Electrochemical Study of V(V)-Substituted Keggin-Type Phosphomolybdates and -Tungstates, *Inorganics*, 2023, **11**, 138.
- 56 J.-C. Raabe, J. Albert and M. J. Poller, Spectroscopic, Crystallographic, and Electrochemical Study of Different Manganese(II)-Substituted Keggin-Type Phosphomolybdates, *Chem. – Eur. J.*, 2022, **28**, e202201084.
- 57 X. Chen, N. Guigo, A. Pizzi, N. Sbirrazzuoli, B. Li, E. Fredon and C. Gerardin, Ambient Temperature Self-Blowing Tannin-Humins Biofoams, *Polymer*, 2020, **12**(11), 2732.
- 58 T. Wilke and M. A. Barteau, Dehydration and Oxidation of Alcohols by Supported Polyoxometalates: Effects of Mono- and Multivalent Cation Exchange on Catalyst Acidity and Activity, *Ind. Eng. Chem. Res.*, 2019, **58**, 14752–14760.
- 59 L. Jing, J. Shi, F. Zhang, Y. Zhong and W. Zhu, Polyoxometalate-Based Amphiphilic Catalysts for Selective Oxidation of Benzyl Alcohol with Hydrogen Peroxide under Organic Solvent-Free Conditions, *Ind. Eng. Chem. Res.*, 2013, **52**, 10095–10104.
- 60 A. M. Khenkin and R. Neumann, Oxidative C–C bond cleavage of primary alcohols and vicinal diols catalyzed by H5PV2Mo10O40 by an electron transfer and oxygen transfer reaction mechanism, *J. Am. Chem. Soc.*, 2008, **130**, 14474–14476.
- 61 A. Djaouida, M. Sadia and H. Smaïn, Direct Benzyl Alcohol and Benzaldehyde Synthesis from Toluene over Keggin-Type Polyoxometalates Catalysts: Kinetic and Mechanistic Studies, *J. Chem.*, 2019, **2019**, 1–11.
- 62 T. Kim, R. S. Assary, C. L. Marshall, D. J. Gosztola, L. A. Curtiss and P. C. Stair, Acid-Catalyzed Furfuryl Alcohol Polymerization: Characterizations of Molecular Structure and Thermodynamic Properties, *ChemCatChem*, 2011, **3**, 1451–1458.
- 63 L. Quinquet, P. Delliere and N. Guigo, Conditions to Control Furan Ring Opening during Furfuryl Alcohol Polymerization, *Molecules*, 2022, **27**(10), 3212.
- 64 M. Hronec, K. Fulajtárová and T. Soták, Kinetics of high temperature conversion of furfuryl alcohol in water, *J. Ind. Eng. Chem.*, 2014, **20**, 650–655.
- 65 G. M. González Maldonado, R. S. Assary, J. Dumesic and L. A. Curtiss, Experimental and theoretical studies of the acid-catalyzed conversion of furfuryl alcohol to levulinic acid in aqueous solution, *Energy Environ. Sci.*, 2012, **5**, 6981.
- 66 G. Falco, N. Guigo, L. Vincent and N. Sbirrazzuoli, Opening Furan for Tailoring Properties of Bio-based Poly(Furfuryl Alcohol) Thermoset, *ChemSusChem*, 2018, **11**, 1805–1812.



- 67 P. Delliere and N. Guigo, Revealed pathways of furan ring opening and surface crosslinking in biobased polyfurfuryl alcohol, *Eur. Polym. J.*, 2023, **187**, 111869.
- 68 J. Zhong, J. Pérez-Ramírez and N. Yan, Biomass valorisation over polyoxometalate-based catalysts, *Green Chem.*, 2021, **23**, 18–36.
- 69 S. Agarwal, D. van Es and H. J. Heeres, Catalytic pyrolysis of recalcitrant, insoluble humin byproducts from C6 sugar biorefineries, *J. Anal. Appl. Pyrolysis*, 2017, **123**, 134–143.
- 70 E. Licsandru, M. Gaysinski and A. Mija, Structural Insights of Humins/Epoxidized Linseed Oil/Hardener Terpolymerization, *Polymer*, 2020, **12(7)**, 1583.
- 71 E. G. Zhizhina and V. Odyakov, Alteration of the physicochemical properties of catalysts based on aqueous solutions of Mo-V-P heteropoly acids in redox processes, *React. Kinet. Catal. Lett.*, 2008, **95(2)**, 301–312.
- 72 E. G. Zhizhina, V. F. Odyakov and M. V. Simonova, Catalytic oxidation of organic compounds with oxygen in the presence of Mo-V-phosphoric heteropoly acid solutions, *Kinet. Catal.*, 2008, **49**, 773–781.
- 73 V. F. Odyakov and E. G. Zhizhina, A novel method of the synthesis of molybdovanadophosphoric heteropoly acid solutions, *React. Kinet. Catal. Lett.*, 2008, **95**, 21–28.



6.4 Process Optimization for the Humin Valorization and Application of an Efficient Downstream Process using Nanofiltration

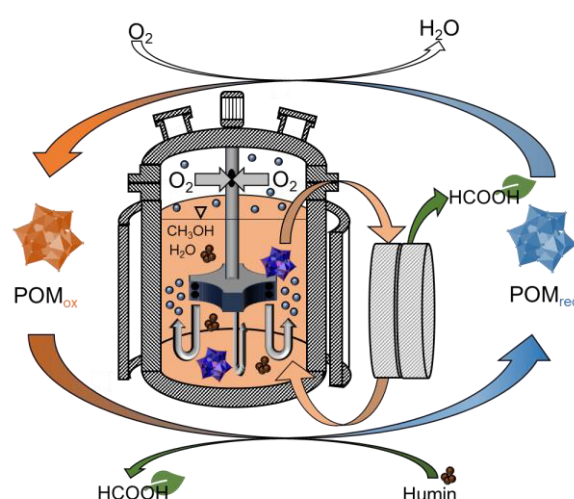
P4

Novel insights into the recovery and recyclability of homogeneous polyoxometalate catalysts applying an efficient nanofiltration process for the selective catalytic oxidation of humins

Tobias Esser, André Wassenberg, Dorothea Voß and Jakob Albert

Esser, T.; Wassenberg, A.; Voß, D.; Albert, J.: Novel insights into the recovery and recyclability of homogeneous polyoxometalate catalysts applying an efficient nanofiltration process for the selective catalytic oxidation of humins. *Chemical Engineering Research and Design*, **2024** (209), 311–322. DOI: 10.1016/j.cherd.2024.08.007

In Section 6.3, the remarkable CO₂ inhibiting effect of methanol in the selective catalytic oxidation of humins using the H₄[PVMo₁₁O₄₀] POM-catalyst was demonstrated. It was found that CO₂ formation is strongly inhibited by methanol addition (5 vol-%), even at elevated temperatures. In combination with pTSA, an optimized reaction system could be created whereby pTSA increases the activity and methanol increases the selectivity. The present section is dedicated to examining the translation of these findings to more active catalysts that are prone to overoxidation and the use of nanofiltration as an efficient downstream process. For this purpose, the more active but less selective disubstituted H₅[PV₂Mo₁₀O₄₀] POM-catalyst (*vide supra*, 6.2), was used to oxidize the glucose-based humin applying the novel reaction system. Not only an increase in the yield of carboxylic acids from 40 % to 50 % was achieved, but at the same time a decrease in the reaction temperature by 30 °C. Hence, it was possible to further optimize the sustainability of the process. In addition, the time-resolved degradation of humins was investigated. Subsequently, the nanofiltration process developed in Section 6.1 was tested as a potential downstream process. To this end, various commercial acid-stable membranes were tested to identify the most suitable one. The selected membrane underwent duration testing and was finally used in recycling studies. Additional supporting information can be found in Appendix 9.5.4.^{213,214} The following section is reproduced from Ref.²¹⁴ published in *Chemical Design and Engineering, Elsevier*.



Publication: *Novel insights into the recovery and recyclability of homogeneous polyoxometalate catalysts applying an efficient nanofiltration process for the selective catalytic oxidation of humins.*²¹⁴



Novel insights into the recovery and recyclability of homogeneous polyoxometalate catalysts applying an efficient nanofiltration process for the selective catalytic oxidation of humins

Tobias Esser, André Wassenberg, Dorothea Voß, Jakob Albert*

Institute of Technical and Macromolecular Chemistry, Universität Hamburg, Bundesstraße 45, Hamburg 20146, Germany

ARTICLE INFO

Keywords:

Biomass
Polyoxometalate
Homogenous catalysis
Humins
Nanofiltration

ABSTRACT

Selective catalytic oxidation (SCO) of humins is a promising strategy to valorize undesired side streams of biomass conversion processes. Keggin-type polyoxometalates are efficient catalysts for the SCO of humins giving platform chemicals like formic acid, acetic acid or their respective esters up to combined yields of 51 %. Moreover, one of the main challenges for establishing continuous processes is the efficient catalyst recycling and product separation. Herein, we combined an optimization study for the process parameters in SCO with an integrated product separation carried out by using nanofiltration membranes. For this purpose, an enhanced reaction system consisting of 5 vol% methanol addition for CO₂ suppression in combination with 1.5 mmol pTSA as solubility promotor was applied using H₅[PV₂Mo₁₀O₄₀] (HPA-2) as a catalyst achieving a maximum humin conversion of 90 % resulting in 57 % carboxylic ester selectivity. In subsequent studies, an appropriate XN 45 nanofiltration membrane was identified allowing for >99 % catalyst and >90 % additive retention efficiently separating the acidic reaction products in the permeate. Furthermore, long-time stability of the membrane and thus of the separation process could be confirmed up to 168 h time on stream. Based on these results, the developed process represents an important milestone in the valorization of humins combined with efficient separation of the molecular polyoxometalate catalyst and could therefore be the basis for future developments.

1. Introduction

To encounter the rising demand for energy, chemicals, and materials, the modern society is consuming an increasing amount of fossil hydrocarbons including petroleum and natural gas (Hou et al., 2021; Chen et al., 2018). However, the over-reliance on non-renewable fossil fuels has led to a number of social, economic, and environmental issues, including resource deficits and energy crisis as well as immense emission of pollutants (Hou et al., 2021; Dincer, 2000). As a result, the interest in industrial utilization of renewable energy and carbon sources for the sustainable production of platform chemicals has grown in recent years (Hou et al., 2021; Román-Leshkov et al., 2007; Wang et al., 2014). Since biomass is the only renewable carbon source, it has tremendous potential to replace fossil resources among renewable energy sources. In particular, lignocellulosic biomass is discussed as a potential feedstock for green fuels and chemicals due to its abundance and availability (Hou et al., 2021; Alonso et al., 2010; Liu et al., 2022). The development of so-called biorefineries, which use lignocellulosic biomass as a source of

sustainable carbon and renewable energy, offers a promising approach for decreasing immoderate dependency on finite fossil resources while also addressing climate and other environmental issues (Hayes and Hayes, 2009; Cherubini, 2010; Maity, 2015). Due to the over-functionalized characteristic of biomass, the conversion into value-added products obligates a number of intricate process steps decreasing competency compared to well-established petroleum refining technologies (Bozell and Petersen, 2010; Weissermel and Arpe, 2003). Therefore, only a few technologies that can convert biomass into value-added products have been established so far. In this regard, one of the most advanced large-scale biorefinery technologies is the Biofine process for the continuous acid-catalyzed hydrolysis of sugars to biogenic levulinic acid (Kapanji et al., 2021; Climent et al., 2014). Unfortunately, the Biofine process also forms insoluble polymeric solids called humins due to thermal-induced reactions of intermediates decreasing the atom efficiency of the process (Liu et al., 2022; Patil et al., 2012).

Serval studies have been conducted with the scope of valorizing

* Corresponding author.

E-mail address: jakob.albert@uni-hamburg.de (J. Albert).

<https://doi.org/10.1016/j.cherd.2024.08.007>

Received 16 April 2024; Received in revised form 26 June 2024; Accepted 4 August 2024

Available online 6 August 2024

0263-8762/© 2024 The Author(s). Published by Elsevier Ltd on behalf of Institution of Chemical Engineers. This is an open access article under the CC BY-NC-ND license (<http://creativecommons.org/licenses/by-nc-nd/4.0/>).

these undesired by-products to increase efficiency, economy and sustainability (Maerten et al., 2017; Wassenberg et al., 2023). Humins exhibit poor solubility and a complex structure hampering their chemical valorization. Therefore, the overall carbon efficiency of biorefineries is limited so far. Maerten et al (Maerten et al., 2017). and Wassenberg et al (Wassenberg et al., 2023). demonstrated the oxidative conversion of humins to short-chain carboxylic acids such as formic acid (FA) as well as acetic acid (AA) using Keggin-type polyoxometalate catalysts (POM) in aqueous phase. Hereby, FA is an interesting product as it is widely used as important chemical and offers an environmental friendly hydrogen source (He et al., 2023; Voß et al., 2020a). Nevertheless, using this approach a large fraction of the carbon provided by the humin was converted into undesired CO_2 . More precisely, in the study of Maerten et al (Maerten et al., 2017). a FA yield of only about 8 %, an AA yield of 4 % and a CO_2 yield of more than 63 % was achieved, using the five times vanadium-substituted phosphomolybdic acid $\text{H}_8[\text{PV}_5\text{Mo}_7\text{O}_{40}]$ (HPA-5). The results correspond to a CO_2 selectivity of about 83 %.

In previous studies, it was demonstrated that the application of the monovanadium-substituted $\text{H}_4[\text{PVMo}_{11}\text{O}_{40}]$ catalyst (HPA-1) provides a relative selectivity advantage compared to higher substituted POMs (Esser et al., 2024a, 2024b). Herein, the yield of CO_2 could be drastically decreased to below 19 %, while the combined yield of carboxylic acids remained almost unchanged at 11 % (Esser et al., 2024b). Furthermore, it was impressively demonstrated that the use of a combination of para-toluene sulfonic acid (pTSA) and methanol enables the efficient SCO of humins. In detail, adding methanol as a co-solvent strongly inhibited CO_2 formation, while pTSA as solubilizer increased humin solubility and therefore conversion. Methanol is known as an efficient additive to inhibit CO_2 formation based on its function as radical scavenger, stabilizer of reactive groups and promotor of new catalytic V-spezies (He et al., 2023; Wesinger et al., 2020). In this way, the monovanadium-substituted HPA-1 catalyst could convert the humins in more value-added products than undesired by-products. A combined yield of carboxylic acids of more than 40 % was achieved (Esser et al., 2024b).

POMs are an intriguing class of anionic metal-oxide cluster with a wide range of structural characteristics and several catalytic applications, particularly in the conversion of complex biogenic feedstock (Zhong et al., 2021; Lechner et al., 2016). They act as bifunctional catalysts due to their function as potent Brønsted acids and as redox catalysts, enabling multiple electron transfer (Zhong et al., 2021). Therefore, POMs have numerous catalytic applications in innovative green processes (Voß et al., 2020a, 2020b; Bertleff et al., 2017; Bukowski et al., 2020). However, downstream processing of molecular POMs in polar solutions is difficult due to their homogeneous nature and represents a hurdle for a sustainable process. To this end, nanofiltration is a promising approach for an efficient separation of molecular POM catalysts. Nanofiltration has a relative sustainability advantage over other separation techniques, mostly due to its cost-effective and safe operation. Furthermore, nanofiltration membranes own unique characteristics such as enhanced ion selectivity, making them ideal for use in the separation of polyvalent POM catalysts. In literature, some studies can be found where nanofiltration has been used for separation of polyvalent POM catalysts with remarkable rejections of over 99 % and low rejections for monovalent substances between 0 % and 10 % (Bertleff et al., 2017; Esser et al., 2022; Raabe et al., 2023a). Fig. 1 visualizes the factual connection of the entire value chain from biomass to levulinic acid and the formation of undesired humins that are subsequently converted by SCO to formic acid. The main scope of the present study was to optimize the SCO of complex humins to value-added carboxylic acids using molecular POM catalysts in combination with the development of an efficient downstream process based on nanofiltration, enabling an overall sustainable green process. For this purpose, the novel approach combining methanol and pTSA as additives was applied for the divanadium-substituted POM catalyst HPA-2 to investigate its efficiency for the optimized SCO of humins. In subsequent studies, an appropriate nanofiltration membrane was selected by screening experiments and applied for recycling experiments of the catalyst. Furthermore, long-time stability of the membrane and thus of the separation process was investigated.

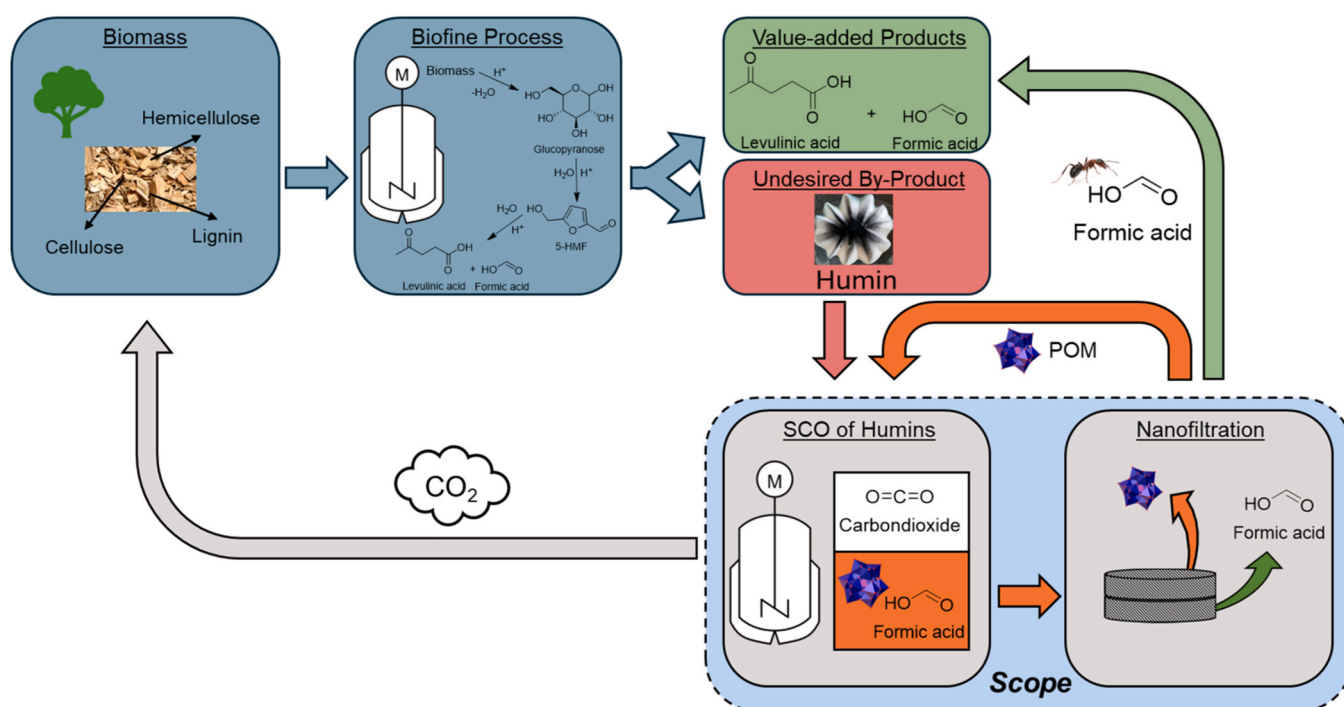


Fig. 1. : Simplified block flow diagram for the entire value chain from biomass to levulinic acid via Biofine process and the conversion of undesired humins into formic acid by SCO.

2. Results and discussion

2.1. Comparing different POM catalysts for SCO of humins in the enhanced reaction system

Combining the addition of pTSA and methanol in the SCO of humins using the monovanadium-substituted HPA-1 catalyst is a promising approach (Esser et al., 2024b). However, its use has not been investigated yet for higher vanadium-substituted Keggin-type POM catalysts. On the one hand, higher vanadium-substituted catalysts exhibit significantly increased activity, most likely due to peroxy ligands between adjacent vanadium atoms (Poller et al., 2022). Due to this fact, it might be possible to decrease the reaction temperature or reaction time. On the other hand, higher vanadium-substituted catalysts tend to overoxidize, increasing the formation of undesired by-products such as CO₂. In order to elucidate if higher vanadium substitution is beneficial for the SCO of humins, the double vanadium-substituted H₅[PV₂Mo₁₀O₄₀] (HPA-2) was used as a catalyst. The experiments were conducted using 1.5 mmol pTSA as solubilizer and a reaction solution consisting of water:methanol = 95:5 vol.-% for temperatures of 90 °C, 105 °C and 120 °C, respectively. A glucose-based humin was used as a substrate. The detailed description of the experiments can be found in the corresponding section of the experimental part.

At reaction temperatures of 105 °C and 120 °C, the carbon balance reached unrealistic values and exceeded 100 % with values of about 119 % and 122 %, respectively (see Figure S1). The results indicate that the stability of the additives was no longer given due to the exceeding carbon balance. In particular, pTSA could be degraded to oxidation products such as formic acid (FA) and acetic acid (AA), since higher vanadium-substituted catalysts are known to efficiently catalyze desulfurization reactions at elevated temperatures (Bertleff et al., 2017; Esser et al., 2022; Bertleff et al., 2018). In this way, the process would be less sustainable, and the results were distorted. Therefore, the stability of the individual additives must be investigated. For this purpose, additional stability experiments, i.e. reactions without substrate at reaction temperatures of 90 °C, 105 °C and 120 °C, were conducted. The liquid phase was analyzed by nuclear magnetic resonance (NMR) spectroscopy and high-performance liquid chromatography (HPLC) to determine if oxidation or other reaction products could be found. In addition, gas samples were analyzed by gas chromatography (GC).

Fig. 2 shows the ¹H NMR spectra of the stability experiments. According to the spectra, FA (δ_H 8.1 ppm) and AA (δ_H 2.0 ppm) were detected presumably as degradation products of pTSA at reaction temperatures of 105 °C and 120 °C. Methoxy methanol (MM) at a chemical shift of 3.4 ppm was also detected as an oxidation product of methanol. Moreover, up to 2 vol.-% CO₂ could be detected in the gas phase by GC measurements. Overall, it is evident that the additives are not stable in a temperature range of 105 °C to 120 °C using HPA-2. The degradation of pTSA most probably led to the formation of FA and AA. Consequently, valuable additive was lost and thus the sustainability as well as resource-efficiency of the process was decreased. However, at a reaction temperature of 90 °C, no hint for the formation of degradation products, other oxidation or reaction products were found in the NMR spectra (Fig. 2). Interestingly, not even the reaction products of methanol such as methane diol (MeOH₂), methoxy methanol (MM), dimethoxy methanol (DMM) or dimethyl ether (DME) could be detected. The results could be confirmed by HPLC measurements, which can be found in the supporting information (Figure S2). consequently, the stability of the additives at a reaction temperature of 90 °C is plausible.

To further confirm this hypothesis, oxidation experiments at 90 °C were performed using a fully reduced catalyst (HPA-2 blue) in nitrogen atmosphere. This was done to eliminate the possibility that the reduced catalyst could interact with the additives due to altered chemical properties. According to the NMR spectra and HPLC measurements, neither the formation of FA nor AA was observed as products of a reaction of the additives and the reduced catalyst at 90 °C. Therefore, the

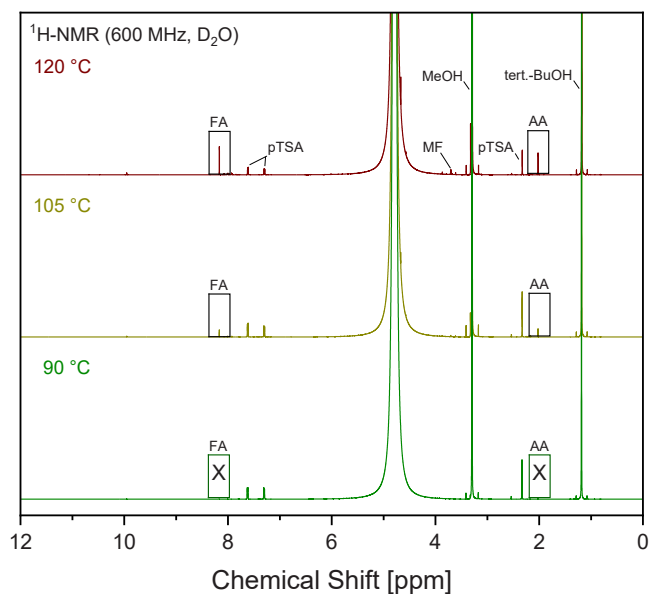


Fig. 2. Comparison of stability experiments for the enhanced system with methanol and pTSA in aqueous solution using HPA-2 as a catalyst for different reaction temperatures. *Experimental conditions:* 3-fold reaction system, 90 °C to 120 °C, 30 bar O₂, 30 h, 1000 rpm, 300 mg solid humin (16.2 mmol carbon), 0.83 mmol of vanadium (20 mol_{carbon} mol⁻¹) and 1.5 mmol pTSA in 30 mL 95:5 vol.-% water:methanol.

sole origin of FA and AA from the substrate could be confirmed. The findings for the stability of pTSA are consistent with the studies of Albert et al (Albert and Wasserscheid, 2015; Albert et al., 2012), where comparable conclusions can be found. Based on these findings, the oxidation experiments of the glucose-based humin using pTSA and methanol as additives in combination with HPA-2 as catalyst at 90 °C are reliable.

The comparison between the results using the HPA-2 catalyst at 90 °C and the reference HPA-1 from a previous study (Esser et al., 2024b) at 120 °C is shown in Fig. 3. In addition, an experiment without catalyst (blank) was conducted at 90 °C. Astonishingly, the reaction using the

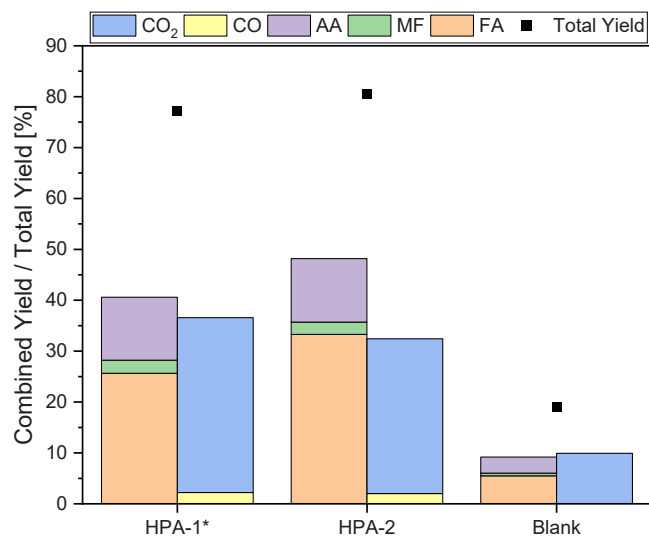


Fig. 3. Oxidation experiments of humin using HPA-1 at 120 °C and HPA-2 at 90 °C, respectively. *Results using HPA-1 are taken from a previous study of Esser et al (Esser et al., 2024b). *Experimental conditions:* 3-fold reaction system, 90 °C or 120 °C, 30 bar O₂, 30 h, 1000 rpm, 300 mg solid humin (16.2 mmol carbon), 0.83 mmol of vanadium (20 mol_{carbon} mol⁻¹) and 1.5 mmol pTSA in 30 mL 95:5 vol.-% water:methanol.

double vanadium-substituted HPA-2 catalyst outperforms the reaction using the monovanadium-substituted catalyst despite the significantly lower reaction temperature of 90 °C. More specific, when the HPA-2 catalyst was used at 90 °C the combined yield of the value-added products FA, its ester methyl formate (MF) and AA increased by more than 8 % compared to the reference reaction. A combined yield of almost 50 % was reached. Overall, the total yield also increased slightly from about 76 % to about 80 % indicating a higher activity of the HPA-2 catalyst even at a lower reaction temperature. Interestingly, the combined yield of the undesired by-products CO and CO₂ decreased slightly about 3 % reaching a value of about 32 %. The yield of MF was in all experiments far below 3 % indicating that the hydrolysis equilibrium is on the side of the free acid due to the high excess of water in the reaction system.

Accordingly, the combined yield of value-added products was 1.5 times higher than the combined yield of undesired by-products. The blank reaction without catalyst at 90 °C showed only a low activity reaching a total yield of below 20 %. On the purpose to further demonstrate the efficiency of the additive combination and HPA-2 as a catalyst, further experiments were performed using the individual additives as well as in water without additives. The results are shown in Fig. 4. The synergetic effects by combining pTSA and methanol are superior to the effect of the individual additives.

When using pTSA or methanol alone, the combined yield of carboxylic acid (esters) was only between 30 % and 40 %, respectively. The lack of inhibition of overoxidation and thus CO₂ formation was noticeable when pTSA was used without methanol. More specifically, the combined yield of the undesired by-products CO and CO₂ reached almost 60 %, which is nearly twice as high as using the combination of pTSA and methanol. However, the activity enhancing effect of pTSA was demonstrated by its action as a solubilizer with the highest total yield of oxidation products of over 90 %. Nevertheless, methanol as an individual additive is superior to pTSA due to its strong inhibition of CO₂ formation. The combined yield of undesired by-products was only about 26 %, which was even about 6 % lower than using the combination of methanol and pTSA. Moreover, the yield of FA of about 29 % when methanol was used as sole additive could compete with the FA yield of about 33 % using the combined reaction system. Still, the combined yield of carboxylic acid (esters) with a value of 36 % was lower when methanol was used than when both additives were used in one reaction

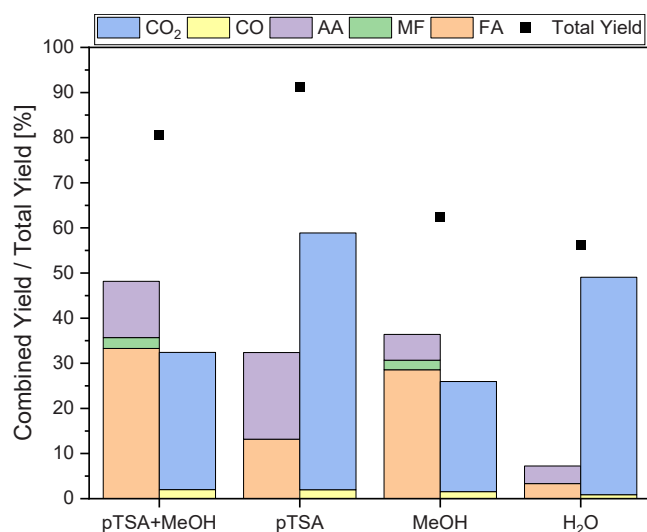


Fig. 4. Oxidation experiments of humin using HPA-2 at 90 °C with different additives compared to pure water. *Experimental conditions:* 3-fold reaction system, 90 °C, 30 bar O₂, 30 h, 1000 rpm, 300 mg solid humin (16.2 mmol carbon), 0.83 mmol of vanadium (20 mol_{carbon} mol⁻¹) and 1.5 mmol pTSA, 5 vol% methanol or without additives in 30 mL water.

with a yield of 48 %. This is mainly due to the increased formation of AA when pTSA is used. Without the CO₂ inhibiting effect of methanol, oxidation of humins in aqueous solution using the HPA-2 catalyst without additives led almost only to the formation of CO₂. Thus, the efficiency of the additives in combination with HPA-2 catalyst was proven. Although methanol could compete as a sole additive in terms of FA yield, the combination of both additives was superior concerning both activity and combined yield of carboxylic acid (esters). To prove the robustness of the results, the experiment using both additives and HPA-2 as catalyst was repeated three times. The results are shown in Fig. 5. It could be demonstrated that the results are reproducible with low deviations reaching an average combined yield of carboxylic acid (esters) of 48.6 % ± 0.9 %, of undesired by-products of 32.2 % ± 0.2 % and a total yield of 80.8 % ± 1 %. More precisely, an average yield of 33.5 % ± 0.5 %, 2.8 % ± 0.3 % and 12.3 % ± 0.3 % was reproduced in liquid phase for FA, MF and AA, respectively. In the gas phase average yields of 1.9 % ± 0.1 % and 30.3 % ± 0.1 % for CO and CO₂ were reproduced.

For the purpose of a deeper understanding of the reaction process, the reaction course between 0 h and 24 h was recorded and displayed in Fig. 6. Individual experiments with reaction times of 0 h, 2 h, 8 h, 16 h and 24 h were conducted and the liquid and gaseous products as well as the solid residue were analyzed. During the first 8 h of the reaction, the increase of the combined yield of carboxylic acid (esters) as well as of the combined yield of gaseous products was the highest. Within this period, the combined yield of carboxylic acid (esters) and gaseous products increased about 27 % or 19 %, respectively. Accordingly, the decrease in solid residues (unreacted humin) was also the highest within the first 8 h. In the subsequent 16 h of the reaction, the yields increased only moderately and approached their maximum values, resulting in strongly flattened curves. In the same manner the decline of solid residues slowed down. In comparison, the color of the solid residues showed a visible change between the period from 0 h to 8 h and the subsequent period from 8 h to 24 h (see upper part of Fig. 6). The color changed from black to brown, indicating a change in the composition of the solid residue.

In order to investigate the changes in the solid residue, the latter was further examined using elemental analysis, which is shown in Fig. 7. Within the first 8 h, the mass fraction of carbon (C) decreased linearly

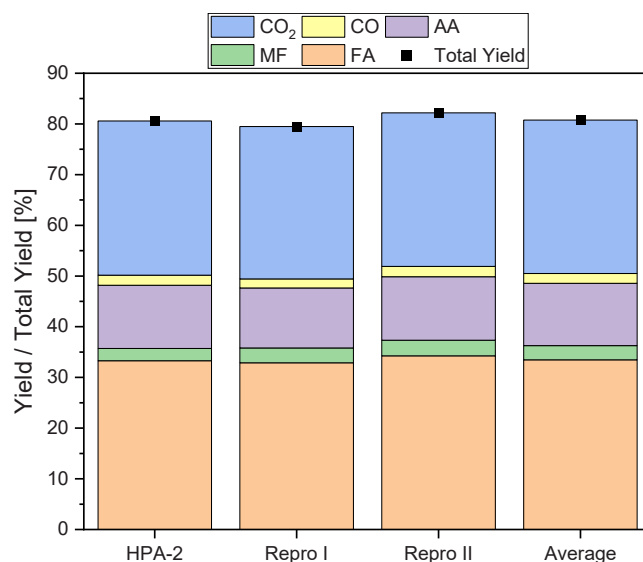


Fig. 5. Reproduction of SCO of glucose-based humin using HPA-2 at 90 °C in the combined system. *Experimental conditions:* 3-fold reaction system, 90 °C, 30 bar O₂, 30 h, 1000 rpm, 300 mg solid humin (16.2 mmol carbon), 0.83 mmol of vanadium (20 mol_{carbon} mol⁻¹) and 1.5 mmol pTSA in 30 mL 95:5 vol.-% water:methanol.

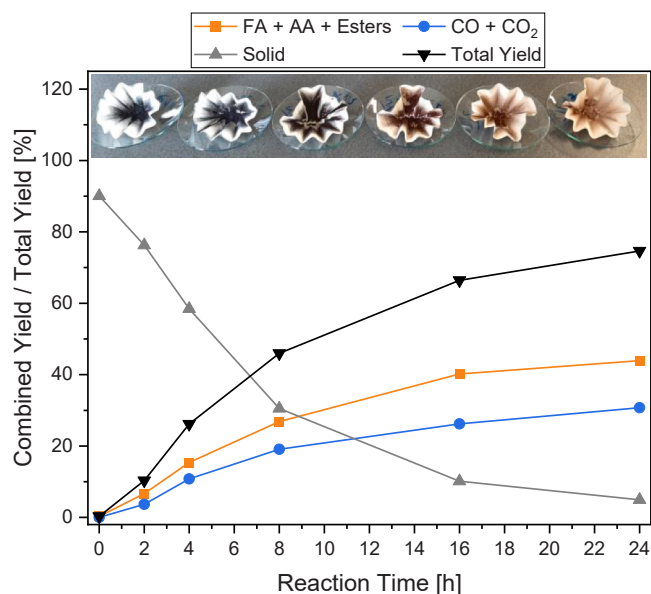


Fig. 6. Reaction course of the SCO of glucose-based humin using HPA-2 at 90 °C in the combined system. *Experimental conditions:* 3-fold reaction system, 90 °C, 30 bar O₂, 0 h to 24 h, 1000 rpm, 300 mg solid humin (16.2 mmol carbon), 0.83 mmol of vanadium (20 mol_{Carbon} mol_V⁻¹) and 1.5 mmol pTSA in 30 mL 95:5 vol.-% water:methanol.

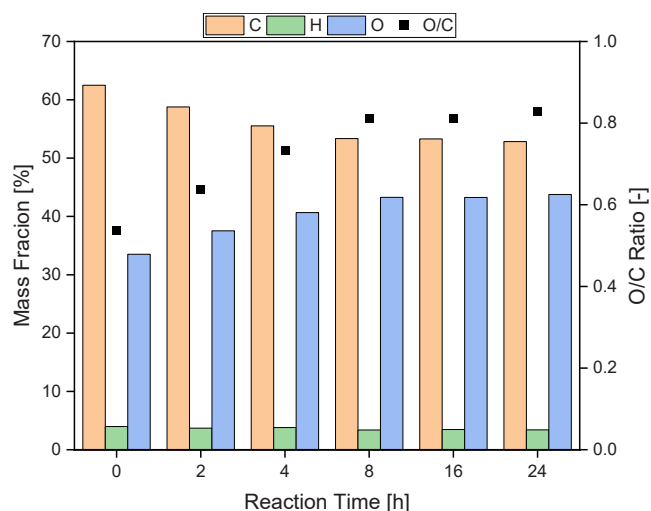


Fig. 7. Elemental analysis of the solid residues for the SCO of glucose-based humin using HPA-2 at 90 °C in the combined system. *Experimental conditions:* 3-fold reaction system, 90 °C, 30 bar O₂, 0 h to 24 h, 1000 rpm, 300 mg solid humin (16.2 mmol carbon), 0.83 mmol of vanadium (20 mol_{Carbon} mol_V⁻¹) and 1.5 mmol pTSA in 30 mL 95:5 vol.-% water:methanol.

with increasing reaction time from over 62 % to about 53 %. In contrast, the mass fraction of oxygen (O) increased from about 33 % to over 43 % and thus the ratio between oxygen and carbon (O/C) increased from 0.5 to over 0.8. In the subsequent reaction time, there were no compositional changes observed. Therefore, it is plausible that bonds and functional groups of the humin structure were oxidized within the first 8 h of the reaction. After 8 h of reaction, presumably the same amount of oxygen was introduced to the humin structure as removed by oxidative C-C bond cleavage.

2.2. Efficient product removal and catalyst recovery using nanofiltration membranes

In the interest of sustainability, the previous results have demonstrated that the reaction temperature in the SCO of humins could be drastically reduced by 30 °C to a mild temperature of only 90 °C using HPA-2 as a catalyst in the combined reaction system containing both 5 vol%MeOH and 1.5 mmol pTSA as additives. For an overall sustainable process, an efficient downstream process is also required. In particular, the homogeneity of the POM catalyst used represents a challenge in this context. To this end, the use of nanofiltration was tested and evaluated. In the first step, various membranes were screened using a model solution based on the liquid product phase of the SCO of humins and the experimental setup described in a previous study (Esser et al., 2022). As the esters are hardly formed in the reaction solution due to the strong excess of water, they were excluded for the initial investigations of the nanofiltration process. This simplified the quantitative analysis as MF co-elutes with FA. The following membranes were selected for the screening experiments: GL-Series (Suez), PuraMem® Selective, Performance and Flux (Evonik) as well as the TRISEP® nanofiltration membranes XN45, UA60 and NADIR® nanofiltration membrane NP030 (Mann+Hummel). Based on results of preliminary experiments, the membranes obtained from Evonik were excluded from further considerations due to a low permeate flux and no selective separation for the present reaction solution. The results for the rejection of the catalyst components of the remaining membranes can be found in Fig. 8. The membranes were evaluated in terms of the rejection of the components phosphorous (P), vanadium (V) and molybdenum (Mo) as well as by the means of the rejection of the products FA and AA. Due to the dissociation of the catalyst, different species can arise, therefore it is necessary to analyze the individual components. This was done by inductively coupled plasma-optical emission spectrometry (ICP-OES). Furthermore, the rejection of pTSA was determined using ICP-OES.

The permeate flux was also measured and used for the evaluation of the membranes. A detailed description of the experimental procedure and the calculation method can be found in the corresponding section of the experimental part. The catalyst should ideally be enriched in the retentate to allow removal of the products and recycling of the catalyst. Consequently, a high rejection of the catalyst components is required. For all membranes tested, P rejection was conspicuously low, with

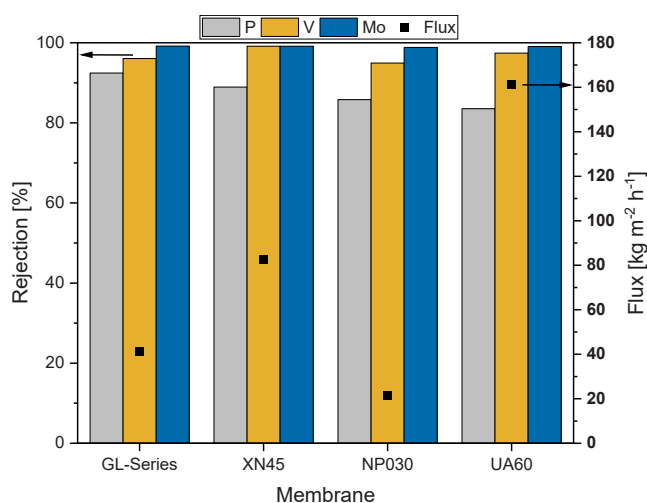


Fig. 8. Rejection for catalyst components P, V, Mo in membrane screening experiments using a model reaction solution from the SCO of glucose-based humin using HPA-2 at 90 °C in the combined system. *Experimental conditions:* pre-wetted membranes, ambient temperature, 30 bar transmembrane pressure, 15 mL min⁻¹ flow rate, 1100 rpm stirring speed, model solution containing HPA-2, FA, AA and pTSA in 95:5 vol.-% water:methanol.

values of about 90 % or less, compared to the other catalyst components. Presumably, some of the P occurred in the form of free phosphate anions due to an excess during catalyst synthesis. Phosphate is a much smaller molecule and has a lower charge than the POM molecules. Therefore, it was less strongly rejected. The molecular weight cut-off (MWCO) increased from about 300 Da, through 500 Da and 600 Da to about 1000 Da using the membranes GL-Series, XN45, NP030 and UA60, respectively. Consequently, the rejection for P decreased linearly from about 92–84 % using the membrane GL-Series or UA60, respectively. It is plausible that this observed trend is due to the increasing MWCO of the membranes. However, since this phosphate is most likely an excess of catalyst synthesis, it is not an indicator of catalyst loss. In contrast, Mo, as framework metal of the catalyst, can indicate catalyst losses. Interestingly, all membranes tested allow high rejection for Mo of 99 % or higher, regardless of the increasing MWCO. Hence, it seems likely that Mo occurs in larger species, probably as a complete POM structure ($> 1800 \text{ g mol}^{-1}$) and therefore is too large to penetrate the membranes. This is consistent with previous studies (Esser et al., 2022; Bertleff et al., 2018). The most important species is V as it is the active component of the catalyst, which can form smaller species due to dissociation. Surprisingly, all membranes tested enable V rejection of 95 % or higher. Nevertheless, the nanofiltration membrane XN45 was superior to the other membranes tested with a high rejection of V of over 99 %. Furthermore, this membrane had the second highest permeate flux of about $83 \text{ kg h}^{-1} \text{ m}^{-2}$.

In Fig. 9 the results for the rejection of value-added products and additives are shown. The products should be discharged with the permeate, therefore low rejection is beneficial. At the same time, the loss of pTSA as a valuable additive should be low and rejection should therefore be high. All tested membranes had almost no rejection of FA as value-added product. The highest but still low rejection for FA of about 2 % was reached using NP030 membrane. AA was rejected by the XN45 membrane with the highest but still low rejection of 8 %. Overall, all membranes tested enable efficient removal of the products. However, the XN45 membrane allowed by far the lowest pTSA loss with a rejection of 93 %. Based on the results, the XN45 membrane was selected for further experiments due to its high rejection of V and pTSA as well as the high permeate flux. The long-term stability of this membrane was tested. The results can be seen in Fig. 10.

Over 168 h, all streams (permeate & retentate) were recycled into

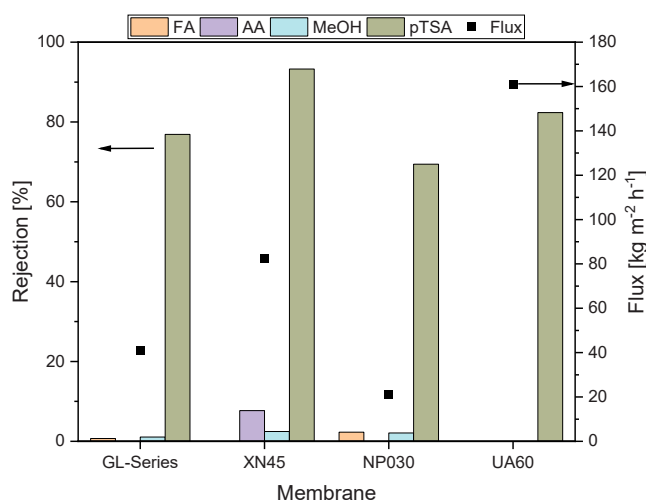


Fig. 9. Rejection for oxidation products as well as for additives in membrane screening experiments using a model reaction solution from the SCO of glucose-based humin and HPA-2 at 90°C in the combined system. *Experimental conditions:* pre-wetted membranes, ambient temperature, 30 bar transmembrane pressure, 15 mL min^{-1} flow rate, 1100 rpm stirring speed, model solution containing HPA-2, FA, AA and pTSA in 95:5 vol.-% water:methanol.

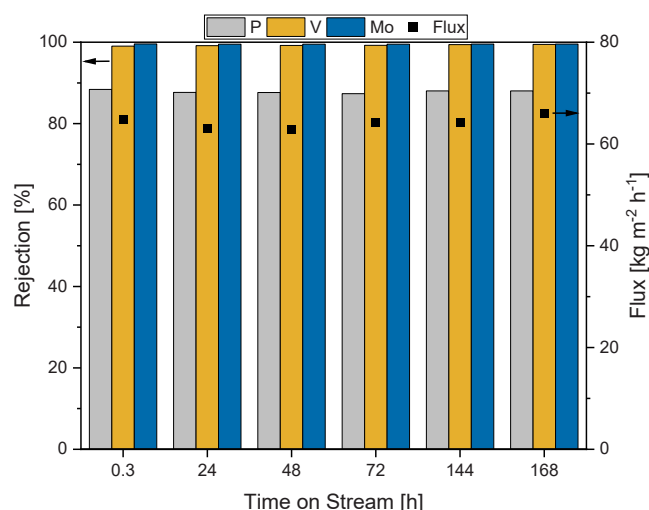


Fig. 10. Development of membrane performance by means of catalyst rejection (P, V, Mo) in dependency of the time on stream using a model reaction solution from SCO of glucose-based humin and HPA-2 at 90°C in the combined system. *Experimental conditions:* pre-wetted XN-45 nanofiltration membrane, ambient temperature, 30 bar transmembrane pressure, 15 mL min^{-1} flow rate, 1100 rpm stirring speed, model solution containing HPA-2, FA, AA and pTSA in 95:5 vol.-% water:methanol.

the storage vessel (feed), simulating a continuous process. Samples were taken at the beginning of the experiment and every 24 h for the following 72 h. In addition, samples were taken after 144 h and 168 h, respectively. The permeate flux was determined and the rejection was calculated for all components. A detailed description of the experimental procedure and the calculation can be found in the corresponding section of the experimental part. Over the entire period of 168 h, the values for the rejection of the catalyst components (P, Mo, V) remained almost unchanged (see Fig. 10). More specifically, the rejection of V and Mo was always over 99 % indicating a stable and selective separation. This could also be confirmed by the results for the rejection of the products and additives, which can be found in the Supporting Information (Figure S3).

After more than 168 h on stream, the membrane was removed from the system and examined. Visual inspection of the membrane at a macroscopic level was conducted and supported by scanning electron microscope (SEM) depicted in Fig. 11. On a macroscopic level, the membrane was white, slightly shiny, smooth, and free of defects prior to the experiment due to the dense polymer film (Fig. 11 a). After the experiment, the color of the membrane was almost unchanged, indicating that there were no deposits adhering to the membrane surface. In fact, the active separation layer of the membrane lost luster and appeared rather dull.

In addition, small defects could be detected on the surface. On a microscopic level, the active separation layer of the membrane consists of a dense layer of spherical particles (Fig. 11 b). This structure remained intact even after the experiment (Fig. 11 c). Due to this structural integrity, it seems plausible that the membrane did not lose performance over the duration of the experiment.

2.3. Enrichment and recycling of HPA-2 using nanofiltration

In order to successfully apply nanofiltration as a downstream process, the catalyst must be enriched without major losses and the products must be removed almost completely with the permeate. In particular, the accumulation of FA and the associated acidification of the reaction solution can have a negative impact on the catalytic process, therefore efficient removal is essential (Esser et al., 2022; Poller et al., 2022; Bertleff et al., 2018). For this purpose, an enrichment experiment

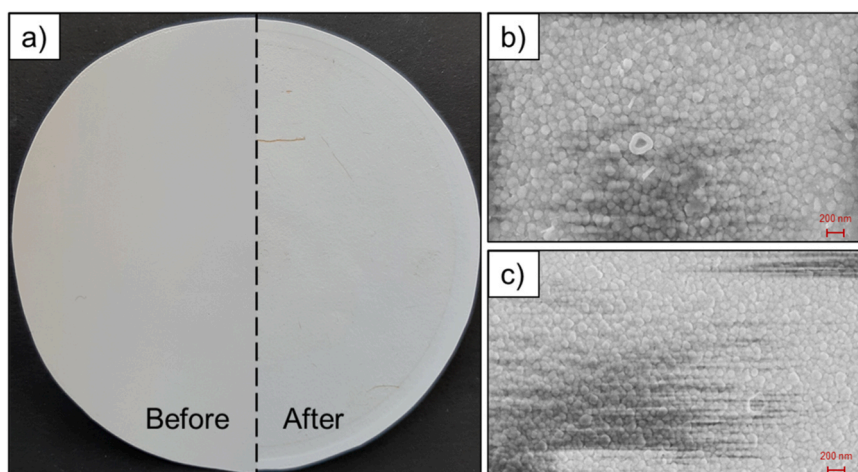


Fig. 11. Visual inspection of the XN45 membrane a) before (left) and after (right) an experiment on a macroscopic level, b) inspection via SEM before the experiment and c) inspection via SEM after the experiment.

was performed. The retentate was recycled into the feed storage and the permeate was withdrawn until the desired decrease in volume of the feed solution was achieved. In this context, the volumetric enrichment is important, which results from the ratio of the volume of the feed solution before and after the experiment. A volumetric enrichment of 5.3 was selected. The theoretical enrichment factor of a component is calculated based on the rejection of the respective component and the volumetric enrichment. A detailed description of the experimental procedure and the calculations can be found in the corresponding section of the experimental part.

The results of the enrichment experiment are shown in Table 1. For all system components, the enrichment factors determined were consistent to the theoretically calculated values. Accordingly, well-rejected components strongly enriched in the retentate. More specifically, for V and Mo, which were rejected to about 99 %, the achieved enrichment was almost equal to the volumetric enrichment of the feed solution of 5.3. For P and pTSA, which were rejected to about 90 %, the enrichment achieved was lower but still high reaching values of about 4.3 and higher. Due to low rejections or no rejection at all, the value-added products and methanol were not enriched in the retentate. As a result, over 80 % of value-added products would be removed from the reaction solution when diluted back to the original reaction volume. In contrast, the concentration of V and Mo in the original reaction volume would be almost unchanged. Therefore, a recycling of the catalyst by an efficient separation of the catalyst and the reaction products would be enabled.

Table 1
Enrichment of catalyst components, value-added products and additives using nanofiltration.

Entry ^a	Component	Type	Rejection / % ^{b,c}	Enrichment / %	
				Theoretic ^b	Determined ^b
1	V	Catalyst	98.6	5.2	5.2
2	Mo	Catalyst	99.7	5.3	5.3
3	P	Catalyst	86.7	4.3	4.5
4	FA	Product	0.0	1.0	1.0
5	AA	Product	0.0	1.1	1.1
6	MeOH	Additive	2.2	>1.0	1.1
7	pTSA	Additive	90.6	4.7	4.6

Experimental Conditions:

^a XN45 membrane, ambient temperature, 30 bar transmembrane pressure, 15 mL min⁻¹ flow rate, 1100 rpm stirring speed, 25.4 g L⁻¹ HPA-2, 6.5 g L⁻¹ FA, 0.8 g L⁻¹ AA, and 9.5 g L⁻¹ pTSA in 95:5 vol.-% water-methanol,

^b calculated as described in the corresponding section of the experimental part

^c determined by ICP-OES.

The removal of the acidic reaction products depends heavily on the enrichment factor. Therefore, the more permeate is removed from the reaction solution, the more of the acidic products can be removed. In principle, a higher enrichment factor would be possible, but it would have to be determined whether there is a threshold value for the enrichment of the catalyst above where it precipitates or changes structurally. The enrichment of the catalyst conducted here was within a range that has already been tested by previous studies (Esser et al., 2022). Alternatively, a diafiltration process can be used where fresh solvent is added to the retentate to dilute it and subsequently reconcentrate it so that further products can be removed without enriching the catalyst beyond a certain concentration. However, this would have the disadvantage that the products would be more diluted. Whether the enrichment factor and the corresponding removal of the acidic products is sufficient has to be tested in the real recycling study.

For further experiments the reaction was scaled up. This was intended to minimize the influences on the process caused by sampling during the planned recycling experiments. Moreover, for the operation of the membrane system, especially if enrichment is conducted, a higher volume is required than was processed in the previous reaction setup. Therefore, the reaction was performed in a 600 mL Hastelloy (C-276) autoclave equipped with a gas entrainment impeller. A reaction volume of 150 mL was used, which is five times larger than in the previous catalytic experiments. All concentrations and ratios were kept constant. In the corresponding section of the experimental part a detailed description of the scale-up experiment can be found. A comparison of

Table 2
Scale-up experiment for SCO of glucose-based humin using HPA-2 at 90 °C.

Entry	Reaction System	Reaction Volume / mL	Total Yield / %	Combined Yield / %		Ratio ^e (Value : Waste) / %
				FA + AA + Esters ^c	CO + CO ₂ ^d	
1 ^a	100 mL	30	74.7	43.9	30.8	59:41
2 ^b	600 mL	150	89.9	50.9	38.6	57:43

Experimental Conditions

^a 30 mL reaction solution in 3-fold reaction system,
^b 150 mL reaction solution in 600 mL autoclave both at 90 °C, 30 bar O₂, 24 h, 1000 rpm containing 50 mmol L⁻¹ pTSA and a carbon to vanadium ratio of 20 mol_{Carbon} mol_V⁻¹ in 95:5 vol.-% water-methanol,

^c determined with quantitative ¹H NMR,

^d determined with GC-TCD,

^e calculated as described in the corresponding section of the experimental part.

the results in the 100 mL autoclave and 600 mL autoclave can be found in Table 2. In the upscaled reaction system, the combined yield of carboxylic acids, undesirable by-products and the total yield increased by approximately a factor of 1.2 (Entry 1, Table 2). Accordingly, scale-up appears to have an impact on activity without affecting selectivity. Thus, the ratio of carboxylic acids (value) and undesired by-products (waste) remained almost unchanged. Reasons for the enhanced activity could be the changed interface between liquid and gas phase, improved homogenization and gas entry through optimized stirring. Even in the enlarged reaction system, a yield for MF of less than 3 % was achieved and no acetic acid methyl ester was detected. Overall, there was no loss in selectivity or activity and the reaction was successfully scaled-up.

Based on the aforementioned results, a recycling experiment was conducted in the up-scaled reaction setup. After each reaction the liquid product phase containing the carboxylic acids, additives and catalyst was processed in the membrane system. The enriched catalyst in the retentate was diluted back to the original reaction volume with aqueous methanol solution and fresh humin was added starting a new cycle. The detailed description of the experimental procedure is attached to the corresponding section of the experimental part. Fig. 12 shows the experimental results of the recycling tests in terms of catalytic performance. All yields were adjusted for the products left from previous tests. The results show a strong decrease in the catalytic performance, which is expressed in a decrease in the total yield from about 90 % after the first test to about 60 % after the third recycling. The yield of valuable products falls drastically from around 50 % to around 29 %. More precisely, the yield of FA drops from 35 % to 18 %, MF from 3 % to 2 % and AA from 12 % to 9 %. Previous studies have demonstrated that the combination of batchwise operating reaction and membrane system leads to the accumulation of oxidation products and acidification of the reaction solution during the reaction (Esser et al., 2022). As a result, the catalytic performance decreased as less active V-species are progressively formed, which could be detected using ^{51}V NMR (Esser et al., 2022). For this reason, the reaction solutions from the recycling experiments were examined after the reaction using ^{51}V NMR. In Fig. 13, the ^{51}V NMR spectra of the consecutive recycle reactions are shown. The signals were assigned according to literature (Wesinger et al., 2020; Bertleff et al., 2018; Albert et al., 2019; Raabe et al., 2023b; Evtugin et al., 1981; Pettersson et al., 1994). Before catalysis, isomers of HPA-1

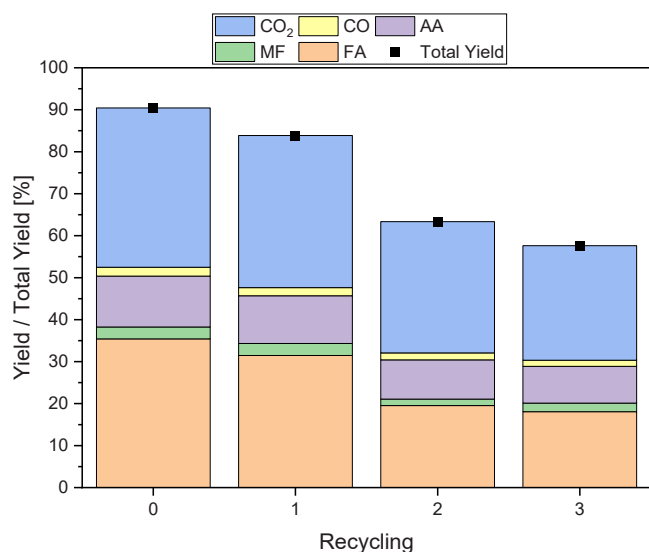


Fig. 12. Recycling experiments for SCO of glucose-based humin using HPA-2 with addition of pTSA. Experimental conditions: 90 °C, 30 bar O₂, 24 h, 1000 rpm, 1500 mg solid humin (81 mmol carbon), 4.15 mmol of vanadium (20 mol_{Carbon} mol⁻¹) in 150 mL 95:5 vol.-% water:methanol.

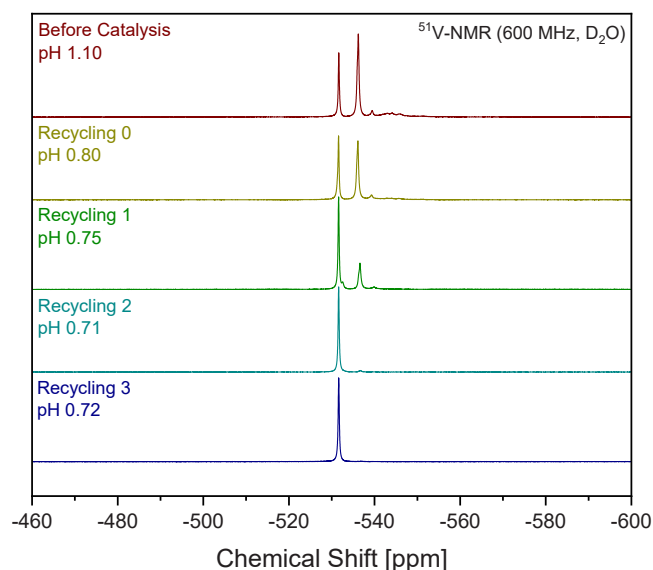


Fig. 13. ^{51}V NMR spectra from recycling experiments for SCO of glucose-based humin using HPA-2. Experimental conditions: 90 °C, 30 bar O₂, 24 h, 1000 rpm, 1500 mg solid humin (81 mmol carbon), 4.15 mmol of vanadium (20 mol_{Carbon} mol⁻¹) and 7.50 mmol pTSA in 150 mL 95:5 vol.-% water:methanol.

and HPA-2 are represented by the signals at about -533 ppm and -537 ppm. Even higher vanadium-substituted HPA isomers could be detected in the range from -540 ppm to -550 ppm inducing a broad signal of very low intensity. With each recycling the intensity shifted between the double as well as higher substituted and the mono substituted isomers in favor of the mono substituted isomers.

At the same time, the pH value decreased from 1.1 before the reaction to 0.8 and lower after the reactions. This sharp drop in pH could explain the change in catalyst structure that causes catalytic performance to decrease. The reaction products were efficiently removed from the reaction solution after reaction, so that the acidification of the reaction solution within the reactor during the catalytic experiment must be responsible for the decreasing activity. Even, MF as a larger molecule (compared to FA) was not accumulated according to the unadjusted yields (including residues of previous experiments), indicating that its rejection is very low or that the concentration of this product is severely limited by the hydrolysis equilibrium. When using pTSA as an additive, the initial pH was 1.1, which is already very low. Accordingly, there is hardly any buffer left to prevent the pH value from dropping too much during the reaction causing most probably the sharp drop in catalytic performance.

Therefore, the recycling experiments were repeated without the use of pTSA and only methanol was used as an additive. It has already been demonstrated in aforementioned experiments that the addition of pTSA primarily increases the yield of AA. However, when only methanol was used as an additive, the yields of FA, which was the main value-added product in both systems, were competitive to yields in the combined system. Thus, the approach is still highly promising. In Fig. 14, the ^{51}V NMR spectra and the corresponding pH values of the repeated experiments without the addition of pTSA are shown. The initial pH value of the system was 1.8, which is significantly higher than in the combined system. Interestingly, an additional signal was detected at below -530 ppm that can be assigned to the vanadium ester $[\text{VO}(\text{OMe})_2]^{2-}$ (Wesinger et al., 2020). This signal slightly shifted after the first reaction, most probably due to decrease in pH to 1.3, but did not disappear. The ratio of the different isomers remained unchanged. Overall, no structural changes of the catalyst could be detected, so that the structural integrity of the catalyst is evident. The pH value could also be stabilized between 1.2 and 1.3, which kept it within the optimal range for the HPA-2 catalyst.

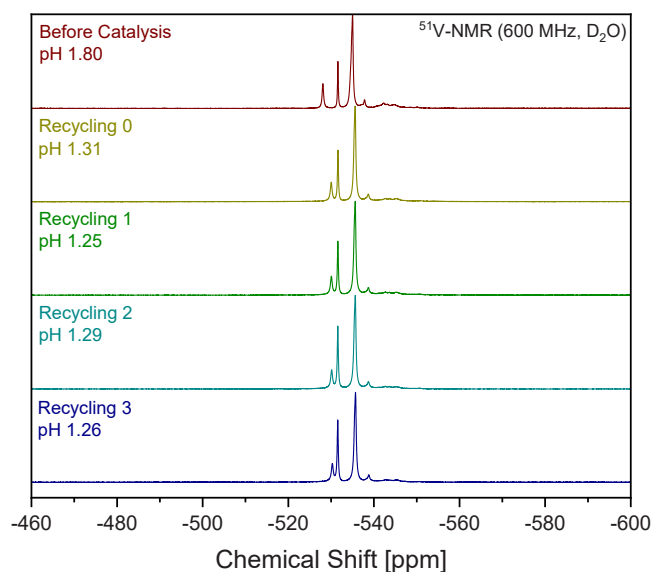


Fig. 14. ^{51}V NMR spectra from recycling experiments for SCO of glucose-based humin using HPA-2 without addition of pTSA. *Experimental conditions:* 90 °C, 30 bar O_2 , 24 h, 1000 rpm, 90 °C, 30 bar O_2 , 24 h, 1000 rpm, 1500 mg solid humin (81 mmol carbon), 4.15 mmol of vanadium ($20 \text{ mol}_{\text{Carbon}} \text{ molV}^{-1}$) in 150 mL 95:5 vol.-% water:methanol.

This fact indicates that the removal of the liquid reaction products was successful and sufficient. The concentration of FA was decreased from 160 mmol L^{-1} after the first reaction (Recycling 0) to 34 mmol L^{-1} before the first recycling (Recycling 1), meaning after nanofiltration and rediluting. This corresponds to a drastically decrease of about 80 %. Furthermore, 74 % of AA and 76 % of MF as large product molecules were removed. Both products were formed in such small quantities or are limited by its hydrolysis equilibrium that no accumulation could be determined during the whole series of experiments. Based on the results, the repeated set of experiments is highly promising.

For a well-founded evaluation, it is also necessary to take into account the SCO results, which are shown in Fig. 15. The results presented

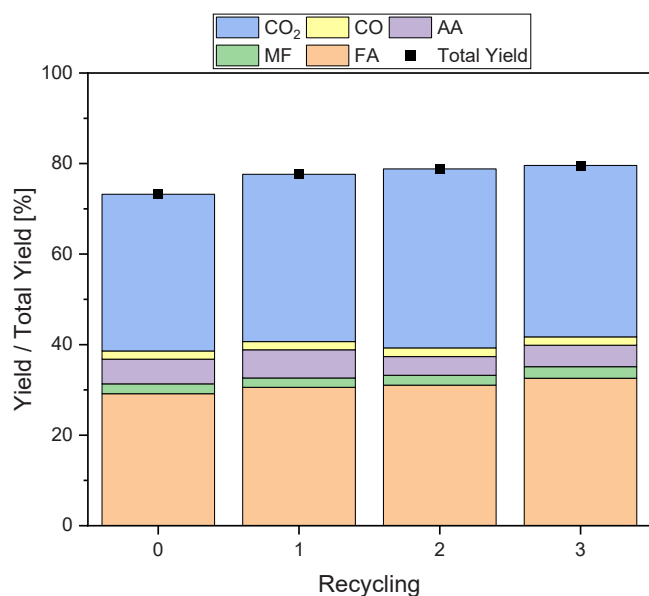


Fig. 15. Recycling experiments for SCO of glucose-based humin using HPA-2 without addition of pTSA. *Experimental conditions:* 90 °C, 30 bar O_2 , 24 h, 1000 rpm, 1500 mg solid humin (81 mmol carbon), 4.15 mmol of vanadium ($20 \text{ mol}_{\text{Carbon}} \text{ molV}^{-1}$) in 150 mL 95:5 vol.-% water:methanol.

were adjusted by the remaining amount of liquid reaction products from the respective previous reactions. The activity remained stable throughout all cycles with total yields of more than 73 %. Apparently, after the first reaction (Recycling 0) the total yield increased to about 80 % and remained at this value in the subsequent recycling experiments (Recycling 1–3). As already mentioned, after nanofiltration, approximately 20 % of the main reaction product FA remained in the reaction solution, therefore the pH value permanently stabilized at values below the initial pH of 1.8. The acidic reaction products could help in the hydrolysis of bonds in the humin structure and thus act as solubilizer or reaction promoter increasing the activity. As long as the pH value does not fall below pH 1, this positive effect seemed to be noticeable. On the one hand, the yield of the main value-added product FA was around 40 % in all experiments. On the other hand, the yield of the main undesired by-product CO_2 was also around 40 % in all experiments. Thus, the ratio of value-added product and undesired by-product was maintained at 50:50 indicating no loss in selectivity.

In summary, the reaction products were efficiently removed, stabilizing pH in the optimal range and the structure, activity as well as selectivity of the catalyst were preserved. Overall, a sustainable and efficient process could be developed representing an important milestone in the efficient separation of homogeneous polyoxometalate catalysts and could therefore be the basis for further developments.

3. Conclusion

In the present study, a sustainable process for the selective catalytic oxidation of humins to short-chain carboxylic acids using molecular polyoxometalate catalysts in aqueous methanolic solution in combination with nanofiltration as efficient downstream process was demonstrated. Replacing the monovanadium-substituted HPA-1 catalyst by a di vanadium-substituted HPA-2 enabled a drastic decrease of the reaction temperature without loss in activity. Furthermore, by using the CO_2 inhibiting effect of methanol and pTSA as solubilizer, a loss of selectivity was prevented, even when a higher substituted catalyst, which usually tend to overoxidation, was used.

The accumulation of acidic products in the liquid reaction solution results in a decreasing pH and finally leads to the formation of less active V-substituted species. Therefore, the efficient separation of value-added products (carboxylic acids) and the catalyst is essential. For the development of a nanofiltration-based downstream process, several acid-stable and commercially available nanofiltration membranes were tested. We discovered that the XN45 nanofiltration membrane (*Mann+Hummel*) outperformed all other tested membranes concerning the rejections of catalyst components and value-added products at a high permeate flux. The XN45 membrane enabled a remarkable rejection for the catalyst components Mo and V of over 99 %. The latter can form smaller species that can penetrate membranes more easily making the results even more promising. In addition, the value-added products were almost not rejected, resulting in a highly selective separation process. Moreover, we demonstrated long-time stability of the membrane by a duration test. Over 168 h on stream, there was no loss in separation performance. Examining the membrane after the experiment using SEM did not reveal any changes in the microscopic membrane structure. Based on enrichment experiments, it was possible to remove about 80 % of acidic reaction products. In the final step, the recycling of the catalyst was tested and could be demonstrated by using the developed nanofiltration process. However, this was only possible if no pTSA was used as an additive, since otherwise the initial pH value of the reaction solution was already very low. Thus, it reached too low values during the batch reaction and nanofiltration process. For this reason, only methanol was used as a CO_2 inhibiting additive in a second recycling study. The pH could be stabilized within the optimal range and thus activity as well as selectivity in the SCO of humins to short-chained carboxylic acids was persevered. We examined the catalyst structure before and after each reaction by ^{51}V NMR proving that its structural integrity is given. These results are

outstanding and represent an important milestone for the chemical valorization of humins and a subsequent downstream processing. Moreover, the developed process can be a generic tool for the separation of molecular POM catalysts enabling efficient and sustainable processes for the valorization of complex biomass.

4. Experimental details

4.1. Chemicals

Alle used chemicals were purchased commercially without further purification. For calibration, as reference or for preparation of model solutions, formic acid (97 %), acetic acid (glacial) and tert.-butanol (97 %) obtained from VWR Chemicals were used.

For the acid catalyzed synthesis of humins, D(+)-glucose (for biochemistry) was purchased from Merck Millipore. The preparation of humins is based on studies of Wassenberg et al (Wassenberg et al., 2023). and was adapted according to literature (Esser et al., 2024b).

The vanadium-substituted Keggin-type polyoxometalate catalysts $H_4[PVMo_{11}O_{40}]$ (HPA-1) and $H_5[PV_2Mo_{10}O_{40}]$ (HPA-2) were synthesized according to literature (Albert et al., 2014; Odyakov and Zhizhina, 2008; Zhizhina et al., 2008). For the optimization studies, methanol (99.8 %) and para- toluenesulfonic acid monohydrate (98 %) supplied by VWR Chemicals and Roth were used.

4.2. Catalyst characterization

Inductively coupled plasma-optical emission spectroscopy (ICP-OES) was used to determine the stoichiometry of the synthesized catalysts. For HPA-1, a stoichiometry of 1.23 P/0.97 V/11 Mo and for HPA-2, a stoichiometry of 1.12 P/1.96 V/10 Mo, were determined. The integrity of the catalysts in solution was proved by ^{51}V NMR and ^{31}P NMR spectroscopy as well as attenuated total reflection Fourier-transform infrared spectroscopy (ATR-FTIR).

4.3. Experimental setup & general method for oxidation experiments

In a 3-fold reaction system consisting of three identical 100 mL autoclaves made of stainless steel, the selective catalytic oxidation of glucose-based humins was conducted. Heating jackets suitable for reaction temperatures up to 200 °C, a gas entrainment impeller and 45 mL glass liners were used.

In a typical experiment, 30 mL of an aqueous methanolic solution with a volumetric methanol content of 5 % was added to 300 mg humin (16.2 mmol carbon) and the appropriate amount of the respective catalyst (0.83 mmol of vanadium) in the glass liner. Before the addition of liquid, 285 mg (1.50 mmol) pTSA monohydrate were added, if used in the experiment. The prepared glass liners were inserted into the autoclaves. Afterwards, the autoclaves were closed and purged three times with 30 bar oxygen to guarantee pure oxygen atmosphere. A pre-pressure of 26.5 bar was set for experiments at a reaction temperature of 90 °C. Subsequently, the heating jackets were put on and a reaction temperature of 90 °C as well as a stirring speed of 300 rpm were set. Reaching the desired reaction temperature and pressure inside the autoclaves, the stirring speed was increased to 1000 rpm, marking the start of the reaction. At the end of the experiment, the stirring speed was decreased to 300 rpm, the temperature was set to 0 °C and the heating jackets were taken off. Below a temperature of 30 °C, samples of the gas phase could be taken using gas bags and the respective valve. The autoclaves were vented and the liquid phase was filtered.

The described methodology was also used for the scale-up experiments, but some adjustments were made. A reaction volume of 150 mL was used increasing the amount of humin to 1.500 g (81.0 mmol carbon), pTSA monohydrate to 1.425 g (7.50 mmol) and vanadium to 4.15 mmol provided by 3.801 g HPA-2 catalyst. The reactions were performed in a 600 mL Hastelloy C276 autoclave equipped with a gas

entrainment impeller. For the recycling experiments, the setup and the methodology were identical to the scale-up experiments. After the first reaction of the recycling study, no fresh catalyst was added to the reaction solution. Furthermore, in one set of experiments no pTSA was used. Before and after each reaction, samples (0.6 mL) for qualitative and quantitative NMR measurements (1H , ^{13}C , HSQC, HMBC, ^{51}V and ^{31}P) were taken. In addition, samples (0.1 mL) were taken and diluted by a factor of 100 for quantitative measurements via ICP-OES before each experiment.

4.4. Experimental setup & general method for nanofiltration experiments

A detailed description of the used setup for nanofiltration experiments can be found in literature (Esser et al., 2022). For membrane screening experiments, a model solution containing about 6.8 g L⁻¹ FA, 0.8 g L⁻¹ AA, 38.0 g L⁻¹ MeOH, 9.5 g L⁻¹ pTSA and about 25.4 g L⁻¹ HPA-2 catalyst was prepared and used. Before each screening experiment, a round cut out of the respective membrane (diameter of 76 mm), was inserted into the membrane cell and pre-wetted with water. For this purpose, the membrane system was rinsed with water at a volume flow of 15 mL min⁻¹. After 5 min, the transmembrane pressure was increased to 30 bar and remained at this level for 2 h. Subsequently, the membrane system was depressurized by switching the pump off. The membrane was stored within the flooded membrane system for 24 h to ensure the sufficient wetting and swelling of the membrane. After 24 h, the membrane system was dried using air and 100 mL of model solution was filled into the system. The membrane system was rinsed with the model solution without pressure for 5 min recycling all streams back into the feed storage. In the subsequent 15 min, the system was rinsed using the desired values of the experimental parameters. The stirrer integrated within the membrane cell was set to a stirring speed of 1100 rpm, the volume flow remained at 15 mL min⁻¹ and a transmembrane pressure of 30 bar was used. Before the actual experiment started, a sample of the feed solution was taken. Afterwards, permeate and retentate were withdrawn into separated vessels (measuring cylinders) and the time measurement was started. The mass of permeate was determined and used for the calculation of the permeate flux. Samples of the permeate and retentate were taken and analyzed by ICP-OES NMR and HPLC. In a final step, the membrane system was cleaned by rinsing with air and water.

The same procedure with some adaptations was applied for the enrichment or recycling experiments. One adaptation was that 150 mL of the model solution or real reaction solution were diluted to 400 mL by aqueous methanol solution (5 vol%). This was done since the autoclaves and the periphery of the reaction setup needed to be cleaned to ensure that all the catalyst was collected after a recycling experiment. The enrichment experiment was intended to replicate the recycling process, which is why this procedure was also followed in the enrichment experiment. Another adaptation was the recycling of the retentate into the feed storage of the membrane system, while the permeate was withdrawn. Thus, the retentate/feed volume was decreased to about 75 mL, corresponding to an enrichment of the catalyst of about 5.3. In the recycling experiments the membrane system was rinsed with about 50 mL of aqueous methanol solution. The rinsing solution contained catalyst and was united with the enriched catalyst solution. Diluted to the original reaction volume of 150 mL, the reaction solution was filled back into the autoclave of the reaction system and fresh humin was added.

4.5. Analytics

ATR-FTIR spectra of the catalysts were measured using a QATRTM-S single reflection ATR. The catalyst's stoichiometry was determined using a Fa. Spectro Ametek Model Arcos ICP-OES spectrometer. Elemental analysis (CHNSO) was conducted on a Model EA-3000 analyzer of Fa. EuroVector (Milano, Italy). HPLC measurements were performed using a

SHIMADZU HPLC system equipped with an Aminex HPX-87 H 300 mm×7.8 mm BIORAD column and a refractive index detector. Aqueous sulfuric acid (5 mmol L⁻¹) with a flow rate of 0.5 mL min⁻¹ was used as eluent. Measurements were conducted at a pressure of about 49 bar and a temperature of 45 °C. For qualitative and quantitative analysis, nuclear magnetic resonance (NMR) was applied using a Bruker AVANCEII 600 MHz spectrometer. 0.6 mL of reaction solution were blended with 0.1 mL of a 10 wt% tert.-butanol solution in D₂O. The gas phase was analyzed by a Varian 450-GC equipped with a thermal conductivity detector (TCD-GC).

4.6. Formulas for calculations

All yields were calculated based on carbon. For quantification by ¹H NMR, a 10 wt% tert.-butanol solution in D₂O was used as a standard solution. The exact mass of the standard solution added was measured, so the molar amount of tert.-butanol in the sample is given by its known mass fraction and molar mass. The molar amount $n_{Pro\ i}$ of a product i results from the ratio of its area $A_{Pro\ i}$ and the area of the standard A_{Stand} multiplied by the known molar amount of the standard n_{Stand} . The number of protons $N_{H,i}$, which generate the signals, must be taken into account, as it is done in Eq. 1:

$$n_{Pro\ i} = \frac{A_{Pro\ i} \cdot N_{H,Stand} \cdot n_{Stand}}{A_{Stand} \cdot N_{H,Pro\ i}} \quad (1)$$

According to known relationships, the mass fraction $w_{Pro\ i}$ of a product i was calculated from its determined molar amount, its molar mass, and the mass of the sample. For the calculation of carbon-based yields, the initial amount of carbon $n_{0,C}$ provided by the substrate had to be calculated. This was done using Eq. 2, where $w_{C,Sub}$ is the known mass fraction of carbon of the substrate, m_{Sub} is its weight in mass for the reaction and M_c is the molar mass of carbon:

$$n_{0,C} = \frac{w_{C,Sub} \cdot m_{Sub}}{M_c} \quad (2)$$

Based on the initial amount of carbon $n_{0,C}$, the amount of carbon $N_{C,i}$ required for the formation of a product i , its molar mass $M_{Pro\ i}$ and the sum of weights of substrate m_{Sub} , pTSA m_{pTSA} , catalyst m_{Cat} as well as solvent m_{Sol} , the theoretical possible mass fraction $w_{theo,Pro\ i}$ of a product i was calculated by Eq. 3:

$$w_{theo,Pro\ i} = \frac{n_{0,C} / N_{C,Pro\ i} \cdot M_{Pro\ i}}{m_{Sub} + m_{pTSA} + m_{cat} + m_{sol}} \quad (3)$$

The yield $Y_{Pro\ i}$ of a product i was calculated by the ratio of its determined and theoretical mass fraction, as shown in Eq. 4:

$$Y_{Pro\ i} = \frac{w_{Pro\ i}}{w_{theo,Pro\ i}} \quad (4)$$

For quantification by HPLC, the measured molar concentration of a product i $c_{Pro\ i}$ was converted to the mass fraction of the product i $w_{Pro\ i}$ using Eq. 5:

$$w_{Pro\ i} = c_{Pro\ i} \cdot \rho_{liq} \cdot M_{Pro\ i} \quad (5)$$

The density of the reaction solution ρ_{liq} after the reaction was measured by weighing an exact defined volume of the solution and calculating the ratio of the measured mass and the volume. The yield could be calculated according to Eq. 4. The combined yields were calculated by the sum of the yields of liquid products or gaseous products, respectively. The sum of those combined yields is the total yield. Dividing the respective combined yield by the total yield results in the ratio of value-added products and undesired by-products.

The rejection R_i for a component i was calculated using Eq. 6, where $\beta_{i,Permeate}$ and $\beta_{i,Feed}$ are the measured mass concentration of the component in the permeate or feed, respectively:

$$R_i = 1 - \frac{\beta_{i,Permeate}}{\beta_{i,Feed}} \quad (6)$$

The volumetric enrichment E_V was calculated based on the ratio of the feed volume at the beginning of the experiment V_0 and the feed volume at the end V_{End} . Based on the volumetric enrichment the theoretical enrichment $E_{theo,i}$ of a component i can be calculated, according to Eq. 7.

$$E_{theo, i} = \left(\frac{V_0}{V_{End}} \right)^{R_i} \quad (7)$$

The determined enrichment E_i of a component i was calculated by the ratio of the determined mass concentration of the component at the end and at the beginning of the experiment.

Appendix. Supporting Information

The calculated yields are based on carbon. The supporting information is accompanied by various additional results and compositions of reaction solutions.

CRedit authorship contribution statement

Jakob Albert: Writing – review & editing, Supervision, Conceptualization. **Dorothea Voss:** Validation, Supervision, Project administration, Methodology. **Andre Wassenberg:** Writing – original draft, Investigation, Formal analysis. **Tobias Esser:** Writing – original draft, Conceptualization.

Declaration of Competing Interest

The authors declare that they have no known competing financial interests or personal relationships that could have appeared to influence the work reported in this paper.

Acknowledgements

J.A., T.E. and A.W. acknowledge financial support from the Deutsche Forschungsgemeinschaft (DFG) via the project AL 2130/5–1. We like to thank the division for electron microscopy, the division for NMR spectroscopy and the division for central element analytics of the Department of Chemistry conducting SEM measurements, NMR experiments and ICP as well as CHNS measurements. We acknowledge scientific support in the first membrane screening phase from Prof. Dr.-Ing. Mirko Skiborowski and Kai Kruber from TUHH. We also thank Suez Water Technologies and Solution for providing membrane samples.

Appendix A. Supporting information

Supplementary data associated with this article can be found in the online version at [doi:10.1016/j.cherd.2024.08.007](https://doi.org/10.1016/j.cherd.2024.08.007).

References

- Hou, Q., Qi, X., Zhen, M., Qian, H., Nie, Y., Bai, C., Zhang, S., Bai, X., Ju, M., 2021. Biorefinery roadmap based on catalytic production and upgrading 5-hydroxymethylfurfural. *Green. Chem.* 23, 119–231.
- Chen, S., Wojcieszak, R., Dumeignil, F., Marceau, E., Royer, S., 2018. How Catalysts and Experimental Conditions Determine the Selective Hydroconversion of Furfural and 5-Hydroxymethylfurfural. *Chem. Rev.* 118, 11023–11117.
- Dincer, I., 2000. Renewable energy and sustainable development: a crucial review. *Renew. Sustain. Energy Rev.* 4, 157–175.
- Román-Leshkov, Y., Barrett, C., Liu, Z., Dumesic, J.A., 2007. Production of dimethylfuran for liquid fuels from biomass-derived carbohydrates. *Nature* 447, 982–985.
- Wang, T., Tan, J., Qiu, S., Zhang, Q., Long, J., Chen, L., Ma, L., Li, K., Liu, Q., Zhang, Q., 2014. Liquid Fuel Production by Aqueous Phase Catalytic Transformation of Biomass for Aviation. *Energy Procedia* 61, 432–435.
- Alonso, D.M., Bond, J.Q., Dumesic, J.A., 2010. Catalytic conversion of biomass to biofuels. *Green. Chem.* 12, 1493–1513.

- Liu, S., Zhu, Y., Liao, Y., Wang, H., Liu, Q., Ma, L., Wang, C., 2022. Advances in understanding the humins: Formation prevention and application. *Appl. Energy Combust. Sci.* 10, 100062.
- Hayes, D.J., Hayes, M.H.B., 2009. The role that lignocellulosic feedstocks and various biorefining technologies can play in meeting Ireland's biofuel targets. *Biofuels, Bioprod. Bioref.* 3, 500–520.
- Cherubini, F., 2010. The biorefinery concept: Using biomass instead of oil for producing energy and chemicals. *Energy Convers. Manag.* 51, 1412–1421.
- Maity, S.K., 2015. Opportunities, recent trends and challenges of integrated biorefinery: Part I. *Renew. Sustain. Energy Rev.* 43, 1427–1445.
- Bozell, J.J., Petersen, G.R., 2010. Technology development for the production of biobased products from biorefinery carbohydrates—the US Department of Energy's "Top 10" revisited. *Green. Chem.* 12, 539.
- Weissermel, K., Arpe, H.-J., 2003. *Industrial organic chemistry*. Wiley-VCH, Weinheim, 4th edn.
- Kapanji, K.K., Haigh, K.F., Görgens, J.F., 2021. Techno-economics of lignocellulose biorefineries at South African sugar mills using the biofine process to co-produce levulinic acid, furfural and electricity along with gamma valeractone. *Biomass- Bioenergy* 146, 106008.
- Climent, M.J., Corma, A., Iborra, S., 2014. Conversion of biomass platform molecules into fuel additives and liquid hydrocarbon fuels. *Green. Chem.* 16, 516.
- Patil, S.K.R., Heltzel, J., Lund, C.R.F., 2012. Comparison of Structural Features of Humins Formed Catalytically from Glucose, Fructose, and 5-Hydroxymethylfurfuraldehyde. *Energy Fuels* 26, 5281–5293.
- Maerten, S.G., Voß, D., Liauw, M.A., Albert, J., 2017. Selective Catalytic Oxidation of Humins to Low-Chain Carboxylic Acids with Tailor-Made Polyoxometalate Catalysts. *ChemistrySelect* 2, 7296–7302.
- Wassenberg, A., Esser, T., Poller, M.J., Albert, J., 2023. Investigation of the Formation, Characterization, and Oxidative Catalytic Valorization of Humins. *Materials* 16 (7), 2864.
- He, Z., Hou, Y., Li, H., Wang, Y., Ren, S., Wu, W., 2023. Novel insights into CO₂ inhibition with additives in catalytic aerobic oxidation of biomass-derived carbohydrates to formic acid. *Renew. Energy* 211, 403–411.
- Voß, D., Kahl, M., Albert, J., 2020a. Continuous Production of Formic Acid from Biomass in a Three-Phase Liquid–Liquid–Gas Reaction Process. *ACS Sustain. Chem. Eng.* 8, 10444–10453.
- Esser, T., Wassenberg, A., Raabe, J.-C., Voß, D., Albert, J., 2024a. Catalytic Valorization of Humins by Selective Oxidation Using Transition-Metal-Substituted Keggin-Type Polyoxometalate Catalysts. *ACS Sustain. Chem. Eng.* 12 <https://doi.org/10.1021/acssuschemeng.3c06539>.
- Esser, T., Wassenberg, A., Voß, D., Albert, J., 2024b. Selective catalytic oxidation of humins to carboxylic acids using the H₄[PVMo₁₁O₄₀] Keggin-type polyoxometalate enhanced by alcohol doping and solubilizer. *React. Chem. Eng.* <https://doi.org/10.1039/D3RE00672G>.
- (a) Wesinger, S., Mendt, M., Albert, J., 2021. Alcohol-Activated Vanadium-Containing Polyoxometalate Complexes in Homogeneous Glucose Oxidation Identified with 51 V-NMR and EPR Spectroscopy. *ChemCatChem* 13, 3662–3670. (b) Maerten, S., Kumpidet, C., Voß, D., Bukowski, A., Wasserscheid, P., Albert, J., 2020. Glucose oxidation to formic acid and methyl formate in perfect selectivity. *Green. Chem.* 22 (13), 4311–4320.
- Zhong, J., Pérez-Ramírez, J., Yan, N., 2021. Biomass valorisation over polyoxometalate-based catalysts. *Green. Chem.* 23, 18–36.
- Lechner, M., Güttel, R., Streb, C., 2016. Challenges in polyoxometalate-mediated aerobic oxidation catalysis: catalyst development meets reactor design. *Dalton Trans.* 45, 16716–16726.
- Voß, D., Dietrich, R., Stuckart, M., Albert, J., 2020b. Switchable Catalytic Polyoxometalate-Based Systems for Biomass Conversion to Carboxylic Acids. *ACS Omega* 5, 19082–19091.
- Bertleff, B., Claußnitzer, J., Korth, W., Wasserscheid, P., Jess, A., Albert, J., 2017. Extraction Coupled Oxidative Desulfurization of Fuels to Sulfate and Water-Soluble Sulfur Compounds Using Polyoxometalate Catalysts and Molecular Oxygen. *ACS Sustain. Chem. Eng.* 5, 4110–4118.
- Bukowski, A., Schill, L., Nielsen, D., Mossin, S., Riisager, A., Albert, J., 2020. NH₃-SCR of NO with novel active, supported vanadium-containing Keggin-type heteropolyacid catalysts. *React. Chem. Eng.* 5, 935–948.
- Esser, T., Huber, M., Voß, D., Albert, J., 2022. Development of an efficient downstream process for product separation and catalyst recycling of a homogeneous polyoxometalate catalyst by means of nanofiltration membranes and design of experiments. *Chem. Eng. Res. Des.* 185, 37–50.
- Raabe, J.-C., Esser, T., Jameel, F., Stein, M., Albert, J., Poller, M.J., 2023a. Study on the incorporation of various elements into the Keggin lacunary-type phosphomolybdate [PMo₉O₃₄] 9– and subsequent purification of the polyoxometalates by nanofiltration. *Inorg. Chem. Front.* 10, 4854–4868.
- Poller, M.J., Bönsch, S., Bertleff, B., Raabe, J.-C., Görling, A., Albert, J., 2022. Elucidating activating and deactivating effects of carboxylic acids on polyoxometalate-catalysed three-phase liquid–liquid–gas reactions. *Chem. Eng. Sci.* 264, 118143.
- Bertleff, B., Goebel, R., Claußnitzer, J., Korth, W., Skiborowski, M., Wasserscheid, P., Jess, A., Albert, J., 2018. Investigations on Catalyst Stability and Product Isolation in the Extractive Oxidative Desulfurization of Fuels Using Polyoxometalates and Molecular Oxygen. *ChemCatChem* 10, 4602–4609.
- Albert, J., Wasserscheid, P., 2015. Expanding the scope of biogenic substrates for the selective production of formic acid from water-insoluble and wet waste biomass. *Green. Chem.* 17, 5164–5171.
- Albert, J., Wölfel, R., Bösmann, A., Wasserscheid, P., 2012. Selective oxidation of complex, water-insoluble biomass to formic acid using additives as reaction accelerators. *Energy Environ. Sci.* 5, 7956.
- Albert, J., Mendt, M., Mozer, M., Voß, D., 2019. Explaining the role of vanadium in homogeneous glucose transformation reactions using NMR and EPR spectroscopy. *Appl. Catal. A: Gen.* 570, 262–270.
- Raabe, J.-C., Poller, M., Voß, D., Albert, J., 2023b. H₈PV₅Mo₇O₄₀ (HPA-5) - a unique polyoxometalate for acid and RedOx catalysis: synthesis, characterization, and modern applications in green chemical processes. *ChemSusChem*, e202300072.
- Evtugin, D.V., Pascoal Neto, C., Rocha, J., Pedrosa de Jesus, J.D., 1981. *Applied catalysis*. *Appl. Catal.* 1, 97–105.
- Pettersson, L., Andersson, I., Grate, J.H., Selling, A., 1994. Multicomponent Polyoxometalates. 46. Characterization of the Isomeric Keggin Decamolybdodivanadophosphate Ions In Aqueous Solution by 31P and 51V NMR. *Inorg. Chem.* 33, 982–993.
- Albert, J., Lüders, D., Bösmann, A., Guldi, D.M., Wasserscheid, P., 2014. Spectroscopic and electrochemical characterization of heteropoly acids for their optimized application in selective biomass oxidation to formic acid. *Green. Chem.* 16, 226–237.
- Odyakov, V.F., Zhizhina, E.G., 2008. A novel method of the synthesis of molybdovanadophosphoric heteropoly acid solutions. *React. Kinet. Catal. Lett.* 95, 21–28.
- Zhizhina, E.G., Odyakov, V.F., Simonova, M.V., 2008. Catalytic oxidation of organic compounds with oxygen in the presence of Mo-V-phosphoric heteropoly acid solutions. *Kinet. Catal.* 49, 773–781.

7 Comprehensive Discussion of Research Results

Selective catalytic oxidation of biogenic feedstock and complex biomass into various chemicals is a crucial approach for the substitution of fossil-based processes and the development of sustainable green processes. The objective of the present study was to develop a conversion process for humins to short chain carboxylic acids based on the selective catalytic oxidation using homogeneous polyoxometalate catalysts and their efficient recycling employing nanofiltration. Thus, humins can be valorized as the undesired by-product of biorefineries, converting nearly every biomass types into various classes of platform chemicals, biofuels and biochemicals, increasing the overall carbon efficiency. This could contribute to the substitution of fossil-based processes alleviating excessive dependence on depleting fossil resources.

Development of a nanofiltration-based downstream process for the recycling of homogenous POM-catalysts

Parallel to the investigation of an efficient recovery process for homogeneous POM-catalysts and product purification, the development of a reaction system for the selective catalytic oxidation of humins was investigated. Due to its unique properties, NF seemed predestined for this task (*vide supra*, 4.5.4). When using homogeneous vanadium-substituted *Keggin*-type POM-catalysts for the oxidative valorization of biomass, FA and AA are recurring products. The efficient separation of these acidic products from the catalysts is essential for a sustainable process, but also challenging. An example is the extraction-coupled oxidative desulfurization (ECODS), in which the accumulation of FA inhibits the catalytic activity of higher vanadium-substituted POM-catalysts. For this purpose, a NF system was designed, constructed, and optimized using a model solution based on the product solution of ECODS (*vide supra*, 6.1). The acid stable NF membrane DK-Series with a MWCO of 200 Da (*Suez Water Technologies & Solution*) was used for the initial experiments.²⁰⁵

The designed NF system has a unique feature compared to classical cross-flow filtration, which is ensured by a stirrer integrated into the membrane cell. The stirrer allows sufficient cross-flow of the membrane and turbulence in the cell without applying high flow rates caused by powerful pumps. After developing a suitable pre-wetting and swelling method for the membranes, the process was optimized.²⁰⁵

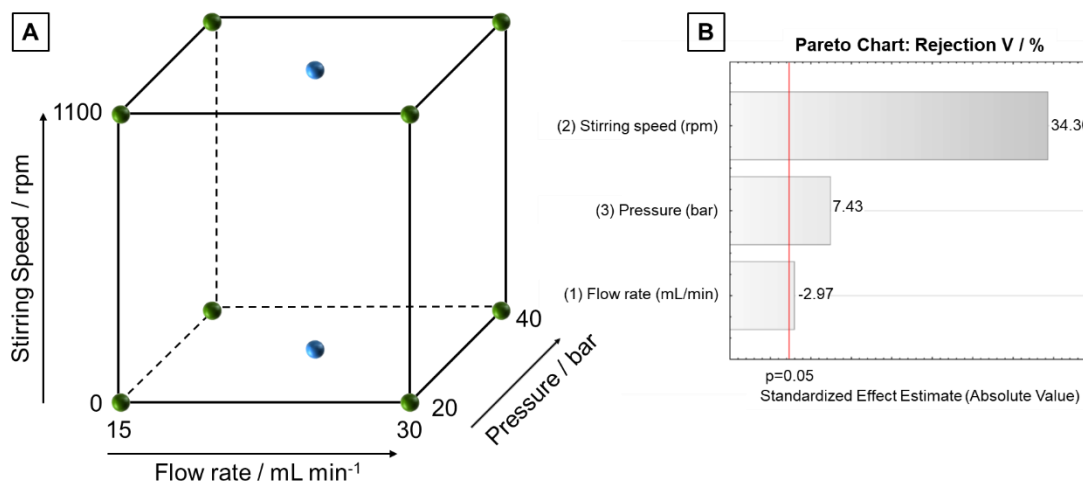


Figure 7.1: A) Statistical design of experiments according to *Box-Hunter-Hunter* for the optimization of nanofiltration process.²⁰⁵ B) Pareto chart comparing the significance of individual parameter exemplary for the rejection of vanadium.

According to *statistical design of experiments* (DoE), a comprehensive study was conducted to optimize the NF process considering the flow rate, transmembrane pressure and stirrer speed as variables using a *Box-Hunter-Hunter* experimental design that is shown in Figure 7.1 A. The target variables were the rejections of the products FA and AA as well as the catalyst components vanadium, molybdenum, and phosphorus. It was shown that the stirring speed has the highest influence on the rejections of all system components (Figure 7.1 B). Increasing the stirring speed to 1100 rpm led above all to a desired increase in the rejection of the catalyst components vanadium and phosphorous. Due to the chosen design of the membrane cell, this result is plausible, as the stirrer ensures sufficient cross-flow of the membrane. Hence, a high stirring speed caused high turbulence and thus minimized effects such as concentration polarization. Molybdenum was hardly affected by the parameter variations, as was FA. It can be assumed that molybdenum, which tends to occur in larger species, could hardly penetrate the membrane. On the other hand, FA is a small molecule and penetrated the membrane almost unhindered. Furthermore, the unique properties of NF membranes based on micro hydrodynamics and interfacial events enable high selectivity between multivalent and monovalent ions (*vide supra*, 4.5.4). Consequently, FA (resp. formate, HCOO^-) was hardly rejected as a monovalent ion and molybdenum species (heteropoly anion) was strongly rejected as a polyvalent ion. Based on the results, the NF process was optimized, selecting the maximum stirring speed of 1100 rpm, a pressure of 30 bar and a pump flow rate of 15 mL min⁻¹. Applying these conditions, rejections of over 97 % for vanadium and over 99 % for molybdenum

as well as a low product rejection (FA, AA) between 3 % and 10 % was achieved enabling selective separation.²⁰⁵

Enrichment experiments demonstrated that a high enrichment of the catalyst in the retentate is possible. NMR analyses confirmed that the structural integrity of the catalyst sustained, during this process. Thus, a removal of over 80 % of the carboxylic acids was obtained. The enriched catalyst solutions of the desulfurization experiments were recycled several times to investigate the recyclability. Figure 7.2 displays the results of the recycling study by means of the development of the degree of desulfurization (Figure 7.2 A) and the corresponding ⁵¹V-NMR spectra (Figure 7.2 B). The catalytic activity was retained in three consecutive reactions. Therefore, recycling is possible if the acidic products are sufficiently removed. Beyond these three cycles, the catalytic activity decreased dramatically indicated by a sharp decrease of the degree of desulfurization from almost 100 % to less than 40 %. On the one hand, the pH value of the reaction solution fell to well below pH 1 during the reaction due to the batch operation. On the other hand, sulfuric acid, which was produced by the desulfurization of the organic sulfur components, was too strongly rejected by the membrane as a larger divalent anion. According to ⁵¹V-NMR analyses, both led to the formation of lower substituted catalyst isomers and thus to lower catalytic activity. Continuous operation and other membranes with larger MWCO that reject less sulfuric acid could enable recyclability. In conclusion, for an efficient downstream process, stabilization of the pH value above pH 1 is crucial.²⁰⁵

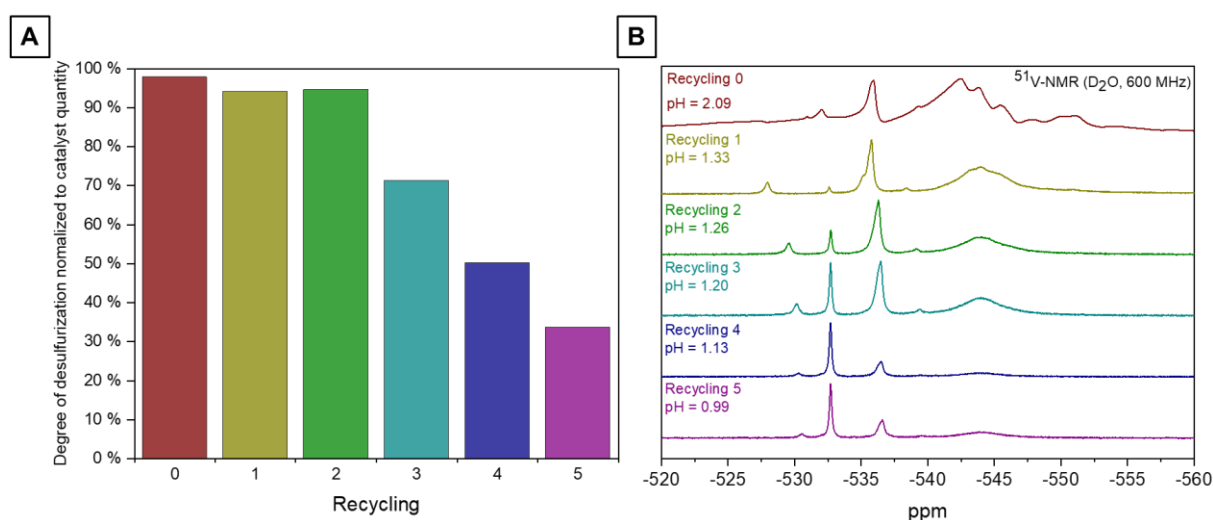


Figure 7.2: A) Normalized degree of desulfurization with reused aqueous catalyst solution. B) ⁵¹V-NMR spectra (600 MHz) of the liquid phase before reaction (after nanofiltration). Figures are adapted from literature²⁰⁵.

The selective separation of homogeneous POM-catalysts from carboxylic acids such as FA and AA, which are also products of the valorization of humins is feasible. In further studies of *Raabe et al.*²¹⁵, the developed NF process was tested for various POM-catalysts to demonstrate the generic efficiency of the new process for the recovery or purification of homogeneous POM-catalysts. More specifically, it was shown that a high rejection and selectivity for the catalyst is possible across systems by using the NF process to purify various POM-catalysts in aqueous phase. This means that the developed NF process is a generic tool for the separation of homogenous POM-catalysts that can be applied to POMs substituted with different transition metals and different degrees of substitution.²¹⁵

Development of a sustainable reaction system for the selective catalytic oxidation of humins

The development of the selective catalytic oxidation of humins to short chain carboxylic acids started with the selection of appropriate model substances that emulate the fundamental structural motifs of humins shown in Figure 7.3. The necessity of using model substances was given due to the high complexity of the humin structure, which has not yet been fully understood. A basic building block are furan rings, which form the complex three-dimensional network of humins through a wide variety of bonding types and functional groups (*vide supra*, 4.2.1.2). Furfural was selected as a commercially available model substance for selective catalytic oxidation using various homogeneous *Keggin*-type POM-catalysts under mild reaction conditions (90 °C, 30 bar O₂) in aqueous media.²¹²

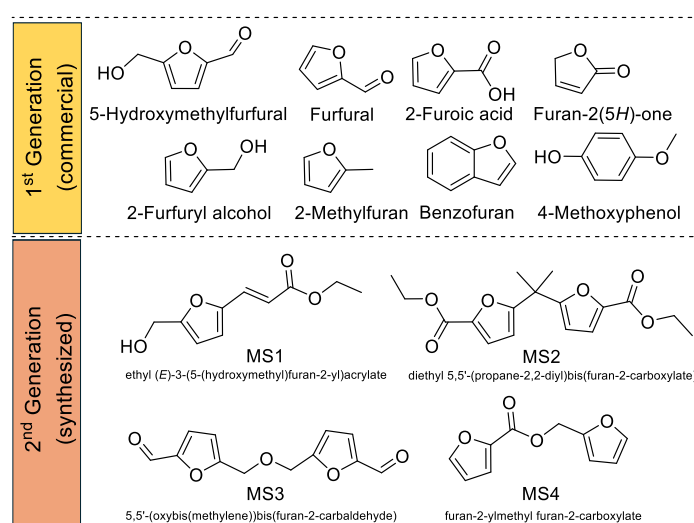


Figure 7.3: Molecular structure of various first-generation (top / yellow section) and second-generation (bottom, orange section) model substrates emulation structural motifs of complex humins.

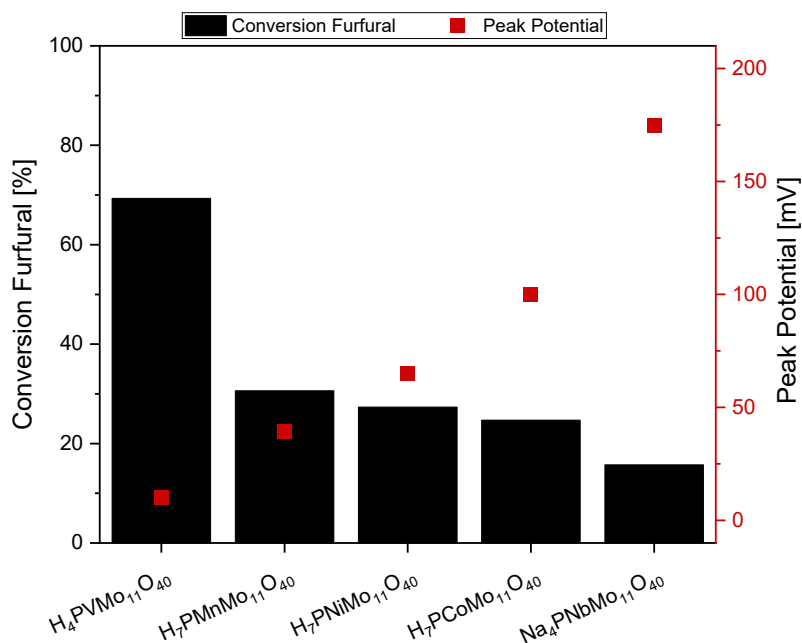


Figure 7.4: Comparison of furfural conversion and peak potentials in dependency of the POM catalysts used.²⁰⁵

In an initial screening series, various mono-substituted POM-catalysts were tested to identify the most suitable transition metal for substitution. In terms of yield of the industrial relevant MA and FA as well as activity, vanadium was superior compared to other transition metals such as nickel, manganese, niobium, and cobalt or no substitution. Furthermore, despite the greatly increased activity, less CO_2 was formed than without the use of a catalyst. The increased activity was attributed to the highly changed redox potential of the *Keggin*-type POM-catalyst upon substitution with vanadium. Based on electrochemical measurements, a correlation could be revealed between the transition metal used for substitution, the resulting redox potential and the conversion achieved. Compared to transition metals such as nickel, cobalt, manganese, and niobium, by far the lowest peak potential was measured in SWV data using vanadium for substitution as shown in Figure 7.4. Accordingly, an adjustment of the redox activity was achieved (*vide supra*, 6.2).²¹²

In a second screening series, the degree of substitution using vanadium in *Keggin*-type phosphomolybdates was varied. For this purpose, molybdenum was substituted as addenda atom in phosphomolybdic acid by up to six vanadium atoms. The results showed that higher degrees of substitution (≥ 1) can dramatically increase the activity by factor two and even higher. More specifically, furfural conversion increased from approximately 30 % without substitution to 70 % with mono-substitution and to 100 % with double or higher substitution. A change in the catalysts properties through multiple

substitution seems plausible. It is assumed that multiple substitutions can result in adjacent vanadium pairs forming peroxo-ligands. According to literature⁹⁹, these peroxo-ligands can oxidize the substrate more efficiently since the activation energy for oxidation is lowered by the single state of peroxo-ligand. However, the increase in activity was accompanied by a decrease in selectivity. While the yield of MA decreased from more than 22 % to less than 5 %, the yield of the overoxidation product CO₂ increased from less than 6 % to more than 20 % by increasing the degree of substitution from one to two. A further increase in the degree of substitution enhanced this effect, so that MA was no longer a product. On the other hand, the yield of CO₂ and FA increased to over 30 % or 42 %, respectively, with a maximum degree of substitution of six. Accordingly, the mono-substituted H₄[PVMo₁₁O₄₀] POM-catalyst represents the best compromise between activity and selectivity.²¹²

In the next step, various commercially available furan derivatives (see Figure 7.3) were tested as substrates in a substrate screening using the selected catalyst under otherwise identical conditions. This ensured that a broad spectrum of different functional groups that occur in the humin structure or can be induced by its oxidative degradation were represented. In addition, benzofuran and 4-methylphenol were tested, which can also occur to a lesser extent as structural elements in humins. The selective catalytic oxidation of water-soluble substrates such as furfural, 2-furoic acid, 2(5H)-furanone and 5-HMF produced MA as one of the main products with yields of about 22 %, 6 %, 12 % and 23 %, respectively. These substrates have some common characteristics such as water solubility. In addition, they are all oxygen-functionalized and therefore offer active positions for catalytic oxidation and thus facilitate the removal of C₁ building blocks or oxidative ring opening. Oxidative C-C bond cleavage on a C₁ building block can produce FA, which was detected as a co-product in all reactions. More specifically, the conversion of furfural resulted in a FA yield of around 15 %. This was in excellent agreement with the theoretical yield of 14 %, assuming that for every mole of furfural converted, one mole of FA must be split off. Therefore, it is not surprising that most FA was formed during the oxidative conversion of 5-HMF as a bifunctional C₆ substrate with yields of over 35 %. Consequently, for the same yield of MA (C₄ product), twice as many C₁ building blocks needed to be removed from the 5-HMF molecule (C₆ substrates) as in the case of furfural. The bifunctionality also increases conversion because the POM-catalyst has two oxygen functionalities as enabling a high conversion of 98 %. Furthermore, the bilateral C₁-bond cleavage could

lead to significantly more reactive intermediates and ultimately to four times higher formation of CO₂ (20 %) compared to furfural as a substrate.²¹²

Based on the results, a reaction pathway for furfural was postulated that is shown in Figure 7.5. It can be assumed that the elimination of FA occurs through a nucleophilic attack of a water molecule in the acidic medium and electron transfer to the catalyst ($V^V \rightarrow V^{IV}$). This creates an extremely unstable furyl radical (I_1), which is converted into 5-hydroxyfuran-2(5H)-one (I_2). Indeed, the apparently less active intermediate 5-hydroxyfuran-2(5H)-one was detected in the oxidative conversion of furfural (10 %), but not for 5-HMF. In this process, the catalyst is reoxidized ($V^{IV} \rightarrow V^V$) under the action of molecular oxygen and water. 5-hydroxyfuran-2(5H)-one is in chemical equilibrium with β -formylacrylic acid (I_3). The terminal aldehyde group of β -formylacrylic acid is readily oxidized to a carboxyl group that forms MA. An analogous reaction path could be assumed for 2-furoic acid. However, the carboxyl group cannot be eliminated as formic acid, but must be cleaved as CO₂ by decarboxylation. The determined CO₂ yield (2 %) is in excellent agreement with the theoretical yield (1.7 %) assuming the above mentioned mechanism.²¹²

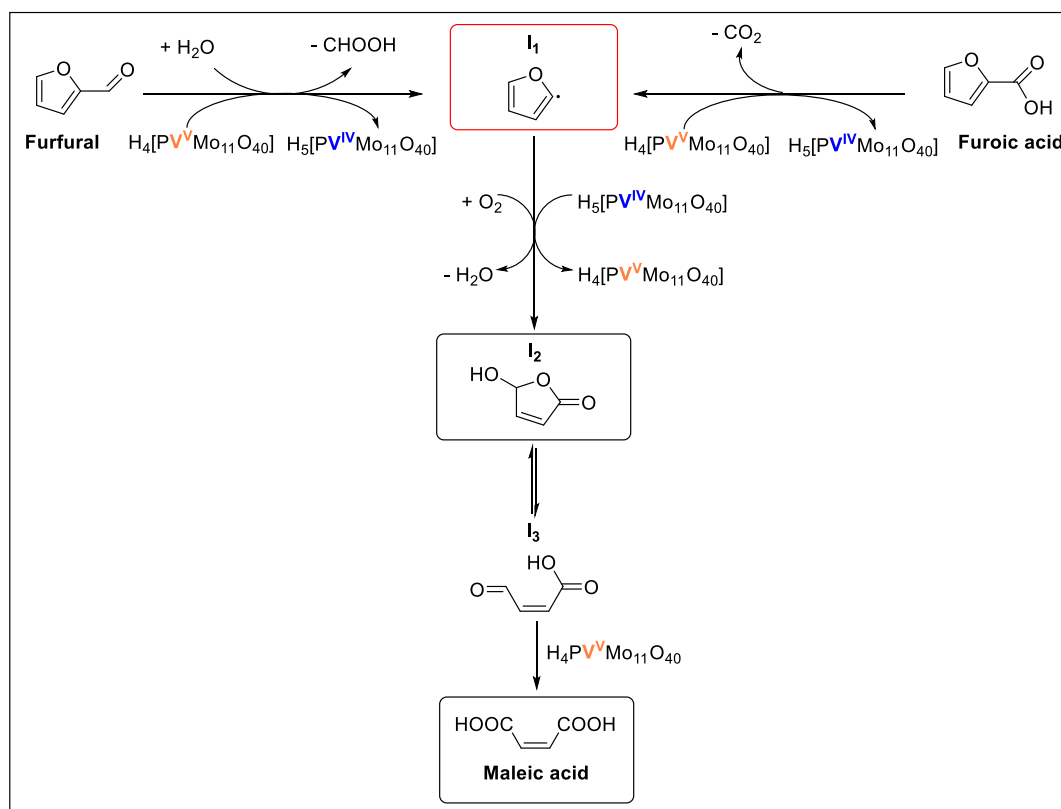


Figure 7.5: Proposed reaction pathways for oxidation of furan derivatives by the means of furfural and 2-furoic acid using H₄[PVMo₁₁O₄₀] in aqueous medium.²¹²

Apparently, the C-C bond cleavage via decarboxylation is more difficult than the elimination of FA, which means that 2-furoic acid is more stable and thus only a conversion of about 10 % was achieved. Furan-2(5H)-one was a similarly stable substrate enabling only low conversions of about 16 %. Nevertheless, the selectivity for MA was high with values of 60 % to 70 % for both substrates.²¹²

Due to its poor water solubility and the lack of suitable oxygen functionalization, 2-methylfuran was oxidized with only a moderate conversion of about 44 %. Interestingly, shorter oxidation products such as FA, AA and CO₂ were predominantly formed, which presumably arise from the oxidative C-C bond cleavage of the side chain. The model substrates benzofuran and 4-methoxyphenol behaved similarly to 2-methylfuran and were only converted moderately due to their lack of water solubility and oxygen functionalization as well as high stability derived from their aromaticity.²¹²

Overall, appropriate oxygen functionalization can be considered as crucial for active conversion using a POM-catalyst. This is even more plausible when considering the conversion of more complex difuran derivatives or branched furan rings in the final screening series. These more complex substrates could also be converted to MA and FA analogous to the monofuran derivatives. Again, it was shown that oxygen-functionalized bond types can be converted much better than non-functionalized bonds. For real humins, where the coexistence of less to non-oxygen-functionalized with strongly oxygen-functionalized bonds and structures can be assumed, the latter represent a crucial access to selective catalytic oxidation by the POM-catalyst. The oxidative C-C bond cleavage at oxygen-functionalized bonds could induce new functionalization at the remaining humin structure, which in turn represent an attack site. In this way, the oxygen functionalization could act as a kind of predetermined breaking point and enable the functionalization of non-oxygen-functionalized bond and thus the successive degradation of humins.²¹²

In summary, a number of important insights, including structure-activity-selectivity relationships, were gained by investigating the oxidative conversion of model substances. Furthermore, plausible reaction pathways were derived from the conversion of these furan-based model substances, which are building blocks of humins. The understanding of the influence of the redox activity of the catalysts was expanded. These findings form an important basis for further investigations and optimizations of the oxidative valorization of humins. In addition to the translation to real humins, further insights could be gained by investigating the conversion of even

more complex model substrates (higher degree of polymerization) and enhanced investigations on non-oxygen-functionalized bond types in future studies. To this end, interesting substances would be for example furan-based polymers, which are created by acid catalyzed polymerization of 2-methylfuran or 2-furfuryl alcohol. Besides to a higher degree of polymerization, these polymers are also characterized by a low oxygen functionalization and could therefore represent the part of the humic structure that is difficult to convert.

Based on the insights of the oxidative conversion of humin-like model substances, real humins were converted (*vide supra*, 6.3). For this purpose, a glucose-based humin was selectively catalytically oxidized using the $H_4[PVMo_{11}O_{40}]$ POM-catalyst at 90 °C and 30 bar O_2 . Due to the lowered conversion during the catalytic oxidation of the more complex model substances, the reaction time for the even more complex humis was increased to 30 h. Here, the relative selectivity advantage of the mono-substituted catalyst compared to higher substituted catalysts could be demonstrated again. Higher substituted catalysts produce predominantly CO_2 (carboxylic acid: CO_2 -ratio of 16:84) due to their higher activity enabled by the peroxo-ligands. A yield of FA of only 12 % was achieved. In contrast, with a CO_2 yield of around 19 % and almost the same yield of FA of around 11 %, less CO_2 was formed when using the singly substituted catalyst (carboxylic acid: CO_2 -ratio of 36:64). In view of the expected lowered conversion, the coarse product distribution, and the relative selectivity advantage of $H_4[PVMo_{11}O_{40}]$ POM-catalyst, the conversion of the complex model substances proved to be a suitable model for the conversion of real humins. However, the results of the conversion of real humins showed that larger structures leading to products such as furfural, 5-HMF and finally also MA could not be made accessible. At least such products could not be detected with the analytics used. This contrasts with the results obtained using the complex model substances as substrates. Consequently, this could mean that the oxygen functionalization in real humins is lower than assumed. According to the possible formation mechanism of humins, this seems conceivable. For example, the aldol condensation of 5-HMF with levulinic acid or DHH leads to structures with a lower oxygen functionalization (*vide supra*, 4.2.1.1 & 4.2.1.2). These structures only exhibit one oxygen functionalization in the immediate vicinity of the furan ring. Figure 7.6 shows a theoretic humin model structure representing the combination of different possible bonds and structures reported by literature^{40,45,216} in one section.²¹³

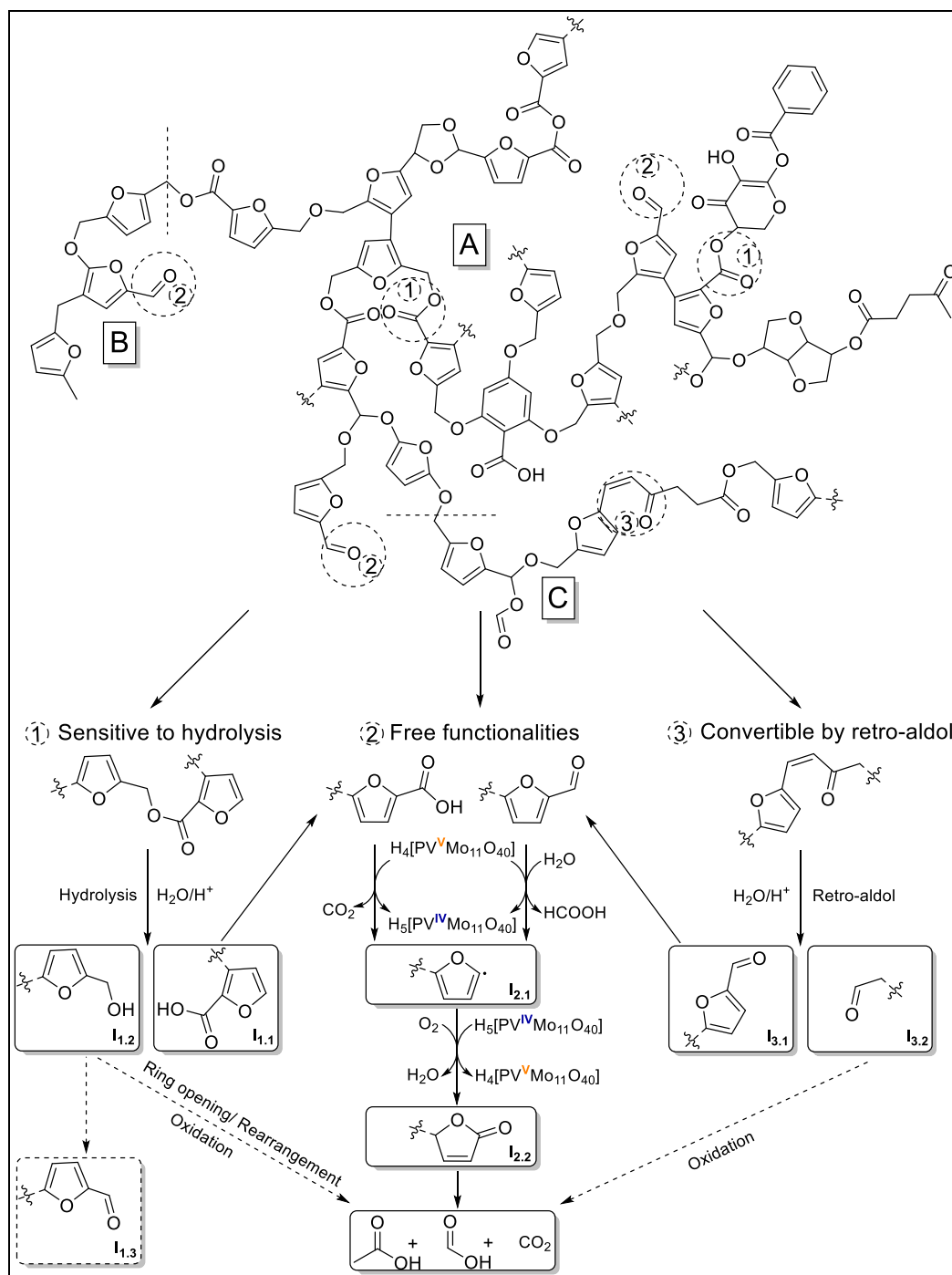


Figure 7.6: Proposed reaction pathway for the selective catalytic oxidation of humins using a modified humin model structure based on structural motifs published by *Filiciotto et al.*⁴⁰ (A), *Wassenberg et al.*²¹⁶ (B) and *Shen et al.*⁴⁵ (C) as example by converting functionalities that are hydrolysis-sensitive (1), free (2) or convertible by retro-aldol (3).²¹³

Analogous to the results of the SCO of model substances, the direct catalytic conversion of freely accessible oxygen functionalities is possible according to the previously postulated reaction pathway. In addition, side reactions can convert structural motifs of the humins into free functionalities, which in turn are oxidized according to the postulated mechanism. In contrast to the model substances, after an initial oxidative cleavage of the C–C bond at an oxygen functionalization, larger

structures would still be bound to the humin network via a non-oxygen-functionalized bond. Hence, further degradation of the humin occurs through the successive oxidative C-C bond cleavage of the newly induced functionality, leading to short chain products such as FA, AA, and CO₂. Thereby, the expected value-added products are FA and AA. Increasing the activity and selectivity of these products was part of further investigations.

Various alcoholic additives were tested in the purpose of inhibiting the formation of CO₂ and enhancing the selectivity. It could be demonstrated that methanol exhibits a remarkable CO₂ inhibiting effect due to its function as radical scavenger, stabilizer of reactive groups and promotor of new catalytic V-species. One conjecture for the latter is the formation of the vanadium ester [VO(OMe)O₂]²⁻, which is more selective and inhibits the overoxidation of the substrate to CO₂. In subsequent experiments the alcohol content as well as reaction temperature could be optimized in terms of conversion and yield of value-added products (carboxylic acids). It was found that a reaction temperature of 120 °C and a low alcohol content of 5 % represent the best conditions in the range investigated. Using these conditions, a high activity and simultaneously for the first time more value-added products (29 %) were produced than undesired CO₂ (28 %) in oxidative conversion of humins.²¹³

An alternative approach investigated was the use of para-toluenesulfonic acid (pTSA) as solubilizer to circumvent the water-insoluble character of humins and thus optimize the activity. Even without the CO₂ inhibiting effect of methanol, almost equal amounts of carboxylic acids (20 %) and undesired by-products (19 %) with an increased total yield of 39 % could be achieved. Thus, the function of pTSA as solubilizer and reaction promoter seems to be evident. Due to the subsequent optimization of the amount of solubilizer and the reaction temperature, the activity of the reaction system could be further enhanced. According to the results, 1.5 mmol pTSA at 120 °C demonstrated the highest activity with a total yield of 94 %. However, the formation of CO₂ (58 %) predominated due to the drastically increased activity. Consequently, the addition of pTSA at elevated reaction temperatures efficiently promotes the activity but exhibit a lack of selectivity compared to methanol, resulting in only a slightly increased yield of value-added products. Therefore, a reaction system where pTSA as a solubilizer increases the activity and methanol increases the selectivity through its CO₂-inhibiting effect seemed to be a promising approach. The results are shown in Figure 7.7 A.

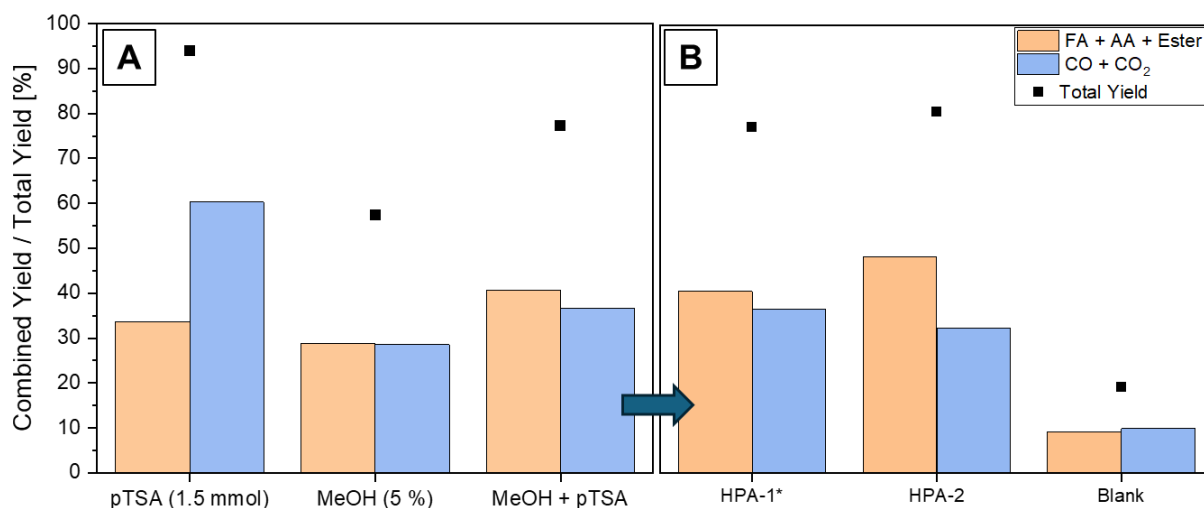


Figure 7.7: A) SCO of humins as catalyst in aqueous methanolic solution, applying solely pTSA as additive and the combination of both additives using HPA-1 catalyst at 120 °C.²¹³ B) Comparison of HPA-1 at 120 °C and HPA-2 at 90 °C for SCO of humins in the combined system.²¹⁴

The combination of both additives applying their optimized amounts and a reaction temperature of 120 °C led to remarkable results (Figure 7.7 A). More specifically, applying this novel approach a low yield of CO₂ (34 %) and simultaneously the highest yields of carboxylic acids (41 %) reported to date in the oxidative conversion of humins were achieved. Additional experiments converting various humins using the novel approach demonstrated the generic efficiency of the novel reaction system. Efficient conversion of all tested humins was possible regardless of the sugar (xylose, glucose, fructose, sucrose) used for the synthesis of the respective humin. The newly developed reaction system is characterized by strong inhibition of CO₂ formation, which opens further optimization potential by applying this system to higher substituted catalysts that tend to overoxidation (*vide supra*, 6.2 & 6.3). In this manner, the reaction time or the reaction temperature could be decreased, which would enable the development of an even more sustainable process. For this purpose, oxidation experiments were conducted at 90 °C, 105 °C and 120 °C using the H₅[PV₂Mo₁₀O₄₀] catalyst under otherwise identical reaction conditions (*vide supra*, 6.4). Stability tests of the additives without substrates revealed that the additives were not stable at temperatures above 90 °C and were oxidized to FA, AA, and CO₂. At a reaction temperature of 90 °C, neither FA nor AA could be detected by HPLC measurements or NMR analyses using both a fully oxidized and a fully reduced H₅[PV₂Mo₁₀O₄₀] catalyst in stability tests. Consequently, the formation of carboxylic acids in oxidation experiments of humins at 90 °C could be attributed to their sole origin from humins. Figure 7.7 B shows the results using H₅[PV₂Mo₁₀O₄₀] catalyst at 90 °C. Using the H₅[PV₂Mo₁₀O₄₀] catalyst the

results exceeded the previous results using $\text{H}_4[\text{PVMo}_{11}\text{O}_{40}]$ catalyst at $120\text{ }^\circ\text{C}$, even though the reaction temperature was lowered by $30\text{ }^\circ\text{C}$. A combined yield of carboxylic acids of 48 % was achieved with a low yield of CO_2 of 32 %. Therefore, the efficiency of the process could be increased and at the same time the energy demand could be decreased enabling a more sustainable process.²¹³

Humine degradation was examined in more detail in time-resolved reaction experiments, with the reaction time broken down from a total of 30 h to 0 h, 2 h, 4 h, 8 h, 16 h and 24 h using $\text{H}_5[\text{PV}_2\text{Mo}_{10}\text{O}_{40}]$ catalyst at $90\text{ }^\circ\text{C}$. The results are shown in Figure 7.8. It was observed that the highest humin degradation and the highest product formation rate was achieved within the first 8 h of the reaction (Figure 7.8 A). Interestingly, CHNSO analyzes also revealed a sharp increase in oxygen content in the solid phase from 30 % to over 40 % (O/C-ratio of 0.8) during this period (Figure 7.8 B). This observation proves to be plausible due to the postulated gradual degradation of the humin structure through oxidative C-C bond cleavage on oxygen-functionalized structural elements and induction of new functionalization. Accordingly, oxygen-functionalized carbon was first removed from the humin structure, but new oxygen was also introduced onto previously unfunctionalized carbon, whereby the mass fraction of carbon decreased, and oxygen increased. This seems to be even more evident concerning the results of ATR-FTIR measurements. Here, the intensity of bands at 1600 cm^{-1} corresponding to carbonyl conjugated C=C double bonds increased within the first hours of reaction.²¹⁴

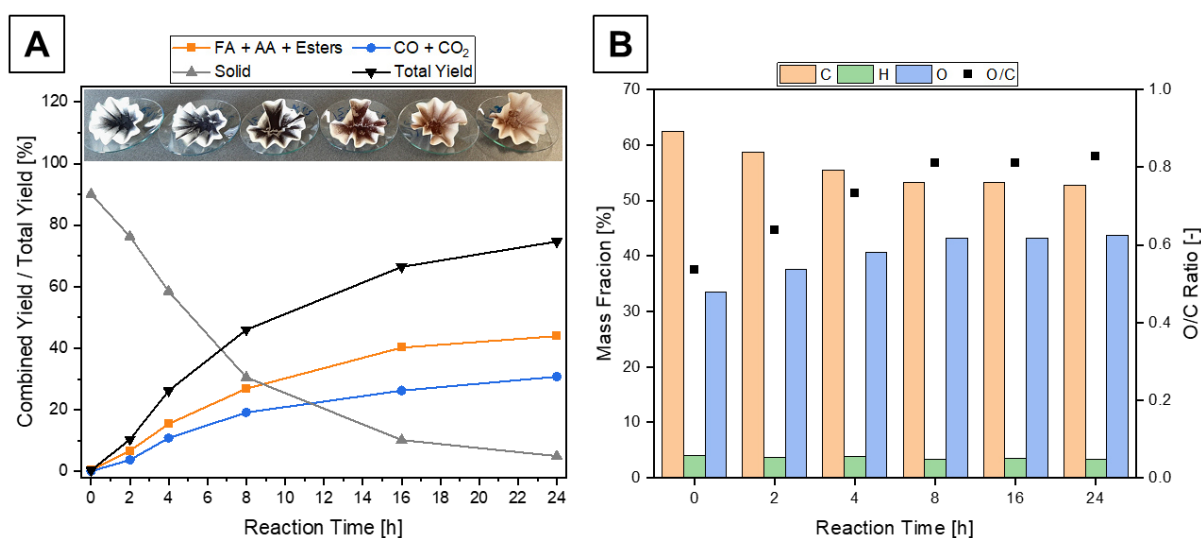


Figure 7.8: A) Reaction course and B) elemental analysis of the solid reaction residues in the SCO of glucose-based humin using HPA-2 at $90\text{ }^\circ\text{C}$ in the combined system.²¹⁴

The increase in intensity might be due to the oxidation of insoluble humin residue consisting of alkyl groups or furan rings that could not be cleaved. In this process, double bonds or ketones were formed. Consequently, double bonds conjugated to carbonyl compound would increase in number. Bands corresponding to C=O bonds in acids, aldehydes, and ketones at 1710 cm^{-1} behaved in the same manner.²¹⁴

The results of the developed reaction system for the selective catalytic conversion of humins are remarkable and promising, but in contrast to the results converting model substances, access to larger structural elements from the humin was not possible. The non-oxygen-functionalized parts of the humins are most likely responsible for this since they only enable the gradual degradation of the humins starting at oxygen-functionalized bonds and the induction of new functionalities. Investigating ways to better target the non-oxygen-functionalized bond types would be an interesting aspect for future studies. Here, the investigation of *Lewis* acidic catalysts would be a possibility with which tandem catalysis can be conducted or new POMs can be synthesized. An example are catalysts based on Al^{3+} . According to the *Hard-Soft-Acid-Base* concept, Al^{3+} is a strong *Lewis* acid. Using Al^{3+} as counterion for the heteropoly acid anion might lead to redox active, *Brønsted* and *Lewis* acidic catalyst enabling multilateral attack of humin structure. Thus, larger fragments of the humin structure might be accessible leading to products such as furfural, 5-HMF and finally MA or 2,5-furandicarboxylic acid (FDCA). Nevertheless, the reaction system developed in the present work exhibit remarkable results for the selective catalytic oxidation of humins to short-chain carboxylic acid.

Adaption of the developed nanofiltration process for the selective catalytic oxidation of humins and its application for the recycling of catalyst

The knowledge gained was used to establish an efficient downstream process for the novel selective catalytic oxidation of humins (*vide supra*, 6.4). In the first step, additional commercial NF membranes with different MWCOs were screened using a model solution based on the selective catalytic oxidation of humins. In Figure 7.9 the results of the screening experiments for the rejection of catalyst components (Figure 7.9 A) and oxidation products as well as additives (Figure 7.9 B) are presented. The acid stable membrane XN45 (*Mann+Hummel*) with a MWCO of 500 Da proved to be the most promising membrane. Rejections of over 99 % were achieved for both the larger molybdenum species and the smaller vanadium species.²¹⁴

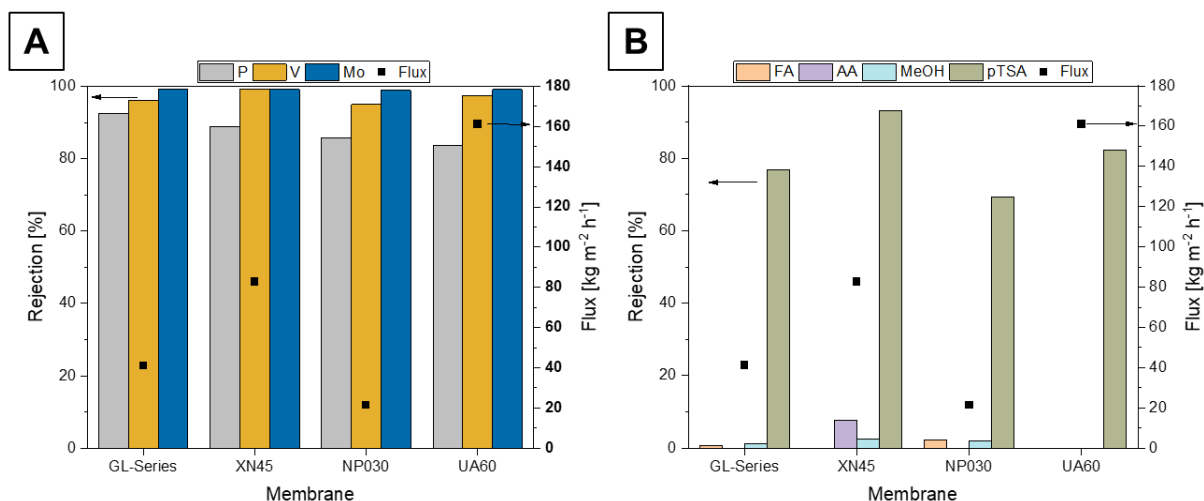


Figure 7.9: A) Rejection for catalyst components P, V, Mo and B) oxidation products as well as additives in membrane screening experiments using a model reaction solution based on the SCO of glucose-based humin using HPA-2 at 90 °C in the combined additive system, adapted from *Esser et al.*²¹⁴.

At the same time, the value-added products (carboxylic acids) were almost not rejected. In contrast, pTSA as additive was rejected with up to 90 %, which means that it can be recycled. The use of the XN45 membrane also had the advantage of allowing a high permeate flux (83 kg h⁻¹ m⁻²) increasing the efficiency of an industrial process. Duration tests have shown that the membrane can be used at least for 168 h on stream without any loss of performance.

In final recycling studies, NF was used for catalyst recycling and product purification for the novel selective catalytic oxidation of humins. Analogous to the results of the recycling study for the ECODS system, the catalytic performance declined as the number of cycles increased. By adding pTSA, the initial pH value was already at 1. Due to the formation and enrichment of the acidic reaction products in batch operation, the pH value in the reactor fell significantly below 1. Here too, the formation of less substituted catalyst isomers (H₄[PVMo₁₁O₄₀]) at the expense of the higher substituted and more active isomers (H₅[PV₂Mo₁₀O₄₀]) was observed using ⁵¹V-NMR. Since continuous operation was not possible, addition of pTSA was relinquished instead. This approach could be justified by the fact that the reaction system without addition of pTSA competes with a system adding pTSA in terms of the yield of the main product, FA. In addition, the initial pH value without the addition of pTSA was around 1.8 and therefore at a significantly more favorable value. The results of this approach are shown in Figure 7.10. Repeating the recycling study under the adapted conditions showed that the catalyst could be recycled.²¹⁴

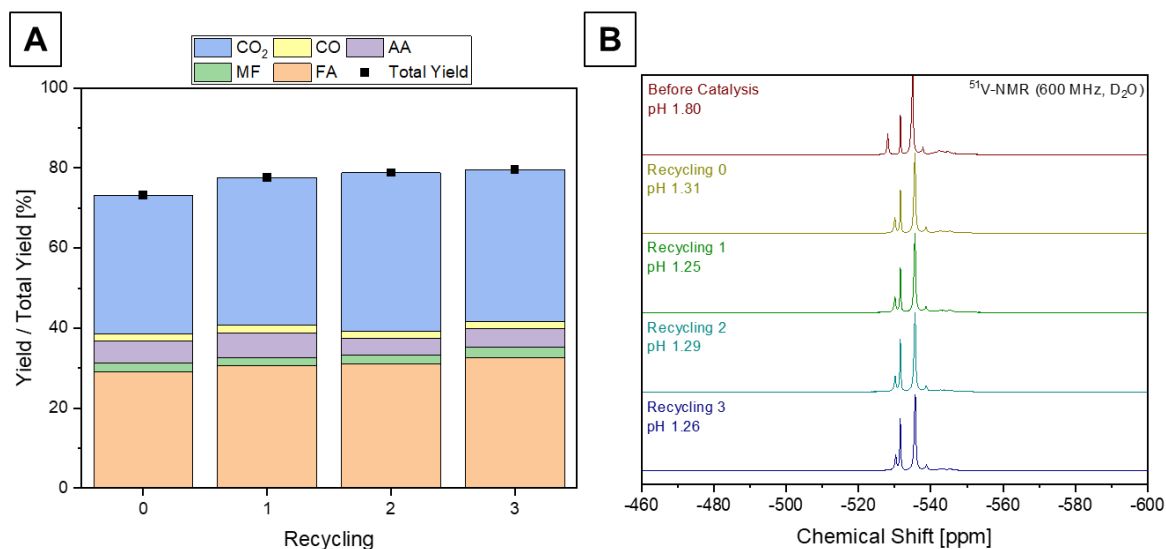


Figure 7.10: A) Comparison of yields of the repeated catalyst recycling study for SCO of glucose-based humin using HPA-2 without addition of pTSA and B) comparison of ⁵¹V-NMR spectra, adapted from Esser *et al.*²¹⁴.

The catalytic activity could be maintained in all cycles and the pH value was stabilized in an optimal range between pH 1.2 and 1.4 (Figure 7.10 A). According to ⁵¹V-NMR measurements, the higher substituted isomers and thus the structural integrity of the catalyst was preserved due to the stabilized pH value (Figure 7.10 B). In conclusion, it could be demonstrated that NF is a generic tool for the recycling of homogenous POM-catalyst and the purification of products. Using the unique properties and inherent advantages of NF combined with the special cell design efficient and sustainable downstream processing is feasible. Hence, the development of a successful downstream process for the selective catalytic oxidation of humins was achieved. Further developments might be the design of a continuous operating system using NF as a downstream process. Furthermore, future studies could investigate the transfer to other process valorizing biomass using homogenous POM-catalyst. A wider range of membranes with different MWCO would be helpful to enable adaptation to the different processes. In the studies of the present work, several commercially available membranes were screened with different MWCOs revealing a wide range of promising membranes. For example, the UA60 membrane (*Mann+Hummel*) with a MWCO of about 1000 Da also enabled a high rejection of POM-catalyst and a high permeate flux. This membrane could even enable the separation of larger products with higher economic value. The insights of the present work represent an important step towards an efficient overall process for humin valorization, but also towards the development of sustainable green processes in general.

8 References

- 1 Chen, S.; Wojcieszak, R.; Dumeignil, F.; Marceau, E.; Royer, S.: How Catalysts and Experimental Conditions Determine the Selective Hydroconversion of Furfural and 5-Hydroxymethylfurfural. *Chemical reviews*, **2018**, *118* (22), 11023–11117. DOI: 10.1021/acs.chemrev.8b00134.
- 2 Hou, Q.; Qi, X.; Zhen, M.; Qian, H.; Nie, Y.; Bai, C.; Zhang, S.; Bai, X.; Ju, M.: Biorefinery roadmap based on catalytic production and upgrading 5-hydroxymethylfurfural. *Green Chem.*, **2021**, *23* (1), 119–231. DOI: 10.1039/D0GC02770G.
- 3 Baskar, C.; Baskar, S.; Dhillon, R. S.: *Biomass Conversion*; Springer Berlin Heidelberg, **2012**. DOI: 10.1007/978-3-642-28418-2.
- 4 Olsen, K. H.: The clean development mechanism's contribution to sustainable development: a review of the literature. *Climatic Change*, **2007**, *84* (1), 59–73. DOI: 10.1007/s10584-007-9267-y.
- 5 Kaltschmitt, M.; Hartmann, H.; Hofbauer, H.: *Energie aus Biomasse*; Springer Berlin Heidelberg, **2016**. DOI: 10.1007/978-3-662-47438-9.
- 6 Behr, A.; Seidensticker, T.: *Chemistry of Renewables*; Springer Berlin Heidelberg, **2020**. DOI: 10.1007/978-3-662-61430-3.
- 7 Weissermel, K.; Arpe, H.-J.: *Industrial organic chemistry*, 4th completely rev. ed.; Wiley-VCH, **2003**. DOI: 10.1002/9783527619191.
- 8 Maerten, S. G.; Voß, D.; Liauw, M. A.; Albert, J.: Selective Catalytic Oxidation of Humins to Low-Chain Carboxylic Acids with Tailor-Made Polyoxometalate Catalysts. *ChemistrySelect*, **2017**, *2* (24), 7296–7302. DOI: 10.1002/slct.201701553.
- 9 Patil, S. K. R.; Heltzel, J.; Lund, C. R. F.: Comparison of Structural Features of Humins Formed Catalytically from Glucose, Fructose, and 5-Hydroxymethylfurfuraldehyde. *Energy Fuels*, **2012**, *26* (8), 5281–5293. DOI: 10.1021/ef3007454.
- 10 Climent, M. J.; Corma, A.; Iborra, S.: Conversion of biomass platform molecules into fuel additives and liquid hydrocarbon fuels. *Green Chem.*, **2014**, *16* (2), 516. DOI: 10.1039/c3gc41492b.

- 11 Hayes, D. J.; Fitzpatrick, S.; Hayes, M. H. B.; Ross, J. R. H.: The Biofine Process – Production of Levulinic Acid, Furfural, and Formic Acid from Lignocellulosic Feedstocks. In *Biorefineries-Industrial Processes and Products: Status Quo and Future Directions*, 1. Aufl.; Kamm, B., Gruber, P. R., Kamm, M., Eds.; Wiley-VCH Verlag GmbH, **2005**; pp 139–164. DOI: 10.1002/9783527619849.ch7.
- 12 Kapanji, K. K.; Haigh, K. F.; Görgens, J. F.: Techno-economics of lignocellulose biorefineries at South African sugar mills using the biofine process to co-produce levulinic acid, furfural and electricity along with gamma valeractone. *Biomass and Bioenergy*, **2021**, *146*, 106008. DOI: 10.1016/j.biombioe.2021.106008.
- 13 Mukherjee, A.; Dumont, M.-J.; Raghavan, V.: Review: Sustainable production of hydroxymethylfurfural and levulinic acid: Challenges and opportunities. *Biomass and Bioenergy*, **2015**, *72*, 143–183. DOI: 10.1016/j.biombioe.2014.11.007.
- 14 Zhai, S.; Jiang, S.; Liu, C.; Li, Z.; Yu, T.; Sun, L.; Ren, G.; Deng, W.: Liquid Sunshine: Formic Acid. *The journal of physical chemistry letters*, **2022**, *13* (36), 8586–8600. DOI: 10.1021/acs.jpcclett.2c02149.
- 15 Klankermayer, J.; Wesselbaum, S.; Beydoun, K.; Leitner, W.: Selektive katalytische Synthesen mit Kohlendioxid und Wasserstoff: Katalyse-Schach an der Nahtstelle zwischen Energie und Chemie. *Angewandte Chemie*, **2016**, *128* (26), 7416–7467. DOI: 10.1002/ange.201507458.
- 16 van Daele, K.; Arenas-Esteban, D.; Choukroun, D.; Hoekx, S.; Rossen, A.; Daems, N.; Pant, D.; Bals, S.; Breugelmans, T.: Enhanced Pomegranate-Structured SnO₂ Electrocatalysts for the Electrochemical CO₂ Reduction to Formate. *ChemElectroChem*, **2023**, *10* (6), 1. DOI: 10.1002/celec.202201024.
- 17 Tanaka, R.; Yamashita, M.; Nozaki, K.: Catalytic hydrogenation of carbon dioxide using Ir(III)-pincer complexes. *Journal of the American Chemical Society*, **2009**, *131* (40), 14168–14169. DOI: 10.1021/ja903574e.
- 18 Baerns, M.; Behr, A.; Brehm, A.; Gmehling, J.; Hinrichsen, K.-O.; Hofmann, H.; Palkovits, R.; Onken, U.; Renken, A.: *Technische Chemie*, Zweite, erweiterte Auflage; Wiley-VCH, **2013**. ISBN: 9783527674084.

- 19 Witzke, L.: *Alternative Kraftstoffe für die dieselmotorische Verbrennung aus kohlenhydrathaltigen Biomassen und basierend auf bio- und chemisch-katalytischen Herstellverfahren*; SpringerLink Bücher, Vol. 100; Springer, **2017**. DOI: 10.1007/978-3-658-17676-1.
- 20 Isikgor, F. H.; Becer, C. R.: Lignocellulosic biomass: a sustainable platform for the production of bio-based chemicals and polymers. *Polym. Chem.*, **2015**, *6* (25), 4497–4559. DOI: 10.1039/C5PY00263J.
- 21 Jensen, C. U.; Rodriguez Guerrero, J. K.; Karatzos, S.; Olofsson, G.; Iversen, S. B.: Fundamentals of Hydrofaction™: Renewable crude oil from woody biomass. *Biomass Conv. Bioref.*, **2017**, *7* (4), 495–509. DOI: 10.1007/s13399-017-0248-8.
- 22 Alonso, D. M.; Bond, J. Q.; Dumesic, J. A.: Catalytic conversion of biomass to biofuels. *Green Chem.*, **2010**, *12* (9), 1493. DOI: 10.1039/c004654j.
- 23 Anwar, Z.; Gulfracz, M.; Irshad, M.: Agro-industrial lignocellulosic biomass a key to unlock the future bio-energy: A brief review. *Journal of Radiation Research and Applied Sciences*, **2014**, *7* (2), 163–173. DOI: 10.1016/j.jrras.2014.02.003.
- 24 Phan, P. T.; Nguyen, B.-S.; Nguyen, T.-A.; Kumar, A.; Nguyen, V.-H.: Lignocellulose-derived monosugars: a review of biomass pre-treating techniques and post-methods to produce sustainable biohydrogen. *Biomass Conv. Bioref.*, **2023**, *13* (10), 8425–8439. DOI: 10.1007/s13399-020-01161-7.
- 25 Prasad, B. R.; Padhi, R. K.; Ghosh, G.: A review on key pretreatment approaches for lignocellulosic biomass to produce biofuel and value-added products. *Int. J. Environ. Sci. Technol.*, **2023**, *20* (6), 6929–6944. DOI: 10.1007/s13762-022-04252-2.
- 26 Dai, L.; Wang, Y.; Liu, Y.; He, C.; Ruan, R.; Yu, Z.; Jiang, L.; Zeng, Z.; Wu, Q.: A review on selective production of value-added chemicals via catalytic pyrolysis of lignocellulosic biomass. *The Science of the total environment*, **2020**, *749*, 142386. DOI: 10.1016/j.scitotenv.2020.142386.
- 27 Michels, J.: Die Nutzung von Biomasse zur Herstellung von Treibstoff und Chemikalien. In *Bioökonomie für Einsteiger*; Pietzsch, J., Ed.; Springer Berlin Heidelberg, **2017**; pp 77–104. DOI: 10.1007/978-3-662-53763-3_4.

- 28 Kohli, K.; Prajapati, R.; Sharma, B.: Bio-Based Chemicals from Renewable Biomass for Integrated Biorefineries. *Energies*, **2019**, *12* (2), 233. DOI: 10.3390/en12020233.
- 29 Voß, D.; Kahl, M.; Albert, J.: Continuous Production of Formic Acid from Biomass in a Three-Phase Liquid–Liquid–Gas Reaction Process. *ACS Sustainable Chem. Eng.*, **2020**, *8* (28), 10444–10453. DOI: 10.1021/acssuschemeng.0c02426.
- 30 Raabe, J.-C.; Poller, M.; Voß, D.; Albert, J.: H₈PV₅Mo₇O₄₀ (HPA-5) - a unique polyoxometalate for acid and RedOx catalysis: synthesis, characterization, and modern applications in green chemical processes. *ChemSusChem*, **2023**, e202300072. DOI: 10.1002/cssc.202300072.
- 31 Dincer, I.: Renewable energy and sustainable development: a crucial review. *Renewable and Sustainable Energy Reviews*, **2000**, *4* (2), 157–175. DOI: 10.1016/S1364-0321(99)00011-8.
- 32 Hayes, D. J.; Hayes, M. H. B.: The role that lignocellulosic feedstocks and various biorefining technologies can play in meeting Ireland's biofuel targets. *Biofuels, Bioprod. Bioref.*, **2009**, *3* (5), 500–520. DOI: 10.1002/bbb.171.
- 33 Cherubini, F.: The biorefinery concept: Using biomass instead of oil for producing energy and chemicals. *Energy Conversion and Management*, **2010**, *51* (7), 1412–1421. DOI: 10.1016/j.enconman.2010.01.015.
- 34 Kamm, B.; Gruber, P. R.; Kamm, M., Eds.: *Biorefineries-Industrial Processes and Products - Status Quo and Future Directions*, 1. Aufl.; Wiley-VCH Verlag GmbH, **2005**. DOI: 10.1002/9783527619849.
- 35 Albert, J.; Wasserscheid, P.: Expanding the scope of biogenic substrates for the selective production of formic acid from water-insoluble and wet waste biomass. *Green Chem.*, **2015**, *17* (12), 5164–5171. DOI: 10.1039/C5GC01474C.
- 36 Albert, J.; Wölfel, R.; Bösmann, A.; Wasserscheid, P.: Selective oxidation of complex, water-insoluble biomass to formic acid using additives as reaction accelerators. *Energy Environ. Sci.*, **2012**, *5* (7), 7956. DOI: 10.1039/c2ee21428h.
- 37 Kashparova, V. P.; Chernysheva, D. V.; Klushin, V. A.; Andreeva, V. E.; Kravchenko, O. A.; Smirnova, N. V.: Furan monomers and polymers from renewable plant biomass. *Russ. Chem. Rev.*, **2021**, *90* (6), 750–784. DOI: 10.1070/RCR5018.

- 38 Cheng, B.; Wang, X.; Lin, Q.; Zhang, X.; Meng, L.; Sun, R.-C.; Xin, F.; Ren, J.: New Understandings of the Relationship and Initial Formation Mechanism for Pseudolignin, Humins, and Acid-Induced Hydrothermal Carbon. *Journal of agricultural and food chemistry*, **2018**, *66* (45), 11981–11989. DOI: 10.1021/acs.jafc.8b04754.
- 39 Cheng, Z.; Everhart, J. L.; Tsilomelekis, G.; Nikolakis, V.; Saha, B.; Vlachos, D. G.: Structural analysis of humins formed in the Brønsted acid catalyzed dehydration of fructose. *Green Chem.*, **2018**, *20* (5), 997–1006. DOI: 10.1039/C7GC03054A.
- 40 Filiciotto, L.; Balu, A. M.; Romero, A. A.; Angelici, C.; van der Waal, J. C.; Luque, R.: Reconstruction of humins formation mechanism from decomposition products: A GC-MS study based on catalytic continuous flow depolymerizations. *Molecular Catalysis*, **2019**, *479*, 110564. DOI: 10.1016/j.mcat.2019.110564.
- 41 Girisuta, B.; Janssen, L. P. B. M.; Heeres, H. J.: Kinetic Study on the Acid-Catalyzed Hydrolysis of Cellulose to Levulinic Acid. *Ind. Eng. Chem. Res.*, **2007**, *46* (6), 1696–1708. DOI: 10.1021/ie061186z.
- 42 Hoang, T. M. C.; van Eck, E. R. H.; Bula, W. P.; Gardeniers, J. G. E.; Lefferts, L.; Seshan, K.: Humin based by-products from biomass processing as a potential carbonaceous source for synthesis gas production. *Green Chem.*, **2015**, *17* (2), 959–972. DOI: 10.1039/C4GC01324G.
- 43 Liu, S.; Zhu, Y.; Liao, Y.; Wang, H.; Liu, Q.; Ma, L.; Wang, C.: Advances in understanding the humins: Formation, prevention and application. *Applications in Energy and Combustion Science*, **2022**, *10*, 100062. DOI: 10.1016/j.jaecs.2022.100062.
- 44 Rasrendra, C. B.; Windt, M.; Wang, Y.; Adisasmito, S.; Makertihartha, I.G.B.N.; van Eck, E.R.H.; Meier, D.; Heeres, H. J.: Experimental studies on the pyrolysis of humins from the acid-catalysed dehydration of C6-sugars. *Journal of Analytical and Applied Pyrolysis*, **2013**, *104*, 299–307. DOI: 10.1016/j.jaap.2013.07.003.
- 45 Shen, H.; Shan, H.; Liu, L.: Evolution Process and Controlled Synthesis of Humins with 5-Hydroxymethylfurfural (HMF) as Model Molecule. *ChemSusChem*, **2020**, *13* (3), 513–519. DOI: 10.1002/cssc.201902799.

- 46 Shi, N.; Liu, Q.; Ju, R.; He, X.; Zhang, Y.; Tang, S.; Ma, L.: Condensation of α -Carbonyl Aldehydes Leads to the Formation of Solid Humins during the Hydrothermal Degradation of Carbohydrates. *ACS omega*, **2019**, *4* (4), 7330–7343. DOI: 10.1021/acsomega.9b00508.
- 47 Shi, N.; Liu, Q.; Liu, Y.; Chen, L.; Chen, N.; Peng, J.; Ma, L.: Formation of Soluble Furanic and Carbocyclic Oxy-Organics during the Hydrothermal Carbonization of Glucose. *Energy Fuels*, **2020**, *34* (2), 1830–1840. DOI: 10.1021/acs.energyfuels.9b03747.
- 48 Sumerskii, I. V.; Krutov, S. M.; Zarubin, M. Y.: Humin-like substances formed under the conditions of industrial hydrolysis of wood. *Russ J Appl Chem*, **2010**, *83* (2), 320–327. DOI: 10.1134/S1070427210020266.
- 49 Tsilomelekis, G.; Orella, M. J.; Lin, Z.; Cheng, Z.; Zheng, W.; Nikolakis, V.; Vlachos, D. G.: Molecular structure, morphology and growth mechanisms and rates of 5-hydroxymethyl furfural (HMF) derived humins. *Green Chem.*, **2016**, *18* (7), 1983–1993. DOI: 10.1039/C5GC01938A.
- 50 van Zandvoort, I.; Koers, E. J.; Weingarh, M.; Bruijninx, P. C. A.; Baldus, M.; Weckhuysen, B. M.: Structural characterization of ^{13}C -enriched humins and alkali-treated ^{13}C humins by 2D solid-state NMR. *Green Chem.*, **2015**, *17* (8), 4383–4392. DOI: 10.1039/C5GC00327J.
- 51 van Zandvoort, I.; van Eck, E. R. H.; Peinder, P. de; Heeres, H. J.; Bruijninx, P. C. A.; Weckhuysen, B. M.: Full, Reactive Solubilization of Humin Byproducts by Alkaline Treatment and Characterization of the Alkali-Treated Humins Formed. *ACS Sustainable Chem. Eng.*, **2015**, *3* (3), 533–543. DOI: 10.1021/sc500772w.
- 52 van Zandvoort, I.; Wang, Y.; Rasrendra, C. B.; van Eck, E. R. H.; Bruijninx, P. C. A.; Heeres, H. J.; Weckhuysen, B. M.: Formation, molecular structure, and morphology of humins in biomass conversion: influence of feedstock and processing conditions. *ChemSusChem*, **2013**, *6* (9), 1745–1758. DOI: 10.1002/cssc.201300332.
- 53 Maerten, S., Dissertation: *Humine: Bildung und Wertschöpfung*, RWTH Aachen, Aachen, **2018**.

- 54 Horvat, J.; Klaić, B.; Metelko, B.; Šunjić, V.: Mechanism of levulinic acid formation. *Tetrahedron Letters*, **1985**, *26* (17), 2111–2114. DOI: 10.1016/S0040-4039(00)94793-2.
- 55 Yang, G.; Pidko, E. A.; Hensen, E. J.M.: Mechanism of Brønsted acid-catalyzed conversion of carbohydrates. *Journal of Catalysis*, **2012**, *295*, 122–132. DOI: 10.1016/j.jcat.2012.08.002.
- 56 Chen, X.; Guigo, N.; Pizzi, A.; Sbirrazzuoli, N.; Li, B.; Fredon, E.; Gerardin, C.: Ambient Temperature Self-Blowing Tannin-Humins Biofoams. *Polymers*, **2020**, *12* (11). DOI: 10.3390/polym12112732.
- 57 Wölfel, R.; Taccardi, N.; Bösmann, A.; Wasserscheid, P.: Selective catalytic conversion of biobased carbohydrates to formic acid using molecular oxygen. *Green Chem.*, **2011**, *13* (10), 2759. DOI: 10.1039/c1gc15434f.
- 58 Hafeez, S.; Harkou, E.; Spanou, A.; Al-Salem, S. M.; Villa, A.; Dimitratos, N.; Manos, G.; Constantinou, A.: Review on recent progress and reactor set-ups for hydrogen production from formic acid decomposition. *Materials Today Chemistry*, **2022**, *26* (14), 101120. DOI: 10.1016/j.mtchem.2022.101120.
- 59 Fellay, C.; Dyson, P. J.; Laurency, G.: A viable hydrogen-storage system based on selective formic acid decomposition with a ruthenium catalyst. *Angewandte Chemie (International ed. in English)*, **2008**, *47* (21), 3966–3968. DOI: 10.1002/anie.200800320.
- 60 Bulushev, D. A.: Advanced Catalysis in Hydrogen Production from Formic Acid and Methanol. *Energies*, **2021**, *14* (20), 6810. DOI: 10.3390/en14206810.
- 61 Voß, D., Dissertation: *Selektive katalytische Umsetzung biogener Rohstoffe zu organischen Säuren unter Einsatz von Polyoxometallat-Katalysatoren*, Friedrich-Alexander-Universität Erlangen-Nürnberg, Erlangen, **2020**.
- 62 Sánchez, F.; Motta, D.; Dimitratos, N.: Catalytic decomposition of carbon-based liquid-phase chemical hydrogen storage materials for hydrogen generation under mild conditions. *Appl Petrochem Res*, **2016**, *6* (3), 269–277. DOI: 10.1007/s13203-016-0159-9.

- 63 Reichert, J.; Brunner, B.; Jess, A.; Wasserscheid, P.; Albert, J.: Biomass oxidation to formic acid in aqueous media using polyoxometalate catalysts – boosting FA selectivity by in-situ extraction. *Energy Environ. Sci.*, **2015**, *8* (10), 2985–2990. DOI: 10.1039/C5EE01706H.
- 64 Reichert, J.; Albert, J.: Detailed Kinetic Investigations on the Selective Oxidation of Biomass to Formic Acid (OxFA Process) Using Model Substrates and Real Biomass. *ACS Sustainable Chem. Eng.*, **2017**, *5* (8), 7383–7392. DOI: 10.1021/acssuschemeng.7b01723.
- 65 OxFA GmbH. [<https://www.oxfa.eu/oxfa/>] (accessed 2024-02-16).
- 66 Albert, J.; Lüders, D.; Bösmann, A.; Guldi, D. M.; Wasserscheid, P.: Spectroscopic and electrochemical characterization of heteropoly acids for their optimized application in selective biomass oxidation to formic acid. *Green Chem*, **2014**, *16* (1), 226–237. DOI: 10.1039/C3GC41320A.
- 67 Albert, J., Dissertation: *Chemische Wertschöpfung aus Biomasse mittels selektiver katalytischer Oxidation zu Ameisensäure (FA) - der Erlanger OxFA-Prozess*, Friedrich-Alexander-Universität Erlangen-Nürnberg, Erlangen, **2015**.
- 68 Piera, J.; Bäckvall, J.-E.: Catalytic oxidation of organic substrates by molecular oxygen and hydrogen peroxide by multistep electron transfer--a biomimetic approach. *Angewandte Chemie (International ed. in English)*, **2008**, *47* (19), 3506–3523. DOI: 10.1002/anie.200700604.
- 69 Maerten, S.; Kumpidet, C.; Voß, D.; Bukowski, A.; Wasserscheid, P.; Albert, J.: Glucose oxidation to formic acid and methyl formate in perfect selectivity. *Green Chem.*, **2020**, *22* (13), 4311–4320. DOI: 10.1039/D0GC01169J.
- 70 Wölfel, R., Dissertation: *Katalytische Erzeugung von Wasserstoff aus biogenen Rohstoffen*, Friedrich-Alexander-Universität Erlangen-Nürnberg, Erlangen, **2012**. [https://www.shaker.de/Online-Gesamtkatalog-Download/2024.06.02-18.40.04-94.134.109.143-rad2FAD9.tmp/3-8440-1104-8_INH.PDF] (accessed 2024-06-02).
- 71 Albert, J.; Mendt, M.; Mozer, M.; Voß, D.: Explaining the role of vanadium in homogeneous glucose transformation reactions using NMR and EPR spectroscopy. *Applied Catalysis A: General*, **2019**, *570*, 262–270. DOI: 10.1016/j.apcata.2018.10.030.

- 72 Kozhevnikov, I. V.: Catalysis by Heteropoly Acids and Multicomponent Polyoxometalates in Liquid-Phase Reactions. *Chemical reviews*, **1998**, *98* (1), 171–198. DOI: 10.1021/cr960400y.
- 73 OxFA GmbH: *Technology*. [<https://www.oxfa.eu/en/technology/>] (accessed 2024-05-19).
- 74 Jbach, H. W.; Kohler, F.; Schmidt, M.; Scholz, G.; Dirauf, M., US Patent US 10,689,320 B2: Method for Separating Formic Acid from a Reaction Mixture by means of Extraction, 16/318,673.
- 75 Zhong, J.; Pérez-Ramírez, J.; Yan, N.: Biomass valorisation over polyoxometalate-based catalysts. *Green Chem.*, **2021**, *23* (1), 18–36. DOI: 10.1039/D0GC03190A.
- 76 Lechner, M.; Güttel, R.; Streb, C.: Challenges in polyoxometalate-mediated aerobic oxidation catalysis: catalyst development meets reactor design. *Dalton transactions (Cambridge, England : 2003)*, **2016**, *45* (42), 16716–16726. DOI: 10.1039/c6dt03051c.
- 77 Deng, W.; Zhang, Q.; Wang, Y.: Polyoxometalates as efficient catalysts for transformations of cellulose into platform chemicals. *Dalton transactions (Cambridge, England : 2003)*, **2012**, *41* (33), 9817–9831. DOI: 10.1039/c2dt30637a. Published Online: Jun. 1, 2012.
- 78 Albert, J.; Mehler, J.; Tucher, J.; Kastner, K.; Streb, C.: One-step Synthesizable Lindqvist–isopolyoxometalates as Promising New Catalysts for Selective Conversion of Glucose as a Model Substrate for Lignocellulosic Biomass to Formic Acid. *ChemistrySelect*, **2016**, *1* (11), 2889–2894. DOI: 10.1002/slct.201600797.
- 79 Pope, M. T.; Müller, A.: Polyoxometalate Chemistry: An Old Field with New Dimensions in Several Disciplines. *Angewandte Chemie International Edition*, **1991** (30), 34–48. DOI: 10.1002/anie.199100341.
- 80 Gumerova, N. I.; Rompel, A.: Polyoxometalates in solution: speciation under spotlight. *Chemical Society reviews*, **2020**, *49* (21), 7568–7601. DOI: 10.1039/d0cs00392a.
- 81 Gumerova, N. I.; Rompel, A.: Synthesis, structures and applications of electron-rich polyoxometalates. *Nat Rev Chem*, **2018**, *2* (2). DOI: 10.1038/s41570-018-0112.

- 82 Ammam, M.: Polyoxometalates: formation, structures, principal properties, main deposition methods and application in sensing. *J. Mater. Chem. A*, **2013**, 1 (21), 6291. DOI: 10.1039/c3ta01663c.
- 83 Long, D.-L.; Tsunashima, R.; Cronin, L.: Polyoxometallate als Bausteine für funktionelle Nanosysteme. *Angewandte Chemie*, **2010**, 122 (10), 1780–1803. DOI: 10.1002/ange.200902483.
- 84 Rompel, A.: *Polyoxometallate: Eine vielfältige Stoffklasse*. [<https://analyticalscience.wiley.com/content/article-do/polyoxometallate-eine-vielf%C3%A4ltige-stoffklasse>] (accessed 2023-10-26).
- 85 Jerschke, H.-G.; Alsdorf, E.; Fichtner, H.; Hanke, W.; Jancke, K.; Öhlmann, G.: Über die thermischen Eigenschaften von Heteropolysäuren des Typs $H_{3+n} [PV_n Mo_{12-n}O_{40}] \cdot x H_2O$ ($n = 0, 1, 2, 3$) I. Thermogravimetrische, UV-VIS- und röntgenographische Untersuchungen. *Zeitschrift anorg allg chemie*, **1985**, 526 (7), 73–85. DOI: 10.1002/zaac.19855260711.
- 86 Hill, C.; Musaev, D. G.: *Complexity in Chemistry and Beyond: Interplay Theory and Experiment*; Springer Netherlands, **2012**. DOI: 10.1007/978-94-007-5548-2.
- 87 López, X.; Carbó, J. J.; Bo, C.; Poblet, J. M.: Structure, properties and reactivity of polyoxometalates: a theoretical perspective. *Chemical Society reviews*, **2012**, 41 (22), 7537–7571. DOI: 10.1039/c2cs35168d.
- 88 Cong, S.; Yan, L.; Song, P.; Guan, W.; Su, Z.; Sun, C.: Electronic properties and stabilities of methoxy-substituted Lindqvist polyoxometalates $[Nb_2W_4O_{19}CH_3]^{3-}$ by DFT. *Chin. Sci. Bull.*, **2012**, 57 (9), 976–982. DOI: 10.1007/s11434-011-4971-4.
- 89 Weinstock, I. A.; Schreiber, R. E.; Neumann, R.: Dioxygen in Polyoxometalate Mediated Reactions. *Chemical reviews*, **2018**, 118 (5), 2680–2717. DOI: 10.1021/acs.chemrev.7b00444.
- 90 Pope, M. T.; Scully, T. F.: Geometrical Isomerism Arising from Partial Substitution of Metal Atoms in Isopoly and Heteropoly Complexes. Possibilities for Keggin Structure. *Inorganic Chemistry*, **1975** (14), 953–954.
- 91 Cronin, L.: High Nuclearity Clusters: Iso and Heteropolyoxoanions and Relatives. In *Comprehensive Coordination Chemistry II*; McCleverty, J., Meyer, T. J., Eds.; Elsevier, **2003**; pp 1–56. DOI: 10.1016/b0-08-043748-6/06146-6.

- 92 Li, G.; Ding, Y.; Wang, J.; Wang, X.; Suo, J.: New Progress of Keggin and Wells-Dawson Type Polyoxometalates Catalyze Acid and Oxidative Reactions. *ChemInform*, **2007**, *38* (47). DOI: 10.1002/chin.200747211.
- 93 Albert, J.; Jess, A.; Kern, C.; Pöhlmann, F.; Glowienka, K.; Wasserscheid, P.: Formic Acid-Based Fischer–Tropsch Synthesis for Green Fuel Production from Wet Waste Biomass and Renewable Excess Energy. *ACS Sustainable Chem. Eng.*, **2016**, *4* (9), 5078–5086. DOI: 10.1021/acssuschemeng.6b01531.
- 94 Li, C.; Zhang, Y.; O'Halloran, K. P.; Zhang, J.; Ma, H.: Electrochemical behavior of vanadium-substituted Keggin-type polyoxometalates in aqueous solution. *J Appl Electrochem*, **2009**, *39* (3), 421–427. DOI: 10.1007/s10800-008-9687-z.
- 95 Ueda, T.: Electrochemistry of Polyoxometalates: From Fundamental Aspects to Applications. *ChemElectroChem*, **2018**, *5* (6), 823–838. DOI: 10.1002/celec.201701170.
- 96 Lu, X.; Geletii, Y. V.; Cheng, T.; Hill, C. L.: Role of Multiple Vanadium Centers on Redox Buffering and Rates of Polyvanadomolybdate-Cu(II)-Catalyzed Aerobic Oxidations. *Inorganic Chemistry*, **2023**, *62* (14), 5822–5830. DOI: 10.1021/acs.inorgchem.3c00469.
- 97 Simms, C.; Kondinski, A.; Parac-Vogt, T. N.: Metal-Addenda Substitution in Plenary Polyoxometalates and in Their Modular Transition Metal Analogues. *Eur J Inorg Chem*, **2020**, *2020* (27), 2559–2572. DOI: 10.1002/ejic.202000254.
- 98 Borrás-Almenar, J. J.; Coronado, E.; Müller, A.; Pope, M. T., Eds.: *Polyoxometalate molecular science - Proceedings of the NATO Advanced Study Institute on Polyoxometalate Molecular Science, Tenerife, Spain, 25 August - 4 September 2001*; NATO science series 2, Mathematics, physics and chemistry, Vol. 98; Kluwer Acad. Publ, **2003**.
- 99 Poller, M. J.; Bönisch, S.; Bertleff, B.; Raabe, J.-C.; Görling, A.; Albert, J.: Elucidating activating and deactivating effects of carboxylic acids on polyoxometalate-catalysed three-phase liquid–liquid–gas reactions. *Chemical Engineering Science*, **2022**, *264*, 118143. DOI: 10.1016/j.ces.2022.118143.
- 100 Kozhevnikov, I. V.; Matveev, K. I.: Homogeneous catalysts based on heteropoly acids (review). *Applied Catalysis*, **1983**, *5* (2), 135–150. DOI: 10.1016/0166-9834(83)80128-6.

- 101 Murmann, R. K.; Giese, K.: Mechanism of Oxygen-18 Exchange between Water and the Vanadium(V) Oxyanion: $V_{10}O_{28}^{6-}$. *Inorganic Chemistry*, **1978** (17), 1160–1166. DOI: 10.1021/ic50183a014.
- 102 Kozhevnikov, I. V.: $PMo_{12-n}V_nO_{(3+n)-40}$ heteropolyanions as catalysts for aerobic oxidation. *Journal of Molecular Catalysis A: Chemical*, **1997**, 117 (1-3), 151–158. DOI: 10.1016/S1381-1169(96)00295-6.
- 103 Kholdeeva, O. A.; Golovin, A. V.; Kozhevnikov, I. V.: Oxidation of 2,3,6-trimethylphenol in the presence of phosphomolybdovanadium heteropoly acids. *React Kinet Catal Lett*, **1992**, 46 (1), 107–113. DOI: 10.1007/BF02096685.
- 104 Kholdeeva, O. A.; Golovin, A. V.; Maksimovskaya, R. I.; Kozhevnikov, I. V.: Oxidation of 2,3,6-trimethylphenol in the presence of molybdovanadophosphoric heteropoly acids. *Journal of Molecular Catalysis*, **1992**, 75 (3), 235–244. DOI: 10.1016/0304-5102(92)80128-4.
- 105 He, Z.; Hou, Y.; Li, H.; Wang, Y.; Ren, S.; Wu, W.: Novel insights into CO_2 inhibition with additives in catalytic aerobic oxidation of biomass-derived carbohydrates to formic acid. *Renewable Energy*, **2023**, 211, 403–411. DOI: 10.1016/j.renene.2023.05.009.
- 106 Wesinger, S.; Mendt, M.; Albert, J.: Alcohol-Activated Vanadium-Containing Polyoxometalate Complexes in Homogeneous Glucose Oxidation Identified with ^{51}V -NMR and EPR Spectroscopy. *ChemCatChem*, **2021**, 13 (16), 3662–3670. DOI: 10.1002/cctc.202100632.
- 107 Hasenknopf, B.: Polyoxometalates: introduction to a class of inorganic compounds and their biomedical applications. *Frontiers in bioscience : a journal and virtual library*, **2005**, 10, 275–287. DOI: 10.2741/1527.
- 108 Guo, H.; Yin, G.: Catalytic Aerobic Oxidation of Renewable Furfural with Phosphomolybdic Acid Catalyst: an Alternative Route to Maleic Acid. *J. Phys. Chem. C*, **2011**, 115 (35), 17516–17522. DOI: 10.1021/jp2054712.
- 109 Gao, N.; Sun, H.; Dong, K.; Ren, J.; Duan, T.; Xu, C.; Qu, X.: Transition-metal-substituted polyoxometalate derivatives as functional anti-amyloid agents for Alzheimer's disease. *Nature communications*, **2014**, 5, 3422. DOI: 10.1038/ncomms4422.

- 110 Bukowski, A.; Schill, L.; Nielsen, D.; Mossin, S.; Riisager, A.; Albert, J.: NH₃-SCR of NO with novel active, supported vanadium-containing Keggin-type heteropolyacid catalysts. *React. Chem. Eng.*, **2020**, *5* (5), 935–948. DOI: 10.1039/d0re00033g.
- 111 Bertleff, B.; Claußnitzer, J.; Korth, W.; Wasserscheid, P.; Jess, A.; Albert, J.: Extraction Coupled Oxidative Desulfurization of Fuels to Sulfate and Water-Soluble Sulfur Compounds Using Polyoxometalate Catalysts and Molecular Oxygen. *ACS Sustainable Chem. Eng.*, **2017**, *5* (5), 4110–4118. DOI: 10.1021/acssuschemeng.7b00087.
- 112 Bertleff, B.; Goebel, R.; Claußnitzer, J.; Korth, W.; Skiborowski, M.; Wasserscheid, P.; Jess, A.; Albert, J.: Investigations on Catalyst Stability and Product Isolation in the Extractive Oxidative Desulfurization of Fuels Using Polyoxometalates and Molecular Oxygen. *ChemCatChem*, **2018**, *10* (20), 4602–4609. DOI: 10.1002/cctc.201801081.
- 113 Huber, M.; Poller, M. J.; Tochtermann, J.; Korth, W.; Jess, A.; Albert, J.: Revealing the nitrogen reaction pathway for the catalytic oxidative denitrification of fuels. *Chemical communications (Cambridge, England)*, **2023**, *59* (27), 4079–4082. DOI: 10.1039/d3cc00648d.
- 114 Huber, M.; Tochtermann, J.; Eller, S.; Korth, W.; Jess, A.; Albert, J.: Extractive Catalytic Oxidative Deoxygenation of Model Fuels Catalyzed by a Vanadium-Substituted Heteropolyacid and Molecular Oxygen. *Energy Fuels*, **2023**, *37* (6), 4544–4551. DOI: 10.1021/acs.energyfuels.2c04136.
- 115 Chen, R.; Xin, J.; Yan, D.; Dong, H.; Lu, X.; Zhang, S.: Highly Efficient Oxidation of 5-Hydroxymethylfurfural to 2,5-Furandicarboxylic Acid with Heteropoly Acids and Ionic Liquids. *ChemSusChem*, **2019**, *12* (12), 2715–2724. DOI: 10.1002/cssc.201900651.
- 116 Voß, D.; Dietrich, R.; Stuckart, M.; Albert, J.: Switchable Catalytic Polyoxometalate-Based Systems for Biomass Conversion to Carboxylic Acids. *ACS omega*, **2020**, *5* (30), 19082–19091. DOI: 10.1021/acsomega.0c02430.
- 117 Preuster, P.; Albert, J.: Biogenic Formic Acid as a Green Hydrogen Carrier. *Energy Technol.*, **2018**, *6* (3), 501–509. DOI: 10.1002/ente.201700572.

- 118 Latscha, H. P.; Kazmaier, U.; Klein, H.: *Organische Chemie*; Springer Berlin Heidelberg, **2016**. DOI: 10.1007/978-3-662-46180-8.
- 119 Mortimer, C. E.; Müller, U.: *Chemie - Das Basiswissen der Chemie ; 520 Formelbilder, 125 Tabellen*, 8., komplett überarb. und erw. Aufl.; Thieme, **2003**. ISBN: 3134843080.
- 120 Bruckner, R.; Harmata, M.: *Organic Mechanisms*; Springer Berlin Heidelberg, **2010**. DOI: 10.1007/978-3-642-03651-4.
- 121 Wollrab, A.: *Organische Chemie*; Springer Berlin Heidelberg, **2014**. DOI: 10.1007/978-3-642-45144-7.
- 122 Hietala, J.; Vuori, A.; Johnsson, P.; Pollari, I.; Reutemann, W.; Kieczka, H.: Formic Acid. In *Ullmann's Encyclopedia of Industrial Chemistry*; Wiley, **2003**; pp 1–22. DOI: 10.1002/14356007.a12_013.pub3.
- 123 Dutta, I.; Chatterjee, S.; Cheng, H.; Parsapur, R. K.; Liu, Z.; Li, Z.; Ye, E.; Kawanami, H.; Low, J. S. C.; Lai, Z.; Loh, X. J.; Huang, K.-W.: Formic Acid to Power towards Low-Carbon Economy. *Advanced Energy Materials*, **2022**, 12 (15), 223. DOI: 10.1002/aenm.202103799.
- 124 Liesivuori, J.: Formic Acid. In *Encyclopedia of Toxicology*; Elsevier, **2014**; pp 659–661. DOI: 10.1016/B978-0-12-386454-3.00989-1.
- 125 Thijs, B.; Rongé, J.; Martens, J. A.: Matching emerging formic acid synthesis processes with application requirements. *Green Chem.*, **2022**, 24 (6), 2287–2295. DOI: 10.1039/D1GC04791D.
- 126 Chao, J.; Hall, K. R.; Marsh, K. N.; Wilhoit, R. C.: Thermodynamic Properties of Key Organic Oxygen Compounds in the Carbon Range C1 to C4. Part 2. Ideal Gas Properties. *Journal of Physical and Chemical Reference Data*, **1986**, 15 (4), 1369–1436. DOI: 10.1063/1.555769.
- 127 Bulushev, D. A.; Ross, J. R. H.: Towards Sustainable Production of Formic Acid. *ChemSusChem*, **2018**, 11 (5), 821–836. DOI: 10.1002/cssc.201702075.
- 128 Sun, R.; Liao, Y.; Bai, S.-T.; Zheng, M.; Zhou, C.; Zhang, T.; Sels, B. F.: Heterogeneous catalysts for CO₂ hydrogenation to formic acid/formate: from nanoscale to single atom. *Energy Environ. Sci.*, **2021**, 14 (3), 1247–1285. DOI: 10.1039/D0EE03575K.

- 129 Schieweck, B. G.; Westhues, N. F.; Klankermayer, J.: A highly active non-precious transition metal catalyst for the hydrogenation of carbon dioxide to formates. *Chemical science*, **2019**, *10* (26), 6519–6523. DOI: 10.1039/c8sc05230a.
- 130 Xing, R.; Qi, W.; Huber, G. W.: Production of furfural and carboxylic acids from waste aqueous hemicellulose solutions from the pulp and paper and cellulosic ethanol industries. *Energy Environ. Sci.*, **2011**, *4* (6), 2193. DOI: 10.1039/c1ee01022k.
- 131 Sorokina, K. N.; Taran, O. P.; Medvedeva, T. B.; Samoylova, Y. V.; Piligaev, A. V.; Parmon, V. N.: Cellulose Biorefinery Based on a Combined Catalytic and Biotechnological Approach for Production of 5-HMF and Ethanol. *ChemSusChem*, **2017**, *10* (3), 562–574. DOI: 10.1002/cssc.201601244.
- 132 Sorokina, K. N.; Samoylova, Y. V.; Piligaev, A. V.; Sivakumar, U.; Parmon, V. N.: New methods for the one-pot processing of polysaccharide components (cellulose and hemicelluloses) of lignocellulose biomass into valuable products. Part 2: Biotechnological approaches to the conversion of polysaccharides and monosaccharides into the valuable industrial chemicals. *Catal. Ind.*, **2017**, *9* (3), 264–269. DOI: 10.1134/S2070050417030126.
- 133 Biermann, C. J.; McGinnis, G. D.; Ingram, L. L.; Kellogg, T. F.: Wet oxidation of radiolabeled D-glucose. *Carbohydrate research*, **1985**, *143*, 256–259. DOI: 10.1016/S0008-6215(00)90716-X.
- 134 McGinnis, G. D.; Prince, S. E.; Biermann, C. J.; Lowrimore, J. T.: Wet oxidation of model carbohydrate compounds. *Carbohydrate research*, **1984**, *128* (1), 51–60. DOI: 10.1016/0008-6215(84)85083-1.
- 135 McGinnis, G. D.; Wilson, W. W.; Prince, S. E.; Chen, C. C.: Conversion of biomass into chemicals with high-temperature wet oxidation. *Ind. Eng. Chem. Prod. Res. Dev.*, **1983**, *22* (4), 633–636. DOI: 10.1021/i300012a022.
- 136 Zhang, J.; Sun, M.; Han, Y.: Selective oxidation of glycerol to formic acid in highly concentrated aqueous solutions with molecular oxygen using V-substituted phosphomolybdic acids. *RSC Adv*, **2014**, *4* (67), 35463–35466. DOI: 10.1039/C4RA05424E.

- 137 Gromov, N. V.; Medvedeva, T. B.; Lukoyanov, I. A.; Panchenko, V. N.; Timofeeva, M. N.; Taran, O. P.; Parmon, V. N.: Formic Acid Production via One-Pot Hydrolysis-Oxidation of Starch over Quaternary Ammonium Salts of Vanadium-Containing Keggin-Type Heteropoly Acids. *Catalysts*, **2022**, *12* (10), 1252. DOI: 10.3390/catal12101252.
- 138 Gromov, N. V.; Taran, O. P.; Delidovich, I. V.; Pestunov, A. V.; Rodikova, Y. A.; Yatsenko, D. A.; Zhizhina, E. G.; Parmon, V. N.: Hydrolytic oxidation of cellulose to formic acid in the presence of Mo-V-P heteropoly acid catalysts. *Catalysis Today*, **2016**, *278* (3), 74–81. DOI: 10.1016/j.cattod.2016.03.030.
- 139 Grasemann, M.; Laurenczy, G.: Formic acid as a hydrogen source – recent developments and future trends. *Energy Environ. Sci.*, **2012**, *5* (8), 8171. DOI: 10.1039/c2ee21928j.
- 140 Cheung, H.; Tanke, R. S.; Torrence, G. P.: Acetic Acid. In *Ullmann's Encyclopedia of Industrial Chemistry*; Wiley-VCH Verlag GmbH & Co. KGaA, **2000**; 602.5000. DOI: 10.1002/14356007.a01_045.
- 141 Sarchami, T.; Batta, N.; Berruti, F.: Production and separation of acetic acid from pyrolysis oil of lignocellulosic biomass: a review. *Biofuels Bioprod Bioref*, **2021**, *15* (6), 1912–1937. DOI: 10.1002/bbb.2273.
- 142 Pal, P.; Nayak, J.: Acetic Acid Production and Purification: Critical Review Towards Process Intensification. *Separation & Purification Reviews*, **2017**, *46* (1), 44–61. DOI: 10.1080/15422119.2016.1185017.
- 143 Jourdin, L.; Grieger, T.; Monetti, J.; Flexer, V.; Freguia, S.; Lu, Y.; Chen, J.; Romano, M.; Wallace, G. G.; Keller, J.: High Acetic Acid Production Rate Obtained by Microbial Electrosynthesis from Carbon Dioxide. *Environmental science & technology*, **2015**, *49* (22), 13566–13574. DOI: 10.1021/acs.est.5b03821.
- 144 Snao, K.-i.; Uchida, H.; Wakabayashi, S.: A new process for acetic acid production by direct oxidation of ethylene. *Catalysis Surveys*, **1999** (3), 55–60. DOI: 10.1023/A:1019003230537.
- 145 Felthouse, T. R.; Burnett, J. C.; Horrell, B.; Mummey, M. J.; Kuo, Y.-J.: Maleic Anhydride, Maleic Acid, and Fumaric Acid. In *Kirk-Othmer Encyclopedia of Chemical Technology*; Wiley, **2001**; p 230. DOI: 10.1002/0471238961.1301120506051220.a01.pub2.

- 146 Lohbeck, K.; Haferkorn, H.; Fuhrmann, W.; Fedtke, N.: Maleic and Fumaric Acids. In *Ullmann's Encyclopedia of Industrial Chemistry*; Wiley, **2003**; p 143. DOI: 10.1002/14356007.a16_053.
- 147 Skinner, W. A.; Tieszen, D.: Production of Maleic Acid by Oxidizing Butenes. *Ind. Eng. Chem.*, **1961**, *53* (7), 557–558. DOI: 10.1021/ie50619a025.
- 148 Wojcieszak, R.; Santarelli, F.; Paul, S.; Dumeignil, F.; Cavani, F.; Gonçalves, R. V.: Recent developments in maleic acid synthesis from bio-based chemicals. *Sustain Chem Process*, **2015**, *3* (1). DOI: 10.1186/s40508-015-0034-5.
- 149 Fang, Z.; Smith, R. L.; Qi, X.: *Production of Platform Chemicals from Sustainable Resources*; Springer Singapore, **2017**. DOI: 10.1007/978-981-10-4172-3.
- 150 Hu, A.; Wang, X.; Wang, X.; Peng, Q.; Wang, H.: Study on the mechanism of furfural to maleic acid oxidized by hydrogen peroxide in formic acid solution. *J. Theor. Comput. Chem.*, **2020**, *19* (05), 2050019. DOI: 10.1142/S0219633620500194.
- 151 Murzin, D. Y.; Bertrand, E.; Tolvanen, P.; Devyatkov, S.; Rahkila, J.; Eränen, K.; Wärnå, J.; Salmi, T.: Heterogeneous Catalytic Oxidation of Furfural with Hydrogen Peroxide over Sulfated Zirconia. *Ind. Eng. Chem. Res.*, **2020**, *59* (30), 13516–13527. DOI: 10.1021/acs.iecr.0c02566.
- 152 Saleem, F.; Müller, P.; Eränen, K.; Wärnå, J.; Yu Murzin, D.; Salmi, T.: Kinetics and modelling of furfural oxidation with hydrogen peroxide over a fibrous heterogeneous catalyst: effect of reaction parameters on yields of succinic acid. *J. Chem. Technol. Biotechnol*, **2017**, *92* (9), 2206–2220. DOI: 10.1002/jctb.5248.
- 153 Lan, J.; Chen, Z.; Lin, J.; Yin, G.: Catalytic aerobic oxidation of renewable furfural to maleic anhydride and furanone derivatives with their mechanistic studies. *Green Chem*, **2014**, *16* (9), 4351–4358. DOI: 10.1039/C4GC00829D.
- 154 Shao, J.; Ni, Y.; Yan, L.: Oxidation of furfural to maleic acid and fumaric acid in deep eutectic solvent (DES) under vanadium pentoxide catalysis. *Journal of Bioresources and Bioproducts*, **2021**, *6* (1), 39–44. DOI: 10.1016/j.jobab.2021.02.005.

- 155 Rezaei, M.; Najafi Chermahini, A.; Dabbagh, H. A.; Saraji, M.; Shahvar, A.: Furfural oxidation to maleic acid with H₂O₂ by using vanadyl pyrophosphate and zirconium pyrophosphate supported on well-ordered mesoporous KIT-6. *Journal of Environmental Chemical Engineering*, **2019**, *7* (1), 102855. DOI: 10.1016/j.jece.2018.102855.
- 156 Da Silva, M. J.; Rodrigues, A. A.: Metal silicotungstate salts as catalysts in furfural oxidation reactions with hydrogen peroxide. *Molecular Catalysis*, **2020**, *493*, 111104. DOI: 10.1016/j.mcat.2020.111104.
- 157 Alonso-Fagúndez, N.; Agirrezabal-Telleria, I.; Arias, P. L.; Fierro, J. L. G.; Mariscal, R.; Granados, M. L.: Aqueous-phase catalytic oxidation of furfural with H₂O₂ : high yield of maleic acid by using titanium silicalite-1. *RSC Adv*, **2014**, *4* (98), 54960–54972. DOI: 10.1039/C4RA11563E.
- 158 Yu, Q.; Bai, R.; Wang, F.; Zhang, Q.; Sun, Y.; Zhang, Y.; Qin, L.; Wang, Z.; Yuan, Z.: A sustainable system for maleic acid synthesis from biomass-derived sugar. *J Chem Technol Biotechnol*, **2020**, *95* (3), 751–757. DOI: 10.1002/jctb.6260.
- 159 Kang, S.; Tang, P.; Fu, J.; Zhou, H.; Wu, X.; Liao, W.; Liu, S.: Sustainable production of organic acids via ozonation of biomass derived 5-hydroxymethylfurfural and furfural. *Sustainable Chemistry and Pharmacy*, **2021**, *20*, 100383. DOI: 10.1016/j.scp.2021.100383.
- 160 Yang, T.; Li, W.; Ogunbiyi, A. T.: The effect of Br⁻ and alkali in enhancing the oxidation of furfural to maleic acid with hydrogen peroxide. *Molecular Catalysis*, **2021**, *504*, 111488. DOI: 10.1016/j.mcat.2021.111488.
- 161 Huang, Y.; Wu, C.; Yuan, Wenwen, Xia, Yongmei; Liu, X.; Yang, H.; Wang, H.: Catalytic Aerobic Oxidation of Biomass-based Furfural into Maleic Acid in Aqueous Phase with metalloporphyrin Catalysts. *Journal of the chinese chemical society*, **2017**, *17* (64), 786–794. DOI: 10.1002/jccs.201700004.
- 162 Palai, Y. N.; Shrotri, A.; Fukuoka, A.: Selective Oxidation of Furfural to Succinic Acid over Lewis Acidic Sn-Beta. *ACS Catal.*, **2022**, *12* (6), 3534–3542. DOI: 10.1021/acscatal.1c05348.
- 163 Kövilein, A.; Kubisch, C.; Cai, L.; Ochsenreither, K.: Malic acid production from renewables: a review. *J of Chemical Tech & Biotech*, **2020**, *95* (3), 513–526. DOI: 10.1002/jctb.6269.

- 164 Román, A. M.; Hasse, J. C.; Medlin, J. W.; Holewinski, A.: Elucidating Acidic Electro-Oxidation Pathways of Furfural on Platinum. *ACS Catal.*, **2019**, *9* (11), 10305–10316. DOI: 10.1021/acscatal.9b02656.
- 165 Gong, L.; Agrawal, N.; Roman, A.; Holewinski, A.; Janik, M. J.: Density functional theory study of furfural electrochemical oxidation on the Pt (1 1 1) surface. *Journal of Catalysis*, **2019**, *373*, 322–335. DOI: 10.1016/j.jcat.2019.04.012.
- 166 Shanmugam Thiyagarajan; David Franciolus; Roel J. M. Bisselink; Tom A. Ewing; Carmen G. Boeriu; and Jacco van Haveren: *Selective Production of Maleic Acid from Furfural via a Cascade Approach Combining Photochemistry and Electro- or Biochemistry*. DOI: 10.1021/acssuschemeng.0c02833.s001.
- 167 Klingler, F. D.; Ebertz, W.: Oxocarboxylic Acids. In *Ullmann's Encyclopedia of Industrial Chemistry*; Wiley, **2003**; p 167. DOI: 10.1002/14356007.a18_313.
- 168 Rackemann, D., Dissertation: *Production of Levulinic Acid and Other Chemicals from Sugarcane Fibre*, Queensland University of Technology, Queensland, **2014**.
- 169 Pyo, S.-H.; Glaser, S. J.; Rehnberg, N.; Hatti-Kaul, R.: Clean Production of Levulinic Acid from Fructose and Glucose in Salt Water by Heterogeneous Catalytic Dehydration. *ACS omega*, **2020**, *5* (24), 14275–14282. DOI: 10.1021/acsomega.9b04406.
- 170 Saeman, J. F.: Kinetics of Wood Saccharification - Hydrolysis of Cellulose and Decomposition of Sugars in Dilute Acid at High Temperature. *Ind. Eng. Chem.*, **1945**, *37* (1), 43–52. DOI: 10.1021/ie50421a009.
- 171 Chang, C.; Ma, X.; Cen, P.: Kinetics of Levulinic Acid Formation from Glucose Decomposition at High Temperature. *Chinese Journal of Chemical Engineering*, **2006**, *14* (5), 708–712. DOI: 10.1016/S1004-9541(06)60139-0.
- 172 Cha, J.Y.; Hanna, M.A.: Levulinic acid production based on extrusion and pressurized batch reaction. *Industrial Crops and Products*, **2002**, *16* (2), 109–118. DOI: 10.1016/S0926-6690(02)00033-X.
- 173 Farone, W. A.; Cuzens, J. E., United States Patent US006054611: Method for the production of levulinic acid and its derivatives, 09/076,941, **1998**.

- 174 Yan, L.; Yang, N.; Pang, H.; Liao, B.: Production of Levulinic Acid from Bagasse and Paddy Straw by Liquefaction in the Presence of Hydrochloride Acid. *Clean Soil Air Water*, **2008**, *36* (2), 158–163. DOI: 10.1002/clen.200700100.
- 175 Chang, C.; Cen, P.; Ma, X.: Levulinic acid production from wheat straw. *Bioresource technology*, **2007**, *98* (7), 1448–1453. DOI: 10.1016/j.biortech.2006.03.031.
- 176 Werpy, T.; Petersen, G.: *Top value added chemicals from biomass volume I - Results of screening for potential candidates from sugars and synthesis gas*, **2004**. DOI: 10.2172/15008859.
- 177 Bozell, J. J.; Moens, L.; Elliott, D.C.; Wang, Y.; Neuenschwander, G.G.; Fitzpatrick, S.W.; Bilski, R.J.; Jarnefeld, J.L.: Production of levulinic acid and use as a platform chemical for derived products. *Resources, Conservation and Recycling*, **2000**, *28* (3-4), 227–239. DOI: 10.1016/S0921-3449(99)00047-6.
- 178 Girisuta, B.; Janssen, L.P.B.M.; Heeres, H. J.: Green Chemicals. *Chemical Engineering Research and Design*, **2006**, *84* (5), 339–349. DOI: 10.1205/cherd05038.
- 179 Bozell, J. J.; Petersen, G. R.: Technology development for the production of biobased products from biorefinery carbohydrates—the US Department of Energy’s “Top 10” revisited. *Green Chem.*, **2010**, *12* (4), 539. DOI: 10.1039/b922014c.
- 180 Mukherjee, A.; Dumont, M.-J.; Raghavan, V.: Review: Sustainable production of hydroxymethylfurfural and levulinic acid: Challenges and opportunities. *Biomass and Bioenergy*, **2015**, *72*, 143–183. DOI: 10.1016/j.biombioe.2014.11.007.
- 181 Baker, R. W.: *Membrane technology and applications*, 3rd ed.; John Wiley & Sons, **2012**. DOI: 10.1002/9781118359686.
- 182 Drioli, E.; Giorno, L., Eds.: *Encyclopedia of Membranes*; Springer Berlin Heidelberg, **2015**. DOI: 10.1007/978-3-642-40872-4.
- 183 Figoli, A.; Criscuoli, A., Eds.: *Sustainable Membrane Technology for Water and Wastewater Treatment*; Green Chemistry and Sustainable Technology; Springer Singapore, **2017**. DOI: 10.1007/978-981-10-5623-9.

- 184 Merlin, T.; Rautenbach, R.: *Membranverfahren - Grundlagen der Modul- und Anlagenauslegung*, 3rd ed.; Springer, **2007**. ISBN: 3-540-00071-2.
- 185 Sikdar, S. K.; Criscuoli, A.: Sustainability and How Membrane Technologies in Water Treatment Can Be a Contributor. In *Sustainable Membrane Technology for Water and Wastewater Treatment*; Figoli, A., Criscuoli, A., Eds.; Green Chemistry and Sustainable Technology; Springer Singapore, **2017**; pp 1–21. DOI: 10.1007/978-981-10-5623-9_1.
- 186 Thiess, H., Dissertation: *Modellierung von Membrantrennverfahren am Beispiel der Ultrafiltration in der biotechnologischen und der Pervaporation in der chemischen Verfahrenstechnik*, Technische Universität Clausthal; Shaker Verlag.
- 187 Cen, Y.; Meckl, K.; Lichtenthaler, R. N.: Nichtporöse Membranen und ihre Anwendung. *Chemie Ingenieur Technik*, **1993**, 65 (8), 901–913. DOI: 10.1002/cite.330650803.
- 188 Hoek, E. M. V., Ed.: *Encyclopedia of membrane science and technology*; Wiley Online Library; Wiley, **2013**.
- 189 Ohlrogge, K.: *Membranen - Grundlagen, Verfahren und Industrielle Anwendungen*, 1st ed.; John Wiley & Sons Incorporated, **2006**. ISBN: 978-3-527-30979-5.
- 190 Rundquist, E. M.; Pink, C. J.; Livingston, A. G.: Organic solvent nanofiltration: a potential alternative to distillation for solvent recovery from crystallisation mother liquors. *Green Chem.*, **2012**, 14 (8), 2197. DOI: 10.1039/c2gc35216h.
- 191 Bøddeker, K. W.: *Liquid Separations with Membranes - An introduction to barrier interference*; SpringerLink Bücher; Springer Berlin Heidelberg, **2008**. DOI: 10.1007/978-3-540-47453-1.
- 192 Cardew, P. T.: *Membrane processes - A technology guide*; Royal Society of Chemistry, **1999**. DOI: 10.1039/9781847551344.
- 193 Assayie, A. A.; Gebreyohannes, A. Y.; Giorno, L.: Municipal Wastewater Treatment by Membrane Bioreactors. In *Sustainable Membrane Technology for Water and Wastewater Treatment*; Figoli, A., Criscuoli, A., Eds.; Green Chemistry and Sustainable Technology; Springer Singapore, **2017**; pp 265–294. DOI: 10.1007/978-981-10-5623-9_10.

- 194 Wang, L.; Violet, C.; DuChanois, R. M.; Elimelech, M.: Derivation of the Theoretical Minimum Energy of Separation of Desalination Processes. *J. Chem. Educ.*, **2020**, *97* (12), 4361–4369. DOI: 10.1021/acs.jchemed.0c01194.
- 195 Mulder, M.: *Basic Principles of Membrane Technology*; Springer Netherlands, **1991**. DOI: 10.1007/978-94-017-0835-7.
- 196 Baker, R. W.; Wijmans, J. G.; Athayde, A. L.; Daniels, R.; Ly, J. H.; Le, M.: The effect of concentration polarization on the separation of volatile organic compounds from water by pervaporation. *Journal of Membrane Science*, **1997**, *137* (1-2), 159–172. DOI: 10.1016/S0376-7388(97)00189-0.
- 197 Uragami, T.: *Science and technology of separation membranes*; Wiley, **2017**. DOI: 10.1002/9781118932551.
- 198 Wijmans, J. G.; Baker, R. W.: The solution-diffusion model: a review. *Journal of Membrane Science*, **1995**, *1995* (107), 1–21.
- 199 Wijmans, J. G.; Baker, R. W.: The Solution–Diffusion Model: A Unified Approach to Membrane Permeation. In *Materials Science of Membranes for Gas and Vapor Separation*; Yampolskii, Y., Pinnau, I., Freeman, B., Eds.; Wiley, **2006**; pp 159–189. DOI: 10.1002/047002903X.ch5.
- 200 Schäfer, A.; Fane, A. G., Eds.: *Nanofiltration - Principles, applications, and new materials*, 2 edition; Wiley, **2020**.
- 201 Mohammad, A. W.; Teow, Y. H.; Ang, W. L.; Chung, Y. T.; Oatley-Radcliffe, D. L.; Hilal, N.: Nanofiltration membranes review: Recent advances and future prospects. *Desalination*, **2015**, *356*, 226–254. DOI: 10.1016/j.desal.2014.10.043.
- 202 Yu, D.; Xiao, X.; Shokoohi, C.; Wang, Y.; Sun, L.; Juan, Z.; Kipper, M. J.; Tang, J.; Huang, L.; Han, G. S.; Jung, H. S.; Chen, J.: Recent Advances in Stimuli-Responsive Smart Membranes for Nanofiltration. *Adv Funct Materials*, **2023**, *33* (9). DOI: 10.1002/adfm.202211983.
- 203 Suhalim, N. S.; Kasim, N.; Mahmoudi, E.; Shamsudin, I. J.; Mohammad, A. W.; Mohamed Zuki, F.; Jamari, N. L.-A.: Rejection Mechanism of Ionic Solute Removal by Nanofiltration Membranes: An Overview. *Nanomaterials (Basel, Switzerland)*, **2022**, *12* (3). DOI: 10.3390/nano12030437.

- 204 Werhan, H.; Farshori, A.; Rudolf von Rohr, P.: Separation of lignin oxidation products by organic solvent nanofiltration. *Journal of Membrane Science*, **2012**, 423-424, 404–412. DOI: 10.1016/j.memsci.2012.08.037.
- 205 Esser, T.; Huber, M.; Voß, D.; Albert, J.: Development of an efficient downstream process for product separation and catalyst recycling of a homogeneous polyoxometalate catalyst by means of nanofiltration membranes and design of experiments. *Chemical Engineering Research and Design*, **2022** (185), 37–50. DOI: 10.1016/j.cherd.2022.06.045.
- 206 Schirg, P., European Patent EP2078556A2: Verfahren und Vorrichtung zur Filtration von Produktgemischen, 09000370.8, **2009**.
- 207 Hackl, T.; Wontorra, C.: *NMR Service - Equipment*. [<https://www.chemie.uni-hamburg.de/service/wissenschaftlicher-service/nmr/equipment.html>] (accessed 2023-11-12).
- 208 Eifler, D.: *ZEA - Equipment*. [<https://www.chemie.uni-hamburg.de/service/wissenschaftlicher-service/elementanalytik/equipment.html>] (accessed 2023-11-12).
- 209 Burger, P.: *AG Burger - Equipment*. [<https://www.chemie.uni-hamburg.de/institute/ac/arbeitsgruppen/burger/equipment.html>] (accessed 2023-11-16).
- 210 Hoffmann, F.: *X-ray structure analysis Service - Equipment*] (accessed 2023-11-16).
- 211 Ruhmlieb, C.: *Electron Microscopy Service - Equipment*. [<https://www.chemie.uni-hamburg.de/service/wissenschaftlicher-service/mikroskopie/equipment/quanta.html>] (accessed 2023-11-16).
- 212 Esser, T.; Wassenberg, A.; Raabe, J.-C.; Voß, D.; Albert, J.: Catalytic Valorization of Humins by Selective Oxidation Using Transition-Metal-Substituted Keggin-Type Polyoxometalate Catalysts. *ACS Sustainable Chem. Eng.*, **2024** (12), 543–560. DOI: 10.1021/acssuschemeng.3c06539.
- 213 Esser, T.; Wassenberg, A.; Voß, D.; Albert, J.: Selective catalytic oxidation of humins to carboxylic acids using the H₄[PVMo₁₁O₄₀] Keggin-type polyoxometalate enhanced by alcohol doping and solubilizer. *React. Chem. Eng.*, **2024**, 86 (7), 357. DOI: 10.1039/d3re00672g.

- 214 Esser, T.; Wassenberg, A.; Voß, D.; Albert, J.: Novel insights into the recovery and recyclability of homogeneous polyoxometalate catalysts applying an efficient nanofiltration process for the selective catalytic oxidation of humins. *Chemical Engineering Research and Design*, **2024** (209), 311–322. DOI: 10.1016/j.cherd.2024.08.007.
- 215 Raabe, J.-C.; Esser, T.; Jameel, F.; Stein, M.; Albert, J.; Poller, M. J.: Study on the incorporation of various elements into the Keggin lacunary-type phosphomolybdate $[\text{PMo}_9\text{O}_{34}]^{9-}$ and subsequent purification of the polyoxometalates by nanofiltration. *Inorg. Chem. Front.*, **2023**, 10 (16), 4854–4868. DOI: 10.1039/D3QI00937H.
- 216 Wassenberg, A.; Esser, T.; Poller, M. J.; Albert, J.: Investigation of the Formation, Characterization, and Oxidative Catalytic Valorization of Humins. *Materials (Basel, Switzerland)*, **2023**, 16 (7), 2864-2682. DOI: 10.3390/ma16072864. Published Online: Apr. 4, 2023.
- 217 Institut für Arbeitsschutz der Deutschen Gesetzlichen Unfallversicherung: *GESTIS-Stoffdatenbank: Gefahrstoffinformationssystem der Deutschen Gesetzlichen Unfallversicherung*. [<https://gestis.dguv.de/search>] (accessed 2023-11-14).

9 Appendix

9.1 List of hazardous substances

Table 9.1: List of hazardous substances (part 1) used according to globally harmonized system of classification and labelling of chemicals (GHS).²¹⁷







Substance	Purity	GHS-Symbol	Hazard & Precautionary Statement
Acetic acid	100.0 %		H226/H314 P280/P301+P330+P331 P303+P361+P353/P305+P351+P338
Amberlyst-15	100.0 %		H318 P280/P305+P351+P338/P310
Benzofuran	99.0 %		H226/H351 P210/P280/P370+P378
Chloroform	99.0 %		H302/H331/H315/H319/H351/H361d/H336/H372 P201/P273/P301+P312+P330/P302+P352 P304+P340+P3011/P308+P313
Cobalt(II) acetate	99.9 %		H302/H319/H334/H317/H341/H350i/H360F/H410 P210/P273/P280/P301+P312+P330/P302+P352 P308+P313
Dimethoxy-methane	98.0 %		H225 P210/P233/P240/P241/P242/P243
Ethanol	99.8 %		H225/H319 P210/P240/P305+P351+P338/P403+P233
Ethyl acetate	99.8 %		H225/H319/H336 P210/P233/P240/P305+P351+P338/P403+P235
Ethyl bromo-acetate	98.0 %		H226/H300+H310+H330 P210/P233/P240/P303+P361+P353 P304+P330+P310
2-Ethyl-furoate	99.0 %		H225/H302+H332/H319/H335 P210/P240/ P305+P351+P338/P403+P233
Formic acid	98.0 %		H226/H302/H331/H314 P210/P280/P303+P361+P353 P305+P351+P338
Fumaric acid	99.0 %		H319 P264/P280/P305+P351+P338/P337+P313
2(5H)-Furanone	95.0 %	-	-
Furfural	98.0 %		H226/H301/H312/H330/H315/H319/H335/H351 P210/P280(P302+P352/P304+P340 P305+P351+P338/P310

Table 9.2: List of hazardous substances (part 2) used according to globally harmonized system of classification and labelling of chemicals (GHS).²¹⁷

Substance	Purity	GHS-Symbol	Hazard & Precautionary Statement
Furfuryl alcohol	98.0 %		H301+H311/H315/H319/H330/H335/H351/H373 P280/P302+P352/P304+P340/P310/P362 P305+P351+P338/P403+P233 H314
Furoic acid	98.0 %		P260/P280/P301+P330+P331/P303+P361+P353 P304+P340+P310/P305+P351+P338
5-HMF	97.0 %		H315/H319 P280/P302+P352/P305+P351+P338
Hydrochloric acid	37.0 %		H290/H314/H335 P280/P303+P361+P353/P305+P351+P338+P310
Hydrogen	99.9 %		H220/H280 P210/P377/P381/P403
5-Hydroxy-furan-2(5H)-one	96.0 %		H302/H315/H319/H335 P261/P264/P270/P271/P280/P301+P3012 P302+P352/P304+P340/ P305+P351+P338
Levulinic Acid	98.0 %		H302/H317/H318 P261/P264/P280/P301+P312/P301+P312 P302+P352/P305+P351+P338
Maleic Acid	99.0 %		H302+H312/H314/H317/H335 P260/P280/P301+P312+P330/P303+P361+P353 P305+P351+P338+P310
Manganese(II) acetate	98.0 %		H315/H319 P280/ P302+P352/P305+P351+P338/P362
Methanol	99.8 %		H225/H301+H311+H331/H370 P210/P233/P280/P301+P310/P303+P361+P353 P304+P340+P311
4-Methoxy-phenol	99.0 %		H302/H317/H319/H412 P261/P273/P280/P301+P312/P302+P352 P305+P351+P338
2-Methyl-furan	99.0 %		H225/H301/H330 P210/P233/P240/P304+P340/P308+P310 P403+P235
Molybdenum(II) oxide	99.9 %		H319/H335/H351 P201/P202/P261/P264/P305+P351+P338/ P308+P313
Oxygen	99.9 %		H270/H280 P220/P244/P370+P376/P403
Sodium	100.0 %		H260/H314 P223/P231+P232/P280/P305+P351+P338 P370+P378/P422
Para-toluene sulfonic acid	98.0 %		H315/H319/H335 P302+P352/ P305+P351+P338

Table 9.3: List of hazardous substances (part 3) used according to globally harmonized system of classification and labelling of chemicals (GHS).²¹⁷

Substance	Purity	GHS-Symbol	Hazard & Precautionary Statement
Succinic acid	99.0 %		H318 P280/P305+P351+P338/P313
Sulfuric acid	95.0 %		H290/H314 P280+P301+P330+P331/P303+P361+P353 P305+P351+P338+P310
Tetrahydrofuran	99.5 %		H225/H302/H319/H335/H336/H351 P210/P280/ P301+P312+P330 P305+P351+P338/ P370+P378/ P403+P235
Tri-n-butylphosphine	98.0 %		H226/H250/H302+H313/H314/H411 P301+P330+P331/P305+P351+P338 P310/P231+P232/P303+P361+P353/P210
Vanadium(V) oxide	99.95 %		H301/H330/H335/H341/H350/H361fd/H362/H372/ H411

9.2 List of Figures

Figure 4.1: Composition and structure of lignocellulosic biomass. ²¹	14
Figure 4.2: Simplified process flow diagram for the Biofine process, according to Kapanji et al. ¹²	19
Figure 4.3: Qualitative energy diagram of the OxFA process, according to Albert ⁶⁷ . ²⁴	
Figure 4.4: Schematic catalytic cycle of the OxFA process, adapted from literature ^{61,67}	25
Figure 4.5: Schematic representation of the concept of in-situ extraction and its potential implementation in continuous OxFA process, adapted from Voß ⁶¹	27
Figure 4.6: Simplified process flow diagram of OxFA process (mini plant). ²⁹	28
Figure 4.7: Polyhedral representation of different polyoxometalate structures. Octahedra of metal oxide units are blue, tetrahedra of heteroatoms are yellow and octahedrally coordinated heteroatoms are magenta. ⁸⁴	30
Figure 4.8: Dependency of vanadium species on pH value in predominance diagram. ¹⁰¹	34
Figure 4.9: Important carboxylic acid derivatives and their functional groups, according to literature ^{118,119}	36
Figure 4.10: Structural formula of maleic acid, its anhydride, and its trans-isomer fumaric acid.	42
Figure 4.11: Structural formula of levulinic acid.	45
Figure 4.12: Schematic illustration of a membrane module naming the essential components, according to Merlin et al. ¹⁸⁴	48
Figure 4.13: Possible flows in membrane modules for dead-end filtration (left) and cross-flow filtration (right), adapted from literature ^{184,186}	52
Figure 4.14: Idealized model for molecular transport across membranes, adapted from Merlin et al. ¹⁸⁴	53
Figure 4.15: Classification of liquid phase membrane processes according to their pore size and possible areas of application, adapted from Schäfer et al. ²⁰⁰	54
Figure 5.1: Process development matrix for the selective catalytic oxidation of humins.	57
Figure 5.2: 10-fold batch reactor A) picture of the system with all reactors, B) picture of one reactor and C) process flow diagram.	58
Figure 5.3: 3-fold batch reactor A) picture of the system with all reactors, B) process flow diagram.	60

Figure 5.4: 600 mL batch reactor A) picture of the system, B) process flow diagram.	61
Figure 5.5: Nanofiltration system (POMMem) A) picture of entire system, B) picture from above C) process flow diagram, adapted from Esser et al. ²⁰⁵	62
Figure 6.1: Classification of humin model substances according to their chemical complexity: From monofuran derivates (first-generation) over difuran derivates (second-generation) to humins (model according to *Maerten et al. ⁸). ²¹²	92
Figure 7.1: A) Statistical design of experiments according to Box-Hunter-Hunter for the optimization of nanofiltration process. ²⁰⁵ B) Pareto chart compering the significance of individual parameter exemplary for the rejection of vanadium.	148
Figure 7.2: A) Normalized degree of desulfurization with reused aqueous catalyst solution. B) ⁵¹ V-NMR spectra (600 MHz) of the liquid phase before reaction (after nanofiltration). Figures are adapted from literature ²⁰⁵	149
Figure 7.3: Molecular structure of various first-generation (top / yellow section) and second-generation (bottom, orange section) model substrates emulation structural motifs of complex humins.	150
Figure 7.4: Comparison of furfural conversion and peak potentials in dependency of the POM catalysts used. ²⁰⁵	151
Figure 7.5: Proposed reaction pathways for oxidation of furan derivates by the means of furfural and 2-furoic acid using H ₄ [PVMo ₁₁ O ₄₀] in aqueous medium. ²¹² ..	153
Figure 7.6: Proposed reaction pathway for the selective catalytic oxidation of humins using a modified humin model structure based on structural motifs published by Filiciotto et al. ⁴⁰ (A), Wassenberg et al. ²¹⁶ (B) and Shen et al. ⁴⁵ (C) as example by converting functionalities that are hydrolysis-sensitive (1), free (2) or convertible by retro-aldol (3). ²¹³	156
Figure 7.7: A) SCO of humins as catalyst in aqueous methanolic solution, applying solely pTSA as additive and the combination of both additives using HPA-1 catalyst at 120 °C. ²¹³ B) Comparison of HPA-1 at 120 °C and HPA-2 at 90 °C for SCO of humins in the combined system. ²¹⁴	158
Figure 7.8: A) Reaction course and B) elemental analysis of the solid reaction residues in the SCO of glucose-based humin using HPA-2 at 90 °C in the combined system. ²¹⁴	159
Figure 7.9: A) Rejection for catalyst components P, V, Mo and B) oxidation products as well as additives in membrane screening experiments using a model reaction	

solution based on the SCO of glucose-based humin using HPA-2 at 90 °C in the combined additive system, adapted from Esser et al.²¹⁴. 161

Figure 7.10: A) Comparison of yields of the repeated catalyst recycling study for SCO of glucose-based humin using HPA-2 without addition of pTSA and B) comparison of ⁵¹V-NMR spectra, adapted form Esser et al.²¹⁴. 162

9.3 List of Tables

Table 4.1: Fragments of humin structure and components of pyrolysates confirmed by mass spectroscopy. 22

Table 4.2: Vanadium-substituted Keggin-type heteropoly acids based on phosphomolybdic acid.^{84,98} 32

Table 4.3: Different process approaches and their yields to produce levulinic acid from various raw materials. 46

Table 4.4: Examples of membrane processes with different driving forces and phases of the material systems to be processed, according to literature^{184,187,191,192}. 51

Table 5.1: Analytical device for gas phase analysis. 63

Table 5.2: Analytical devices for liquid phase analysis. 64

Table 5.3: Analytical devices for solid analysis – part 1. 65

Table 5.4: Analytical devices for solid analysis – part 2. 66

Table 5.5: List of used chemicals for the synthesis of humins. 70

Table 5.6: List of used chemicals for the synthesis of complex model substances. . 71

Table 5.7: List of used chemicals for the synthesis of POM catalysts (part I). 71

Table 5.8: List of used chemicals for the synthesis of POM catalysts (part II). 72

Table 5.9: List of used chemicals for the oxidation experiments (part I). 72

Table 5.10: List of used chemicals for the oxidation experiments (part II). 73

Table 5.11: List of used gases. 73

Table 9.1: List of hazardous substances (part 1) used according to globally harmonized system of classification and labelling of chemicals (GHS).²¹⁷ 187

Table 9.2: List of hazardous substances (part 2) used according to globally harmonized system of classification and labelling of chemicals (GHS).²¹⁷ 188

Table 9.3: List of hazardous substances (part 3) used according to globally harmonized system of classification and labelling of chemicals (GHS).²¹⁷ 189

9.4 List of Schemes

Scheme 4.1: Photosynthetic formation of glucose.....	12
Scheme 4.2: Ring closure of glucose and fructose as industrially relevant representatives of hexoses, adapted from Behr et al. ⁶	13
Scheme 4.3: Simplified process route of levulinic acid from lignocellulose in the Biofine process, according to Climent et al. ¹⁰	18
Scheme 4.4: Schematic presentation of the reaction pathway from glucose to levulinic acid and formation of humins. A. Pathway to levulinic acid, B. Pathway to DHH, according to literature ^{9,46,53–55}	20
Scheme 4.5: Reaction types of 5-HMF leading to the formation of humins, according to literature ^{9,45,53,54}	21
Scheme 4.6: Indirect hydrogen production from solar energy by converting biomass to formic acid, adapted from Wölfel et al. ⁵⁷	24
Scheme 4.7: Proposed reaction mechanism for the POM catalyzed oxidation of glucose to formic acid, adapted from literature ^{67,69}	25
Scheme 4.8: Pervanadyl-catalyzed oxidation of substrate and subsequent reoxidation of catalyst. ^{102–104}	33
Scheme 4.9: Reaction system of methyl formate hydrolysis to formic acid, according to literature ^{18,121,125}	38
Scheme 4.10: General reaction equation for the carbonylation of methanol to acetic acid.....	41

9.5 Supporting Information (ESI)

9.5.1 ESI of 1st Publication (Chapter 6.1)

Content

Supporting Notes:

1 Characterization of Catalyst	Page S1
2 DOE for Parameter Optimization	Page S2
3 Enrichment Experiments	Page S2 – S3
4 Catalyst Recycling Experiments	Page S3 – S8

The following section is reproduced from Ref.²⁰⁵ published in *Chemical Engineering Research and Design*, Elsevier.

Supporting Information

Characterization of $H_5PV_5Mo_7O_{40}$ catalyst (HPA-5) in aqueous solution

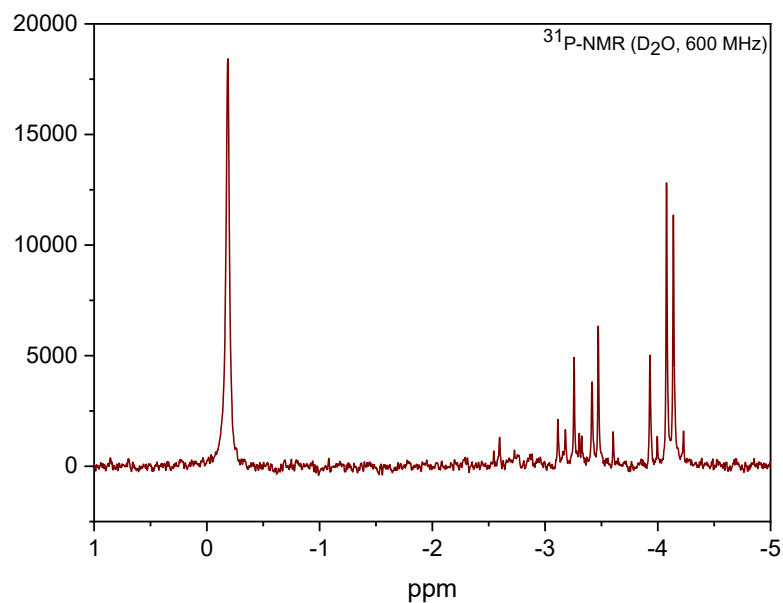


Figure S1: ^{31}P -NMR spectra (600 MHz) of $H_5PV_5Mo_7O_{40}$ catalyst (HPA-5) in aqueous solution. (Solution: 2.5 mmol HPA-5 catalyst in 500 mL water (9.4 g L^{-1}), 13.0 g L^{-1} formic acid, 3.1 g L^{-1} acetic acid and 8.4 g L^{-1} sulfuric acid.)

DOE for parameter optimization

Table S1: Experiments and results of the parameter optimization using Box, Hunter & Hunter design of experiments in randomized order.

Entry	Flow rate / mL min ⁻¹	Stirring speed / rpm	Pressure / bar	Rejection / % ^a					
				P ^b	V ^b	Mo ^b	FA ^c	AA ^c	H ₂ SO ₄ ^c
1	22.5	1100	30	85.5	97.3	99.3	3.0	9.5	85.5
2	30.0	0	40	83.4	95.2	98.6	4.6	9.8	81.5
3	15.0	1100	40	88.7	98.0	99.4	4.0	11.2	88.8
4	30.0	0	20	82.1	94.7	98.6	3.1	5.9	78.3
5	22.5	1100	30	88.8	97.7	99.6	5.2	13.8	89.4
6	15.0	0	40	84.8	95.7	96.0	3.9	7.7	84.8
7	30.0	1100	20	85.0	97.1	99.3	2.6	8.2	86.2
8	22.5	0	30	83.3	95.0	98.8	3.3	6.5	82.6
9	15.0	0	20	82.3	94.8	98.9	5.4	9.7	78.8
10	30.0	1100	40	89.7	97.8	99.6	4.0	12.1	91.3
11	15.0	1100	20	85.9	97.3	99.4	3.1	8.5	87.9
12	22.5	0	30	83.1	95.0	99.0	2.1	5.0	82.9

Experimental conditions: pre-wetted DK-series membrane, ambient temperature, 10 mmol H₅PV₅Mo₇O₄₀ catalyst in 2000 mL water (9.4 g L⁻¹), 13.2 g L⁻¹ formic acid, 3.1 g L⁻¹ acetic acid and 8.8 g L⁻¹ sulfuric acid a) calculated as described in the corresponding section of the experimental part b) determined with ICP-OES for catalyst components and c) analyzed with IC and HPLC.

Enrichment experiments with different concentration factors

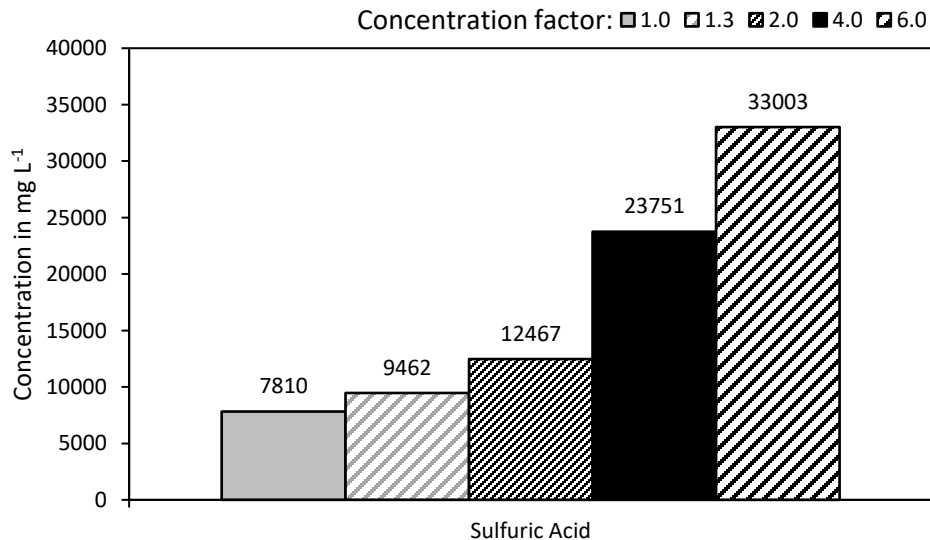


Figure S 2: Comparison of several enrichment experiments concerning the development of sulfuric acid concentration in the retentate depending on the concentration factors.

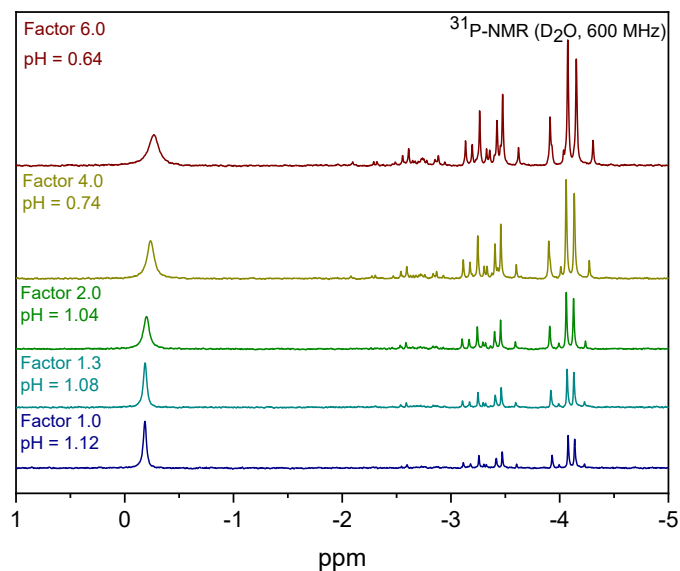


Figure S3: ^{31}P -NMR spectra (600 MHz) of the liquid phase before and after enrichment via nanofiltration membrane. (Conditions: DK-Series membrane, 15 mL min^{-1} flow rate, 30 bar pressure, 1100 rpm stirring speed, concentration factors from 1.0 to 6.0 Feed: 2.5 mmol HPA-5 catalyst in 500 mL water (9.4 g L^{-1}), 13.0 g L^{-1} formic acid, 3.1 g L^{-1} acetic acid and 8.4 g L^{-1} sulfuric acid.).

Catalyst recycling experiments

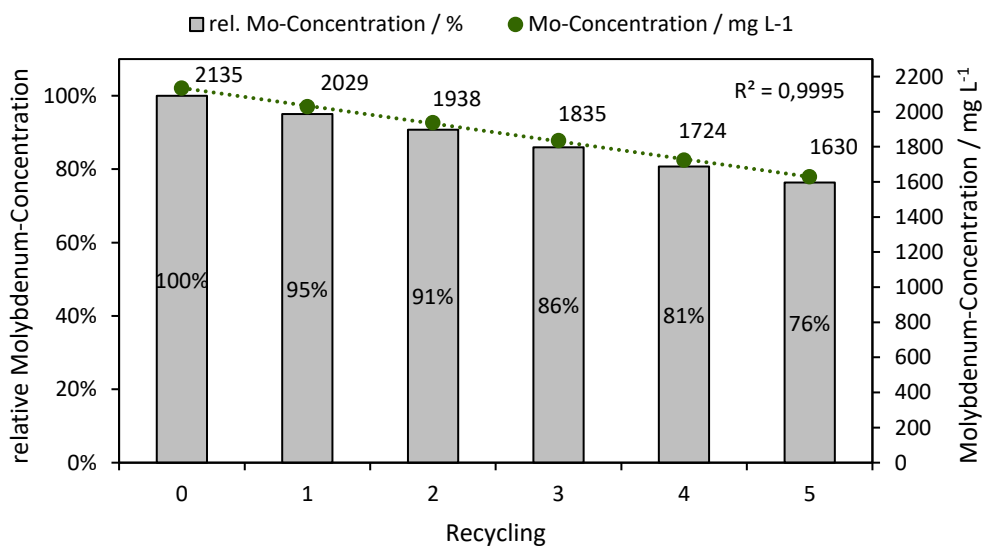


Figure S4: Development of molybdenum concentration in aqueous catalyst solution depending on the recycling. Determined by ICP-OES.

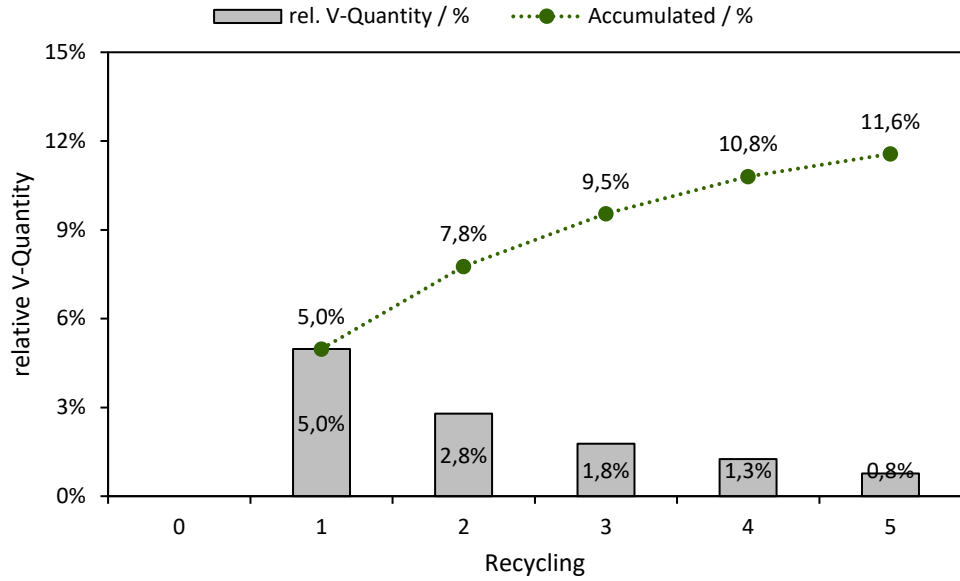


Figure S5: Development of relative vanadium loss via the permeate depending on the recycling. Determined by ICP-OES.

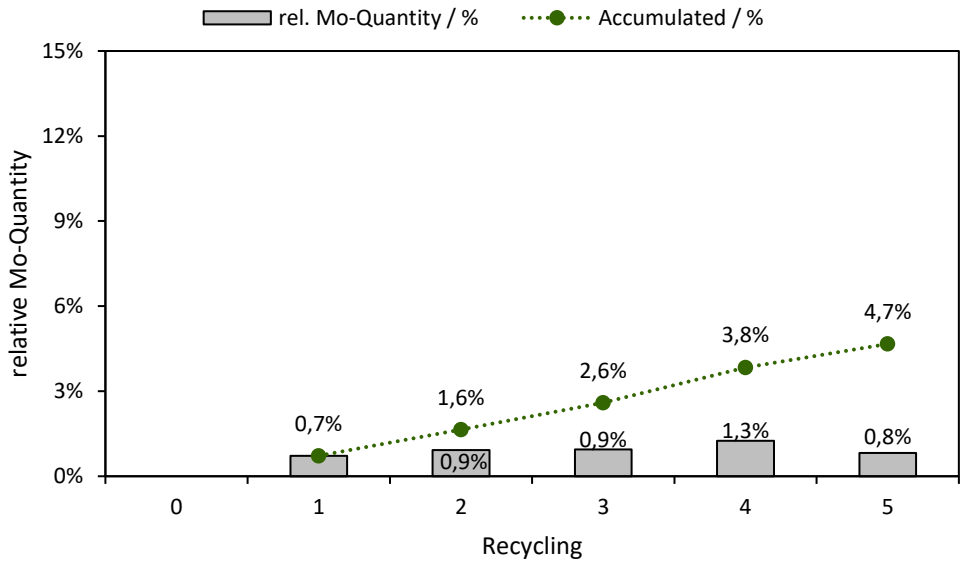


Figure S6: Development of relative molybdenum loss via the permeate depending on the recycling. Determined by ICP-OES.

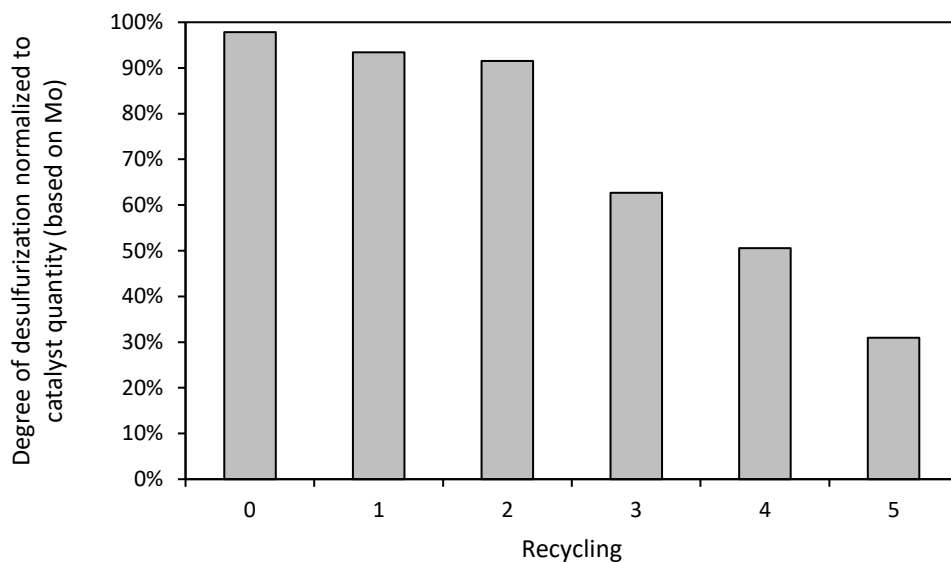


Figure S7: Normalized degree of desulfurization based on molybdenum concentration with reused aqueous catalyst solution. (Reaction *conditions*: 0.5 mmol HPA-5 in 200 mL water, 13.8 mmol benzothiophene in 40 mL 2,2,4-trimethylpentane (15900 ppmw S), 120 °C, 20 bar O₂, 1000 rpm, 6 h).

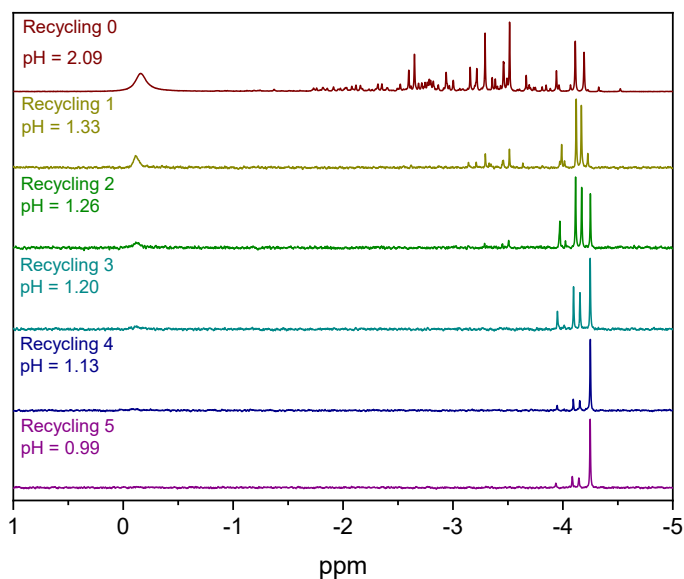


Figure S8: ³¹P-NMR spectra (600 MHz) of the liquid phase before reaction (after nanofiltration). (Reaction *conditions*: 0.5 mmol HPA-5 in 200 mL water, 13.8 mmol benzothiophene in 40 mL 2,2,4-trimethylpentane (15900 ppmw S), 120 °C, 20 bar O₂, 1000 rpm, 6 h).

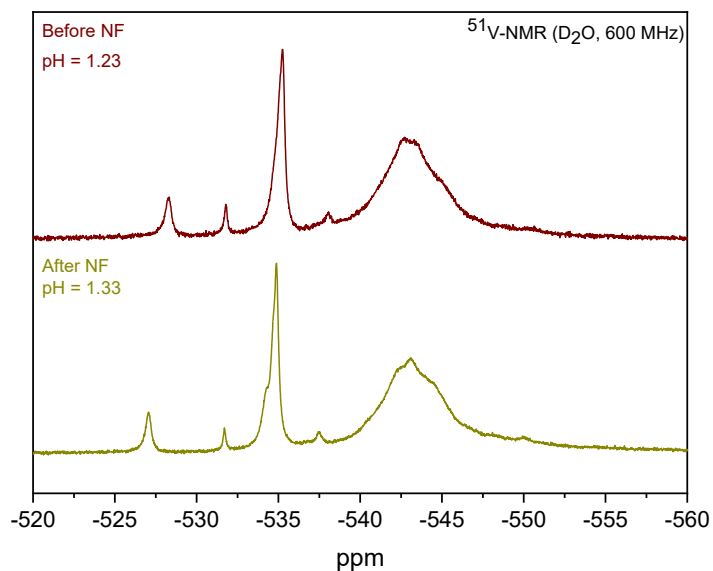


Figure S9: ^{51}V -NMR spectra (600 MHz) of the liquid phase before and after first nanofiltration NF (Membrane Cycle 1). (Reaction conditions: 0.5 mmol HPA-5 in 200 mL water, 13.8 mmol benzothiophene in 40 mL 2,2,4-trimethylpentane (15900 ppmw S), 120 °C, 20 bar O_2 , 1000 rpm, 6 h).

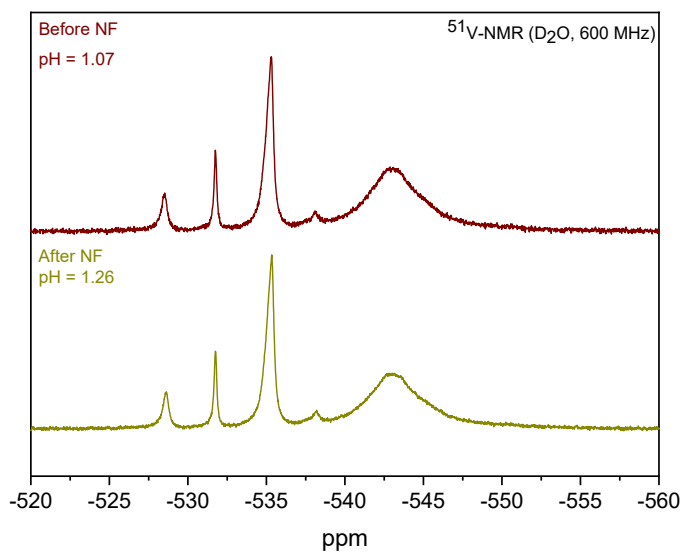


Figure S10: ^{51}V -NMR spectra (600 MHz) of the liquid phase before and after second nanofiltration NF (Membrane Cycle 2). (Reaction conditions: 0.5 mmol HPA-5 in 200 mL water, 13.8 mmol benzothiophene in 40 mL 2,2,4-trimethylpentane (15900 ppmw S), 120 °C, 20 bar O_2 , 1000 rpm, 6 h).

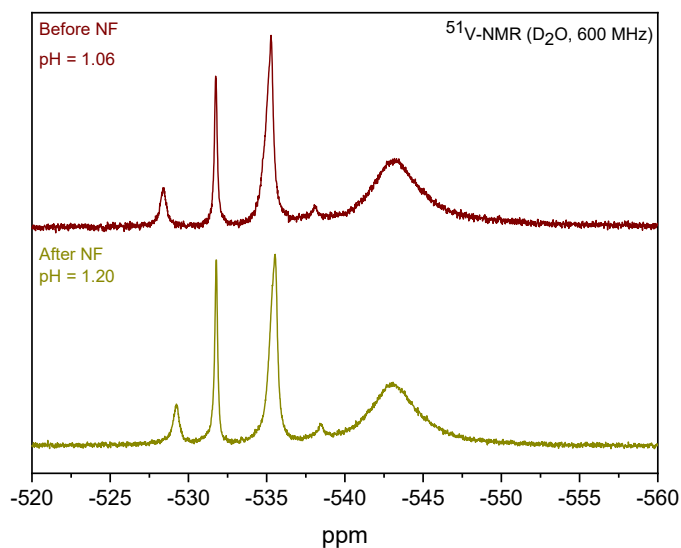


Figure S11: ^{51}V -NMR spectra (600 MHz) of the liquid phase before and after third nanofiltration NF (Membrane Cycle 3). (Reaction conditions: 0.5 mmol HPA-5 in 200 mL water, 13.8 mmol benzothiophene in 40 mL 2,2,4-trimethylpentane (15900 ppmw S), 120 °C, 20 bar O_2 , 1000 rpm, 6 h).

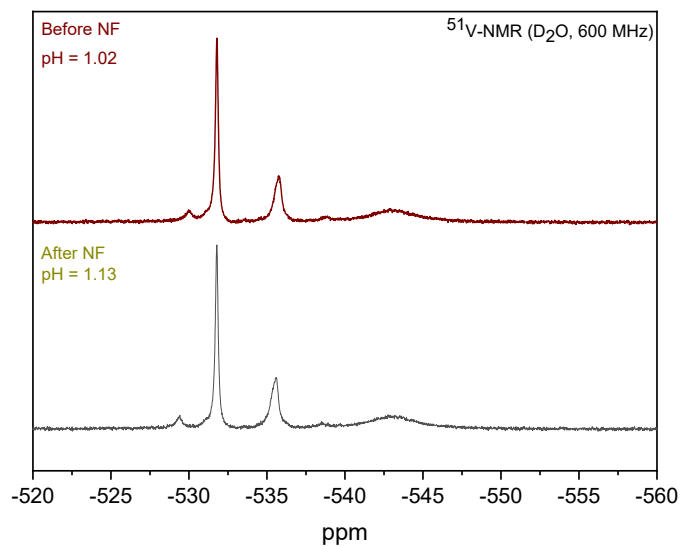


Figure S12: ^{51}V -NMR spectra (600 MHz) of the liquid phase before and after fourth nanofiltration NF (Membrane Cycle 4). (Reaction conditions: 0.5 mmol HPA-5 in 200 mL water, 13.8 mmol benzothiophene in 40 mL 2,2,4-trimethylpentane (15900 ppmw S), 120 °C, 20 bar O_2 , 1000 rpm, 6 h).

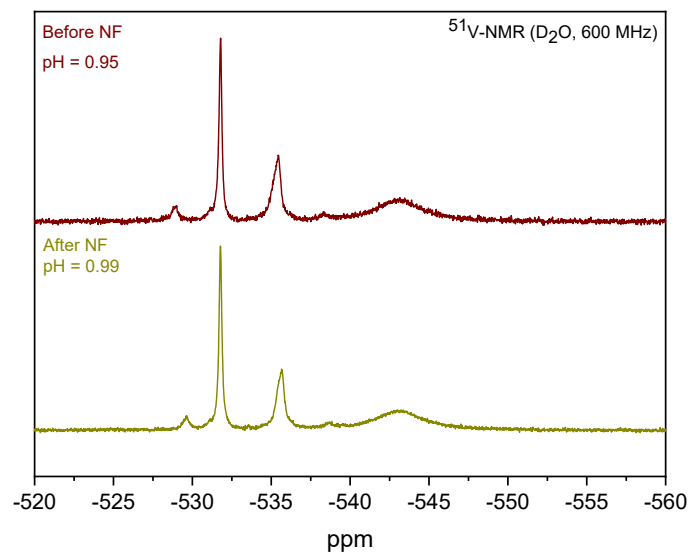


Figure S13: ^{51}V -NMR spectra (600 MHz) of the liquid phase before and after fifth nanofiltration NF (Membrane Cycle 5). (Reaction conditions: 0.5 mmol HPA-5 in 200 mL water, 13.8 mmol benzothiophene in 40 mL 2,2,4-trimethylpentane (15900 ppmw S), 120 °C, 20 bar O_2 , 1000 rpm, 6 h).

9.5.2 ESI of 2nd Publication (Chapter 6.2)Content*Supporting Notes:*

1 Catalyst Screening Experiments (Transition Metal)	Page S2 – S3
2 Electrochemical Characterization of Catalysts	Page S4 – S6
3 NMR Spectroscopy of Product Solution	Page S7 – S8
4 Catalyst Screening Experiments (Degree of Substitution)	Page S9
5 Substrate Screening Experiments (1 st Generation)	Page S10
6 Substrate Screening Experiments (2 nd Generation)	Page S11 – S12
7 Characterization of 2 nd Generation Model Substances	Page S12 – S14
8 Catalyst Characterization	Page S15 – S21
9 Further Analytics	Page S22 – S24

Reprinted from Ref.²¹² with permission of the *American Chemical Society*. Copyright 2023 *American Chemical Society*.

Supporting Information for

Catalytic valorization of humins by selective oxidation using transition-metal substituted Keggin-type polyoxometalate catalysts

Tobias Esser^a, André Wassenberg^a, Jan-Christian Raabe^a, Dorothea Voß^a and Jakob Albert^{a*}

^a Institute of Technical and Macromolecular Chemistry, Universität Hamburg, Bundesstraße 45, 20146 Hamburg, Germany

*e-mail: jakob.albert@uni-hamburg.de

This document contains 5 Tables and 34 Figures on 25 pages.

Catalyst screening experiments for the oxidation of furfural with different mono-substituted Keggin-type POMs

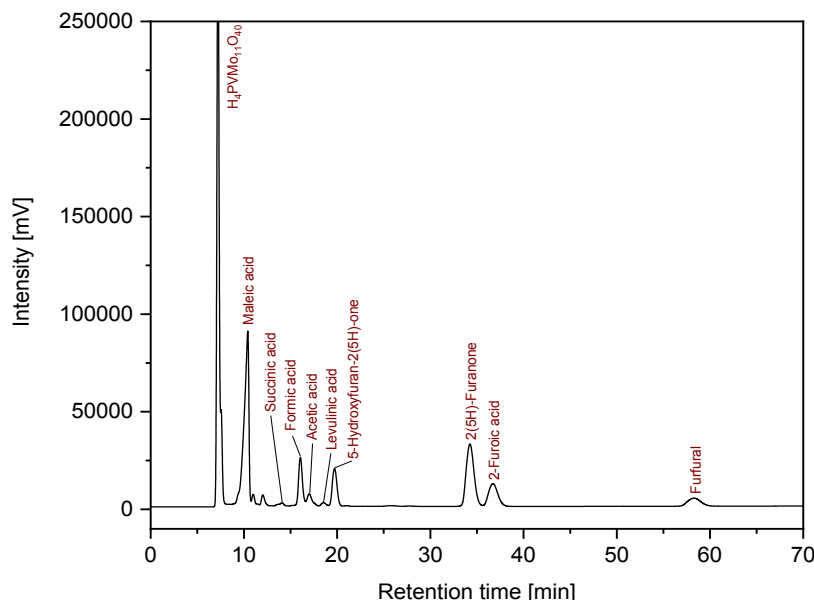


Figure S1: Exemplary chromatogram for the liquid product phase of the oxidation of the substrate mixture using $H_4[PVMo_{11}O_{40}]$ as a catalyst. *Experimental conditions:* 10-fold reaction system, 90 °C, 30 bar (O_2), 15 h, 1000 rpm, 10 mL substrate mixture with furfural, 2-furoic acid and 2(5H)-furanone containing a total of 25.5 mmol carbon (8.5 mmol carbon each), 0.277 mmol vanadium ($92 \text{ mol}_{\text{Carbon}} \text{ mol}^{-1}_{\text{Vanadium}}$).

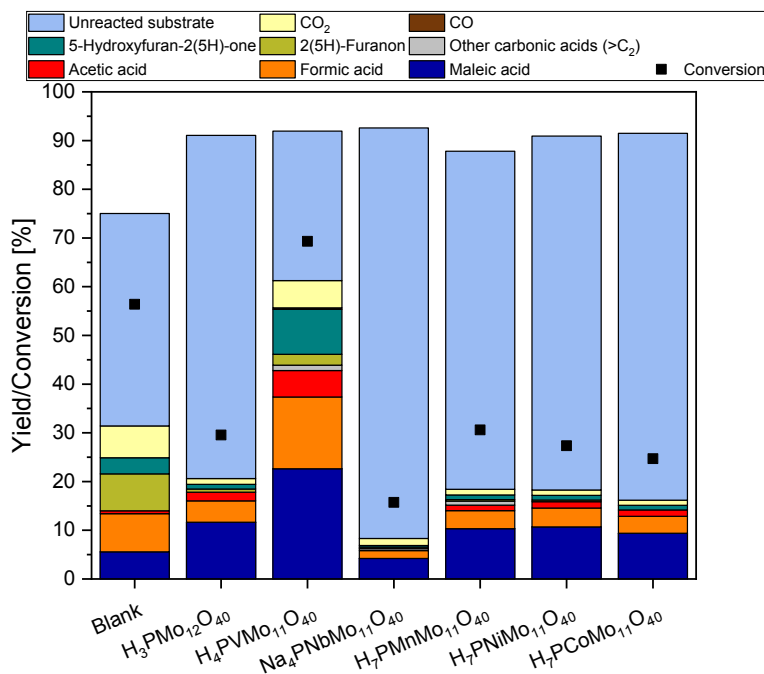


Figure S2: Comparison of product distribution in experiments on furfural using Keggin-type POM catalysts substituted by different transition metals. *Experimental conditions:* 10-fold reaction system, 90 °C, 30 bar (O_2), 15 h, 1000 rpm, 10 mL stock solution with furfural (12.5 mmol carbon), 0.14 mmol substituted metal M ($90 \text{ mol}_{\text{Carbon}} \text{ mol}^{-1}_{\text{M}}$).

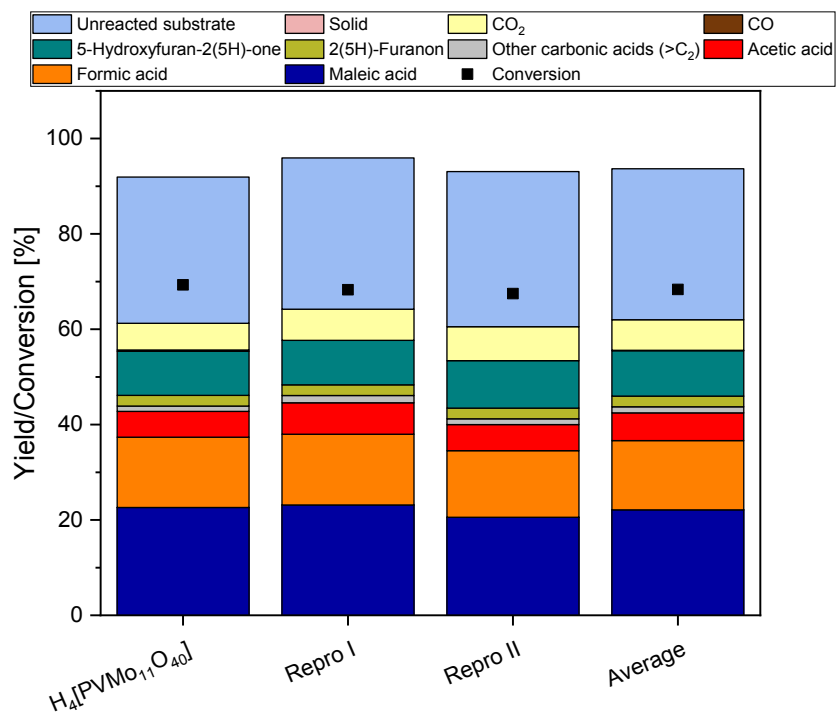


Figure S3: Reproduction of experiments on the catalytic selective oxidation of furfural using Keggin-type polyoxometalate catalysts substituted by vanadium. *Experimental conditions:* 10-fold reaction system, 90 °C, 30 bar (O₂), 15 h, 1000 rpm, 10 mL stock solution with furfural (12.5 mmol carbon), 0.14 mmol substituted metal M (90 mol_{Carbon} mol⁻¹_M).

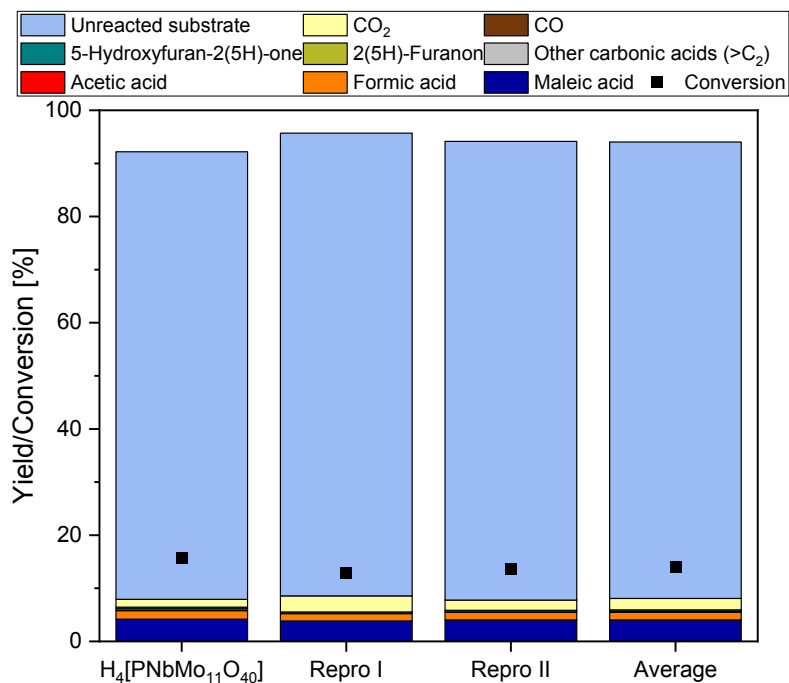


Figure S4: Reproduction of experiments on the catalytic selective oxidation of furfural using Keggin-type polyoxometalate catalysts substituted by niobium. *Experimental conditions:* 10-fold reaction system, 90 °C, 30 bar (O₂), 15 h, 1000 rpm, 10 mL stock solution with furfural (12.5 mmol carbon), 0.14 mmol substituted metal M (90 mol_{Carbon} mol⁻¹_M).

Electrochemical characterization of the used POM catalysts

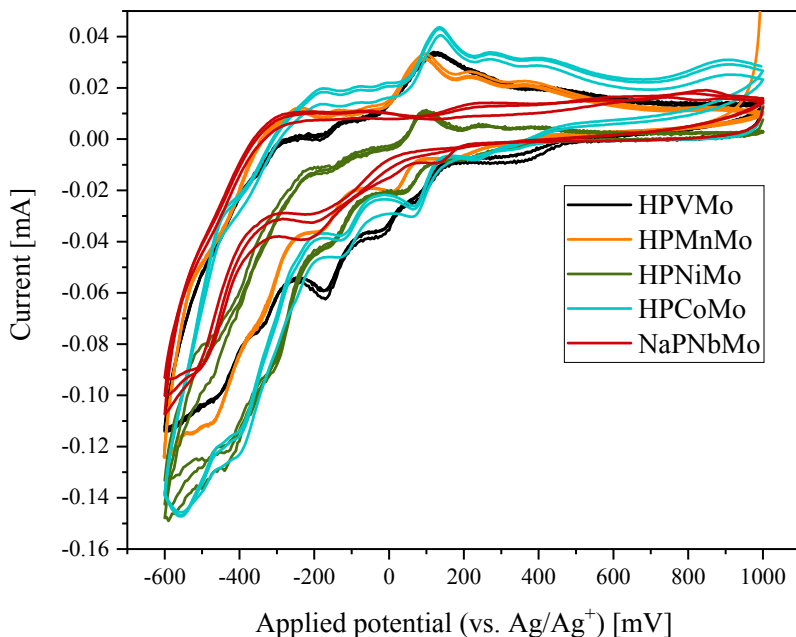


Figure S5: CV data of the M(z) substituted phosphomolybdates $H_x[PMo_{11}O_{40}]$ with $x = 4, 7$ and $M = V^V, Mn^{II}, Ni^{II}, Co^{II}, Nb^V$ (concentration 1 mmol L^{-1} , scan rate 100 mV s^{-1} (CV) at pH 1).

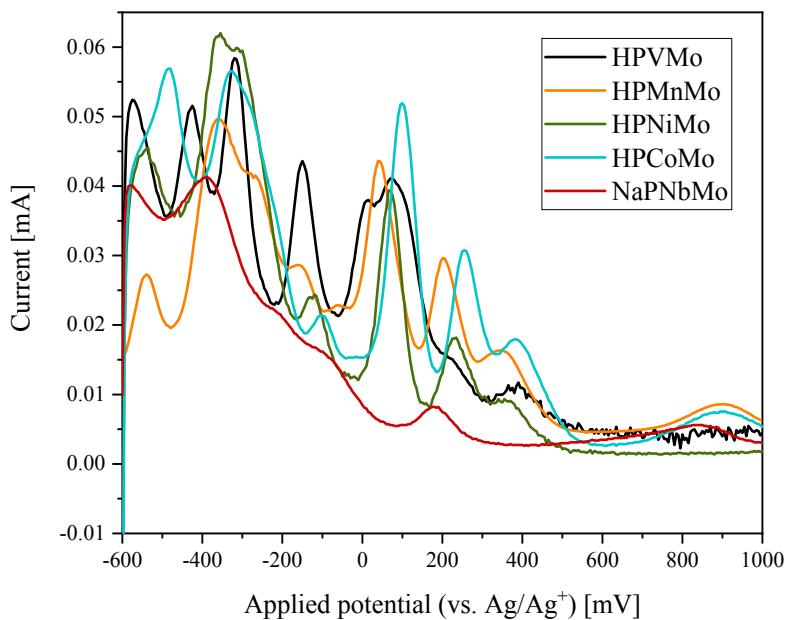


Figure S6: SWV data of the M(z) substituted phosphomolybdates $H_x[PMo_{11}O_{40}]$ with $x = 4, 7$ and $M = V^V, Mn^{II}, Ni^{II}, Co^{II}, Nb^V$ (concentration 1 mmol L^{-1} , scan rate 5 mV s^{-1} (CV) at pH 1).

Table S1: Peak maxima from SWV data, peak maxima (oxidation pathway) and peak minima (reduction pathway) from the CV data of the POMs in solution.

Entry	Maximum oxidation pathway CV [mV]	Minimum oxidation pathway CV [mV]	Mean value CV [mV]	Peak maxima SWV [mV]
H₄[PVMo₁₁O₄₀]				
1	-	-	-	-575
2	-485	-445	-465	-425
3	-270	-335	-303	-320
4	-120	-25	-73	-150
5	-	-	-	10
6	120	85	103	70
7	-	-	-	215
8	440	340	390	390
H₇[PMnMo₁₁O₄₀]				
9	-521	-528	-525	-540
10	-	-365	-	-358
11	-243	-194	-219	-268
12	-	-	-156	-162
13	-	-	-	-66.2
14	99.2	11.3	55.3	39.5
15	214	171	193	201
16	368	-	-	342
17	-	-	-	906

Experimental Conditions: Water as solvent at pH 1 (HCl), concentration 1 mmol L⁻¹, scan rate 100 mV s⁻¹ (CV) and 5 mV s⁻¹ (SWV)

Table S2: Peak maxima from SWV data, peak maxima (oxidation pathway) and peak minima (reduction pathway) from the CV data of the POMs in solution.

Entry	Maximum oxidation pathway CV [mV]	Minimum oxidation pathway CV [mV]	Mean value CV [mV]	Peak maxima SWV [mV]
H₇[PNiMo₁₁O₄₀]				
18	-495	-	-	-535
19	-	-	-	-355
20	-	-	-	-315
21	-200	-160	-180	-120
22	100	10	55	65
23	240	180	210	235
24	390	-	-	355
H₇[PCoMo₁₁O₄₀]				
25	-435	-425	-430	-485
26	-	-	-330	-330
27	-175	-125	-105	-105
28	-75	65	-5	-
29	-5	-	-	-
30	135	-	-	100
31	270	215	243	255
32	400	-	-	385
33	900	775	838	895
Na₄[PNbMo₁₁O₄₀]				
34	-515	-520	-518	-580
35	-	-	-	-395
36	-245	-230	-238	-225
37	-	-	-	-105
38	60	-	-	-
39	230	120	178	175
40	620	-	-	-
41	845	-	-	840

Experimental Conditions: Water as solvent at pH 1 (HCl), concentration 1 mmol L⁻¹, scan rate 100 mV s⁻¹ (CV) and 5 mV s⁻¹ (SWV)

Structure investigations using NMR spectroscopy

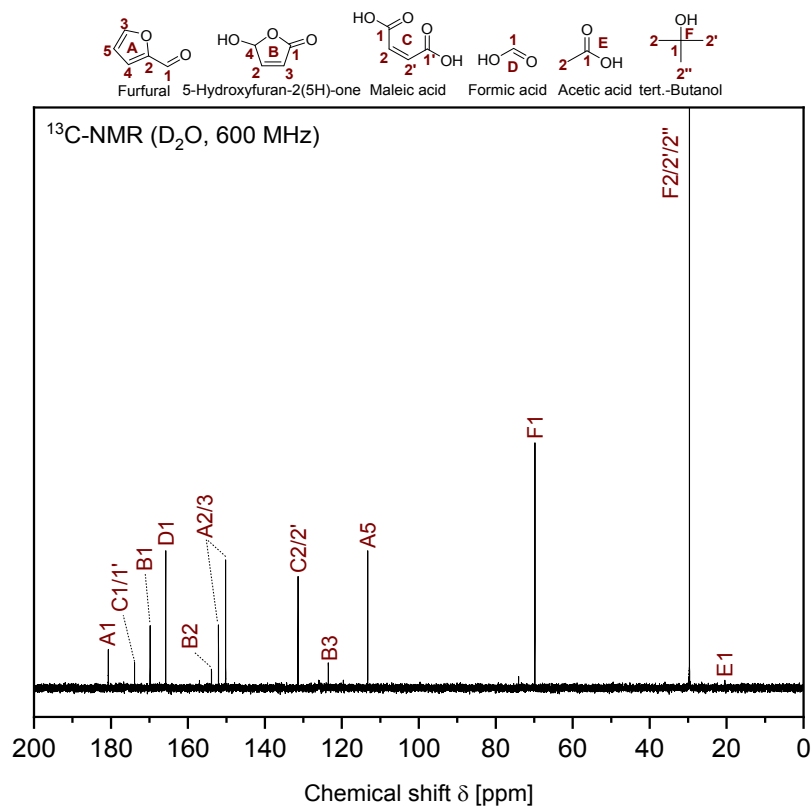


Figure S7: Exemplary ¹³C-NMR spectra (D₂O, 600 MHz) of reaction solution of catalyst screening experiment using H₄[PVMo₁₁O₄₀]. *Experimental Conditions:* a) 10-fold reaction system, 90 °C, 30 bar (O₂), 15 h, 1000 rpm, 10 mL stock solution with furfural (12.5 mmol carbon), 0,14 mmol substituted metal M (90 mol_{Carbon} mol⁻¹_M).

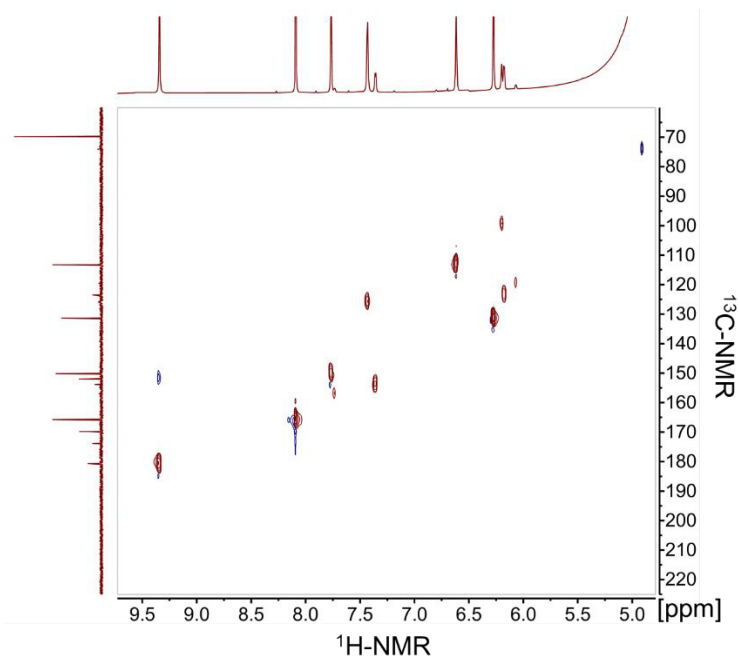


Figure S8: Exemplary HSQC spectra (D_2O , 600 MHz) of reaction solution of catalyst screening experiment using $H_4[PVMo_{11}O_{40}]$. *Experimental Conditions:* a) 10-fold reaction system, 90 °C, 30 bar (O_2), 15 h, 1000 rpm, 10 mL stock solution with furfural (12.5 mmol carbon), 0,14 mmol substituted metal M ($90 \text{ mol}_{\text{Carbon}} \text{ mol}^{-1}_{\text{M}}$).

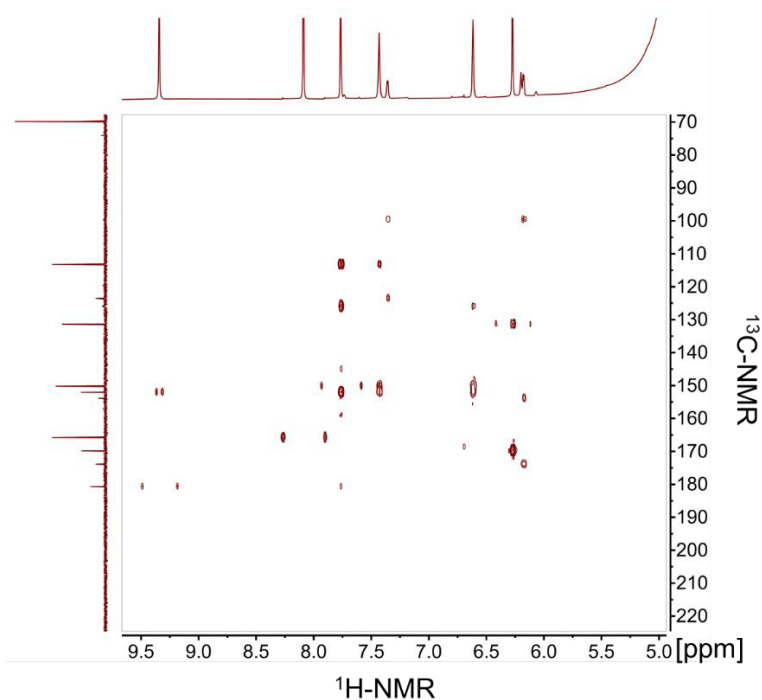


Figure S9: Exemplary HMBC spectra (D_2O , 600 MHz) of reaction solution of catalyst screening experiment using $H_4[PVMo_{11}O_{40}]$. *Experimental Conditions:* a) 10-fold reaction system, 90 °C, 30 bar (O_2), 15 h, 1000 rpm, 10 mL stock solution with furfural (12.5 mmol carbon), 0,14 mmol substituted metal M ($90 \text{ mol}_{\text{Carbon}} \text{ mol}^{-1}_{\text{M}}$).

Catalyst screening experiments for the oxidation of furfural by Keggin-type POMs with different degrees of substitution

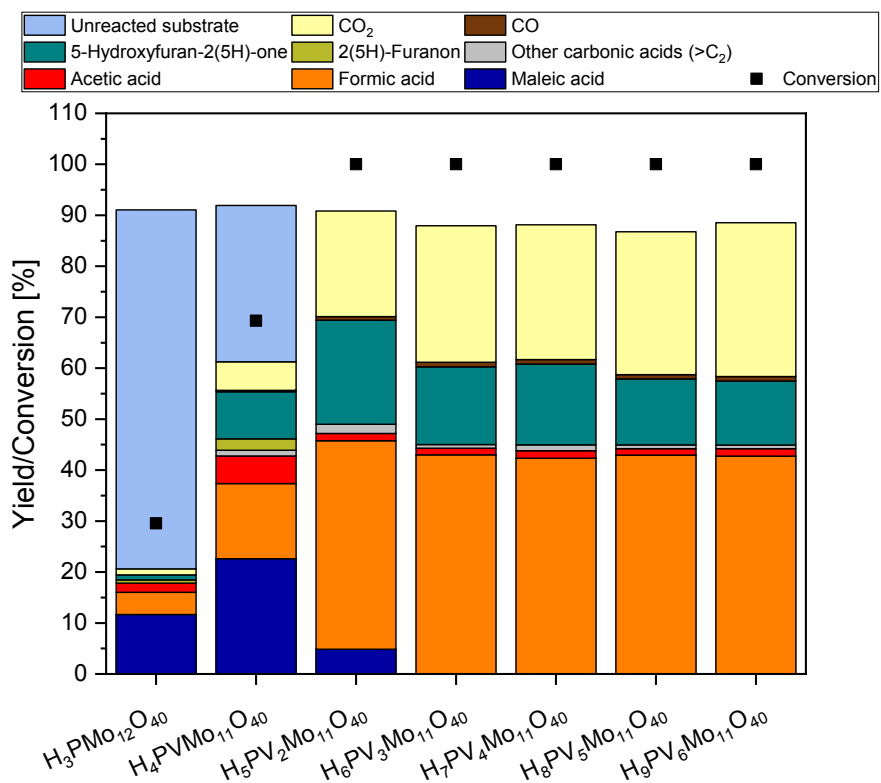


Figure S10: Comparison of product distribution in experiments on furfural using Keggin-type polyoxometalate catalysts substituted by vanadium with different degree of substitution. *Experimental conditions:* 10-fold reaction system, 90 °C, 30 bar (O_2), 15 h, 1000 rpm, 10 mL stock solution with furfural (12.5 mmol carbon), 0.14 mmol substituted metal M ($90 \text{ mol}_{\text{Carbon}} \text{ mol}^{-1}_{\text{M}}$).

Table S3: Stability experiments using $H_4PVMo_{11}O_{40}$ as a catalyst.

Entry ^a	Substrate	Catalyst	X ^b / %	Yield / %	
				FA ^c	CO_2 ^d
1	Maleic acid	-	4.2	3.7	0.5
2		$H_4PVMo_{11}O_{40}$	5.9	4.2	1.7
3	Formic acid	-	0.1	99.9	0.1
4		$H_4PVMo_{11}O_{40}$	0.3	99.7	0.3

a) Experimental conditions: 10-fold reaction system, 90 °C, 30 bar (O_2), 15 h, 1000 rpm, 7.5 mL, $90 \text{ mol}_{\text{Carbon}} \text{ mol}^{-1}_{\text{Vanadium}}$ b) analyzed as described in corresponding section of the experimental part c) determined with HPLC-RID d) determined with GC-TCD

Selective catalytic oxidation of 1st generation substrates using $H_4[PVMo_{11}O_{40}]$ as a catalyst

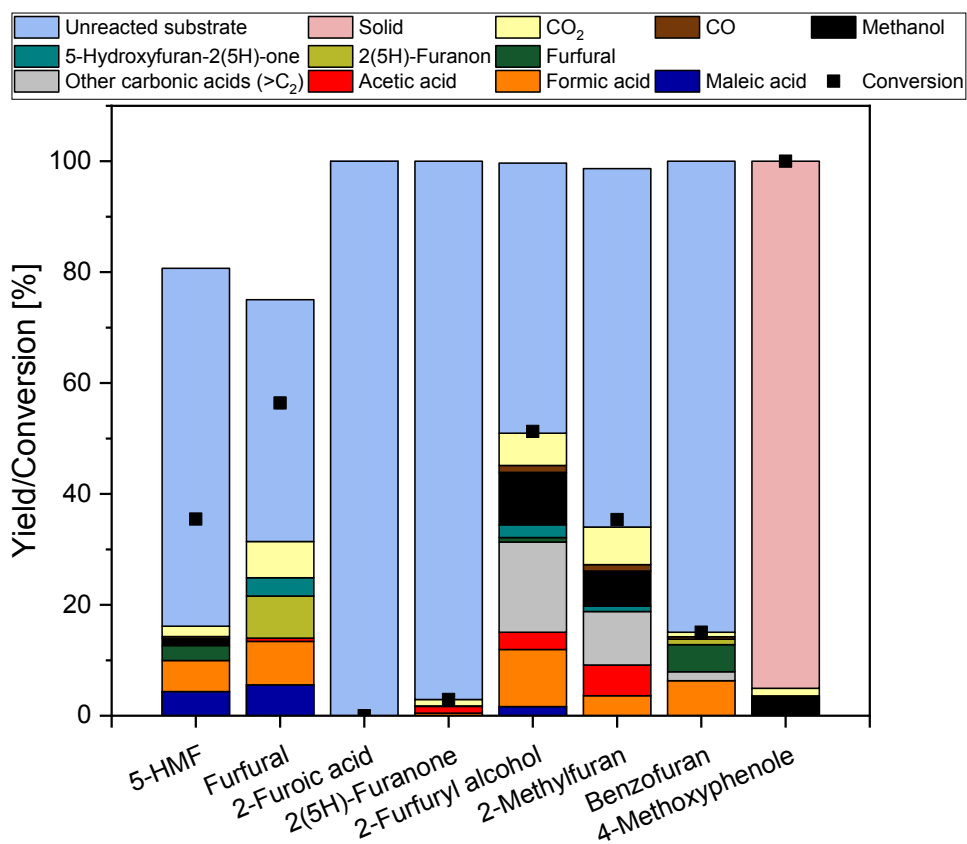


Figure S11: Comparison of product distribution in experiments on different first-generation substrates without catalyst. *Experimental conditions:* 10-fold reaction system, 90 °C, 30 bar (O₂), 15 h, 1000 rpm, 10 mL water, 12.5 mmol carbon from the respective substrate, 0.14 mmol V for substitution (90 mol_{Carbon} mol⁻¹V).

Catalytic oxidation of 2nd generation substrates using H₄[PVMo₁₁O₄₀] as a catalyst

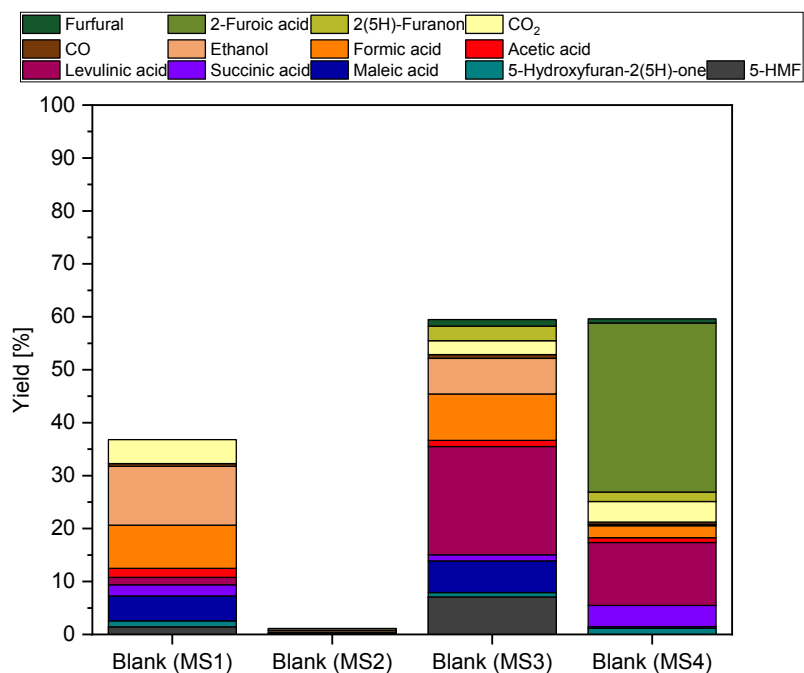


Figure S12: Comparison of product distribution of oxidative conversion of different second-generation substrates without catalyst. *Experimental conditions:* 10-fold reaction system, 90 °C, 30 bar (O₂), 15 h, 1000 rpm, 7.5 mL substrate solution with a) furfural (Fu), b) 2-furoic acid (FuroA) and c) 2(5H)-furanone (FuOn), 92 mol_{Carbon} mol⁻¹_{Vanadium}.

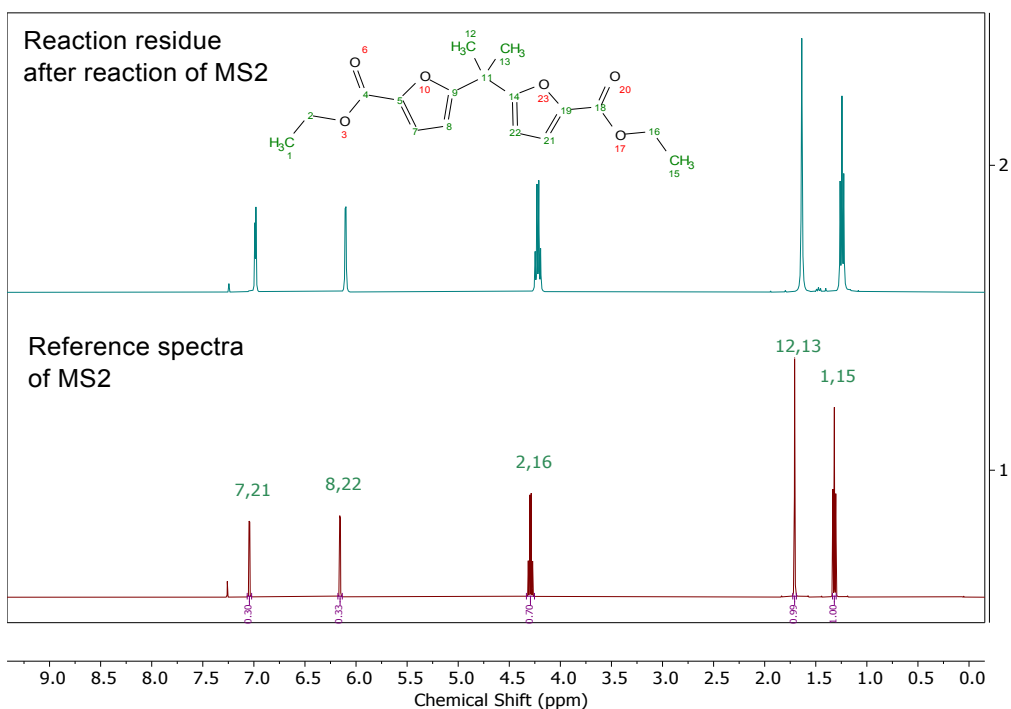


Figure S13: ¹H-NMR spectra (CDCl₃, 400 MHz) of MS2 after reaction (upper part) and before reaction (lower part).

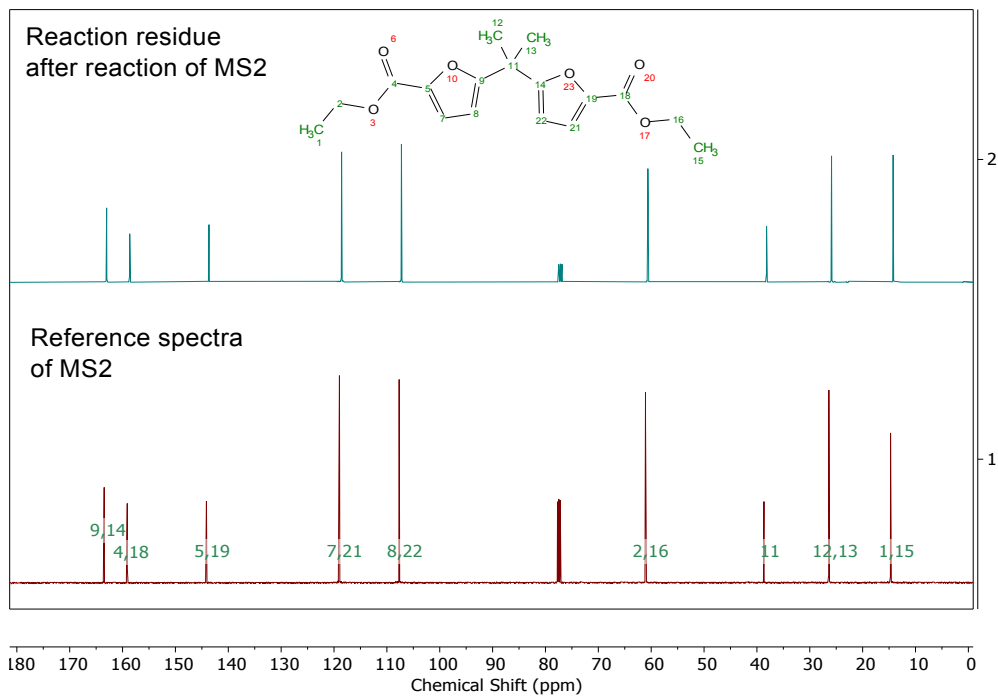


Figure S14: ^{113}C -NMR spectra (CDCl_3 , 400 MHz) of MS2 after reaction (upper part) and before reaction (lower part).

Characterization of 2nd generation model substances

Table S4: Result of CHNS analysis for the model substances MS1 to MS4

Entry	Model substance	Mass fraction [wt.-%]			
		C	H	N	S
1	MS1	60.2	6.0	<0.2	0.5
2	MS2	63.8	6.2	0.0	0.0
3	MS3	61.9	4.4	0.0	0.0
4	MS4	61.6	4.2	<0.2	0

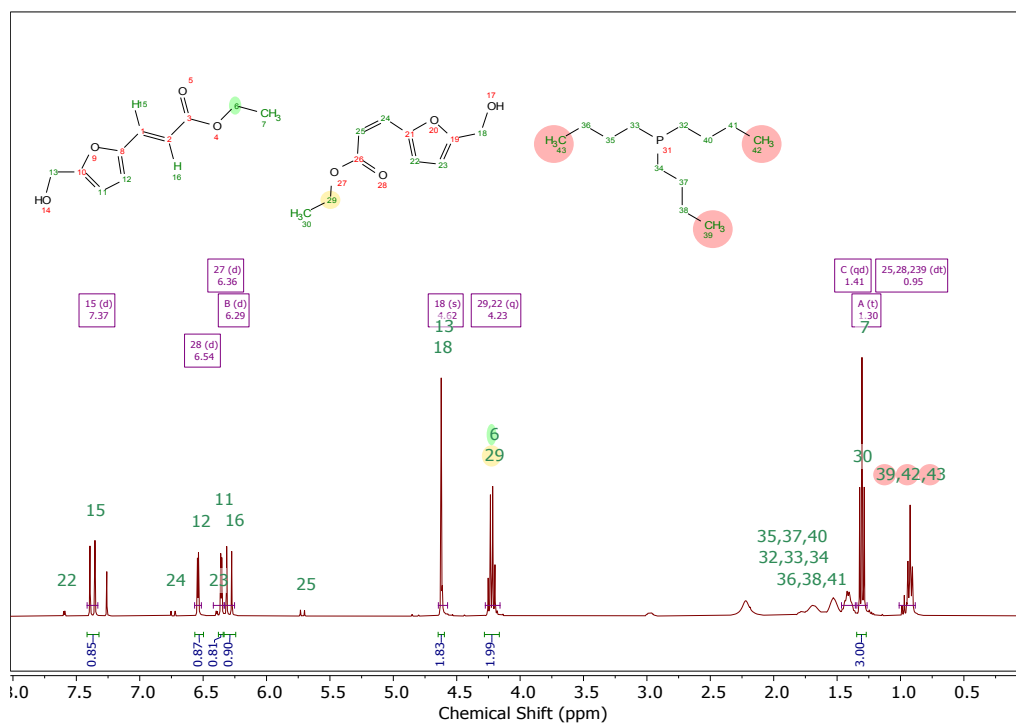


Figure S15: ¹H-NMR spectra (CDCl₃, 400 MHz) of MS1.

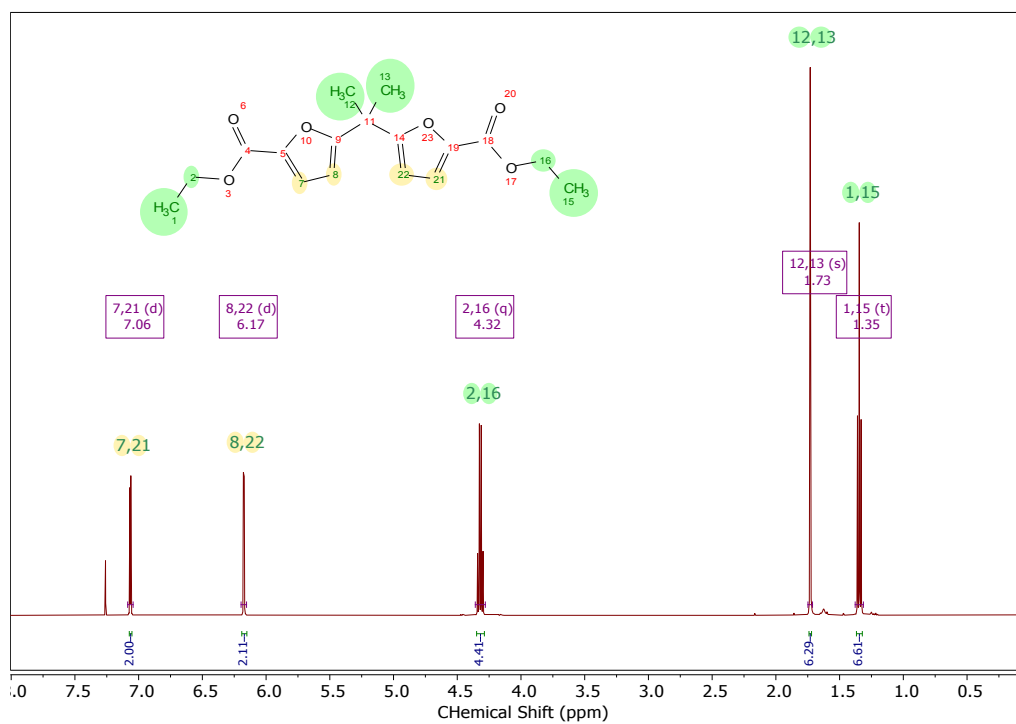


Figure S16: ¹H-NMR spectra (CDCl₃, 400 MHz) of MS2.

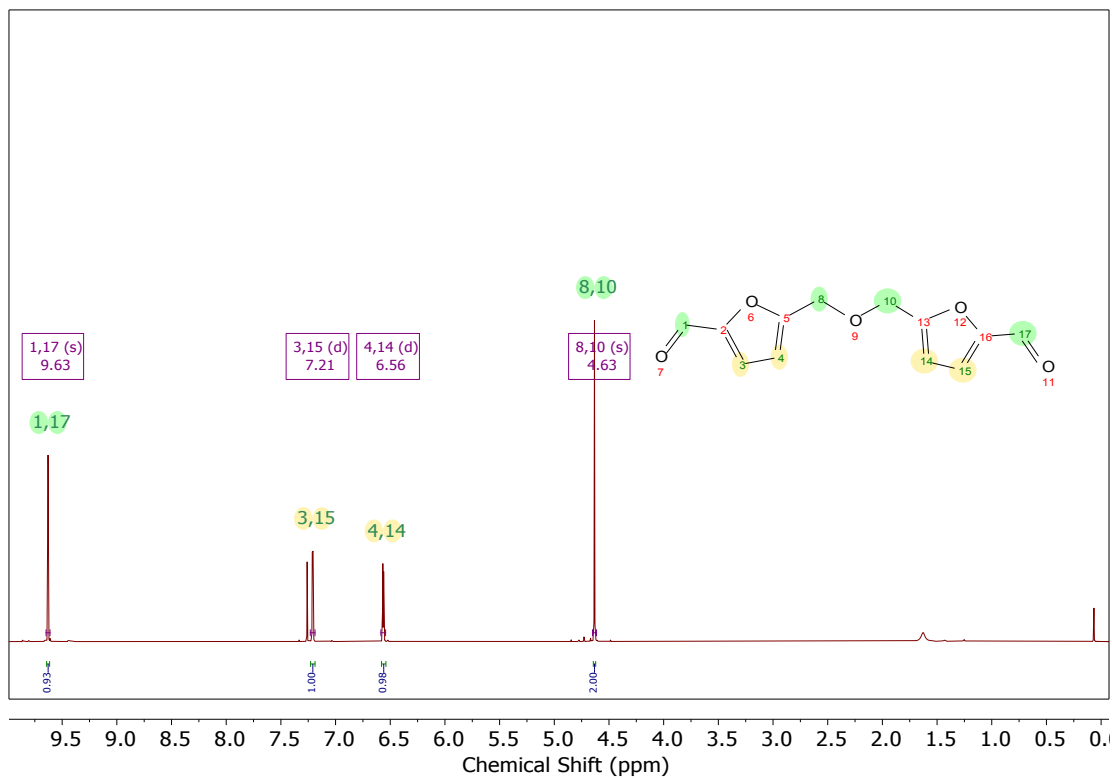


Figure S17: ¹H-NMR spectra (CDCl₃, 400 MHz) of MS3.

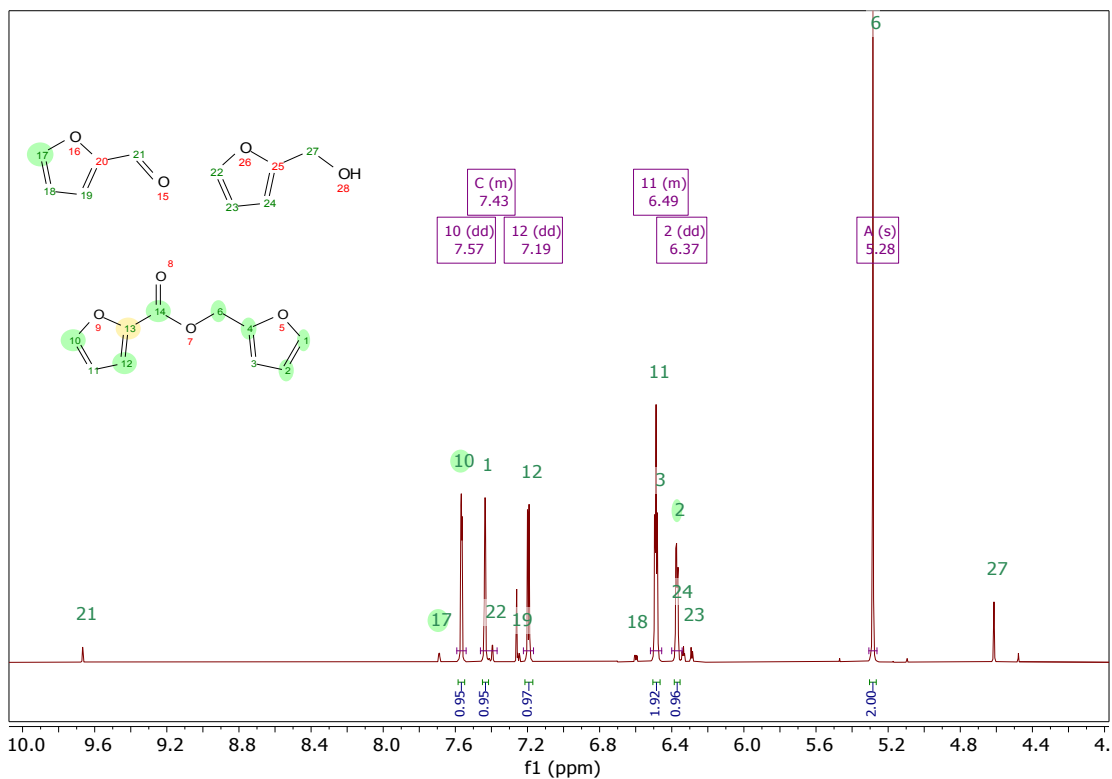


Figure S18: ¹H-NMR spectra (CDCl₃, 400 MHz) of MS4.

Catalyst characterization

Table S5: Result of ICP-OES and TGA analysis for the POM catalysts

Entry	POM	Target molecular composition	Element ratio ^a	Hydration water ^b [mol mol ⁻¹]
Keggin				
1	HPVMo	H ₄ [PVMo ₁₁ O ₄₀]	P/V/Mo 1.23 ^c /0.967/11	7
2	HPV ₂ Mo	H ₅ [PV ₂ Mo ₁₀ O ₄₀]	P/V/Mo 1.28 ^c /2.01/10	9
3	HPV ₃ Mo	H ₆ [PV ₃ Mo ₉ O ₄₀]	P/V/Mo 1.10 ^c /3.03/9	
4	HPV ₄ Mo	H ₇ [PV ₄ Mo ₈ O ₄₀]	P/V/Mo 1.41 ^c /4.03/8	
5	HPV ₅ Mo	H ₈ [PV ₅ Mo ₇ O ₄₀]	P/V/Mo 1.21 ^c /5.02/7	
6	HPV ₆ Mo	H ₉ [PV ₆ Mo ₆ O ₄₀]	P/V/Mo 1.28 ^c /6.11/6	11
7	HPMnMo	H ₇ [PMnMo ₁₁ O ₄₀]	P/Mn/Mo 1.14/1.07/11	8
8	HPNiMo	H ₇ [PNiMo ₁₁ O ₄₀]	P/Ni/Mo 1.09/0.987/11	8
9	HPCoMo	H ₇ [PCoMo ₁₁ O ₄₀]	P/Co/Mo 0.972/1.03/11.0	8
10	NaPNbMo	Na ₄ [PNbMo ₁₁ O ₄₀]	Na/K/P/Nb/Mo 4.96/0.45/0.893/1.10/11	6

a) The element ratios were determined by ICP-OES analysis. The data were normalized to the targeted W/Mo content. b) The content of hydration water was determined by TGA analysis. c) The P content is higher due to the slight excess of H₃PO₄ used during synthesis. d) However, the sodium content seems to be higher than expected, due to a co-crystallization of the POM and NaCl.

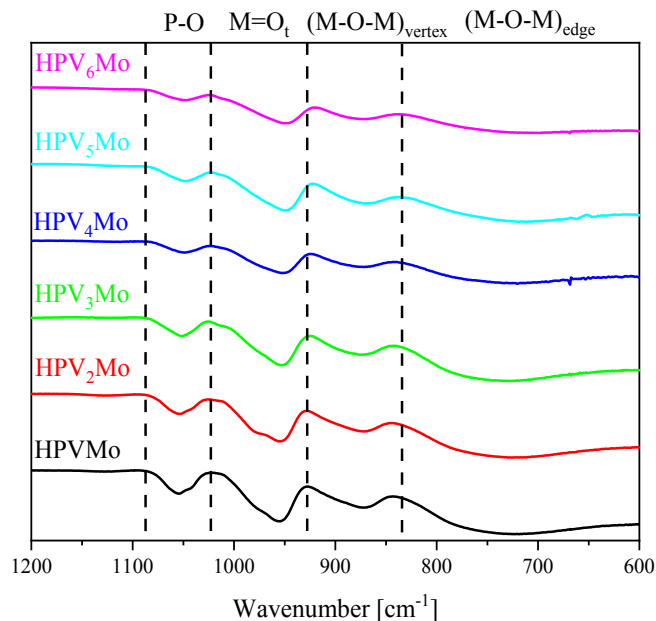


Figure S19: FT-IR (ATR) spectra of the $H_{3+x}[PV_xMo_{12-x}O_{40}]$ POMs with $x = 1$ to 6 . Vibration modes: $1060-1045\text{ cm}^{-1}$ (P-O), $960-950\text{ cm}^{-1}$ ($M=O_t$), $875-865\text{ cm}^{-1}$ ($(M-O-M)_{\text{vertex}}$), $741-710\text{ cm}^{-1}$ ($(M-O-M)_{\text{edge}}$).¹

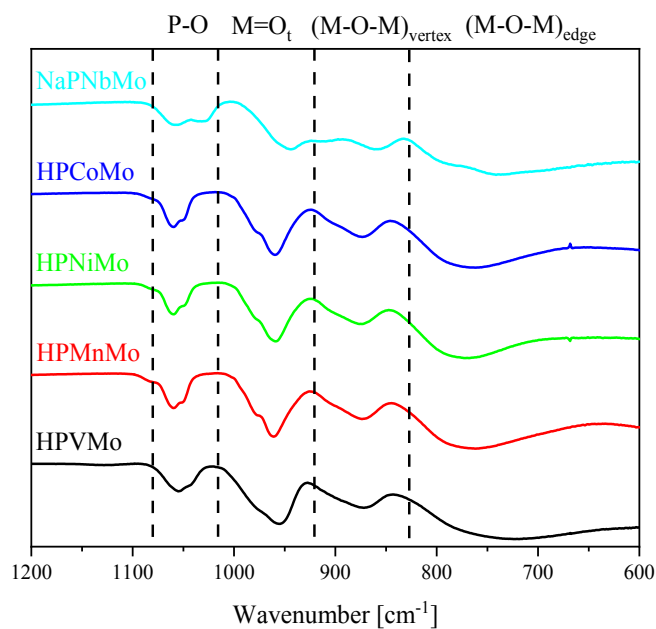


Figure S20: FT-IR (ATR) spectra of the $H_{2z}[PMMo_{11}O_{40}]$ POMs with $M = \text{Mn(II), Co(II), Ni(II), Nb(V)}$ and $z = 4, 7$. Vibration modes: $1060-1030\text{ cm}^{-1}$ (P-O), $960-945\text{ cm}^{-1}$ ($M=O_t$), $870-860\text{ cm}^{-1}$ ($(M-O-M)_{\text{vertex}}$), $770-730\text{ cm}^{-1}$ ($(M-O-M)_{\text{edge}}$).¹

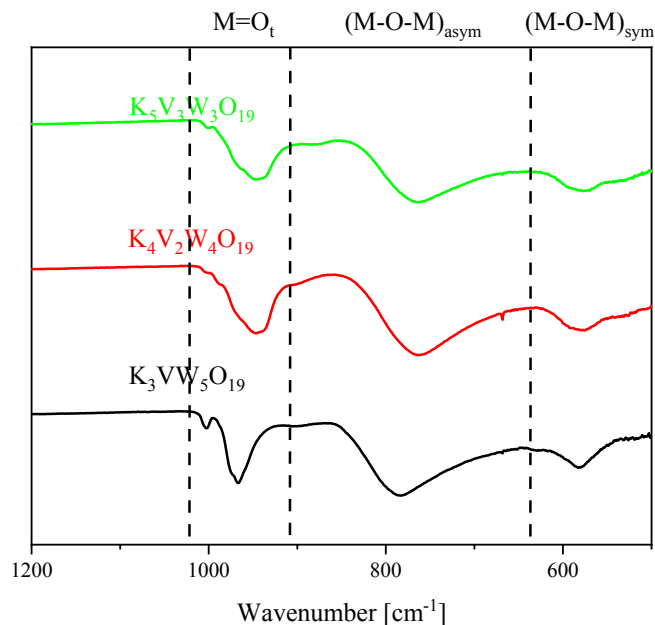


Figure S21: FT-IR (ATR) spectra of the $K_{2+x}[PV_xW_{6-x}O_{19}]$ POMs with $x = 1$ to 3. Vibration modes: 970-940 cm^{-1} ($M=O_t$), 790-770 cm^{-1} ($(M-O-M)_{asym}$), 590-570 cm^{-1} ($(M-O-M)_{sym}$).²

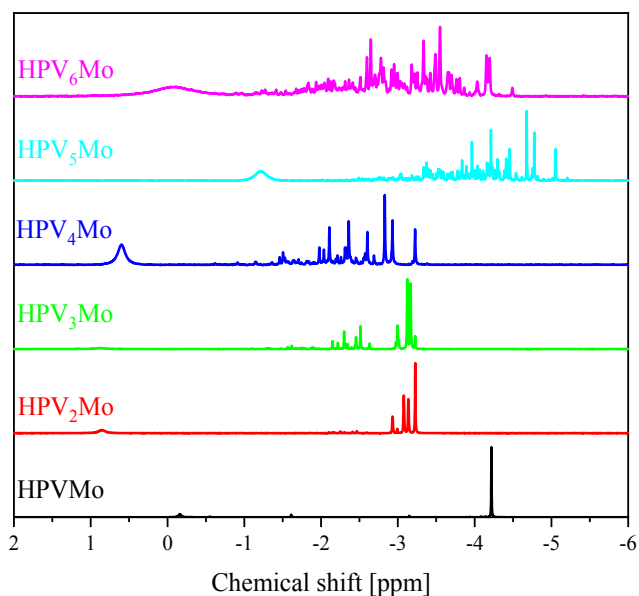


Figure S22: ^{31}P NMR spectra of the $H_{3+x}[PV_xMo_{12-x}O_{40}]$ POMs with $x = 1$ to 6 in a mixture of 90 % H_2O (pH 1) and 10 % acetone- d_6 . The spectra were measured at 242.9 MHz. 85 % H_3PO_4 was used as external standard.

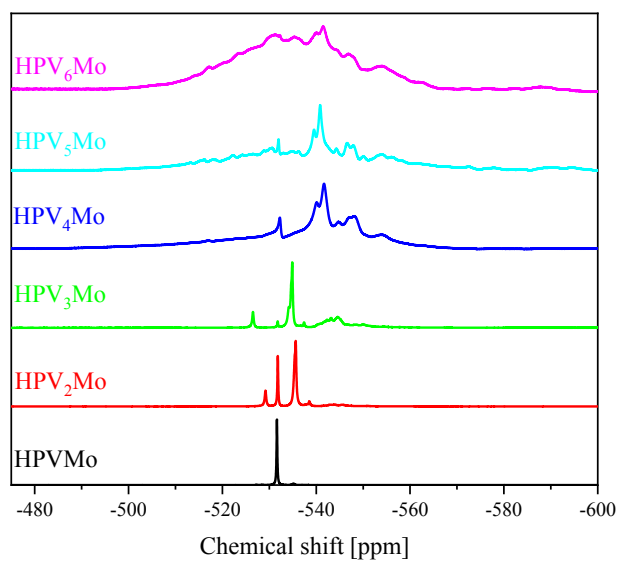


Figure S23: ^{51}V NMR spectra of the $\text{H}_{3+x}[\text{PV}_x\text{Mo}_{12-x}\text{O}_{40}]$ POMs with $x = 1$ to 6 in a mixture of 90% H_2O ($\text{pH } 1$) and 10% $\text{acetone-}d_6$. The spectra were measured at 157.8 MHz. NaVO_3 was used as external standard.

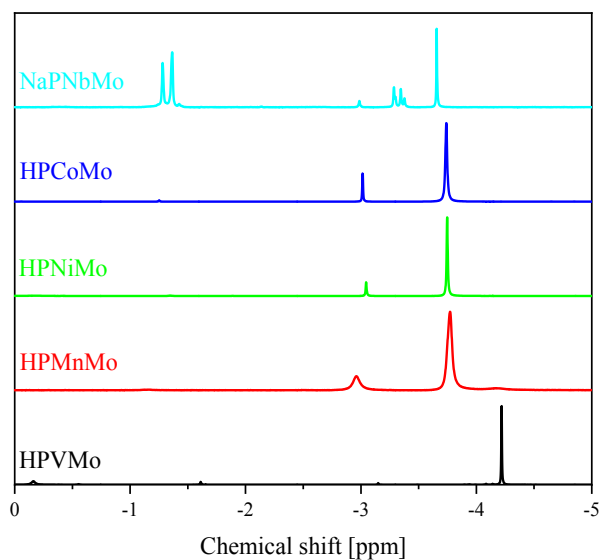


Figure S24: ^{31}P NMR spectra of the $\text{H}_z[\text{PMMo}_{11}\text{O}_{40}]$ POMs with $\text{M} = \text{Mn(II)}, \text{Co(II)}, \text{Ni(II)}, \text{Nb(V)}$ and $z = 4, 7$ in a mixture of 90% H_2O ($\text{pH } 1$) and 10% $\text{acetone-}d_6$. The spectra were measured at 242.9 MHz. 85% H_3PO_4 was used as external standard

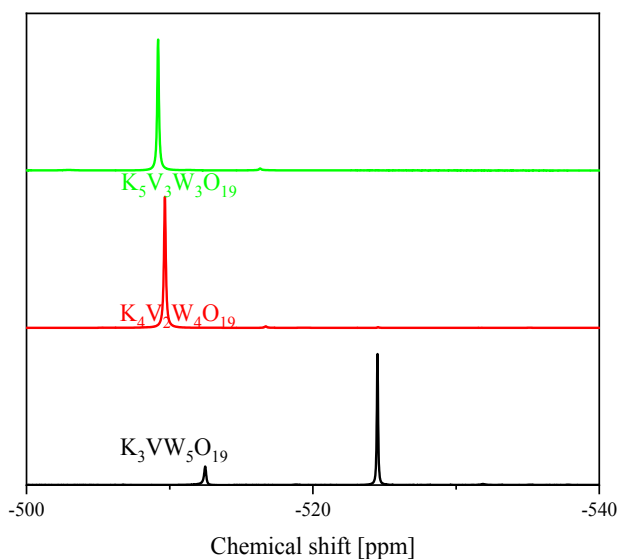


Figure S25: ^{51}V NMR spectra of the $\text{K}_{2+x}[\text{PV}_x\text{W}_{6-x}\text{O}_{19}]$ POMs with $x = 1$ to 3 in a mixture of 90 % H_2O (pH 1) and 10 % acetone- d_6 . The spectra were measured at 242.9 MHz. 85 % H_3PO_4 was used as external standard.

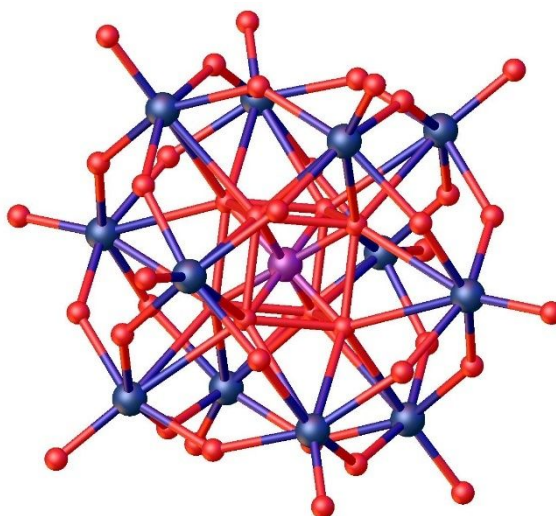


Figure S26: Solid-state structure of the monosubstituted Keggin type POM HPVMo determined using X-ray crystallography. The compound crystallized in space group $P4/mnc$ (128). There are nine atoms in the asymmetric unit. Residual electron density attributed to hydration water has been refined with a solvent mask (aka SQUEEZE). R_1 : 3.91 %, wR_2 : 9.47 %, R_{int} : 3.78 %, Goof : 1.091. Color code: purple: phosphorous, red: oxygen, and blue: metals (Mo, V).

The solid-state structure of HPVMo is shown in Figure S18: The compound was crystallized in space group $P4/mnc$ (128), with lattice parameters $a = 12.76142(19)$ Å, $b = 12.76142(19)$ Å, and $c = 18.0280(4)$ Å, and lattice angles $\alpha = \beta = \gamma = 90^\circ$. It is further evident from the solid-state structure that the central phosphorous atom is subject to a pronounced disorder, originated by dislocations of the central PO_4 tetrahedron in successive unit cells.

Therefore, the occupancies of the oxygen atoms directly bonded to the central phosphorus atom were each refined to 0.5. The metals are all in octahedral coordination through six oxygen atoms each and carry one terminal oxygen atom each. The bond length of the P1-O1 bond is 1.536 Å, the bond of the phosphorus/metal bridging oxygen atom O1-M1,2 is 2.442 Å, the bond O2,3,5-M1,2 (of the metal/metal bridging oxygen atoms) is 1.873 Å, and the bond of the terminal metal/oxygen bond M1,2=O4,6 is 1.640 Å. Compared to the sum of covalent radii (O-V: 1.97 Å; O-Mo: 2.01 Å)³, the M1,2=O4,6 bond is significantly shortened due to the double bond character, while the O₁-M_{1,2} bond is significantly lengthened, indicating coordinative bond character. The .cif file of the single crystal structures is available in the CCDC database with the deposition numbers 2220346 (for HPVMo).

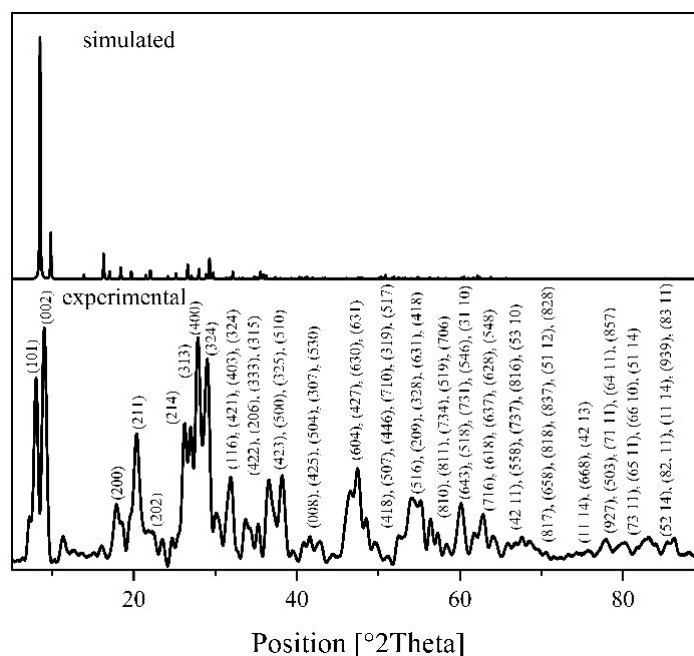


Figure S27: Comparison of simulated and measured powder XRD diffractograms of H₄[PVMoO₄₀] catalyst.

The powder XRD diffractogram was simulated from the single-crystal XRD data and compared with the experimentally measured diffractogram in Figure S27. As reported in our previous publication, a study of POMs using powder XRD is difficult, because there are always numerous solid-state phases of a POM present.⁴ The different solid-state phases, resulting after solvent evaporation, differ greatly in their hydration water content. For every mole of POM there are sometimes 8 to 20 moles of hydration water molecules, which are often highly disordered. Thus, the strong disorder of the hydration water can contribute to a significant non-crystallinity of the material. In addition, various non-crystalline phases are resulting after solvent evaporation, all of which complicate the interpretation of the diffractograms. It is therefore understandable that the presented single-crystal structure of H₄[PVMo₁₁O₄₀] only represents one solid-phase with a defined hydration water content. Due to the disorder of hydration water molecules, the single-crystal XRD data set was treated with a solvent mask (aka SQUEEZE). However, by carefully comparing the simulated and experimentally determined powder XRD data, some Miller planes could be assigned to the experimentally measured reflexes. Miller planes (101) and (002) can be assigned particularly well, which are located at 8° and 9° and differ from the simulated data only in their intensity.

The Miller planes given above the reflexes represent only a small amount of the most intense of all reflexes that can be assigned from the simulated data. It can be seen from both diffractograms that particularly intense reflexes are only observed at small angles, while mainly low-intensity reflexes are measured at larger angles. From the experimental data the reflexes measured at similar angles often merge to form one broad reflex. A similar observation is made for the powder XRD diffractograms of the remaining POMs, which are shown in Figure S28.

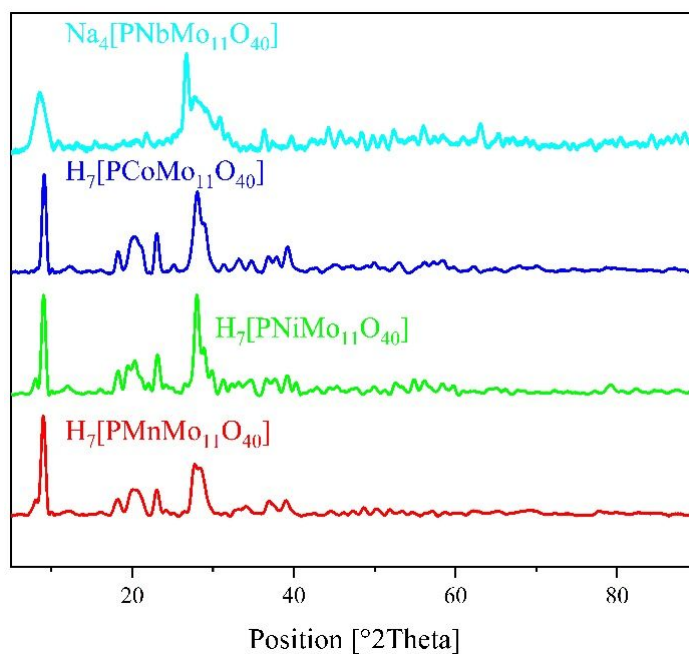


Figure S28: Powder XRD diffractograms for H₇[PMnMo₁₁O₄₀], H₇[PNiMo₁₁O₄₀], H₇[PCoMo₁₁O₄₀] and Na₄[PNbMo₁₁O₄₀] catalysts.

Analytics

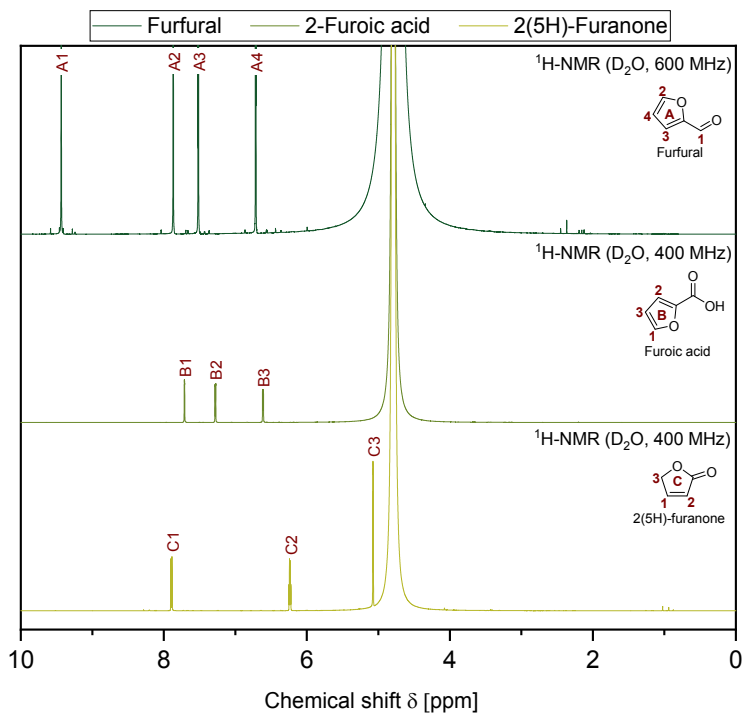


Figure S29: ¹H-NMR spectra (D₂O, 400 MHz) of the educts furfural, 2-furoic acid and 2(5H)-furanone.

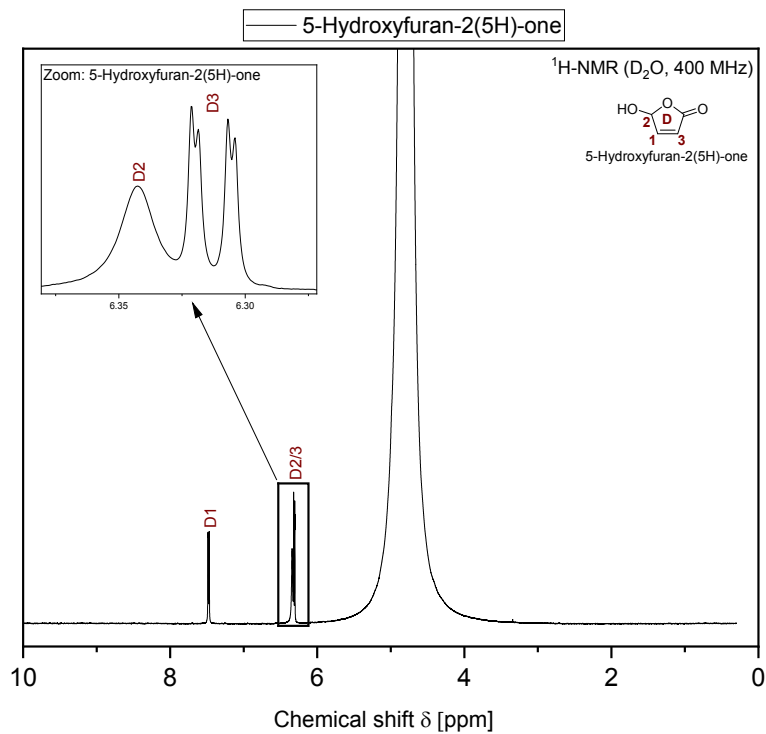


Figure S30: ¹H-NMR spectra (D₂O, 400 MHz) of the intermediate 5-Hydroxyfuran-2(5H)-one.

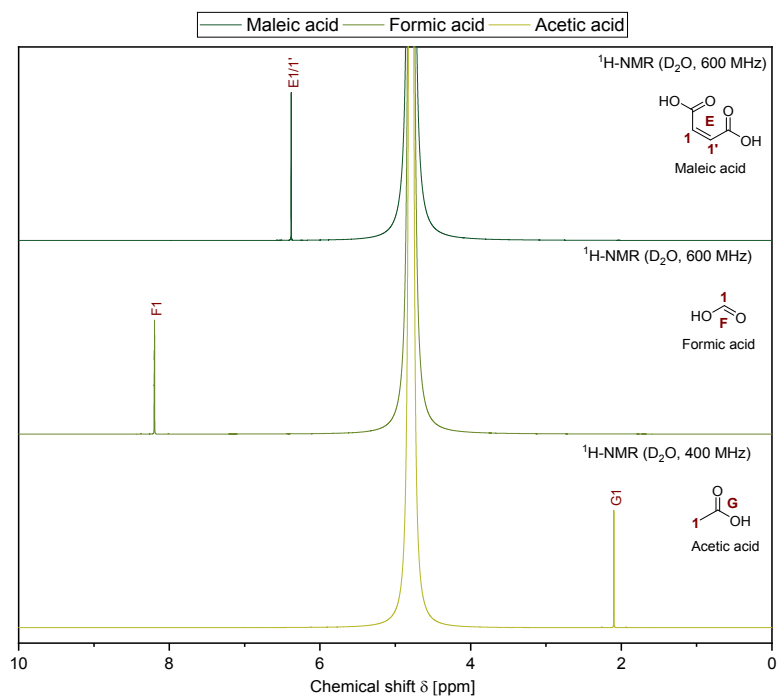


Figure S31: $^1\text{H-NMR}$ spectra (D_2O , 400 MHz) of products maleic acid, formic acid and acetic acid.

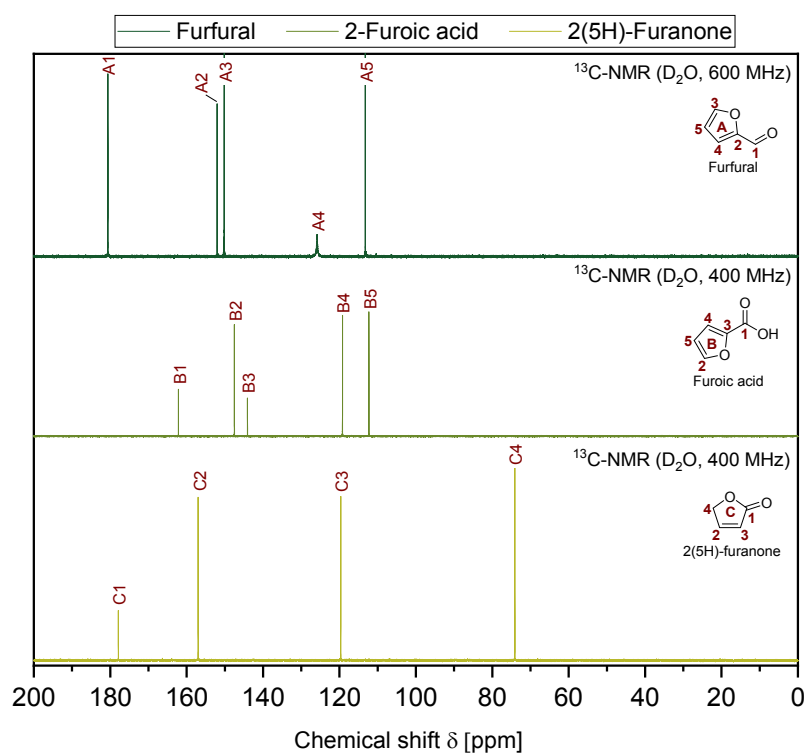


Figure S32: $^{13}\text{C-NMR}$ spectra (D_2O , 400 MHz) of products maleic acid, formic acid and acetic acid.

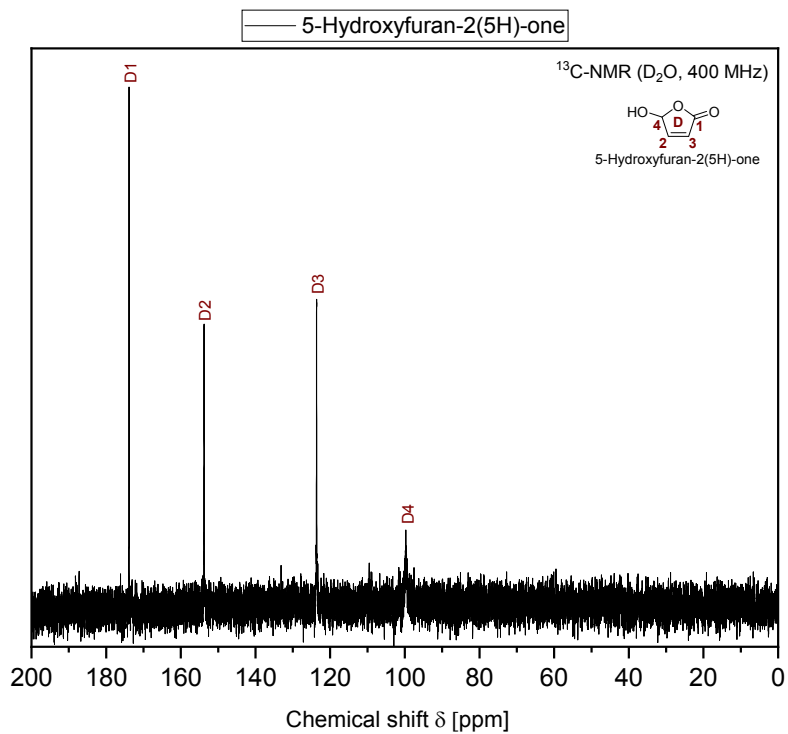


Figure S33: $^{13}\text{C-NMR}$ spectra (D_2O , 400 MHz) of the intermediate 5-hydroxyfuran-2(5H)-one.

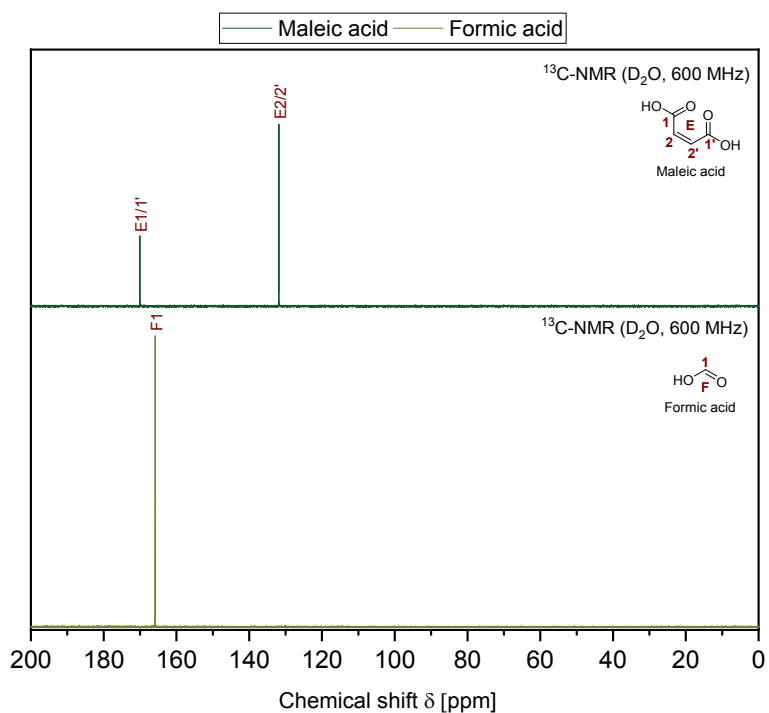


Figure S34: $^{13}\text{C-NMR}$ spectra (D_2O , 600 MHz) of products maleic acid and formic acid.

References

- 1 J. K. Lee, J. Melsheimer, S. Berndt, G. Mestl, R. Schlögl and K. Köhler, *Applied Catalysis A: General*, 2001, **214**, 125–148.
- 2 R. Mattes, H. Bierbsse and J. Fuchs, *Z. Anorg. Allg. Chem.*, 1971, **385**, 230–242.
- 3 P. Pyykkö and M. Atsumi, *Chemistry (Weinheim an der Bergstrasse, Germany)*, 2009, **15**, 186–197.
- 4 J.-C. Raabe, J. Albert and M. J. Poller, *Chemistry (Weinheim an der Bergstrasse, Germany)*, 2022, **28**, e202201084.

9.5.3 ESI of 3rd Publication (Chapter 6.3)

Content

Supporting Notes:

1 Selective Catalytic Oxidation of Humins (HPA-1)	Page 2 – 4
2 Stability Experiments for Additives (Alcohols)	Page 4 – 5
3 Reaction Experiments using Additives (pTSA)	Page 5 – 7
4 Reaction Experiments using Additives (pTSA & MeOH)	Page 8
5 Catalyst Characterization	Page 8 – 9

The following section is reproduced from Ref.²¹³ with permission of the *Royal Society of Chemistry*.

Supporting Information for

Selective catalytic oxidation of humins to carboxylic acids using the $H_4[PVMO_{11}O_{40}]$ Keggin-type polyoxometalate enhanced by alcohol doping and solubilizer

Tobias Esser^a, André Wassenberg^a, Dorothea Voß^a and Jakob Albert^{a*}

^a Institute of Technical and Macromolecular Chemistry, Universität Hamburg, Bundesstraße 45, 20146 Hamburg, Germany

*e-mail: jakob.albert@uni-hamburg.de

This document contains 1 Table and 15 Figures on 10 pages.

SCO of humins using the $H_4[PVMO_{11}O_{40}]$ Keggin-type polyoxometalate

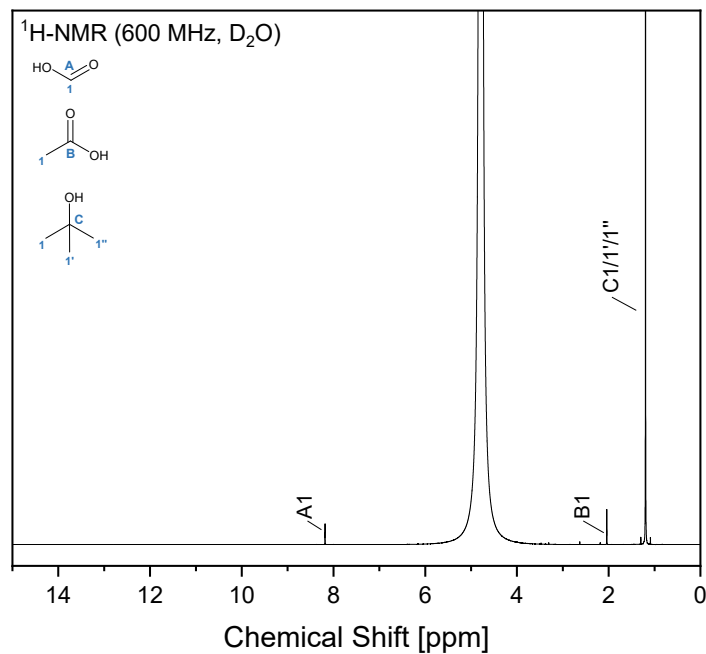


Figure S1: Exemplary 1H -NMR spectra (600 MHz, D_2O) for the liquid product phase of the selective catalytic oxidation of humin using $H_4[PVMO_{11}O_{40}]$ catalyst (HPA-1) in aqueous phase. *Experimental conditions:* 3-fold reaction system, 90 °C, 30 bar O_2 , 30 h, 1000 rpm, 830 mmol of vanadium (V) for substitution in 30 mL water.

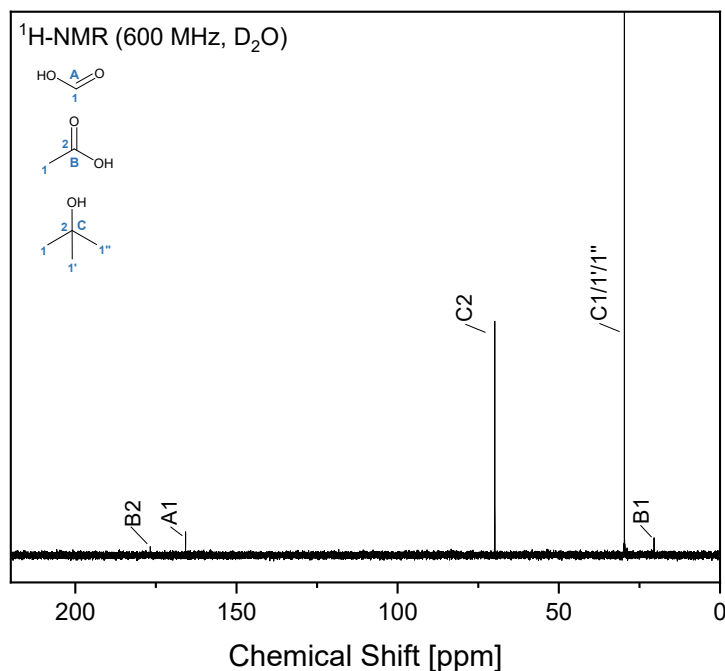


Figure S2: Exemplary ^{13}C -NMR spectra (600 MHz, D_2O) for the liquid product phase of the selective catalytic oxidation of humin using HPA-1 as catalyst in aqueous phase. *Experimental conditions:* 3-fold reaction system, 90 °C, 30 bar O_2 , 30 h, 1000 rpm, 83 mmol of vanadium (V) for substitution in 30 mL water.

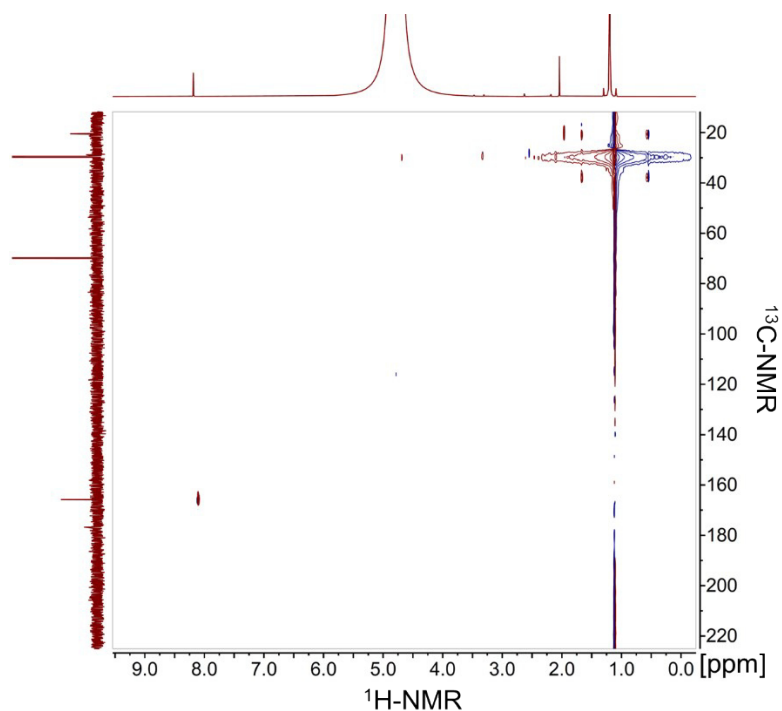


Figure S3: Exemplary HSQC spectra (600 MHz, D₂O) for the liquid product phase of the selective catalytic oxidation of humin using HPA-1 as catalyst in aqueous phase. *Experimental conditions:* 3-fold reaction system, 90 °C, 30 bar O₂, 30 h, 1000 rpm, 83 mmol of vanadium (V) for substitution in 30 mL water.

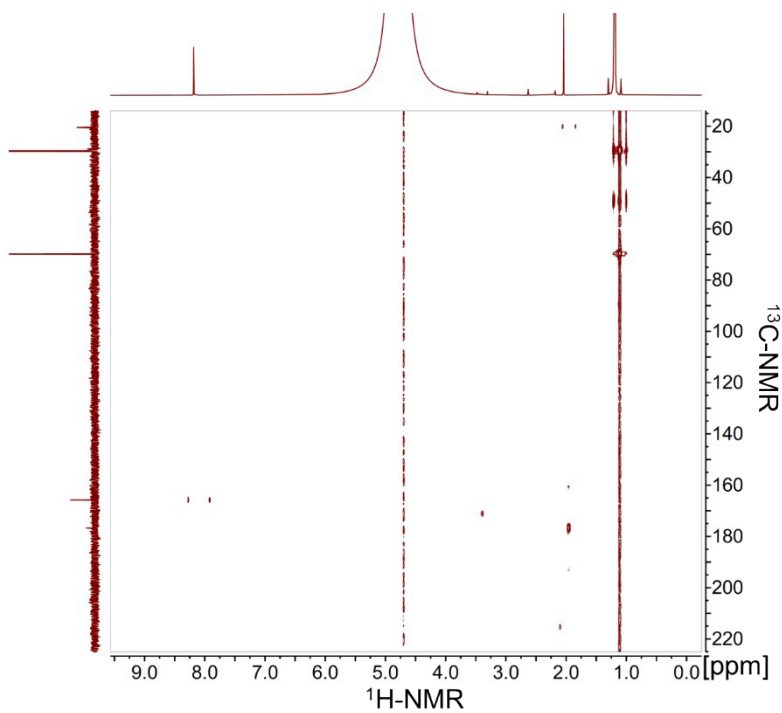


Figure S4: Exemplary HMBC spectra (600 MHz, D₂O) for the liquid product phase of the selective catalytic oxidation of humin using HPA-1 as catalyst in aqueous phase. *Experimental conditions:* 3-fold reaction system, 90 °C, 30 bar O₂, 30 h, 1000 rpm, 83 mmol of vanadium (V) for substitution in 30 mL water.

Table S1: Comparison of quantification via $^1\text{H-NMR}$ and HPLC for the selective catalytic oxidation of humins using HPA-1 as catalyst in aqueous phase.

Entry	Catalyst	Total Yield / %		Combined Yield / % (FA + AA)	
		$^1\text{H-NMR}^b$	HPLC ^c	$^1\text{H-NMR}^b$	HPLC ^c
1 ^a	Blank	11.2	11.3	3.2	3.3
2 ^a	$\text{H}_4[\text{PVMo}_{11}\text{O}_{40}]$	30.1	29.8	10.9	10.6

Experimental Conditions: a) 3-fold reaction system, 90 °C, 30 bar O_2 , 30 h, 1000 rpm, 300 mg solid humin (16.20 mmol carbon), 0.83 mmol of vanadium (V) for substitution (20 mol_{Carbon} mol⁻¹_V) in 30 mL water, b) determined with quantitative $^1\text{H-NMR}$ and tert.-butanol as standard, c) determined with HPLC according to the corresponding section of the experimental part.

Selection of a suitable additive for the suppression of CO_2 formation in SCO of humins

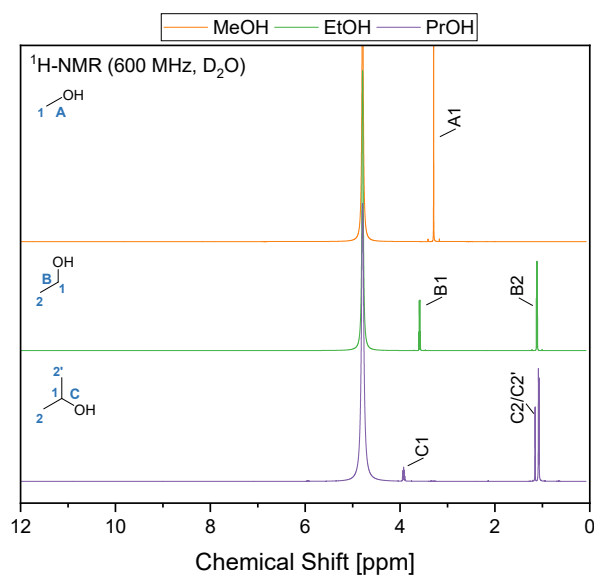


Figure S5: $^1\text{H-NMR}$ spectra (600 MHz, D_2O) for the liquid product phase of the additive stability experiments using HPA-1 as catalyst in alcohol-doped aqueous phase. *Experimental conditions:* 3-fold reaction system, 90 °C, 30 bar O_2 , 30 h, 1000 rpm, 83 mmol of vanadium (V) for substitution in 30 mL of 10-vol.% aqueous solution of the respective alcohol.

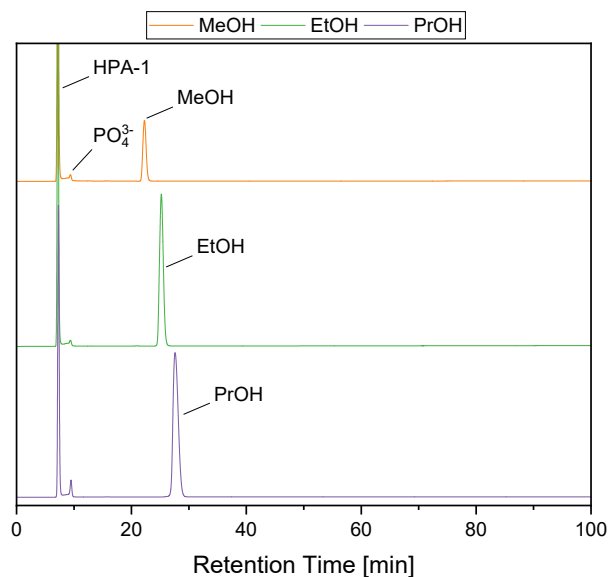


Figure S6: Chromatograms for the liquid product phase of the additive stability experiments using HPA-1 as catalyst in alcohol-doped aqueous phase. *Experimental conditions:* 3-fold reaction system, 90 °C, 30 bar O₂, 30 h, 1000 rpm, 0.83 mmol of vanadium (V) for substitution in 30 mL of 10-vol.% aqueous solution of the respective alcohol.

The effect of para-toluene sulfonic acid as solubilizer on the SCO of humins

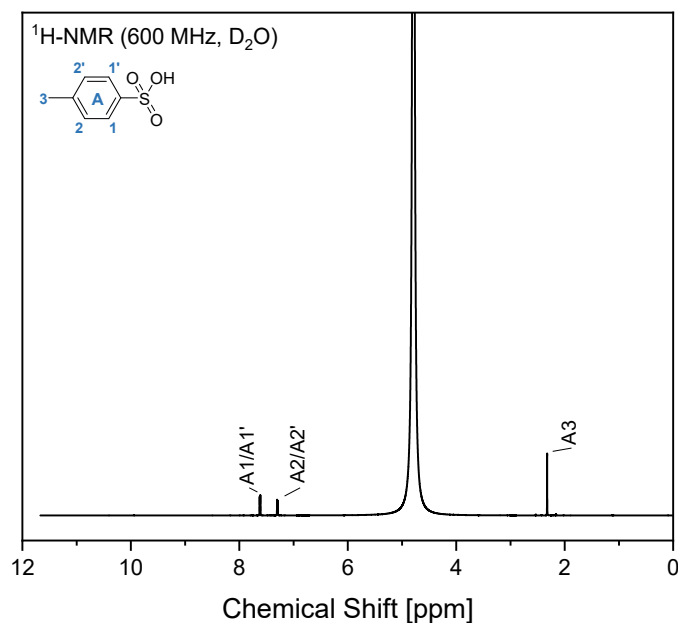


Figure S7: ¹H-NMR spectra (600 MHz, D₂O) for the liquid product phase of the pTSA stability experiment using HPA-1 as catalyst in aqueous phase. *Experimental conditions:* 3-fold reaction system, 90 °C, 30 bar O₂, 30 h, 1000 rpm, 0.83 mmol of vanadium (V) for substitution and 3.0 mmol pTSA in 30 mL aqueous phase.

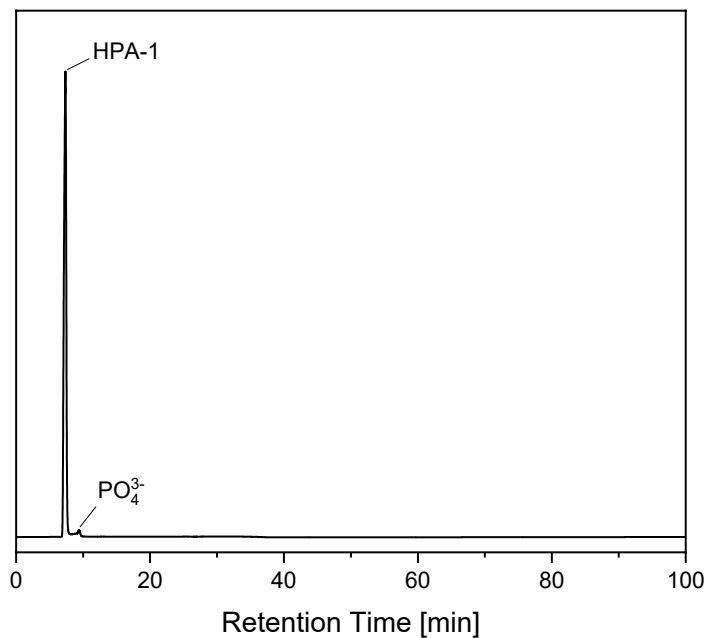


Figure S8: Chromatogram for the liquid product phase of the pTSA stability experiment using HPA-1 as catalyst in aqueous phase. *Experimental conditions:* 3-fold reaction system, 90 °C, 30 bar O₂, 30 h, 1000 rpm, 0.83 mmol of vanadium (V) for substitution and 3.0 mmol pTSA in 30 mL aqueous phase.

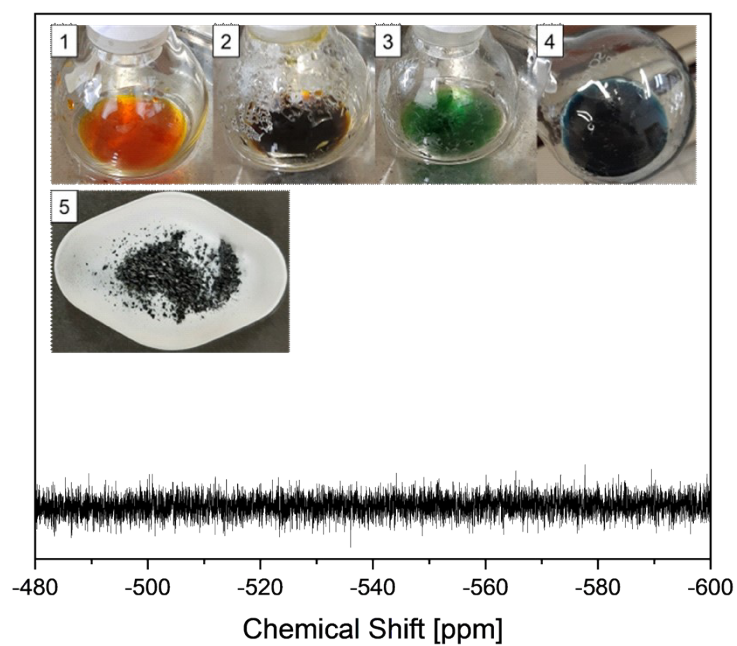


Figure S9: ⁵¹V-NMR spectra (600 MHz, D₂O) for the reduced HPA-1 catalyst in aqueous phase.

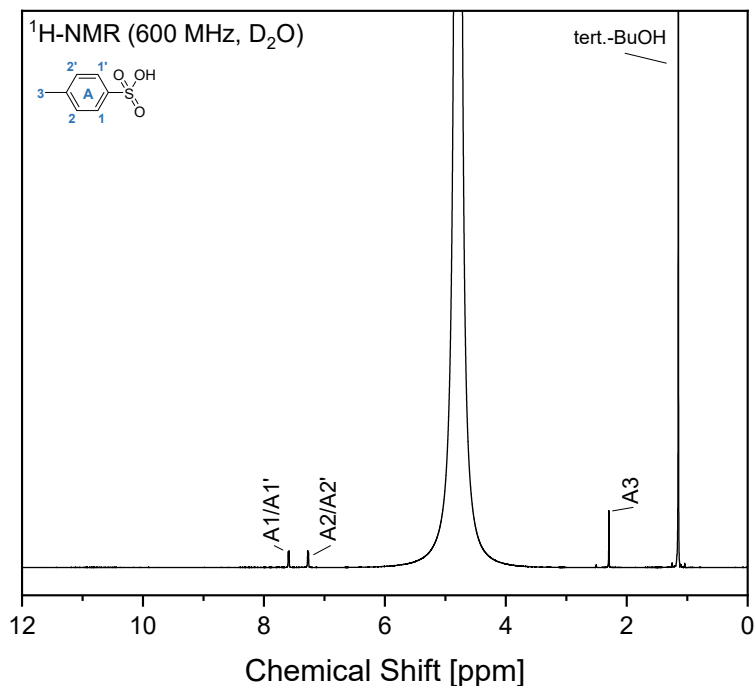


Figure S 10: ¹H-NMR spectra (600 MHz, D₂O) for the liquid product phase of the pTSA stability experiment using fully reduced HPA-1 blue as catalyst in aqueous phase. *Experimental conditions:* 3-fold reaction system, 90 °C, 30 bar O₂, 30 h, 1000 rpm, 0.83 mmol of vanadium (V) for substitution and 3.0 mmol pTSA in 30 mL aqueous phase.

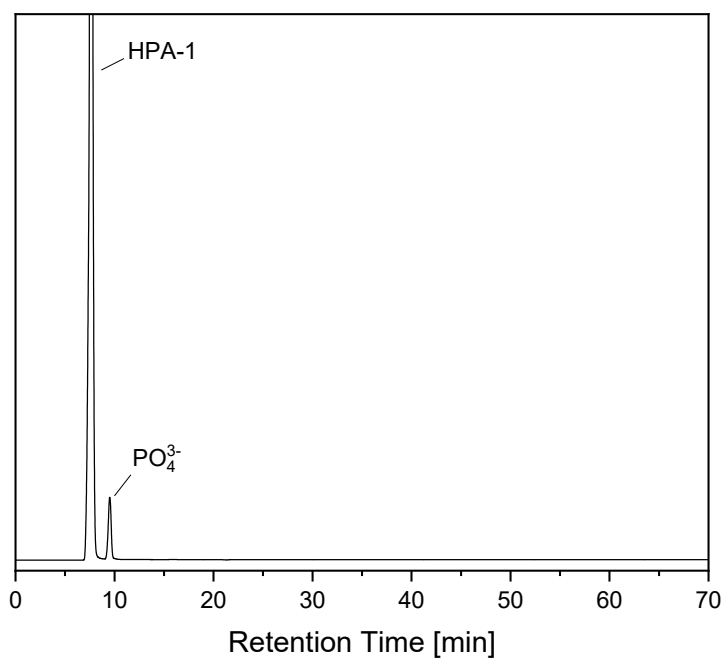


Figure S 11: Chromatogram for the liquid product phase of the pTSA stability experiment using fully reduced HPA-1 blue as catalyst in aqueous phase. *Experimental conditions:* 3-fold reaction system, 90 °C, 30 bar O₂, 30 h, 1000 rpm, 0.83 mmol of vanadium (V) for substitution and 3.0 mmol pTSA in 30 mL aqueous phase.

Optimization of SCO of humins by synergetic combination of MeOH and pTSA

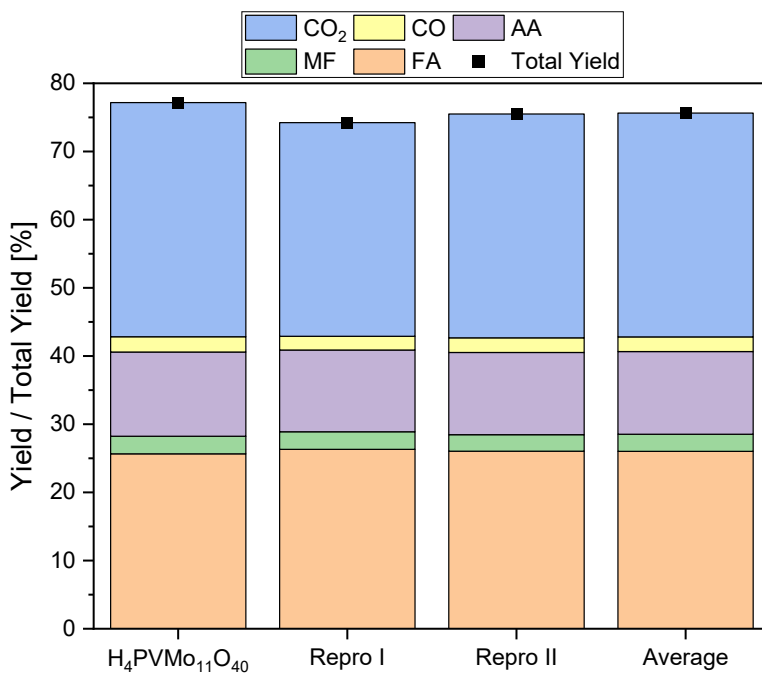


Figure S12: Reproduction for selective catalytic oxidation of humin using HPA-1 as catalyst in aqueous methanol solution with pTSA (combined system). *Experimental conditions:* 3-fold reaction system, 120 °C, 30 bar O₂, 30 h, 1000 rpm, 300 mg solid solid humin (16.20 mmol carbon), 0.83 mmol of vanadium (V) for substitution (20 mol_{Carbon} mol⁻¹_V) in 5 vol.-% methanol with 1.5 mmol pTSA.

Catalyst characterization

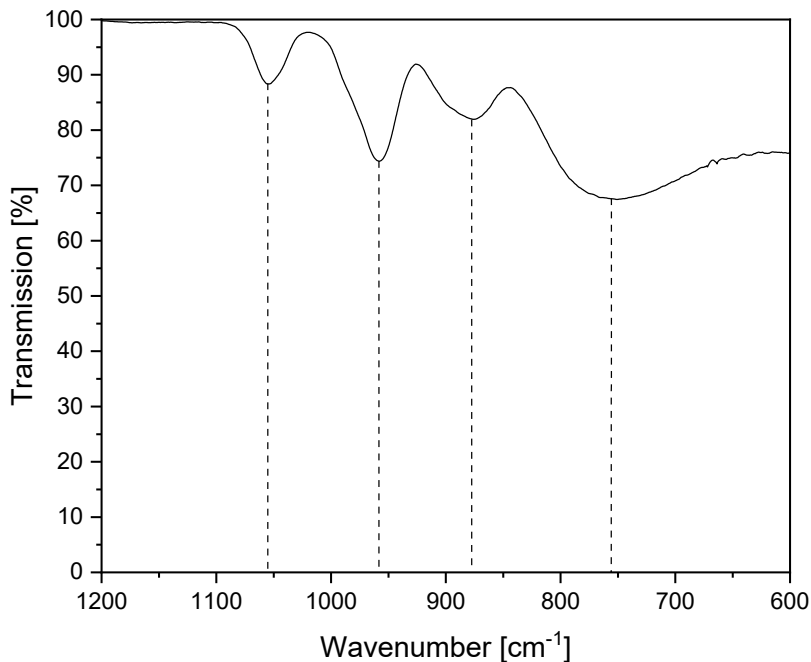


Figure S13: FT-IR (ATR) spectrum of the H₄[PVMo₁₁O₄₀] POM-catalyst. Vibration modes: 1055 cm⁻¹ (P-O), 958 cm⁻¹ (M=O_i), 877 cm⁻¹ ((M-O-M)_{vertex}), 756 cm⁻¹ ((M-O-M)_{edge}).¹

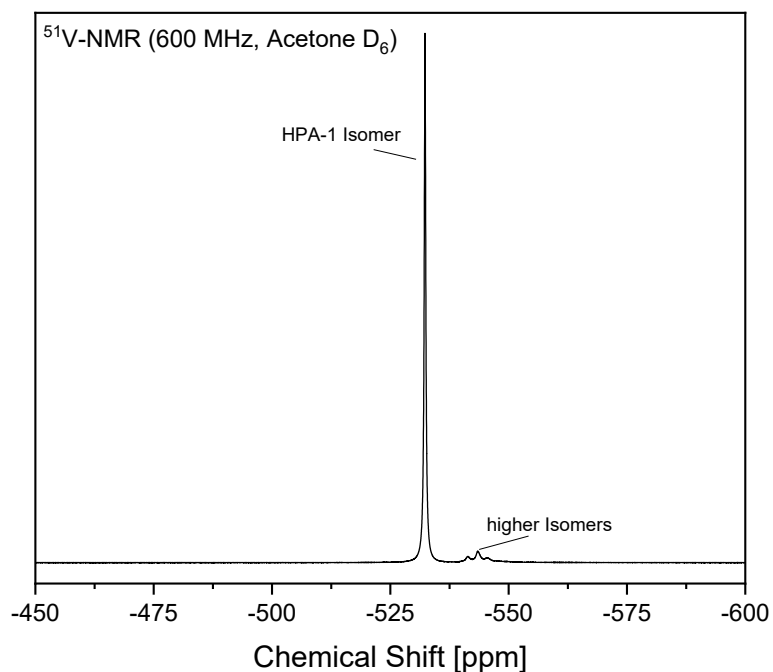


Figure S14: ^{51}V NMR spectrum of the $\text{H}_4[\text{PVMo}_{11}\text{O}_{40}]$ POM-catalyst in a mixture of 90 % H_2O (pH 1) and 10 % acetone- d_6 . NaVO_3 was used as external standard.

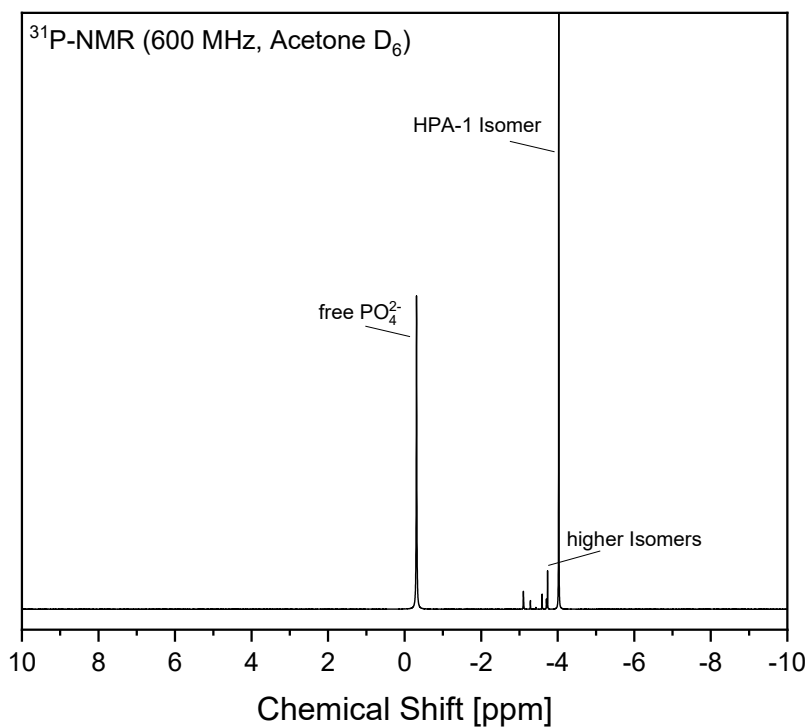


Figure S15: ^{31}P NMR spectrum of the $\text{H}_4[\text{PVMo}_{11}\text{O}_{40}]$ POM-catalyst in a mixture of 90 % H_2O (pH 1) and 10 % acetone- d_6 . 85 % H_3PO_4 was used as external standard.

References

- 1 J. K. Lee, J. Melsheimer, S. Berndt, G. Mestl, R. Schlögl and K. Köhler, *Applied Catalysis A: General*, 2001, **214**, 125–148.

9.5.4 ESI of 4th Publication (Chapter 6.4)

Content

Supporting Notes:

1 Oxidation of humins using HPA-2	Page 1
2 Stability experiments using HPA-2	Page 1
3 Separation of products and catalyst	Page 2
4 Recycling experiments	Page 2

The following section is reproduced from Ref.²¹⁴ published in *Chemical Engineering Research and Design*, Elsevier.

Supporting Information

SCO of humins using HPA-2 as catalyst

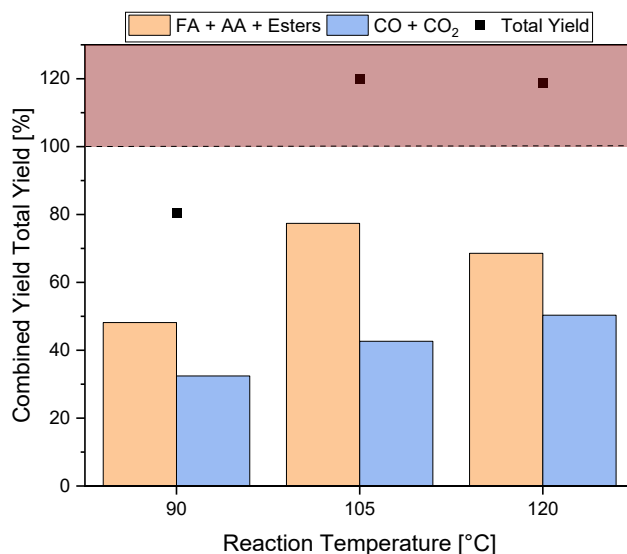


Figure S1: Oxidation experiments of glucose-based humin using HPA-2 as catalyst in aqueous solution at reaction temperatures of 90 °C to 120 °C in the combined system. *Experimental conditions:* 3-fold reaction system, 90 °C – 120 °C, 30 bar O₂, 30 h, 1000 rpm, 300 mg solid humin (16.2 mmol carbon), 0.83 mmol of vanadium (20 mol_{Carbon} mol⁻¹_V) in 95:5 vol.-% water-methanol with 1.50 mmol pTSA.

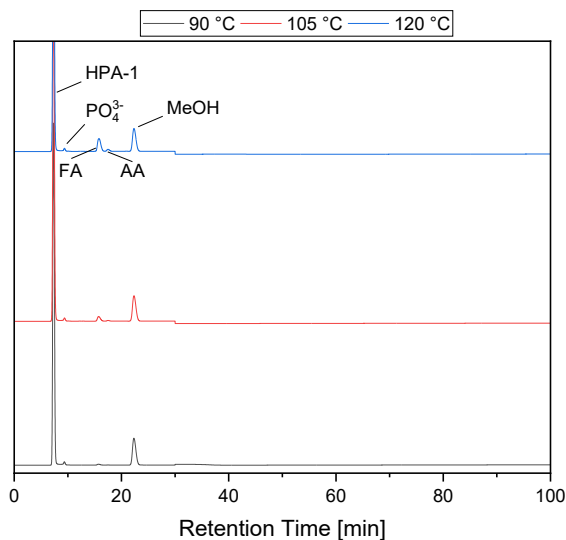


Figure S2: Chromatograms for the liquid product phase of the additive stability experiments using HPA-2 in the enhanced system. *Experimental conditions:* 3-fold reaction system, 90 °C - 120 °C, 30 bar O₂, 30 h, 1000 rpm, 300 mg solid humin (16.2 mmol carbon), 0.83 mmol of vanadium (20 mol_{Carbon} mol⁻¹_V) in 95:5 vol.-% water-methanol with 1.50 mmol pTSA.

Efficient product removal and catalyst recovery using nanofiltration

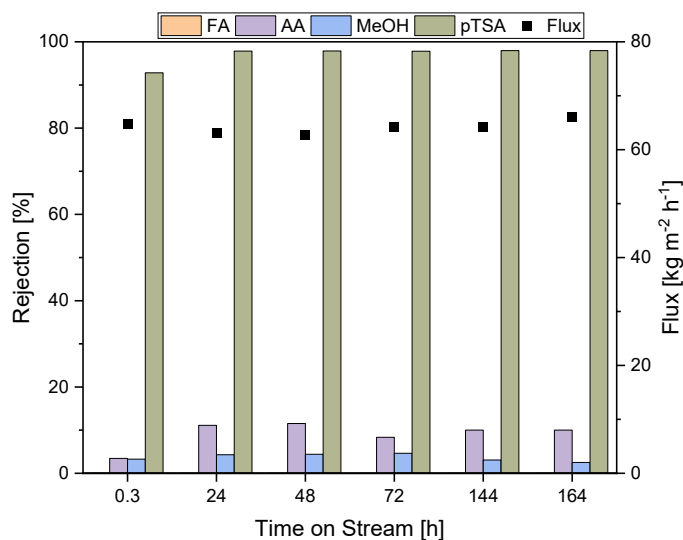


Figure S3: Development of membrane performance by means of product and additive rejection in dependency of the time on stream in membrane stability experiments using a model solution *Experimental conditions:* pre-wetted XN-45 nanofiltration membrane, ambient temperature, 30 bar transmembrane pressure, 15 mL min⁻¹ flow rate, 1100 rpm stirring speed, model solution containing HPA-2, FA, AA and pTSA in 95:5 vol.-% water-methanol.

Enrichment and recycling of HPA-2 using nanofiltration

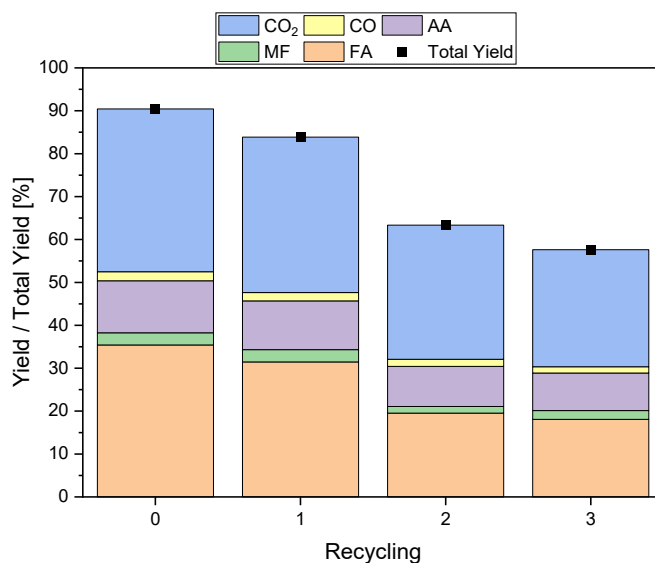


Figure S4: Recycling experiments for selective catalytic oxidation of glucose-based humin using HPA-2 with addition of pTSA. *Experimental conditions:* 90 °C, 30 bar O₂, 24 h, 1000 rpm, 1500 mg solid humin (81.0 mmol carbon), 4.15 mmol of vanadium (20 mol_{Carbon} mol⁻¹_v) and 7.50 mmol pTSA in 150 mL 95:5 vol.-% water-methanol.

Acknowledgments

This study was conducted between October 2020 and September 2023 at the Institute of Technical and Macromolecular Chemistry of the University Hamburg (UHH). I would like to take this opportunity to thank all those who have contributed to the success of the present work in recent years.

First, I would like to express my gratitude to Prof. Dr.-Ing. Jakob Albert, my doctorate supervisor and leader of the Albert research group, for the intriguing topic as well as the numerous technical discussions. Many thanks also for the freedom to shape my research and the support in publishing the results in recognized journals. I particularly enjoyed the joint participation in conferences and thus the change from everyday laboratory work.

I would like to thank Prof. Dr.-Ing. Mirko Skiborowski for the preparation of the second opinion to the present work and the opportunity to conduct initial membrane screening experiments in his research group at the Institute of Process Systems Engineering at the Hamburg University of Technology (TUHH). I would also like to take this opportunity to thank Dr.-Ing. Kai Kruber and the colleagues at the TUHH who supported me during my stay in the research group.

A special thanks goes to our senior engineer Dr.-Ing. Dorothea Voß for the many productive discussions and her open ear. Doro accompanied me on this journey as a supervisor, colleague and friend. The value of her support and encouragement cannot be put into words. A big thank you goes to our post-docs Dr.-Ing. Anna Bukowski and Dr. Maximilian Poller. I would particularly like to emphasize Anna's energetic and motivating manner as well as technical expertise, which often provided a welcome tailwind. Max's impressive wealth of knowledge and pragmatic nature have often helped to find workable solutions.

Furthermore, I would like to thank all my colleagues in the Albert research group for the hours spent together in the labs, but also for the time spent outside of work. A special thanks go to my colleagues of the former D29 office, André Wassenberg and Michael Huber. I would like to thank Hubsy for the helpful discussions. André, as my project partner, supported me in the preparation of humins, which he referred to affectionately as „new batch of dirt“ and also I am thankful for the discussions regarding publications and further progress of our overall project. Also, I am grateful for the

friendship that has grown over the years and the change of perspective in forms of relaxed / funny evenings.

I would also like to thank Steffanie Wesinger for her diligent efforts when the HPLC was not working, for her conscientious cutting of membranes and her collegial nature. I enjoyed the time “rocking” with Steffi, especially outside of the lab to good rock music. I would also like to thank Jan-Christian Raabe for his inspiring nature. Infinity is incomprehensible to the human mind, but nevertheless describes Jan's boundless enthusiasm for research and especially for polyoxometalates.

I would also like to express my sincere thanks to the permanent staff at the institute. I would particularly like to highlight Michael Gröger's efforts in converting laboratory equipment. I thank him for the always good cooperation.

At last, a big thank you goes to my family and friends. Above all I would like to thank my father, who always made the effort to visit me, no matter where I went. I would like to thank my closest friends Andi, Eddy, André, Timo, Arthur and Nikola for their open ears, the fun times and trips. There is little that can encourage me more in stormy times than spending time with them. A special thank you goes to my partner Jessica. No one has experienced the ups and downs of completing this work as closely as she has. I am grateful for the support when things didn't go as planned and for celebrating successes together. The list of things I would like to thank for is too long to write down here, so all that remains is a simple thank you for all.

Eidesstattliche Versicherung

„Hiermit versichere ich an Eides statt, die vorliegende Dissertationsschrift selbst verfasst und keine anderen als die angegebenen Quellen und Hilfsmittel benutzt zu haben. Sofern im Zuge der Erstellung der vorliegenden Dissertationsschrift generative Künstliche Intelligenz (gKI) basierte elektronische Hilfsmittel verwendet wurden, versichere ich, dass meine eigene Leistung im Vordergrund stand und dass eine vollständige Dokumentation aller verwendeten Hilfsmittel gemäß der Guten wissenschaftlichen Praxis vorliegt. Ich trage die Verantwortung für eventuell durch gKI generierte fehlerhafte oder verzerrte Inhalte, fehlerhafte Referenzen, Verstöße gegen das Datenschutz- und Urheberrecht oder Plagiate.“

Unterschrift:



Tobias Esser

Datum: 21.08.2024

Declaration on Oath

"I hereby declare on oath that I have written this dissertation myself and have not used any sources or aids other than those specified. Insofar as electronic resources based on generative artificial intelligence (gKI) were used in the preparation of this thesis, I declare that my own work was in the foreground and that all resources used are fully documented in accordance with good scientific practice. I am responsible for any erroneous or distorted content, incorrect references, violations of data protection and copyright law or plagiarism that were generated by gKI."

Signature:



Tobias Esser

Date: 21.08.2024